

GEORGIA INSTITUTE OF TECHNOLOGY
OFFICE OF CONTRACT ADMINISTRATION

NOTICE OF PROJECT CLOSEOUT

Closeout Notice Date 03/24/93

Project No. E-16-654 _____ Center No. R6101-0A0 _____

Project Director ARMANIOS E A _____ School/Lab AERO ENGR _____

Sponsor NASA/LANGLEY RESEARCH CTR, VA _____

Contract/Grant No. NAG-1-637 _____ Contract Entity GTRC

Prime Contract No. _____

Title ANALYSIS OF DELAMINATION RELATED FRACTURE PROCESSES IN COMPOSITES _____

Effective Completion Date 921225 (Performance) 921225 (Reports)

Closeout Actions Required:	Y/N	Date Submitted
Final Invoice or Copy of Final Invoice	Y	_____
Final Report of Inventions and/or Subcontracts	Y	_____
Government Property Inventory & Related Certificate	N	_____
Classified Material Certificate	N	_____
Release and Assignment	N	_____
Other _____	N	_____

Comments LETTER OF CREDIT APPLIES. EFFECTIVE DATE 2-12-86. _____
CONTRACT VALUE \$345,000. _____

Subproject Under Main Project No. _____

Continues Project No. _____

Distribution Required:

Project Director	Y
Administrative Network Representative	Y
GTRI Accounting/Grants and Contracts	Y
Procurement/Supply Services	Y
Research Property Management	Y
Research Security Services	N
Reports Coordinator (OCA)	Y
GTRC	Y
Project File	Y
Other HARRY VANN-FMD _____	Y
FRED CAIN-OOD _____	Y

NOTE: Final Patent Questionnaire sent to PDPI.

E-13-1-11

SEMI-ANNUAL REPORT

ANALYSIS OF DELAMINATED RELATED
FRACTURE PROCESSES IN COMPOSITES

NASA GRANT NAG-1-637
GEORGIA TECH PROJECT E16-654

PRINCIPAL INVESTIGATORS
Lawrence W. Rehfield and Erian A. Armanios

This report covers the research work performed under Grant NAG-1-637 for the period starting February 1986 and ending August 1986. The work described herein was performed at the School of Aerospace Engineering, Georgia Institute of Technology. The research objectives are:

- (1) Develop an analysis of a symmetric edge delamination specimen including residual strain effects due to temperature and moisture;
- (2) Compare predictions with those of Ref. 1 for the example cases;
- (3) Develop an analysis for delamination in tapered specimens; and
- (4) Create appropriate computer programs and documentation for the NASA Langley Research Center.

In relation to the first objective, the computer code for the edge delamination (ED) analysis without residual strains has been modified to deal with hybrid laminates (plies of different materials). The code has been exercised through comparison with the finite element results provided by NASA Langley. A complete validation study of this version is underway.

The sublaminates analysis of the ED specimen is modified to include residual strain effects. The governing equations have been established. They are being checked before including them in the computer code.

An equilibrium analytical model has been developed for tapered specimens. The interlaminar stresses predicted by this model have been validated through comparison with the finite element results of Ref. 2. The total energy release rate will be compared with the recent simple analysis method of Ref. 3.

Final results for the tapered specimens and residual strain effects in the ED specimens are expected at the end of the year grant.

REFERENCES

1. O'Brien, T.K., Raju, I.S. and Garber, D.P., "Residual Thermal and Moisture Influences on the Strain Energy Release Rate Analysis of Edge Delamination," NASA TM 86437, USAAVSCOM TM 85-B-4, NASA Langley Research Center, June 1985.
2. Chan, W.S., Private Communication, Bell Helicopter Textron Incorporated, August 1985.
3. O'Brien, T.K., "Delamination Durability of Composite Materials for Rotorcraft: Analysis, Characterization and Design," RPI Workshop on Composite Materials and Structures for Rotorcraft, Rensselaer Polytechnic Institute, Troy, NY, September 10-11, 1986.

E-16-654

SEMIANNUAL REPORT

ANALYSIS OF DELAMINATED RELATED
FRACTURE PROCESSES IN COMPOSITES

NASA GRANT NAG-1-637
GEORGIA TECH PROJECT E16-654

PRINCIPAL INVESTIGATORS

Lawrence W. Rehfield and Erian A. Armanios

Overview:

This report covers the research work performed under Grant NAG-1-637 for the period starting August 1986 and ending February 1987. The work described herein was performed at the School of Aerospace Engineering, Georgia Institute of Technology. The research objectives are:

- (1) Develop an analysis of a symmetric edge delamination specimen including residual strain effects due to temperature and moisture;
- (2) Compare predictions with those of Ref. 1 for the example cases;
- (3) Develop an analysis for delamination in tapered specimens; and
- (4) Create appropriate computer programs and documentation for the NASA Langley Research Center.

The first objective is completed. A computer program and documentation has been developed based on the analysis. The code has been checked and the second objective is under completion. A summary paper describing the analysis and the validation study through comparisons with the results of Ref. 1 will be sent to the technical monitor for his review. Also a computer tape will be provided to run cases of interest.

The total energy release rate analysis for the tapered specimens is underway. This represents the final phase of work associated with the third objective. A validation study of the analysis will be performed by comparison with the results of Ref. 2 and other available test cases.

In analyzing the ED specimen, emphasis is given to the evaluation of the total energy release rate as well as the energy release rate components. Based on these modal components, the onset and growth of edge delaminations can be predicted using an appropriate fracture law. The present analysis provides also estimates of the interlaminar shear stress distribution ahead of the delamination front. These distributions can be sensitive to hygrothermal conditions. A preliminary assessment of hygrothermal conditions on interlaminar stresses has been performed and the results are summarized in the following.

Effect of Hygrothermal Conditions on Interlaminar Stresses

To investigate the influence of residual and moisture conditions on interlaminar stresses, the case of $[35/-35/0/90]_S$, $[35/0/-35/90]_S$ and $[0/35/-35/90]_S$ ED specimens are considered. The specimens are subjected to a mechanical strain of 0.00254 at a room temperature of 70°F. The specimens are made of T300/5208 graphite/epoxy material with a cure temperature of 350°F. The moisture weight gain is 0.6 percent. The material properties are those of Reference 1. A comparison of the interlaminar shear stress (σ_{yz}) distributions is presented in Figures 1-3. Labels M, M+T and M+T+H denotes Mechanical, Mechanical and Thermal and Mechanical, Thermal and Moisture effects, respectively. For the layups considered M+T and M+T+H distributions are indistinguishable at this level of moisture weight gain. In contrast, the shape of σ_{yz} distribution ahead of the delamination front is drastically changed due to thermal effects as well as the maximum value at the crack front. The maximum shear stress due to hygrothermal effect is 3.20, 3.25 and 3.35 times the mechanical shear stress at the crack front for the first, second and third layups, respectively. This is due to the fact that hygrothermal residual stresses produce considerable mismatch between the effective thermal and moisture expansion between the upper ply units and the 90 ply in each layup.

A similar finding is presented in Reference 3 for a bidirectional graphite/epoxy laminate subjected to a mechanical strain $\epsilon=0.01$, with a temperature differential from cure temperature to test temperature of -243°F (-117°C). The laminate layup is $[0_3/90_3]_S$. Moisture effects were not considered in this work. The ratio of the maximum peel stress (σ_{zz}) due to thermal residual stress is 2.8 the mechanical stress as shown in Fig. 4 of the Reference.

Closing Remarks

Residual stresses due to fabrication and moisture can have a significant influence on the interlaminar stress distribution at the delamination front. Preliminary results on their effect on the total energy release rate and the energy release rate components show a similar trend. The interlaminar stress increase associated with hygrothermal effects can lead to premature failure and should be considered in the design stage. The present study points to new directions and inquiries. For example, the cases of nonuniform distribution of moisture through-the-thickness and the variation of ambient temperature with the laminate thickness. In this situation, the hygrothermal gradients through-the-thickness may create an unbalance effect in an originally balanced construction. This additional consideration should be accounted for specially for aerospace structural components subjected to a large temperature difference between their upper and lower surfaces.

REFERENCE

1. O'Brien, T.K., Raju, I.S. and Garber, D.P., "Residual Thermal and Moisture Influences on the Strain Energy Release Rate Analysis of Edge Delamination," Journal of Composites Technology & Research, Vol. 8, No. 2, Summer 1986, pp. 37-47.
2. O'Brien, T.K., "Delamination Durability of Composite Materials for Rotorcraft: Analysis, Characterization and Design," RPI Workshop on Composite Materials and Structures for Rotorcraft, Rensselaer Polytechnic Institute, Troy, NY, September 10-11, 1986.
3. Whitney, J.M., "Stress Analysis of a Mode I Edge Delamination Specimen for Composite Materials," Proceedings of the AIAA/ASME/AHS 26th Structures, Structural Dynamics, and Materials (SDM) Conference, Orlando, Florida, 15-17 April 1985. AIAA paper No. 85-0611, pp. 34-40.

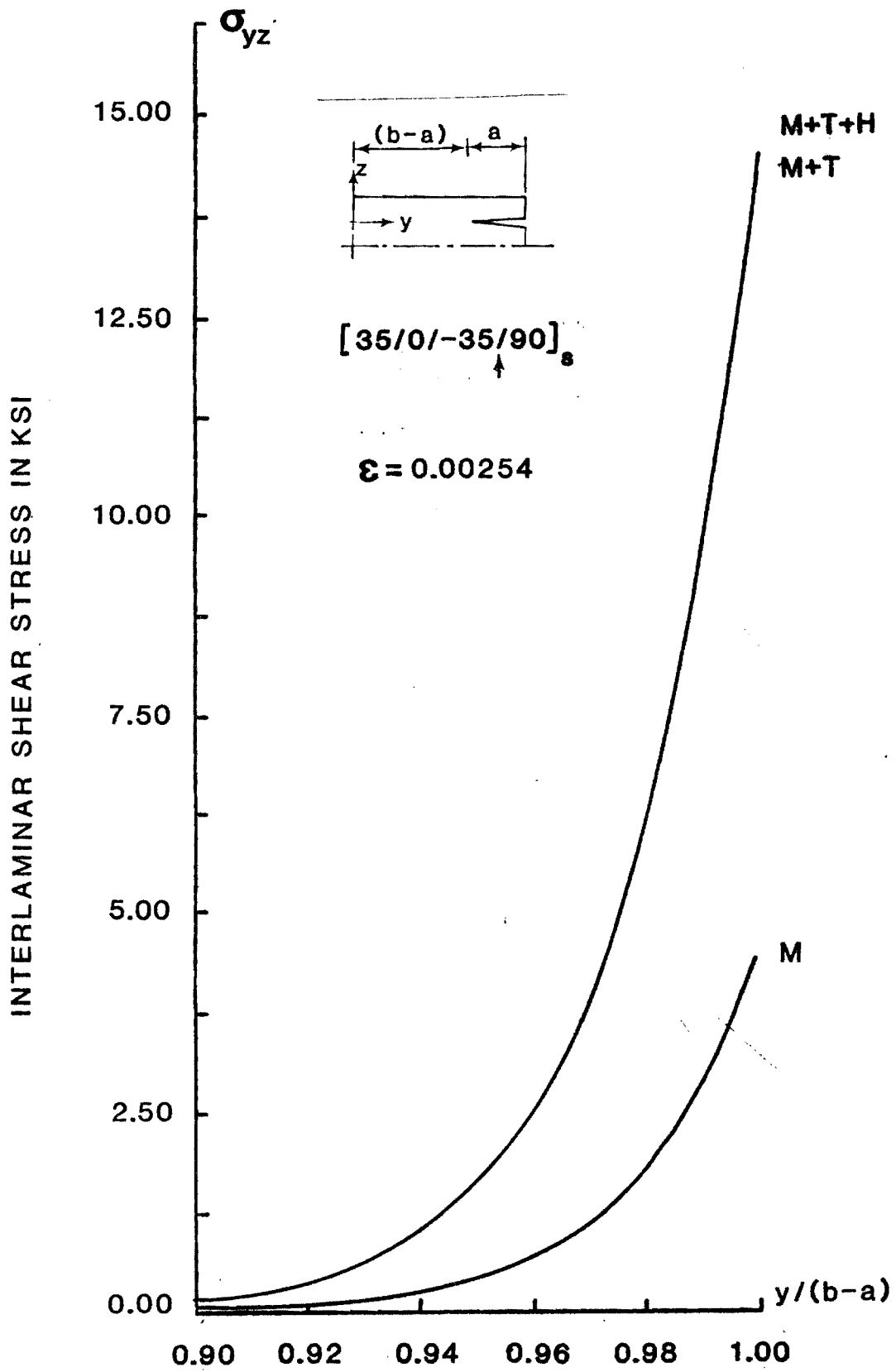


FIGURE 1

INTERLAMINAR SHEAR STRESS IN KSI

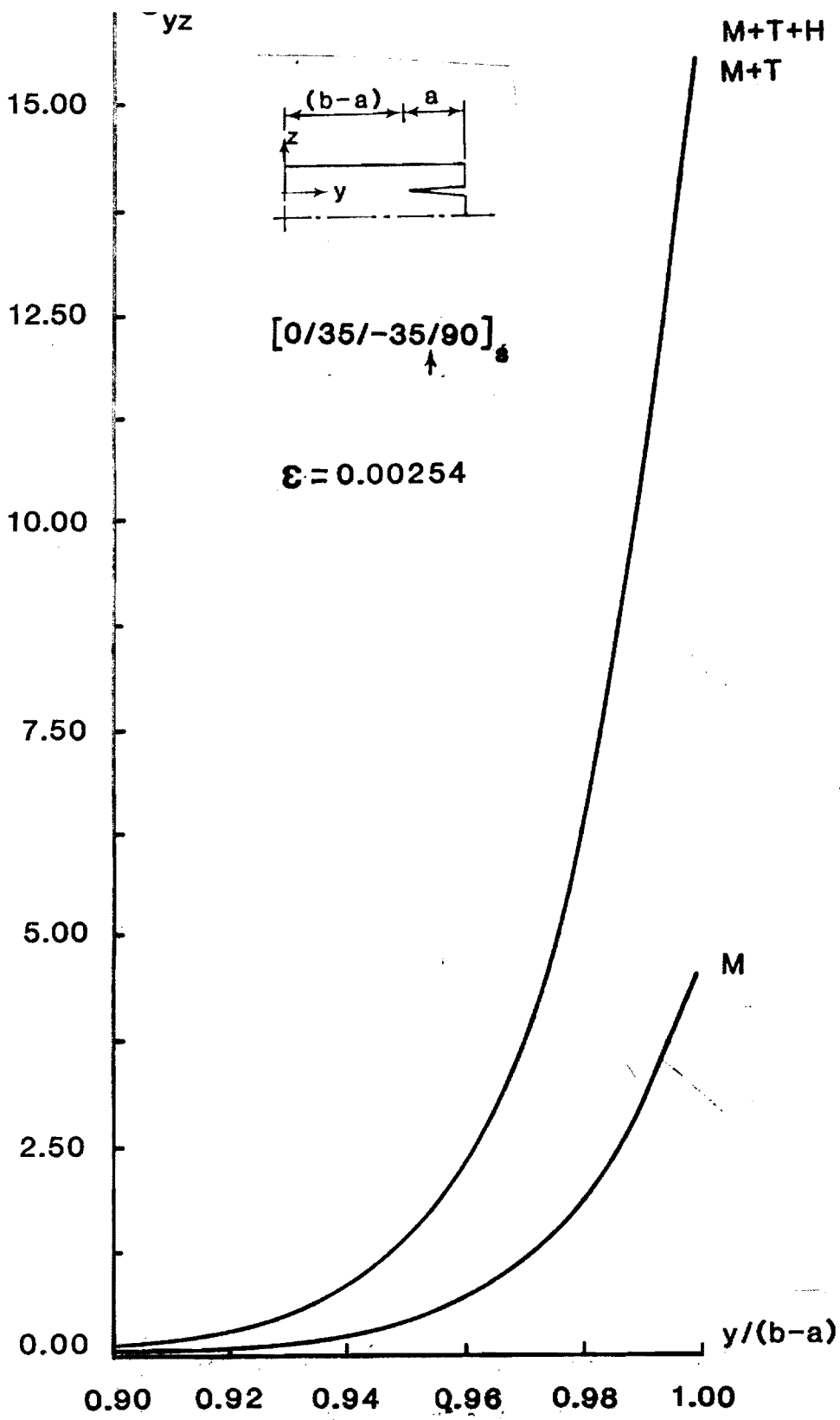


FIGURE 2

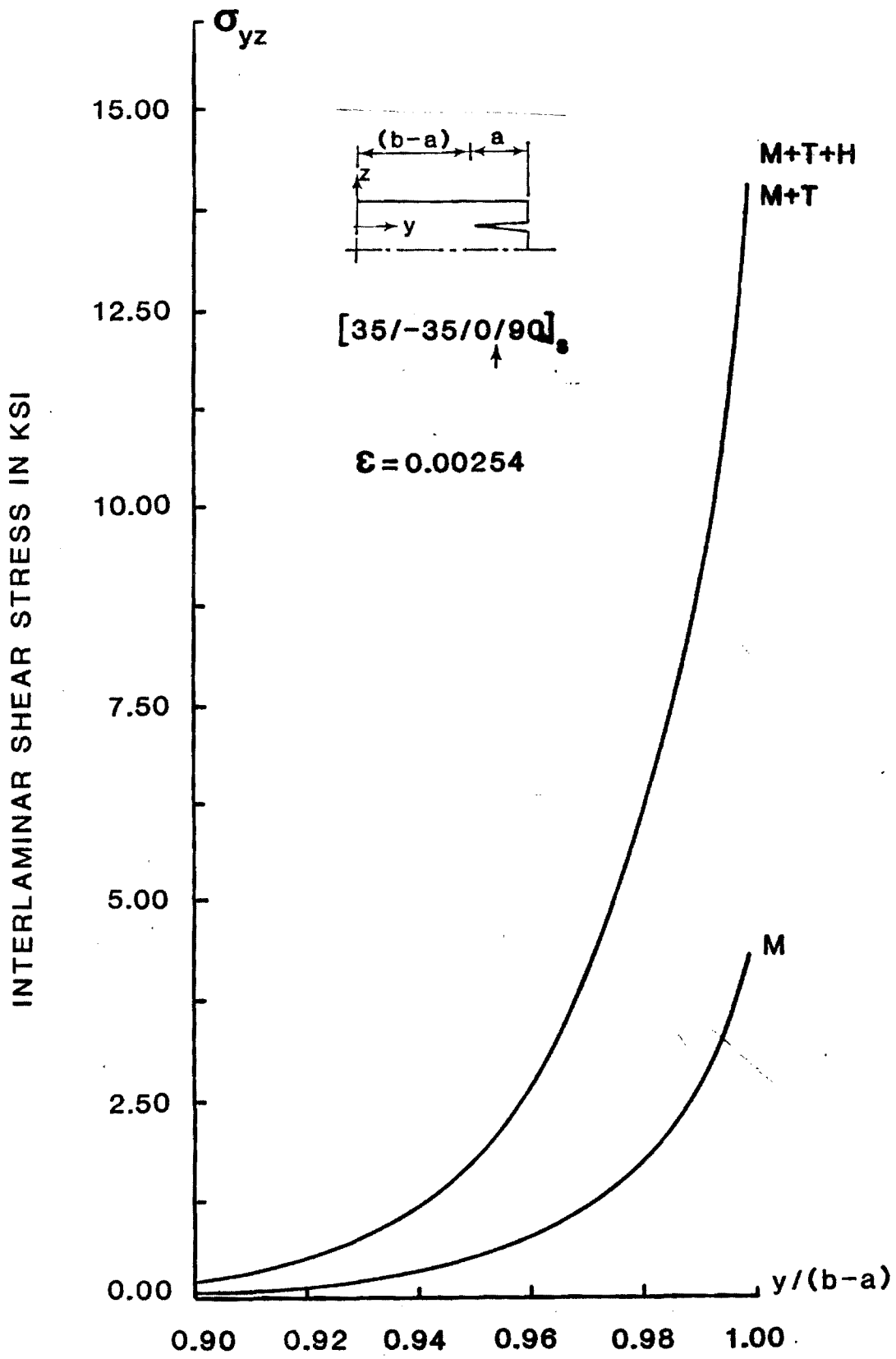


FIGURE 3

SEMIANNUAL REPORT

ANALYSIS OF DELAMINATED RELATED
FRACTURE PROCESSES IN COMPOSITES

NASA GRANT NAG-1-637
GEORGIA TECH PROJECT E16-654

PRINCIPAL INVESTIGATORS
Lawrence W. Rehfield and Erian A. Armanios

Overview

This report covers the research work performed under Grant NAG-1-637 for the period starting February 12, 1987 and ending August 11, 1987. The work described herein was performed at the School of Aerospace Engineering, Georgia Institute of Technology. The research objectives for the first year were:

- (1) Develop an analysis of a symmetric edge delamination (ED) specimen including residual strain effects due to temperature and moisture;
- (2) Compare predictions with those of Reference 1 for the example cases;
- (3) Develop an analysis for delamination in tapered specimens; and
- (4) Create appropriate computer programs and documentation for the NASA Langley Research Center.

The research objectives for the second year are:

- (1) Extend the sublaminar analysis for the delamination in tapered specimens to predict the energy release rate components under tensile loading;
- (2) Develop an analysis for the delamination in tapered specimens subjected to bending loading;
- (3) Develop an analysis for isolated, internal ply cracks;
- (4) Compare predictions in (1), (2) and (3) with available results in the literature or with finite element simulations;

(5) Create appropriate computer programs and documentation for the NASA Langley Research Center.

A summary of the first year program is presented first. This is followed by the work accomplished to date for the second year and a discussion of some issues regarding the influence of residual thermal and moisture strains on the energy release rate and the discrepancy between the results of this research work and those of Reference 1.

Summary of First Year Progress

The objectives of the first year focused on two geometric configurations, the edge delamination specimen and the tapered specimen. A simple analysis methodology predicting the interlaminar stresses in a tapered configuration was developed. The predictions of the method are in good agreement with a finite element simulation.

The influence of residual thermal and moisture strains on interlaminar stresses and total energy release rate in the edge delamination specimen was studied. Of major importance are the findings that: (1) the interlaminar stress distribution and total energy release rate are sensitive to hygrothermal conditions; (2) residual moisture strain tends to alleviate the thermal influence for both the interlaminar stresses and total energy release rate; and (3) the moisture content producing complete alleviation from the thermal effect is the same for the total energy release rate and interlaminar stresses. While the first two findings are in agreement with the results of previous investigators^{1,2} the third finding is new. It establishes a similarity in behavior between a delamination analysis expressed in terms of the energy release rate³ and the strength approach⁴ expressed by the interlaminar stresses.

An illustration of these findings is provided in Figures 1-3. The influence of hygrothermal condition on the interlaminar shear stresses τ_{yz} and τ_{xz} and total energy release rate appears in Figures 1 and 2. The labels M, M+T and M+T+H in the figures stand for mechanical, mechanical and thermal and mechanical, thermal and moisture, respectively. The material considered is T300/5208 graphite/epoxy. Its material properties are those of Reference 1. The cure temperature for this material is 350° F while the operating temperature is 70° F. The moisture weight gain percent is 0.4 in Figure 1. The mechanical strain is 0.00254 which represents a practical value for this material. In Figure 2, the moisture level for total alleviation of the energy release rate from thermal effects is 0.76 for a $[-35/55/10/-80]_s$ layup with delamination at the 55/10 interface.

A comparison of the interlaminar shear stresses at this level of moisture with the case of mechanical loading alone appears in Figure 3. It is seen that a level of moisture of 0.76 results in the total alleviation of the interlaminar shear stresses also. The same conclusion is reached studying eight other layups.

Second Year Progress

Due to the discrepancy between the results of the hygrothermal effects on the ED specimen mentioned earlier, an extensive investigation has been performed in order to resolve the disagreement. A study of the computer program and the details of the analytical method used in Appendix A of Reference 1 clarified these differences. The computer program and the analytical expressions used in Reference 1 were provided at our request by Donald Garber of Kentron International Inc. A description of our findings is given in the following section.

Hygrothermal Effects on Interlaminar Fracture

Some deviation from the proposed research plan has been made due to some unanticipated findings. In attempting to correlate our new delamination analysis⁵ results for test cases analyzed previously at the Langley Research Center¹, we found discrepancies. A thorough investigation revealed that there is a fundamental mistake in the equations appearing in Appendix A of Reference 1. The strain energy is defined in Equation (A₁) of the Appendix as:

$$U = \frac{1}{2} \int_V \epsilon_{ij} \sigma_{ij} dV \quad (1)$$

where the stress tensor for a given ply is defined as the product of the transformed reduced stiffness matrix and the mechanical strain of the ply. The strain tensor however, is taken to be the total strain rather than the mechanical strain. Due to this error the expressions for strain energy and, hence, strain energy release rate are incorrect. As a result, the conclusions drawn and the fundamental nature of the process are actually different than those presented in Reference 1. This situation is depicted in Figure 4 where the variation of the energy release rate with moisture percentage content is shown for a $[35/-35/0/90]_S$ layup with delamination at the 0/90 interface. The agreement is good for the case of mechanical loading. When hygrothermal effects are included however, there is a difference in the distribution as well as the numerical values. The moisture content corresponding to total alleviation from thermal effects is close for both predictions.

In the course of investigating the discrepancy, it was found that an analysis by Whitney⁶ for a Mode I example agrees with our predictions for the same analysis. Whitney's analysis is considered to be correct, so this provides important substantiating evidence.

Additional substantiating evidence is expected from analysis results to be provided by Dr. Wen Chan of Bell Helicopter Textron Inc. The test case

represented by results in Fig. 3 of Reference 1 will be independently reanalyzed by Dr. Chan at our request.

As a result of the above unanticipated problem, in the first six months work on tapered specimen analysis has been deferred.

Progress has been made in modeling the situation caused by isolated transverse cracks in laminates. A description of our preliminary work follows.

Analysis of Progressive Damage Initiated by Isolated Ply Cracks

Considerable attention has been devoted to transverse matrix microcracking for first generation brittle epoxy matrix composites. One characteristic that has been documented is the crack characteristic spacing or, conversely, crack density. In the usual characteristic damage patterns, the intercept of transverse cracks with neighboring ply surfaces often serve as sites for the initiation of delamination cracks. As delamination cracks isolate individual plies and sublaminates, failure of the isolated units by fiber fracture occurs in the terminal stages of the process. Currently, we are concerned with modeling and analyzing the early stages of the process through the onset of delamination.

There is no consensus on methods for predicting transverse cracking. A key assumption has been utilized in creating our analysis methodology. It is that matrix microcracking is predicted by strain level only. This is valid for damage characteristic dimensions greater than a ply thickness. For damage on a smaller scale, fracture mechanics concepts and means for detecting sub-ply microcracks are required. For most purposes, strain level predictions are quite satisfactory.

A model for an isolated ply crack has been created. We call it the Membrane Ply-Sublamine Model. The analysis is quite simple to perform as local bending of the modeling units is neglected.

The isolated cracked ply of a laminate under tensile loading causes a redistribution of loading locally. The axial stress at the crack surface of the cracked ply drops to zero. The interlaminar shear stresses are very large at interply surfaces on either side of the cracked ply and tend to decay away from the crack front. As load is again picked up by the cracked ply through shear transfer, it approaches the original level, which was sufficient to produce the original crack. Consequently, a characteristic pattern of periodic cracks is produced.

The next phase of the damage process is the onset of delamination at the intercepts of the transverse cracks with neighboring plies. For the onset of delamination, it seems that the strain energy release rate can be predicted on the basis that the cracks are isolated. This is because they are situated at the shear stress decay distance apart.

A stress analysis based upon our Membrane Ply-Sublaminar model has been performed. For the case analyzed, a $[0,90]_s$ laminate of AS/3501 graphite-epoxy, the predicted transverse crack spacing is 1.160 mm. The average value of measured crack spacings for this configuration is 1.131 mm as determined by Reifsnider. Consequently, at least to this extent, our model appears very promising.

An energy release rate analysis is underway. After it is completed and validated, a correlation study with experimental data in the literature will be performed. At a later time, an extensive finite element, numerical correlation may be undertaken.

References

1. O'Brien, T.K., Raju, I.S. and Garber, D.P., "Residual Thermal and Moisture Influences on the Strain Energy Release Rate Analysis of Edge Delamination," Journal of Composites Technology & Research, Vol. 8, No. 2, Summer 1986, pp. 37-47.

2. Whitney, J.M., "Stress Analysis of a Mode I Edge Delamination Specimen for Composite Materials," AIAA Paper 85-0611, presented at the 26th AIAA/ASME/ASCE/AHS Structures, Structural Dynamics and Materials Conference, April 15-17, 1985, Orlando, Florida.
3. O'Brien, T.K., "Characterization of Delamination Onset and Growth in a Composite Laminate," Damage in Composite Materials, ASTM STP 775, K.L. Reifsnider, Ed., American Society for Testing and Materials, 1982, pp. 140-167.
4. Lagace, P.A., "Delamination in Composites is Toughness the Key?," SAMPE, November/December 1986, pp. 53-60.
5. Armanios, E.A. and Mahler, M.A., "Residual Thermal and Moisture Influences on the Free-edge Delamination of Laminated Composites," to be presented at the AIAA/ASME/ASCE/AHS/ASC 29th SDM Conference, April 18-30, 1988, Williamsburg, VA.
6. Whitney, J.M. and Knight, M., "A Modified Free-Edge Delamination Specimen," Delamination and Debonding of Materials, ASTM STP 876, W. S. Johnson, Ed., American Society for Testing and Materials, Philadelphia, 1985, pp. 298-314.

INTERLAMINAR SHEAR STRESSES IN KSI

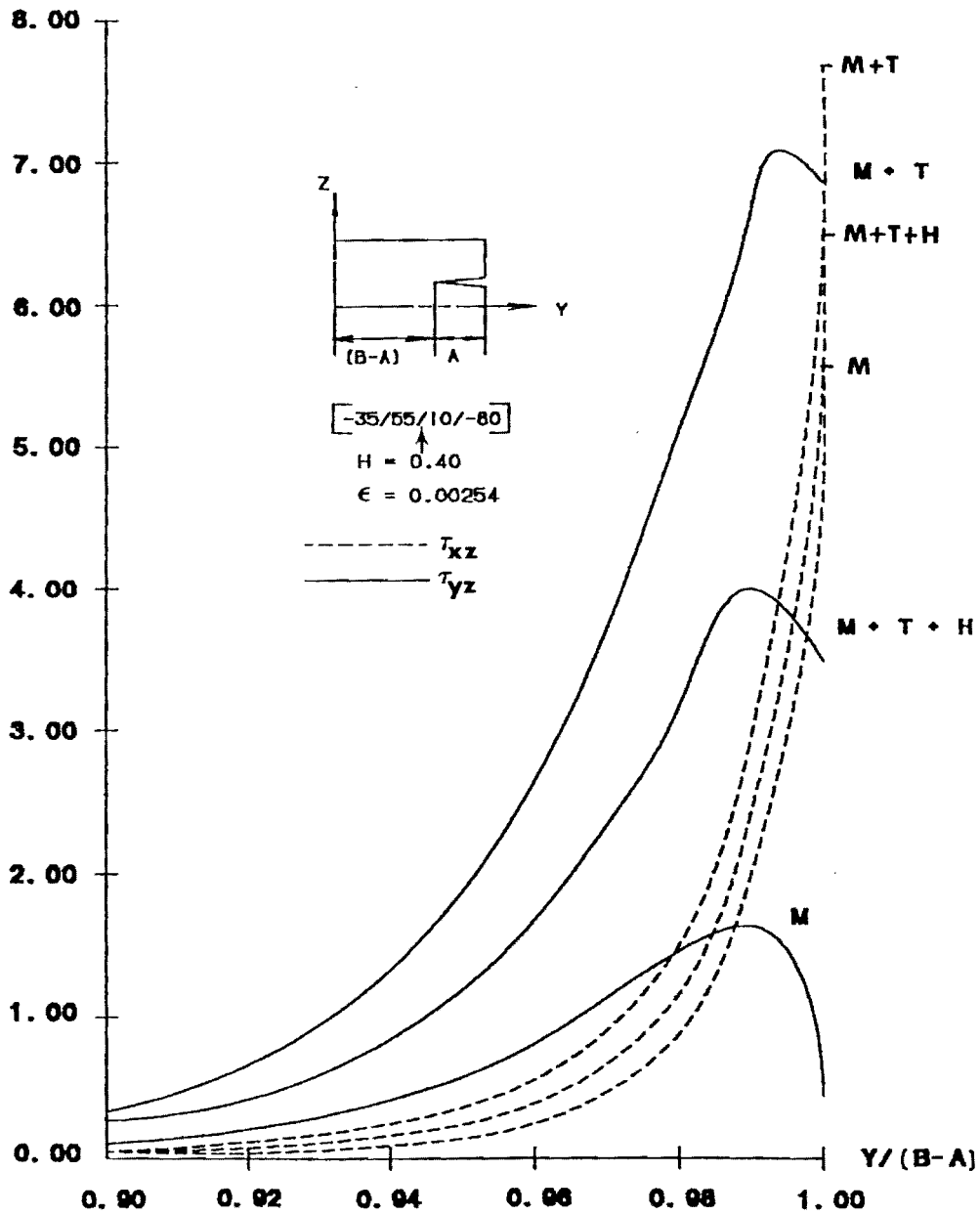


FIGURE 1 - COMPARISON OF INTERLAMINAR STRESSES

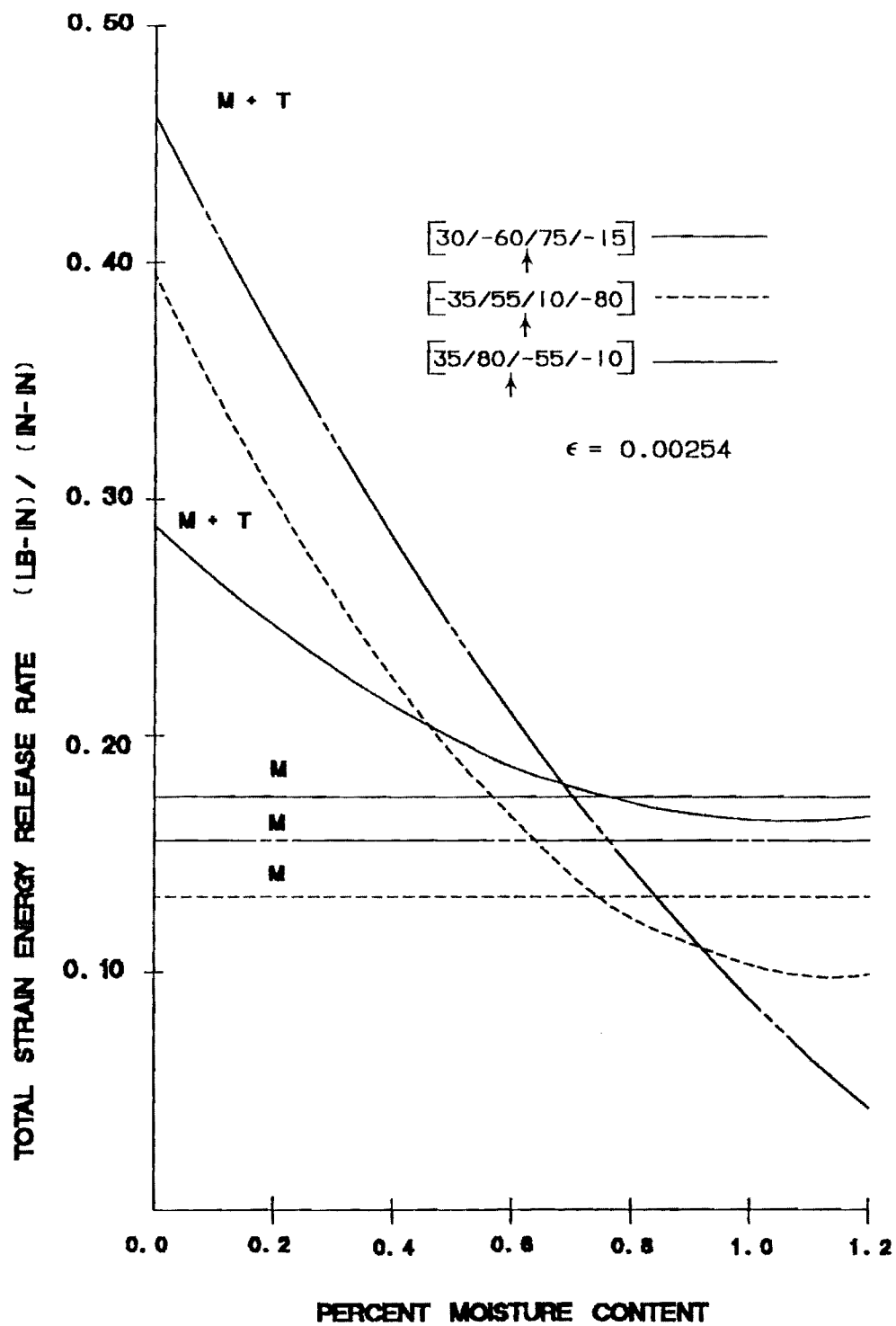


FIGURE 2 - ENERGY RELEASE RATE DISTRIBUTION FOR LAMINATES WITH MODE III

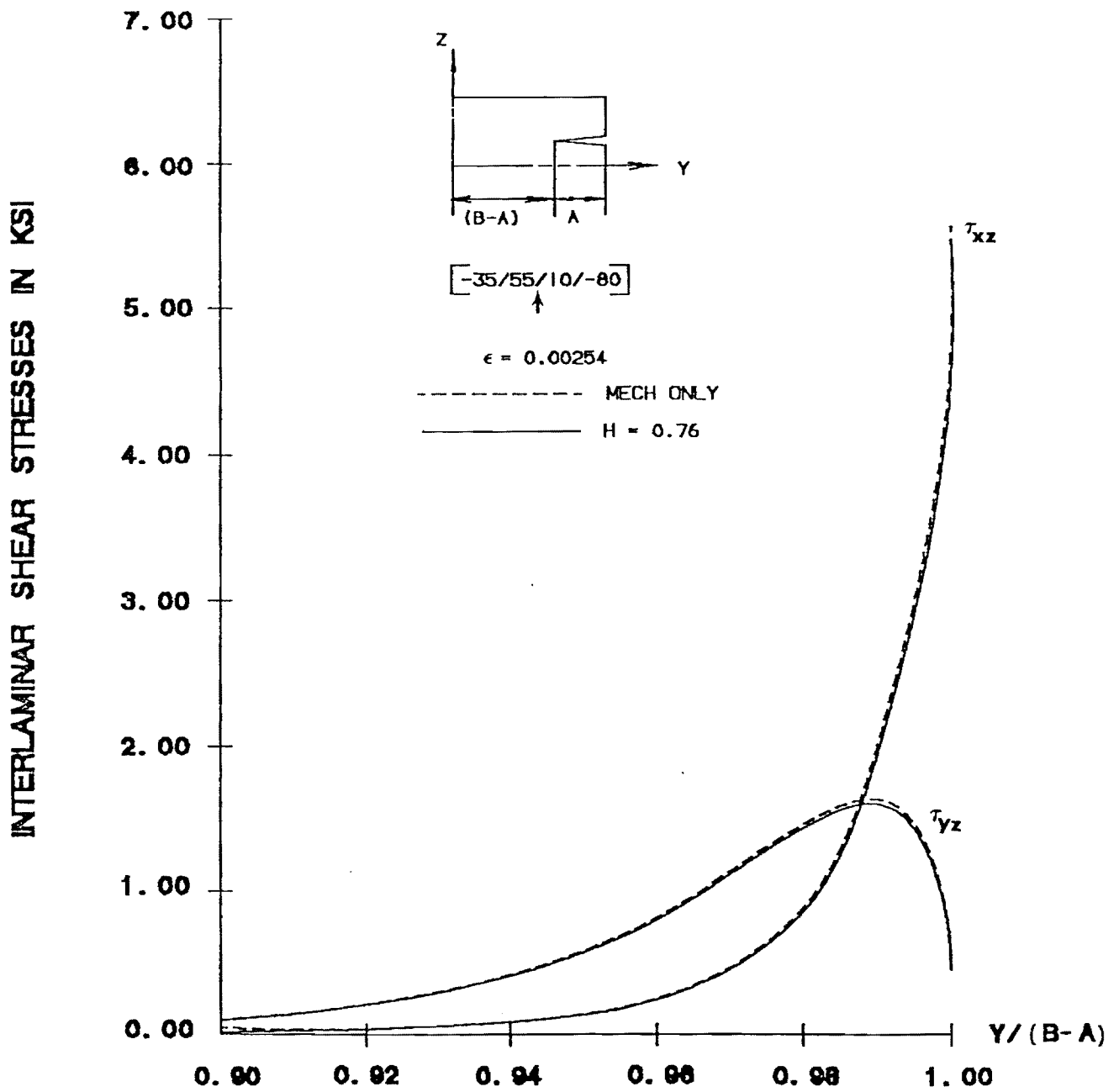


FIGURE 3 - TOTAL ALLEVATED STATE STRESS DISTRIBUTION

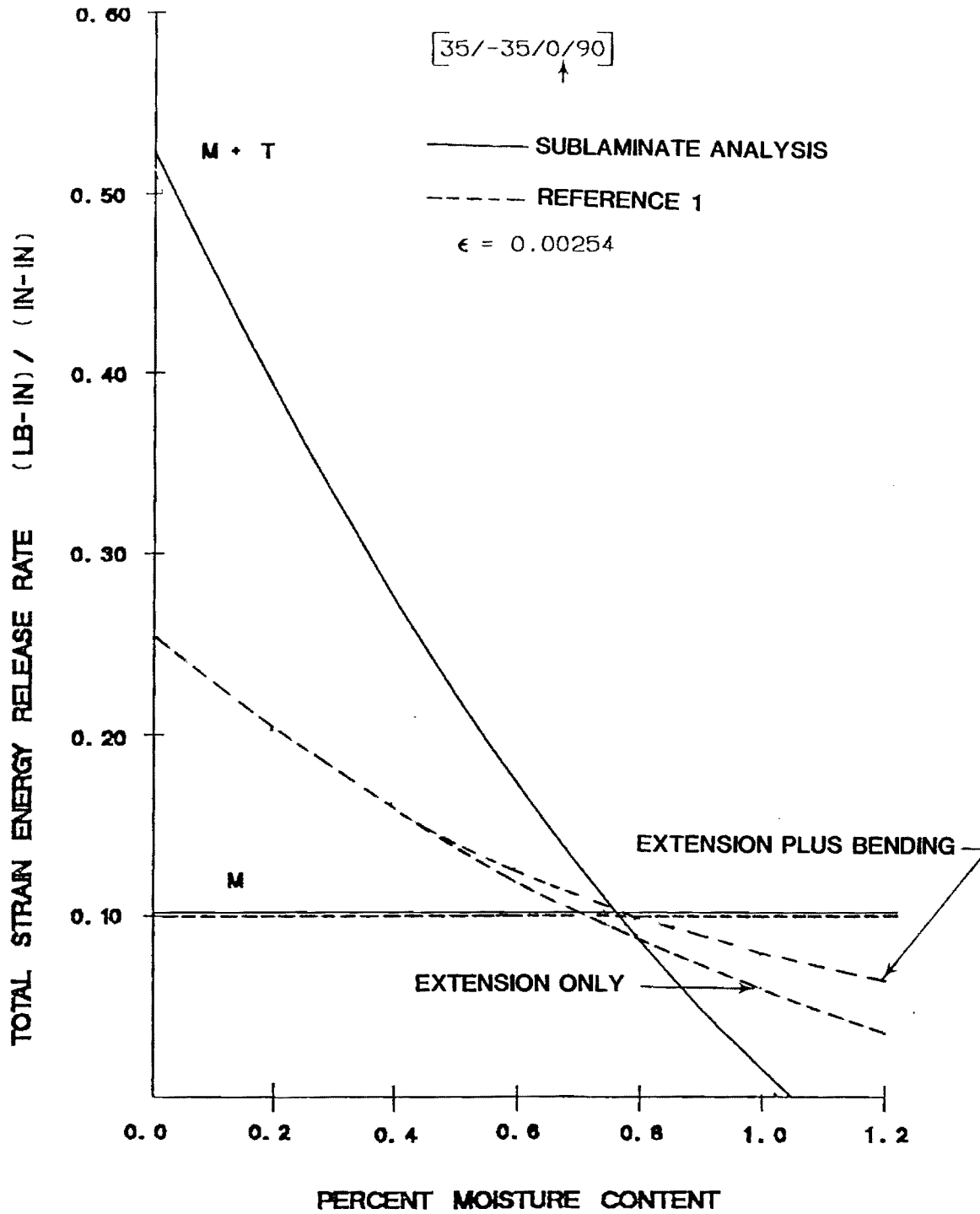


FIGURE 4 - ENERGY RELEASE RATE DISTRIBUTION FOR LAMINATES WITHOUT MODE III

SEMI-ANNUAL REPORT

**ANALYSIS OF INTERLAMINAR FRACTURE IN COMPOSITES
UNDER COMBINED LOADING**

NASA GRANT

NAG-1-637

GEORGIA TECH PROJECT

E-16-654

PRINCIPAL INVESTIGATOR

ERIAN A. ARMANIOS

Overview

This report covers the research work performed under Grant NAG-1-637 for the period ending February 28, 1989. A detailed description of the fracture analysis of transverse crack tip delaminations is presented in the following sections. This work was performed during the first six months of the grant period and has been accepted for presentation at the 30th Structures, Structural Dynamics and Materials Conference (Mobile, Alabama, April 1989). The following sections are adapted from the aforementioned paper.

Abstract

Delamination is a predominant failure mode in continuous fiber reinforced laminated composite structures. One type of delamination is the transverse crack tip delamination which originates at the tip of transverse matrix cracks. An analytical model based on the sublaminar approach and fracture mechanics is developed in this paper to study the growth of such delaminations. Plane strain conditions are assumed and estimates are provided for the total strain energy release rate as well as the mode I and mode II contributions. The energy release rate estimates are used in combination with a simple failure law to predict critical delamination growth strains and stresses. These predictions are compared with experimental data on T300/934 Graphite Epoxy $[\pm 25/90_n]_s$ laminates in the range $n=5$ to 8. A good agreement is demonstrated for the range of n where the experimental observations indicate transverse crack tip delamination to be the predominant failure mode.

Introduction

Fiber reinforced composites are now being used in a wide variety of engineering structures. The concept of directional strength and stiffness has been, for the most part, understood sufficiently to enable efficient load bearing designs. One of the current major issues in composite structures is the understanding and prediction of damage modes and failure mechanisms. A thorough knowledge of the failure mechanisms is bound to lead to the design of efficient and durable structures. Failures in these materials often initiate in the form of matrix cracks or delaminations. Matrix cracks refer to intralaminar failures whereas delaminations refer to interlaminar failures.

Matrix cracks usually occur within laminates where the fibers run at an angle to the primary load direction. Hence, such matrix cracks are also called transverse cracks. Based on the location and direction of growth, two distinct types of delamination can be discerned. These two types are called edge delamination and local or transverse crack tip delamination. Edge delaminations initiate at the load free edges of the laminate whereas local delaminations start from a transverse matrix crack. In many cases, both types occur concurrently with varying levels of interaction. It has been observed in simple tension tests of uniform rectangular cross section specimen (Edge Delamination tests) that delaminations initiate along the load free edges and propagate normal to the load direction. Transverse matrix cracks running parallel to the fibers have also been observed in off axis plies such as 90° plies. Such transverse cracks terminate where the ply orientation changes. Delaminations can also originate at the interfaces where transverse cracks terminate. These delaminations, called

transverse crack tip delaminations or local delaminations, grow normal to the transverse crack from which they originate. In the case of 90° plies, the growth direction is parallel to the load.

The growth process of edge delaminations and local delaminations is often modelled using a fracture mechanics approach leading to the calculation of a strain energy release rate. This is because the strain energy release rate can correlate delamination behavior from different loading conditions and can account for geometric dependencies. The strain energy release rate associated with a particular growth configuration is a measure of the driving force behind that failure mode. In combination with appropriate failure criteria, the strain energy release rate provides a means of predicting the failure loads of the structure.

Several methods are available in the literature for analyzing edge delaminations. These include finite element modelling¹⁻³, complex variable stress potential approach⁴, simple classical laminate theory based technique⁵ and higher order laminate theory including shear deformations⁶. Finite element models provide accurate solutions but involve intensive computational effort. Classical laminate theory (CLT) provides simple closed form solutions and is thus well suited for preliminary design evaluation. However, CLT provides only the total energy release rate, and thus, in a mixed mode situation, there is insufficient information to completely assess the delamination growth tendency. A higher order laminate theory including shear deformations has the ability to provide the individual contributions of the three fracture modes while retaining the simplicity of a closed form solution. A

shear deformation model is available for edge delamination and has been shown to agree well with finite element predictions⁶.

Crossman and Wang⁷ have tested T300/934 Graphite epoxy $[\pm 25/90_n]_s$ specimens in simple tension and reported a range of behavior including transverse cracking, edge delamination and local delamination. O'Brien⁸ has presented classical laminate theory solutions for these specimen, demonstrating reasonable agreement in the case of edge delamination but with some discrepancies in the local delamination predictions. A finite element model combining edge and local delaminations has been proposed by Law⁹. His predictions, however, do not fully explain the dependency of the critical strain on the number of 90° plies.

In this paper, a shear deformation model is developed for the analysis of local delaminations originating from transverse cracks in 90° plies located in and around the specimen midplane. Plane strain conditions are assumed and thickness strain is neglected. Delaminations are assumed to grow from both ends of the transverse crack tip. The transverse crack is treated as a free boundary and the delamination is considered to be the crack whose growth behavior is to be modelled. The sublaminate approach^{10,11} is used to model different regions of the specimen. The resulting boundary value problem is solved to obtain the interlaminar stresses, total strain energy release rate and energy release rate components. Critical local delamination growth loads are predicted for $[\pm 25/90_n]_s$ specimens.

Analytical Model

The formulation is based on the sublaminate approach detailed in Ref. 10. A longitudinal section illustrating the geometry of a generic

configuration is shown in fig. 1. The central region is assumed to be made of 90° plies with an isolated transverse crack in the middle. Delaminations are assumed to grow from both ends of the transverse crack, and towards both ends as shown. From symmetry considerations, only one quarter of the configuration is modelled. The modelled portion is divided into four sublaminates as shown in fig. 2. The top surface (sublaminates 1 and 4) is stress free. In order to simplify the analysis, plane strain conditions are assumed and the thickness strain (ϵ_z) is set to zero. The consequence of this, combined with the fact that the w displacement is zero along the center line, is that w is zero in sublaminates 1, 2 and 3. Also, this approximation does not allow for the enforcement of boundary conditions on the shear stress resultants, leading to incorrect estimates of the interlaminar normal stresses. The interlaminar shear stresses, however, are not affected by this assumption^{6,10}. These assumptions lead to considerable simplifications in the analysis. In spite of the simplifications, reliable energy release rate components can be estimated based on the interlaminar shear stress distributions^{6,10}.

A generic sublamininate is shown in fig. 3 along with the notations and sign conventions. The peel and interlaminar shear stresses are denoted by P and T , respectively, with t and b subscripts for the top and bottom surfaces, respectively. The axial stress resultant, shear stress resultant and bending moment resultant are denoted by N , Q and M , respectively. A summary of the governing equations is presented in the following paragraphs for convenience. These equations are derived for a generic sublamininate using the principle of virtual work in Ref.12.

The x and z displacements within the sublaminates are assumed to be of the form

$$u(x,z) = U(x) + z\beta(z) \quad (1)$$

$$w(x,z) = W(x) \quad (2)$$

Here U represents the axial midplane stretching and W is the transverse displacement. The shear deformation is recognized through the rotation β . The origin of the coordinate axes for the sublaminates is taken at the delamination tip as shown in fig. 4. The equilibrium equations take the form

$$N_{,x} + T_t - T_b = 0 \quad (3)$$

$$Q_{,x} + P_t - P_b = 0 \quad (4)$$

$$M_{,x} - Q + \frac{h}{2}(T_t + T_b) = 0 \quad (5)$$

where h is the thickness of the sublaminates. The constitutive relations in terms of the force and moment resultants are

$$N = A_{11}U_{,x} + B_{11}\beta_{,x} \quad (6)$$

$$Q = A_{55}(\beta + W_{,x}) \quad (7)$$

$$M = B_{11}U_{,x} + D_{11}\beta_{,x} \quad (8)$$

where A_{ij} , B_{ij} and D_{ij} are the classical laminate theory axial, coupling and bending stiffnesses, respectively. The boundary variables to be prescribed at the sublaminates edges are

N or U

M or β

Q or W

Additionally, at the interfaces between sublaminates, reciprocal traction and displacement matching boundary conditions have to be specified.

Solution Procedure

A detailed solution is provided in the Appendix. A summary is provided in this section for convenience. The variables are subscripted to indicate the sublaminates in which they occur. The solutions in sublaminates 1 and 2 are coupled by the reciprocal interlaminar stresses denoted T_1 and P_1 and by displacement continuity at the common interface. Assuming exponential solutions for the axial force and bending moment resultants leads to an eigenvalue problem involving the exponential parameter s . The eigenvalues turn out to be 0 and two nonzero values (say s_1 and s_2) occurring in positive and negative pairs. Since the response decays from the delamination (crack) tip, only the exponentially decaying terms are considered in the solutions.

The following boundary conditions from the ends of the modelled region are enforced.

$$N_2(0) = 0 \quad (9)$$

$$Q_4(a) = 0 \quad (10)$$

$$\beta_4(a) = 0 \quad (11)$$

$$N_1 + N_2 = \text{Applied Load} \quad (12)$$

Further, the following displacement matching conditions are applied.

$$u_1\left(x, -\frac{h_1}{2}\right) = u_2\left(x, \frac{h_2}{2}\right) \quad (13)$$

$$U_1(0) = U_4(0) \quad (14)$$

$$U_2(0) = U_3(0) \quad (15)$$

$$\beta_1(0) = \beta_4(0) \quad (16)$$

It should be noted that a β_2 and β_3 matching condition cannot be applied at this level of modeling since it would amount to specifying both W and Q ^{6,12}. Consequently, there is a displacement discontinuity

at the delamination tip. The effect of this will be discussed subsequently. To eliminate rigid body displacements, U_1 is set to zero at the left end. The following solutions can then be obtained for the resultants in sublaminates 1 and 2.

$$N_1 = a_1 e^{s_1 x} + a_2 e^{s_2 x} + \varepsilon A_{11(1)} \quad (17)$$

$$N_2 = -a_1 e^{s_1 x} - a_2 e^{s_2 x} + \varepsilon A_{11(2)} \quad (18)$$

$$M_1 = a_1 k_1 e^{s_1 x} + a_2 k_2 e^{s_2 x} \quad (19)$$

$$M_2 = a_1 k_3 e^{s_1 x} + a_2 k_4 e^{s_2 x} \quad (20)$$

The interlaminar shear and peel stresses between sublaminates 1 and 2 can be obtained from equilibrium as

$$T_1 = a_1 s_1 e^{s_1 x} + a_2 s_2 e^{s_2 x} \quad (21)$$

$$P_1 = \left(k_1 + \frac{h_1}{2} \right) (a_1 s_1^2 e^{s_1 x}) + \left(k_2 + \frac{h_1}{2} \right) (a_2 s_2^2 e^{s_2 x}) \quad (22)$$

In the above solutions, the k_i parameters are dependent on the eigenvalues and the stiffness of sublaminates 1 and 2, the a_j parameters depend on the k_i parameters and the crack length a , and ε is defined as

$$\varepsilon = \frac{P}{2b} \frac{1}{A_{11(1)} + A_{11(2)}} \quad (23)$$

where P is the uniform axial force applied on the specimen and b is the specimen width. Expressions for the eigenvalues and the a_j and k_i parameters are provided in the Appendix.

Proceeding on to sublaminates 3 and 4, the following solutions can be written.

$$N_3 = 0 \quad (24)$$

$$M_3 = \phi_1 \sinh(\omega_3 x) + \phi_2 \cosh(\omega_3 x) \quad (25)$$

where
$$\phi_2 = a_1 k_3 + a_2 k_4, \quad (26)$$

$$\phi_1 = -\phi_2 \coth(\omega_3 a), \quad (27)$$

and

$$\omega_3 = \sqrt{\frac{A_{55(2)}}{D_{11(2)}}} \quad (28)$$

$$N_4 = \varepsilon (A_{11(1)} + A_{11(2)}) \quad (29)$$

$$M_4 = a_1 k_1 + a_2 k_2 \quad (30)$$

The corresponding displacement solutions are provided in the Appendix. The compliance of the specimen can be evaluated as

$$C = 2 \frac{U_4(a)}{P} \quad (31)$$

The total energy release rate, G_T , per crack is then given by

$$G_T = \frac{P^2}{2b} \frac{dC}{da} \quad (32)$$

Use of the previously described solutions leads to the following expression.

$$G_T = \frac{P^2}{2b^2} \left(\frac{1}{A_{11(1)}} - \frac{1}{A_{11(1)} + A_{11(2)}} + I_1 - I_2 \right) \quad (33)$$

where the quantities I_1 and I_2 contain exponential terms dependent on the delamination length. Using the virtual crack closure technique, from the relative displacements in the cracked portion and the interlaminar stresses ahead of the crack tip, the mode I and mode II energy release rate contributions can be obtained. The mode III energy release rate is zero from the assumption of plane strain. The mode II energy release rate is given by

$$G_{II} = \lim_{\delta \rightarrow 0} \frac{1}{2\delta} \int_0^\delta T_{II}(x-\delta) \Delta u(x) dx \quad (34)$$

where δ is the virtual crack step size. The result of the limiting process is zero if there is no singularity in the stress field¹⁰. So, the limit is usually taken as the crack step size d tends to a small value, say Δ , based on the decay length or the length required to capture the

essential features of the stress and displacement fields near the crack tip. The decay length is dependent on the eigen values s_1 and s_2 . In this study, the value of Δ has been set to

$$\Delta = \frac{1}{4} \left(\frac{1}{s_1} + \frac{1}{s_2} \right) \quad (35)$$

since it reasonably fulfills the criterion given above. In a similar fashion, the mode I energy release rate can be obtained based on the normal stress (P) and the w displacements near the crack front. The normal (peel) stress estimate is inaccurate due to the absence of thickness strain. Hence, an alternate approach was used to estimate G_I , the mode I energy release rate. The total energy release rate for this problem is made up entirely of G_I and G_{II} ($G_{III}=0$). From an estimate of G_T and G_{II} , an estimate for G_I can be obtained simply as

$$G_I = G_T - G_{II} \quad (36)$$

The critical load for a given specimen can then be evaluated based on an appropriate fracture law. This is illustrated in the following section.

Results and Discussion

The solutions derived in the previous section have been used to model the behavior of $[\pm 25/90_n]_s$ T300/934 Graphite Epoxy specimen for n values of .5,1,2,3,4,6,and 8. These correspond to the specimen tested by Crossman and Wang⁷. The specimen width and length were fixed at .0381m and .015m, respectively, as in the tests and the applied uniform axial stress was 100MPa. The solutions were generated using a simple computer program based on the closed form expressions for the interlaminar stress and energy release rates.

An example of the total energy release rate variation with the crack length is presented in fig. 5. The asymptotic value of G_T is denoted by G_{T0} in the figure. It can be observed that after a certain crack length, the G_T is independent of the crack length. On the basis of curves like the one shown in fig. 5, the crack length was fixed at 10 ply thicknesses for the remainder of the study. The dependence of the mode II contribution of the energy release rate on crack length (a) is depicted in fig. 6. Typical interlaminar shear and normal stress profiles are presented in figs. 7 and 8, respectively. The corresponding energy release rates have also been calculated and are presented in Table I and fig. 9.

In order to evaluate the critical loads, an appropriate mixed mode fracture law has to be applied, based on the calculated energy release components. Since the calculated mode split shows only a small variation with n , the simple Griffith criterion $G_T = G_{Tc}$ has been used to scale the stresses to obtain the critical delamination growth stress (σ_c) and strain (ϵ_c) values. The critical energy release rate G_{Tc} was chosen as 415 J/m^2 to obtain the critical stresses and strains listed in Table I. This value of G_{Tc} is larger than G_{Ic} to account for the presence of mode II and the fact that for the material system under consideration, G_{IIc} is about four times G_{Ic} . The critical strains are plotted against n , the number of 90° plies in fig. 10. The experimental results of Ref. 7 and the predictions of Refs. 8 and 9 are also presented in the figure for comparison. The predictions of the model developed in this paper are represented by the solid line while the experimental results are shown as filled squares. The classical laminate theory and finite element critical strain predictions of Refs. 8 and 9

are represented by triangles with a connecting line and a dotted line respectively. The CLT based model agrees well with the shear deformation model in terms of the total energy release rate. However, the CLT based model does not provide information on the mode split and thus, the value of $G_c (=G_{IC})$ used leads to bias in the predictions.

In the experiments, the local delamination phenomenon was observed as the predominant failure mode only for the $n=4, 6$ and 8 specimens. The shear deformation model presented in this paper provides good agreement with the experimental data in this range. For $n < 4$, edge delamination either in the mid plane or in the $25/90$ interface was observed in the tests. Hence, the predictions of the local delamination models in this region are not of consequence as long as they do not predict critical loads lower than those predicted by edge delamination models. Thus, it can be seen that the shear deformation model predicts the observed behavior with reasonable accuracy and can be used in conjunction with an appropriate edge delamination model to predict critical loads accurately for the complete range of n values. The edge delamination model presented in Refs. 6 and 12 can be used for this purpose. However, a separate model is required to account for the midplane (Mode I) edge delamination behavior. The development of such a model is described in Ref. 13.

Conclusions

A shear deformation model has been developed to analyze local delaminations growing from transverse cracks in 90° plies located around the mid plane of symmetric laminates. The total energy release rate calculations yield the same results as in the case of CLT based models. The predictions of the shear deformation model agree

reasonably with critical strain experimental data from $[\pm 25/90]_n$ T300/934 Graphite Epoxy laminates. The predicted behavior is such that, in combination with an edge delamination model, the critical loads can be predicted accurately in the range of n from .5 to 8.

Acknowledgements

The authors gratefully acknowledge the financial support provided by NASA under grant NAG-1-637 for performing the research reported in this paper. The authors also wish to thank Mr. A. Badir for help in verifying the analytical model.

References

- [1] Wilkins, D.J., Eisemann, J.R., Camin, R.A., Margolis, W.S. and Benson, R.A., "Characterizing Delamination Growth in Graphite-Epoxy," in *Damage in Composite Materials*, ASTM STP 775, K.L. Reifsnider, Ed., pp. 168-183 (1982).
- [2] O'Brien, T.K., "Mixed-Mode Strain Energy Release Rate Effects on Edge Delamination of Composites," in *Effects of Defects in Composite Materials*, ASTM STP 836, pp. 125-142 (1984).
- [3] Wang, S.S. and Choi, I., "The Mechanics of Delamination in Fiber Reinforced Composite Materials. Part II - Delamination Behavior and Fracture Mechanics Parameters," NASA CR-172270 (1983).
- [4] Wang, S.S., "Edge Delamination in Angle Ply Composite Laminates," *Proceedings of the 22nd AIAA/ASME/ASCE/AHS Structures, Structural Dynamics and Materials Conference*, Atlanta, Georgia, 6-8 April, 1981, pp. 473-484.
- [5] O'Brien, T.K., "Characterization of Delamination Onset and Growth in a Composite Laminate," in *Damage in Composite*

- Materials, ASTM STP 775, K.L. Reifsnider, Ed., pp. 140-167 (1982).
- [6] Armanios, E.A., and Rehfield, L.W., "Interlaminar Analysis of Laminated Composites using a Sublaminar Approach," Proceedings of the 27th AIAA/ASME/ASCE/AHS Structures, Structural Dynamics and Materials Conference, San Antonio, Texas, 19-21 May, 1986, Part 1, pp. 442-452. AIAA Paper 86-0969CP.
- [7] Crossman, F.W., and Wang, A.S.D., "The Dependence of Transverse Cracking and Delamination on Ply Thickness in Graphite/Epoxy Laminates," in Damage in Composite Materials, ASTM STP 775, K.L. Reifsnider, Ed., pp. 118-139 (1982).
- [8] O'Brien, T.K., "Analysis of Local Delaminations and Their Influence on Composite Laminate Behavior," in Delamination and Debonding of Materials, ASTM STP 876, Johnson, W.S., Ed., pp. 282-297 (1985).
- [9] Law, G.E., "A Mixed Mode Fracture Analysis of $(\pm 25/90_n)_s$ Graphite/Epoxy Composite Laminates," in Effects of Defects in Composite Materials, ASTM STP 836, pp. 143-160 (1984).
- [10] Armanios, E.A., "New Methods of Sublaminar Analysis for Composite Structures and Applications to Fracture Processes," Ph.D. Thesis, Georgia Institute of Technology (1984).
- [11] Armanios, E.A., Rehfield, L.W., and Reddy, A.D., "Design Analysis and Testing for Mixed-Mode and Mode II Interlaminar Fracture of Composites," in Composite Materials: Testing and Design (Seventh Conference), ASTM STP 893, J.M. Whitney, Ed., pp. 232-255 (1986).

- [12] Armanios, E.A., and Rehfield, L.W., "Sublaminar Analysis of Interlaminar Fracture in Composites: Part I - Analytical Model," submitted for publication in the Journal of Composites Technology and Research (July, 1988).
- [13] Armanios, E.A., Badir, A., and Sriram, P., "Sublaminar Analysis of Mode I Edge Delamination in Laminated Composites," 30th AIAA/ASME/ASCE/AHS Structures, Structural Dynamics and Materials Conference, Mobile, Alabama (April 1989).

Appendix

Sublaminar Analysis for Local Delaminations

A generic sublaminar is shown in fig. 3 along with the notations and sign conventions: The interlaminar normal (peel) and shear stresses are denoted by P and T respectively with the t and b subscripts for the top and bottom surfaces respectively. The axial force resultant, shear force resultant and bending moment resultant are denoted by N , Q and M respectively. Plane strain conditions are assumed to prevail in the x - z plane and the thickness strain ϵ_{zz} is neglected. These assumptions lead to considerable simplification in the analysis. The displacements in the x and z directions are assumed to be of the form

$$u = U(x) + zb(x) \quad (A.1)$$

$$w = W(x) \quad (A.2)$$

Here U represents the axial stretching and W is the transverse (thickness direction) displacement. This formulation recognizes shear deformation through the rotation β . The equilibrium equations take the form

$$N_{,x} + T_t - T_b = 0 \quad (A.3)$$

$$Q_{,x} + P_t - P_b = 0 \quad (\text{A.4})$$

$$M_{,x} - Q + \frac{h}{2} (T_t + T_b) = 0 \quad (\text{A.5})$$

where h is the thickness of the sublaminates. The constitutive equations in terms of the force and moment resultants are

$$N = A_{11}U_{,x} + B_{11}\beta_{,x} \quad (\text{A.6})$$

$$Q = A_{55}(\beta + W_{,x}) \quad (\text{A.7})$$

$$M = B_{11}U_{,x} + D_{11}\beta_{,x} \quad (\text{A.8})$$

where A, B and D are the classical laminate theory axial, coupling and bending stiffnesses defined in the customary manner as

$$(A_{ij}, B_{ij}, D_{ij}) = \int_{-h/2}^{h/2} C_{ij}(1, z, z^2) dz$$

Here, the C_{ij} s are the material moduli. For the case of plane strain in the x - z plane, the C s are defined as follows.

$$\begin{Bmatrix} \sigma_{xx} \\ \sigma_{zz} \\ \tau_{xz} \end{Bmatrix} = \begin{bmatrix} C_{11} & C_{13} & 0 \\ C_{13} & C_{22} & 0 \\ 0 & 0 & C_{55} \end{bmatrix} \begin{Bmatrix} \epsilon_{xx} \\ \epsilon_{zz} \\ \gamma_{xz} \end{Bmatrix} \quad (\text{A.9})$$

The boundary quantities to be prescribed at the sublaminates edges are

N or U

M or β

Q or W

Further, at the interfaces between sublaminates, reciprocity of tractions and continuity of displacements have to be enforced.

The four sublaminates along with the loads acting on each are shown in fig. 4. Setting P_1 and T_1 as shown automatically satisfies the traction matching boundary condition at the 1-2 interface. From symmetry, we get $w=0$ and zero shear stress along the bottom faces of

sublaminates 2 and 3. This leads to $w=0$ in sublaminates 1, 2 and 3. Thus, W has been prescribed in these sublaminates and the vertical shear force resultant Q cannot be prescribed on these sublaminates. Consequently, the calculated peel stress distribution will not be correct. In addition, at the 2-3 interface, the β s cannot be matched, since in these sublaminates, specifying β is equivalent to specifying Q (through Eq. A.7). In spite of these simplifications, reliable energy release rate components can be estimated based on the interlaminar shear stress distributions. The mode I contribution can then be evaluated using the total energy release rate, which is not affected significantly by these simplifications.

For the $(\pm 25/90_n)_s$ laminates under consideration, B_{11} is zero in all the four sublaminates. For sublaminates 1 and 2, the equilibrium equations and constitutive relationships can be written as

$$N_{1,x} - T_1 = 0 \quad (A.10)$$

$$N_{2,x} + T_1 = 0 \quad (A.11)$$

$$Q_{1,x} - P_1 = 0 \quad (A.12)$$

$$Q_{2,x} + P_1 - P_2 = 0 \quad (A.13)$$

$$M_{1,x} + \frac{h_1}{2} T_1 - Q_1 = 0 \quad (A.14)$$

$$M_{2,x} + \frac{h_2}{2} T_1 - Q_2 = 0 \quad (A.15)$$

$$N_1 = A_{11(1)} U_{1,x} \quad (A.16)$$

$$N_2 = A_{11(2)} U_{2,x} \quad (A.17)$$

$$Q_1 = A_{55(1)} \beta_1 \quad (A.18)$$

$$Q_2 = A_{55(2)} \beta_2 \quad (A.19)$$

$$M_1 = D_{11(1)} \beta_{1,x} \quad (A.20)$$

$$M_2 = D_{11(2)} \beta_{2,x} \quad (A.21)$$

The subscripts in parentheses refer to the sublaminates to which the stiffness coefficients correspond. Eqs. A.14, A.15 and A.12 can be rewritten in a modified form as

$$M_{1,x} + \frac{h_1}{2} N_{1,x} = A_{55(1)}\beta_1 \quad (\text{A.22})$$

$$M_{2,x} - \frac{h_2}{2} N_{2,x} = A_{55(2)}\beta_2 \quad (\text{A.23})$$

$$\begin{aligned} P_1 &= Q_{1,x} \\ &= M_{1,xx} + \frac{h_1}{2} T_{1,x} \end{aligned} \quad (\text{A.24})$$

Matching the u displacement along the 1-2 interface implies

$$u_1\left(x, -\frac{h_1}{2}\right) = u_2\left(x, \frac{h_2}{2}\right)$$

or

$$U_1 - \frac{h_1}{2} b_1 = U_2 + \frac{h_2}{2} b_2 \quad (\text{A.25})$$

Combining the equations to eliminate the displacement and interlaminar stress terms leads to the following system of homogeneous coupled ordinary differential equations.

$$N_{1,x} + N_{2,x} = 0 \quad (\text{A.26})$$

$$M_{1,xx} + \frac{h_1}{2} N_{1,xx} - \frac{A_{55(1)}}{D_{11(1)}} M_1 = 0 \quad (\text{A.27})$$

$$M_{2,xx} - \frac{h_2}{2} N_{2,xx} - \frac{A_{55(2)}}{D_{11(2)}} M_2 = 0 \quad (\text{A.28})$$

$$\frac{N_1}{A_{11(1)}} - \frac{h_1 M_1}{2D_{11(1)}} - \frac{N_2}{A_{11(2)}} - \frac{h_2 M_2}{2D_{11(2)}} = 0 \quad (\text{A.29})$$

The solution is assumed of the form

$$\begin{Bmatrix} N_1 \\ N_2 \\ M_1 \\ M_2 \end{Bmatrix} = \begin{Bmatrix} A_1 \\ A_2 \\ A_3 \\ A_4 \end{Bmatrix} e^{sx} \quad (\text{A.30})$$

Substitution of this solution into Eqs. A.26-A.29 leads to an eigenvalue problem with the following characteristic equation.

$$s[B_1s^4+B_2s^2+B_3] = 0 \quad (A.31)$$

where the B's involve the stiffness and thickness parameters A, D and h. For the material system and ply stacking sequence considered, $B_2^2 > 4B_1B_3$. Hence, the roots can be written as

$$s=0, \pm \sqrt{\frac{-B_2 \pm \sqrt{B_2^2 - 4B_1B_3}}{2B_1}} \quad (A.32)$$

Only the zero and positive roots of eq. A.32 are considered as they give solutions decaying exponentially from the crack tip. Then, the axial force and moment resultants can be written as

$$N_1 = a_1e^{s_1x} + a_2e^{s_2x} + a_1 \quad (A.33)$$

$$N_2 = -a_1e^{s_1x} - a_2e^{s_2x} + a_2 \quad (A.34)$$

$$M_1 = a_1k_1e^{s_1x} + a_2k_2e^{s_2x} \quad (A.35)$$

$$M_2 = a_1k_3e^{s_1x} + a_2k_4e^{s_2x} \quad (A.36)$$

The k parameters in the above solutions involve the eigenvalues and the stiffness coefficients (A,D). For example, we have the definition for k_1 as

$$k_1 = \frac{\frac{h_1}{2} s_1^2}{\frac{A_{55(1)}}{D_{11(1)}} - s_1^2} \quad (A.37)$$

Using the equilibrium Eqs. A.10, A.12 and A.14 along with the applied axial force P and specimen width b, the axial force resultants and interlaminar stresses can be written as

$$N_1 = a_1e^{s_1x} + a_2e^{s_2x} + \frac{P}{2b} \frac{A_{11(1)}}{A_{11(1)}+A_{11(2)}} \quad (A.38)$$

$$N_2 = -a_1e^{s_1x} - a_2e^{s_2x} + \frac{P}{2b} \frac{A_{11(2)}}{A_{11(1)}+A_{11(2)}} \quad (A.39)$$

$$T_1 = N_{1,x} = a_1s_1e^{s_1x} + a_2s_2e^{s_2x} \quad (A.40)$$

$$P_1 = M_{1,xx} + \frac{h_1}{2} T_{1,x}$$

$$= \left(k_1 + \frac{h_1}{2}\right) a_1 s_1^2 e^{s_1 x} + \left(k_2 + \frac{h_1}{2}\right) a_2 s_2^2 e^{s_2 x} \quad (\text{A.41})$$

The constitutive equations are used to write down the displacement solutions. The arbitrary constants associated with the displacements and rotations are determined from the matching conditions between sublaminates 1 and 2 and the end conditions. Proceeding to sublaminate 3, the governing equations are

$$N_{3,x} = 0 \quad (\text{A.42})$$

$$Q_{3,x} + P_3 = 0 \quad (\text{A.43})$$

$$M_{3,x} - Q_3 = 0 \quad (\text{A.44})$$

$$N_3 = A_{11(2)} U_{3,x} \quad (\text{A.45})$$

$$Q_3 = A_{55(2)} \beta_3 \quad (\text{A.46})$$

$$M_3 = D_{11(2)} \beta_{3,x} \quad (\text{A.47})$$

Matching U at the 2-3 interface and applying the boundary condition at the free end, $N_3(a) = 0$, gives

$$N_3 = 0 \quad (\text{A.48})$$

$$U_3 = U_2(0) = -\frac{a_1}{s_1 A_{11(2)}} - \frac{a_2}{s_2 A_{11(2)}} + a_3 \quad (\text{A.49})$$

In order to solve for the bending moment, Eqs. A.44, A.46 and A.47 are combined to yield

$$M_3 = \varphi_1 \sinh \omega_3 x + \varphi_2 \cosh \omega_3 x \quad (\text{A.50})$$

where ω_3 is defined by

$$\omega_3 = \sqrt{\frac{A_{55(2)}}{D_{11(2)}}} \quad (\text{A.51})$$

Since the β matching condition cannot be used at the 2-3 interface, the (remaining) boundary conditions are

$$M_3(a) = 0 \quad (\text{A.52})$$

$$M_3(0) = M_2(0) \quad (\text{A.53})$$

The φ s can be solved using the boundary conditions A.52 and A.53 as

$$\varphi_2 = a_1 k_3 + a_2 k_4 \quad (\text{A.54})$$

$$\varphi_1 = -\varphi_2 \coth \omega_3 a \quad (\text{A.55})$$

The solution for sublaminates 3 can be completed by writing the expressions for Q_3 , β_3 and P_3 based on the M_3 solution.

The equilibrium equations for sublaminates 4 are

$$N_{4,x} = 0 \quad (\text{A.56})$$

$$Q_{4,x} = 0 \quad (\text{A.57})$$

$$M_{4,x} - Q_4 = 0 \quad (\text{A.58})$$

The constitutive relations take the form

$$N_4 = A_{11(1)} U_{4,x} \quad (\text{A.59})$$

$$Q_4 = A_{55(1)} (\beta_4 + W_{4,x}) \quad (\text{A.60})$$

$$M_4 = D_{11(1)} \beta_{4,x} \quad (\text{A.61})$$

Using Eq. A.56 with the boundary condition $N_4(a) = \frac{P}{2b}$ yields

$$N_4 = \frac{P}{2b} \quad (\text{A.62})$$

Similarly, using Eq. A.57 with $Q_4(a) = 0$ results in

$$Q_4 = 0 \quad (\text{A.63})$$

Matching M_1 and M_4 at the 1-4 interface and using Eq. A.58 gives

$$M_4 = a_1 k_1 + a_2 k_2 \quad (\text{A.64})$$

The U_4 displacement is obtained by integrating Eq. A.59 and using the displacement matching boundary condition $U_4(0) = U_1(0)$.

$$U_4 = \frac{1}{A_{11(1)}} \left(\frac{P}{2b} x + \frac{a_1}{s_1} + \frac{a_2}{s_2} \right) + a_3 \quad (\text{A.65})$$

Similarly, integrating Eq. A.64 and setting $\beta_4(a)$ to zero gives the solution for β_4 . Using the solutions for Q_4 and β_4 and the boundary condition $W_4(0) = 0$ in Eq. A.63 yields the solution for W_4 .

In order to determine a_1 , a_2 and a_3 , the following boundary conditions are used.

$$N_1(0) = \frac{P}{2b}$$

$$\beta_1(0) = \beta_4(0)$$

$$U_1(-L+a) = 0$$

It is convenient to define the following parameters.

$$\theta_1 = \frac{s_1}{A_{55(1)}} \left(k_1 + \frac{h_1}{2} \right) \quad (\text{A.66})$$

$$\theta_2 = \frac{k_1}{D_{11(1)}} \quad (\text{A.67})$$

$$\theta_3 = \frac{s_2}{A_{55(1)}} \left(k_2 + \frac{h_1}{2} \right) \quad (\text{A.68})$$

$$\theta_4 = \frac{k_2}{D_{11(1)}} \quad (\text{A.69})$$

$$\theta_d = \theta_3 - \theta_1 + (\theta_4 - \theta_2)a \quad (\text{A.70})$$

The nominal (far field) strain is given by

$$\epsilon = \frac{P}{2b} \frac{1}{A_{11(1)} + A_{11(2)}} \quad (\text{A.71})$$

The a parameters are obtained as

$$a_1 = A_{11(2)} \epsilon \frac{\theta_3 + \theta_4 a}{\theta_d} \quad (\text{A.72})$$

$$a_2 = -A_{11(2)} \epsilon \frac{\theta_1 + \theta_2 a}{\theta_d} \quad (\text{A.73})$$

$$a_3 = \epsilon (L-a) - \frac{a_1}{s_1 A_{11(1)}} e^{-s_1(L-a)} - \frac{a_2}{s_2 A_{11(1)}} e^{-s_2(L-a)} \quad (\text{A.74})$$

The specimen compliance C is defined as the ratio of specimen extension to applied load. This is obtained as

$$C = \frac{2U_4(a)}{P}$$

$$= \frac{2}{PA_{11(1)}} \left\{ \frac{Pa}{2b} + \frac{a_1}{s_1} + \frac{a_2}{s_2} + a_3 A_{11(1)} \right\} \quad (\text{A.75})$$

The total energy release rate associated with the crack (delamination) growth under a constant load P is given by

$$G_T = \frac{P^2}{2b} \frac{dC}{da} \quad (\text{A.76})$$

Substituting the compliance expression from Eq. A.75 in Eq. A.76 yields the following expression for the total energy release rate.

$$G_T = \frac{P^2}{2b^2} \left(\frac{1}{A_{11(1)}} - \frac{1}{A_{11(1)} + A_{11(2)}} + I_1 - I_2 \right) \quad (\text{A.77})$$

where

$$I_1 = \chi \frac{\theta_2 \theta_3 - \theta_1 \theta_4}{\theta_d^2} \left(\frac{1 - e^{-s_1(L-a)}}{s_1} - \frac{1 - e^{-s_2(L-a)}}{s_2} \right) \quad (\text{A.78})$$

$$I_2 = \chi \frac{(\theta_3 + \theta_4 a)e^{-s_1(L-a)} - (\theta_1 + \theta_2 a)e^{-s_2(L-a)}}{\theta_d} \quad (\text{A.79})$$

with

$$\chi = \frac{1}{A_{11(1)} + A_{11(2)}} \frac{A_{11(2)}}{A_{11(1)}} \quad (\text{A.80})$$

The individual fracture mode contributions to the energy release rate can be calculated using the virtual crack closure method, based on the interlaminar stresses and displacements in the vicinity of the crack tip. From the assumed plane strain condition, the mode III contribution is zero ($G_{III}=0$). The mode II energy release rate, G_{II} , is calculated using the virtual crack closure technique while G_I is evaluated using

$$G_I = G_T - G_{II} \quad (\text{A.81})$$

G_{II} is calculated from the interlaminar shear stress and relative sliding displacement as

$$G_{II} = \lim_{\delta \rightarrow 0} \frac{1}{2\delta} \int_0^{\delta} T_1(x-\delta) \Delta u(x) dx \quad (\text{A.82})$$

In the absence of a singularity in the stress field, the limiting process leads to the trivial result $G_{II}=0$. Hence, the limit is calculated as δ tends to some finite value, say Δ . The value of Δ is chosen depending on the decay length associated with the problem i.e. the length within which the presence of the crack significantly alters the specimen response in comparison with the corresponding far field values. The decay length in this problem is dependent on the eigenvalues s_1 and s_2 . The following value of Δ has been chosen in order to reasonably fulfil the decay length criterion.

$$\Delta = \frac{1}{4} \left(\frac{1}{s_1} + \frac{1}{s_2} \right) \quad (\text{A.83})$$

The relative sliding displacement Δu is based only on the difference U_4-U_3 so that the kinematic condition of zero relative displacement at the crack tip is fulfilled. This also simplifies the calculations. If the true value of Δu (based on u_4-u_3) is used, the β mismatch at the 3-4 interface leads to a kinematically inadmissible displacement discontinuity at the interface. This discontinuity causes a non trivial limiting value G_{II} as $\delta \rightarrow 0$. But this value is an artifact of the modeling assumptions and cannot be used as the true value of G_{II} . The mode II energy release rate component, using $\Delta u=U_4-U_3$, is obtained as

$$G_{II} = \frac{I_3}{2\Delta} \quad (\text{A.84})$$

where the parameter I_3 depends on $A_{11(1)}$, $A_{11(2)}$, s_1 , s_2 , a_1 , a_2 , Δ and the specimen nominal strain ϵ .

Table I Summary of Results

number of 90° plies	G_T J/m ²	G_{II}/G_T	σ_c MPa	ϵ_c %
1/2	2.404	0.276	1313.9	1.6747
1	6.752	0.275	784.0	1.1685
2	22.849	0.267	426.2	0.8058
3	51.049	0.261	285.1	0.6427
4	93.603	0.256	210.6	0.5444
6	228.871	0.250	134.7	0.4264
8	440.065	0.247	97.1	0.3555

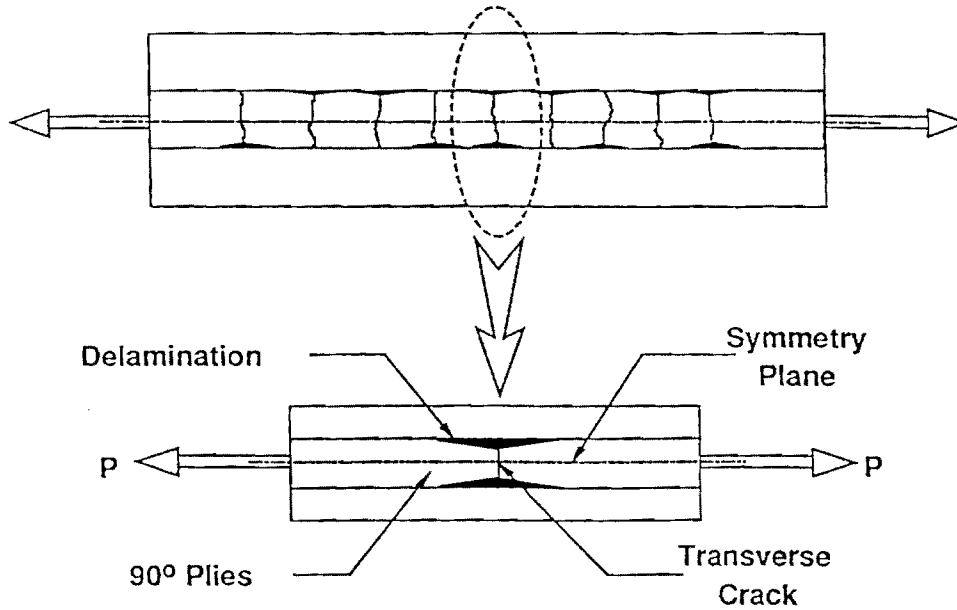


Fig. 1 Specimen Cross Section

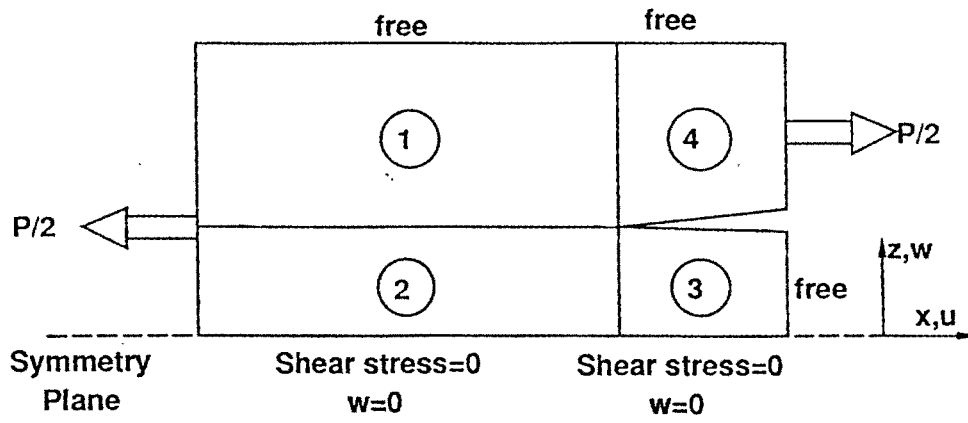


Fig. 2 Modelled Region and Sublaminar Scheme

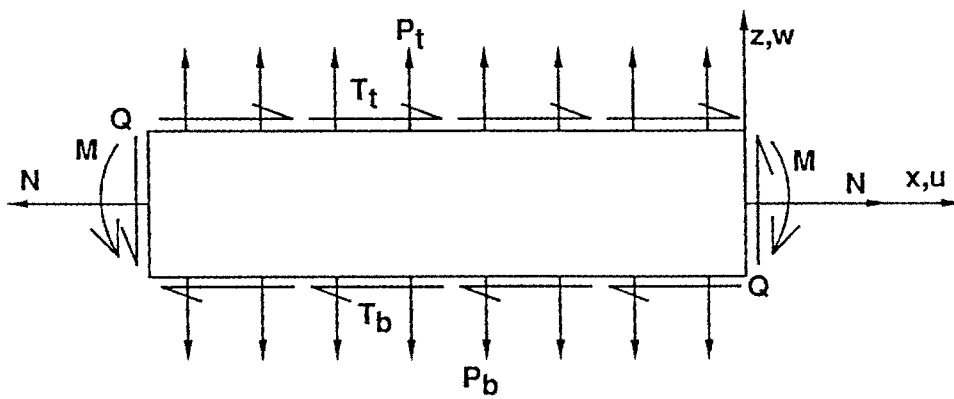


Fig. 3 Generic Sublaminar

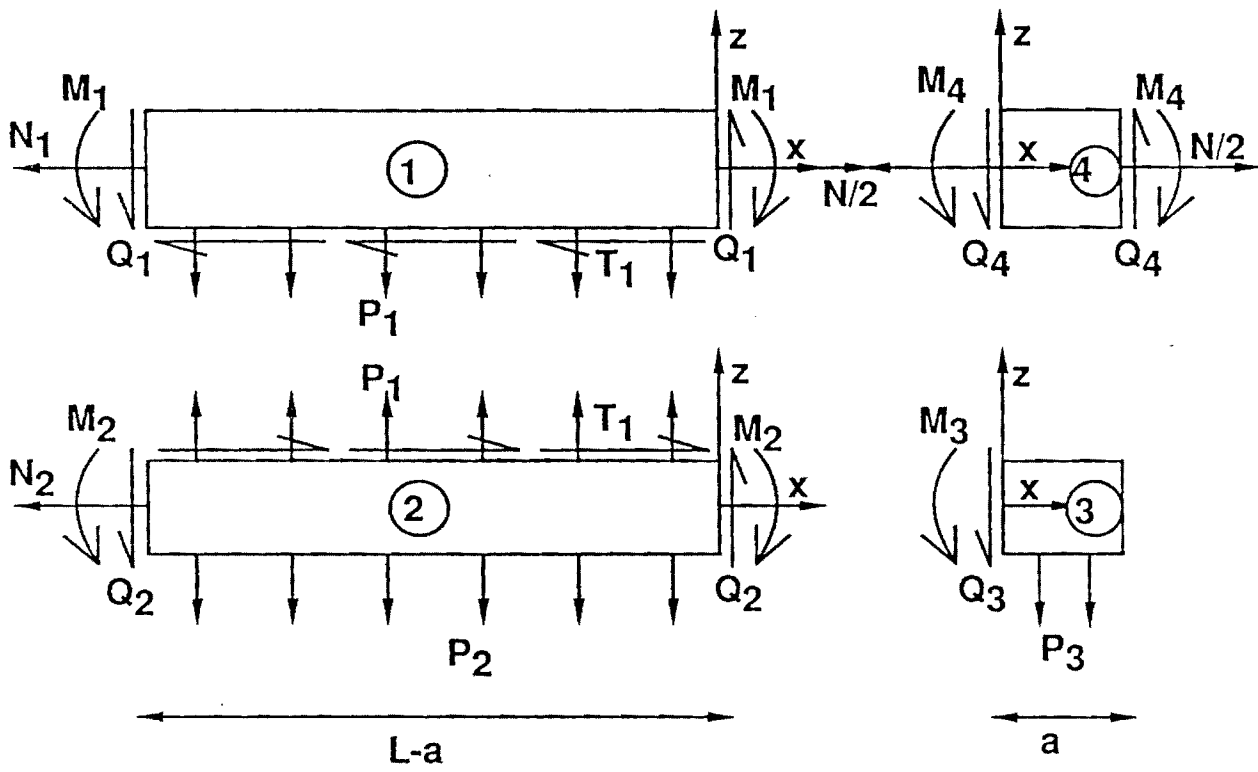


Fig. 4 Sublaminates Forces and Coordinate Systems

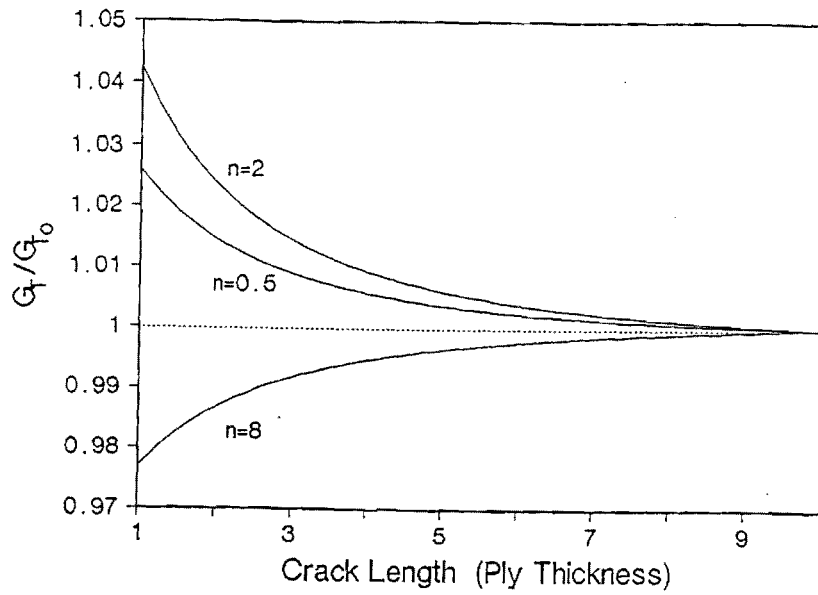


Fig. 5 Total Energy Release Rate Variation with Crack Size

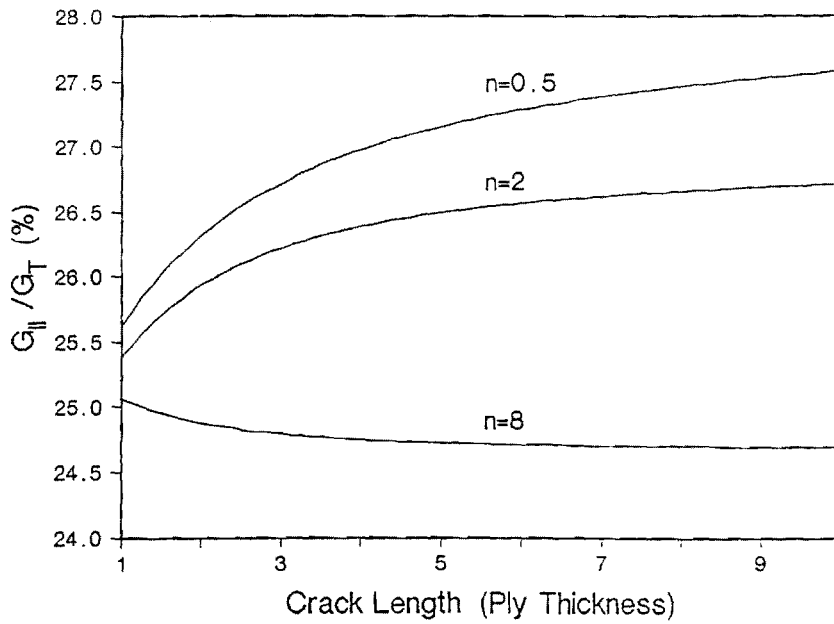


Fig. 6 Mode II Energy Release Rate Dependence on Crack Size

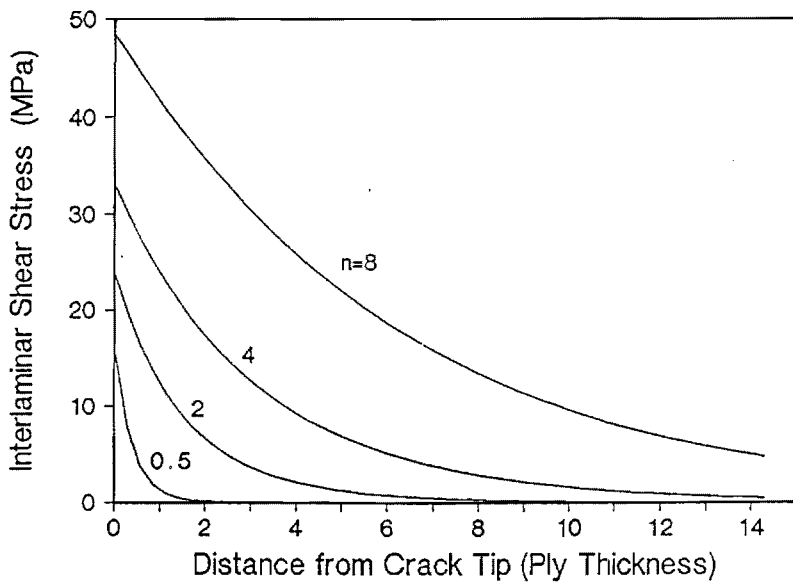


Fig. 7 Interlaminar Shear Stress Distribution

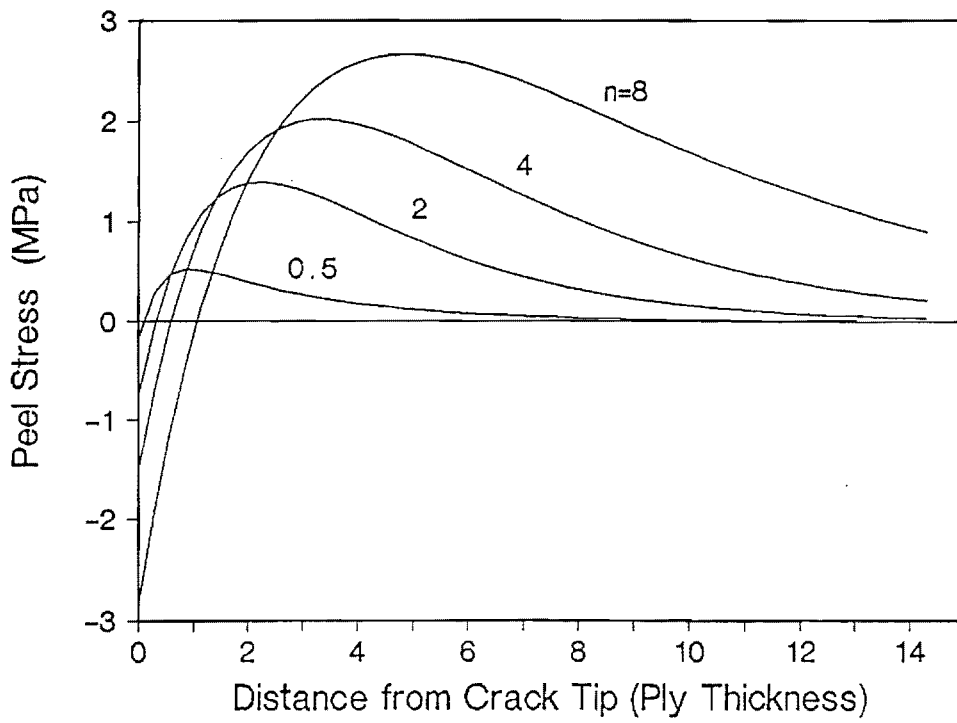


Fig. 8 Interlaminar Normal Stress (Peel Stress) Distribution

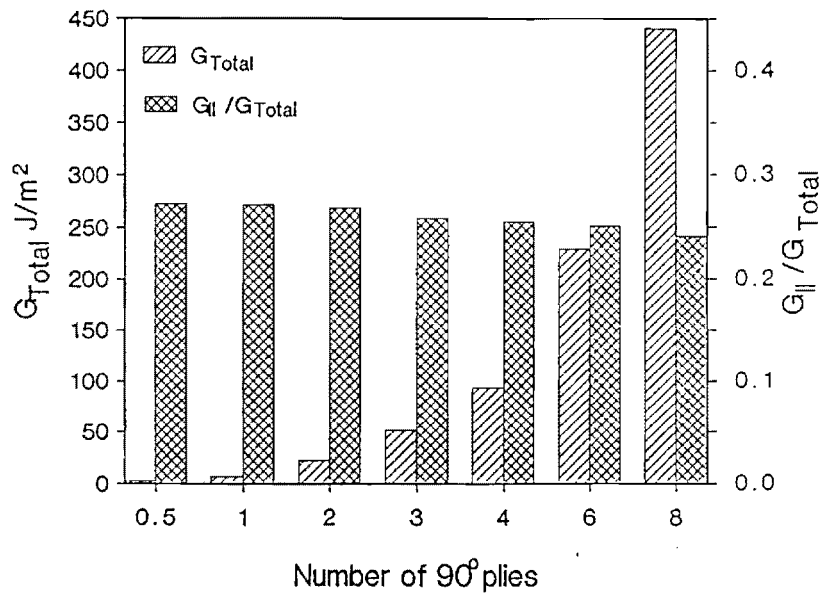


Fig. 9 Energy Release Rate Comparison

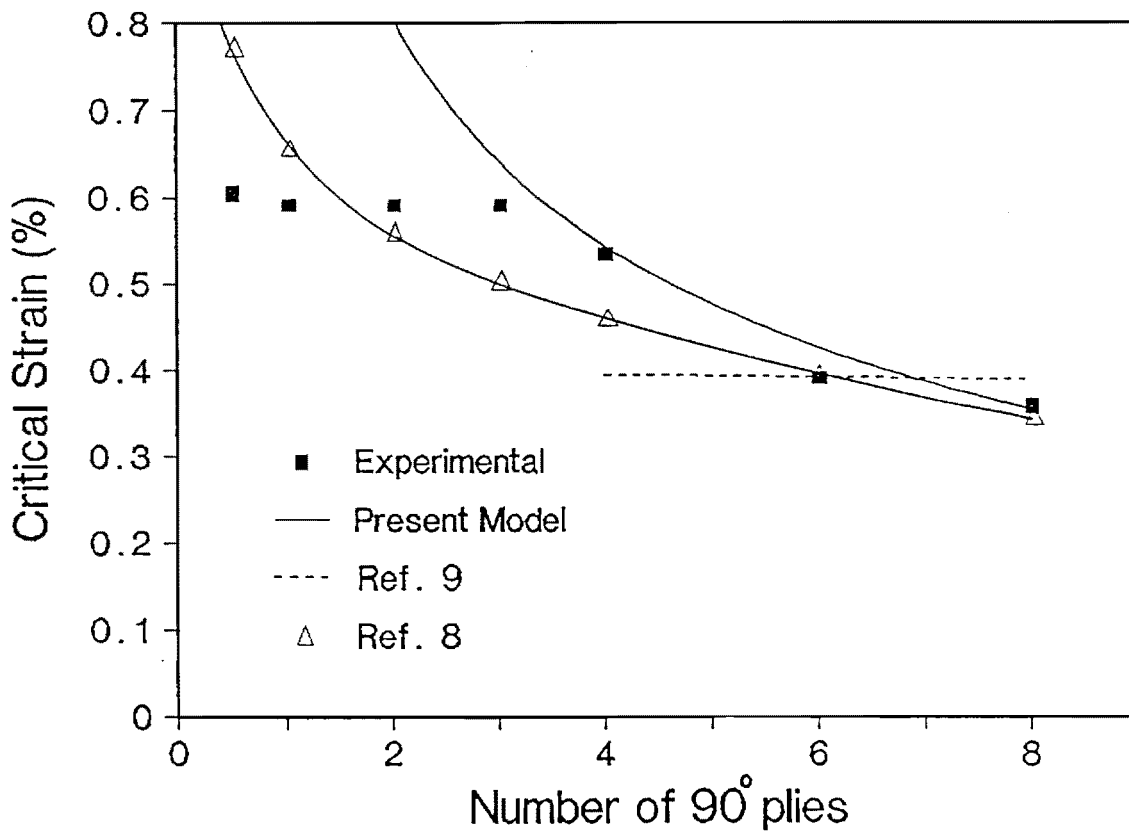


Fig. 10 Critical Delamination Growth Strain Variation

E-16-654

Research Proposal Submitted to
NASA Langley Research Center

Attention: Mrs. Gretchen Bostaph Murri
Mail Stop 188 E
NASA Langley Research Center
Hampton, VA 23665
(804) 864-3466

by the

Georgia Institute of Technology
Atlanta, Georgia 30332

ANALYSIS OF INTERLAMINAR FRACTURE IN
COMPOSITES UNDER COMBINED LOADING
(Renewal of Grant NAG-1-637)

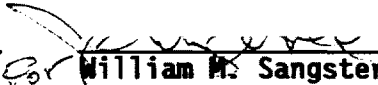
Principal Investigator:

.1

Erian A. Armanios
Assistant Professor
School of Aerospace
Engineering
SSN: 260-35-6743
(404) 894-8202

Endorsements:

Don P. Giddens
Director
School of Aerospace
Engineering
(404) 894-3000


William M. Sangster
Dean
College of Engineering
(404) 894-3350

Dennis Farmer
Grant & Contract Officer
Office of Contract
Administration
(404) 894-4817

INTRODUCTION

This is a proposal to extend the sublaminar analysis method^{1,2} developed under the current Grant NAG-1-637, to the interlaminar failure analysis of laminated tapered composites under combined loading. Tapered laminates are used in composite rotorcraft and airframe components. An example is the flapping flexure region of the Bell 680 tapered hub. In the airframe context tapered laminates are the result of inserting internal plies at locations of stress concentrations such as holes, cut outs and connections between structural members in order to tailor stiffness and strength. The potential increase in stiffness and strength in tapered laminates is often limited by premature failure initiated by interlaminar fracture. An accurate knowledge of interlaminar stresses and strain energy release rate in tapered laminates is essential in predicting and designing against interlaminar fracture.

The sublaminar analysis methods provides accurate prediction of interlaminar stresses and strain energy release rate. They are intended to be used for preliminary design studies where a large number of candidate configurations need to be evaluated quickly and economically. The methods are effective in developing insight and understanding fundamental behavior by isolating the parameters controlling the damage mechanisms.

A brief summary of the status of the current research work under the present grant is given in the next section. This is followed by a discussion of some issues associated with the research and a presentation of the proposed research program. Biographical and budgetary information appear in appendices.

SUMMARY OF ACCOMPLISHMENTS

The sublaminar analysis of tapered rotor hubs made of glass/epoxy material subjected to tensile loading is under completion. A generic configuration of a tapered hub appears in Figure 1 where a 38 ply thick laminate is reduced to 26 ply by dropping three inner sets of plies. The basic analysis approach that is adopted utilizes two levels of modeling, a global scale and a local scale. The global scale is concerned with overall generalized forces and strains such as axial force and extension. A simple consistent deformation assumption is the foundation of this model. Global equilibrium equations are written and solved.

The generalized strains determined from the global analysis served to provide estimates for the key primary stresses in the belt of the tapered section. Local estimates of interlaminar stresses are determined on the basis of equilibrium condition.

The total strain energy release rate is computed from the work done by the external applied loads. It is based on the axial stiffness of the different elements in the tapered configurations. This work is the subject of Reference 3.

The second objective of the research under the current grant is the analysis of local or transverse crack-tip delamination. This damage mode appears in Figure 2 along with a representation of the predominant damage modes in laminated composites.

Three analytical models, sublaminar shear, membrane and shear lag have been developed in order to estimate the transverse crack spacing distance. The saturation crack spacing corresponds to the distance from the crack where the broken plies regain their uniform stress/strain state i.e. where the interlaminar shear stress has decayed down to its far field (uniform) value.

The analysis of transverse crack tip delamination is based on the sublaminar shear model. Closed form expressions for the interlaminar stresses, total strain energy release rate and energy release rate components are obtained. A computer code based on this analysis is developed and implemented into an earlier mixed-mode edge delamination code developed under the previous NASA grant NAG-1-558 and presented in References 4 and 5. This code was used to estimate the critical strain levels and the associated delamination damage mode with increasing number of 90° plies in a $[\pm 25/90_n]_s$ laminate. Since mid-plane edge delamination is a possible damage mode in this type of laminates a mid-plane delamination analysis was developed and presented in Reference 6. A computer code based on this analysis is developed and implemented in the mixed-mode edge delamination code. The critical strain and associated delamination damage modes predicted appear in Figure 3.

Experimental results⁷ show that the local (crack-tip) delamination phenomenon is the predominant damage mode only for $n=4, 6$ and 8 specimens. For $n<4$ edge delamination either in the mid-plane or in the $25/90$ interface were observed in tests. The present analysis predicts mid-plane edge delamination for $n=1/2$ and 1 and mixed mode edge delamination for $n=2$ and 3 ,

respectively. For $n=4, 6$ and 8 local delaminations are predicted to be the controlling damage mode. The critical strains in Figure 3 are computed based on a fracture toughness values of 415 J/m^2 , 140 J/m^2 , and 120 J/m^2 for local delamination, mixed mode edge delamination and mid-plane edge delamination, respectively. A detailed description of this work is presented in References 8 and 9.

An assessment of the influence of residual thermal and moisture stresses is underway. The effects of hygrothermal stresses on mid-plane edge delamination has been completed⁶ and final results for mixed-mode edge delamination are expected by the end of the grant year.¹⁰

PROPOSED RESEARCH

Background Information

Tapered laminates constructions are used in rotorcraft dynamic components as well as airframe members. The flapping flexure region of composite rotor hubs are tapered in order to create an effective hinge for elastic tailoring. The tapered design is achieved by dropping a number of plies at discrete locations. The ply drop creates large interlaminar stresses causing delaminations. This is illustrated in Figure 4 where the transverse normal stress resultants between the belt and the core region of the tapered laminate appearing in Figure 1 is plotted. The applied tensile load is denoted by P in Figure 4. Peak values occur at the ply drop locations and precipitate delaminations.

Tapered composite laminates used in dynamic rotorcraft components are subjected to centrifugal tensile and combined bending-extension-torsion loading. A sublaminates analysis¹¹ of a uniform laminate subjected to bending and combined bending and extension loading indicated that bending loading is not as critical as tension or combined bending and extension. However, the energy release rates under a combined bending-extension loading can be more critical than tension loading only. This is shown in Table I from Reference 11 where the strain energy release rates for a $[0_8/90_4]_s$ laminate made of T300/5208 graphite/epoxy laminated is presented. The strain ϵ_0 in the table is $1\mu\text{in/in}$. For a delamination occurring at the $0/90$ interface, the presence of bending loading

in addition to in-plane extension results in a 68% increase in the total strain energy release rate (G_T) and a 3% in the Mode I ratio (G_I/G_T). These results were found to be in good agreement with the finite element formulation of Wen Chan¹².

While these findings are limited to uniform laminates they indicate, however, the potential detrimental effect of combined loading.

Statement of the work

The research program consists of the following elements:

- (1) Develop a delamination analysis for tapered laminates under bending and combined bending and tension loading.
- (2) Validate the predictions in item (1) through comparison with numerical simulation and test results performed at the NASA Langley Research Center and Bell Helicopter Textron Inc
- (3) Create appropriate computer codes and documentation based on the analysis in item (1).

Interaction with Dr. Wen Chan of the University of Texas at Arlington and Mr. Ed Lee of Bell Helicopter Textron, Inc., is planned through this research work in order to adapt and apply the developed analysis and computer codes to the practical design needs. Computer codes developed under NASA Grant NAG-1-558 are being implemented for the preliminary design of laminates prone to mixed-mode free edge delaminations at Bell Helicopter and the University of Texas.

REFERENCES

1. Armanios, E.A. and Rehfield, L.W., "Sublaminar Analysis of Interlaminar Fracture in Composites: Part I - Analytical Model," accepted for publication in the Journal of Composites Technology and Research.
2. Armanios, E.A., Rehfield, L.W., O'Brien, T.K. and Raju, I.S., "Sublaminar Analysis of Interlaminar Fracture in Composites: Part II - Applications," accepted for publication in the Journal of Composites Technology and Research.
3. Armanios, E.A. and Parnas, L., "Delamination Analysis of Tapered Laminated Composites Under Tensile Loading," to be presented at the third ASTM Symposium on Composite Materials: Fatigue and Fracture, November 6-9, 1989, Orlando, Florida.
4. Armanios, E.A. and Rehfield, L.W., "Interlaminar Analysis of Laminated Composites Using a Sublaminar Approach," Proceedings of the AIAA/ASME/ASCE/AHS 27th Structures, Structural Dynamics, and Materials (SDM) Conference, San Antonio, Texas, 19-21 May, 1986. AIAA Paper No. 86-0969CP, Part 1, pp. 442-452.
5. Armanios, E.A. and Rehfield, L.W., "Sublaminar Analysis of Interlaminar Fracture in Composites," Final Report, NASA Grant NAG-1-558, March 1986.
6. Armanios, E.A., Badir, A. and Sriram, P., "Sublaminar Analysis of Mode I Edge Delamination in Laminated Composites," Proceedings of the AIAA/ASME/ASCE/AHS/ASC 30th SDM Conference, Mobile, Alabama, April 3-5, 1989, pp. 2109-2116.
7. Crossman, F.W., and Wang, A.S.D., "The Dependence of Transverse Cracking and Delamination on Ply Thickness in Graphite/Epoxy Laminates," in Damage in Composite Materials, ASTM STP 775, K.L. Reifsnider, Ed., pp. 118-139 (1982).

8. Sriram, P., and Armanios, E.A., "Fracture Analysis of Local Delaminations in Laminated Composites," Proceedings of the AIAA/ASME/ASCE/AHS/ASC 30th SDM Conference, Mobile, Alabama April 3-5, 1989, pp. 2109-2116.
9. Armanios, E.A., Sriram, P. and Badir, A., "Fracture Analysis of Matrix Crack-tip and free edge delamination in Laminated Composites" to be presented at the third ASTM Symposium on Composite Materials: Fatigue and Fracture, November 6-9, 1989, Orlando, Florida.
10. Armanios, E.A. and Badir, A., "Hygrothermal Influence on the Edge Delamination of Laminated Composites," to be presented at the ASC Fourth Technical Conference on Composite Materials, October 3-5, 1989, Blacksburg, VA.
11. Armanios, E.A. and Rehfield, L.W., "Interlaminar Fracture Analysis of Composite Laminates Under Bending and Combined Bending and Extension," Composite Materials: Testing and Design (Eighth Conference). ASTM STP 972, J.D. Whitcomb, Eds., American Society for Testing and Materials, Philadelphia, 1988, pp. 81-94.
12. Chan, W.S. and Ochoa, O.O., "An Integrated Finite Element Model of Edge - Delamination Analysis for Laminates due to Tension, Bending, and Torsion Loads," Proceedings of the AIAA/ASME/ASCE/AHS 28th SDM Conference, Monterey, CA, April 6-8, 1987, pp. 27-35.

TABLE I - Energy release rate comparison for a $[0_8/90_4]_s$ laminate-graphite/epoxy material.

Energy Release Rate	Uniform Extension $\epsilon_1 = \epsilon_2 = \epsilon_0$	Uniform Bending $\epsilon_1 = -\epsilon_2 = \epsilon_0$	Combined Bending Extension $\epsilon_1 = 2\epsilon_0, \epsilon_2 = 0$
G_I/G_T	0.61	0.82	0.63
$10^6 G_T$ (J/m ²)	0.34	0.05	0.57

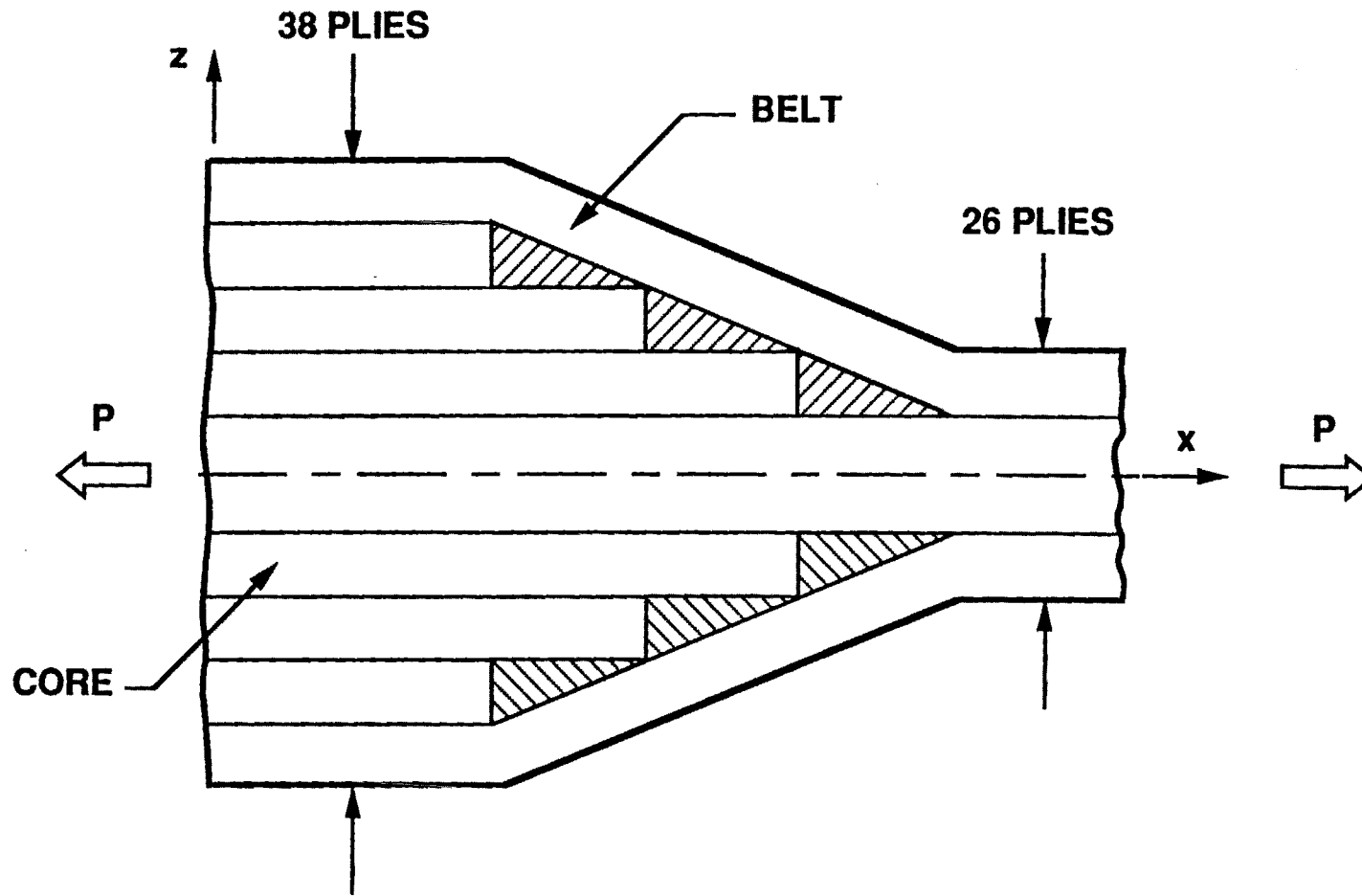


Figure 1. Tapered Laminate Configuration

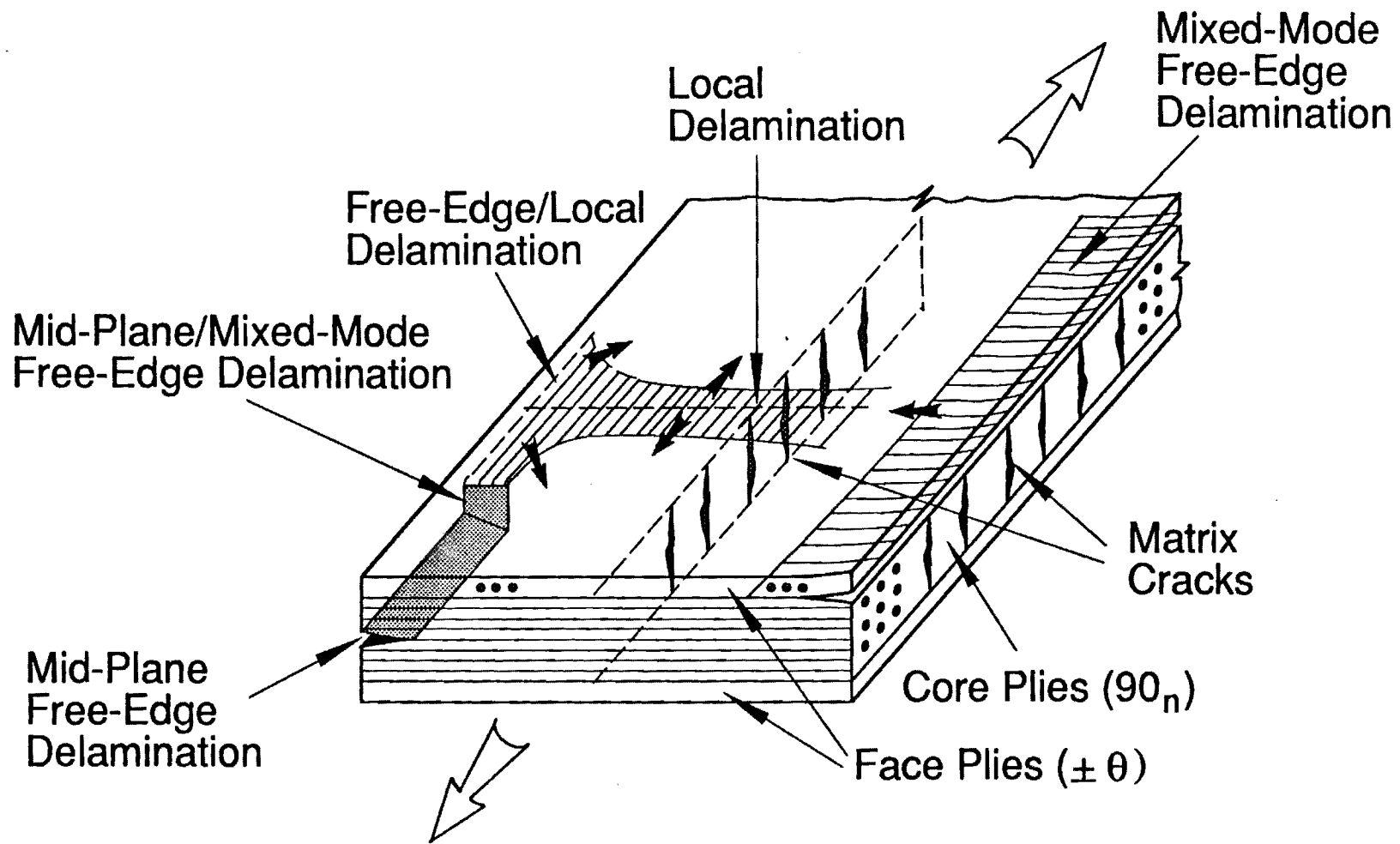


Figure 2. DAMAGE MODES

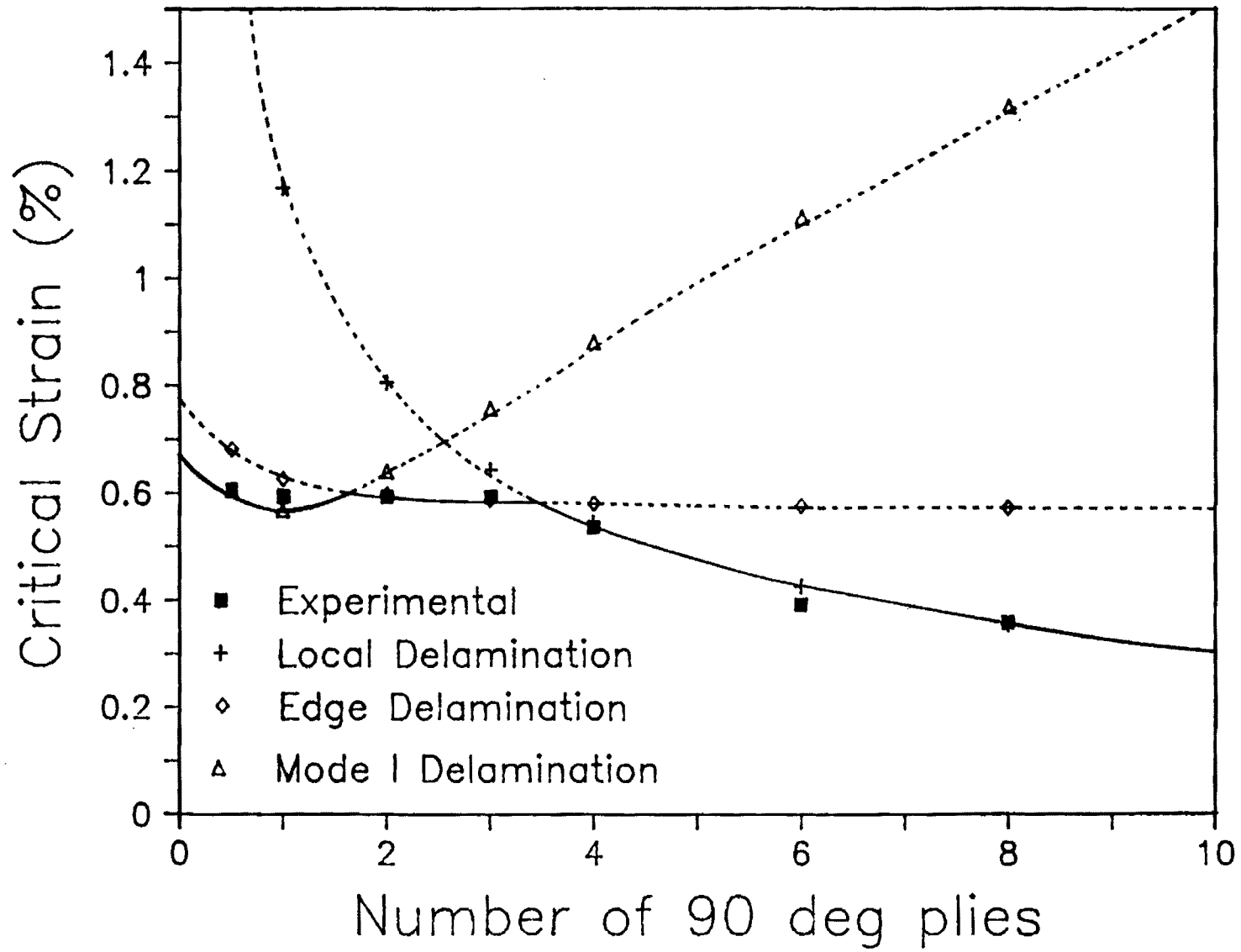


Figure 3. Damage Prediction

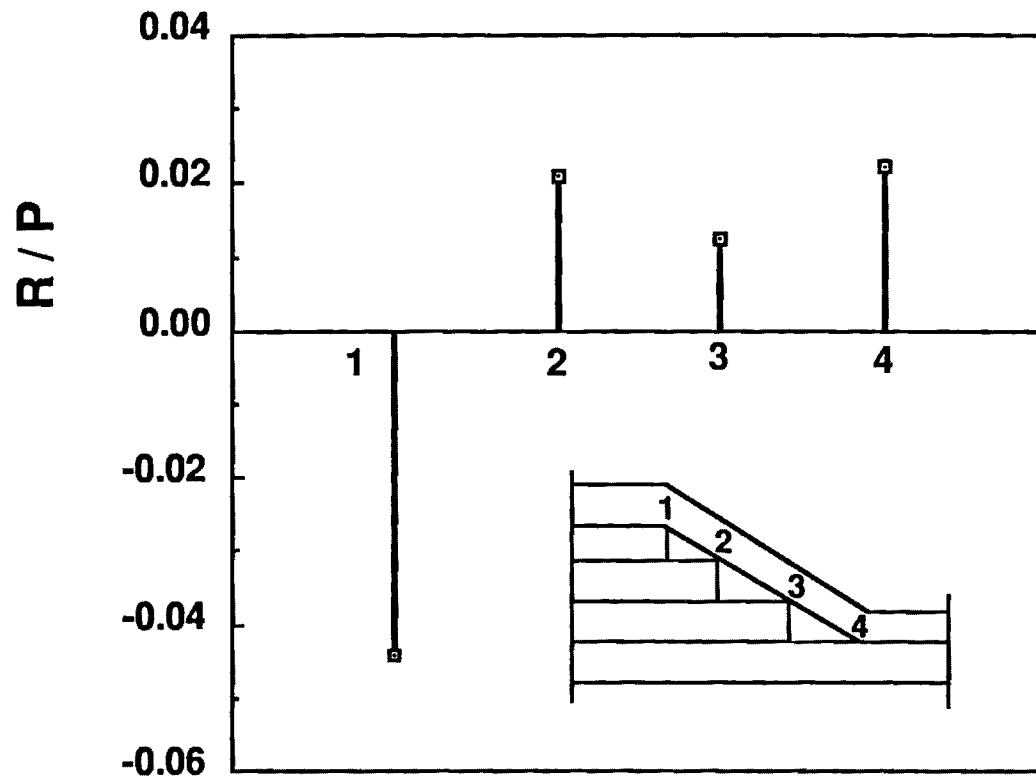


Figure 4. Interlaminar Transverse Normal Stress Resultant Distribution

SEMI-ANNUAL REPORT

ANALYSIS OF DELAMINATION RELATED FRACTURE PROCESSES IN COMPOSITES

NASA GRANT NAG-1-637
GEORGIA TECH PROJECT E16-654

PRINCIPAL INVESTIGATOR
Erian A. Armanios

This report covers the research work performed for the period starting September 1989 and ending February 1990. In the first phase of the program, a study was conducted to analyze tapered composite laminates under tensile loading. A simple extensional model was used to calculate the total strain energy release rate from the work done by the external forces. The model used is concerned with overall generalized forces and strains such as axial force and displacements leading to the global energy balance of the laminate. A simple consistent deformation assumption is the foundation of this model.

The sublaminates modelling of cracked laminate configurations and corresponding sublaminates stiffnesses are shown in Fig 1. These stiffnesses change from one ply drop group to another with crack growth. The tapered laminate shown in Fig. 1 is assumed to be fixed at $x=0$, and subjected to an axial load at $x=c$.

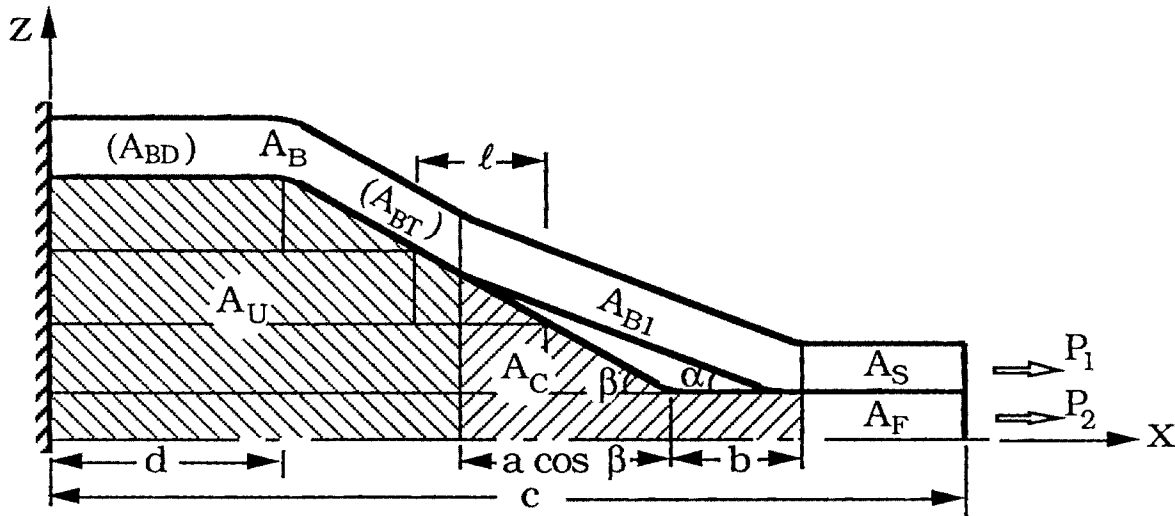


Figure 1. Dependency of Core and Belt Stiffnesses on Delamination

The stress and displacement fields used in the strain energy release rate calculations were determined based on the effective section stiffnesses. The load share between the core and belt portions is based on their relative stiffness ratios and on the continuity of displacements at the *belt-core* interface. The analysis resulted in the following expressions for the end displacements¹

$$U_1 = \frac{P A_B c}{A_S(A_B + A_U)} + \frac{P(d + 3\ell + b)}{(A_B + A_U)} \left(\frac{A_B}{A_{B1}} - \frac{A_B}{A_F} \right) + \frac{P(d + 3\ell - a')}{(A_B + A_U)} \left(1 - \frac{A_B}{A_{B1}} \right)$$

$$U_2 = \frac{P A_U c}{A_F(A_B + A_U)} + \frac{P(d + 3\ell + b)}{(A_B + A_U)} \left(\frac{A_U}{A_C} - \frac{A_U}{A_F} \right) + \frac{P(d + 3\ell - a')}{(A_B + A_U)} \left(1 - \frac{A_U}{A_C} \right)$$

where

$$a' = a \cdot \cos\beta$$

and section stiffnesses are denoted by A with their respective subscripts.

The solution resulted in a mismatch between the axial end displacements. This is due to the membrane modeling approach where the interlaminar stresses are neglected. The model leads to a configuration which is schematically shown in Fig. 2. The delamination extends from the crack front in the taper section to the end of the uniform thin section.

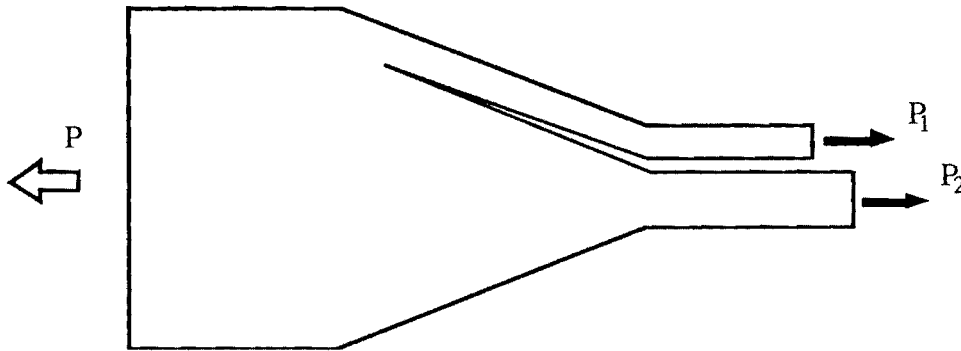


Figure 2. Discontinuity of End Displacements

Although there is an agreement with the FE strain energy release rate distributions for delamination growth in the tapered section, there is a quantitative difference in the thin uniform region. Some efforts were undertaken to investigate this discrepancy. These are summarized in the following.

- The strain energy stored due to the interlaminar stresses between core-belt interface in the uniform section is added to the strain energy release rate calculation. The interlaminar shear stresses are calculated by a local sublaminar analysis. This seems to alleviate the problem, but a considerable difference in both G_T values continued to exist.
- In another attempt, the axial displacements are determined in such a way that the end displacements become continuous. In this model as opposed to the original one, belt and core stiffnesses are treated together all along the belt-core interface. The solution led to an increase in the difference between the FE and current G_T values.
- Finally, an attempt is made to see the effect of the location where the load share is performed. The results showed that this effect is negligible.

This investigation is still continuing.

TAPERED LAMINATES UNDER COMBINED LOADING

Rotor hubs are subjected to combined extension, bending and torsion loadings. Combined extension and bending are considered in this phase of the program. The problem of bending load is treated first.

A schematic view of the tapered laminate under bending load is shown in Fig. 3. According to the bending moment distribution, the upper section of the laminate is under tensile and the lower section is under compressive load. In contrast to the uniaxial loading case, the laminate is not symmetric in terms of loading and therefore the whole laminate should be considered in the analysis. Under this load distribution, the upper section is expected to have a mixed-mode delamination originating at the junction between the taper and thin uniform regions. In the lower section, however, delamination initiates at the thick uniform and taper junction due to high interlaminar stress concentration around this location. This is a Mode II dominated delamination behavior.

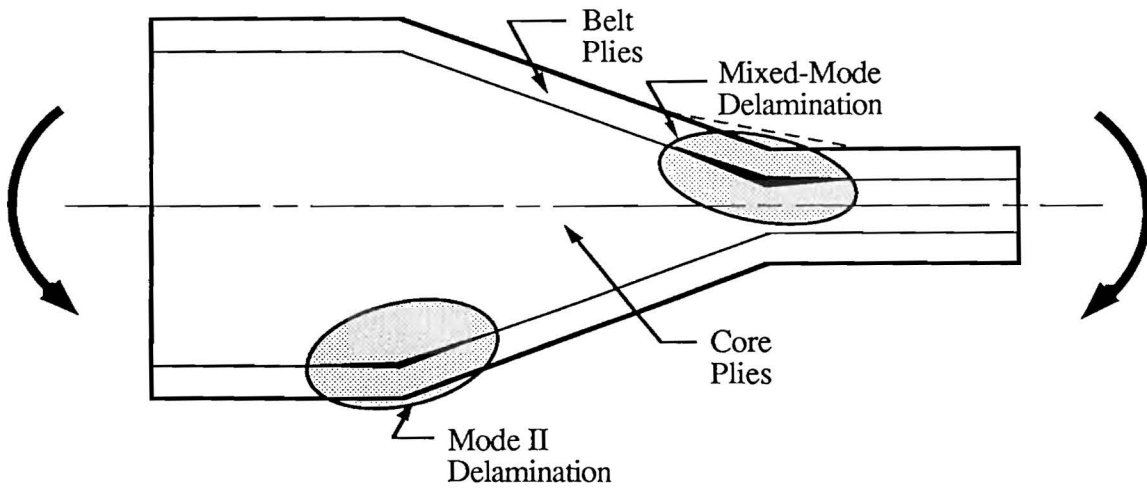


Figure 3. Tapered Laminate under Combined Loading

A sublaminates modelling approach is used in the analysis. The tapered laminate is represented with 7 sublaminates as shown in Fig. 4. Each sublaminates has its corresponding axial and bending stiffnesses. The stiffness properties of each generic section are smeared to obtain the effective sublaminates stiffness values. A linear stress distribution is assumed as shown Fig. 4. The analysis is underway, closed form expressions for the interlaminar stresses and total energy release rate are expected by the end of the grant.

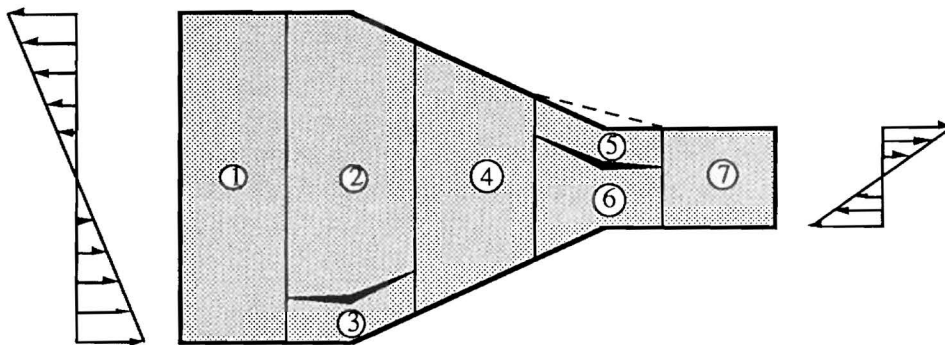


Figure 4. Modelling of Tapered Laminate

REFERENCE

Armanios, E. A. and Parnas, L. , "Delamination Analysis of Tapered Laminated Composites Under Tensile Loading " presented at the Third Symposium on Composite Materials: Fatigue and Fracture, Lake Buena Vista, Florida, November 6-7, 1989.

A Research Proposal Entitled
**EFFECT OF DAMAGE ON ELASTICALLY
TAILORED COMPOSITES**

Research Proposal Submitted to the
NASA Langley Research Center


Attention: Dr. T. Kevin O'Brien
Mail Stop 188E
NASA Langley Research Center
Hampton, VA 23665
(804) 864 3465

by the
Georgia Institute of Technology
Atlanta, Georgia 30332


EFFECT OF DAMAGE ON ELASTICALLY
TAILORED COMPOSITES

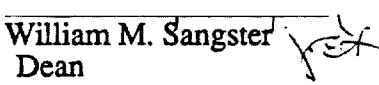
(renewal of Grant NAG-1-637)

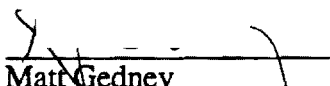
Principal Investigator:


Erian A. Armanios
Assistant Professor
School of Aerospace
Engineering
SSN: 260-35-6743
(404) 894 8202

Endorsements:


Don P. Giddens
Director
School of Aerospace
Engineering
(404) 894 3000


William M. Sangster
Dean
College of Engineering
(404) 894 3350


Matt Gedney
Grant & Contract Officer
Office of Contract
Administration
(404) 894 4817

BACKGROUND

Elastically tailored composite designs are being used to achieve favorable deformation modes under a given loading environment. Coupling between deformation modes such as extension-twist or bending-twist is created by an appropriate selection of fiber orientation, stacking sequence and materials. An example is the X-29 swept forward wing aircraft where a laminated composite skin is used to create the bending-twist coupling required to handle divergence. This design uses AS-1/3501-5A graphite/epoxy wing covers with -45° outboard plies 9° forward of the wing's 40% chord line.

Elastically tailored composite rotor blades can be used in rotorcraft structures in order to control twisting motions at different rotor speeds. This concept can be utilized in tilt rotor aircraft in order to achieve a compromise between hover performance and forward flight propulsive efficiency [1]. A change in the blade twist between flight modes can be developed through the use of extension-twist coupling as outlined in Ref. 2 for the XV-15 tilt rotor aircraft. Twist control was achieved by assuming a 15 percent change in operating rpm between hover and forward flight regimes.

The fundamental mechanism producing elastic tailoring in composite beams is a result of their anisotropy. Several theories have been developed for the analysis of thin-walled anisotropic beams. A review is provided in Ref.3. A pertinent element in the analytical modeling development is the inclusion of section warping. The major difference between various theories lies in the methodology used to eliminate warping and consequently obtain a one-dimensional theory. A description of the major approaches is provided in Refs.4-13. The works described in Refs.11-13 are based on a finite element formulation.

The finite element analysis developed in Ref.13 is based on the anisotropic beam theory of Ref. 6. This simple theory includes shear deformation and provides closed form expressions of coupling stiffnesses in terms of familiar laminate parameters. While this theory accounts for torsional warping, It does not, however, include the effects of bending-related section warping which can be significant in thin-walled laminated composites. A modification was proposed in Ref. 13 in order to minimize the error associated with neglect of bending-related warping. This modification was based on shear stiffness correction factors determined by numerical comparison of results with an MSC/NASTRAN simulation. However, these correction factors are based on the beam configurations considered and require an alternative approach which includes section warping such as the MSC/NASTRAN model to validate.

The potential of elastically tailored composite rotor blade designs to achieve weight and performance benefits was shown in Refs.1 and 14. An optimization methodology was presented in Ref.14 for a minimum-weight structural design of composite main rotor blades subject to aerodynamic performance, material strength, autorotation, and frequency constraints. Damage tolerance constraints were not considered. This may explain the fact that the resulting multiple composite-spar design was heavier than the comparably designed single composite-spar. The author concludes that if ballistic tolerance is considered in the design, the multispar design will probably have the minimum weight .

The behavior of elastically tailored structures in the presence of damage should therefore be investigated in order to ensure their damage tolerance and durability. While a local damage mode may have a negligible effect on the structure's overall strength it can however, significantly reduce its elastic coupling and consequently fail to perform as designed. The primary objective of this work is to assess the effect of the damage modes relevant to laminated composite structures on their elastic coupling and performance.

PRELIMINARY INVESTIGATION Design Configurations

In order to investigate the effect of damage in elastically tailored structures. Two designs have been considered. The first is a closed cell designed to exhibit extension-twist coupling. This is representative of single cell rotor blade sections where blade twist distribution is adjusted according to rotor speed. The second is a flat laminated composite with bending-extension coupling similar to a swept forward wing skin design.

A simple analytical methodology based on Rehfield's model [6] has been developed in order to determine the optimum stacking sequence that produces maximum extension-twist coupling in a generic closed cell. A similar procedure was developed for the flat laminate configuration. The optimum stacking sequence for both constructions was unidirectional with a fiber orientation of approximately 30° to the loading axis. This is due to the fact that the controlling parameter for extension-twist coupling in a closed cell is strongly influenced by A_{16} while bending-twist coupling in a flat laminate is controlled by D_{16} . The variation of the extension-twist coupling parameter, S_{14} , with fiber orientation is shown in Figure 1 for several material systems. Maximum coupling occurs at approximately $+30^\circ$ or -30° .

A similar result is achieved for a multilayered laminate as illustrated in Figure 2 for the case of a two-ply laminate. The coupling parameter is plotted on the vertical axis against the two ply angles denoted by α and β in the figure. The material system is T300/5208 graphite/epoxy. The maxima depicted in the figure correspond to a unidirectional construction with a fiber angle of approximately $+30^\circ$ or -30° . It can be shown that the fiber orientation corresponding to maximum coupling in a single ply is a local maximum for the multilayered construction. Moreover, the coupling corresponding to a single ply is at the most 5% smaller compared to the global maximum. Minimization of residual curing stresses was not considered in the optimization scheme. Residual thermal coupling due to curing can be avoided when the laminate is composed of 0/90 set of plies stacked symmetrically even if some of the sets are rotated[15].

Damage Models

Two damage modes have been considered in the analysis. The first is matrix dominated where the stiffness components controlled by matrix properties are progressively reduced. These are Q_{12} , Q_{22} and Q_{66} . In the limiting case when Q_{12} , Q_{22} and Q_{66} tend to zero the stiffness component Q_{11} will be equal to E_{11} . This damage mode can be significant in elastically tailored designs due to the use of a larger number of off-axis plies. The second damage mode is fiber dominated. This mode ultimately precipitates final failure. The effect of damage on E_{11} and G_{12} appears in Figure 3 and Figure 4, respectively. The horizontal axis shows the accumulation of damage percentage. Each damage mode (matrix or fiber dominated) varies from 0 to 100% with solid diamond symbol representing fiber damage. As expected, the longitudinal modulus is primarily affected by fiber damage while the shear modulus is influenced by both fiber and matrix dominated damage modes.

In order to gain confidence in this simple engineering model a comparison of predictions is provided in Figure 5. The variation of the longitudinal modulus ratio relative to the undamaged state is plotted against matrix damage percent in the 90° plies of a $[0/90_3]_S$ laminate. The percent of matrix damage is based on the crack density per mm.[16]. Hashin's analysis[16] is based on a complementary energy variational approach and an admissible stress field which satisfy equilibrium and all boundary and interface conditions. Halpin-Tsai and Ekvall's equations are given in Ref.17. Test data from Ref.18 are represented by the solid dots in Figure 5. The present model shows a distribution similar to the Halpin-Tsai model with a slightly improved correlation compared to the test data.

These damage modes have been applied to the single cell laminate shown in Figure 6 with a $[30]_3$ layout. Three damage mode sequence are considered. The first, or case A,

represents a partial damage in the outer ply at one side of the cell while the second, is a damage in all the plies of that side. The third, denoted as case C, is a peripheral damage of the outer ply. This damage sequence is shown schematically in Figure 7.

Results and Discussion

The effect of progressive fiber damage on the extension-twist coupling is shown in Figure 8. The normalized coupling parameter in Figure 8 is defined as the ratio of damaged to the undamaged section coupling. As fiber damage increases the coupling is enhanced for all three damage sequences. At 100% fiber damage cases A, B and C show 8%, 37% and 50% increase in coupling, respectively. The same trend is also found for matrix damage progression as shown in Figure 9. The increase in normalized coupling is 8%, 37% and 55% for cases A, B and C, respectively at 100% matrix damage. Also appearing in the figure is the combined effect of matrix and fiber damage. While fiber damage alone results in a coupling increase its interaction with matrix damage has a negligible effect on the coupling. At 100% fiber damage in addition to matrix damage the coupling increase remains at 8% for case A while it decreases by 5% for case C. For case B, however, the coupling vanishes since the cell becomes an open section.

The results appearing in Figures 8 and 9 are significant in assessing the failure of elastically coupled composite structures. An increase in the laminate coupling with damage progression may result in an increase of the aerodynamic loading which ultimately can lead to an aeroelastic divergence. Furthermore, the damage effect on coupling is a nonlinear phenomenon. This is depicted in Figure 9 where the combined influence of fiber and matrix dominated damage does not follow a superposition law. It is even more significant in the limit where a damage mode results in an opening of the section. In this case the coupling drops to zero.

The findings of this preliminary work show the significance of investigating the influence of damage on the behavior of elastically tailored structures. Moreover, this investigation is essential in establishing a damage tolerance design procedure for this types of structures.

OVERVIEW OF THE RESEARCH PROGRAM

A research program to investigate the effect of damage in elastically tailored structures consists of the following tasks:

- (1) Develop a thin-walled laminated composite analysis including the effect of section warping. The analysis should consider moderate and large deformations in order to account for the effects of damage.
- (2) Develop a mechanics model that accounts for matrix and fiber dominated damage in elastically tailored generic composite sections.
- (3) Verify the model developed in task #2 with predictions from other models and available test data.
- (4) Incorporate the damage model in #2 with the thin-walled analysis in #1 in order to study the effect of damage on the elastic coupling.
- (5) Verify the predictions in #4 with selected tests of extension-twist and bending-twist laminated sections.

In developing the thin-walled composite beam theory described in task #1 a variational-asymptotic approach [19] will be adopted in order to ensure the consistency of the theory. This approach is outlined in Ref. 19 in connection with the development of a nonlinear shell theory. It allows investigating the influence of small, moderate and large deformation kinematic assumptions on the response in a variationally consistent manner.

Based on the preliminary results obtained, these tasks will provide a sound scientific and technological basis for predicting and managing damage in elastically tailored composite structures. Interaction with Dr. Raymond Kvaternik, Mr. Mark Nixon and Mrs. Renee Lake of the Army Aerostructures Directorate is planned throughout this work.

REFERENCES

- [1] Nixon, Mark W., "Improvements to Tilt Rotor Performance Through Passive Blade Twist Control," NASA TM 100583, USAAVSCOM TM 88-B-010, April 1988.
- [2] Bauchau, O.A., Loewy, R.G., and Bryan, P.S., "An Approach to Ideal Twist Distribution in Tilt Rotor VSTOL Blade Designs," AHS 39th Annual Forum Proceedings, May 1983.
- [3] Hodges, D.H., "Review of Composite Rotor Blade Modeling," *AIAA Journal*, Vol.28, No. 3, 1990, pp. 561-565.
- [4] Berdichevsky, V. L., and Staroselsky, L. A., "On the Theory of Curvilinear Timoshenko-type Rods," *PMM*, Vol. 47, No. 6, 1983, pp. 809-817.
- [5] Borri, M., and Merlini, T., "A large Displacement Formulation for Anisotropic Beam Analysis," *Meccanica*, Vol.21, 1986, pp. 30-37.
- [6] Rehfield, L.W., "Design Analysis Methodology for Composite Rotor Blades," Presented at the 17th DoD/NASA Conference on Fibrous Composites in Structural Design, Denver, Colorado, June 17-20, 1985.
- [7] Bauchau, O.A., and Hong, C.H., "Large Displacement Analysis of Naturally Curved and Twisted Composite Beams," *AIAA Journal*, Vol. 25, No.11, pp. 1469-1475.
- [8] Bauchau, O.A., and Hong, C.H., "Nonlinear Composite Beam Theory," *Journal of Applied Mechanics*, Vol.55, No.1, 1988, pp. 156-163.
- [9] Rehfield, L.W., and Atilgan, A.R., and Hodges, D.H., "Nonclassical Behavior of Composite Thin-walled Beams with Closed Cross Sections," *Journal of American Helicopter Society*, Vol.35, No.2, 1990, pp. 42-50.
- [10] Librescu, L. and Song, O., "Static Aeroelastic Tailoring of Composite Aircraft Wings Modeled as Thin-Walled Beam Structure," Presented at the Fifth Japan-US Conference on Composite Materials, June 24-27, 1990, Tokyo, Japan.
- [11] Kosmatka, J.B., "Structural Dynamic Modeling of Advanced Composite Propellers by the Finite Element Method," Ph.D. Dissertation, University of California, Los Angeles, 1986.
- [12] Lee, S.W., and Stemple, A.D., "A Finite Element Model for Composite Beams with Arbitrary Cross-Sectional Warping," Proceedings of the 28th Structures, Structural Dynamics and Materials Conference, April 6-8, 1987, Monterey, California, AIAA Paper No. 87-0773, pp. 304-313.
- [13] Nixon, M.W., "Analytical and Experimental Investigations of Extension-Twist-Coupled Structures," M.Sc. Thesis, George Washington University, May 1989.
- [14] Nixon, M.W., "Preliminary Structural Design of Composite Main Rotor Blades for Minimum Weight," NASA TP 2730, AVSCOM TM 87-B-6, July 1987.
- [15] Winckler, S.J., "Hygrothermally Curvature Stable Laminates with Tension-torsion Coupling", *Journal of the American Helicopter Society*, Vol.30, No.3, 1985, pp. 56-58.
- [16] Hashin, Z., "Analysis of Stiffness Reduction of Cracked Cross-ply Laminates," *Engineering Fracture Mechanics*, Vol.25, Nos 5/6, pp. 771-778, 1986.
- [17] Jones, R.M., Mechanics of Composite Materials, Mc Graw-Hill Book Co., New York, 1975.
- [18] Highsmith, A.L. and Reifsnider, K.L., "Stiffness-Reduction Mechanisms in Composite Laminates," *Damage in Composite Materials*, ASTM STP 115, K.L. Reifsnider, Ed., American Society for Testing and Materials, Philadelphia, 1982, pp. 103-117.

[19] Berdichevsky, V.L., "Variational-Asymptotic Method of Constructing the Nonlinear Shell Theory," W.T. Koiter and G.K. Mikhailov, Eds., Theory of Shells, North-Holland Publishing Co., 1980, pp. 137-161.

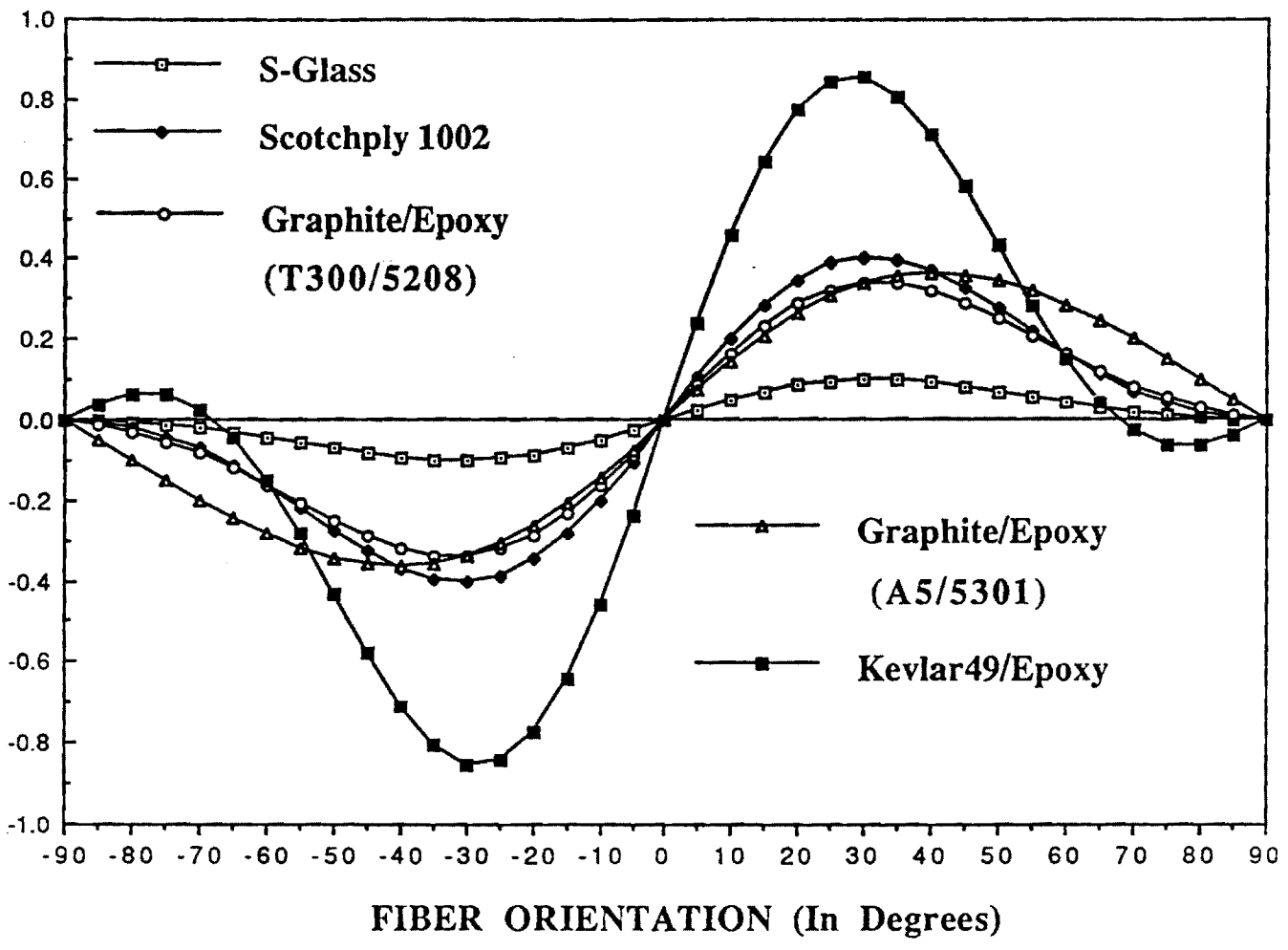


Figure 1. Effect of Fiber Orientation on Extension - Twist Coupling

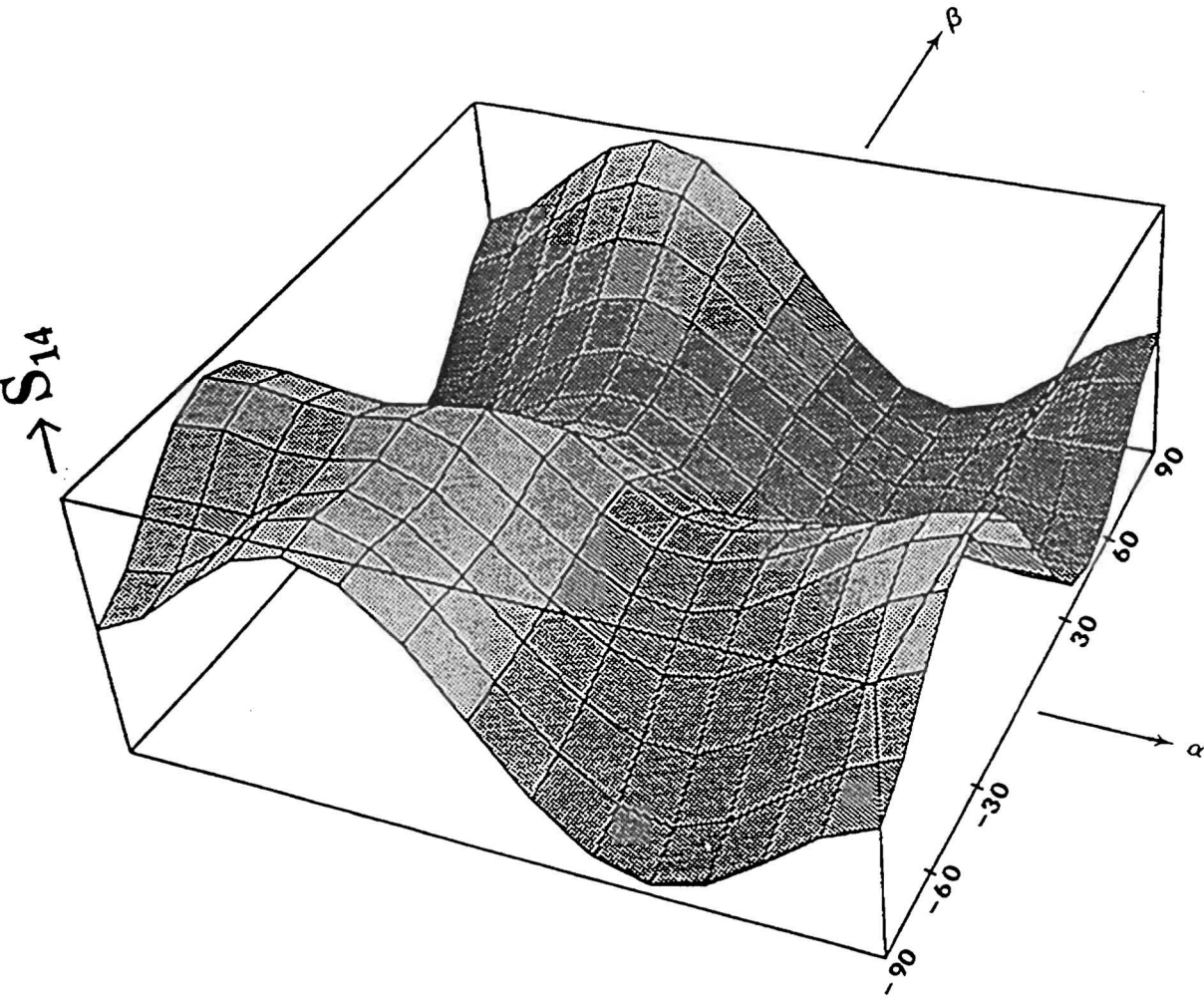


Figure 2. Effect of Fiber Orientation on Extension - Twist Coupling in a two - Ply Construction

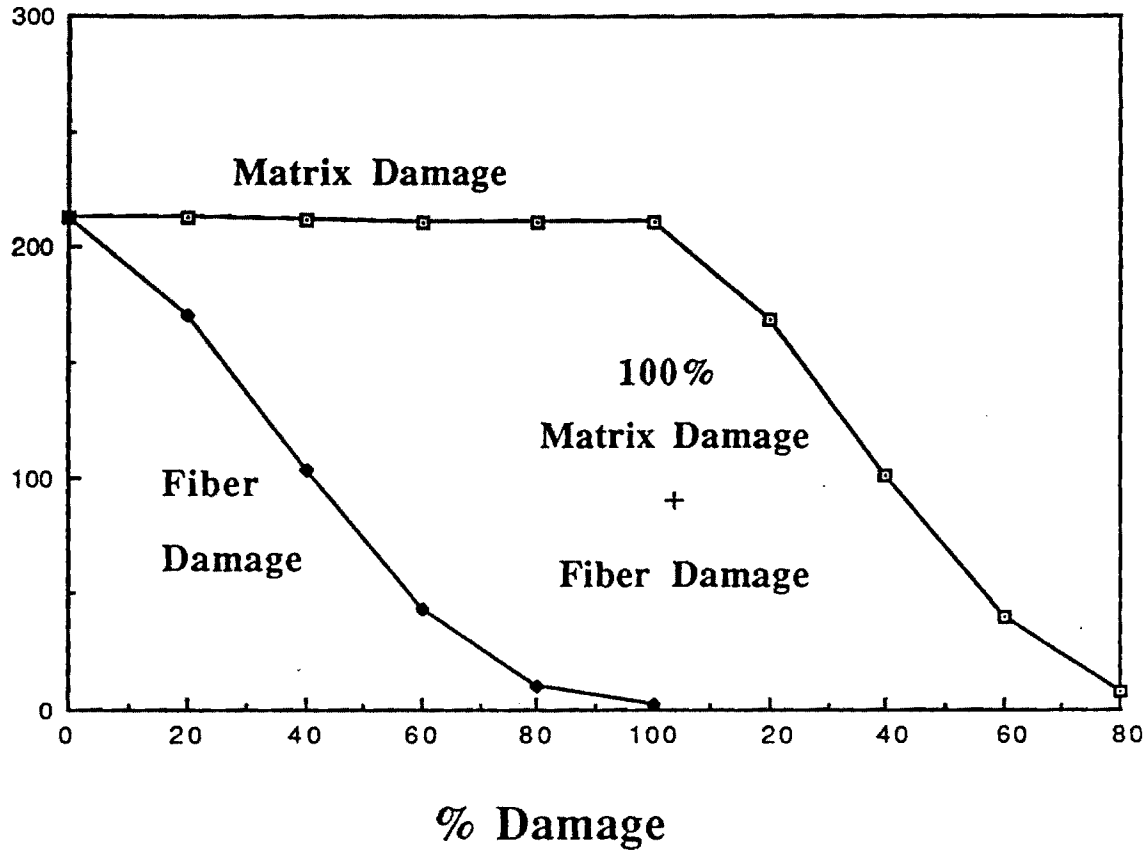


Figure 3. Effect of Damage on Longitudinal Modulus E_{11}

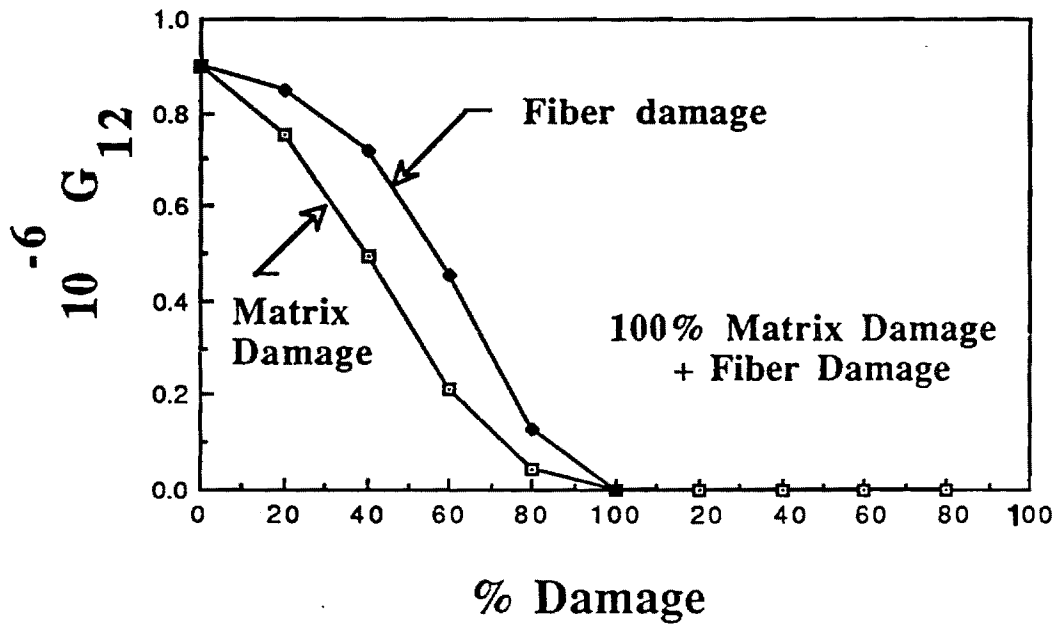
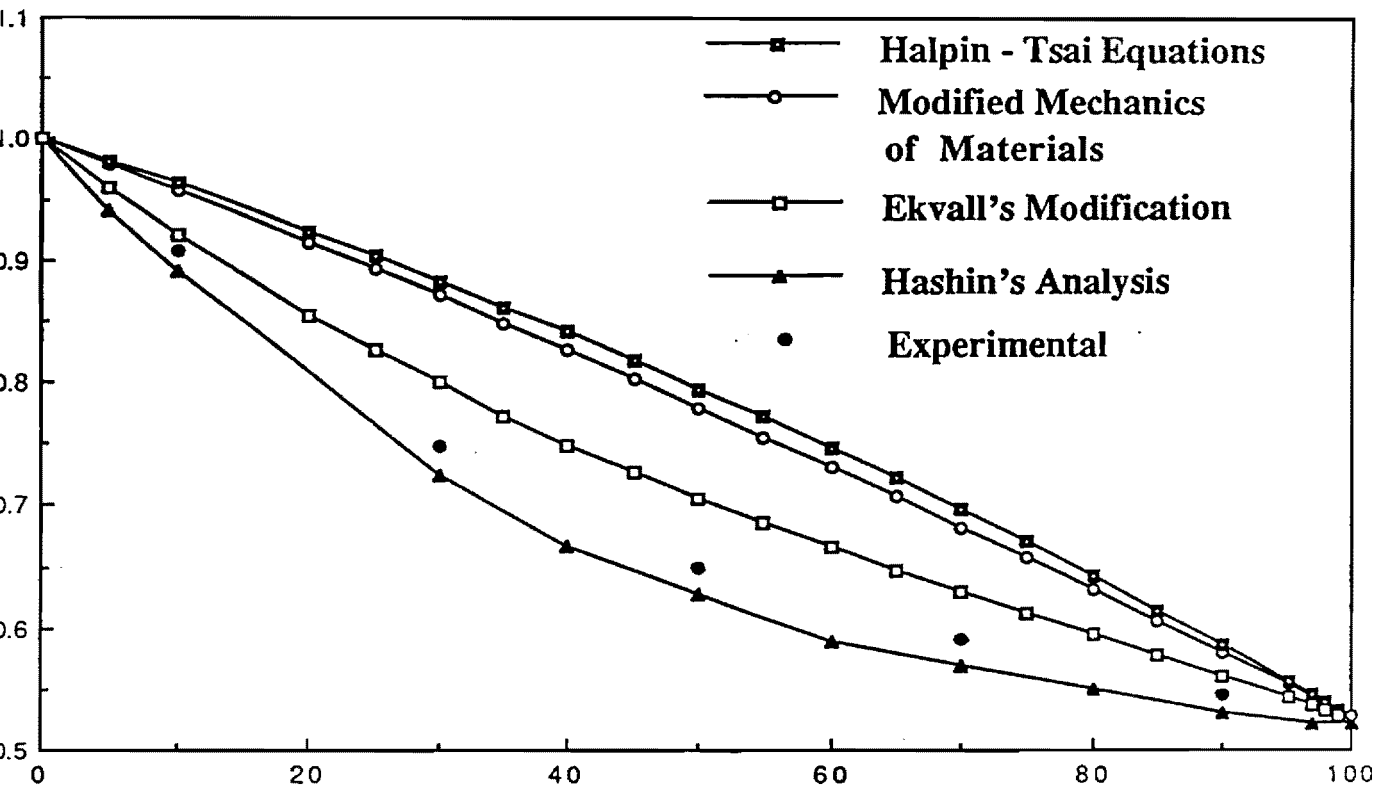


Figure 4. Effect of Damage on Shear Modulus G_{12}



% Matrix Damage in 90 Plies

100 * Crack Density, per mm (Hashin's Analysis)

Figure 5. Stiffness Reduction of $(0/90)_3^s$ Glass/Epoxy Laminate

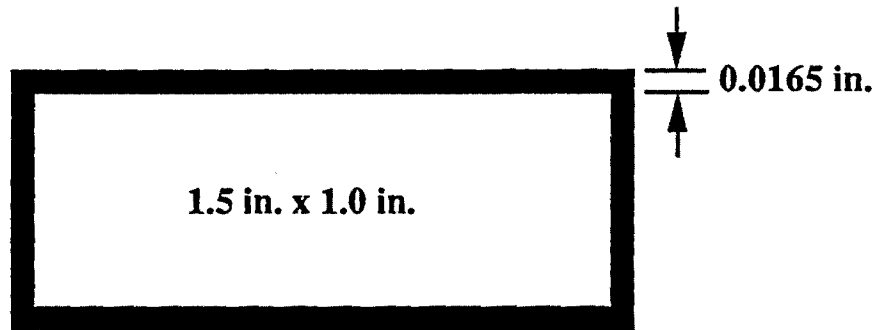


Figure 6. Single Closed Cell Configuration
with $[30]_3$ Layup

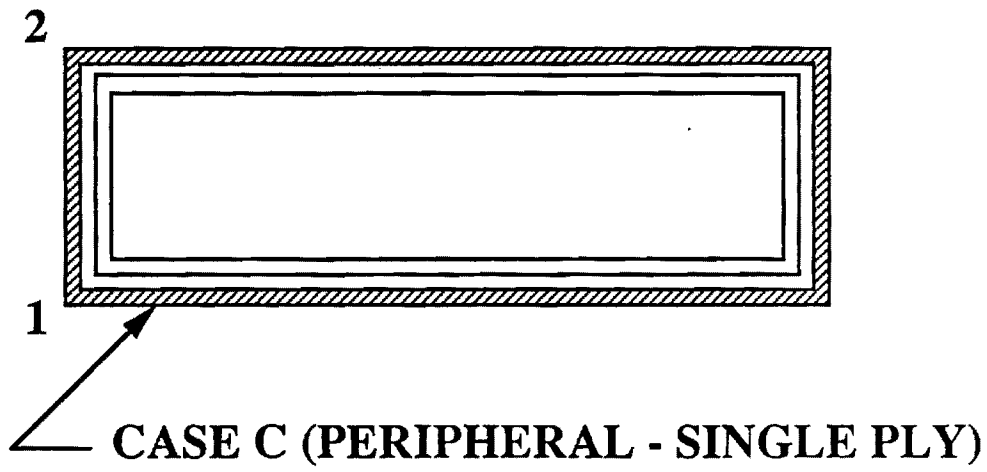
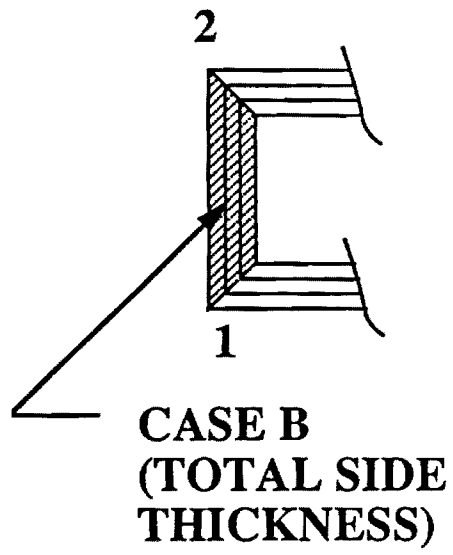
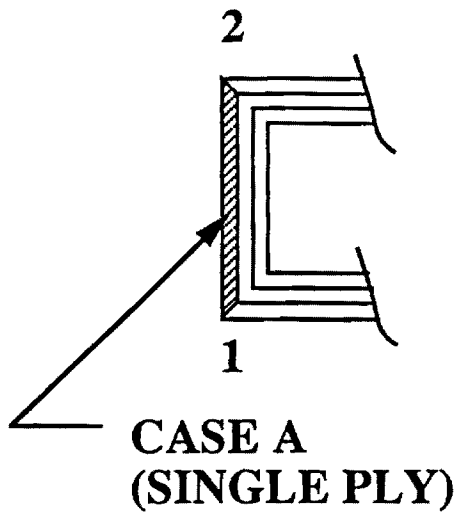


Figure 7. Damage Modes

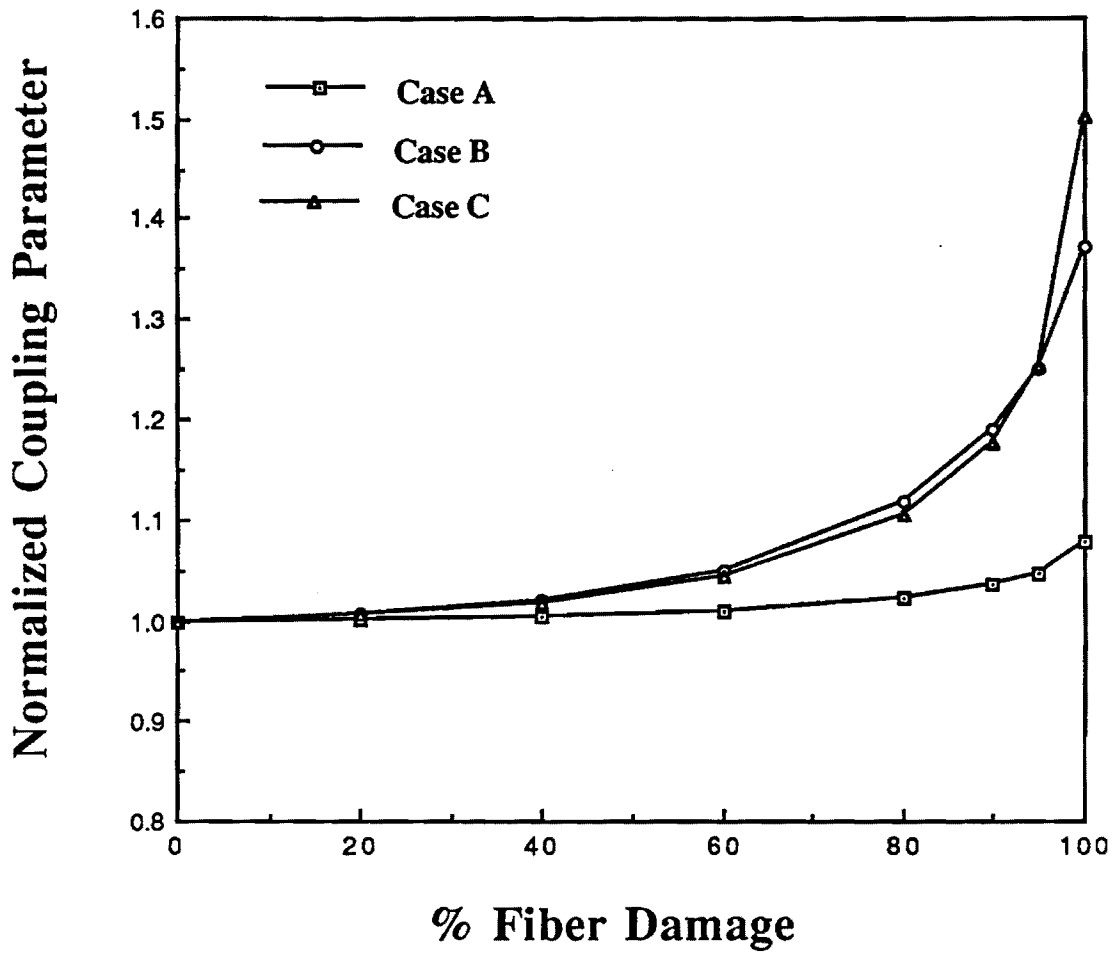


Figure 8. Effect of Fiber Damage on Extension - Twist Coupling

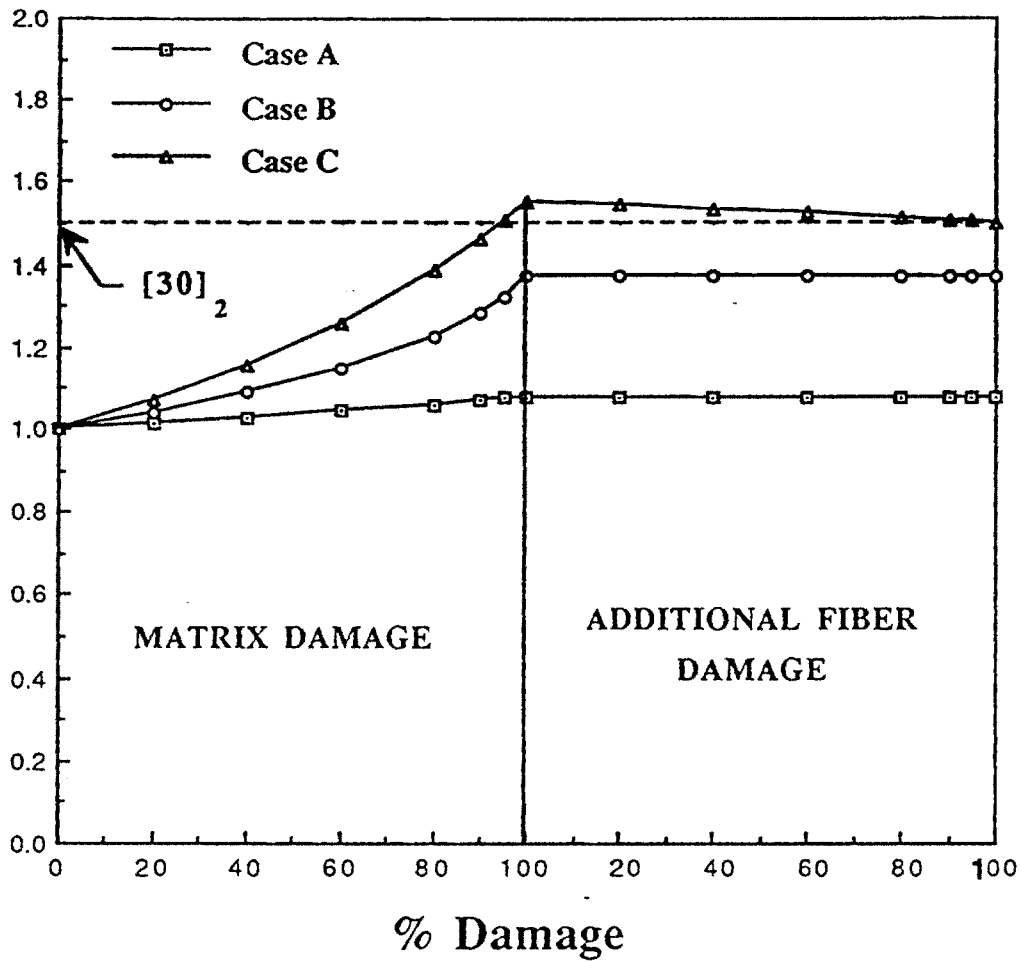


Figure 9. Effect of Combined Matrix and Fiber Damage

BIOGRAPHICAL INFORMATION

ERIAN A. ARMANIOS

**School of Aerospace Engineering
Georgia Institute of Technology
Atlanta, Georgia 30332
(404) 894-8202**

SUMMARY OF EXPERIENCE:

Works in the area of structural analysis and design of advanced composite structures. Has broad experience in analysis methodology ranging from classical methods to finite element and advanced optimization techniques. Current research interests are new structural concepts for aerospace systems: modeling, stress analysis and failure processes for advanced composite structures.

EXPERIENCE:

- Georgia Institute of Technology, Atlanta, Georgia.
Assistant Professor of Aerospace Engineering (1986-Present).
- Georgia Institute of Technology, Atlanta, Georgia.
Research Engineer in Aerospace Engineering (1985 - 1986).
- Georgia Institute of Technology, Atlanta, Georgia.
Graduate Research Assistant in Aerospace Engineering (1980 - 1984).
- University of Cairo, Giza, Egypt.
Assistant Lecturer in Aeronautical Engineering (1979 - 1980).
- Steel Structure Consulting Office, Cairo Egypt.
Consulting Engineer (1979 - 1980).
- University of Cairo, Giza, Egypt.
Teaching Assistant in Aeronautical Engineering (1974 - 1979).
- French National Railways (SNCF), Bischheim, Strasbourg, France.
Engineering Trainee (Summer 1973).

EDUCATION:

- Ph. D. , Aerospace Engineering, Georgia Institute of Technology (1985).
- M.S., Aeronautical Engineering, College of Engineering, University of Cairo (1979).
- B. of Aeronautical Engineering (Distinction with Honor Degree), College of Engineering, University of Cairo (1974).

PROFESSIONAL ACTIVITIES:

Memberships:

American Institute of Aeronautics and Astronautics , Associate Fellow.
American Society for Testing and Materials, Member.
American Society for Composites, Member .

Reviewer for Articles, Books or Proposals:

AIAA Journal
Journal of the American Helicopter Society
ASTM STP Volumes, Composite Materials
Journal of Aerospace Engineering
Journal of Composites Technology and Research
ARO, Structures Program

Editor:

Trans Tech Publications Ltd., Key Engineering Materials series.

Conference/Session Chairs:

Chairman, Session on Delamination, ASTM Second Symposium on Composite Materials: Fatigue and Fracture, Cincinnati, Ohio, April 27-28, 1987.

Invited lecturer on Advanced Materials and Composites, Spotlight on Research at Georgia Tech, Georgia Tech, Georgia Institute of Technology, Atlanta, Georgia, 9-10 June, 1987.

Chairman, Session on Structures and Materials, Fifth Annual Aerospace Technology Symposium, Atlanta, Georgia, February 19-20, 1988.

Chairman, Session on Interlaminar Fracture Toughness, ASTM Third Symposium on Composite Materials: Fatigue and Fracture, Orlando, Florida, November 6-7, 1989.

Chairman, Session on Considerations Within Composite Material Structures, Fifteenth Southeastern Conference on Theoretical and Applied Mechanics (SECTAM), Atlanta, Georgia, March 22-23, 1990.

Committee Activities:

Member, ASTM Technical Committee D-30 on High Modulus Fibers and their Composites.
Council Member, AIAA Atlanta Section (1987-1990).

Consulting:

Bell Helicopter Textron, Inc.

Rolls-Royce, Inc.

HONORS, AWARDS AND SPECIAL RECOGNITION:

CETL/Amoco Junior Faculty Teaching Excellence Award (1990).

SAIC Award in honor of contribution made to outstanding technical paper for originality, significance of research and effectiveness of presentation style.

AIAA Atlanta Section Certificate of Appreciation (1990).

First author of ASTM Best Presented Paper Award, Third Symposium on Composite Materials: Fatigue and Fracture (1989).

AIAA Outstanding Faculty Advisor Citation, Georgia Tech Student Branch (1988-1989).

AIAA Faculty Advisor Award, Region II - Southeastern United States (1988-1989).

Sigma Xi Award for Outstanding Ph.D. Thesis in Engineering, Georgia Institute of Technology (1985).

Distinction with Honor Degree, B. of Aeronautical Engineering (1974).

Medal of Excellence in Aeronautical Studies (1973).

College of Engineering Scholarship (1969-1974).

SPONSORED RESEARCH PROJECTS (Contributor):

1. "Sublaminar Damage Mechanisms in Composite Structures," Air Force Office of Scientific Research, 1985, Research Engineer, \$175,700.
2. "Design Analysis for Structurally Efficient Composite Hub Flexure Program," Bell Helicopter Textron, Inc., 1985, Research Engineer, 12 months, \$22,000.

SPONSORED RESEARCH PROJECTS (Principal, Co-Principal Investigator):

3. "Sublaminar Analysis of Interlaminar Fracture in Composites," NASA Langley Research Center, Grant NAG-1-558, 1985, Co-Principal Investigator, 12 months, \$57,200.
4. "Analysis of Delamination Related Fracture Processes in Composites," NASA Langley Research Center, Grant NAG-1-637, 1986, Co-Principal Investigator, 24 months, \$120,000.
5. "Center of Excellence for Rotary Wing Aircraft Technology (CERWAT)": Composite Structures Task, Army Research Office, 1988, Principal Investigator, 60 months, \$298,718.
6. "Analysis of Interlaminar Fracture in Composites Under Combined Loading," Grant NAG-1-637, 1988, Principal Investigator, 24 months, \$110,000.
7. "Design Analysis and Development Testing of the MH-53J," United States Air Force/Warner Robins Air Force Base, Grant F09603-85-G-3104-0034, 1988, Co-Principal Investigator, 5 months, \$75,487.

SELECTED PUBLICATIONS

Books and Parts of Books:

Interlaminar Fracture of Composites, E.A. Armanios Ed., Key Engineering Materials, 1989, Trans Tech Publications, Switzerland.

Also author of section entitled "Interlaminar Fracture in Graphite/Epoxy in Composites," pp. 85-102.

Refereed Papers:

1. Armanios, E.A., and Negm, H.M., "An Improved Rectangular Element for Plate Bending Analysis," Computers and Structures, Vol. 16, No. 5, pp. 677-686, 1983.
2. Armanios, E.A., Negm, H.M. and Smith, C.V., "A Technical Comment on the Determination of the Optimal Parametric Rectangular Plate Element," Computers and Structures, Vol. 16, No. 5, pp. 687, 1983.
3. Negm, H.M. and Armanios, E.A., "Calculation of the Natural Frequencies and Steady State Response of Thin Plates in Bending by an Improved Rectangular Element," Computers and Structures, Vol. 16, No. 5, pp. 687-1983.
4. Rehfield, L.W., Armanios, E.A. and Changli, Q., "Analysis of Behavior of Fibrous Composite Compression Specimen," Recent Advances in Composites in the United States and Japan, ASTM STP 864, J.R. Vinson and M. Taya, Eds., American Society for Testing and Materials, Philadelphia, 1985, pp. 236-252.
5. Rehfield, L.W., Armanios, E.A. and Valisetty, R.R., "Simplified Sublaminar Analysis of Composites and Applications," Computers and Structures, Vol. 20, 1985, pp. 401-411.
6. Armanios, E.A., Rehfield, L.W. and Reddy, A.D., "Design Analysis and Testing for Mixed-Mode and Mode II Interlaminar Fracture of Composites," in Composite Materials: Testing and Design (Seventh Conference), ASTM STP 893. J.M. Whitney, Ed., American Society for Testing and Materials, Philadelphia, 1986, pp. 232-255.
7. Armanios, E.A. and Rehfield, L.W., "Interlaminar Fracture Analysis of Composite Laminates Under Bending and Combined Bending and Extension," Composite Materials: Testing and Design (Eight Conference), ASTM STP 972, J.D. Whitcomb, Ed., American Society for Testing and Materials, Philadelphia, 1988, pp. 81-94.
8. Reddy, A.D., Rehfield, L.W., Weinstein, F., and Armanios, E.A., "Interlaminar Fracture Processes in Resin Matrix Composites Under Static and Fatigue Loading," Composite Materials: Testing and Design (Eight Conference), ASTM STP 972, J.D. Whitcomb, Ed., American Society for Testing and Materials, Philadelphia, 1988, pp. 340-355.

9. Armanios, E.A., Rehfield, L.W. and Weinstein, F., "Understanding and Predicting Sublaminar Damage Mechanisms in Composite Structures," Composite Materials: Testing and Design (Ninth Volume), ASTM STP 1059, S. Garbo, Ed., American Society for Testing and Materials, Philadelphia, 1990, pp. 231-249.
10. Armanios, E.A., Rehfield, L.W., Weinstein, F. and Reddy, A.D., "Interlaminar Fracture of Composites under Tension and Compression," Journal of Aerospace Engineering, ASCE, Vol. 3, No. 1, January 1990, pp. 30-45.
11. Armanios, E.A. and Rehfield, L.W., "Sublaminar Analysis of Interlaminar Fracture in Composites: Part I - Analytical Model," Journal of Composites Technology & Research, Vol. 11, No. 4, Winter 1989, pp. 135-146.
12. Armanios, E.A. Rehfield, L.W., Raju, I.S., and O'Brien, T.K. "Sublaminar Analysis of Interlaminar Fracture in Composites: Part II--Applications," Journal of Composites Technology & Research, Vol. 11, No. 4, Winter 1989, pp. 147-153.
13. Armanios, E.A., "Delamination Analysis Models for Laminated Composites - Fundamentals," accepted for publication Journal of Aerospace Engineering, ASCE, 1990.
14. Armanios, E.A., "Delamination Analysis Models for Laminated Composites-Numerical Verification," accepted for publication Journal of Aerospace Engineering, ASCE, 1990.
15. Armanios, E.A. and Badir, A.M., "Hygrothermal Influence on Mode I Edge Delamination in Composites," Journal of Composite Structures, Vol. 15, No. 4, 1990, pp. 323-342.
16. *Armanios, E.A., Sriram, P., and Badir, A.M., "Fracture Analysis of Transverse Crack-Tip and Free Edge Delamination in Laminated Composites," accepted for publication in Composite Materials: Fatigue and Fracture (Third Volume), ASTM Special Technical Publication.
17. Armanios, E.A., and Parnas, L., "Delamination Analysis of Tapered Laminated Composites Under Tensile Loading," accepted for publication in Composite Materials: Fatigue and Fracture (Third Volume), ASTM Special Technical Publication.

Conference Proceedings

1. Rehfield, L.W., Reddy, A.D., Yehezkely, O. and Armanios, E., "Buckling of Continuous Filament Composite Isogrid Panels: Theory and Experiment," in Progress in Science and Engineering of Composites, Proceedings of ICCM-IV, Tokyo, Vol. 1, pp. 545-554, 1982.
2. Armanios, E.A. and Rehfield, L.W., "Interlaminar Analysis of Laminated Composites Using a Sublaminar Approach," Proceedings of the AIAA/ASME/ASCE/AHS 27th Structures, Structural Dynamics, and Materials (SDM) Conference, San Antonio, Texas, 19-21 May, 1986. AIAA Paper No. 86-0969CP, Part 1, pp. 442-452.

*Winner of ASTM Best Presented Paper Award, third Symposium on Composite Materials: Fatigue and Fracture 1989. Award based on quality of presentation, long-term value of paper and technical innovation.

3. Rehfield, L.W., Armanios, E.A. and Weinstein, F., "Analytical Modeling of Interlaminar Fracture in Laminated Composites," Composites '86: Recent Advances in Japan and the United States, Proceedings of the Third Japan-U.S. Conference on Composite Materials, K. Kawata, S. Umekawa, and A. Kobayashi, Eds., pp. 331-340, 1986.
4. Armanios, E.A. and Mahler, M.A., "Residual Thermal and Moisture Influences on the Free-Edge Delamination of Laminated Composites," Proceedings of the AIAA/ASME/ASCE/AHS 19th Structures, Structural Dynamics and Materials (SDM) Conference, Part 1, pp. 371-381, 1988.
5. Armanios, E.A. and Rehfield, L.W., "A Simplified Approach to Strain Energy Release Computations for Interlaminar Fracture of Composites," Proceedings of the Fourth Japan-U.S. Conference on Composite Materials, June 27-29, 1988, Washington, D.C., Technomic Publishing Co., pp. 285-296.
6. Fortson, B., Webb, G., and Armanios, E.A., "Fracture Surface Morphology and Crack Arrest in Cracked Lap Shear Composite Specimens," Proceedings of the International Symposium on Testing and Failure Analysis, ASM International, Metals Park, OH, 1988, pp. 299-306.
7. Armanios, E.A., Badir, A. and Sriram, P., "Sublaminar Analysis of Mode I Edge Delamination in Laminated Composites," Proceedings of the AIAA/ASME/AHS/ASC 30th Structures, Structural Dynamics and Materials (SDM) Conference, Mobile, Alabama, April 3-5, 1989, pp. 2109-2116.
8. Sriram, P., and Armanios, E.A., "Fracture Analysis of Local Delaminations in Laminated Composites," Proceedings of the AIAA/ASME/ASCE/AHS/ASC 30th (SDM) Conference, Mobile, Alabama, April 3-5, 1989, pp. 2109-2116.
9. Armanios, E.A. and Badir, A.M., "Hygrothermal Influence on the Edge Delamination in Composites," proceedings of the American Society for Composites Fourth Technical Conference, V.P.I. Blacksburg, VA, October 3-5, 1989, pp. 944-950.
10. Armanios, E.A. and Li, Jian, "Interlaminar Stress Analysis for Laminated Composites Under Torsion Loads," Proceedings of the Fifteenth Southeastern Conference on Theoretical and Applied Mechanics (SECTAM), Atlanta, Georgia, March 22-23, 1990, Volume XV, pp. 7-14.

E-16-654

SEMI-ANNUAL REPORT

**ANALYSIS OF DELAMINATION RELATED
FRACTURE PROCESSES IN COMPOSITES**

**NASA GRANT NAG-1-637
GEORGIA TECH PROJECT E16-654**

**PRINCIPAL INVESTIGATOR
Erian A. Armanios**

SEMI-ANNUAL REPORT

ANALYSIS OF DELAMINATION RELATED FRACTURE PROCESSES IN COMPOSITES

NASA GRANT NAG-1-637
GEORGIA TECH PROJECT E16-654

PRINCIPAL INVESTIGATOR
Erian A. Armanios

This report covers the research work performed for the period starting September 1990 and ending February 1991. In the first phase of the program, a variationally consistent theory for thin-walled composite beams has been developed. Three major aspects are considered in the development: the first is concerned with its simplicity and ease of implementation in any existing rotorcraft code such as TAIL [1]. The second, deals with its ability to be applied to the investigation of damage. Consequently, restrictions on the uniformity of stiffness and thickness along the periphery of the section have been relaxed. Finally, consistency of the assumptions used is ensured by deriving the theory from a variationally asymptotic energy principle. Comparisons of stiffness coefficients and response with Rehfield's theory [2] and finite element solutions have been performed.

The details of the derivation and comparisons of predictions is provided in the attached paper which will be presented at the AHS International Specialists' meeting on Rotorcraft Basic Research. A summary of the significant aspects of this work is outlined in the following.

Stiffness Coefficients

The derivation is based on an energy formulation where the contribution of in-plane shear stresses and out-of-plane bending and twisting curvatures are identified. An order of magnitude analysis shows that the contribution of the out-of-plane terms is asymptotically small compared to the in-plane terms. This provides a consistent basis for deriving a one-dimensional theory from the two-dimensional thin shell theory.

The resulting constitutive relationships are obtained in terms of four generalized force and deformation-related variables.

$$\begin{Bmatrix} N \\ M_x \\ M_y \\ M_z \end{Bmatrix} = \begin{bmatrix} C_{11} & C_{12} & C_{13} & C_{14} \\ C_{12} & C_{22} & C_{23} & C_{24} \\ C_{13} & C_{23} & C_{33} & C_{34} \\ C_{14} & C_{24} & C_{34} & C_{44} \end{bmatrix} \begin{Bmatrix} U_1' \\ \phi' \\ U_3'' \\ U_2'' \end{Bmatrix} \quad (1)$$

where N , M_x , M_y , and M_z , denote the axial force, torsional moment, and bending moments about y and z axis, respectively. The deformation-related variables U_1' , ϕ' , U_3'' and U_2'' represent the axial strain, twist rate and bending curvatures associated with the xz and xy planes, respectively. The stiffness coefficients in Eq. (1) are obtained in closed form in terms of familiar parameters such as stacking sequence and geometry.

$$\begin{aligned}
C_{11} &= \oint \left[K_{11} - \frac{K_{12}^2}{K_{22}} \right] ds + \frac{[\oint (K_{12} / K_{22}) ds]^2}{\oint (1 / K_{22}) ds} \\
C_{12} &= 2A_e \frac{\oint (K_{12} / K_{22}) ds}{\oint (1 / K_{22}) ds} \\
C_{13} &= -\oint \left[K_{11} - \frac{K_{12}^2}{K_{22}} \right] z ds - \frac{\oint (K_{12} / K_{22}) ds \oint (K_{12} / K_{22}) z ds}{\oint 1 / K_{22} ds} \\
C_{14} &= -\oint \left[K_{11} - \frac{K_{12}^2}{K_{22}} \right] y ds - \frac{\oint (K_{12} / K_{22}) ds \oint (K_{12} / K_{22}) y ds}{\oint 1 / K_{22} ds} \\
C_{22} &= 4A_e^2 \frac{1}{\oint (1 / K_{22}) ds} \\
C_{23} &= -2A_e \frac{\oint (K_{12} / K_{22}) z ds}{\oint (1 / K_{22}) ds} \\
C_{24} &= -2A_e \frac{\oint (K_{12} / K_{22}) y ds}{\oint (1 / K_{22}) ds} \\
C_{33} &= \oint \left(K_{11} - \frac{K_{12}^2}{K_{22}} \right) z^2 ds + \frac{[\oint (K_{12} / K_{22}) z ds]^2}{\oint (1 / K_{22}) ds} \\
C_{34} &= \oint \left(K_{11} - \frac{K_{12}^2}{K_{22}} \right) y z ds + \frac{\oint (K_{12} / K_{22}) y ds \oint (K_{12} / K_{22}) z ds}{\oint 1 / K_{22} ds} \\
C_{44} &= \oint \left(K_{11} - \frac{K_{12}^2}{K_{22}} \right) y^2 ds + \frac{[\oint (K_{12} / K_{22}) y ds]^2}{\oint (1 / K_{22}) ds}
\end{aligned} \tag{2}$$

where

$$\begin{aligned}
K_{11} &= A_{11} - \frac{(A_{12})^2}{A_{22}} \\
K_{12} &= A_{16} - \frac{A_{12}A_{26}}{A_{22}} \\
K_{22} &= A_{66} - \frac{(A_{26})^2}{A_{22}}
\end{aligned} \tag{3}$$

The axial stiffnesses from CLT are denoted by A_{ij} in Eq. (3). In order to compare the stiffness coefficients in Eq. (2) with those of Rehfield's theory, the 7x7 stiffness matrix in Rehfield's theory is reduced to a 4x4 matrix by first neglecting the kinematical variable associated with restrained torsional warping. The resulting 6x6 matrix is then reduced by minimizing the associated energy expression with respect to the transverse shear strains. For the case of a Circumferentially Uniform Stiffness (CUS) configuration the result is

PRESENT

$$\begin{aligned}
C_{11} &= \oint \left[K_{11} - \frac{K_{12}^2}{K_{22}} \right] ds + \frac{[\oint (K_{12} / K_{22}) ds]^2}{\oint (1 / K_{22}) ds} \\
C_{12} &= 2A_e \frac{\oint (K_{12} / K_{22}) ds}{\oint (1 / K_{22}) ds} \\
C_{22} &= 4A_e^2 \frac{1}{\oint (1 / K_{22}) ds} \\
C_{33} &= \oint \left(K_{11} - \frac{K_{12}^2}{K_{22}} \right) z^2 ds + \frac{[\oint (K_{12} / K_{22}) z ds]^2}{\oint (1 / K_{22}) ds} \\
C_{44} &= \oint \left(K_{11} - \frac{K_{12}^2}{K_{22}} \right) y^2 ds + \frac{[\oint (K_{12} / K_{22}) y ds]^2}{\oint (1 / K_{22}) ds} \\
C_{13} &= C_{14} = C_{23} = C_{24} = C_{34} = 0
\end{aligned}$$

REHFIELD'S THEORY

$$\begin{aligned}
C_{11} &= \oint K_{11} ds \\
C_{12} &= 2A_e \frac{\oint K_{12} ds}{\oint ds} \\
C_{22} &= 4A_e^2 \frac{\oint K_{22} ds}{(\oint ds)^2} \\
C_{33} &= \oint K_{11} z^2 ds - \frac{[\oint K_{12} \frac{dy}{ds} z ds]^2}{\oint K_{22} (\frac{dy}{ds})^2 ds} \\
C_{44} &= \oint K_{11} y^2 ds - \frac{[\oint K_{12} \frac{dz}{ds} y ds]^2}{\oint K_{22} (\frac{dz}{ds})^2 ds} \\
C_{13} &= C_{14} = C_{23} = C_{24} = C_{34} = 0
\end{aligned}$$

(4)

It is worth noting that in Rehfield's theory the K_{ij} coefficients are assumed to be constant and consequently independent of the circumferential coordinate s in Eq. (4). This is a result of the displacement function adopted in Rehfield's work. In the present theory, the displacement derived from the energy principle is a function of the anisotropy of the section. This displacement function coincides with

Rehfield's expression when isotropic materials' constraints are enforced. That is, the anisotropic stiffness coefficients in Rehfield's theory are based on the classical St. Venant's displacement function used in the analysis of thin-walled isotropic beams. If the K_{ij} coefficients are considered constant in the present theory, C_{11} , C_{12} and C_{22} become identical to those of Rehfield's. However, C_{33} and C_{44} will be different. For the case of a circular section all C_{ij} 's are the same. A comparison between these stiffness coefficients and their effect on the response is illustrated in the following applications.

Applications

A comparison of the flexibility coefficients S_{ij} for the box-beam shown below [3] with the predictions from two models is provided in Table I.

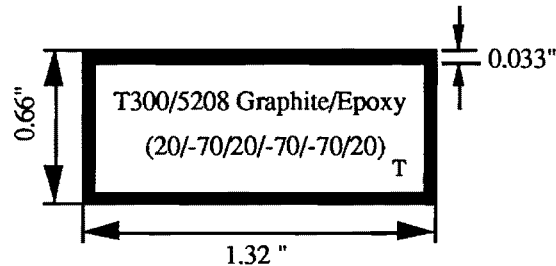


Fig. 1. Beam Cross Section

The flexibility coefficients are obtained by inverting the 4x4 matrix in Eq. (1). The NABSA (Nonhomogeneous Anisotropic Beam Section Analysis) is a finite element model based on an extension of the work presented in *Ref. 4*. In this model all possible types of warping are accounted for. The TAIL model is based on Rehfield's theory with the restrained torsional warping ignored. The predictions of the NABSA and TAIL models are provided in *Ref. 3*. The percentage differences appearing in Table I are relative to the NABSA predictions. The present theory is in good agreement with NABSA. Its predictions show a difference ranging from +0.7 to +3.6 percent while those of TAIL range from +3.6 to -18.4 percent.

Table I. Comparison of Flexibility Coefficients of NABSA, TAIL and Present

Flexibility	NABSA	PRESENT	%Diff.	TAIL	% Diff.
S_{11} , lb ⁻¹	0.143883E-05	0.14491E-05	+0.7	0.14491E-05	+0.7
S_{22} , lb ⁻¹ -in ⁻²	0.312145E-04	0.32364E-04	+3.6	0.32364E-04	+3.6
S_{12} , lb ⁻¹ -in ⁻¹	-0.417841E-05	-0.43010E-05	+2.9	-0.43010E-05	+2.9
S_{33} , lb ⁻¹ -in ⁻²	0.183684E-04	0.1886E-04	+2.6	0.17291E-04	-5.8
S_{44} , lb ⁻¹ -in ⁻²	0.614311E-05	0.63429E-05	+3.2	0.50157E-05	-18.4

The present theory is applied to the prediction of the tip deflection in a cantilevered beam made of Graphite/Epoxy and subjected to different loading types. The beam has a square cross section with [12]₄ lay-up.

Table II. MSC/NASTRAN and Present Solutions for a Cantilevered Beam* with [+12]₄ Layups Subjected to Various Tip Load Cases

Load Type	Tip Load		Tip Deformation		% Diff.
			NASTRAN	Present	
Axial Force	100 lb	Axial Dis.:	0.002189 in.	0.002202 in.	+0.6 %
Axial Force	100 lb	Twist :	0.3178 deg.	0.32325 deg.	+1.7 %
Torsional	100 lb-in	Twist :	2.959 deg.	2.998 deg.	+1.32 %
Moment					
Transverse	100 lb	Deflection :	1.866 in	1.853 in.	-0.7 %
Force					

*Geometry of Beam (Ref. 1): Thin-walled square cross section; length=24.0 in., width=depth=1.17 in.; ply thickness=0.0075 in., number of plies=4, wall thickness=0.03 in. Mechanical Properties: $E_{11}=11.65$ Msi., $E_{22}=11.65$ Msi., $G_{12}=0.82$ Msi., $\nu_{12}=0.05$

Comparison of results with the MSC/NASTRAN finite element analysis of *Ref. 1* is provided in Table II. The predictions of the present theory range from +0.6 to -1.7 percent difference relative to the finite element results. Since the cross section has a CUS layup the predictions of the present model coincide with values calculated from Rehfield's theory, not shown in Table II, except for the tip deflection due to transverse force. The tip deflection predicted from Rehfield's theory is 1.6917 inch resulting in 9.34 percentage difference compared to the NASTRAN result.

A comparison of the present theory predictions with experimental data appears in Figs. (2) and (3). The Experimental results are obtained from *Ref. 5* for two cantilevered beams. Their geometry and material properties are given in Table III. The spanwise variation of the bending slope in a symmetric [30]₆ beam under a transverse tip load appears in Fig. (2).

Table III. Cantilever Geometry and Properties

Ply Thickness=0.005 in
Width=0.953 in.
Depth=0.53 in.
E_{11} =20.59 Msi.
E_{22} =1.42 Msi.
G_{12} =0.89 Msi.
ν_{12} =0.42

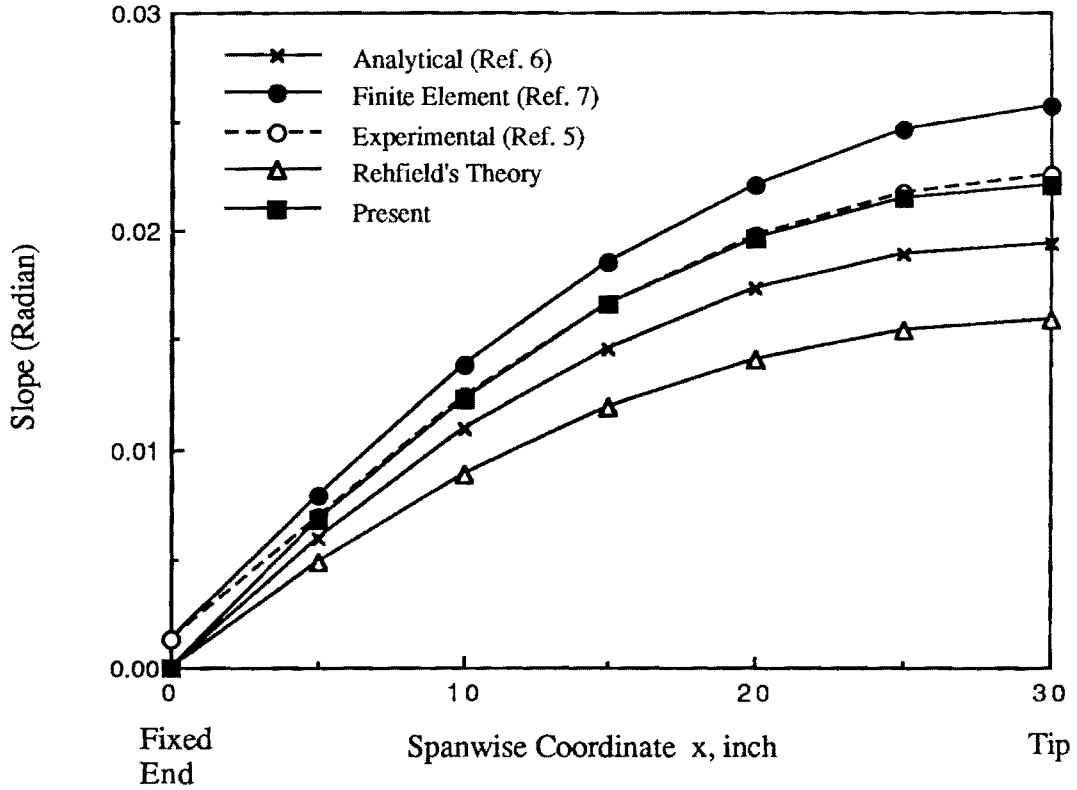


Fig. 2. Bending Slope of a Symmetric [30]₆ Cantilever Under 1 lb Transverse Tip Load

Analytical predictions from a simplified linear analysis (*Ref. 6*) and the refined finite element analysis of *Ref. 7* are provided. The spanwise twist distribution in an antisymmetric [15]₆ beam under tensile loading is shown in Fig. (2). Figures (2) and (3) show that the predictions of the present theory are in good agreement with the experimental data and the closest when compared to the other analytical approaches. For the extension-twist variation appearing in Fig. (3), the prediction of Rehfield's theory coincides with the present theory this is because the section is a CUS and S_{12} is identical.

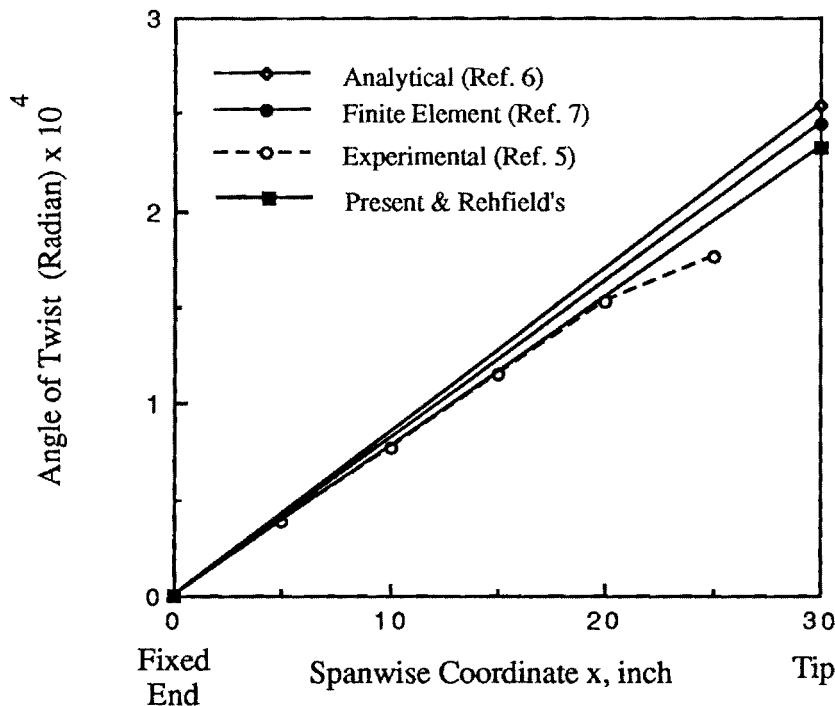


Fig. 3. Twist of an Antisymmetric [15]₆ Cantilever under 1 lb Tensile Load

Closing Remarks

Applications of the present theory to the effect of damage on the elastic coupling of tailored composite beams is underway . A preliminary investigation is provided in the attached paper. The development of a thin-walled theory for composite beams with open cross sections is necessary in order to assess damage modes that lead to an opening of an initially closed cross section. The influence of restrained warping is expected to be significant for thin-walled composite beams with open cross section.

REFERENCES

- [1]. Nixon, M.W., "Analytical and Experimental Investigations of Extension-Twist-Coupled Structures," M.Sc. Thesis, George Washington University, May 1989.
- [2]. Rehfield, L. W., " Design Analysis Methodology for Composite Rotor Blades," Proceedings of the Seventh DoD/NASA Conference on Fibrous Composites in Structural Design, AFWAL-TR-85-3094, June 1985, pp. (V(a)-1)-(V(a)-15).
- [3]. Hodges, D. H., Atilgan A. R., Fulton M. V., and Rehfield L. W., "Free-Vibration Analysis of Composite Beams," *Journal of the American Helicopter Society*, to appear, 1991.
- [4]. Giavotto, V., Borri, M., Mantegazza, P. and Ghiringhelli, G., "Anisotropic Beam Theory and Applications," *Computers and Structures*, Vol. 16, No. 1-4, pp. 403-413, 1983.
- [5] Chandra, R., Stemple, A. D., and Chopra, I., "Thin-walled Composite Beams under Bending, Torsional, and Extensional Loads," *Journal of Aircraft*, Vol. 27, No. 7, July 1990, pp. 619-626.
- [6] Hong, C. H., and Chopra, I., "Aeroelastic Stability of a Composite Blade," *Journal of the American Helicopter Society*, Vol. 30, No. 2, 1985, pp. 57-67.
- [7] Stemple, A. D., and Lee, S. W., "A Finite Element Model for Composite Beams with Arbitrary Cross-Sectional Warping," *AIAA Journal*, Vol. 26, No. 12, 1988.

APPENDIX

Paper to be Presented at the AHS International Specialists' Meeting on
Rotorcraft Basic research, Atlanta, Georgia, March 25-27, 1991

Effect of Damage On Elastically Tailored Composite Laminates

Erian Armanios, Ashraf Badir and Victor Berdichevsky
School of Aerospace Engineering
Georgia Institute of Technology
Atlanta, Georgia

ABSTRACT

A variationally consistent theory is derived in order to predict the response of anisotropic thin-walled closed sections subjected to axial load, torsion and bending. The theory is valid for arbitrary cross-sections made of laminated composite materials with variable thickness and stiffness. Closed form expressions for the stiffness coefficients are provided as integrals in terms of lay-ups parameters and cross-sectional geometry. A comparison of stiffness coefficients and response with finite element predictions and a closed form solution is performed. The theory is applied to the investigation of the effect of damage on the extension-twist coupling in a thin-walled closed section beam. The damage is simulated as a progressive ply-by-ply failure. Results show that damage can have a significant effect on the extension-twist coupling.

INTRODUCTION

Elastically tailored composite designs are being used to achieve favorable deformation modes under a given loading environment. Coupling between deformation modes such as extension-twist or bending-twist is created by an appropriate selection of fiber orientation, stacking sequence and materials.

The fundamental mechanism producing elastic tailoring in composite beams is a result of their anisotropy. Several theories have been developed for the analysis of thin-walled anisotropic beams. A review is provided in Ref. (1). A pertinent element in

the analytical modeling development is the inclusion of section warping. The major difference among various theories lies in the methodology used to eliminate warping and consequently obtain a one-dimensional theory. A description of the major approaches is provided in Refs. (2)-(13). The works described in Refs. (11)-(13) are based on a finite element formulation.

The finite element analysis developed in Ref. (13) is based on the anisotropic beam theory of Ref. (4). This simple theory includes shear deformation and provides closed form expressions of stiffness coefficients in terms of familiar laminate parameters. While this theory accounts for torsional warping and transverse shear deformation, It does not however, include the effects of bending-related section warping. The theory also assumes implicitly that the cross-section stiffness and thickness are constant. A modification was proposed in Ref.(13) in order to minimize the error associated with neglect of bending-related warping. This modification was based on shear stiffness correction factors determined by numerical comparison of results with an MSC/NASTRAN solution of cantilevered beam configurations loaded transversely at the free end.

The potential of elastically tailored composite rotor blade designs to achieve weight and performance benefits was shown in Refs. (14) and (15). An optimization methodology was presented in Ref. (15) for a minimum-weight structural design of composite main rotor blades subject to aerodynamic performance, material strength, autorotation, and

frequency constraints. Damage tolerance constraints were not considered. This may explain the fact that the resulting multiple composite-spar design was heavier than the comparably designed single composite-spar. The author concludes that if ballistic tolerance is considered in the design, the multispar design will probably have the minimum weight .

The behavior of elastically tailored structures in the presence of damage needs to be investigated in order to ensure their damage tolerance and durability. While a local damage mode may have a negligible effect on the structure's overall strength it can however, significantly influence its elastic coupling and consequently alter its designed performance.

The primary objective of this work is to assess the effect of damage in thin-walled laminated composite closed-section beams on their elastic coupling. A prerequisite is the development of a consistent theory for predicting the response of anisotropic thin-walled beams . The theory should be simple and suitable for parametric studies. The derivation is based on the asymptotically variational analysis provided in Refs. (16) and (17). In the present approach, the one dimensional theory for thin-walled closed-cell anisotropic beam is derived from the two-dimensional shell analysis.

An outline of the analysis is presented first. This is followed by a comparison of the predicted stiffness coefficients and response with closed form solutions and finite element results. Finally, the analysis is applied to the prediction of the extension-twist coupling in a composite beam with various stages of damage.

ANALYSIS

Consider in a three dimensional space R the prismatic shell shown in Fig. 1. The shell has a thin-walled closed cross-section with variable thickness $h(\xi^2)$. The cartesian

coordinates x^i in R are related to the curvilinear frame ξ^1, ξ^2 and ξ by

$$x^i = r^i(\xi^\alpha) + \xi n^i(\xi^\alpha) \quad (1)$$

The curvilinear frame is associated with the undeformed shell configuration V and the equation of the mid-surface Ω is given by $x^i = r^i(\xi^\alpha)$. Latin superscripts run from 1 to 3, while Greek superscripts run from 1 to 2. The components of the outward normal \bar{n} are denoted by n^i in Eq.(1). The curvilinear coordinates associated with the mid-surface Ω are denoted by ξ^α with the third component $\xi^3 = \xi$. The displacement components associated with ξ^α and ξ are denoted by v_α and v , respectively.

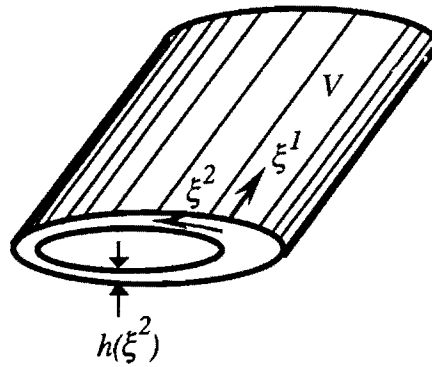


Fig. 1. Curvilinear Coordinate System

The shell strain-displacement equations can be written as (Ref.18):

$$\begin{aligned} \gamma_{11} &= \frac{dv_1}{d\xi^1} \\ \gamma_{22} &= \frac{dv_2}{d\xi^2} + \frac{v}{R} \\ 2\gamma_{12} &= \frac{dv_1}{d\xi^2} + \frac{dv_2}{d\xi^1} \end{aligned} \quad (2)$$

where R is the radius of curvature. The mid-surface of the shell is determined by the position vector \bar{r} as

$$\bar{r} = x\bar{i}_x + y(s)\bar{i}_y + z(s)\bar{i}_z \quad (3)$$

where \bar{i}_x , \bar{i}_y and \bar{i}_z are unit vectors associated with the cartesian coordinate system x , y and z shown in Fig. 2. The circumferential coordinate s is measured along the mid-surface of the cross section. The displacement vector corresponding to the cartesian system is given by

$$\bar{u} = u_1\bar{i}_x + u_2\bar{i}_y + u_3\bar{i}_z \quad (4)$$

where u_1 , u_2 and u_3 are the displacements in the direction of x , y and z , respectively, as shown in Fig. 2. The unit tangent vector \bar{t} along s , and the unit outward normal \bar{n} to the mid-surface of the cross section are defined by

$$\bar{t} = \frac{d\bar{r}}{ds} = \frac{dy}{ds}\bar{i}_y + \frac{dz}{ds}\bar{i}_z \quad (5)$$

and

$$\bar{n} = \bar{t} \times \bar{i}_x = \frac{dz}{ds}\bar{i}_y - \frac{dy}{ds}\bar{i}_z \quad (6)$$

The projection of the position vector \bar{r} in the normal and tangential directions to the surface of the shell are given by r_n and r_t , respectively, where

$$r_n = \bar{r} \cdot \bar{n} = y \frac{dz}{ds} - z \frac{dy}{ds} \quad (7)$$

and

$$r_t = \bar{r} \cdot \bar{t} = y \frac{dy}{ds} + z \frac{dz}{ds} \quad (8)$$

The displacements in both the curvilinear and cartesian systems are related by

$$\begin{aligned} v_2 = \bar{u} \cdot \bar{t} &= u_2 \frac{dy}{ds} + u_3 \frac{dz}{ds} \\ v_3 = \bar{u} \cdot \bar{n} &= u_2 \frac{dz}{ds} - u_3 \frac{dy}{ds} \end{aligned} \quad (9)$$

Displacement Field

The displacement field in the cartesian coordinate system may be expressed as

$$\begin{aligned} u_1 &= U_1(x) + \bar{u}_1(s, x) \\ u_2 &= U_2(x) - z\varphi(x) \\ u_3 &= U_3(x) + y\varphi(x) \end{aligned} \quad (10)$$

where $U_1(x)$, $U_2(x)$ and $U_3(x)$ represent the rigid body translation and $\varphi(x)$ represents the rigid body rotation, i.e. the angle of twist. The unknown function $\bar{u}_1(s, x)$ is determined from energy considerations.

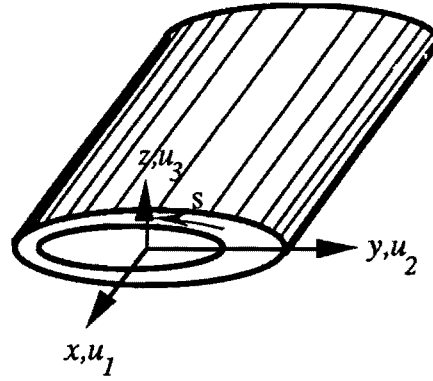


Fig. 2 Cartesian Coordinate System

The energy density, Φ , of the two-dimensional classical anisotropic shell is given by

$$\begin{aligned} 2\Phi &= hC^{\alpha\beta\gamma\delta}\gamma_{\alpha\beta}\gamma_{\gamma\delta} + h^2C_1^{\alpha\beta\gamma\delta}\gamma_{\alpha\beta\rho}\gamma_{\rho\gamma\delta} \\ &+ \frac{h^3}{12}C_2^{\alpha\beta\gamma\delta}\rho_{\alpha\beta\rho}\rho_{\rho\gamma\delta} \end{aligned} \quad (11)$$

where $C^{\alpha\beta\gamma\delta}$, $C_1^{\alpha\beta\gamma\delta}$ and $C_2^{\alpha\beta\gamma\delta}$ are "two-dimensional projection" of the elastic moduli tensor. The in-plane strain components are denoted by $\gamma_{\alpha\beta}$ and the change in curvatures of the reference surface by $\rho_{\alpha\beta}$. The energy of the shell is given by

$$I = \int_{\Omega} \Phi d\omega \quad (12)$$

where $d\omega$ is the area element of Ω . The first terms in Eq. (11) represents the energy associated with the in-plane strains. Their contribution to the energy is much larger than the bending contribution expressed by the remaining terms. Therefore, the strain energy density can be approximated by

$$2\Phi \cong hC^{\alpha\beta\gamma\delta}\gamma_{\alpha\beta}\gamma_{\gamma\delta} \quad (13)$$

This approximation enables the derivation of a one-dimensional theory from the two-dimensional energy function. Furthermore, in the case of no internal pressure acting on the shell, the hoop stress resultant is negligibly small and may be ignored, thus

$$\frac{\partial\Phi}{\partial\gamma_{22}} = 0 \quad (14)$$

Combine Eq. (14) with Eq. (13) to obtain

$$\gamma_{22} = -\frac{1}{C^{2222}}(C^{1122}\gamma_{11} + 2C^{1222}\gamma_{12}) \quad (15)$$

The energy density takes the form

$$2\Phi_1 = \min_{\gamma_{22}} 2\Phi = S_1\gamma_{11}^2 + 2S_{12}\gamma_{11}\gamma_{12} + S_2\gamma_{12}^2 \quad (16)$$

where

$$\begin{aligned} S_1 &= [C^{1111} - \frac{(C^{1122})^2}{C^{2222}}]h \\ S_{12} &= 2[C^{1112} - \frac{C^{1122}C^{1222}}{C^{2222}}]h \\ S_2 &= 4[C^{1212} - \frac{(C^{1222})^2}{C^{2222}}]h \end{aligned} \quad (17)$$

and the shear flow N_{12} can be written as

$$\frac{\partial\Phi_1}{\partial\gamma_{12}} = S_{12}\gamma_{11} + S_2\gamma_{12} = 2N_{12} \quad (18)$$

thus,

$$2\gamma_{12} = a\gamma_{11} + bN_{12} \quad (19)$$

where

$$a = -2\frac{S_{12}}{S_2} \quad \text{and} \quad b = \frac{4}{S_2} \quad (20)$$

Combine Eqs. (9) and (10) with Eqs. (7) and (8), to get

$$\begin{aligned} v_1 &= U_1(x) + \bar{u}_1 \\ v_2 &= U_2(x)\frac{dy}{ds} + U_3(x)\frac{dz}{ds} + r_n(s)\varphi(x) \\ v &= U_2(x)\frac{dz}{ds} - U_3(x)\frac{dy}{ds} - r_t(s)\varphi(x) \end{aligned} \quad (21)$$

The strain-displacement relations take the form

$$\begin{aligned} \gamma_{11} &= U_1'(x) + \bar{u}_1'(s,x) \\ 2\gamma_{12} &= \frac{d\bar{u}_1}{ds} + U_2'(x)\frac{dy}{ds} + U_3'(x)\frac{dz}{ds} \\ &\quad + r_n(s)\varphi'(x) \end{aligned} \quad (22)$$

where a prime in Eqs. (22) and (23) denotes differentiation with respect to x . From Eqs. (19) and (23) get

$$\begin{aligned} 2\gamma_{12} &= \frac{d\bar{u}_1}{ds} + U_2'(x)\frac{dy}{ds} + U_3'(x)\frac{dz}{ds} \\ &\quad + r_n(s)\varphi'(x) = a\gamma_{11} + bN_{12} \end{aligned} \quad (24)$$

By expressing \bar{u}_1 as

$$\bar{u}_1 = -U_2'(x)y - U_3'(x)z + g(s,x) \quad (25)$$

where $g(s,x)$ is an unknown function of s and x , Eq. (24) takes the form

$$\begin{aligned} \frac{dg}{ds} &= -r_n(s)\varphi'(x) \\ &\quad + a[U_1'(x) - U_2''(x)y - U_3''(x)z + g'(s,x)] \\ &\quad + bN_{12} \end{aligned} \quad (26)$$

For long shells, $L/d \gg 1$, where L and d are measures of the shell length and the

cross section size, respectively. Thus $\partial(\)/\partial x \ll \partial(\)/\partial s$. Consequently $a\partial g/\partial x$ is asymptotically small compared to $\partial g/\partial s$ and hence can be neglected in Eq. (26).

The shear flow N_{12} is determined from the condition that $g(s,x)$ should be a single valued continuous function, i.e.

$$\oint \frac{dg}{ds} ds = 0 \quad (27)$$

Therefore, N_{12} is independent of s . Substitute Eq. (26) into Eq. (27) to get

$$N_{12} = \frac{1}{\oint b ds} [2A_e \varphi'(x) - \oint a(U_1'(x) - U_2''(x)y - U_3''(x)z) ds] \quad (28)$$

where A_e is the enclosed area of the cross section given by

$$A_e = \frac{1}{2} \oint r_n(s) ds \quad (29)$$

Integrate Eq. (26) and use Eq. (28) to obtain

$$g(s,x) = \varphi'(x) \left[\frac{2A_e}{\oint b ds} \int_0^s b ds - \int_0^s r_n(s) ds \right] + \int_0^s a[U_1'(x) - U_2''(x)y - U_3''(x)z] ds - \frac{\oint a[U_1'(x) - U_2''(x)y - U_3''(x)z] ds}{\oint b ds} \int_0^s b ds \quad (30)$$

the axial displacement takes the form

$$u_1 = U_1(x) - U_2'(x)y - U_3'(x)z + \varphi'(x)\psi(s) + \int_0^s a[U_1'(x) - U_2''(x)y - U_3''(x)z] ds - \frac{\oint a[U_1'(x) - U_2''(x)y - U_3''(x)z] ds}{\oint b ds} \int_0^s b ds \quad (31-a)$$

The coefficient of $\varphi'(x)$ in Eq. (30) represents the torsion-related warping

function $\psi(s)$ in Eq. (31-a). This function emerges naturally and is expressed as

$$\psi(s) = \left[\frac{2A_e}{\oint b ds} \int_0^s b ds - \int_0^s r_n(s) ds \right] \quad (31-b)$$

Force-Deformation Relationships

The displacement field is now completely defined. The expression for the u_1 component is provided in Eqs. (31) while u_2 and u_3 are given in Eq. (10). Combining Eqs. (16) and (19) the energy density takes the form

$$2\Phi_1 = E\gamma_{11}^2 + GN_{12}^2 \quad (32)$$

where

$$E = S_1 - \frac{S_{12}^2}{S_2} \quad (33)$$

and

$$G = \frac{4}{S_2} \quad (34)$$

Using Eqs. (35) and (28), the axial strain can be written as

$$\gamma_{11} = U_1'(x) - U_2''(x)y - U_3''(x)z + g'(x,s) \quad (35)$$

Substitute Eqs. (35) and (28) into Eq.(32), and use Eq. (12), while neglecting $\partial g/\partial x$, to get the following expression for the energy of the shell

$$I = \frac{1}{2} (C_{11}U_1'^2 + C_{22}\varphi'^2 + C_{33}U_3''^2 + C_{44}U_2''^2) + C_{12}U_1'\varphi' + C_{13}U_1'U_3'' + C_{14}U_1'U_2'' + C_{23}\varphi'U_3'' + C_{24}\varphi'U_2'' + C_{34}U_2''U_3'' \quad (36)$$

For a laminated section made of N plies, with arbitrary fiber orientations, an appropriate transformation of the elastic moduli $C^{\alpha\beta\gamma\delta}$ is required. Summation of the plane stress stiffnesses for each ply

leads to the following explicit expressions for the stiffness coefficients C_{ij} in terms of the laminate axial stiffness A_{ij} (Ref. 19)

$$\begin{aligned}
C_{11} &= \oint \left[K_{11} - \frac{K_{12}^2}{K_{22}} \right] ds + \frac{[\oint (K_{12}/K_{22}) ds]^2}{\oint (1/K_{22}) ds} \\
C_{12} &= 2A_e \frac{\oint (K_{12}/K_{22}) ds}{\oint (1/K_{22}) ds} \\
C_{13} &= -\oint \left[K_{11} - \frac{K_{12}^2}{K_{22}} \right] z ds \\
&\quad - \frac{\oint (K_{12}/K_{22}) ds \oint (K_{12}/K_{22}) z ds}{\oint 1/K_{22} ds} \\
C_{14} &= -\oint \left[K_{11} - \frac{K_{12}^2}{K_{22}} \right] y ds \\
&\quad - \frac{\oint (K_{12}/K_{22}) ds \oint (K_{12}/K_{22}) y ds}{\oint 1/K_{22} ds} \\
C_{22} &= 4A_e^2 \frac{1}{\oint (1/K_{22}) ds} \\
C_{23} &= -2A_e \frac{\oint (K_{12}/K_{22}) z ds}{\oint (1/K_{22}) ds} \\
C_{24} &= -2A_e \frac{\oint (K_{12}/K_{22}) y ds}{\oint (1/K_{22}) ds} \\
C_{33} &= \oint \left(K_{11} - \frac{K_{12}^2}{K_{22}} \right) z^2 ds + \frac{[\oint (K_{12}/K_{22}) z ds]^2}{\oint (1/K_{22}) ds} \\
C_{34} &= \oint \left(K_{11} - \frac{K_{12}^2}{K_{22}} \right) y z ds \\
&\quad + \frac{\oint (K_{12}/K_{22}) y ds \oint (K_{12}/K_{22}) z ds}{\oint 1/K_{22} ds} \\
C_{44} &= \oint \left(K_{11} - \frac{K_{12}^2}{K_{22}} \right) y^2 ds + \frac{[\oint (K_{12}/K_{22}) y ds]^2}{\oint (1/K_{22}) ds}
\end{aligned} \tag{37}$$

where

$$\begin{aligned}
K_{11} &= A_{11} - \frac{(A_{12})^2}{A_{22}} \\
K_{12} &= A_{16} - \frac{A_{12}A_{26}}{A_{22}} \\
K_{22} &= A_{66} - \frac{(A_{26})^2}{A_{22}}
\end{aligned} \tag{38}$$

The constitutive relationships between the stress resultants and deformation-related variables can be written as

$$\begin{Bmatrix} N \\ M_x \\ M_y \\ M_z \end{Bmatrix} = \begin{bmatrix} C_{11} & C_{12} & C_{13} & C_{14} \\ C_{12} & C_{22} & C_{23} & C_{24} \\ C_{13} & C_{23} & C_{33} & C_{34} \\ C_{14} & C_{24} & C_{34} & C_{44} \end{bmatrix} \begin{Bmatrix} U_1' \\ \varphi' \\ U_3'' \\ U_2'' \end{Bmatrix} \tag{39}$$

where N , M_x , M_y , and M_z , represent the axial force, torsional moment, and the bending moments about y and z axis, respectively.

The classical St. Venant's theory of bending and torsion may be recovered if Eq. (39) is applied to isotropic materials. For the case of isotropic sections with constant thickness h , the coefficients a and b in Eq. (20) take the values

$$a = 0 \quad \text{and} \quad b = \text{constant} \tag{40}$$

Substitute Eq. (40) into Eqs. (31), to get the axial displacement for isotropic material as

$$\begin{aligned}
u_1 &= U_1(x) - U_2'(x)y - U_3'(x)z \\
&\quad + \varphi'(x) \left[\frac{2A_e}{\oint ds} \int_0^s ds - \int_0^s r_n(s) ds \right]
\end{aligned} \tag{41}$$

which coincides with the expression given in Ref. (4). This displacement function associated with isotropic materials was adopted in Ref. (4) for composite materials. As a result, the stiffness expressions obtained in Ref. (4) are different from those of Eqs.(37).

By neglecting the kinematical variable associated with restrained warping, the 6x6 stiffness matrix in Ref. (4) can be compared with the 4x4 stiffness matrix of Eqs. (39). This is done by minimizing the energy expression with respect to the transverse shear strains. The resulting stiffness expressions are all different from Eqs. (37).

It is worth noting that for the case of Circumferentially Uniform Stiffness (CUS) layups, the stiffness coefficients in Eqs. (37) coincide with those of Ref. (4), except for the bending stiffnesses C_{33} and C_{44} and the coupling coefficient C_{45} . Moreover, the stiffness coefficients coincide fully in the case of a circular CUS configuration.

APPLICATIONS

In order to assess the accuracy of the predictions, the present theory is applied to the box beam given in Ref. (20). The cross sectional configuration is shown in Fig. 3 and the material properties in Table I. A comparison of the flexibility coefficients S_{ij} obtained by inverting the 4x4 matrix in Eqs. (39) with the predictions from two models is provided in Table II. The NABSA (Nonhomogeneous Anisotropic Beam Section Analysis) is a finite element model based on an extension of the work presented in Ref. (6). In this model all possible types of warping are accounted for. The TAIL model is based on Ref. (4) where the restrained torsional warping is ignored. The predictions of the NABSA and TAIL models are provided in Ref. (20). The percentage differences appearing in

Table II are relative to the NABSA predictions. The present theory is in good agreement with NABSA. Its predictions show a difference ranging from +0.7 to +3.6 percent while those of Ref. (4) range from +3.6 to -18.4 percent.

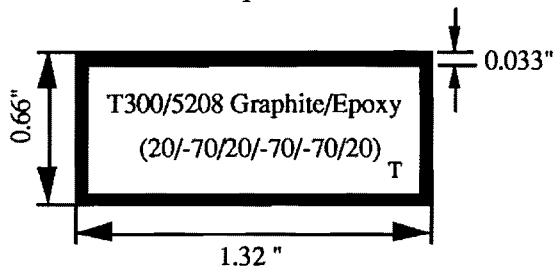


Fig. 3. Beam Cross Section

Table I. Properties of T300/5208 Graphite/Epoxy

E_{11}	= 21.3 Msi
$E_{22} = E_{33}$	= 1.6 Msi
$G_{12} = G_{13}$	= 0.9 Msi
G_{23}	= 0.7 Msi
$\nu_{12} = \nu_{13}$	= 0.28
ν_{23}	= 0.5

Table II. Comparison of Flexibility Coefficients of NABSA, TAIL and Present

Flexibility	NABSA	PRESENT	%Diff.	TAIL	% Diff.
S_{11} , lb ⁻¹	0.143883E-05	0.14491E-05	+0.7	0.14491E-05	+0.7
S_{22} , lb ⁻¹ -in ⁻²	0.312145E-04	0.32364E-04	+3.6	0.32364E-04	+3.6
S_{12} , lb ⁻¹ -in ⁻¹	-0.417841E-05	-0.43010E-05	+2.9	-0.43010E-05	+2.9
S_{33} , lb ⁻¹ -in ⁻²	0.183684E-04	0.1886E-04	+2.6	0.17291E-04	-5.8
S_{44} , lb ⁻¹ -in ⁻²	0.614311E-05	0.63429E-05	+3.2	0.50157E-05	-18.4

Table III. MSC/NASTRAN and Present Solutions for a Cantilevered Beam* with [+12]₄ Layups Subjected to Various Tip Load Cases

Load Type	Tip Load		Tip Deformation		% Diff.
			NASTRAN	Present	
Axial Force	100 lb	Axial Disp.:	0.002189 in.	0.002202 in.	+0.6 %
Axial Force	100 lb	Twist :	0.3178 deg.	0.32325 deg.	+1.7 %
Torsional Moment	100 lb-in	Twist :	2.959 deg.	2.998 deg.	+1.32 %
Transverse Force	100 lb	Deflection :	1.866 in	1.853 in.	-0.7 %

*Geometry of Beam (Ref. 13): Thin-walled square cross section; length=24.0 in., width=depth=1.17 in.; ply thickness=0.0075 in., number of plies=4, wall thickness=0.03 in. Mechanical Properties: $E_{11}=11.65$ Msi., $E_{22}=11.65$ Msi., $G_{12}=0.82$ Msi., $\nu_{12}=0.05$

The present theory is applied to the prediction of the tip deformation in a cantilevered beam made of Graphite/Epoxy and subjected to different loading types. The beam has a square cross section with [+12]₄ lay-up. Comparison of results with the MSC/NASTRAN finite element analysis of Ref. (13) is provided in Table III. The MSC/NASTRAN analysis is based on a 2-D plate model accounting for both shear deformation and warping. The predictions of the present theory range from +1.7 to -0.7 percent difference relative to the finite element results. Since the cross section has a CUS layup the predictions of the present model coincide with values calculated on the basis of Ref. (4), not shown in Table III, except for the tip deflection due to the transverse force. The tip deflection predicted from the theory of Ref. (4) is 1.6917 inch resulting in -9.34 percentage difference compared to the NASTRAN result .

In order to investigate the effect of damage on the extension-twist coupling, the theory is applied to a thin-walled composite beam with a rectangular cross section. The layup is [40₅ / 80]_T and the dimensions of the cross section are shown in Fig. (3). This stacking sequence maximizes the extension-twist coupling for

a T300/5208 Graphite-Epoxy laminate made up of six plies as reported in Ref. (21). Damage is simulated by progressive ply failure in the upper member of the cross section. The variation of the normalized coupling parameter S_{12} with damage appears in Fig. (4).

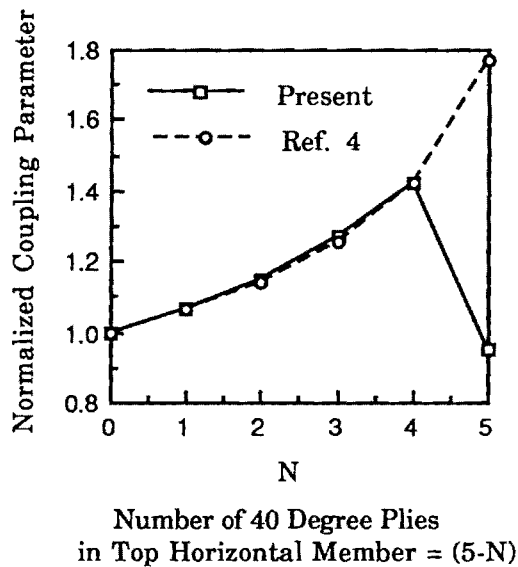


Figure 4. Effect of Ply Reduction on The Extension-Twist Coupling

The normalized coupling parameter is defined as the ratio of extension-twist

flexibility coefficient of the damaged relative to the undamaged laminate. The number of failed plies starting from the top portion of the cross section is denoted by N along the horizontal axis. The lay-up of the top flange is $[40_{(5-N)} / 80]_T$, while the layups of the bottom flange and both vertical webs are unaltered.

Results obtained on the basis of Ref. (4) and the present theory show a gradual increase in the extension-twist coupling parameter reaching a 42 percent increase when the upper flange is reduced to a $[40 / 80]_T$ laminate, i.e. at $N=4$. Further damage results in a sharp decrease in the coupling according to the present theory. A value of 0.95 is predicted when the top five plies in the upper flange fail. The theory of Ref. (4) shows a continuous increase in coupling with a maximum of 1.77. This difference in behavior is due to the fact that the stiffness, K_{ij} , vary with damage while the theory of Ref. (4) is developed for a cross section with uniform thickness. Since for an open section with a $[40_5 / 80]_T$ lay-up the extension-twist coupling is considerably small compared to the closed section, the abrupt drop in the coupling parameter suggests that the prediction of the present model approaches the behavior of the opened section as damage progresses.

The influence of damage progression in one of the webs when the load carrying capacity of the upper flange is reduced to one ply, appears in Fig. (5). Damage progression in the web portion corresponds to values of N ranging from 5 to 10. Additional damage in the web region shows similar behavior with an initial increase at a slightly smaller gradient followed by a sharp drop. The predictions of Ref. (4) show a steady increase at a smaller rate compared to damage progression in the flange portion.

For a rotor blade construction using a box beam as shown in Fig. (3), the behavior depicted in Figs. (4) and (5) indicate that at the initial stages of damage

the extension-twist coupling increases. The resulting loss in torsional stiffness or shift in the effective shear center may lead to divergence. This consideration should be accounted for when establishing the static margins in damage tolerant rotor blades.

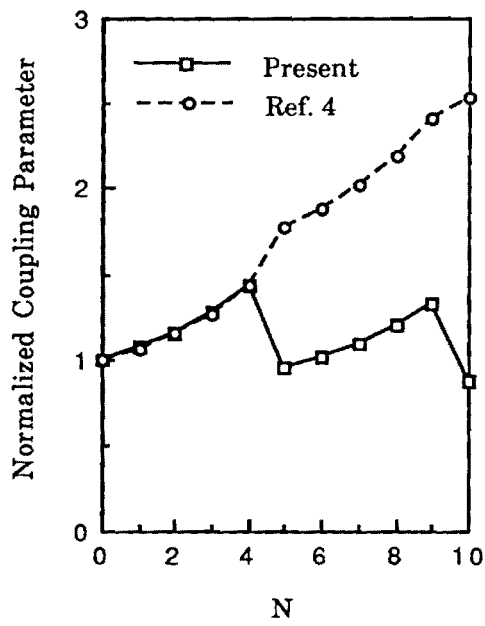


Fig. 5. Effect of Ply Reduction on The Extension-Twist Coupling

CONCLUSION

A Variationally consistent theory has been developed for the analysis of thin-walled anisotropic composite beams. Closed form expressions for the stiffness coefficients in terms of geometry, material and layup parameters are obtained. The theory has been validated by comparison of predictions with finite element analyses and a closed form solution.

The theory has been applied to the investigation of the influence of damage on the extension-twist coupling in laminated composite beam configuration. Results indicate that damage progression results in an initial increase in the coupling followed by a sharp decrease at the final stage. This effect should be accounted for when establishing the static margins for the damage tolerance design of composite rotor blades.

ACKNOWLEDGMENTS

The authors gratefully acknowledge the support provided by the NASA Langley Research Center under Grant NAG-1-637 of which Dr. T. Kevin O'Brien is the technical monitor. The authors would like also to thank Dr. Ali Atilgan for his enlightening discussions and suggestions.

REFERENCES

- (1) Hodges, D.H., "Review of Composite Rotor Blade Modeling," *AIAA Journal*, Vol.28, No. 3, 1990, pp. 561-565.
- (2) Mansfield, E. H., and Sobey, A. J., "The Fibre Composite Helicopter Blade - Part 1: Stiffness Properties - Part 2: Prospect for Aeroelastic Tailoring," *Aeronautical Quarterly*, Vol. 30, May 1979, pp. 413-449.
- (3) Libove, C., "Stresses and Rate of Twist in Single-Cell Thin-Walled Beams with Anisotropic Walls," *AIAA Journal*, Vol. 26, No. 9, September 1988, pp. 1107-1118.
- (4) Rehfield, L. W., "Design Analysis Methodology for Composite Rotor Blades," Proceedings of the Seventh DoD/NASA Conference on Fibrous Composites in Structural Design, AFWAL-TR-85-3094, June 1985, pp. (V(a)-1)-(V(a)-15).
- (5) Borri, M., and Merlini, T., "A large Displacement Formulation for Anisotropic Beam Analysis," *Meccanica*, Vol.21, 1986, pp. 30-37.
- (6) Giavotto, V., Borri, M., Mantegazza, P. and Ghiringhelli, G., "Anisotropic Beam Theory and Applications," *Computers and Structures*, Vol. 16, No. 1-4, pp. 403-413, 1983.
- (7) Bauchau, O.A., and Hong, C.H., "Large Displacement Analysis of Naturally Curved and Twisted Composite Beams," *AIAA Journal*, Vol. 25, No.11, pp. 1469-1475.
- (8) Bauchau, O.A., and Hong, C.H., "Nonlinear Composite Beam Theory," *Journal of Applied Mechanics*, Vol.55, No.1, 1988, pp. 156-163.
- (9) Rehfield, L.W., and Atilgan, A.R., and Hodges, D.H., "Nonclassical Behavior of Composite Thin-walled Beams with Closed Cross Sections," *Journal of American Helicopter Society*, Vol.35, No.2, 1990, pp. 42-50.
- (10) Librescu, L. and Song, O., "Static Aeroelastic Tailoring of Composite Aircraft Wings Modeled as Thin-Walled Beam Structure," Presented at the Fifth Japan-US Conference on Composite Materials, June 24-27, 1990, Tokyo, Japan.
- (11) Kosmatka, J.B., "Structural Dynamic Modeling of Advanced Composite Propellers by the Finite Element Method," Ph.D. Dissertation, University of California, Los Angeles, 1986.
- (12) Lee, S.W., and Stemple, A.D., "A Finite Element Model for Composite Beams with Arbitrary Cross-Sectional Warping," Proceedings of the 28th Structures, Structural Dynamics and Materials Conference, April 6-8, 1987, Monterey, California, AIAA Paper No. 87-0773, pp. 304-313.
- (13) Nixon, M.W., "Analytical and Experimental Investigations of Extension-Twist-Coupled Structures," M.Sc. Thesis, George Washington University, May 1989.
- (14) Nixon, Mark W., "Improvements to Tilt Rotor Performance Through Passive Blade Twist Control," NASA TM 100583,

USAAVSCOM TM 88-B-010, April 1988.

(15) Nixon, M.W., "Preliminary Structural Design of Composite Main Rotor Blades for Minimum Weight," NASA TP 2730, AVSCOM TM 87-B-6, July 1987.

(16) Berdichevskii, V. L. "Variational-Asymptotic Method of Constructing the Nonlinear Shell Theory," W. T. Koiter and G. K. Mikhailov, Eds., *Theory of Shells*, North-Holland Publishing Company, 1980, pp. 137-161.

(17) Berdichevskii, V. L. "On the Energy of an Elastic Rod," *PMM U.S.S.R.*, Vol. 45, pp.518-529, 1981.

(18) Kraus, H., *Thin Elastic Shells*, John Wiley & Sons, 1967, p. 30.

(19) Jones, R.M., *Mechanics of Composite Materials*, McGraw Hill Book Co., New York, 1975, p. 163.

(20) Hodges, D. H., Atilgan A. R., Fulton M. V., and Rehfield L. W., "Free-Vibration Analysis of Composite Beams," *Journal of the American Helicopter Society*, to appear, 1991.

(21) Bezerril, C. P., "A Study on The Extension-Twist Coupling for Thin-Walled Closed Cross-Section Beams," A Special Problem Report submitted in partial fulfillment for a Master of Science, Georgia Institute of Technology, School of Aerospace Engineering, August 1990.

INTRODUCTION

This is a proposal to apply the thin-walled anisotropic beam theory developed under the current Grant NAG-1-637 to the interlaminar fracture analysis in elastically tailored composites. The work has two major objectives. The first, is to investigate the influence of delamination on the elastic stiffnesses and specially elastic couplings. The second, is to obtain the interlaminar stresses and strain energy release rate in order to predict delamination onset. Combined loading conditions associated with composite rotorcraft components will be considered. The analysis will include also the influence of residual thermal and moisture stresses.

A major emphasis of the work is to maintain simplicity and provide closed form expressions for the stiffness coefficients, stresses and strain energy release rate. This approach is effective in developing insight, understanding of fundamental behavior and evaluating competitive design configurations.

A summary of the status of the current research under the present work is given in the next section. This is followed by a discussion of some issues associated with the research and a presentation of the proposed research program. Biographical and budgetary information appear in appendices.

SUMMARY OF ACCOMPLISHMENTS

A variationally consistent theory for thin-walled composite beams has been developed [1]. Its predictions have been validated by comparisons with available finite element [2-4], analytical [5,6] and test results [7]. These comparisons are given in *Ref. 1* and in the semi-annual report [8].

More importantly an understanding of the reasons for the predictions of Rehfield's [5] and Chopra's [6] models was achieved. Both models are based on an a priori assumed displacement field that does not account accurately for the anisotropy of the material. In *Ref. 5* the assumed warping function is identical to the one used for isotropic materials while in *Ref. 6* the material's shear rigidity only is considered in an approximate manner. Consequently the predicted rigidities and response are inaccurate for a generally anisotropic beam with varying circumferential stiffnesses. This key issue is presented in some detail in the following section.

Warping Function:

In our approach the functional form of the beam's displacement emerges naturally and the effect of the material's anisotropy is accounted for from the variationally asymptotic thin shell energy. The warping function obtained has the following form.

$$g(s, x) = \varphi'(x) \psi(s) + \int_0^s a(\xi) U(x, y, z) d\xi - \frac{\int_0^s a(\xi) U(x, y, z) ds}{\int_0^s b(\xi) d\xi} \int_0^s b(\xi) d\xi \quad (1)$$

where

$$\begin{aligned}
\psi(s) &= \frac{2A_e}{\oint b(\xi)d\xi} \int_0^s b(\xi)d\xi - \int_0^s r_n(\xi)d\xi \\
U(x,y,z) &= U_1'(x) - yU_2''(x) - zU_3''(x) \\
a &= \frac{(A_{16} - A_{12}A_{26})}{(A_{66} - A_{26}^2)} \\
b &= \frac{I}{(A_{66} - \frac{A_{26}^2}{A_{22}})}
\end{aligned} \tag{2}$$

The enclosed area is denoted by A_e in Eq. (2) and the projection of the position vector in the normal direction to the surface of the beam is given by r_n . Parameter b represents the shear flexibility contribution to the warping while parameter a the in-plane coupling. Both parameters are a results of the material's anisotropy. The function $U(x,y,z)$ in Eq.(1) represents the axial strain due to uniform extension along the x-axis and bending about the y- and z- axes. A comparison of Eq. (1) with the corresponding warping functions show that the first term only is considered in the formulations of *Refs. 5 and 6*. The absence of the second and third terms which include bending effects leads to significant error in the bending flexibilities as illustrated in Table II of *Ref.1*. Moreover, the function $\psi(s)$ in *Ref. 5* is given as

$$\psi(s) = \frac{2A_e}{\oint d\xi} \int_0^s d\xi - \int_0^s r_n(\xi)d\xi \tag{3}$$

which implies that the section is circumferentially uniform. In *Ref. 6* this function is considered as

$$\psi(s) = \frac{2A_e}{\oint \frac{d\xi}{G(\xi)t(\xi)}} \int_0^s \frac{d\xi}{G(\xi)t(\xi)} - \int_0^s r_n(\xi)d\xi \tag{4}$$

where

$$G(s) = t_w [A_{66}' - \frac{(A_{16}')^2}{A_{11}'A_{66}'}] \tag{5}$$

and

$$\begin{bmatrix} A_{11}' & A_{16}' \\ A_{16}' & A_{66}' \end{bmatrix} = \begin{bmatrix} A_{11} - \frac{A_{16}^2}{A_{22}} & A_{16} - \frac{A_{12}A_{26}}{A_{22}} \\ A_{16} - \frac{A_{12}A_{26}}{A_{22}} & A_{66} - \frac{A_{26}^2}{A_{22}} \end{bmatrix} \tag{6}$$

The wall thickness is denoted by t_w in Eq.(5). The shear contribution expression given in Eqs. (5) and (6) was determined using a "practical approximate manner" as mentioned by the authors. This expression however, is different from the b parameter in Eq.(3). Moreover, Eq. (5) is dimensionally incorrect.

The circumferential uniform stiffness constraint implied in Eq.(3) was relaxed in *Refs.9* and *10* by considering the pure torsion of a thin-walled beam of isotropic material. A correction factor α was introduced in the warping function as follows.

$$\psi(s) = \frac{2A_e}{\int_0^s \frac{d\xi}{\alpha(\xi)}} \int_0^s \frac{d\xi}{\alpha(\xi)} - \int_0^s r_n(\xi) d\xi \quad (7)$$

with

$$\alpha(s) = \left[A'_{66} - \frac{(A'_{16})^2}{A'_{11}A'_{66}} \right] \quad (8)$$

The A'_{ij} coefficients are identical to those defined in Eq.(6). This corrected warping function was created by using the principle of virtual work. It is similar to Eqs.(4) and (5) when $G(s)t(s)$ is replaced by $\alpha(\xi)$.

This correction was used to modify the torsion-related stiffness only. An illustration of its influence is shown for the case of a cantilevered beam under a transverse tip load in Fig.1. The spanwise variation of the bending slope in a symmetric [30]₆ box-beam is depicted. The predictions of the corrected warping function are closer to the experimental data.

This is not the case however, for the tip bending deflection where Rehfield's theory prediction with and without α correction show an 8% difference compared to the NASTRAN solution [2]. This is because the α correction does not affect the bending-related stiffness coefficients. This comparison is for a [12]₄ beam made of Graphite/Epoxy with a square cross section.

Ongoing Research:

A proof of convergence of the developed theory is underway. This is based on the dual variational principle. In addition to providing a rigorous proof of convergence of predictions from the present theory compared to a general nonlinear formulation, this approach provides closed form expressions of the stress field in terms of familiar stiffness parameters. The governing differential equations of motion and consistent boundary conditions are derived for the general case of combined loading. This enables the solution of boundary value problems including the effects of dynamic loading.

to 10-10-88

SEMI-ANNUAL REPORT

**ANALYSIS OF DELAMINATION RELATED
FRACTURE PROCESSES IN COMPOSITES**

**NASA GRANT NAG-1-637
GEORGIA TECH PROJECT E16-654**

**PRINCIPAL INVESTIGATOR
Erian A. Armanios**

SEMI-ANNUAL REPORT

EFFECT OF DAMAGE ON ELASTICALLY TAILORED COMPOSITES

**NASA GRANT NAG-1-637
GEORGIA TECH PROJECT E16-654**

**PRINCIPAL INVESTIGATOR
Erian A. Armanios**

This report covers the research work performed for the period starting September 1991 and ending February 1992. An investigation of the different physical contributions in the displacement field derived from the variationally asymptotical analysis is performed. The analytical approach along with the derived displacement field and stiffness coefficients for a generally anisotropic thin-walled beam is presented in detail in Ref.1. A copy is attached in the Appendix for convenience.

Significance of Out-of-plane Warping

The variationally asymptotical approach does not require an a priori assumed displacement field and the warping function emerges as natural result. It follows an iterative process. The displacement function corresponding to the zeroth order approximation is obtained first by keeping the leading order terms in the energy functional. A set of successive corrections is added and the associated energy functional is determined. Corrections generating terms of the same order in the energy functional as previously obtained, are kept. The process is terminated when the new contributions generate terms of smaller order. The displacement field converges to the following expression:

$$\begin{aligned}v_1 &= U_1(x) - y(s)U_2'(x) - z(s)U_3' + G(s)\phi'(x) \\ &\quad + \underline{g_1(s)U_1'(x) + g_2(s)U_2''(x) + g_3(s)U_3''(x)} \\ v_2 &= U_2(x)\frac{dy}{ds} + U_3(x)\frac{dz}{ds} + \phi(x)r_n \\ v &= U_2(x)\frac{dz}{ds} - U_3(x)\frac{dy}{ds} - \phi(x)r_t\end{aligned}\tag{1}$$

The axial displacement is denoted by v_1 while v_2 and v denote the displacement along the tangent and normal to the cross section mid-surface, respectively as shown in Fig.1. The average displacement over the cross section along the x , y and z Cartesian coordinate system is denoted by $U_1(x)$, $U_2(x)$ and $U_3(x)$, respectively. The cross sectional rotation is denoted by $\phi(x)$. The underlined terms in Eq.(1) represent the extension and bending-related warping. These new terms emerges naturally in addition to the classical torsional-related warping $G(s)\phi'$. They are strongly

influenced by the material's anisotropy and vanish for materials that are either orthotropic or whose properties are antisymmetric relative to middle surface of the cross section wall. These out-of-plane warping functions were derived earlier and presented in Ref.2.

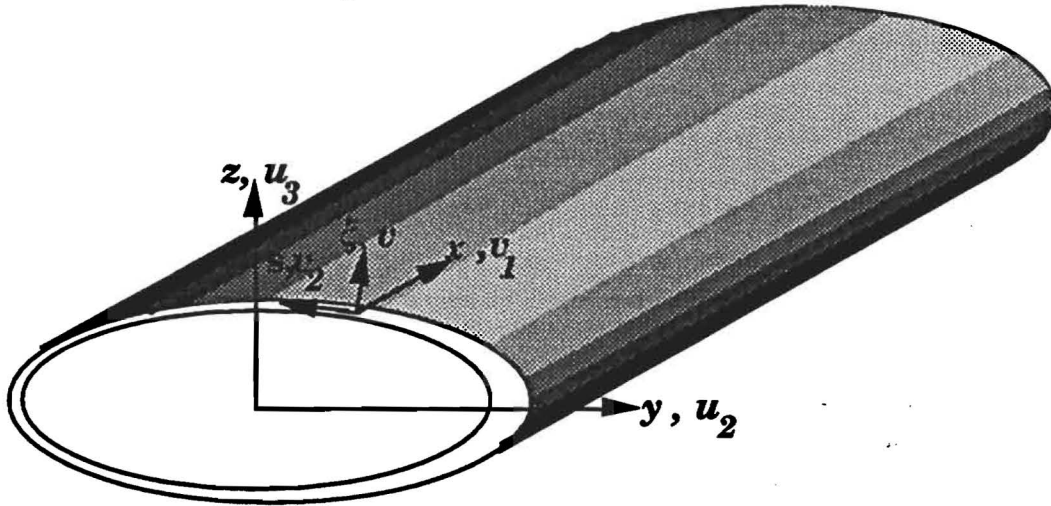


Fig.1 Coordinate system

The contribution of out-of-plane warping was considered recently by Kosmatka [3]. Local in-plane deformations and out-of-plane warping of the cross section were expressed in terms of unknown functions. These functions were assumed to be proportional to the axial strain, bending curvature and twist rate within the cross section and were determined using a finite element modeling. In our formulation, the out-of-plane warping is shown to be proportional to the axial strain, bending curvature and twist rate. Moreover, the functions associated with each physical behavior are expressed in closed-form by $g_1(s)$ for the axial strain, $g_2(s)$ and $g_3(s)$ for the bending curvatures and $G(s)$ for the twist rate.

An illustration of their effect appears in Figs. 2 and 3 where the bending slope in a cantilevered beam is plotted along the span. The beam is subjected to a unit bending load at the tip and has a rectangular cross section with $[15]_6$ (Fig.2) and $[30]_6$ (Fig.3) layup. Two types of predictions are compared to the experimental results [4, 5]. In the first, the torsional-related warping is considered only while in the second the contribution of bending-related warping is included. Extension-related warping is negligible for this construction. Neglecting bending-related warping leads to significant errors in predictions for this case.

Shear Deformation Contribution

A similar behavior to the one illustrated in Figs. 2 and 3 was found in the theory of Ref. 5 when the shear deformation contribution is neglected. This may indicate that the out-of-plane warping due to bending includes implicitly the shear deformation contribution. In the theory of Ref.5 the cross section stiffness coefficients are predicted from a finite element

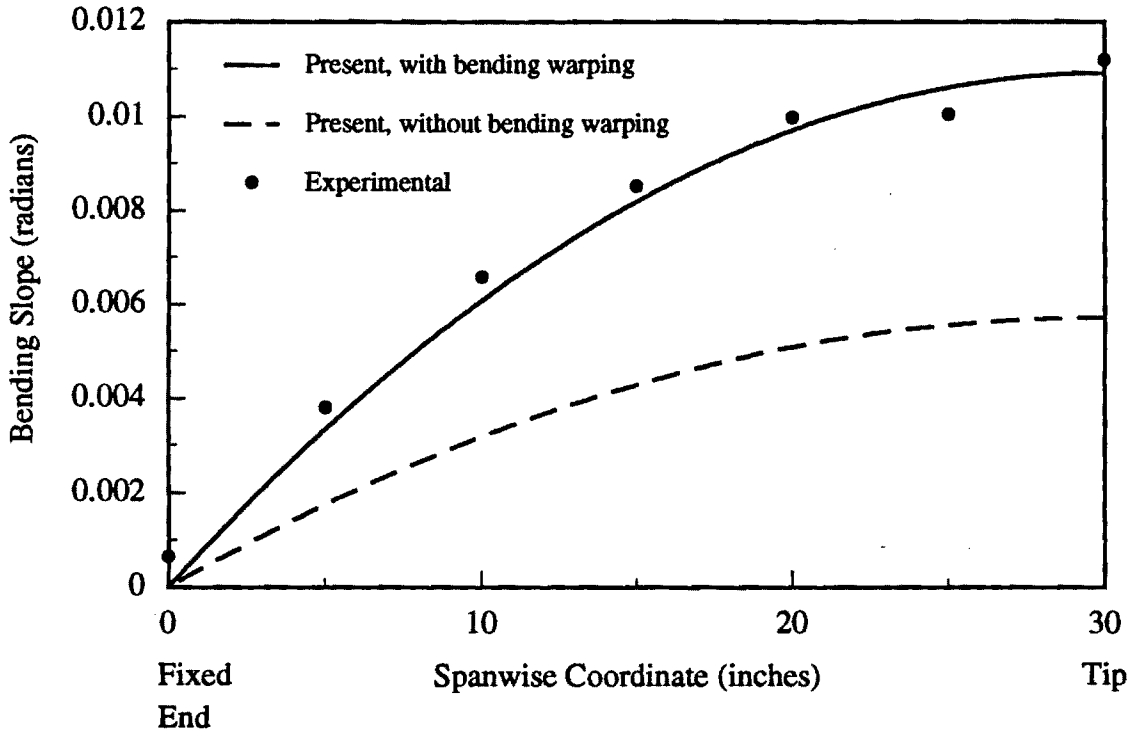


Fig. 2 Bending slope in a [15]₆ cantilevered beam under unit tip load

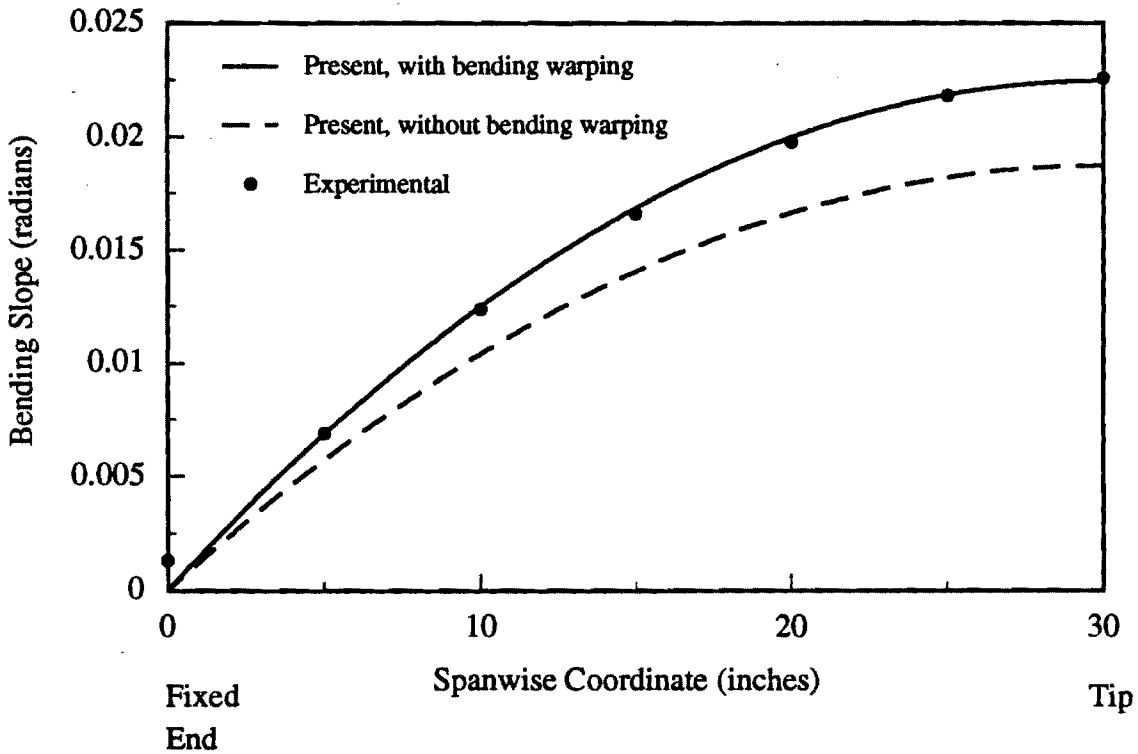


Fig. 3 Bending slope in a [30]₆ cantilevered beam under unit tip load

simulation. The theory is not restricted to thin-walled configurations. In order to assess the similarity between the shear deformation contribution and the out-of-plane warping, the present theory and the numerical work of Ref. 5 are applied to the prediction of the deflection curve in a cantilevered beam made of graphite/epoxy material and subjected to a transverse tip load of 1 lb. The beam has a [15]₆ layup with a rectangular cross section. The geometry and mechanical properties are similar to those of Ref. 5 and are provided in Table I.

Table I. Cantilever Geometry and Properties

Ply Thickness = 0.005 in
Width = 0.923 in.
Depth = 0.50 in.
E ₁₁ = 20.6 Msi.
E ₂₂ = E ₃₃ = 1.42 Msi.
G ₁₂ = G ₁₃ = 0.87 Msi.
G ₂₃ = 0.696 Msi
ν ₁₂ = ν ₁₃ = 0.30
ν ₂₃ = 0.34

Figure 4 shows a similar behavior suggesting that in the present theory, shear deformation is implicitly accounted through bending-related warping. The prediction of Ref.5 are referred to as Classical when shear deformation is neglected. Further evidence could be provided by estimating the equivalent shear deformation strain in the present theory which can be expressed in terms of the slope of the plane that approximates the cross section warping. This slope is given by

$$2\gamma_{xy} = -\frac{\int yv_1 dA}{I_{zz}} \quad (2)$$

where A and I_{zz} denote the cross-sectional area and second moment of area about the z -axis, respectively. A comparison of the shear strain γ_{xy} over the length of the beam with the prediction of Ref. 5. is shown in Fig. 5.

The shear strain at the fixed end is 4.5924×10^{-4} based on Eq.(2) which is within 2 % of 4.6857×10^{-4} calculated on the basis of Ref. 5.

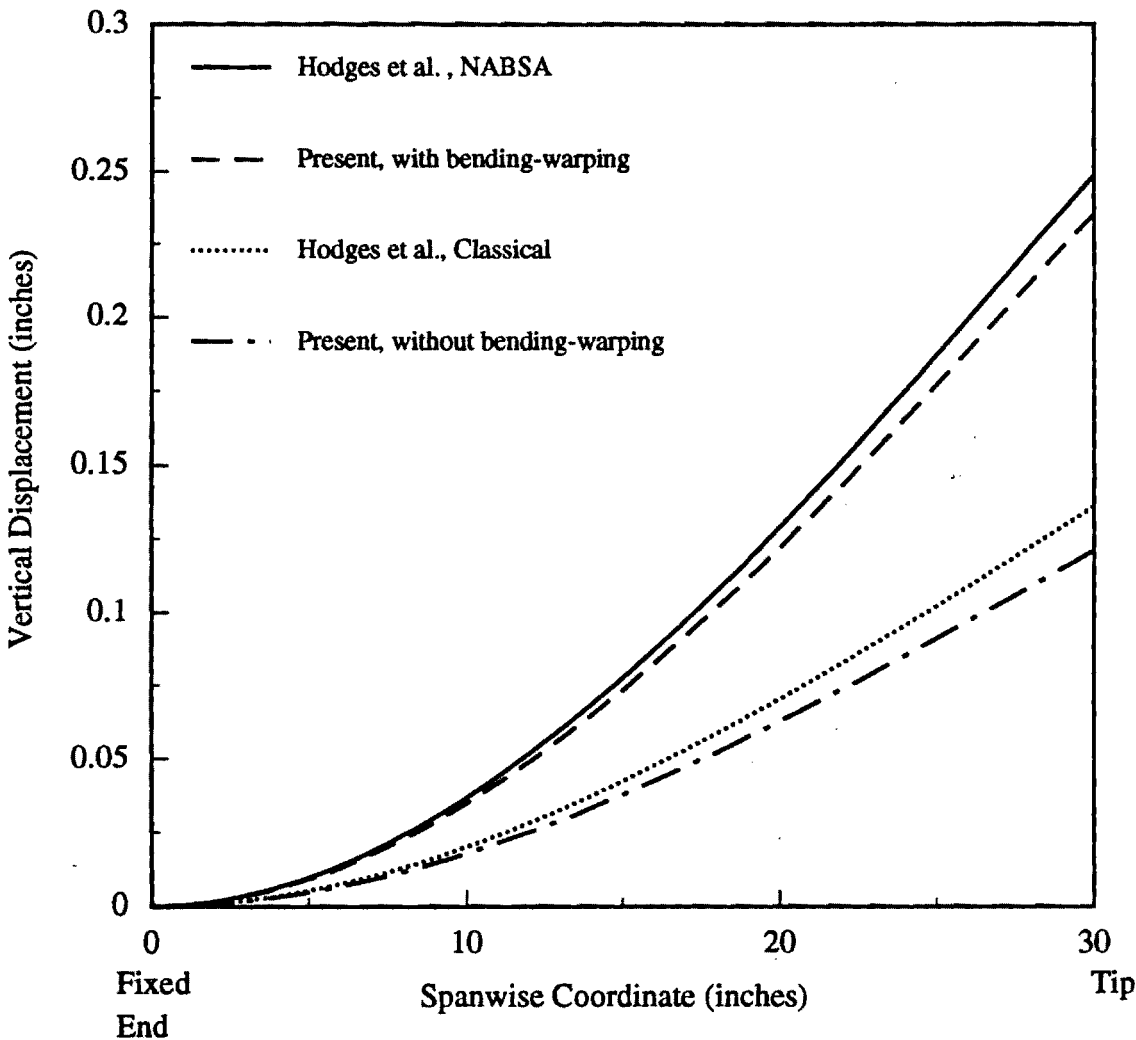


Fig. 4 Deflection of a $[15]_6$ cantilevered beam under unit tip load

Closing Remarks

The variationally asymptotical theory developed provides a consistent means for including the effects of the material's anisotropy in thin-walled beams. Two issues have been addressed in this progress report. The first, is concerned with the functional form of in-plane deformation and out-of-plane warping contributions to the displacement field. The second, is concerned with the significance of shear deformation effects.

A rigorous proof is provided for the assumed displacement field in Kosmatka's work [3]. Local in-plane deformations and out-of-plane warping of the cross section are indeed shown to be proportional to the axial strain, bending curvature and twist rate within the cross section. Moreover, their closed form functions are determined.

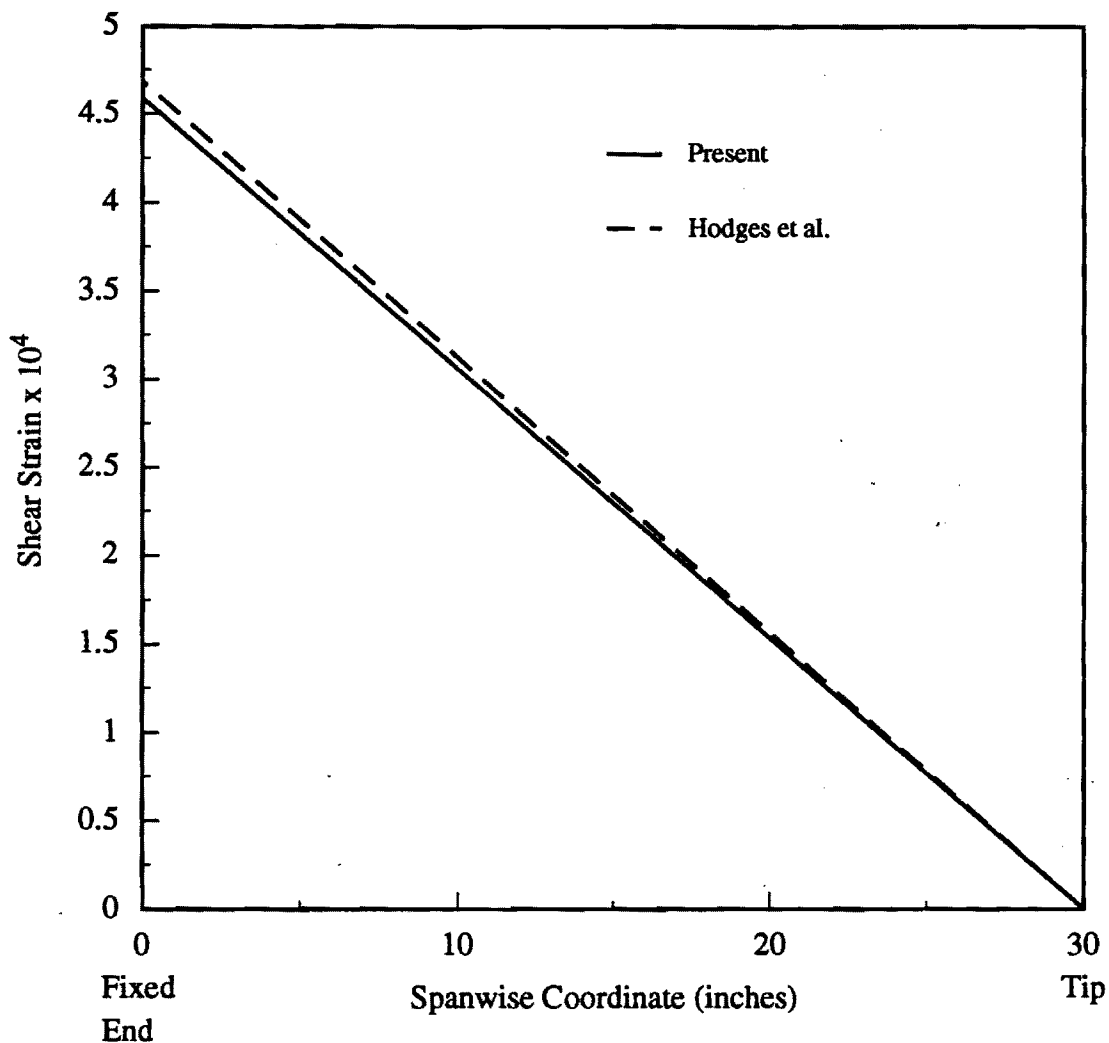


Fig. 5 Shear strain in a $[15]_6$ cantilevered beam under unit tip load

The significance of shear deformation in the modeling of laminated composites was recognized in the early work of Rehfield and was followed by Chopra et al. by adopting a Timoshenko-type shear deformation formulation. The displacement field developed in the present work is shown to include shear deformation through the out-of-plane warping terms. A closed form expression for the slope of the plane that approximates the cross section warping is derived and shown to be within 2% of the shear strain in a cantilever beam problem.

REFERENCES

- [1]. Berdichevsky, V., Armanios, E., and Badir, A., "Theory of Anisotropic Thin-Walled Closed Cross-Section Beams", To appear in a special issue of *Composites Engineering*, May 1992.
- [2] Armanios, E., Badir, A., and Berdichevsky, V., "Effect of damage on Elastically Tailored Composite Laminates", *Proceedings of the AHS International Technical Specialists' Meeting on Rotorcraft Basic Research*, Georgia Institute of Technology, Atlanta, Georgia, March 25-27, 1991, pp. 48(1)-48(11).
- [3]. Kosmatka, J. B., "Extension-bend-Twist Coupling Behavior of Thin-walled Advanced Composite Beams with Initial Twist," *Proceedings of the 32st AIAA/ASME/AHS/ASC Structures, Structural Dynamics and Materials Conference*, 1991, pp. 1037-1049.
- [4]. Smith, E. C., and Chopra, I., "Formulation and Evaluation of an Analytical Model for Composite Box-Beams," in *Proceedings of the 31st AIAA/ASME/AHS/ASC Structures, Structural Dynamics and Materials Conference*, 1990, pp. 759-782
- [5]. Smith, E. C., and Chopra, I., "Formulation and Evaluation of an Analytical Model for Composite Box-Beams," *Journal of the American Helicopter Society*, July 1991, pp. 23-35.
- [6]. Hodges, D. H., Atilgan, A. R., Cesnik, C. S., and Fulton, M. V., "On a Simplified Strain Energy Function for Geometrically Nonlinear Behavior of Anisotropic Beams," Presented at the Seventeenth European Rotorcraft Forum, September 24-26, 1991, Berlin, Germany. To appear in a special issue of *Composites Engineering*, May 1992

APPENDIX

Paper to appear in a special issue of *Composites Engineering*, May 1992

Theory of Anisotropic Thin-Walled Closed Cross-Section Beams

Victor Berdichevsky, Erian Armanios, and Ashraf Badir *
School of Aerospace Engineering
Georgia Institute of Technology
Atlanta, Georgia 30332-0150

ABSTRACT

A variationally and asymptotically consistent theory is developed in order to derive the governing equations of anisotropic thin-walled beams with closed sections. The theory is based on an asymptotical analysis of two-dimensional shell theory. Closed-form expressions for the beam stiffness coefficients, stress and displacement fields are provided. The influence of material anisotropy on the displacement field is identified. A comparison of the displacement fields obtained by other analytical developments is performed. The stiffness coefficients and static response are also compared with finite element predictions, closed form solutions and test data.

INTRODUCTION

Elastically tailored composite designs are being used to achieve favorable deformation behavior under a given loading environment. Coupling between deformation modes such as extension-twist or bending-twist is created by an appropriate selection of fiber orientation, stacking sequence and materials. The fundamental mechanism producing elastic tailoring in composite beams is a result of their anisotropy. Several theories have been developed for the analysis of thin-walled anisotropic beams.

*Professor, Associate Professor, and Graduate Research Assistant, respectively.

A review is provided in Hodges (1990). A basic element in the analytical modeling development is the derivation of the effective stiffness coefficients and governing equations which allows the three-dimensional (3D) state of stress to be recovered from a one-dimensional (1D) beam formulation. For isotropic or orthotropic materials this is a classical problem, which is considered in a number of text books such as Timoshenko and Goodier (1951), Sokolnikoff (1956), Washizu (1968), Crandall *et al.* (1978), Wempner (1981), Gjelsvik (1981), Libai and Simmonds (1988), and Megson (1990).

For generally anisotropic materials a number of 1D theories have been developed by Reissner and Tsai (1972), Mansfield and Sobey (1979), Rehfield (1985), Libove (1988), Rehfield and Atilgan (1989), and Smith and Chopra (1990;1991). A discussion of these works is provided in the comparison section of this paper.

The objective of this work is to develop a consistent theory for thin-walled beams made of anisotropic materials. The theory is an asymptotically correct first order approximation. The accuracy of previously developed theories is assessed by comparing the resulting displacement fields. A comparison of stiffness coefficients and static response with finite element predictions, closed form solutions and test data is also performed.

A detailed derivation of the theory is presented first. This is followed by a summary of governing equations. Finally a comparison of results with previously developed theories is provided.

DEVELOPMENT OF THE ANALYTICAL MODEL

Coordinate Systems

Consider the slender thin-walled elastic cylindrical shell shown in Fig. 1. The length of the shell is denoted by L , its thickness by h , the radius of curvature of the middle surface by R and the maximum cross sectional dimension by d . It is assumed that

$$d \ll L \quad h \ll d \quad h \ll R \quad (1)$$

The shell is loaded by external forces applied to the lateral surfaces and at the ends. It is assumed that the variation of the external forces and material properties over distances of order d in the axial direction and over distances of order h in the

circumferential direction, is small. The material is anisotropic and its properties can vary in the direction normal to the middle surface.

It is convenient to consider simultaneously two coordinate systems for the description of the state of stress in thin-walled beams. The first one is the Cartesian system x, y and z shown in Fig. 1. The axial coordinate is x while y and z are associated with the beam cross section. The second coordinate system, is the curvilinear system x, s and ξ shown in Fig. 2. The circumferential coordinate s is measured along the tangent to the middle surface in a counter-clockwise direction whereas ξ is measured along the normal to the middle surface. A number of relationships have a simpler form when expressed in terms of curvilinear coordinates. A relationship between the two coordinate systems can be established as follows.

Define the position vector \vec{r} of the shell middle surface as

$$\vec{r} = x\vec{i}_x + y(s)\vec{i}_y + z(s)\vec{i}_z$$

where $\vec{i}_x, \vec{i}_y, \vec{i}_z$ are unit vectors associated with the cartesian coordinate system x, y and z . Equations $y = y(s)$ and $z = z(s)$ define the closed contour Γ in the y, z plane. The normal vector to the middle surface \vec{n} has two nonzero components

$$\vec{n} = n_y(s)\vec{i}_y + n_z(s)\vec{i}_z \quad (2)$$

The position vector \vec{R} of an arbitrary material point can be written in the form

$$\vec{R} = \vec{r} + \xi\vec{n} \quad (3)$$

Equations (2) and (3) establish the relations between the cartesian coordinates x, y, z and the curvilinear coordinates x, s, ξ . The coordinate ξ lies within the limits

$$-\frac{h(s)}{2} \leq \xi \leq \frac{h(s)}{2}$$

The shell thickness varies along the circumferential direction and is denoted by $h(s)$.

The tangent vector \vec{t} , the normal vector \vec{n} and the projection of the position vector \vec{r} on \vec{t} and \vec{n} are expressed in terms of the cartesian and curvilinear coordinates as

$$\begin{aligned} \vec{t} &= \frac{d\vec{r}}{ds} = \frac{dy}{ds}\vec{i}_y + \frac{dz}{ds}\vec{i}_z \\ \vec{n} &= \vec{t} \times \vec{i}_x = \frac{dz}{ds}\vec{i}_y - \frac{dy}{ds}\vec{i}_z \end{aligned}$$

$$r_t = \vec{r} \cdot \vec{t} = y \frac{dy}{ds} + z \frac{dz}{ds}$$

$$r_n = \vec{r} \cdot \vec{n} = y \frac{dz}{ds} - z \frac{dy}{ds}$$

An asymptotical analysis is used to model the slender thin-walled shell as a beam with effective stiffnesses. The method follows an iterative process. The displacement function corresponding to the zeroth-order approximation is obtained first by keeping the leading order terms in the energy functional. A set of successive corrections is added to the displacement function and the associated energy functional is determined. Corrections generating terms of the same order as previously obtained in the energy functional, are kept. The process is terminated when the new contributions do not generate any additional terms of the same order as previously obtained.

Shell Energy Functional

Consider in a $3D$ space the prismatic shell shown in Fig. 2. A curvilinear frame x , s , and ξ is associated with the undeformed shell configuration. Values 1, 2 and 3 denoting x , s , and ξ , respectively are assigned to the curvilinear frame. Throughout this section, Latin superscripts (or subscripts) run from 1 to 3, while Greek superscripts (or subscripts) run from 1 to 2, unless otherwise stated.

The energy density of a $3D$ elastic body is a quadratic form of the strains

$$U = \frac{1}{2} E^{ijkl} \varepsilon_{ij} \varepsilon_{kl}$$

The material properties are expressed by the Hookean tensor E^{ijkl} . Following classical shell formulation (Koiter (1959), and Sanders (1959)) the through-the-thickness stress components σ^{i3} are considerably smaller than the remaining components $\sigma^{\alpha\beta}$ therefore

$$\sigma^{i3} = 0 \tag{4}$$

The strains can be written as

$$\varepsilon_{\alpha\beta} = \gamma_{\alpha\beta} + \xi \rho_{\alpha\beta} \tag{5}$$

where $\gamma_{\alpha\beta}$ and $\rho_{\alpha\beta}$ represent the in-plane strain components and the change in the shell middle surface curvatures, respectively. For a cylindrical shell these are related to the displacement variables by

$$\gamma_{11} = \frac{\partial v_1}{\partial x}$$

$$\begin{aligned}
2\gamma_{12} &= \frac{\partial v_1}{\partial s} + \frac{\partial v_2}{\partial x} \\
\gamma_{22} &= \frac{\partial v_2}{\partial s} + \frac{v}{R} \\
\rho_{11} &= \frac{\partial^2 v}{\partial x^2} \\
\rho_{12} &= \frac{\partial^2 v}{\partial s \partial x} + \frac{1}{4R} \left(\frac{\partial v_1}{\partial s} - 3 \frac{\partial v_2}{\partial x} \right) \\
\rho_{22} &= \frac{\partial^2 v}{\partial s^2} - \frac{\partial}{\partial s} \left(\frac{v_2}{R} \right)
\end{aligned} \tag{6}$$

where v_1 , v_2 and v represent the displacements in the axial, tangential and normal directions, respectively as shown in Fig. 2. These are related to the displacement components in cartesian coordinates by

$$\begin{aligned}
v_1 &= u_1 \\
v_2 &= u_2 \frac{dy}{ds} + u_3 \frac{dz}{ds} \\
v &= u_2 \frac{dz}{ds} - u_3 \frac{dy}{ds}
\end{aligned} \tag{7}$$

where u_1 , u_2 , and u_3 denote the displacements along the x , y and z coordinates, respectively.

The energy density of the 2D elastic body is obtained in terms of $\gamma_{\alpha\beta}$ and $\rho_{\alpha\beta}$ by the following procedure.

The 3D energy is first minimized with respect to ϵ_{i3} . This is equivalent to satisfying Eq. (4). The result is

$$\hat{U} = \min_{\epsilon_{i3}} U = \frac{1}{2} D^{\alpha\beta\gamma\delta} \epsilon_{\alpha\beta} \epsilon_{\gamma\delta} \tag{8}$$

where $D^{\alpha\beta\gamma\delta}$ represents the components of the 2D moduli. The expressions for $D^{\alpha\beta\gamma\delta}$ are given in terms of $E^{\alpha\beta\gamma\delta}$ in the Appendix.

The strain $\epsilon_{\alpha\beta}$ from Eq. (5) is substituted into Eq. (8). After integration of the result over the thickness ξ one obtains the energy of the shell Φ per unit middle surface area

$$2\Phi = h C^{\alpha\beta\gamma\delta} \gamma_{\alpha\beta} \gamma_{\gamma\delta} + h^2 C_1^{\alpha\beta\gamma\delta} \gamma_{\alpha\beta} \rho_{\gamma\delta} + \frac{h^3}{12} C_2^{\alpha\beta\gamma\delta} \rho_{\alpha\beta} \rho_{\gamma\delta}$$

where

$$\begin{aligned}
C^{\alpha\beta\gamma\delta} &= \frac{1}{h} \langle D^{\alpha\beta\gamma\delta} \rangle \\
C_1^{\alpha\beta\gamma\delta} &= \frac{2}{h^2} \langle D^{\alpha\beta\gamma\delta} \xi \rangle \\
C_2^{\alpha\beta\gamma\delta} &= \frac{12}{h^3} \langle D^{\alpha\beta\gamma\delta} \xi^2 \rangle
\end{aligned}$$

and a function of ξ , say $\alpha(\xi)$, between pointed brackets is defined as an integral through the thickness, viz.,

$$\langle \alpha \rangle = \int_{-h(s)/2}^{+h(s)/2} \alpha(\xi) d\xi \quad (9)$$

For an applied external loading P_i , the displacement field u_i determining the deformed state is the stationary point of the energy functional

$$I = \int \Phi dx ds - \int P_i u_i dx ds \quad (10)$$

Asymptotical Analysis of the Shell Energy Functional

Zeroth-Order Approximation

Let Δ and E be the order of displacements and stiffness coefficients $C^{\alpha\beta\gamma\delta}$, respectively. Assume that the order of the external forces is

$$P \sim O\left(\frac{E\Delta h}{L^2}\right)$$

This assumption is shown later to be consistent with the equilibrium equations. An alternative would be to assume the order of the external force as some quantity P and derive the order of the displacements as PL^2/Eh from an asymptotical analysis of the energy functional.

For a thin-walled slender beam whose dimensions satisfy Eq. (1) the rate of change of the displacements along the axial direction is much smaller than their rate of change along the circumferential direction. That is, for each displacement component

$$\left| \frac{\partial v_i}{\partial x} \right| \ll \left| \frac{\partial v_i}{\partial s} \right|$$

Using Eq. (6) and assuming that d is of the same order as R , the order of magnitude of the in-plane strains and curvatures is

$$\gamma_{11} \sim O\left(\frac{\Delta}{L}\right)$$

$$2\gamma_{12} \sim O\left(\frac{\Delta}{d}\right)$$

$$\gamma_{22} \sim O\left(\frac{\Delta}{d}\right)$$

$$\rho_{11} \sim O\left(\frac{\Delta}{L^2}\right)$$

$$\rho_{12} \sim O\left(\frac{\Delta}{d^2}\right)$$

$$\rho_{22} \sim O\left(\frac{\Delta}{d^2}\right)$$

Since γ_{11} and ρ_{11} are much smaller than γ_{12} , γ_{22} and ρ_{12} , ρ_{22} , respectively, their contribution to the elastic energy is neglected.

By keeping the leading order terms in the strain-displacement relationships, Eq. (6) can be written as

$$\begin{aligned} 2\gamma_{12} &= \frac{\partial v_1}{\partial s} \\ \gamma_{22} &= \frac{\partial v_2}{\partial s} + \frac{v}{R} \\ \rho_{12} &= \frac{1}{4R} \frac{\partial v_1}{\partial s} \\ \rho_{22} &= \frac{\partial^2 v}{\partial s^2} - \frac{\partial}{\partial s} \left(\frac{v_2}{R} \right) \end{aligned} \tag{11}$$

The order of magnitude of the shell energy per unit area and the work done by external forces is

$$\begin{aligned} \Phi &\sim O\left(\frac{E\Delta^2 h}{d^2}\right) \\ P_i u_i &\sim O\left(\frac{E\Delta^2 h}{L^2}\right) \end{aligned}$$

Since $P_i u_i \ll \Phi$, the contribution of external forces is neglected. The energy functional takes the form

$$\begin{aligned}
2I = \int_0^L \oint \{ & 4hC^{1212}(\gamma_{12})^2 + 4hC^{1222}\gamma_{12}\gamma_{22} + hC^{2222}(\gamma_{22})^2 + 4h^2C_1^{1212}\gamma_{12}\rho_{12} \\
& + 2h^2C_1^{1222}\gamma_{12}\rho_{22} + 2h^2C_1^{2212}\gamma_{22}\rho_{12} + h^2C_1^{2222}\gamma_{22}\rho_{22} \\
& + \frac{h^3}{3}C_2^{1212}(\rho_{12})^2 + \frac{h^3}{3}C_2^{1222}\rho_{12}\rho_{22} + \frac{h^3}{12}C_2^{2222}(\rho_{22})^2 \} ds dx \quad (12)
\end{aligned}$$

The integrand in Eq. (12) is a positive quadratic form, therefore the minimum of the functional is reached by functions v , v_1 , and v_2 for which $\gamma_{12} = \gamma_{22} = \rho_{12} = \rho_{22} = 0$. From Eq. (11) this corresponds to

$$\frac{\partial v_1}{\partial s} = 0 \quad (13)$$

$$\frac{\partial v_2}{\partial s} + \frac{v}{R} = 0 \quad (14)$$

$$\frac{\partial^2 v}{\partial s^2} - \frac{\partial}{\partial s} \left(\frac{v_2}{R} \right) = 0 \quad (15)$$

The function v in Eqs. (14) and (15) should be single valued, i. e.

$$\overline{\left(\frac{\partial v}{\partial s} \right)} \equiv \frac{1}{l} \oint \frac{\partial v}{\partial s} ds = 0 \quad (16)$$

The integral in Eq. (16) is performed along the cross sectional mid-plane closed contour Γ . The length of contour Γ is denoted by l . The bar in Eq. (16) and in the subsequent derivation denotes averaging along the closed contour Γ .

Equation (13) implies that v_1 is a function of x only, i.e.

$$v_1 = U_1(x) \quad (17)$$

Integrate Eq. (15) to get

$$\frac{\partial v}{\partial s} - \frac{v_2}{R} = -\varphi(x) \quad (18)$$

where $\varphi(x)$ is an arbitrary function which is shown later to represent the cross sectional rotation about the x -axis. From Eq. (16) and (18), one obtains the relation between $\varphi(x)$ and v_2 .

$$\varphi(x) = \overline{\left(\frac{v_2}{R} \right)}$$

Substitute v from Eq. (14) into Eq. (18), to get the following second-order differential equation for v_2

$$\frac{\partial}{\partial s}(R \frac{\partial v_2}{\partial s}) + \frac{v_2}{R} = \varphi(x) \quad (19)$$

To solve this equation, one has to recall the relations between the radius of curvature R and the components $y(s)$ and $z(s)$ of the position vector associated with contour Γ

$$\begin{aligned} \frac{d^2 z}{ds^2} &= \frac{1}{R} \frac{dy}{ds} \\ \frac{d^2 y}{ds^2} &= -\frac{1}{R} \frac{dz}{ds} \end{aligned} \quad (20)$$

It follows from Eq. (20) that $\frac{dy}{ds}$ and $\frac{dz}{ds}$ are solutions of the homogeneous form of Eq. (19) and $v_2 = \varphi(x)r_n$ is its particular solution. The general solution is therefore given by

$$v_2 = U_2(x) \frac{dy}{ds} + U_3(x) \frac{dz}{ds} + \varphi(x)r_n \quad (21)$$

where U_2 and U_3 are arbitrary functions of x . Substitute from Eq. (21) into Eq. (14) to get

$$v = U_2(x) \frac{dz}{ds} - U_3(x) \frac{dy}{ds} - \varphi(x)r_t \quad (22)$$

Equations (17), (21) and (22) represent the curvilinear displacement field that minimizes the zeroth order approximation of the shell energy. Using Eq. (7) the curvilinear displacement field is written in Cartesian coordinates as

$$u_1 = U_1(x)$$

$$u_2 = U_2(x) - z\varphi(x)$$

$$u_3 = U_3(x) + y\varphi(x)$$

The variables $U_1(x)$, $U_2(x)$ and $U_3(x)$ represent the average cross-sectional translation while $\varphi(x)$ the cross-sectional rotation normally referred to in beam theory as the torsional rotation. This displacement field corresponds to the zeroth-order approximation and does not include bending behavior. For a centroidal coordinate system $U_1(x)$, $U_2(x)$, $U_3(x)$ and $\varphi(x)$ can be expressed as

$$U_1(x) = \bar{u}_1$$

$$U_2(x) = \bar{u}_2$$

$$U_3(x) = \bar{u}_3$$

$$\varphi(x) = \frac{(\vec{u} \cdot \vec{t})}{r_n}$$

First-Order Approximation

A first-order approximation can be constructed by rewriting the displacement field in Eqs. (17), (21) and (22) in the form

$$\begin{aligned} v_1 &= U_1(x) + w_1(s, x) \\ v_2 &= U_2(x) \frac{dy}{ds} + U_3(x) \frac{dz}{ds} + \varphi(x) r_n + w_2(s, x) \\ v &= U_2(x) \frac{dz}{ds} - U_3(x) \frac{dy}{ds} - \varphi(x) r_t + w(s, x) \end{aligned} \quad (23)$$

where w_1, w_2 and w can be regarded as correction functions to be determined based on their contributions to the energy functional.

Substitute Eq. (23) into Eq. (6) to obtain the strains and curvatures in terms of the displacement corrections

$$\begin{aligned} \gamma_{11} &= \overset{\circ}{\gamma}_{11} + \frac{\partial w_1}{\partial x} \\ 2\gamma_{12} &= 2\overset{\circ}{\gamma}_{12} + \frac{\partial w_2}{\partial x} + 2\hat{\gamma}_{12} \quad , \quad 2\hat{\gamma}_{12} = \frac{\partial w_1}{\partial s} \\ \gamma_{22} &= \overset{\circ}{\gamma}_{22} + \hat{\gamma}_{22} \quad , \quad \hat{\gamma}_{22} = \frac{\partial w_2}{\partial s} + \frac{w}{R} \\ \rho_{11} &= \overset{\circ}{\rho}_{11} + \frac{\partial^2 w}{\partial x^2} \\ \rho_{12} &= \overset{\circ}{\rho}_{12} + \frac{\partial^2 w}{\partial s \partial x} - \frac{3}{4R} \frac{\partial w_2}{\partial x} + \hat{\rho}_{12} \quad , \quad \hat{\rho}_{12} = \frac{1}{4R} \frac{\partial w_1}{\partial s} \\ \rho_{22} &= \overset{\circ}{\rho}_{22} + \hat{\rho}_{22} \quad , \quad \hat{\rho}_{22} = \frac{\partial^2 w}{\partial s^2} - \frac{\partial}{\partial s} \left(\frac{w_2}{R} \right) \end{aligned} \quad (24)$$

where $\gamma^\circ_{\alpha\beta}$ and $\rho^\circ_{\alpha\beta}$ are the strains and curvatures corresponding to the zeroth-order approximation. These are expressed as

$$\begin{aligned} \overset{\circ}{\gamma}_{11} &= U_1'(x) \\ 2\overset{\circ}{\gamma}_{12} &= U_2'(x) \frac{dy}{ds} + U_3'(x) \frac{dz}{ds} + \varphi'(x) r_n \\ \overset{\circ}{\gamma}_{22} &= 0 \end{aligned}$$

$$\begin{aligned}
\overset{\circ}{\rho}_{11} &= U_2''(x) \frac{dz}{ds} - U_3''(x) \frac{dy}{ds} - \varphi''(x) r_t \quad (25) \\
\overset{\circ}{\rho}_{12} &= \frac{1}{4R} \left[U_2'(x) \frac{dy}{ds} + U_3'(x) \frac{dz}{ds} + \varphi'(x) r_n \right] - \varphi'(x) \\
\overset{\circ}{\rho}_{22} &= 0
\end{aligned}$$

The prime in Eq. (25) denotes differentiation with respect to x . The order of w_i is $(\frac{\Delta d}{L})$. Among the new terms introduced by the function w_i , the leading ones are denoted by superscript $\hat{\cdot}$ in Eq. (24). By keeping their contribution over the other terms, the energy functional can be represented by

$$\Phi(\overset{\circ}{\gamma}_{11}, 2\overset{\circ}{\gamma}_{12} + 2\hat{\gamma}_{12}, \hat{\gamma}_{22}, 0, \hat{\rho}_{12}, \hat{\rho}_{22})$$

where terms of order $(\frac{\Delta^2 h}{L^2 d})$ or smaller such as

$$h\overset{\circ}{\rho}_{11}\hat{\gamma}_{12}, h\overset{\circ}{\rho}_{11}\hat{\gamma}_{22}, h^2\overset{\circ}{\rho}_{11}\hat{\rho}_{12}, h^2\overset{\circ}{\rho}_{11}\hat{\rho}_{22}$$

$$h\overset{\circ}{\rho}_{12}\hat{\gamma}_{12}, h\overset{\circ}{\rho}_{12}\hat{\gamma}_{22}, h^2\overset{\circ}{\rho}_{12}\hat{\rho}_{12}, h^2\overset{\circ}{\rho}_{12}\hat{\rho}_{22}$$

are neglected in comparison with the following terms

$$\overset{\circ}{\gamma}_{11}\hat{\gamma}_{12}, \overset{\circ}{\gamma}_{11}\hat{\gamma}_{22}, \overset{\circ}{\gamma}_{12}\hat{\gamma}_{12}, \overset{\circ}{\gamma}_{12}\hat{\gamma}_{22}$$

of order $(\frac{\Delta^2}{L^2})$. Similarly, the contribution of the work done by external forces, $P_i w_i$, is neglected since its order is $(Eh \frac{\Delta^2}{L^2} (\frac{d}{L}))$ in comparison with the order of the remaining terms in the energy functional $(Eh \frac{\Delta^2}{L^2})$. Therefore in order to determine the functions w_i one has to minimize the functional

$$\oint \Phi(\overset{\circ}{\gamma}_{11}, 2\overset{\circ}{\gamma}_{12} + 2\hat{\gamma}_{12}, \hat{\gamma}_{22}, 0, \hat{\rho}_{12}, \hat{\rho}_{22}) ds$$

If the rigid body motion is suppressed the solution is unique. The terms $\hat{\rho}_{12}$, $\hat{\rho}_{22}$ are essential to the uniqueness of the solution; however, their contribution to the energy is of order $(Eh \frac{\Delta^2}{L^2} (\frac{h}{d}))$ and is consequently dropped. This aspect is discussed by Berdichevsky and Misiura (1991) with regard to the accuracy of classical shell theory. The shell energy can therefore be represented by

$$I = \int_0^L \oint \Phi(\overset{\circ}{\gamma}_{11}, 2\overset{\circ}{\gamma}_{12} + 2\hat{\gamma}_{12}, \hat{\gamma}_{22}, 0, 0, 0) ds dx \quad (26)$$

It is worth noting that the bending contribution does not appear in Eq. (26). That is, to the first order approximation the shell energy corresponds to a membrane state.

The first variation of the energy functional is

$$\delta I = \int_0^L \oint \left\{ \frac{\partial \Phi}{\partial (2\gamma_{12})} \delta \left(\frac{\partial w_1}{\partial s} \right) + \frac{\partial \Phi}{\partial \gamma_{22}} \delta \left(\frac{\partial w_2}{\partial s} + \frac{w}{R} \right) \right\} ds dx \quad (27)$$

Equation (27) can be written in terms of the shear flow N_{12} and hoop stress resultant N_{22} by recalling that $N_{12} = \frac{\partial \Phi}{\partial (2\gamma_{12})}$ and $N_{22} = \frac{\partial \Phi}{\partial \gamma_{22}}$. The result is

$$\delta I = \int_0^L \oint \left\{ N_{12} \frac{\partial(\delta w_1)}{\partial s} + N_{22} \left(\frac{\partial(\delta w_2)}{\partial s} + \frac{1}{R} \delta w \right) \right\} ds dx$$

Set the first variation of the energy to zero, to obtain the following

$$\frac{\partial N_{12}}{\partial s} = 0$$

$$\frac{\partial N_{22}}{\partial s} = 0$$

$$\frac{N_{22}}{R} = 0$$

which result in

$$N_{12} = \text{constant} \quad (28)$$

and

$$N_{22} = 0 \quad (29)$$

This is similar to the classical solution of constant shear flow and vanishing hoop stress. By setting N_{22} to zero the energy density is expressed in terms of γ_{11} and γ_{12} only

$$2\Phi_1 = \min_{\gamma_{22}} 2\Phi = A(s)(\gamma_{11})^2 + 2B(s)\gamma_{11}\gamma_{12} + C(s)(\gamma_{12})^2 \quad (30)$$

The variables $A(s)$, $B(s)$ and $C(s)$ represent the axial, coupling and shear stiffnesses, respectively. They are defined in terms of the 2D shell moduli in the Appendix.

Equation (30) indicates that, to the first order, the energy density function is independent of functions w_2 and w . That is the in-plane warping contribution to the shell energy is negligible. The function w_1 however, can be determined from Eqs. (28) and (30) and by enforcing the condition on w_1 to be single valued as follows

$$N_{12} = \frac{\partial \Phi_1}{\partial (2\gamma_{12})} = \frac{1}{2} (B(s)\gamma_{11} + C(s)\gamma_{12}) = \text{constant} \quad (31)$$

Substitute the leading terms from Eqs. (24) and (25) into Eq. (31) to get

$$\frac{1}{2}BU_1'(x) + \frac{1}{4}C \left(U_2'(x)\frac{dy}{ds} + U_3'(x)\frac{dz}{dx} + \varphi'(x)r_n(s) + \frac{\partial w_1}{\partial s} \right) = \text{constant} \quad (32)$$

In deriving Eq. (32) the term $B\frac{\partial w_1}{\partial x}$ has been neglected in comparison with $\frac{1}{2}C\frac{\partial w_1}{\partial s}$. This is possible if $|B|$ is less or of the same order of magnitude as C . For the case when $|B| \gg C$ additional investigation is needed. Since the elastic energy is positive definite, $B^2 \leq AC$, and B could be greater than C only if $A \gg C$. In practical laminated composite designs $|B| < C$, as the shear stiffness is greater than the extension-shear coupling.

Equation (32) is a first-order ordinary differential equation in w_1 . The value of the constant in the right hand side of Eq. (32) can be found from the single value condition of function w_1 :

$$\overline{\left(\frac{\partial w_1}{\partial s} \right)} \equiv \frac{1}{l} \oint \frac{\partial w_1}{\partial s} ds = 0$$

The solution of Eq. (32) is determined within an arbitrary function of x . This function can be specified from various conditions. Each one yields a specific interpretation of the variable U_1 . For example if $\bar{w}_1 = 0$ the variable $U_1 = \bar{v}_1$ according to Eq. (23). The choice of these conditions does not affect the final form of the 1D beam theory and therefore will not be specified in this formulation. The result is the following simple analytical solution of Eq. (32)

$$w_1 = -yU_2'(x) - zU_3'(x) + G(s)\varphi'(x) + g_1(s)U_1'(x) \quad (33)$$

where

$$\begin{aligned} G(s) &= \int_0^s \left[\frac{2A_e}{l\bar{c}}c(\tau) - r_n(\tau) \right] d\tau \\ g_1(s) &= \int_0^s \left[b(\tau) - \frac{\bar{b}}{\bar{c}}c(\tau) \right] d\tau \\ b(s) &= -2\frac{B(s)}{C(s)} \quad c(s) = \frac{1}{C(s)} \quad A_e = \frac{l}{2}\bar{r}_n \end{aligned} \quad (34)$$

The area enclosed by contour Γ is denoted by A_e in Eq. (34).

The displacement field corresponding to the first correction is obtained by substituting Eq. (33) into Eq. (23) and dropping w_2 and w since their contribution to

the shell energy is negligible compared to w_1 . The result referred to as first-order approximation is given by

$$\begin{aligned}v_1 &= U_1(x) - y(s)U_2'(x) - z(s)U_3'(x) + G(s)\varphi'(x) + g_1(s)U_1'(x) \\v_2 &= U_2(x)\frac{dy}{ds} + U_3(x)\frac{dz}{ds} + \varphi(x)r_n \\v &= U_2(x)\frac{dz}{ds} - U_3(x)\frac{dy}{ds} - \varphi(x)r_t\end{aligned}$$

Displacement Field

The displacement field corresponding to the next correction is found in the same way. A third correction can also be performed. However, subsequent corrections yield only smaller terms, as shown in Badir (1992), and the displacement field converges to the following expression

$$\begin{aligned}v_1 &= U_1(x) - y(s)U_2'(x) - z(s)U_3'(x) + G(s)\varphi'(x) \\&\quad + g_1(s)U_1'(x) + g_2(s)U_2''(x) + g_3(s)U_3''(x) \\v_2 &= U_2(x)\frac{dy}{ds} + U_3(x)\frac{dz}{ds} + \varphi(x)r_n \\v &= U_2(x)\frac{dz}{ds} - U_3(x)\frac{dy}{ds} - \varphi(x)r_t\end{aligned}\tag{35}$$

where

$$\begin{aligned}g_2(s) &= -\int_0^s \left[b(\tau)y(\tau) - \frac{\overline{by}}{\overline{c}}c(\tau) \right] d\tau \\g_3(s) &= -\int_0^s \left[b(\tau)z(\tau) - \frac{\overline{bz}}{\overline{c}}c(\tau) \right] d\tau\end{aligned}\tag{36}$$

It is seen from expressions (34) and (36) that $G(s)$, $g_1(s)$, $g_2(s)$, and $g_3(s)$ are single-valued functions, that is

$$G(0) = G(l) = g_1(0) = g_1(l) = g_2(0) = g_2(l) = g_3(0) = g_3(l) = 0$$

The expressions for the displacements v_2 , v and the first four terms in v_1 are analogous to the classical theory of extension, bending and torsion of beams. The additional terms $g_1(s)U_1'$, $g_2(s)U_2''$ and $g_3(s)U_3''$ in the expression of v_1 in Eq. (35) represent warping due to axial strain and bending. These new terms emerge naturally in addition to the classical torsional related warping $G(s)\varphi'$. They are strongly

influenced by the material's anisotropy, and vanish for materials that are either orthotropic or whose properties are antisymmetric relative to the shell middle surface. These out-of-plane warping functions were first derived by Armanios *et al.* (1991) for laminated composites.

The contribution of out-of-plane warping was considered recently by Kosmatka (1991). Local in-plane deformations and out-of-plane warping of the cross section were expressed in terms of unknown functions. These functions were assumed to be proportional to the axial strain, bending curvature and twist rate within the cross section and were determined using a finite element modeling. In the present formulation, the out-of-plane warping is shown to be proportional to the axial strain, bending curvature and torsion twist rate. The functions associated with each physical behavior are expressed in closed-form by $g_1(s)$ for the axial strain, $g_2(s)$ and $g_3(s)$ for the bending curvatures and $G(s)$ for the torsion twist rate.

Strain Field

The strain field is obtained by substituting Eq. (35) into Eq. (6) and neglecting terms of smaller order in the shell energy. The result is

$$\begin{aligned}
 \gamma_{11} &= U_1'(x) - y(s)U_2''(x) - z(s)U_3''(x) \\
 2\gamma_{12} &= \frac{2A_e}{l\bar{c}}c(s)\varphi' + \left[b(s) - \frac{\bar{b}}{c}c(s) \right] U_1' \\
 &\quad - \left[b(s)y(s) - \frac{\bar{b}y}{c}c(s) \right] U_2'' \\
 &\quad - \left[b(s)z(s) - \frac{\bar{b}z}{c}c(s) \right] U_3'' \\
 \gamma_{22} &= 0
 \end{aligned} \tag{37}$$

It is worth noting that the vanishing of hoop stress resultant in Eq. (29) and hoop strain in Eq. (37) should be interpreted as negligible contribution relative to other parameters. The longitudinal strain γ_{11} is a linear function of y and z . This result was adopted as an assumption in the work of Libove (1988).

In deriving Eq. (37), higher order terms associated with $G\varphi''$ in the energy functional have been neglected in comparison with $C \left(\frac{A_e}{l\bar{c}}c\varphi' \right)^2$ as shown in Badir (1992). This is possible if the following inequalities are satisfied

$$\frac{A}{C} \left(\frac{d}{L} \right) \ll 1 \quad \frac{B}{C} \left(\frac{d}{L} \right) \ll 1$$

Constitutive Relationships

Substitute Eq. (37) in the energy density, Eq. (30), and integrate over s to get the energy of 1D beam theory

$$I = \int_0^L \Phi_2 dx - \int P_i u_i dx ds \quad (38)$$

where

$$\begin{aligned} \Phi_2 = & \frac{1}{2} [C_{11}(U_1')^2 + C_{22}(\varphi')^2 + C_{33}(U_3'')^2 + C_{44}(U_2'')^2] \\ & + C_{12}U_1'\varphi' + C_{13}U_1'U_3'' + C_{14}U_1'U_2'' \\ & + C_{23}\varphi'U_3'' + C_{24}\varphi'U_2'' + C_{34}U_2''U_3'' \end{aligned} \quad (39)$$

Explicit expressions for the stiffness coefficients C_{ij} ($i, j = 1, 4$) are given in the Appendix.

The constitutive relationships can be written in terms of stress resultants and kinematic variables by differentiating Eq. (39) with respect to the associated kinematic variable or by relating the traction T , torsional moment M_x , and bending moments M_y and M_z to the shear flow and axial stress as follows

$$\begin{aligned} T &= \frac{\partial \Phi_2}{\partial U_1'} = \oint \int \sigma_{11} d\xi ds = \oint N_{11} ds \\ M_x &= \frac{\partial \Phi_2}{\partial \varphi'} = \oint \int \sigma_{12} r_n(s) d\xi ds = \oint N_{12} r_n(s) ds \\ M_y &= \frac{\partial \Phi_2}{\partial U_3''} = - \oint \int \sigma_{11} z d\xi ds = - \oint N_{11} z(s) ds \\ M_z &= \frac{\partial \Phi_2}{\partial U_2''} = - \oint \int \sigma_{11} y d\xi ds = - \oint N_{11} y(s) ds \end{aligned} \quad (40)$$

The shear flow N_{12} is derived from the energy density in Eq. (31) and the axial stress resultant N_{11} is given by

$$N_{11} = \frac{\partial \Phi_1}{\partial \gamma_{11}} = A(s)\gamma_{11} + B(s)\gamma_{12} \quad (41)$$

and the associated axial and shear stresses are uniform through the wall thickness.

Substitute Eq. (37) into Eqs. (31) and (41) and use Eq. (40) to get

$$\begin{Bmatrix} T \\ M_x \\ M_y \\ M_z \end{Bmatrix} = \begin{bmatrix} C_{11} & C_{12} & C_{13} & C_{14} \\ C_{12} & C_{22} & C_{23} & C_{24} \\ C_{13} & C_{23} & C_{33} & C_{34} \\ C_{14} & C_{24} & C_{34} & C_{44} \end{bmatrix} \begin{Bmatrix} U_1' \\ \varphi' \\ U_3'' \\ U_2'' \end{Bmatrix} \quad (42)$$

Equilibrium Equations

The equilibrium equations can be derived by substituting the displacement field in Eq. (35) into the energy functional in Eq. (10) and using the principle of minimum total potential energy to get

$$\begin{aligned}T' + \oint P_x ds &= 0 \\M_x' + \oint (P_x y - P_y z) ds &= 0 \\M_y'' + (\oint P_x z ds)' + \oint P_z ds &= 0 \\M_z'' + (\oint P_x y ds)' + \oint P_y ds &= 0\end{aligned}\tag{43}$$

where P_x , P_y and P_z are surface tractions along the x , y and z directions, respectively.

One of the member of each of the following four pairs must be prescribed at the beam ends :

$$T \text{ or } U_1, M_x \text{ or } \varphi, M_y \text{ or } U_3', \text{ and } M_z \text{ or } U_2'\tag{44}$$

SUMMARY OF GOVERNING EQUATIONS

The development presented in this work encompasses five equations. The first, is the displacement field given in Eq. (35). Its functional form was determined based on an asymptotical expansion of shell energy. The associated strain field is given in Eq. (37) and the stress resultants in Eqs. (31), (40) and (41). The fourth, are the constitutive relationships in Eq. (42) with the stiffness coefficients expressed as integrals of material properties and cross sectional geometry in Eq. (56) of the Appendix. Finally the equilibrium equations and boundary conditions are given in Eq. (43) and (44), respectively.

In the present development the determination of the displacement field is essential in obtaining accurate expressions for the beam stiffnesses. A comparison of the derived displacement field with results obtained by previous investigators is presented in the following section.

COMPARISON OF DISPLACEMENT FIELDS

The pioneering work of Reissner and Tsai (1972) is based on developing an exact solution to the governing equilibrium, compatibility and constitutive relationships of shell theory. Closed as well as open cross-sections were considered. The derived constitutive relationships are similar to Eq. (42). However, the authors left to the reader the derivation of the explicit expressions for the stiffness coefficients. This may be the reason for their work to have been overlooked. These expressions are important in identifying the parameters controlling the behavior and in performing parametric design studies. Furthermore, the explicit form of the displacement field helps evaluate and understand predictions of other analytical and numerical models.

A number of assumptions were adopted in Reissner and Tsai's development regarding material properties such as neglecting the coupling between in-plane strains and curvatures which can be significant in anisotropic materials. It is important to assess the influence of these assumptions on the accuracy. This has been done in the present work by using an asymptotical expansion of the shell energy and proving that the coupling and curvatures contributions to the energy are small in comparison with the in-plane contribution.

Mansfield and Sobey (1979) and Libove (1988) obtained the beam flexibilities relating the stretching, twisting and bending deformations to the applied axial load, torsional and bending moments for a special origin and axes orientation. They adopted the assumptions of a negligible hoop stress resultant $N_{\theta\theta}$ and a membrane state in the thin-walled beam section. Although they did not refer to the work of Reissner and Tsai (1972), their stiffnesses coincide for the special case outlined in Reissner and Tsai (1972). This special case refers to the one where the classical assumptions of neglecting shear and hoop stresses and considering the shear flow to be constant is adopted. However, one has to carry out the details to show this fact.

The work of Rehfield (1985) has been used in a number of composite applications. Rehfield's displacement field is of the form

$$\begin{aligned} u_1 &= U_1(x) - y(s) [U_2'(x) - 2\gamma_{xy}(x)] - z(s) [U_3'(x) - 2\gamma_{xz}(x)] + g(s, x) \\ u_2 &= U_2(x) - z(s)\varphi(x) \\ u_3 &= U_3(x) + y(s)\varphi(x) \end{aligned} \quad (45)$$

where γ_{xz} and γ_{xy} are the transverse shear strains. The warping function $g(s, x)$ is given as

$$g(s, x) = \bar{G}(s)\varphi'(x) \quad (46)$$

with

$$\bar{G}(s) = 2A_c \frac{s}{l} - \int_0^s r_n(\tau) d\tau \quad (47)$$

A comparison of the displacement fields in Eq. (35) and (45) shows that the warping function in Rehfield's formulation comprises the torsional-related contribution but does not include explicit terms that express the bending-related warping. The torsional warping function $G(s)$ in Eq. (34) is different from the function in Eq. (47). The two expressions coincide when $c = \text{constant}$ that is, when the wall stiffness and thickness are uniform along the cross section circumference.

The torsional warping function in Eq. (47) was modified by Atilgan (1989) and Rehfield and Atilgan (1989) as

$$\hat{G}(s) = \int_0^s \left[\frac{2A_e}{l c_1} c_1 - r_n(\tau) \right] d\tau \quad (48)$$

where

$$c_1 = \frac{1}{A'_{66} - \frac{(A'_{16})^2}{A'_{11}}} \quad (49)$$

and

$$\begin{bmatrix} A'_{11} & A'_{16} \\ A'_{16} & A'_{66} \end{bmatrix} = \begin{bmatrix} A_{11} - \frac{(A_{12})^2}{A_{22}} & A_{16} - \frac{A_{12}A_{26}}{A_{22}} \\ A_{16} - \frac{A_{12}A_{26}}{A_{22}} & A_{66} - \frac{(A_{26})^2}{A_{22}} \end{bmatrix} \quad (50)$$

The A_{ij} in Eq. (50) are the in-plane stiffnesses of Classical Lamination Theory (Jones (1975) and Vinson and Sierakowski (1987)). They are related to the modulus tensor by

$$\begin{aligned} A_{11} &= \langle E^{1111} \rangle, & A_{12} &= \langle E^{1122} \rangle, & A_{22} &= \langle E^{2222} \rangle \\ A_{16} &= \langle E^{1112} \rangle, & A_{26} &= \langle E^{1222} \rangle, & A_{66} &= \langle E^{1212} \rangle \end{aligned}$$

A comparison of the modified torsional warping function in Eq. (48) and $G(s)$ in Eq. (34) shows that they coincide for laminates with no extension-shear coupling ($\langle D^{1112} \rangle = \langle D^{1222} \rangle = 0$, in Eq. (54) of the Appendix). For the case where the through-the-thickness contribution is neglected in Eq. (54), this reduces to $A_{16} = A_{26} = 0$.

The warping function obtained by Smith and Chopra (1990, 1991) for composite box-beams is identical to the expression of Rehfield and Atilgan (1989) and Atilgan (1989) given in Eqs. (46) and (48).

An assessment of all the previous warping expressions can be made by checking whether they reduce to the exact expression for isotropic materials (see, for example,

Megson (1990))

$$\bar{G}(s) = \int_0^s \left[\frac{2A_e}{l c_2} c_2 - r_n(\tau) \right] d\tau \quad (51)$$

with

$$c_2 = \frac{1}{\mu h(s)}$$

where μ is the shear modulus.

For isotropic materials the in-plane coupling b is zero and consequently g_1 , g_2 and g_3 in Eqs. (34) and (36) vanish. That is the warping is torsion-related and reduces to $G(s)\varphi'$. Moreover, the shear parameter c is equal to $\frac{1}{4\mu h(s)}$ and the expressions for $G(s)$ and $\bar{G}(s)$ in Eqs. (34) and (51) coincide.

Rehfield's warping function in Eq. (47) coincides with Eq. (51) when the material properties and the thickness are uniform along the wall circumference. Atilgan's (1989), Rehfield and Atilgan's (1989), and Smith and Chopra's (1991) formulations reduce to Eq. (51) for isotropic materials.

APPLICATIONS

Two special layups: the circumferentially uniform stiffness (CUS) and circumferentially asymmetric stiffness (CAS) have been considered by Atilgan (1989), Rehfield and Atilgan (1989), Hodges *et al.* (1989), Rehfield *et al.* (1990), Chandra *et al.* (1990), and Smith and Chopra (1990, 1991).

CUS Configuration

This configuration produces extension-twist coupling. The axial, coupling and in-plane stiffnesses A , B , and C given in Eq. (53) of the Appendix are constant throughout the cross section, and hence the name circumferentially uniform stiffness (CUS) was adopted by Atilgan (1989), Rehfield and Atilgan (1989), Hodges *et al.* (1989), and Rehfield *et al.* (1990). For a box-beam, the ply lay-ups on opposite sides are of reversed orientation, and hence the name antisymmetric configuration was adopted by Chandra *et al.* (1990), and Smith and Chopra (1990,1991).

Since A , B , and C are constants, the stiffness matrix in Eq. (42), for a centroidal

coordinate system, reduces to

$$\begin{bmatrix} C_{11} & C_{12} & 0 & 0 \\ C_{12} & C_{22} & 0 & 0 \\ 0 & 0 & C_{33} & 0 \\ 0 & 0 & 0 & C_{44} \end{bmatrix}$$

The nonzero stiffness coefficients are given by

$$C_{11} = Al$$

$$C_{12} = BA_e$$

$$C_{22} = \frac{C}{l} A_e^2 \quad (52)$$

$$C_{33} = A \oint z^2 ds - \frac{B^2}{C} \oint z^2 ds$$

$$C_{44} = A \oint y^2 ds - \frac{B^2}{C} \oint y^2 ds$$

For such a case the out-of-plane warping due to axial strain vanishes and g_1 does not affect the response.

CAS Configuration

This configuration produces bending-twist coupling. The stiffness A is constant throughout the cross section. For a box beam, the coupling stiffness, B in opposite members is of opposite sign and hence the name circumferentially asymmetric stiffness (CAS) was adopted by Atilgan(1989), Rehfield and Atilgan(1989), Hodges *et al.*(1989), and Rehfield *et al.*(1990). For a box-beam, the ply lay-ups along the horizontal members are mirror images, and hence the name symmetric configuration was adopted by Chandra *et al.*(1990), and Smith and Chopra(1990,1991). The stiffness C in opposite members is equal. The stiffness matrix, for a centroidal system of axes, reduces to

$$\begin{bmatrix} C_{11} & 0 & 0 & 0 \\ 0 & C_{22} & C_{23} & 0 \\ 0 & C_{23} & C_{33} & 0 \\ 0 & 0 & 0 & C_{44} \end{bmatrix}$$

The nonzero stiffness coefficients are expressed by

$$C_{11} = Al - 2\frac{B_t^2}{C_t}d$$

Table 1: Properties of T300/5208 Graphite/Epoxy

$$\begin{aligned}
 E_{11} &= 21.3 \text{ Msi} \\
 E_{22} &= E_{33} = 1.6 \text{ Msi} \\
 G_{12} &= G_{13} = 0.9 \text{ Msi} \\
 G_{23} &= 0.7 \text{ Msi} \\
 \nu_{12} &= \nu_{13} = 0.28 \\
 \nu_{23} &= 0.5
 \end{aligned}$$

$$\begin{aligned}
 C_{22} &= \frac{C_t}{2 \left[d + a \left(\frac{C_t}{C_v} \right) \right]} A_e^2 \\
 C_{23} &= \frac{B_t}{2 \left[d + a \left(\frac{C_t}{C_v} \right) \right]} A_e^2 \\
 C_{33} &= A \oint z^2 ds - \frac{B_t^2}{2C_t} \left\{ a - \frac{A_e}{\left[d + a \left(\frac{C_t}{C_v} \right) \right]} \right\} A_e \\
 C_{44} &= A \oint y^2 ds - \frac{B_t^2 d^3}{6C_t}
 \end{aligned}$$

Subscripts t and v denote top and vertical members, respectively. The box width and height are denoted by d and a , respectively. For the CAS configuration and with reference to the Cartesian coordinate system in Fig. 1, bending about the y -axis is coupled with torsion while extension and bending about the z -axis are decoupled.

In order to assess the accuracy of the predictions the present theory is applied to the box beam studied by Hodges *et al.* (1989). The cross sectional configuration is shown in Fig. 3 and the material properties in Table 1.

Flexibility Coefficients

A comparison of the flexibility coefficients S_{ij} with the predictions from two models is provided in Table 2. The flexibility coefficients S_{ij} are obtained by inverting the 4×4 matrix in Eq. (42). The NABSA (Nonhomogeneous Anisotropic Beam Section Analysis) is a finite element model based on an extension of the work of Giavotto

Table 2: Comparison of Flexibility Coefficients of NABSA, TAIL and Present (lb,in units)

Flexibility	NABSA	PRESENT	% Diff.	TAIL	% Diff.
$S_{11} \times 10^5$	0.143883	0.14491	+0.7	0.14491	+0.7
$S_{22} \times 10^4$	0.312145	0.32364	+3.6	0.32364	+3.6
$S_{12} \times 10^5$	-0.417841	-0.43010	+2.9	-0.43010	+2.9
$S_{33} \times 10^4$	0.183684	0.1886	+2.6	0.17294	-5.8
$S_{44} \times 10^5$	0.614311	0.63429	+3.2	0.50157	-18.4

Table 3: Geometry and Mechanical Properties of Thin-Walled Beam with $[+12]_4$ CUS square cross-section

Length = 24.0 in.	$E_{11} = E_{22} = E_{33} = 11.65$ Msi
Width = depth = 1.17 in.	$G_{12} = G_{13} = 0.82, G_{23} = 0.7$ Msi
Ply thickness = 0.0075 in.	$\nu_{12} = \nu_{13} = 0.05, \nu_{23} = 0.3$

et al.(1983). In this model all possible types of warping are accounted for. The TAIL model is based on the theory of Rehfield (1985) while neglecting the restrained torsional warping. The predictions of the NABSA and TAIL models are provided by Hodges *et al.*(1989). The percentage differences appearing in Table 2 are relative to the NABSA predictions. The present theory is in good agreement with NABSA. Its predictions show a difference ranging from +0.7 to +3.6 percent while those based on Rehfield's theory (1985) range from +3.6 to -18.4 percent.

The present theory is applied to the prediction of the tip deformation in a cantilevered beam made of Graphite/Epoxy and subjected to different types of loading. The beam has a CUS square cross section with $[+12]_4$ lay-up. The geometry and mechanical properties are given in Table 3. Comparison of results with the MSC/NASTRAN finite element analysis of Nixon (1989) is provided in Table 4. The MSC/NASTRAN analysis is based on a 2D plate model. The predictions of the present theory range from +1.7 to -0.7 percent difference relative to the finite ele-

Table 4: MSC/NASTRAN and Present Solutions for a CUS Cantilevered Beam with $[+12]_4$ Layups Subjected to Various Tip Load Cases

Tip Load	Tip Deformation		% Diff.
	NASTRAN	Present	
Axial Force (100 lb)	Axial Disp. : 0.002189 in.	0.002202 in.	+0.6 %
Axial Force (100 lb)	Twist : 0.3178 deg.	0.32325 deg.	+1.7 %
Torsional Moment (100 lb-in)	Twist : 2.959 deg.	2.998 deg.	+1.32 %
Transverse Force (100 lb)	Deflection : 1.866 in.	1.853 in.	-0.7 %

Table 5: Cantilever Geometry and Properties

Width = 0.953 in.	$E_{11} = 20.59$ Msi, $E_{22} = E_{33} = 1.42$ Msi
Depth = 0.53 in.	$G_{12} = G_{13} = 0.87$ Msi, $G_{23} = 0.7$ Msi
Ply thickness = 0.005 in.	$\nu_{12} = \nu_{13} = 0.42$, $\nu_{23} = 0.5$

ment results.

For a CUS configuration, the extension-torsional response is decoupled from bending. Since C is constant and g_1 does not affect the stiffness coefficients, the flexibility coefficients controlling extension and twist response, S_{11} , S_{12} and S_{22} coincide with those of Atilgan (1989), and Rehfield and Atilgan (1989). As a consequence, the axial displacement and twist angle predictions coincide. However, the lateral deflection under transverse load differs. The tip lateral deflection predicted using the theory of Rehfield (1985), and Atilgan (1989), and Rehfield and Atilgan (1989), is 1.724 inch resulting in -7.6 percentage difference compared to the NASTRAN result.

The test data appearing in the comparisons of Figs. 4-9, are reported by Chandra *et al.* (1990), and Smith and Chopra (1990, 1991). Figures 4 and 5 show the bending slope variation along the beam span for antisymmetric and symmetric cantilevers under a 1 lb transverse tip load. The beam geometry and material properties are given in Table 5. The analytical predictions reported by Chandra *et al.* (1990), and Smith and Chopra (1990, 1991) together with results obtained on the basis of the

analyses of Rehfield (1985), Rehfield and Atilgan (1989), Atilgan (1989), and the present work are combined in Figs. 4 and 5. Results show that the predictions of the present theory are the closest to the test data when compared to the other analytical approaches.

The bending slope in Figs. 4 and 5 is defined in terms of the cross section rotation for theories including shear deformation. For the geometry and material properties considered, this effect is negligible as shown in Figs. 4 and 5 where the spanwise slope at the fixed end predicted by theories with shear deformation, is indistinguishable from zero. The nonzero value shown by the test data may be due to the experimental set up used to achieve clamped end conditions.

The spanwise twist distribution of symmetric cantilevered beam with $[30]_6$ and $[45]_6$ lay-ups is plotted in Figs. 6 and 7, respectively. The beams are subjected to a transverse tip load of 1 lb. Their dimensions and material properties are given in Table 5. Results show that the present theory and the works of Rehfield and Atilgan (1989) and Atilgan (1989) are the closest to the test data. A similar behavior is found for the bending slope and the twist angle at the mid-span of the symmetric cantilevered beams appearing in Figs. 8 and 9. The beams are subjected to a tip torque of 1 lb-in.

CONCLUSION

An anisotropic thin-walled closed section beam theory has been developed based on an asymptotical analysis of the shell energy functional. The displacement field is not assumed a priori and emerges as a result of the analysis. In addition to the classical out-of-plane torsional warping, two new contributions are identified namely, axial strain and bending warping. A comparison of the derived governing equations confirms the theory developed by Reissner and Tsai. In addition, explicit closed-form expressions for the beam stiffness coefficients, the stress and displacement fields are provided. The predictions of the present theory have been validated by comparison with finite element simulation, other closed form analyses and test data.

ACKNOWLEDGMENT

This work was supported by the NASA Langley Research Center under grant NAG-1-637. This support is gratefully acknowledged.

REFERENCES

Atilgan, Ali Rana, "Towards A Unified Analysis Methodology For Composite Rotor Blades," *Ph. D. Dissertation*, School of Aerospace Engineering, Georgia Institute of Technology, August 1989.

Armanios, Erian, Badir, Ashraf, and Berdichevsky, Victor, "Effect of Damage on Elastically Tailored Composite Laminates," *Proceedings of the AHS International Technical Specialists' Meeting on Rotorcraft Basic Research*, Georgia Institute of Technology, Atlanta, Georgia, March 25-27, 1991, pp. 48(1)-48(11).

Badir, Ashraf M., "Analysis of Advanced Thin-Walled Composite Structures," *Ph. D. Dissertation*, School of Aerospace Engineering, Georgia Institute of Technology, February 1992.

Berdichevsky, V. L., and Misiura, V., "Effect of Accuracy Loss in Classical Shell Theory," *Journal of Applied Mechanics*, December 1991.

Chandra, R., Stemple, A. D., and Chopra, I., "Thin-walled Composite Beams under Bending, Torsional, and Extensional Loads," *Journal of Aircraft*, Vol. 27, No. 7, July 1990, pp. 619-626.

Crandall, Stephen H., Dahl, Norman C., and Lardner, Thomas J., *An Introduction to the Mechanics of Solids*, McGraw-Hill Book Company, 1978.

Giavotto, V., Borri, M., Mantegazza, P., Ghiringhelli, G., Carmashi, V., Maffioli, G.C., and Mussi, F., "Anisotropic Beam Theory and Applications," *Computers and Structures*, Vol. 16, No. 1-4, pp. 403-413, 1983.

Gjelsvik, Atle, *The Theory of Thin Walled Bars*, John Wiley & Sons, 1981.

Hodges, D. H., "Review of Composite Rotor Blade Modeling," *AIAA Journal*, Vol. 28, No. 3, 1990, pp. 561-565.

Hodges, D. H., Atilgan A. R., Fulton M. V., and Rehfield L. W., "Dynamic Characteristics of Composite Beam Structures," *Proceedings of the AHS National Specialists' Meeting on Rotorcraft Dynamics*, Fort Worth, Texas, Nov. 13-14, 1989.

Jones, R. M., *Mechanics of Composite Materials*, McGraw Hill Book Co., New York, 1975, p. 163.

Koiter, W. T., "A Consistent First Approximation in the General Theory of Thin Elastic Shells," *Proc. IUTAM Symp on the Theory of Thin Shells*, Delft, August 1959, 12-33, North-Holland Publ. Amsterdam, 1960, Edited by W. T. Koiter.

Kosmatka, J. B., "Extension-Bend-Twist Coupling Behavior of Thin-Walled Advanced Composite Beams with Initial Twist," *Proceedings of the 32nd AIAA/ASME/AHS/ASC Structures, Structural Dynamics and Materials Conference*, Baltimore, Maryland, April 8-10, 1991, pp. 1037-1049.

Libai, A., and Simmonds, J. G., *The Nonlinear Theory of Elastic Shells : One Spatial Dimension*, Academic Press, Inc., 1988.

Libove, C., "Stresses and Rate of Twist in Single-Cell Thin-Walled Beams with Anisotropic Walls," *AIAA Journal*, Vol. 26, No. 9, September 1988, pp. 1107-1118.

Mansfield, E. H., and Sobey, A. J., "The Fibre Composite Helicopter Blade - Part 1: Stiffness Properties - Part 2: Prospect for Aeroelastic Tailoring," *Aeronautical Quarterly*, Vol. 30, May 1979, pp. 413-449.

Megson, T. H. G., *Aircraft Structures for Engineering Students*, Second Edition, Halsted Press, 1990.

Nixon, M.W., "Analytical and Experimental Investigations of Extension-Twist-Coupled Structures," M.Sc. Thesis, George Washington University, May 1989.

Rehfield, L. W., "Design Analysis Methodology for Composite Rotor Blades," *Proceedings of the Seventh DoD/NASA Conference on Fibrous Composites in Structural Design*, AFWAL-TR-85-3094, June 1985, pp. (V(a)-1)-(V(a)-15).

Rehfield, L. W., and Atilgan, A. R., "Shear Center and Elastic Axis and Their Usefulness for Composite Thin-Walled Beams," *Proceeding of The American Society For Composites*, Fourth Technical Conference, Blacksburg, Virginia, October 3-5, 1989, pp. 179-188.

Rehfield, L. W., Atilgan, A. R., and Hodges, D. H., "Nonclassical Behavior of Thin-Walled Composite Beams with Closed Cross Sections." *Journal of the American Helicopter Society*, Vol. 35, (2), April 1990, pp. 42-50.

Reissner E., and Tsai, W. T., "Pure Bending, Stretching, and Twisting of Anisotropic Cylindrical Shells," *Journal of Applied Mechanics*, Vol. 39, March 1972, pp. 148-154.

Sanders, J. L., "An Improved First-Approximation Theory for Thin Shells," *NASA - TR - R24*, 1959.

Smith, Edward C., and Chopra Inderjit, "Formulation and Evaluation of an Analytical Model for Composite Box-Beams," *Proceedings of the 31st AIAA/ASME/AHS/ASC Structures, Structural Dynamics and Materials Conference*, Long Beach, California, April 2-4,1990, pp. 759-782.

Smith, Edward C., and Chopra Inderjit, "Formulation and Evaluation of an Analytical Model for Composite Box-Beams," *Journal of The American Helicopter Society*, July 1991, pp. 23-35.

Sokolnikoff, I. S., *Mathematical Theory of Elasticity*, McGraw-Hill, New York, 1956.

Timoshenko, S., and Goodier, J. N., *Theory of Elasticity*, McGraw-Hill, New York, 1951.

Vinson, J. R., and Sierakowski, R. L., *The Behavior of Structures Composed of Composite Materials*, Martinus Nijhoff Publishers, 1987., p.54.

Washizu, K., *Variational Methods in Elasticity and Plasticity*, Pergamon, New York, 1968.

Wempner, G., *Mechanics of Solids with Applications to Thin Bodies*, Sijthoff & Noordhoff International Publishers, 1981.

APPENDIX

In this appendix explicit expressions for some of the relevant variables used in the development as well as the stiffnesses C_{ij} ($i, j = 1, 4$) in Eq. (42) are provided.

The three stiffness parameters A , B and C in Eq. (30) are expressed in terms of the Hookean tensor E^{ijkl} as follows

$$\begin{aligned}
 A(s) &= \langle D^{1111} \rangle - \frac{(\langle D^{1122} \rangle)^2}{\langle D^{2222} \rangle} \\
 B(s) &= 2 \left(\langle D^{1112} \rangle - \frac{\langle D^{1122} \rangle \langle D^{1222} \rangle}{\langle D^{2222} \rangle} \right)
 \end{aligned}
 \tag{53}$$

$$C(s) = 4 \left(\langle D^{1212} \rangle - \frac{(\langle D^{1222} \rangle)^2}{\langle D^{2222} \rangle} \right)$$

The 2D Young's moduli $D^{\alpha\beta\gamma\delta}$ are given by

$$D^{\alpha\beta\gamma\delta} = E^{\alpha\beta\gamma\delta} - \frac{E^{\alpha\beta 33} E^{\gamma\delta 33}}{E^{3333}} - H_{\mu\lambda} G^{\alpha\beta\mu} G^{\gamma\delta\lambda} \quad (54)$$

where

$$G^{\alpha\beta\mu} = E^{\alpha\beta\mu 3} - \frac{E^{\alpha\beta 33} E^{\mu 333}}{E^{3333}}$$

and $H_{\mu\lambda}$ are components of the inverse of the 2D matrix $\left\| E^{\mu 3\lambda 3} - \frac{E^{\mu 333} E^{\lambda 333}}{E^{3333}} \right\|$.

Combining Eq. (34) and (53) the variables b and c can be written as

$$b(s) = - \frac{\langle D^{1112} \rangle - \frac{\langle D^{1122} \rangle \langle D^{1222} \rangle}{\langle D^{2222} \rangle}}{\langle D^{1212} \rangle - \frac{(\langle D^{1222} \rangle)^2}{\langle D^{2222} \rangle}}$$

and

$$c(s) = \frac{1}{4 \left(\langle D^{1212} \rangle - \frac{(\langle D^{1222} \rangle)^2}{\langle D^{2222} \rangle} \right)} \quad (55)$$

where the pointed brackets denote integration over the thickness as defined in Eq. (9).

Expressions for the stiffness coefficients C_{ij} ($i, j = 1, 4$) in terms of the cross section geometry and materials properties are as follows

$$\begin{aligned} C_{11} &= \oint \left(A - \frac{B^2}{C} \right) ds + \frac{[\oint (B/C) ds]^2}{\oint (1/C) ds} \\ C_{12} &= \frac{\oint (B/C) ds}{\oint (1/C) ds} A_e \\ C_{13} &= - \oint \left(A - \frac{B^2}{C} \right) z ds - \frac{\oint (B/C) ds \oint (B/C) z ds}{\oint (1/C) ds} \\ C_{14} &= - \oint \left(A - \frac{B^2}{C} \right) y ds - \frac{\oint (B/C) ds \oint (B/C) y ds}{\oint (1/C) ds} \\ C_{22} &= \frac{1}{\oint (1/C) ds} A_e^2 \\ C_{23} &= - \frac{\oint (B/C) z ds}{\oint (1/C) ds} A_e \end{aligned} \quad (56)$$

$$C_{24} = -\frac{\oint (B/C)yds}{\oint (1/C)ds} A_e$$

$$C_{33} = \oint \left(A - \frac{B^2}{C} \right) z^2 ds + \frac{[\oint (B/C)zds]^2}{\oint (1/C)ds}$$

$$C_{34} = \oint \left(A - \frac{B^2}{C} \right) yz ds + \frac{\oint (B/C)yds \oint (B/C)zds}{\oint (1/C)ds}$$

$$C_{44} = \oint \left(A - \frac{B^2}{C} \right) y^2 ds + \frac{[\oint (B/C)yds]^2}{\oint (1/C)ds}$$

Figure Legend:

Figure 1: Cartesian Coordinate System

Figure 2: Curvilinear Coordinate System

Figure 3: Beam Cross Section

Figure 4: Bending Slope of an Anti-Symmetric $[15]_6$ Cantilever Under 1 lb Transverse Tip Load

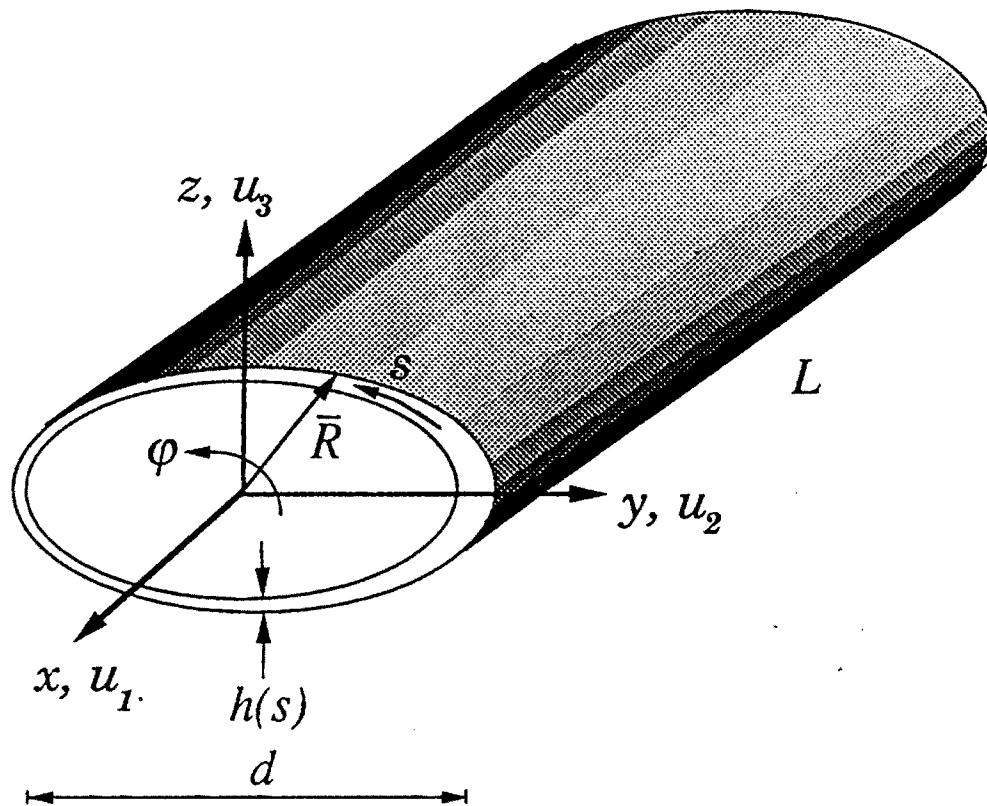
Figure 5: Bending Slope of a Symmetric $[30]_6$ Cantilever Under 1 lb Transverse Tip Load

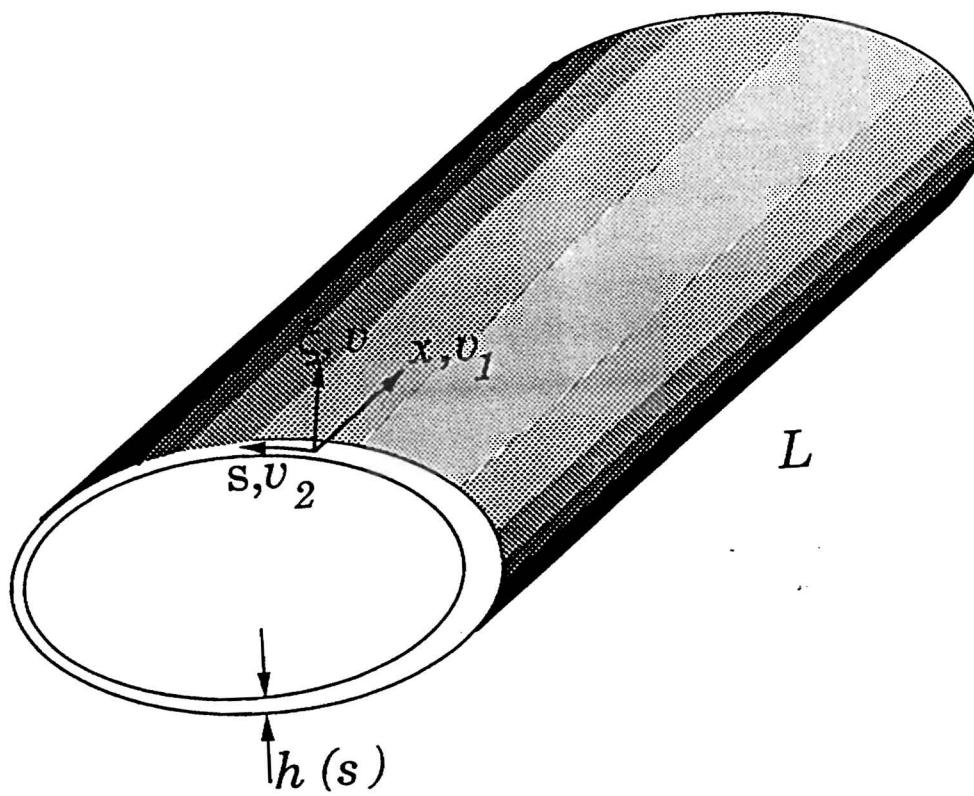
Figure 6: Twist of a Symmetric $[30]_6$ Cantilever Under 1 lb Transverse Tip Load

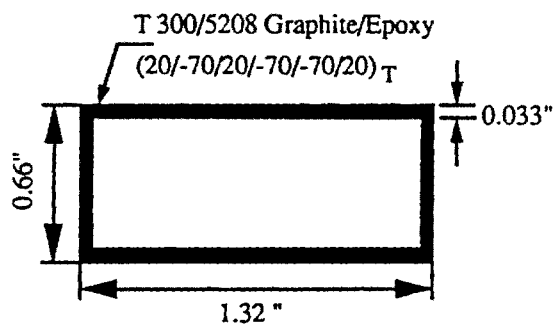
Figure 7: Twist of a Symmetric $[45]_6$ Cantilever Under 1 lb Transverse Tip Load

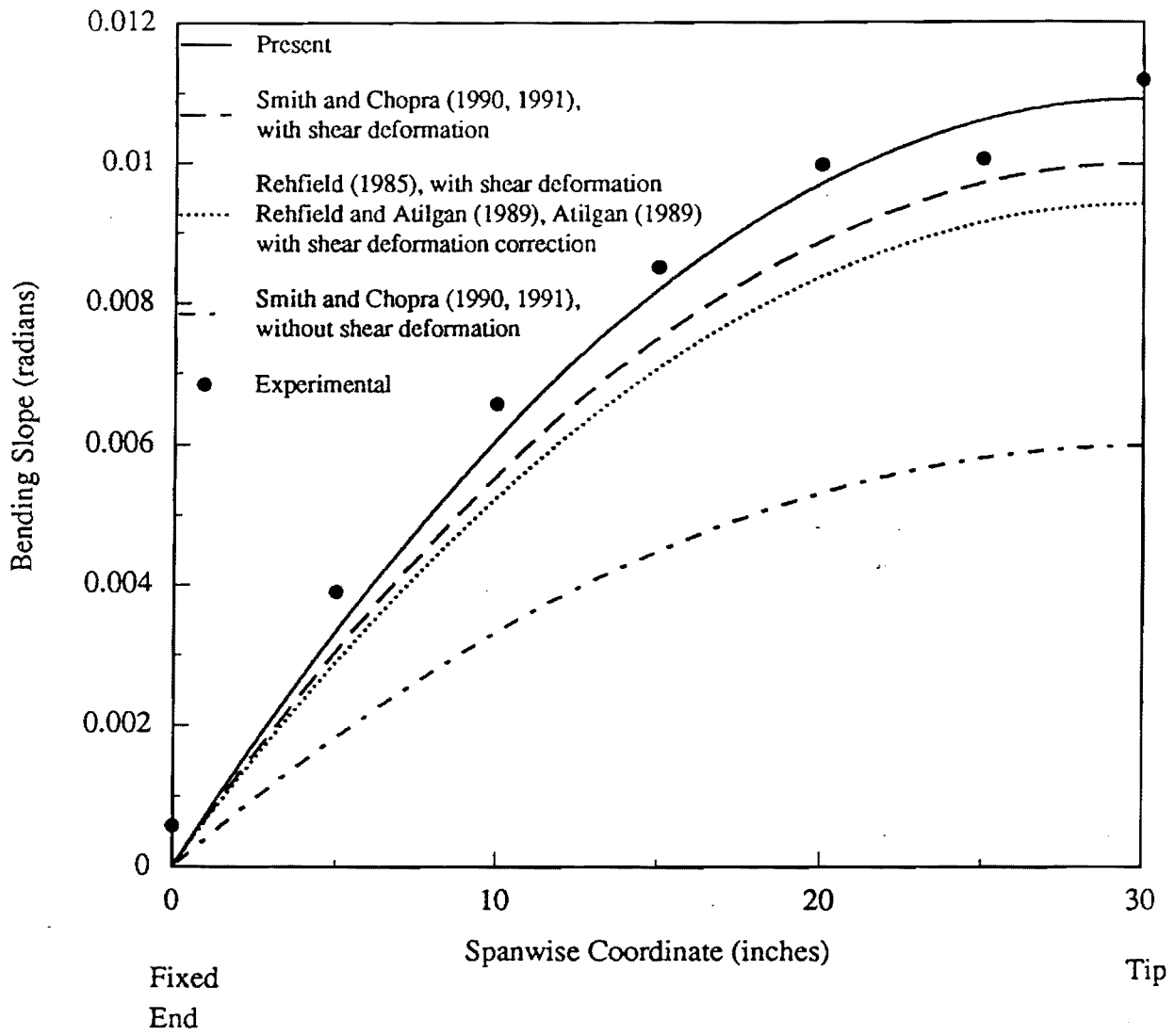
Figure 8: Bending slope at mid-span under unit tip torque of Symmetric lay-up Cantilever beams

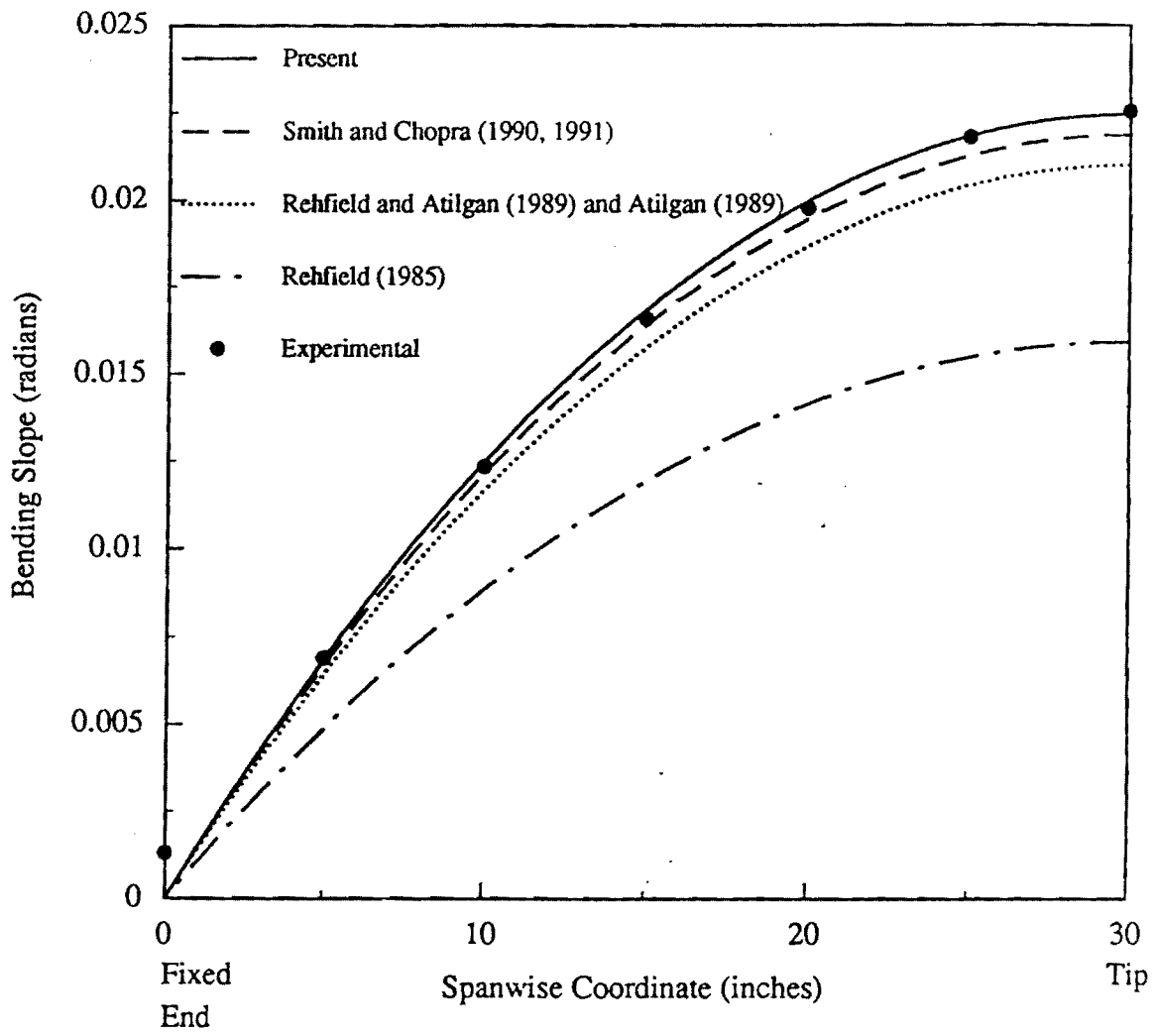
Figure 9: Twist at mid-span under unit tip torque of Symmetric lay-up Cantilever beams

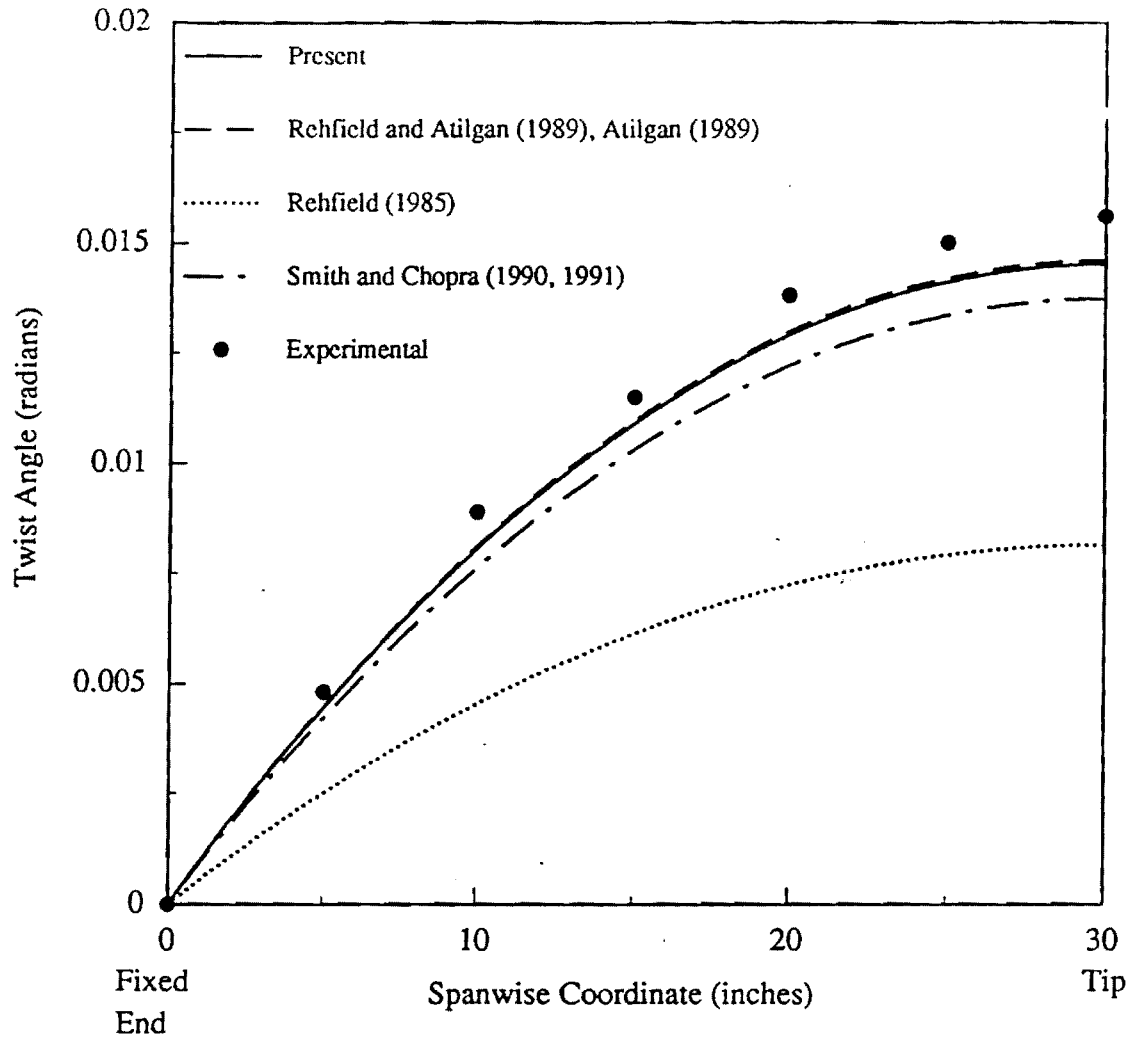


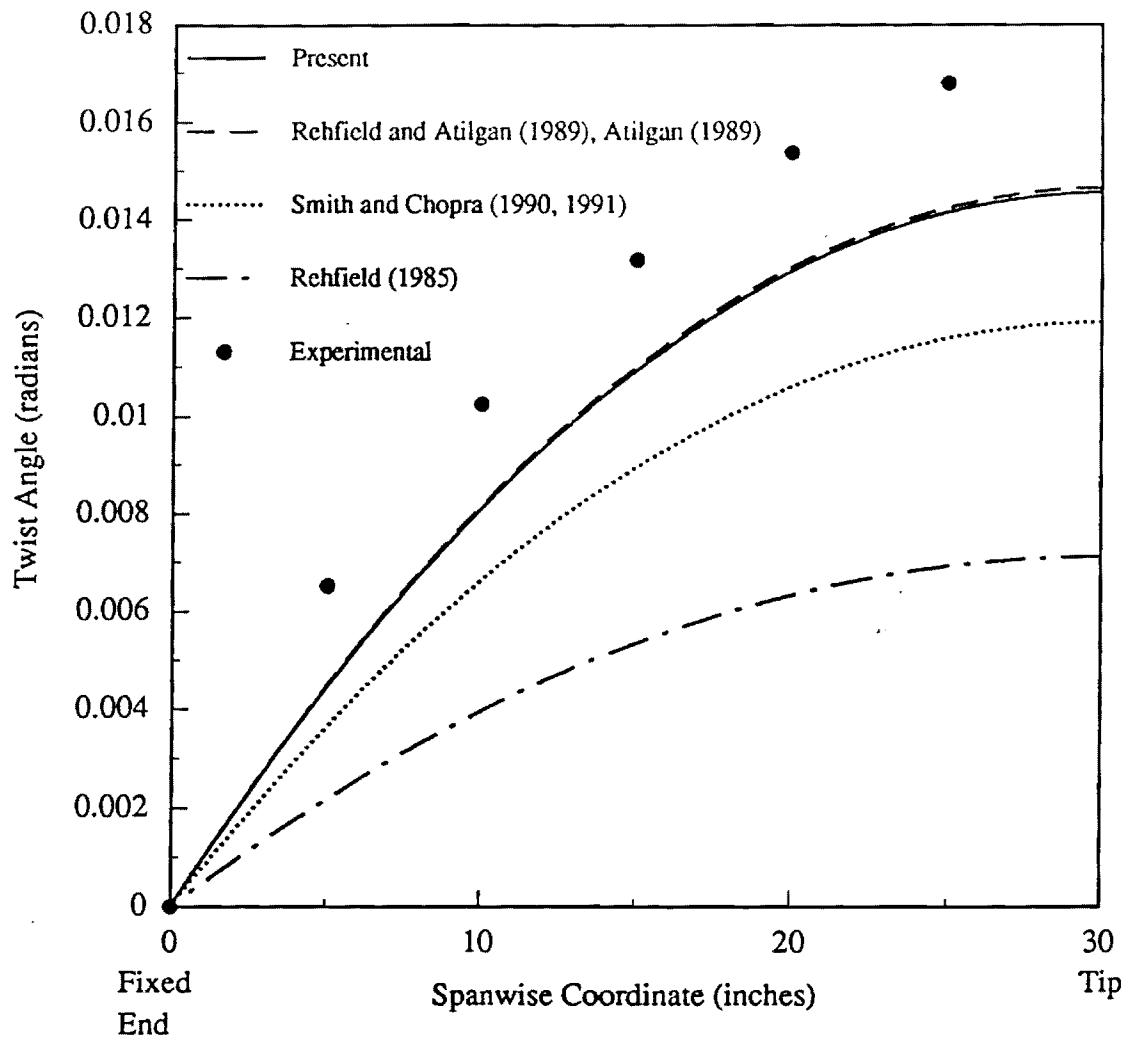


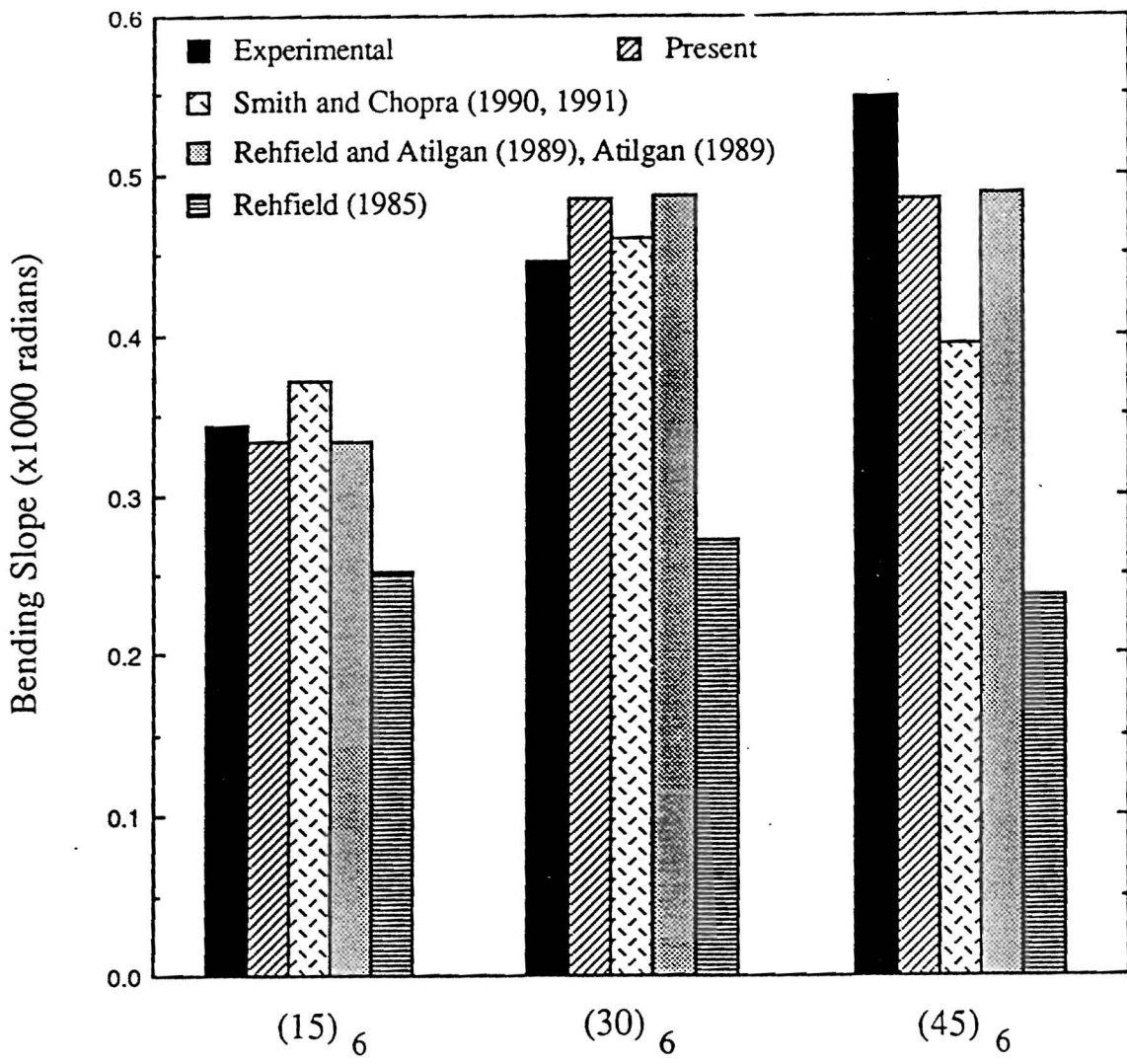


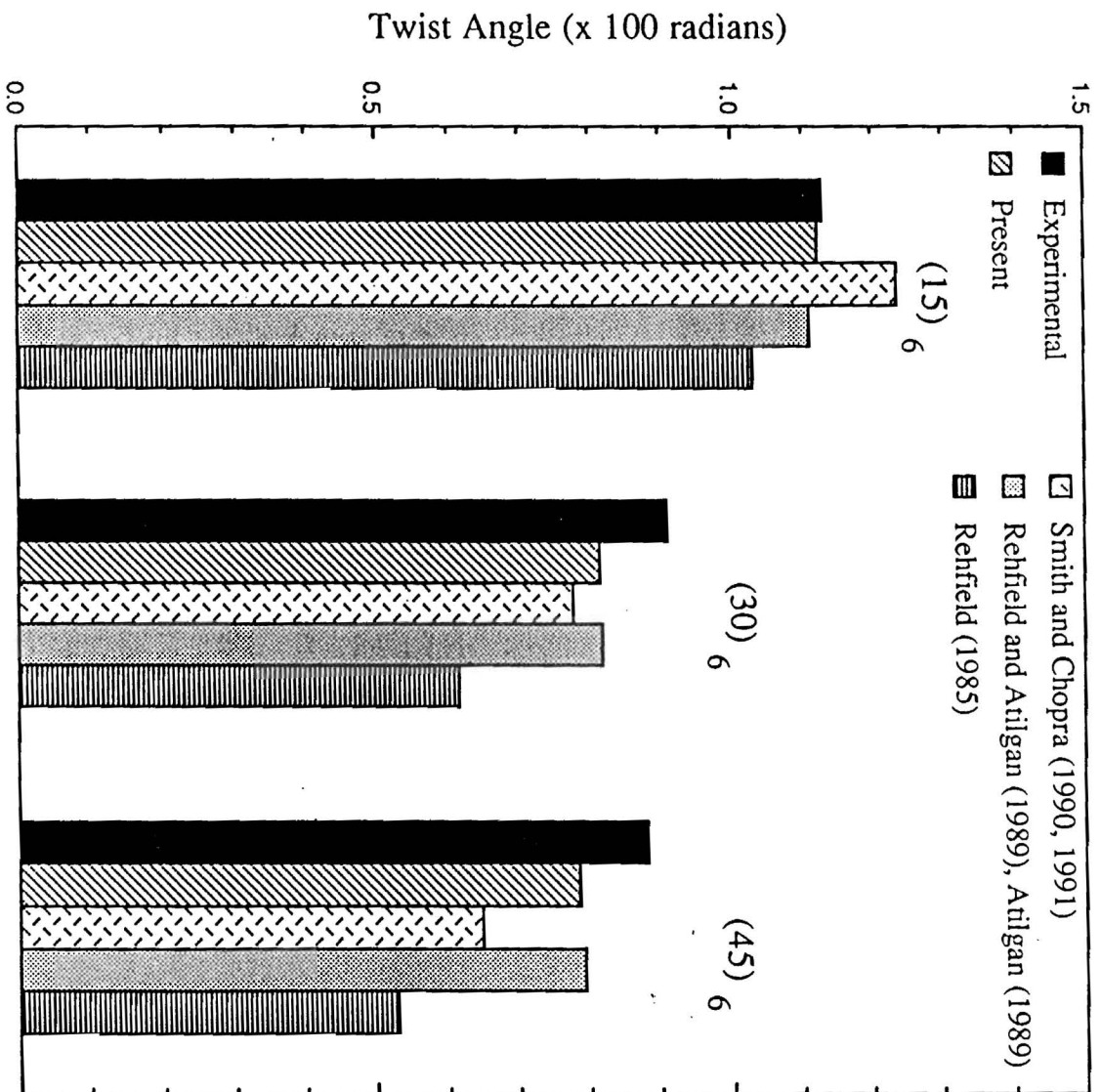












E. Armanios

**ANALYSIS OF DELAMINATION RELATED FRACTURE
PROCESSES IN COMPOSITES**

Erian A. Armanios

**School of Aerospace Engineering
Georgia Institute of Technology
Atlanta, Georgia 30332-0150**

**Preliminary Final Report
NASA Grant NAG-1-637**

**ANALYSIS OF DELAMINATION RELATED FRACTURE
PROCESSES IN COMPOSITES**

Erian A. Armanios

**School of Aerospace Engineering
Georgia Institute of Technology
Atlanta, Georgia 30332-0150**

**Preliminary Final Report
NASA Grant NAG-1-637**

INTRODUCTION

The work described herein was performed at the School of Aerospace Engineering, Georgia Institute of Technology during the period 12 February 1986 - September 1988. Professors Erian A. Armanios and Lawrence W. Rehfield were the Principal Investigators.

This research concerns the analysis and prediction of delamination damage that occur in composite structure on the on the sublaminar scale --that is the scale of individual plies or groups of plies. The objective have been to develop analytical models for mixed-mode delamination in composites. These includes:

- (1) the influence of residual thermal and moisture strains
- (2) local or transverse crack tip delamination originating at the tip of transverse matrix cracks
- (3) delamination in tapered composite under tensile loading.

Computer codes based on the analytical models in (1) and (2) have been developed and comparisons of predictions with available experimental and analytical results in the literature have been performed. A simple analysis for item (3) has been developed and comparisons of predictions with finite element simulation is underway.

The usual approach to dealing with localized phenomena is large scale numerical simulation and analysis, mostly by general purpose finite element codes. This approach is often supplemented by a "build and test" demonstration, or series of demonstrations if repeated failures are encountered. While such approaches are often costly and inefficient, their major drawback is that fundamental principles are not discovered which provide the means to produce better results. Furthermore, the steps must be repeated all over again the next time a similar situation arises.

Overview of the Research

The research program can be separated into three elements: The influence of residual thermal and moisture stresses on the mixed-mode edge delamination of composites. The analyses of transverse crack-tip delamination and delamination analysis in tapered laminates under tensile loading. A detailed account of the analysis and applications of each element is provided in Appendices I through III. A brief description and summary of the major findings of each research element is presented in the following sections.

Influence of Hygrothermal Stresses

The sublaminar edge delamination analysis and code which had its origin in the research conducted under the earlier grant NAG-1-558 has been modified to include the effects of hygrothermal stresses.

The model is applied to mixed mode edge delamination specimens made of T300/5208 graphite/epoxy material. Residual thermal and moisture stresses significantly influenced the strain energy release rate and interlaminar stresses. Both experienced large increases when thermal conditions were added to the mechanical strains. These effects were alleviated when moisture stresses were included. Thermal effects on the interlaminar shear stress and total energy release rate were totally alleviated for the same specific moisture content. Moreover, this value of moisture content was not significantly affected by the stacking sequence for the laminates considered. This work is presented in accomplishments 3,4 and 12. A complete derivation of the analytical model, Fortran program listing and applications are provided in an accomplishment 3 and Appendix I.

Transverse Crack Tip Analysis

Transverse crack tip delaminations originate at the tip of transverse matrix cracks. This situation appears in Figure 1 where a symmetric laminate made of 90° plies in the core region and angle plies in the top and bottom portions is subjected to a tensile loading. Under tensile loading transverse

matrix cracks initiate in the core region reaching a saturation level at a crack spacing denoted by λ in the figure. Delamination often initiate at the tip of these transverse cracks. This situation is depicted in the generic model shown in Figure 1 of a symmetric delamination growing from a transverse crack tip.

Three analytical models, sublaminar shear, membrane and shear lag have been developed in order to estimate the saturated crack spacing distance. The saturation crack spacing corresponds to the distance from the crack where the broken plies regain their uniform stress/strain state i.e. where the interlaminar shear stress has decayed down to its far field (uniform) value. Based on the closed form expression for the interlaminar shear stress the crack spacing predicted by each model is presented in Table I. The experimental result in the table is based on Reifsnider's work for a $[0/90]_S$ laminate. A complete derivation of these models is provided in Appendix II.

The analysis of transverse crack tip delamination is presented in Appendix II and applied to $[\pm 25/90_n]_S$ laminates in the range $n=0.5$ to 8 made of T300/934 graphite/epoxy material. Closed form expressions for the interlaminar stresses, total strain energy release rate and energy release rate components are obtained. A computer code based on this analysis is developed and implemented into an earlier mixed-mode edge delamination code developed under the previous NASA grant NAG-1-558 and presented in accomplishment 6 and 7. This code was used to estimate the critical strain levels and the associated delamination damage mode with increasing number of 90° plies in the $[\pm 25/90_n]_S$. Since mid-plane edge delamination is a possible damage mode in this type of laminates a mid-plane delamination analysis was developed and presented in accomplishment 10. A computer code based on this analysis is developed and implemented in the mixed-mode edge delamination code. The critical strain and associated delamination damage modes predicted appear in Figure 2 and Table II. The critical stresses and associated delamination damage mode are provided in Table III.

Experimental results show that the local (crack tip) delamination phenomenon is the predominant damage mode only for $n=4, 6$ and 8 specimens. For $n < 4$ edge delamination either in the mid-plane or in the 25/90 interface were observed in tests. The present analysis predicts mid-plane edge delamination for $n=1/2$ and 1 and mixed mode edge delamination for $n=2$ and 3 , respectively. For $n=4, 6$ and 8 local delaminations are predicted to be the controlling damage mode with approximately 25 percent Mode II for the three specimens. The critical strains in Figure 2 and Table II are computed based on a fracture toughness values of 415 J/m^2 , 140 J/m^2 and 120 J/m^2 for local delamination, mixed mode edge delamination and mid-plane edge delamination, respectively. A complete account of this work appears in Appendix II.

Analysis of Tapered Composites

A generic configuration of a tapered laminated composite is shown in Figure 3 where a 38 ply thick laminate is reduced to 26 ply by dropping three inner sets of plies. The basic analysis approach that is adopted utilizes two levels of modeling, a global scale and a local scale. The global scale is concerned with overall generalized forces and strains such as axial force and extension. A simple consistent deformation assumption is the foundation of this model. Global equilibrium equations are written and solved.

The generalized strains determined from the global analysis serve to provide estimates for the key primary stresses in the belt of the tapered section. Local estimates of interlaminar stresses are determined on the basis of equilibrium condition.

The total strain energy release rate is computed from the work done by the external applied loads. The work done by the external forces is based on the axial stiffness of the different elements in the tapered configurations. These elements are represented by the six sublaminates shown in Figure 4 where A_B denote the effective axial stiffness of the uncracked belt portion, A_{B1} the effective axial stiffness of the cracked belt portion. The uncracked belt portion in the tapered region makes an angle β with the loading axis while the

cracked portion makes an angle α due to delaminations along the taper and the uniform regions. These are denoted by a and b in Figure 4. The effective axial stiffness of the uncracked and cracked dropped plies are denoted by A_u and A_c respectively. The axial stiffness of the straight portion is denoted by A_s for the belt and A_f for the core plies.

The extent of delamination along the tapered and the uniform portion of the laminate has a significant influence on the axial stiffnesses A_u , A_c and A_{B1} . This is due to the discrete number of ply drops in the core region as illustrated in Figure 5 and the pop-off of the delaminated belt region.

A three-dimensional transformation is required in order to estimate the effective axial stiffness of the belt regions A_B and A_{B1} . This is due to the belt layup and the orientation of the different belt portions to the loading axis as shown in Figure 6.

The interlaminar stresses between the belt and the core plies are predicted by considering the equilibrium of the belt region. The equilibrium equations are derived using a complementary potential energy formulation of the belt on an elastic foundation. The elastic foundation is made of two contributions. The first, is a continuous shear restraint provided by the resin pocket regions at the interface between the belt and the inner core plies. The second, is a discrete number of concentrated transverse normal (R_i) and shear (T_i) forces at the ply drop locations as shown in figure 7 for $i=1-4$. The distributed shear stiffness is denoted by G in Figure 8 while the transverse normal and shear stiffnesses at the ply drop locations are denoted by k_i and g_i ($i=1-4$), respectively.

The variation of the total strain energy release rate G with delamination a growing along the tapered region appears in Figure 9. The effect of delamination b along the uniform portion on a is also shown in the figure. The discrete jumps at a/h equal 20 and 40 correspond to the ply drop. A plot of the concentrated transverse normal and shear forces and the interface between the belt and the inner core appears in Figure 10.

A detailed description of the analysis, closed form expressions for the total energy release rate and interlaminar stresses is provided in Appendix III. Additional refinements are planned within this general framework such as accounting for shear strains in the belt and increasing the number of sublaminar elements in the analysis.

ACCOMPLISHMENTS

Publications

1. Armanios, E.A. and Rehfield, L.W., "Interlaminar Analysis of Laminated Composites Using a Sublaminar Approach," Proceedings of the AIAA/ASME/ASCE/AHS 27th Structures, Structural Dynamics, and Materials (SDM) Conference, San Antonio, Texas, 19-21 May, 1986. AIAA Paper No. 86-0969CP, Part 1, pp. 442-452.
2. Rehfield, L.W., Armanios, E.A. and Weinstein, F., "Analytical Modeling of Interlaminar Fracture in Laminated Composites," Composites '86: Recent Advances in Japan and the United States, Proceedings of the Third Japan-U.S. Conference on Composite Materials, K. Kawata, S. Umekawa, and A. Kobayashi Eds., 1986 pp. 331-340.
3. Mahler, M.A., "A Study on the Thermal and Moisture Influences on the Free-edge Delamination of Laminated Composites," Special Problem in Partial Fulfillment for M. Sc., School of Aerospace Engineering, Georgia Institute of Technology, September, 1987.
4. Armanios, E.A. and Mahler, M.A., "Residual Thermal and Moisture Influences on the Free-Edge Delamination of Laminated Composites," Proceedings of the AIAA/ASME/ASCE/AHS 29th Structures, Structural Dynamics and Materials (SDM) Conference, Part 1, pp. 371-381, 1988.
5. Armanios, E.A. and Rehfield, L.W., "Interlaminar Fracture Analysis of Composite Laminates Under Bending and Combined Bending and Extension," Composite Materials: Testing and Design (Eighth Conference), ASTM STP 972, J. D. Whitcomb, Eds., American Society for Testing and Materials, Philadelphia, 1988, pp. 81-94.

Publications Pending

6. Armanios, E.A. and Rehfield, L.W., "Sublaminar Analysis of Interlaminar Fracture in Composites: Part I-Analytical Model," Journal of Composites Technology and Research, July, 1988.
7. Armanios, E.A., Rehfield, L.W., Raju, I.S. and O'Brien, T.K., "Sublaminar Analysis of Interlaminar Fracture in Composites: Part II - Applications," Journal of Composites Technology and Research, July, 1988.
8. Armanios, E.A. and Rehfield, L.W., "A Simplified Approach to Strain Energy Release Rate Computations for Interlaminar Fracture of Composites," Composites '88: Recent Advances in Japan and the United States, Proceedings of the Fourth Japan - U.S. Conference on Composite Materials.
9. Sriram, P. and Armanios, E.A., "Fracture Analysis of Local Delaminations in Laminated Composites," to appear in the proceedings of the AIAA/ASME/ASCE/AHS/ASC 30th Structures, Structural Dynamics and Materials (SDM) Conference, April, 1989.
10. Armanios, E.A., Sriram, P. and Badir, A., "Sublaminar Analysis of Mode I Edge Delamination in Laminated Composites," to appear in the proceedings of the AIAA/ASME/ASCE/AHS/ASC 30th Structures, Structural Dynamics and Materials (SDM) Conference, April, 1989.

Presentations

11. Armanios, E.A. and Mahler, M.A., "Residual Thermal and Moisture Influences on the Free-edge Delamination of Laminated Composites," presented at the 29th Structures, Structural Dynamics and Materials (SDM) Conference, Williamsburg, VA, April 18-20, 1988.

Table I Comparison of Transverse Crack Spacing

Model		Saturated Crack Spacing (mm)
Shear	2 Sublaminates	1.651
	4 sublaminates, $a \rightarrow 0$	1.105
Membrane		1.004
Shear Lag		1.160
Experimental		1.131

Table II Critical Strains and Associated Delamination Damage Modes

Critical Strains (%)

Number of 90° plies	Experimental	Local Delamination	Edge Delamination	
			Mixed Mode	Mid-Plane
1/2	0.6058	1.6747	0.6819	0.6058
1	0.5936	1.1685	0.6262	0.5677
2	0.5934	0.8058	0.5964	0.6402
3	0.5934	0.6427	0.5862	0.7582
4	0.5369	0.5444	0.5810	0.8815
6	0.3914	0.4264	0.5757	1.1133
8	0.3589	0.3555	0.5731	1.3199

Table III Critical Stresses and Associated Delamination Damage Modes

Critical Stresses (MPa)

Number of 90° plies	Experimental	Local Delamination	Edge Delamination	
			Mixed Mode	Mid-Plane
1/2	438	1313.9	535.0	475.3
1	409	784.0	420.1	380.9
2	324	426.2	315.4	338.6
3	270	285.1	260.1	336.4
4	211	210.6	224.7	341.0
6	128	134.7	181.8	351.6
8	94.4	97.1	156.6	360.5

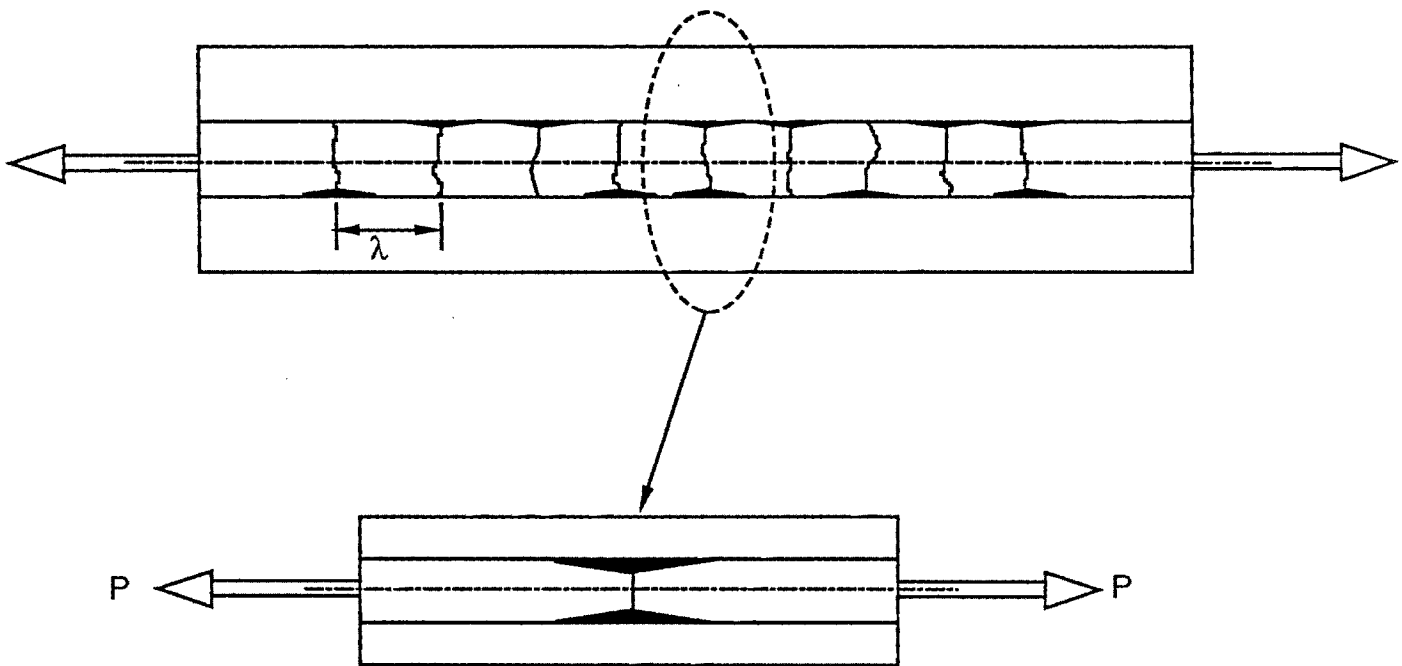


Fig. 1 Generic Crack-tip Delamination

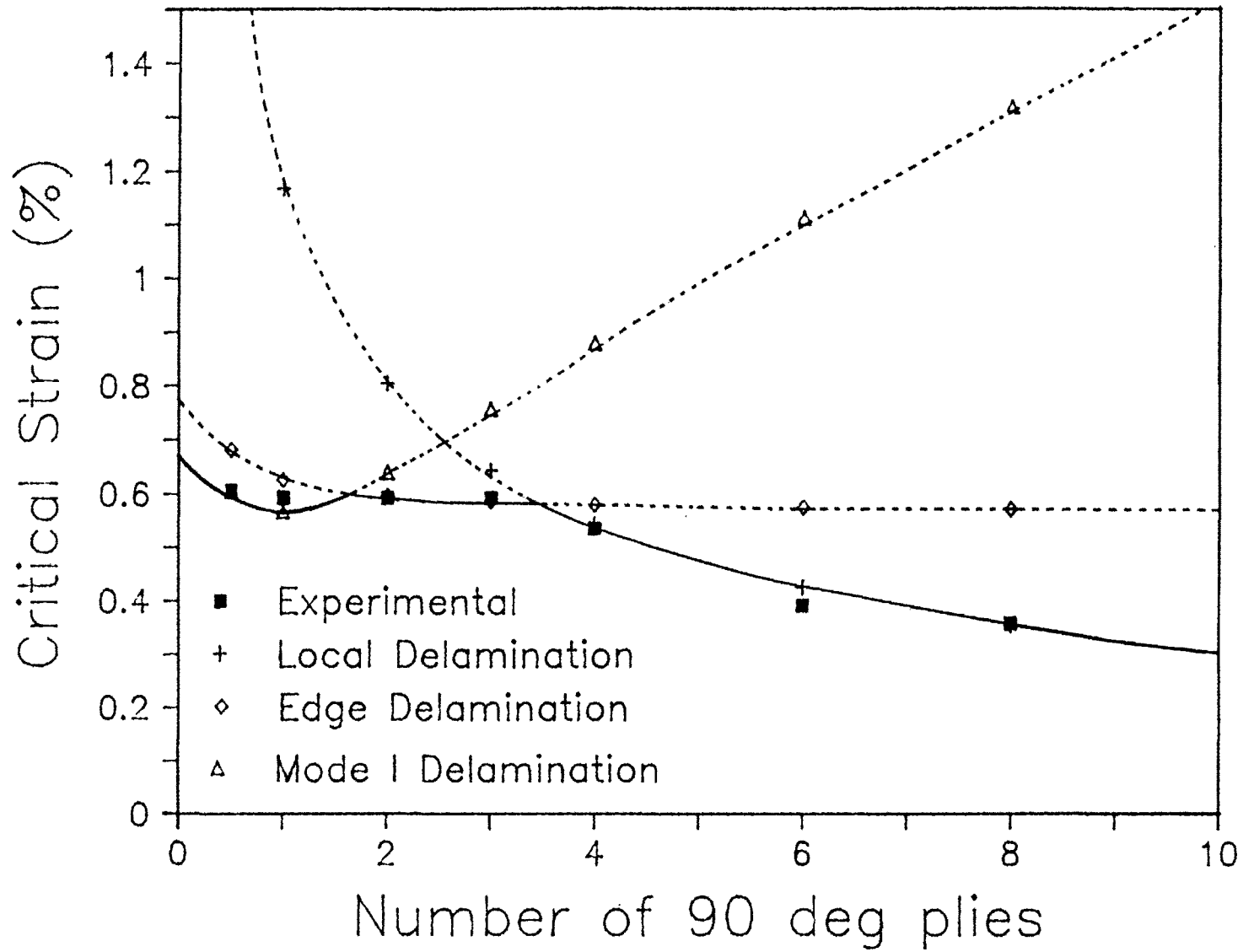


Fig. 2 Critical Strains and Associated Delamination Damage Modes

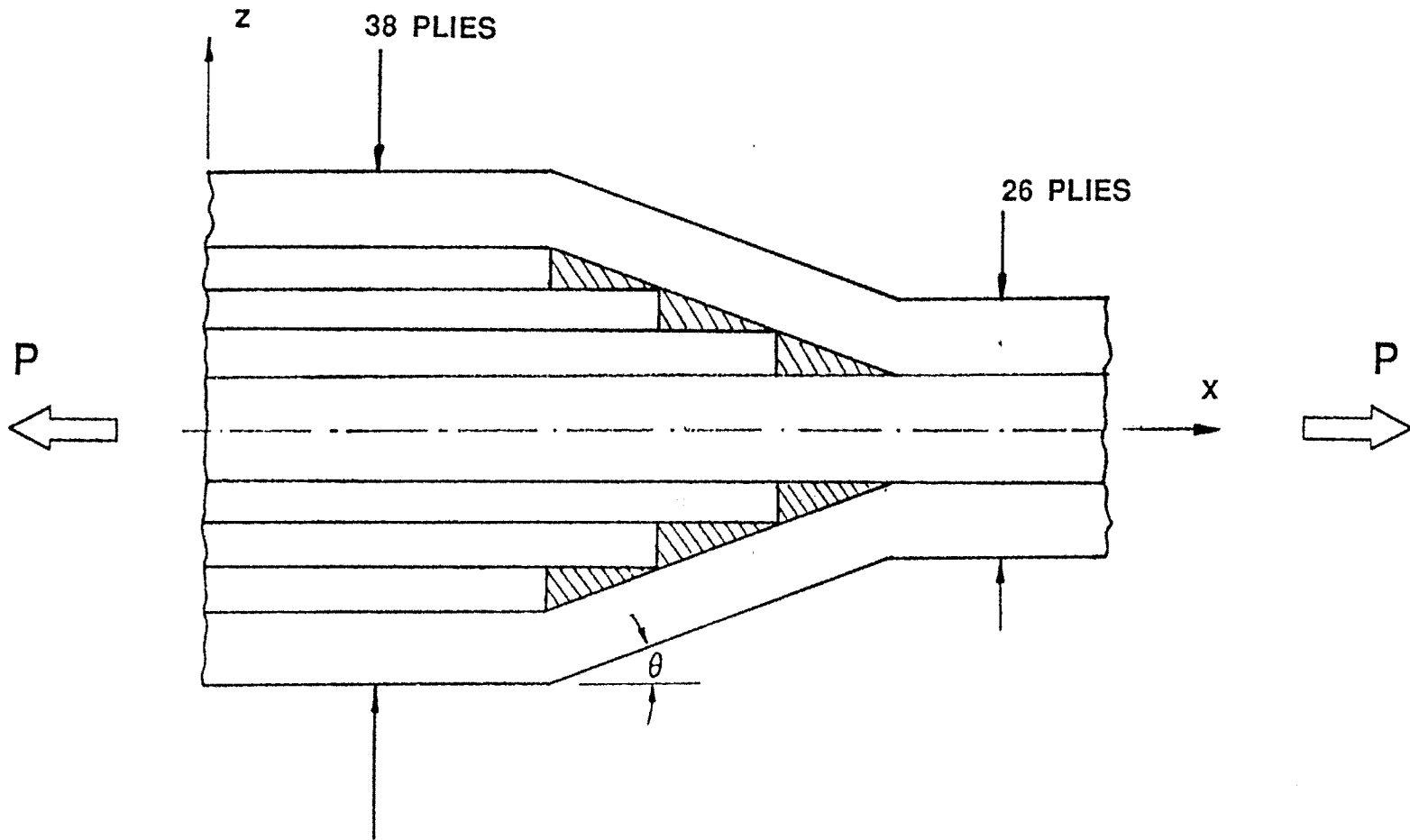


Figure 3. Edge View of the Tapered Structure

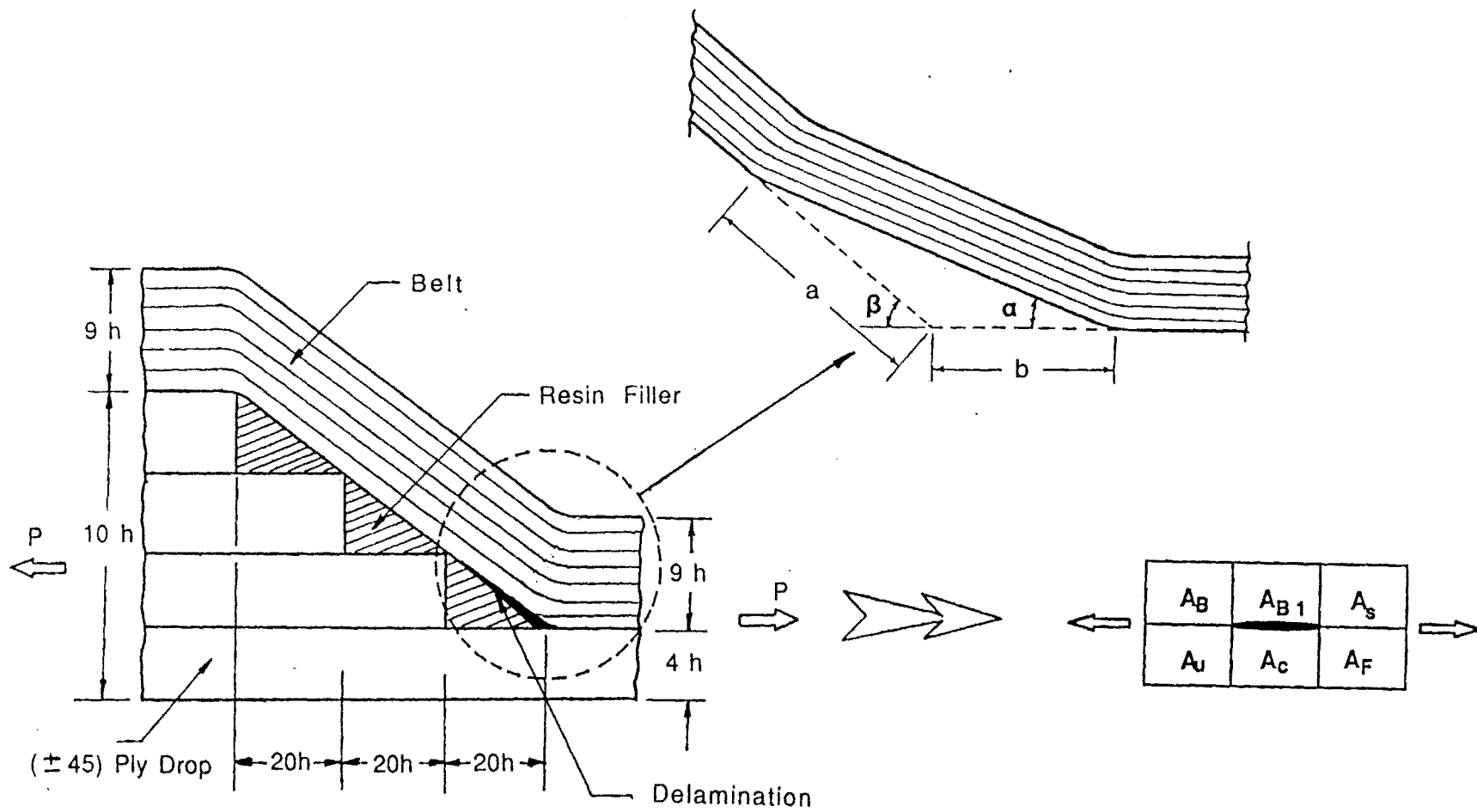


Figure 4. Modelling Approach

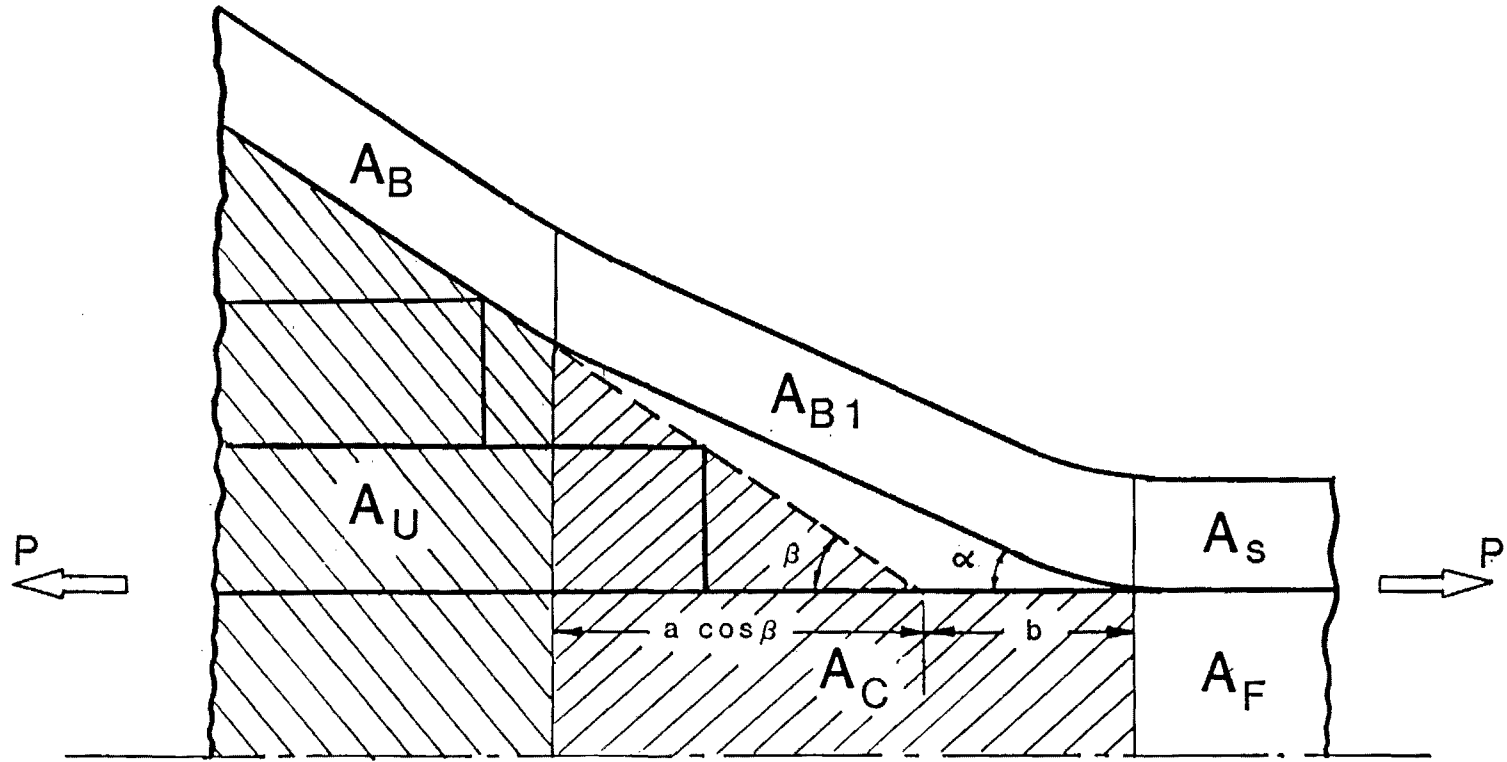


Figure 5. Dependency of Core and Belt Stiffnesses on Delamination

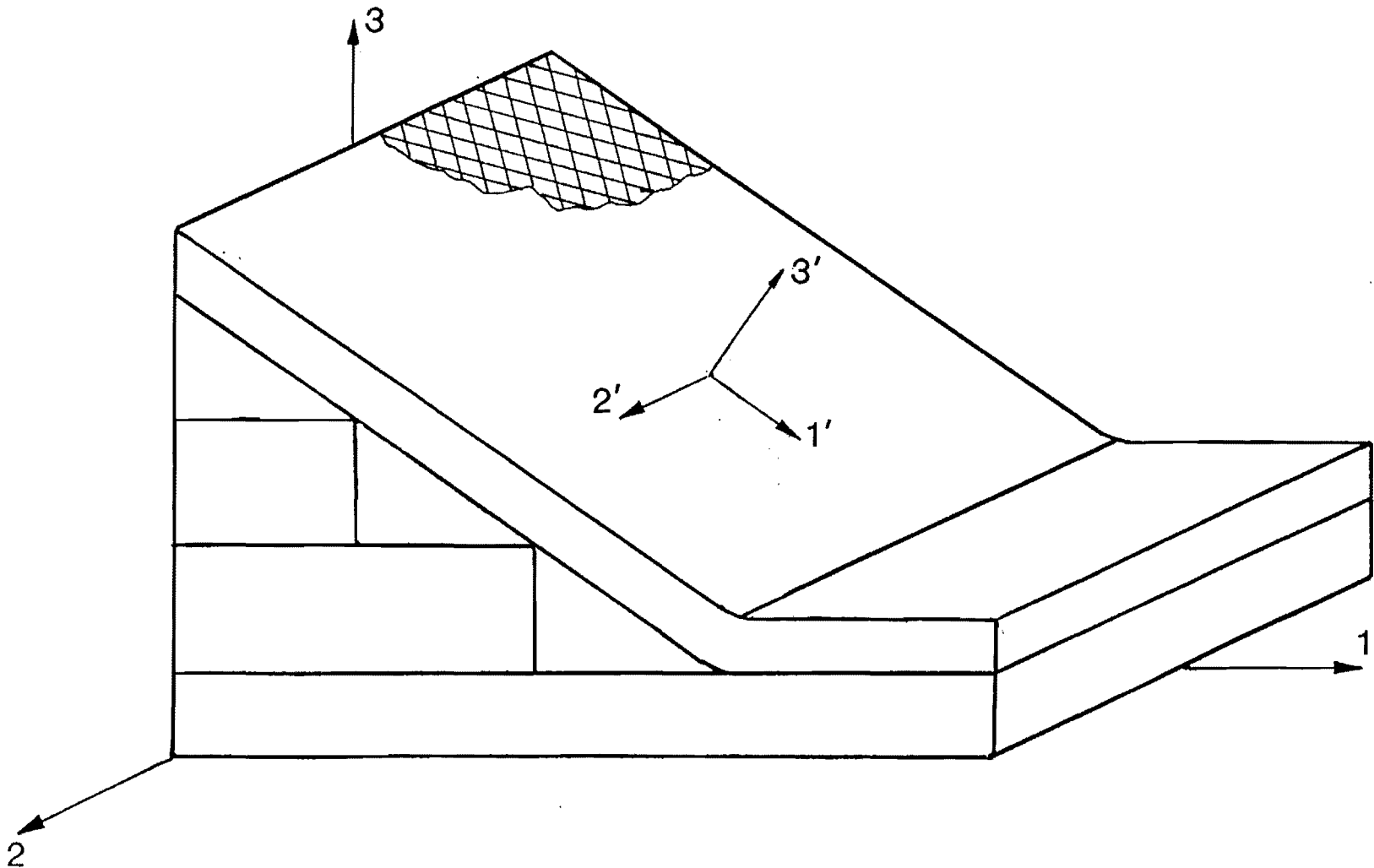


Figure 6. Three Dimensional Coordinates in the belt Region

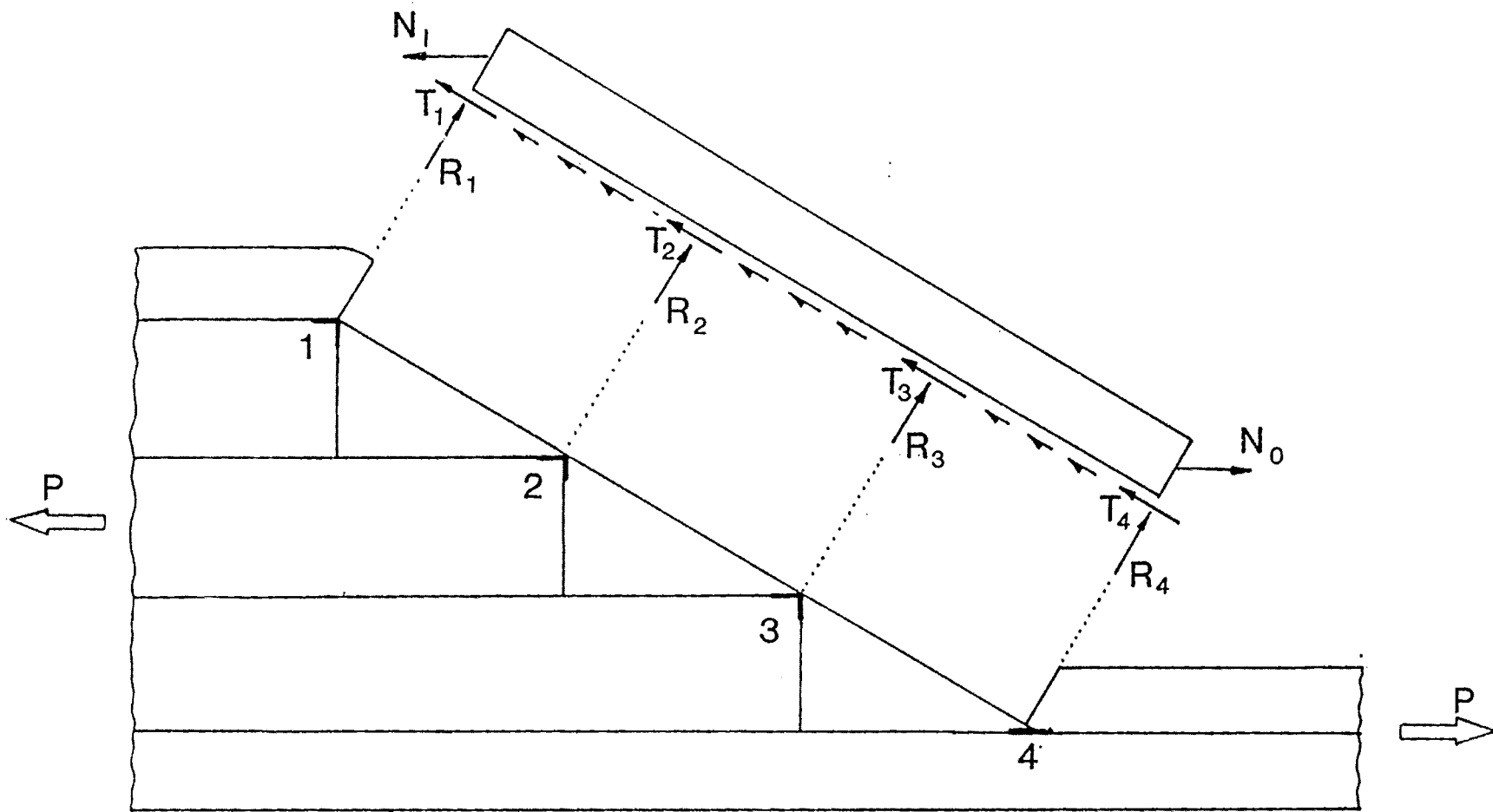


Figure 7. Interlaminar Stresses

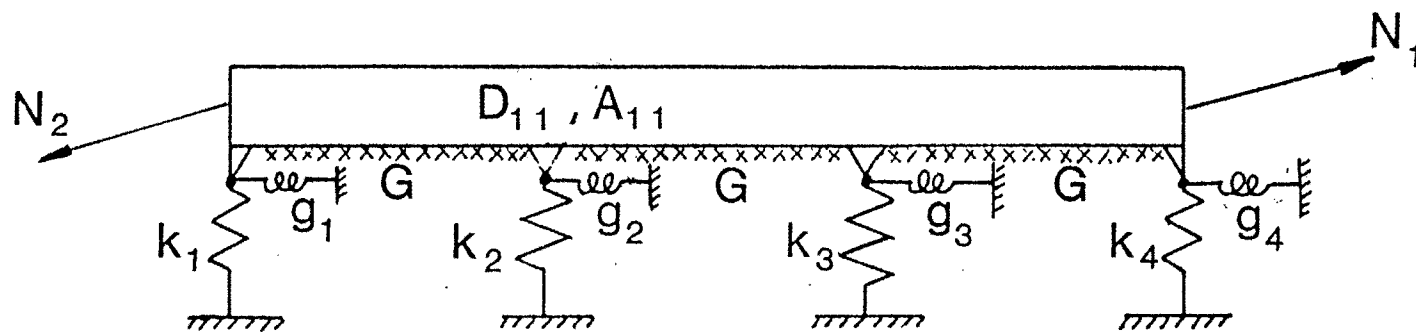


Figure 8. Elastic Stiffnesses and Supporting Conditions

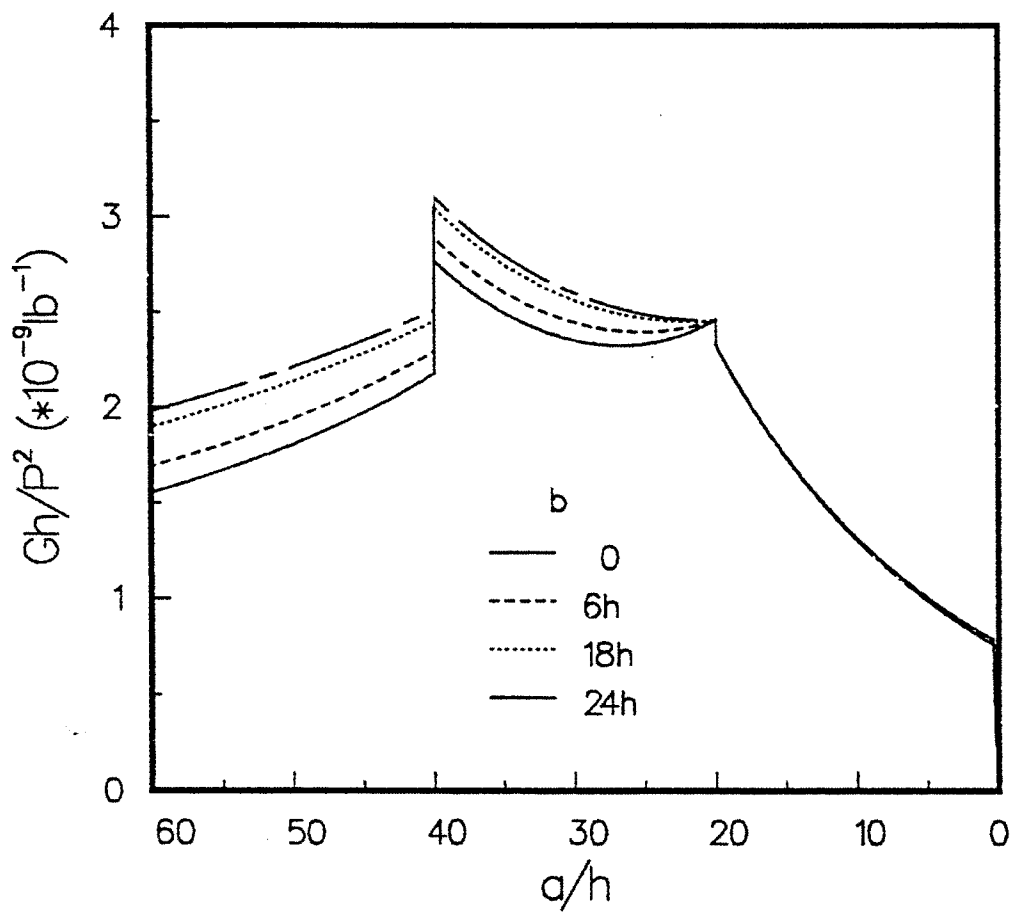


Figure 9. Variation of Total Strain Energy Release Rate with Delamination

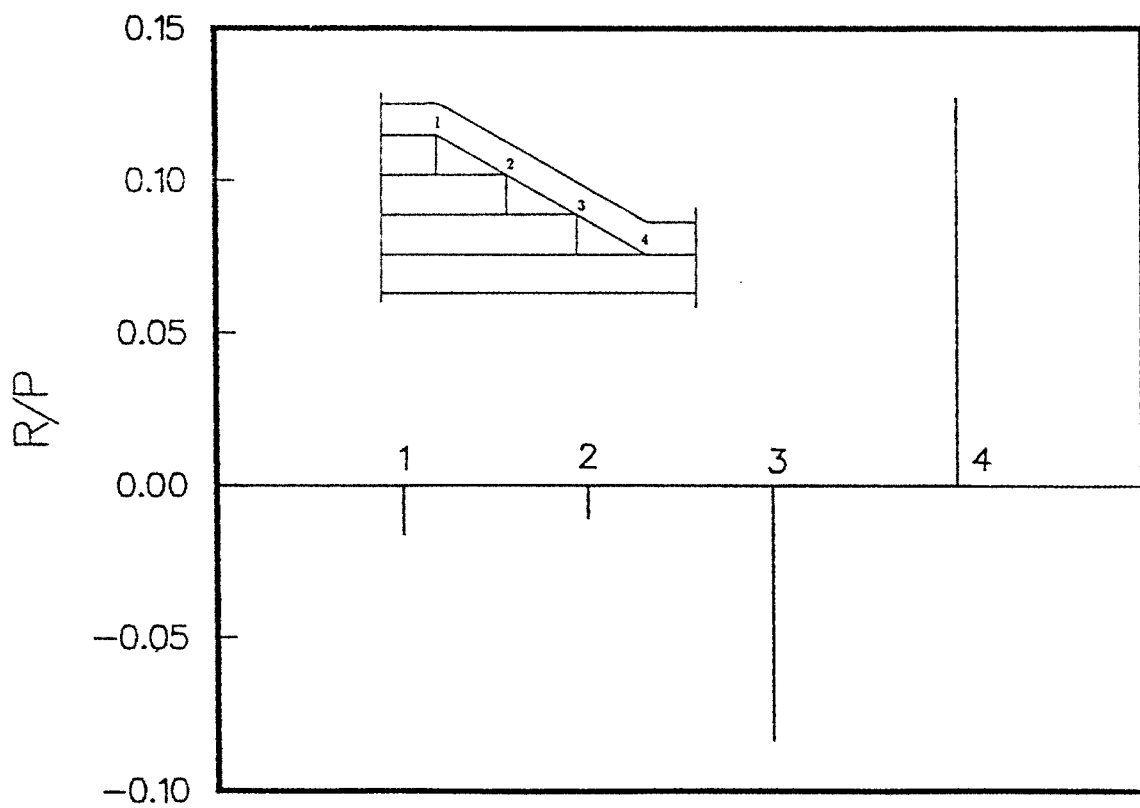


Figure 10 a. Distribution of Concentrated Normal Forces Along the Belt

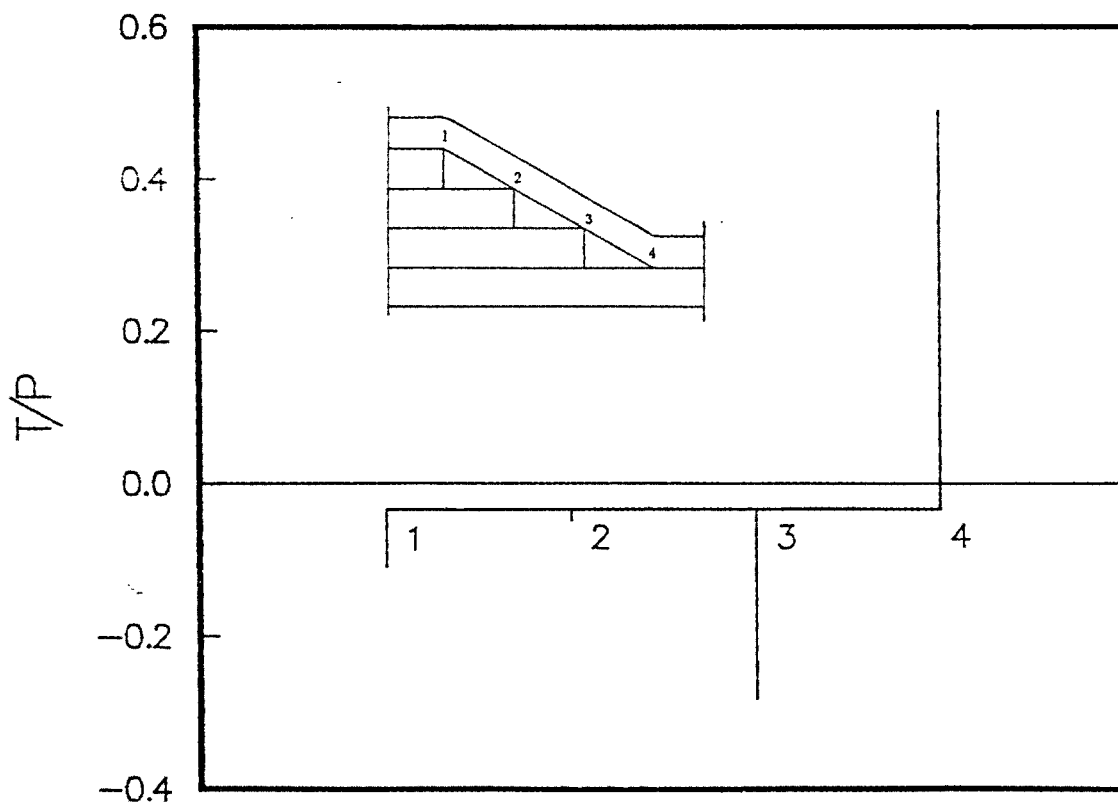


Figure 10 b. Distribution of Concentrated Shear Forces Along the Belt

APPENDIX I

A Study on the
Thermal and Moisture Influences on the Free-Edge
Delamination of Laminated Composites

By:

Mary A. Mahler

September 1987

A Special Problem Report:
Submitted in Partial Fulfilment for a
--- Master of Science ---
--- Aerospace Engineering Degree ---

Georgia Institute of Technology
School of Aerospace Engineering
Atlanta, Georgia 30332

Acknowledgments

It is with great pleasure that I express my deepest gratitude to my Advisor, Dr. Erian A. Armanios. Without his guidance, encouragement, and patience this work would not have been possible. Our enlightening discussions on delamination, composites, and related matters gave me the incentive to work harder. Throughout my graduate studies, I have learnt a great deal more from him than just the material presented in this report.

I am also indebted to Dr. Lawrence W. Rehfield for his classes and discussions with the Advance Composite Group. His talks about his past experiences were found to be very enhancing to my studies and research.

This research has been sponsored by the NASA Langley Research Center under Grant NAG-1-558. This support is gratefully acknowledged.

The patience of my roommate, Ruth Dolenga, for listening to my frustrations was sincerely appreciated. It was a privilege to have studied and worked with my officemates of the Advance Composites Group. Their words of encouragement, advice, and questions certainly enhanced my year at Georgia Institute of Technology.

At the foundation of all my work is the continuous support and encouragement from my parents, for which I am very grateful for.

Index

<u>Subject</u>	<u>Page</u>
Acknowledgments	
Index	
List of Figures	1
List of Tables.	2
Abstract.	3
Introduction.	4
Literature Summary.	7
Analytical Approach	
Overview of the Analysis	10
Interlaminar Shear Stresses.	14
Energy Release Rate.	15
Results & Discussion	
Benchmark Study.	19
Interlaminar Shear Stresses.	20
Energy Release Rate.	21
Conclusions	23
Recommendations	25
References.	27
Tables.	29
Figures	30
Appendices.	47

List of Figures

No.	Subject
1.	Glass/Epoxy Rotor Hub after Delamination.
2.	Graphite/Epoxy Single Crack-lap-shear Specimen
3.	Graphite/Epoxy Post-buckled I-Beam
4.	Compressive and Tensile Delamination Specimens
5.	Free edge Delamination Specimen
6.	Sublaminates Description and Coordinate Systems
7.	Notations and Sign Convention for Generic Sublaminates
8.	Comparison of Interlaminar Stress -- $[35/-35/0/90]_s$ layup
9.	Comparison of Interlaminar Stress -- $[35/0/-35/90]_s$ layup
10.	Comparison of Interlaminar Stress -- $[0/35/-35/90]_s$ layup
11.	Comparison of Interlaminar Stresses -- $[30/-60/75/15]_s$ layup
12.	Comparison of Interlaminar Stresses -- $[-35/55/10/-80]_s$ layup
13.	Comparison of Interlaminar Stresses -- $[35/80/-55/-10]_s$ layup
14.	Energy Release Rate Distribution for Laminates without Mode III
15.	Energy Release Rate Distribution for Laminates with Mode III
16.	Total Alleviation State of Interlaminar Shear Stresses

List of Tables

No.

Title

1. Properties of T300/5208 Graphite Epoxy
2. Geometric Dimensions of Benchmark Specimen

Abstract

Laminated composite structures exhibit a number of different failure modes. These include fiber-matrix debonding within individual layers, delamination or separation of the layers, transverse cracks through one or more layers and fiber fracture. These failures are influenced by environmental conditions. Thermal and moisture conditions are significant factors in interlaminar delamination as well as the other modes of failures.

A simple delamination analysis method is presented here. It is based on a shear-type deformation theory and includes hygrothermal effects. These environmental conditions are applied to the strain energy release rate and interlaminar shear stresses.

The method is applied to mixed mode edge delamination specimens made of T300/5208 graphite/epoxy material. Residual thermal and moisture stresses significantly influenced the strain energy release rate and interlaminar stresses. Both experienced large increases when thermal conditions were added to the mechanical strains. These effects were alleviated when moisture stresses were included. Thermal effects on the interlaminar shear stress and total energy release rate were totally alleviated for the same specific moisture content. Moreover, this value of moisture content was not significantly affected by the stacking sequence for the laminates considered.

Introduction

Composites have been used in the aircraft industry since 1969. One aspect of concern for using composites in structures is separation of plies or delamination. This occurs in regions of stress raisers such as holes, ply terminations, cut-outs and free edges. Delamination along the free edge of laminates have been observed during testing and service. The presence of delamination, initiated by interlaminar stresses, causes redistribution of the stresses among the plies in a laminate. Thus, it usually results in a reduction of stiffness and strength.

Figure 1 shows delamination in a rotor hub made of S2/SP250 glass/epoxy. The specimen has delaminated in two places that can be depicted by the dark lines. Figure 2 shows delamination in a single cracked-lap-shear test specimen made of AS4/3502 graphite/epoxy[1]. The specimen layup is $[\pm 45/0/90]_{6S}$ quasi-isotropic with 8 plies in the strap and 40 plies in the lap. The tests were performed on a displacement controlled machine. Fiber glass tabs were attached to the specimen ends. Multiple, isolated free edge delaminations occur in the neighborhood of the lap/strap junction and the tab. Figure 3 illustrates an I-beam section made of C3000/5225 graphite/epoxy woven cloth in the post-buckled regime. Free edge delamination depicted in the flanges precipitated the final failure in the specimen. Figure 4 shows how delamination can take place in single cracked-lap-shear specimens subjected to compressive and tensile loading. Specimens A and B delaminated under compressive loading while C experienced a

tensile loading. These examples illustrate the importance of investigating delamination problems in composites.

Thermal residual and moisture effects on a composite are practical environmental conditions. Determining the response of these conditions on interlaminar stresses and energy release rates in laminated composites is the primary objective of this work.

Delamination analysis can be based on two approaches. They are the strain energy release rate and interlaminar stresses. The interlaminar stresses are due to Poisson's ratio mismatch and difference in the coefficients of thermal and moisture expansion between plies. Delamination occurs when these stresses reach the interlaminar strength of the material. An alternative approach is based on the actual process of fracture rather than the strength concept. Delamination can propagate when the strain energy release rate at the crack front is sufficient to overcome the material's fracture resistance or toughness.

The strain energy release rate can be obtained for three particular modes of crack action. These three modes are known as Mode I or opening mode, Mode II or forward shearing mode and Mode III or tearing mode. Several failure laws are formulated in terms of these modes [2].

A simple analysis predicting interlaminar shear stresses and total energy release rate with the influence of thermal and moisture effects is developed. This simple approach is useful in understanding the basic mechanics of the problem and predicting the factors controlling the behavior. The method is directed to the needs of a practical

design environment. It is not intended to compete with large-scale numerical approaches, but rather to serve as the means for selecting and screening candidate configurations and providing trend information. Simple codes for a desktop computer have been created to analyze laminate configurations.

Literature Summary

A historical discussion of previously developed work for predicting interlaminar stresses and energy release rates is presented to establish a basis for the proposed model and to permit the present work to be placed in proper perspective.

Earlier analyses have reflected the prediction of interlaminar stress and energy release rate without hygrothermal conditions. O'Brien[3,4] investigated delamination onset and growth in graphite/epoxy laminates under uniform extension. A simple expression was developed for the total energy release rate based on classical lamination theory. Whitney and Knight[5] used classical laminated plate theory to develop an edge delamination specimen analysis. This work was limited to Mode I behavior.

An analysis based on a shear deformation theory and a sublaminar formulation [6] was developed by Armanios and Rehfield[7,8]. This method provides good estimates for the interlaminar shear stresses. Energy release rate components are estimated based on these stresses. However, this method does not provide reliable estimates of peel stress since thickness strain is neglected. This analysis was limited to mechanical strain only.

O'Brien[9] modified his analysis to include thermal and moisture conditions. The influence of thermal effects was considered by Whitney[10].

The work of Reference 9 was based on a classical laminated plate theory. It was applied to mixed-mode edge delamination specimens.

The results were limited to strain energy release rate. Finite element modeling was used to determine the strain energy release rate components. O'Brien's results reflected an increase in the strain energy release rate due to thermal effects. It decreased with the addition of moisture considerations. For a T300/5208 graphite/epoxy laminate with $[\pm 30/\pm 30/90/90]_s$ layup, the thermal effect increased the total energy release rate by 170 percent when compared to mechanical loading alone. However, a specific moisture level of 0.75 percent completely alleviated this increase. In calculating the total strain energy he showed that bending and coupling effects became important at high levels of moisture content.

In Reference 10 a higher-order plate theory with transverse normal strain effects was developed. Peel as well as interlaminar shear stresses could be predicted by this method. The thermal influence on total energy release rate and interlaminar stresses was investigated using a Mode I specimen. Residual thermal effects showed a significant influence on the stresses and release rates. For a graphite/epoxy laminate of $[0_3, 90_3]_s$ layup, thermal effects increased the maximum peel stress by a factor of 2.7 over that of pure mechanical strains.

In the present work both thermal and moisture influences are studied in a mixed-mode delamination specimen. The analysis includes total energy release rate as well as interlaminar stresses. Similarities between the interlaminar stresses and total energy release predictions with hygrothermal effects is investigated.

In the subsequent sections, the analytical approach is developed.

The method is then applied to six graphite/epoxy laminates. A discussion of the hygrothermal effects on interlaminar shear stress and total energy release rate predictions is provided. Recommendations for further investigations are proposed. Appendices are included for completeness. The first provides detailed expressions of the governing equations. Appendix II defines the hygrothermal expressions and their use in the analysis. The last appendix shows a listing of the program used and sample output.

Analytical Approach

Overview

The sublaminar modeling approach describes the essential features of the laminate behavior in a simple way. A free edge delamination specimen is shown in Figure 5. A uniform strain, ϵ , is applied in the axial direction. From symmetry, only one quarter of the specimen is considered. In Figure 6, the specimen is modeled as if it were composed of four distinct sublaminae. Sublaminae 2 and 3 represent the group of plies above and below the crack, respectively in the cracked portion of the laminate, while sublaminae 1 and 4 denote the same group of plies in the uncracked portion of the laminate.

The use of sublaminae -- groups of plies that are conveniently treated as laminated units -- simplifies the analysis considerably. This approach is applied with confidence when the characteristic length of the response is large compared to the individual sublaminar thickness[6]. This sublaminar modeling approach has been verified in Reference 7 by comparison with a ply-by-ply finite element solution. These sublaminae are connected by enforcing the proper continuity conditions on stresses and displacements at their interfaces.

Displacement fields within each sublaminar are defined as:

$$\begin{aligned}
 u &= x\epsilon + U(y) + z\beta_x(y) \\
 v &= V(y) + z\beta_y(y) \\
 w &= W(y)
 \end{aligned}
 \tag{1}$$

where u, v , and w denote the displacements relative to the x, y , and z axes, respectively. Shear deformation is recognized through the rotations β_x and β_y . The governing equations for each sublaminar are derived using a virtual work approach. The derivation of the governing equations used in the development appears in Appendix I. The derivation is an extension of the work of Reference 8 with hygrothermal effects included.

The constitutive relationships in terms of these force and moment resultants can be written as

$$\begin{aligned} N_i &= A_{ij} \epsilon_j + B_{ik} \kappa_k - N_i^{NM} & (i, j, k = 1, 2, 6) \\ M_i &= B_{ij} \epsilon_j + D_{ik} \kappa_k - M_i^{NM} & (i, j, k = 1, 2, 6) \\ Q_i &= A_{ij} \epsilon_j & (i, j = 4, 5) \end{aligned} \quad (2)$$

where the subscripts x, y, z, yz, xz , and xy are replaced by the subscripts 1-6 respectively. The force and moment resultants are denoted by N_i and M_i , respectively. Non-mechanical forces and moments resulting from the hygrothermal effects are labeled with a superscript NM. They are defined as:

$$(N_i^{NM}, M_i^{NM}) = \int_{-h/2}^{h/2} Q_{ij}(1, z) (\alpha_j \Delta T + b_j C) dz \quad (3)$$

The swelling coefficient is denoted by b_j in Equation (3), the thermal coefficient by α_j . The change in temperature is denoted by ΔT and moisture weight gain by C .

The elastic stiffnesses A_{ij} , B_{ij} , and D_{ij} are defined in terms of the sublaminar reduced stiffness Q_{ij} for a plane stress situation. These bear the classical definition.

$$(A_{ij}, B_{ij}, D_{ij}) = \int_{-h/2}^{h/2} (1, z, z^2) Q_{ij} dz \quad (4)$$

The equilibrium equations are:

$$\begin{aligned} N_{xy,y} + (t_{2x} - t_{1x}) &= 0 \\ N_{y,y} + (t_{2y} - t_{1y}) &= 0 \\ Q_{y,y} + (p_2 - p_1) &= 0 \\ M_{xy,y} - Q_x + h/2 (t_{2x} + t_{1x}) &= 0 \\ M_{y,y} - Q_y + h/2 (t_{2x} + t_{1x}) &= 0 \end{aligned} \quad (5)$$

where t_{2x} , t_{2y} , p_2 and t_{1x} , t_{1y} , p_1 denote the interlaminar stress components in the x-z, y-z and z directions at the sublaminar upper and lower surfaces, respectively. These stress components appear in Figure 7.

The displacements, resultant forces and moments, and interlaminar shear stresses in each sublaminar is governed by the displacement distribution (1), constitutive (2), and equilibrium (5) equations. These equations are applied to each sublaminar. The variables associated with each sublaminar are coupled through the continuity requirements at their interfaces. Enforcement of the boundary conditions lead to a solution for these variables. This procedure

discussed in general terms above is applied to the analysis of the edge delamination specimen shown in Figure 2 in the following sections.

The response associated with sublaminates 1 and 0 shown in Figure 2 is coupled through the continuity conditions at their common interface. The situation is different with sublaminate 2 and 3 where the continuity conditions are relaxed due to the presence of the crack.

Uncracked Region: Sublaminates 0 and 1

From symmetry conditions at the sublaminate bottom surface the shear stresses are zero. Interlaminar stresses at the top surface of sublaminate 0 are equal to those on the bottom of sublaminate 1. Substituting these conditions into the equilibrium and constitutive relations and enforcing continuity of displacements at their common interface yields a homogeneous system of ordinary differential equations. These can be expressed in terms of the sublaminate rotations β_x and β_y . Assuming an exponential solution of the form

$$(\beta_{1x}, \beta_{0x}, \beta_{1y}, \beta_{0y}) = (\beta_{1x}^*, \beta_{0x}^*, \beta_{1y}^*, \beta_{0y}^*) e^{sy} \quad (6)$$

results in a characteristic equation of the form

$$E_8 s^8 + E_6 s^6 + E_4 s^4 + E_2 s^2 + E_0 = 0 \quad (7)$$

Parameter E_0 depends only on the stiffness coefficients A_{44} , A_{55} and A_{45} for both sublaminates while E_8 is predominantly influenced by the bending and coupling coefficients D_{ij} and B_{ij} . Thus, its

numerical value can be orders of magnitude smaller than the other coefficients. This results in the presence of a boundary zone in the response.

The characteristic roots controlling the behavior of the laminate are determined from Equation 7 which has a closed-form solution.

Crack Region of the Laminate: Sublaminates 2 and 3

With this group of laminates, there are free surfaces at both the top and bottom of sublaminates 0 and 1 respectively. This is due to the presence of the crack. With the crack dividing the sublaminates, continuity conditions are not enforced at the boundary interface. This results in zero shear stresses at the surfaces of each sublaminate. Thus, the equilibrium and constitutive relations combine to produce a second order differential equation in terms of the sublaminate rotations β_{2X} for sublaminate 2 and β_{3X} for sublaminate 3.

Interlaminar Stresses

The arbitrary constants that are obtained from the eighth degree polynomial are determined by enforcing the stress free boundary conditions at the free edges of sublaminates 2 and 3, and the continuity of force, moment, displacement and rotations between sublaminates 0 and 3, as well as between 1 and 2. This yields the following expression for the interlaminar shear stresses.

$$\tau_X = N_{XY_1, Y} = G_j e^{-s_j y} \quad (8)$$

$$\tau_Y = N_{Y_1, Y} = T_j e^{-s_j y} \quad (j = 1 - 4) \quad (9)$$

Parameters T_j and G_j represent the amplitude of the response.

Energy Release Rate

A complete formulation of the strain energy release rate appears in Appendix II. The total energy release rate can be determined by considering the work done by external forces.

$$G = -1/2 * dW/da \quad (10)$$

The total energy release rate is denoted by G and the crack length by a . The work done is defined as

$$W = L/2 \int_0^b N_{xi} \epsilon_{mi} dy \quad (11)$$

where subscript i denotes the sublaminates being referenced. The term ϵ_{mi} represents the mechanical strain in each ply. This is defined as the difference between the total strain and the strain corresponding to free expansion for each ply. This strain is estimated by using a procedure similar to Reference 5. However, in Reference 5 the free expansion strain was determined by considering groups of plies in the cracked and uncracked regions of a Mode I edge delamination specimen. This approach is valid for a limited class of laminates. A ply-by-ply analysis rather than a sublaminates modeling should be used. In the following analysis, free expansion strains are determined on a ply-by-ply basis.

From the symmetric conditions that exist in the uncracked section of the laminate, there exist no curvature. In the cracked portion,

the moment about the y-axis is assumed to be zero. Using both of these boundary conditions in Equation (2) yields the following.

$$N_{x1} = A_{11} \epsilon + A_{12} \epsilon_y + A_{16} \epsilon_z - N_{x1}^{NM} \quad (12)$$

$$N_{x1} = A_{11} \epsilon + A_{12} \epsilon_y + A_{16} \epsilon_z + B_{12} \kappa_y - N_{x2}^{NM}$$

Strain components ϵ_y and ϵ_z in Equation 12 are expressed in terms of the applied strain by

$$\epsilon_y = C_v \epsilon + C_v^{NM} \quad (13)$$

$$\epsilon_z = C_u \epsilon + C_u^{NM}$$

The terms C_v , C_u , C_v^{NM} and C_u^{NM} are functions of the extensional stiffness components A_{ij} of sublaminates 1 and 0.

Using these expressions, Equation 12 can be re-written in the form.

$$N_{xc}^k = (E_c^k \epsilon_c^k + T_c^k) \quad (14)$$

$$N_{xu}^k = (E_u^k \epsilon_u^k + T_u^k)$$

Parameters E_c^k , T_c^k , E_u^k and T_u^k are defined in Appendix II. Superscript k denotes the individual ply. Subscripts u and c represent the uncracked and cracked portions, respectively. The non-mechanical strain in each ply corresponding to a state of free

expansion is obtained by allowing the stress in each ply to vanish. This yields the following.

$$\epsilon_u^k = -T_u^k / E_u^k \quad (15)$$

$$\epsilon_c^k = -T_c^k / E_c^k$$

The strain corresponding to free expansion of the entire laminate is obtained by letting the resultant force vanish. The non-mechanical strain is

$$\epsilon^{NM} = \left\{ T_u^* - (T_u^* - T_c^*) 2a/b \right\} / \left\{ E_u^* - (E_c^* - E_u^*) 2a/b \right\} \quad (16)$$

The terms T_u^* , T_c^* , E_u^* and E_c^* represent the summation of T_u^k , T_c^k , E_u^k and E_c^k over their respective sublaminates. These strain definitions for the effects of moisture and temperature can now be used in the general expression for the strain energy. The strain field is altered to represent the hygrothermal effects. The total strain for a sublaminate is expressed as:

$$\epsilon^T = \epsilon + \epsilon^{NM} \quad (17)$$

The strain energy expression is given below showing the use of Equations (13) and (17).

$$W = \frac{L}{2} \left[\sum (E_c^k \epsilon^T + T_c^k) (\epsilon^T - \epsilon_c^k) + (E_u^k \epsilon^T + T_u^k) (\epsilon^T - \epsilon_u^k) \right] \quad (18)$$

Substituting this into Equation (11) yields the total strain energy release rate per crack.

Results and Discussion

Benchmark Study

The analytical model is applied to the edge delamination specimen shown in Figure 5. The material considered is T300/5208 graphite/epoxy. Its mechanical properties are listed in Table I. The coefficients of swelling and thermal expansions are also stated. The geometry of the specimen is given in Table II. Cure temperature for this material is 350°F. The ambient operating temperature is 70°F. The moisture level for all cases was allowed to vary from 0 to 1.2 percent of the laminate weight. This moisture level reflects feasible conditions. The mechanical strain is taken as 0.00254. This particular value of strain was taken from test experiments[9]. It is considered a practical value for the material.

Six laminates have been analyzed. They can be divided into two groups. The first group is composed of laminates $[35/-35/0/90]_s$, $[35/0/-35/90]_s$, and $[0/35/-35/90]_s$. These laminates are prone to delaminate at the interfaces indicated by the arrow[9]. The Mode III in these laminates is negligible. This is due to the fact that relative sliding at the crack front and the interlaminar shear stress in the x-z direction, τ_{xz} , is negligible. The second group of laminates is $[30/-60/75/15]_s$, $[-35/55/10/-80]_s$, and $[35/80/-55/-10]_s$. In these laminates Mode I, Mode II, and Mode III are finite. The Mode III strain energy release rate component due to mechanical loading in these laminates are significantly large, ranging from 60 to 90

percent[7].

Interlaminar Shear Stresses

The interlaminar stress τ_{yz} at the delamination interface appear in Figure 8 - 10, for the first group of laminates. The interlaminar shear stresses τ_{xz} and τ_{yz} for the second group of laminates appear in Figures 11 - 13. The labels M, M+T, and M+T+H stand for mechanical, mechanical and thermal, and mechanical, thermal and moisture respectively.

The boundary layer of decay for all laminates ranged from 0.85 to 0.93 of the laminate semi-width. In this context the boundary layer decay length is defined as the distance where the stress decays to 5 percent of its maximum value. The stress boundary zone is not significantly influenced by the environmental conditions.

The magnitude of shear stress however showed a strong dependency on thermal and moisture conditions. At the delamination front, the ratio of stress with thermal effects as compared to pure mechanical loading ranged from 3.22 to 3.36 for the first group of laminates. This maximum was experienced at the crack tip. For the laminates where Mode III was present, this ratio ranged from 4.16 to 5.23 for τ_{yz} . The shear in the x-z direction showed a ratio of 1.4 to 2.16 for the maximum stresses. The maximum τ_{yz} stress for the second group of laminates was experienced at the crack front. However, the maximum τ_{xz} stress occurred slightly ahead of the crack. This can be seen in Figures 11 - 13.

The addition of moisture alleviated the thermal effect. A moisture content of 0.4 has reduced the stress of thermal influence by approximately 40 percent as compared to thermal influences alone. This trend is similar to the results of Reference 9.

Numerical values of interlaminar shear stress at various moisture levels are provided in the sample output of Appendix III. Interlaminar shear stresses show numerical decrease with increase of moisture levels.

Energy Release Rate

The hygrothermal effect on total energy release rate appears in Figures 14 -15. The hygrothermal effects on total energy release rate show a similar trend to that of interlaminar shear stresses. Residual thermal stress tends to increase total energy release rate while residual moisture alleviates this effect. The figures show that for total alleviation of the thermal effect, the specific moisture content ranges between 0.70 and 0.77 for all laminates. This indicates there exist a weak dependency on the stacking sequence.

The effects of thermal conditions alone on the energy release rate does not correspond to the same numerical value as the interlaminar shear stresses. The total energy release rate of layups where Mode III was negligible showed a ratio of 5.1 for mechanical and thermal compared to mechanical conditions only. For the laminates where Mode III is finite, this ratio varied from 1.6 in the $[30/-60/75/-15]_s$ layup to 3.37 in the $[35/80/55/-10]_s$ layup.

The total energy release rate in the first group of laminates is approximately the same for mechanical loading as shown in Figure 14. The influence of thermal and moisture does not appear to alter this trend. The energy release rate for the $[35/-35/0/90]_s$ laminate is indistinguishable from the $[0/35/-35/90]_s$ layup. The rate of alleviation due to moisture is the same for the three laminates. This is in contrast with the alleviation rate of the laminates where Mode III is finite as shown in Figure 15. For this class of laminates, the rate of alleviation due to moisture is different for each laminate.

In some of the laminates, the rate of alleviation is not constant. There is a steep gradient in the rate of alleviation until the moisture content approaches the totally alleviated state. After such moisture content, the decrease in total energy release rate with respect to moisture addition is not as significant.

It is worth noting there is a similarity between the strain energy release rate prediction and the interlaminar stresses for the totally alleviated state. This is shown in Figure 16 for a $[-35/55/10/-80]_s$ layup. The specific moisture percent producing complete alleviation of the total energy release rate from the thermal effect is 0.76 as seen in Figure 15. The interlaminar shear stress distribution corresponding to this level of moisture is indistinguishable from the mechanical loading alone. The same conclusion was reached studying the other laminates.

Conclusions

A simple analysis was developed that predicted the influence of thermal and moisture effects on the interlaminar shear stresses and strain energy release rate. The analysis was applied to six mixed-mode edge delamination specimens. The results provide several significant findings.

1. Residual thermal strain has a significant influence on the interlaminar shear stress and total energy release rate. The interlaminar stress and total energy release rate increased by 330 and 510 percent respectively over that of pure mechanical loading.
2. Moisture tends to alleviate the thermal effect for both the interlaminar stress and energy release rate. At a specific moisture content of approximately 0.75 percent, the thermal influence is totally alleviated.
3. The moisture content for total alleviation found from the total energy release rate analysis also produced an interlaminar stress distribution similar to pure mechanical loading conditions.

The first two findings are in agreement with the results of previous investigators. The third finding is new. It establishes a similarity in behavior between a delamination analysis expressed in terms of the energy release rate and the strength approach expressed

by the interlaminar stresses.

These findings point to new directions for further inquiry. These are discussed in the following section.

Recommendations

The thermal effects on the laminates showed a large increase in both the interlaminar shear stresses and strain energy release rate. The analysis should be supplemented with experimental tests to verify the result. Several fracture laws are expressed in terms of the strain energy release components, as well as the total strain energy. Further analysis should include predictions of these components in the presence of hygrothermal conditions.

Throughout this work the temperature is assumed to be uniform through the thickness of the laminate. The same is true with the moisture. An approach corresponding to a practical environment method should account for temperature and moisture gradients in the laminate. In this situation, the hygrothermal gradients through the thickness may create an unbalance effect in an originally balanced construction. This consideration is of significant importance in aerospace structural components subjected to a large temperature difference between the upper and lower surface.

The loading considered here is uniaxial extension. However, it is known that the load transfer points are not always in the plane of the laminate. Therefore, investigating laminate response under combined loads is of great practical importance. It is recommended that bending, torsion as well as their combined effect be addressed.

Findings by previous investigators suggested that delamination behavior in laminates subjected to fatigue loading follows static loading conditions. Further work is needed to investigate the

influence of hygrothermal conditions on the delamination of laminates under fatigue loading.

Finally, the present analysis is applied to the mixed-mode edge delamination specimen. Extension of this work to other specimens such as the single- and double-crack-lap shear and the Mode II edge notch flexure specimen is recommended.

When accomplished, these recommendations, together with the present research will provide a better understanding of the delamination problem in composites. Consequently, this will enable predicting, managing and ultimately preventing interlaminar fracture in laminated composites.

References

1. Armanios, E.A., Rehfield, L.W., and Reddy, A.D., "Design Analysis and Testing for Mixed-Mode and Mode II Interlaminar Fracture of Composites," Composite Materials: Testing and Design (Seventh Conference), ASTM STP 893, J.M. Whitney, Ed., American Society for Testing and Materials, Philadelphia, 1986, pp. 232-255.
2. Russel, A.J. and Street, K.N., "Moisture and Temperature Effects on the Mixed-Mode Delamination Fracture of Unidirectional Graphite/Epoxy", Delamination and Debonding of Materials, ASTM STP 876, W.S. Johnson, Ed., American Society for Testing and Materials, 1985, pp. 349-370.
3. O'Brien, T.K., "Characterization of Delamination Onset and Growth in a Composite Laminate," Damage in Composite Materials, ASTM STP 775, K.L. Reifsnider, Ed., American Society for Testing and Materials, 1982, pp. 140-167.
4. O'Brien, T.K., "Mixed-Mode Strain-Energy-Release Rate Effects on Edge Delamination of Composites," Effects of Defects in Composite Materials, ASTM STP 836, American Society for Testing and Materials, 1984, pp. 125-142.
5. Whitney, J.M. and Knight, M., "A Modified Free-Edge Delamination Specimen," Delamination and Debonding of Materials, ASTM STP 876. W.S. Johnson. Ed., American Society for Testing and Materials, Philadelphia, 1985, pp. 298-314.
6. Armanios, E.A., "New Methods of Sublaminar Analysis for Composite Structures and Applications to Fracture Processes," Ph.D. Thesis, Georgia Institute of Technology, March 1985.
7. Armanios, E.A. and Rehfield, L.W., "Interlaminar Analysis of Laminated Composites Using a Sublaminar Approach," Proceedings of the AIAA/ ASME/ASCE/ASH 27th Structures, Structural Dynamics, and Materials (SDM) Conference, San Antonio, Texas, 19-21 May 1986. AIAA Paper No. 86-0969CP, Part 1, pp. 442-452.
8. Armanios, E.A. and Rehfield, L.W., "Sublaminar Analysis of Interlaminar Fracture in Composites," Final Report, NASA Grant NAG-1-558, March 1986. Also to be published as a NASA Contractor Report.
9. O'Brien, T.K., Raju, I.S., and Garber, D.P., "Residual Thermal and Moisture Influences on the Strain Energy Release Rate Analysis of Edge Delamination," Journal of Composites Technology and Research, Vol. 8, No. 2, Summer 1986, pp. 37-47.

10. Whitney, J.M. "Stress Analysis of a Mode I Edge Delamination Specimen for Composite Materials," AIAA Paper 85-0611, presented at the 26th AIAA/ASME/ASCE/AHS Structures, Structural Dynamics and Materials Conference, April 15-17, 1985, Orlando, Florida.

TABLE I - T300/5208 GRAPHITE/EPOXY PROPERTIES

$$E_{11} = 18.7 \text{ MSI}$$

$$E_{22} = 1.23 \text{ MSI}$$

$$G_{12} = 0.832 \text{ MSI}$$

$$\text{Poisson Ratio} = 0.292$$

Swelling Coefficients of the Material direction:

$$b(1\text{-direction}) = 0$$

$$b(2\text{-direction}) = 55604\epsilon/\% \text{weight}$$

Thermal Coefficients of the Material direction:

$$\alpha(1\text{-direction}) = -23 \mu\epsilon/^{\circ}\text{F}$$

$$\alpha(2\text{-direction}) = 14.9 \mu\epsilon/^{\circ}\text{F}$$

TABLE II - GEOMETRIC DIMENSIONS OF SPECIMEN

$$\text{Ply thickness} = 0.0054 \text{ inch}$$

$$\text{Width} = 1.5 \text{ inch}$$

$$\text{Crack length} = 6 \times \text{ply thickness} = 0.0324 \text{ inch}$$

FIGURES 1-16

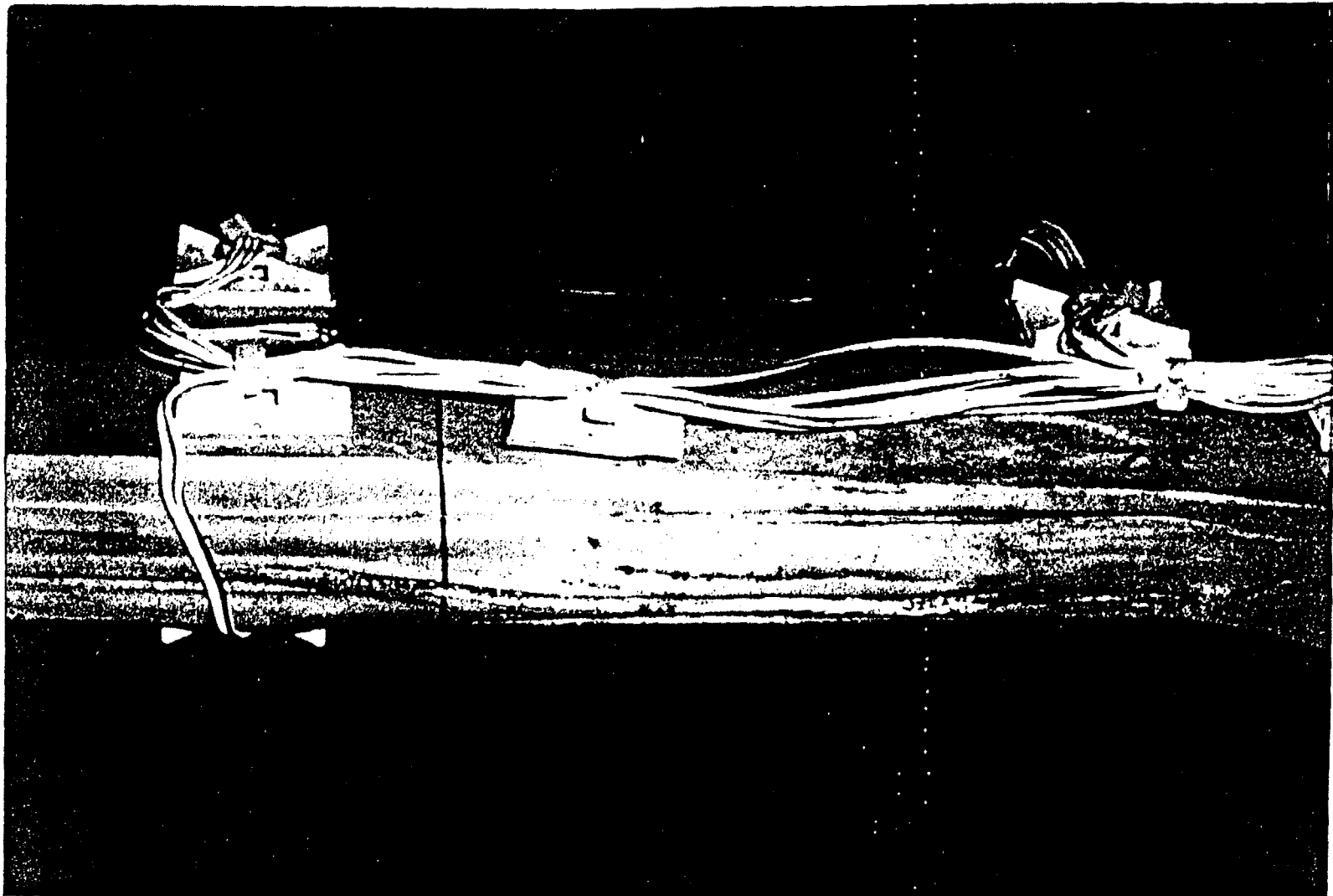


FIGURE 1 - GLASS/EPOXY ROTOR HUB AFTER DELAMINATION

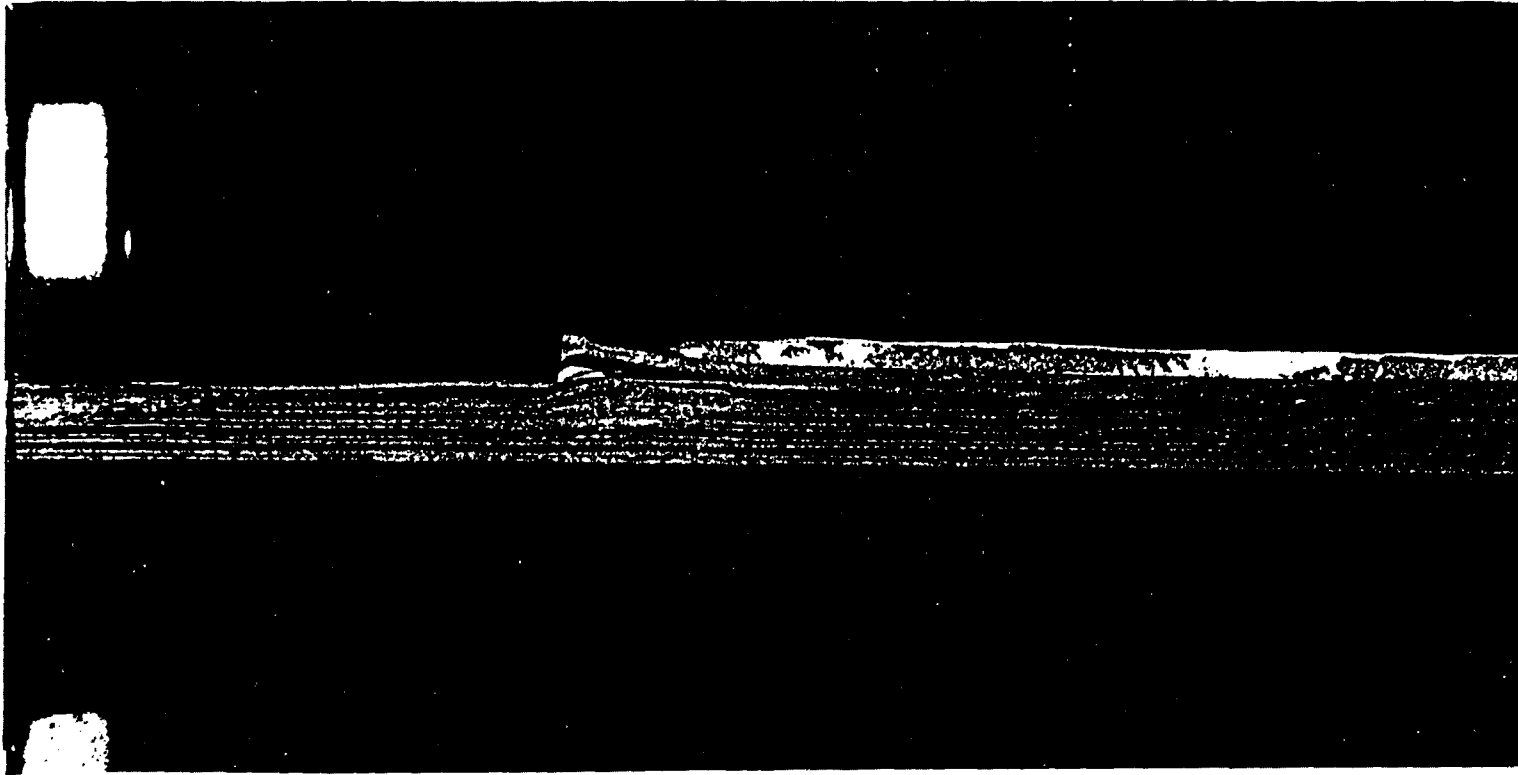


FIGURE 2 - GRAPHITE/EPOXY SINGLE CRACK-LAP-SHEAR SPECIMEN

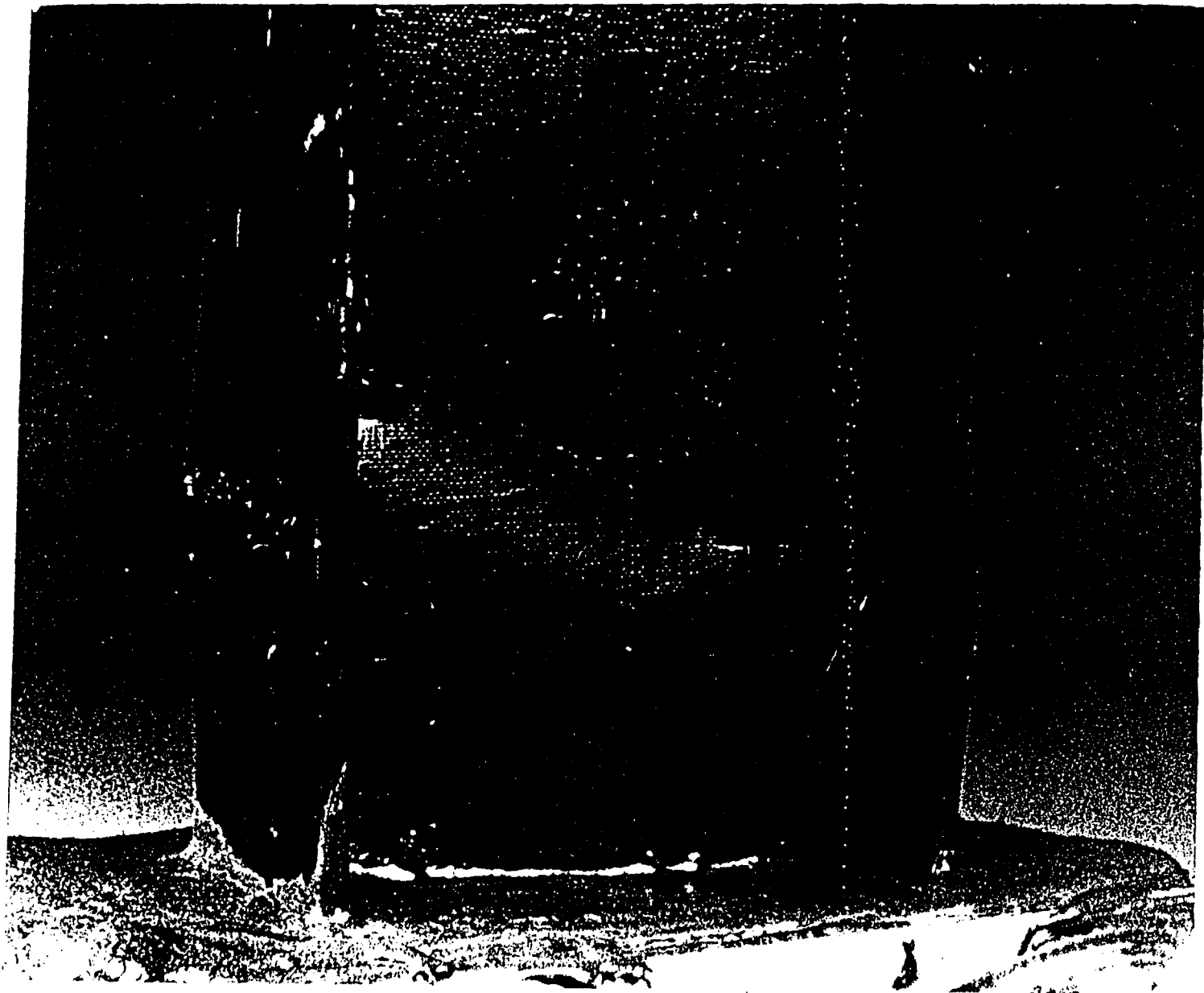


FIGURE 3 - GRAPHITE/EPOXY POST-BUCKLED I - BEAM

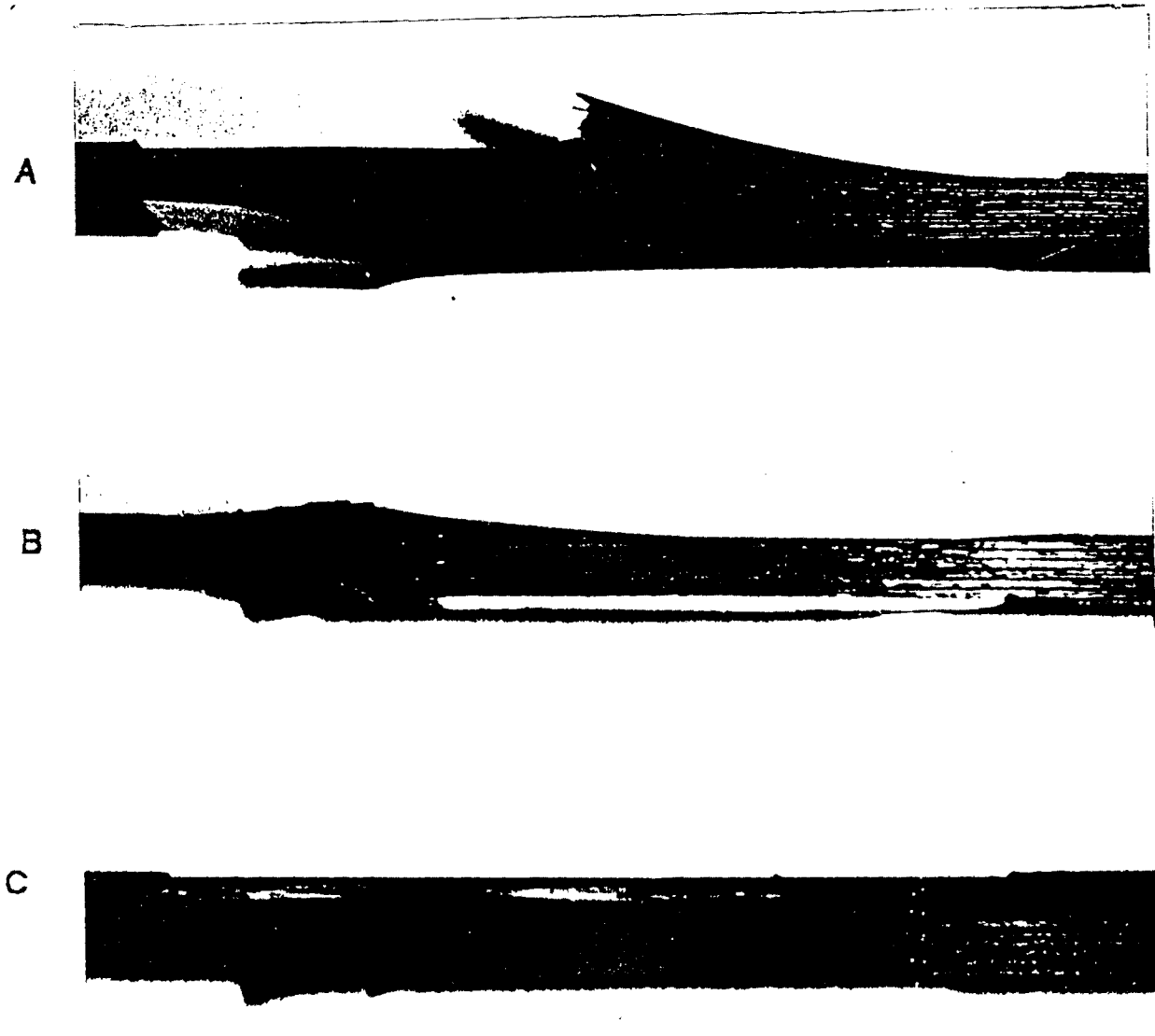


FIGURE 4 - COMPRESSIVE AND TENSILE DELAMINATION SPECIMENS

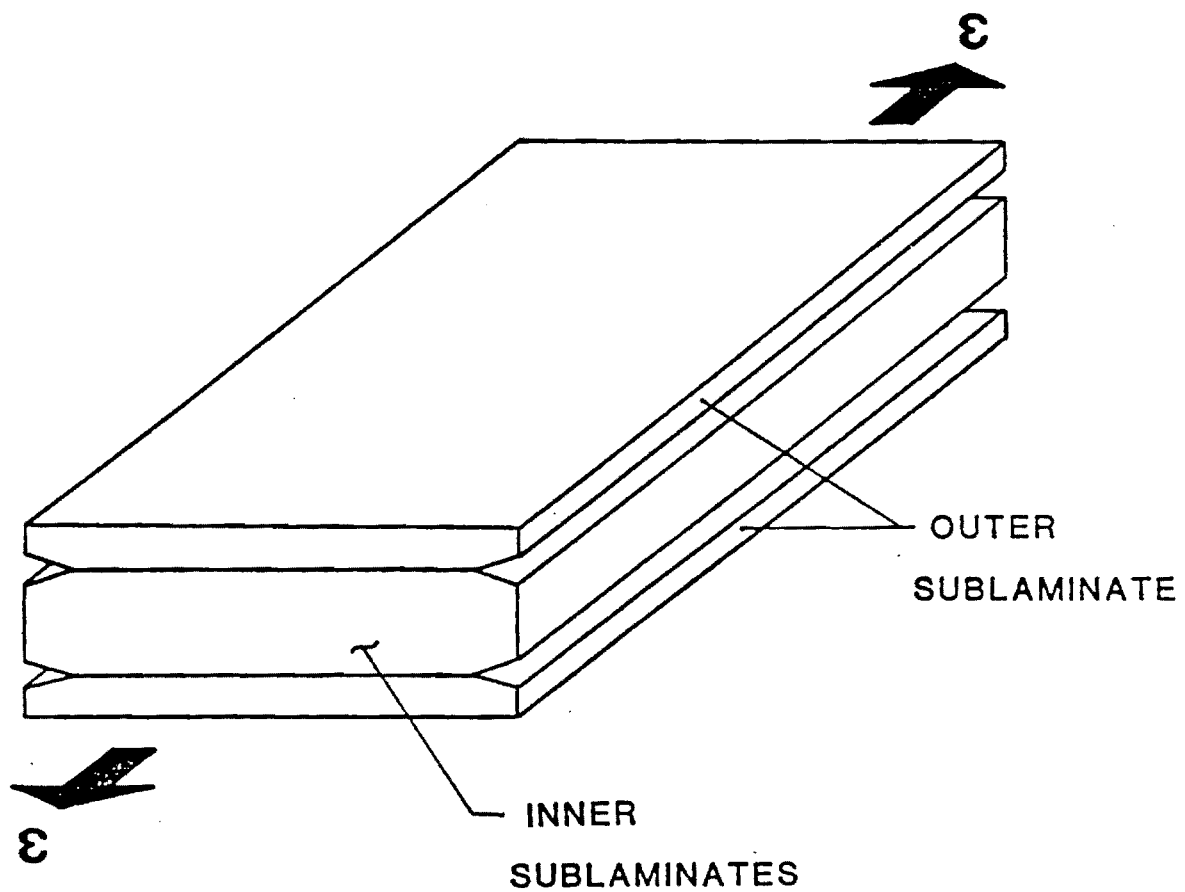


FIGURE 5 - FREE EDGE DELAMINATION SPECIMEN

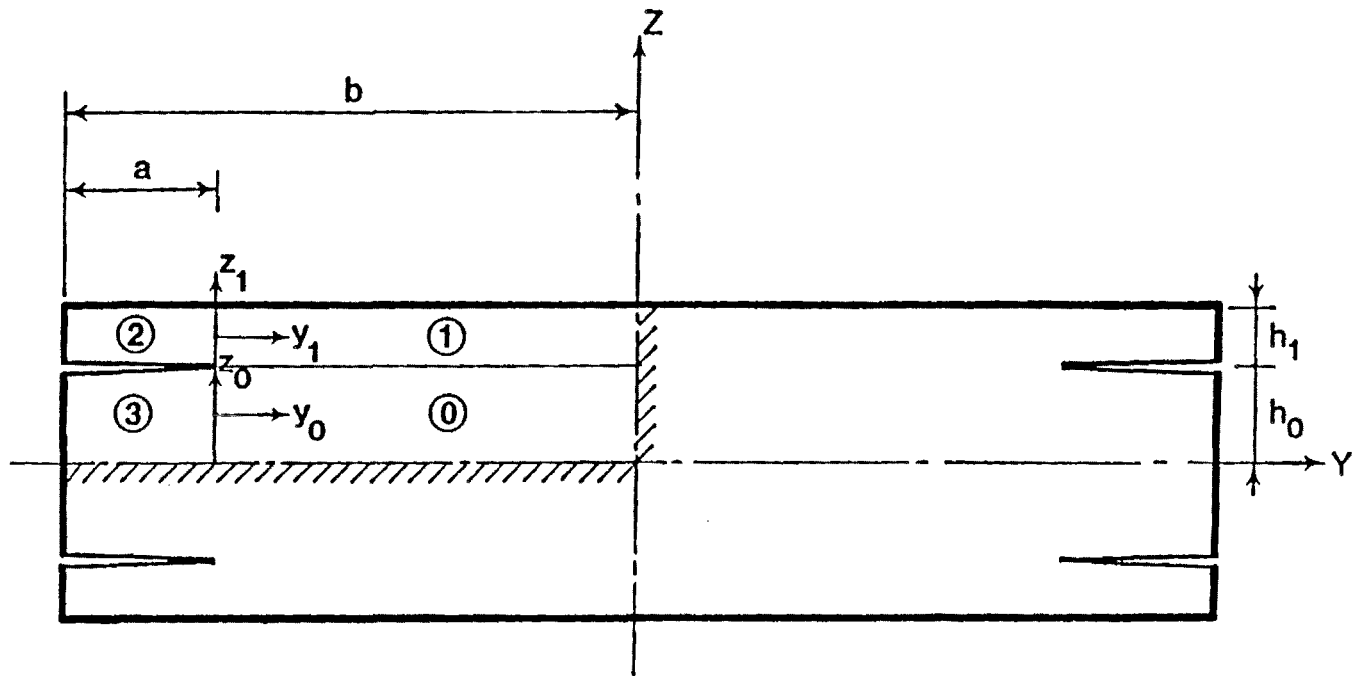


FIGURE 6 - SUBLAMINATE DESCRIPTION AND COORDINATE SYSTEM

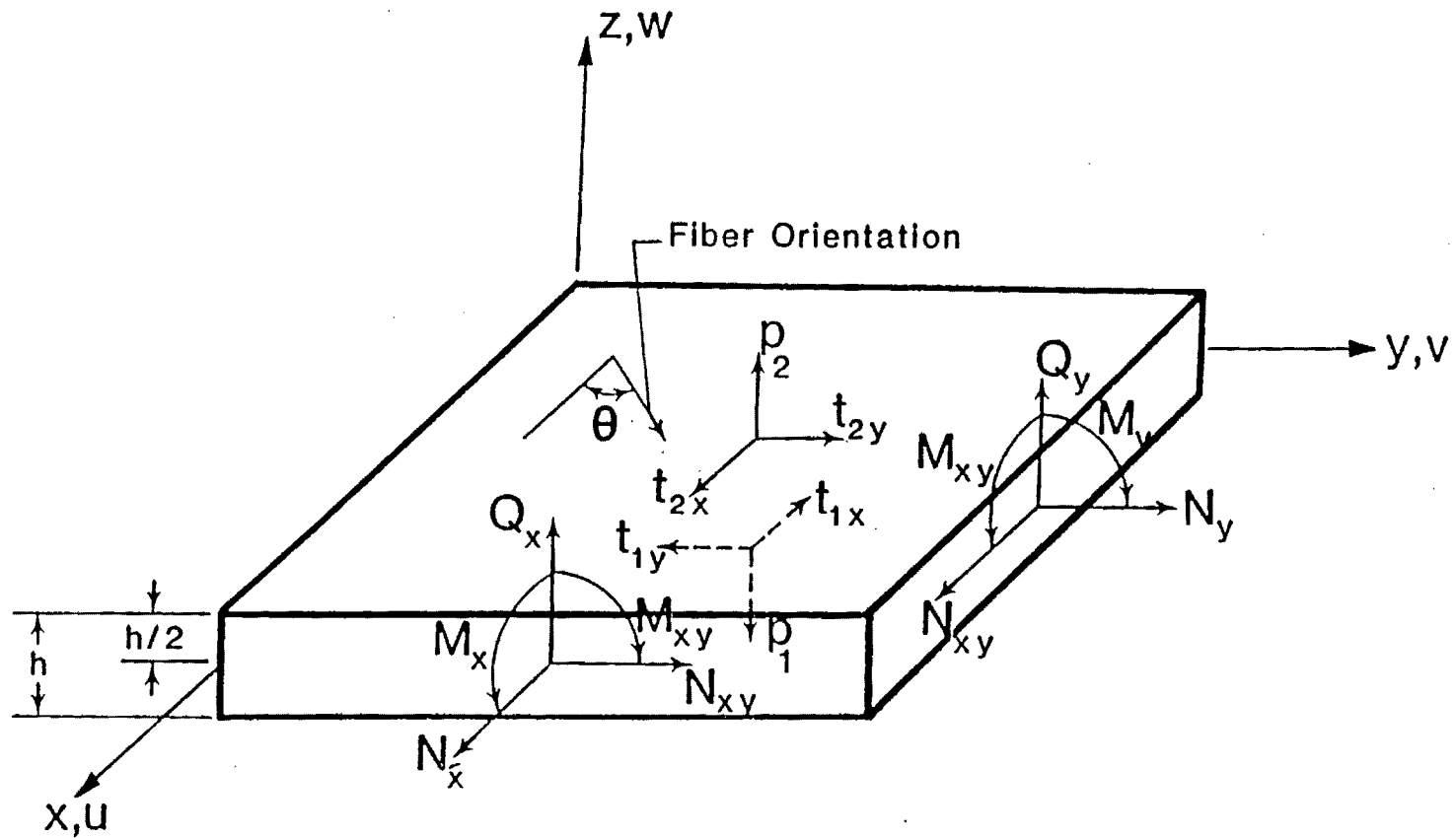


FIGURE 7 - NOTATIONS AND SIGN CONVENTION FOR GENERIC SUBLAMINATE

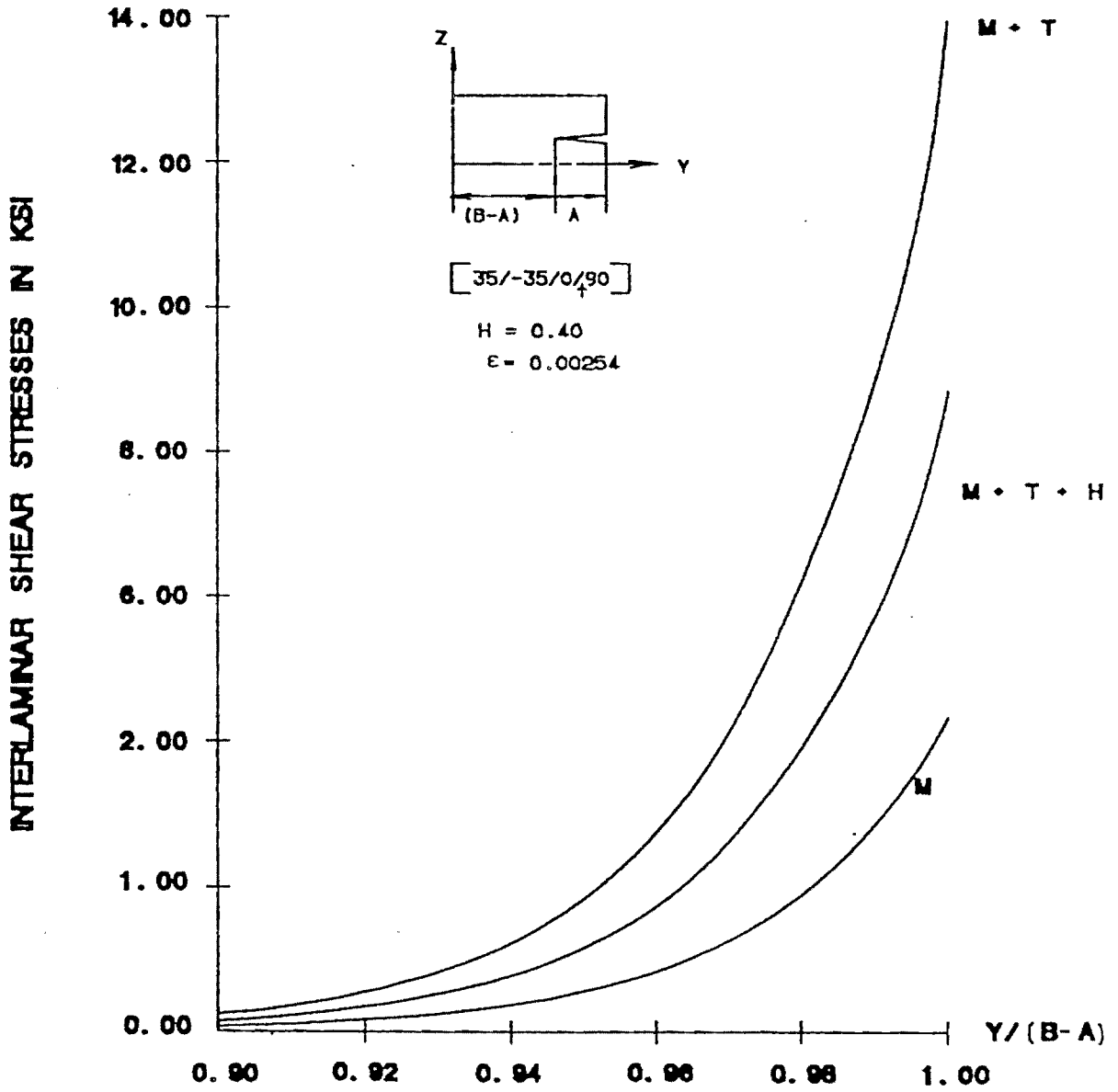


FIGURE 8 - COMPARISON OF INTERLAMINAR STRESSES

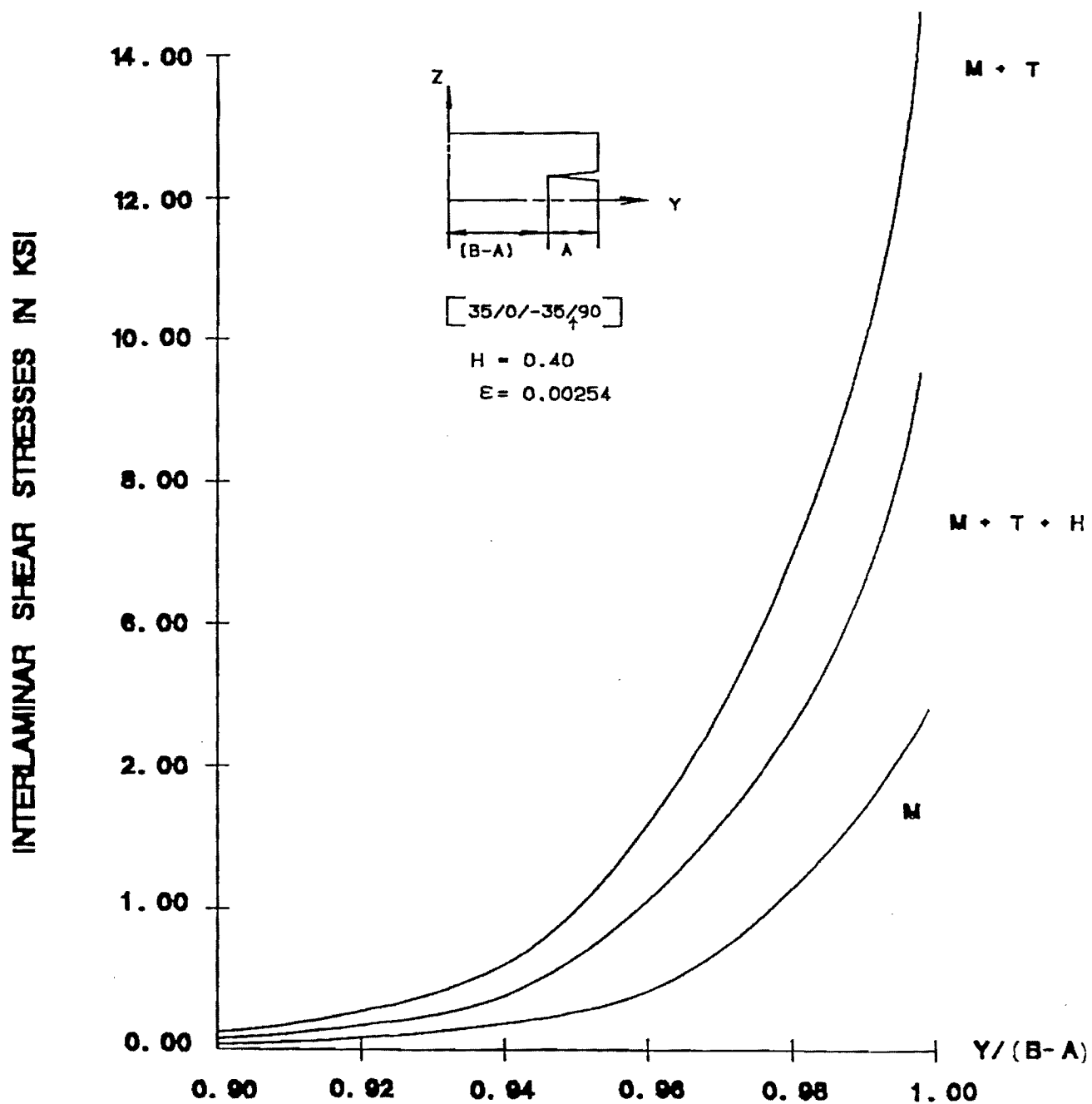


FIGURE 9 - COMPARISON OF INTERLAMINAR STRESS

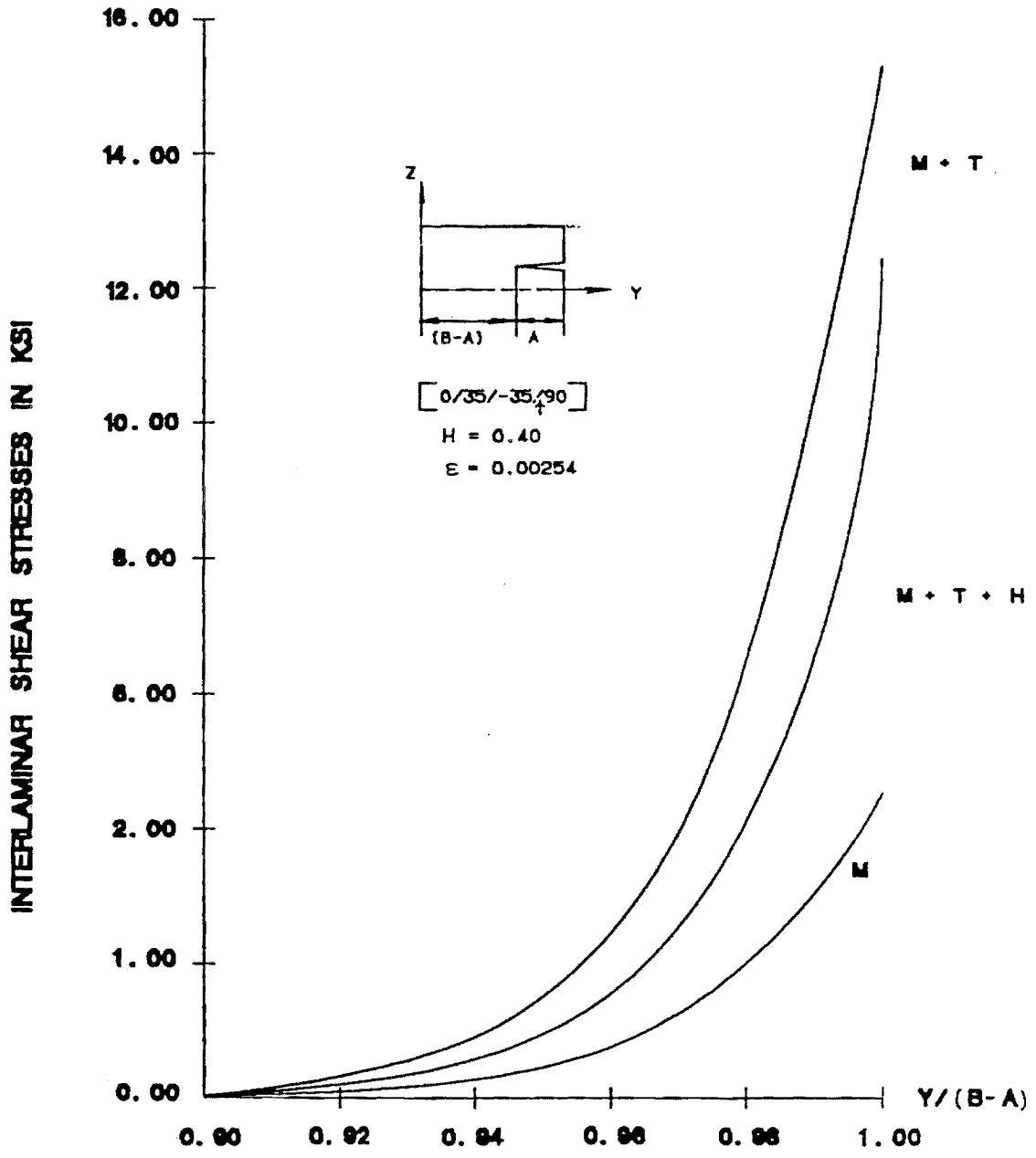


FIGURE 10 - COMPARISON OF INTERLAMINAR STRESS

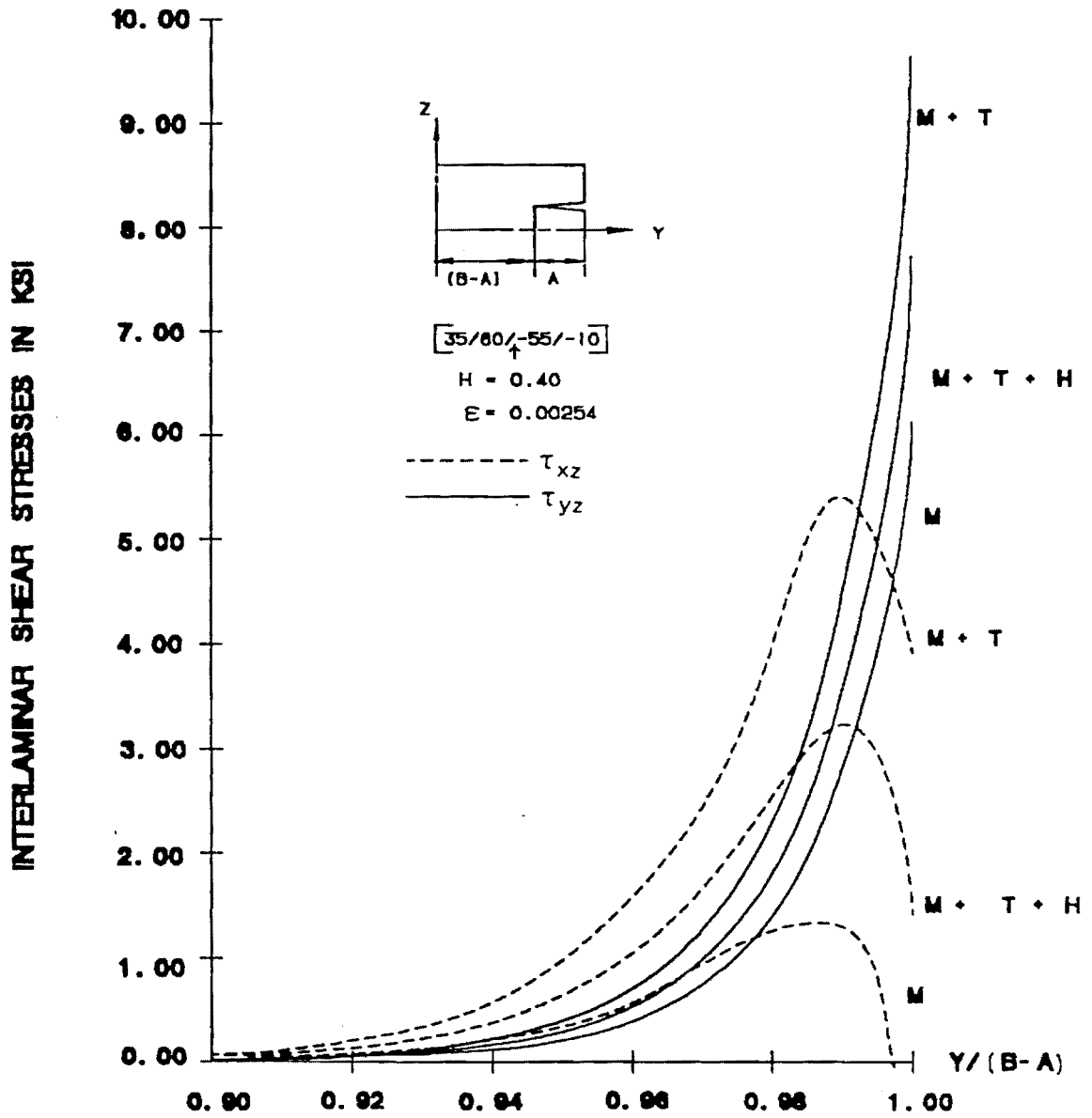


FIGURE 11 - COMPARISON OF INTERLAMINAR STRESSES

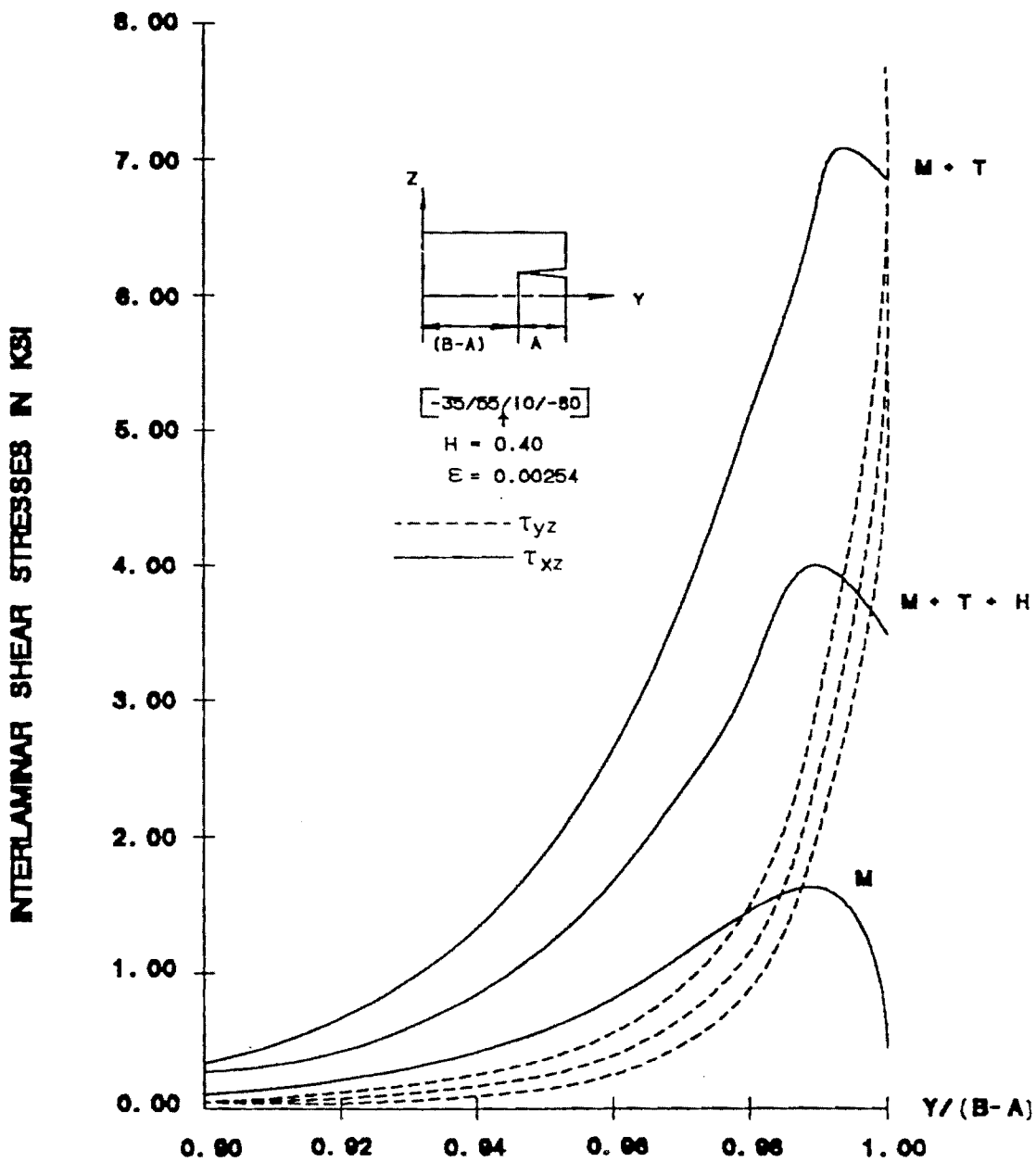


FIGURE 12 - COMPARISON OF INTERLAMINAR STRESSES

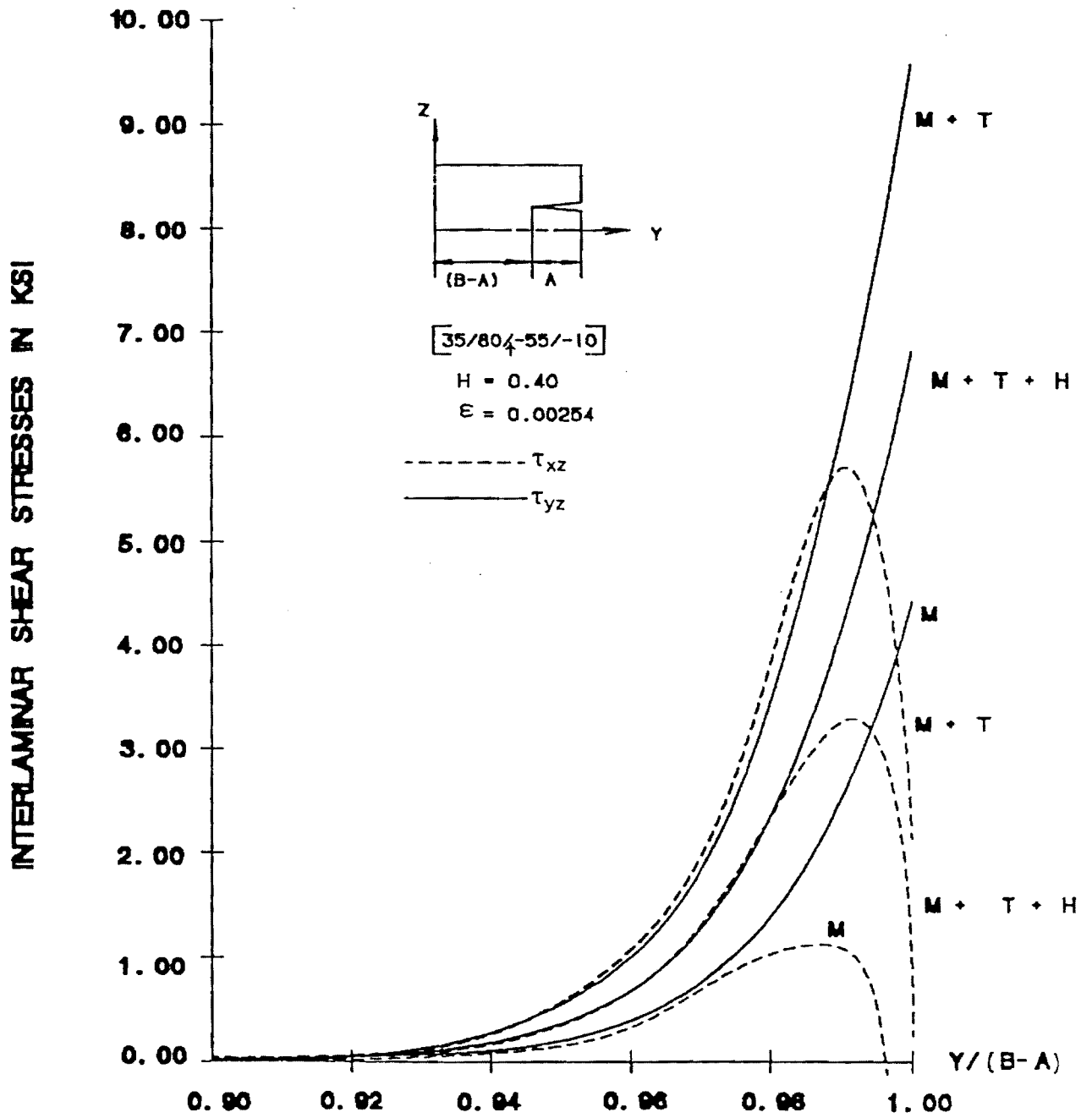


FIGURE 13 - COMPARISON OF INTERLAMINAR STRESSES

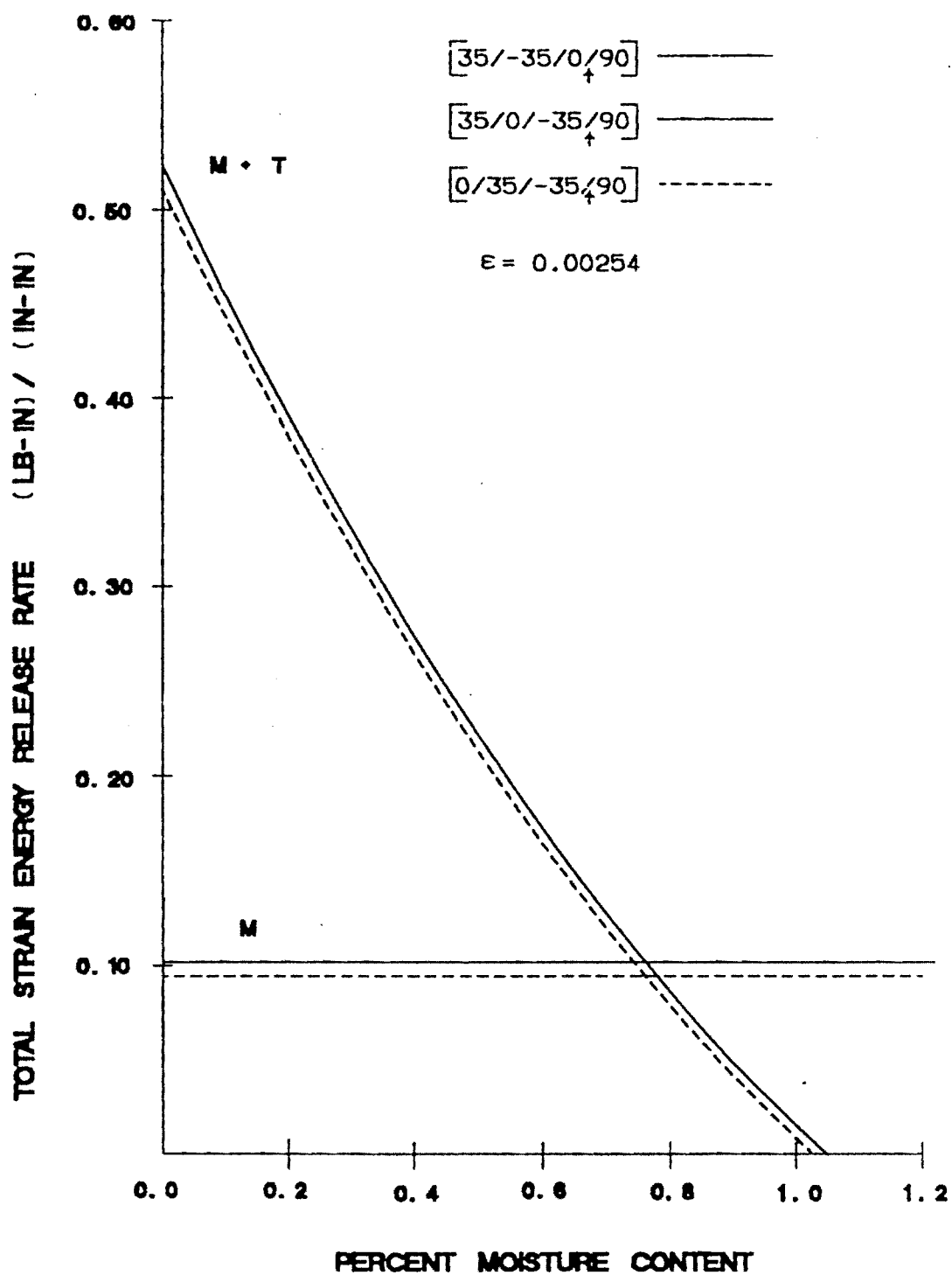


FIGURE 14 - ENERGY RELEASE RATE DISTRIBUTION
 FOR LAMINATES WITHOUT MODE III

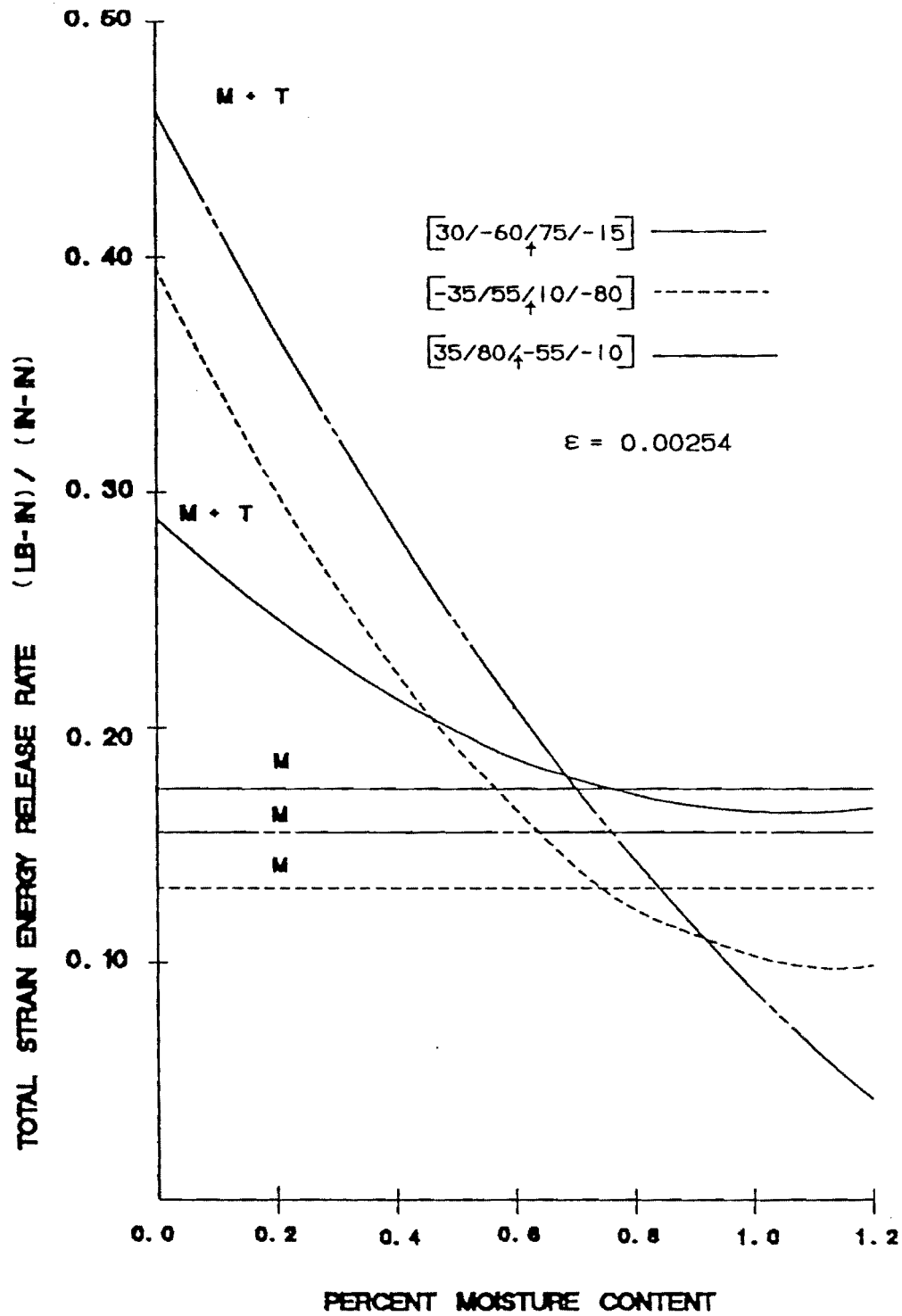


FIGURE 15 - ENERGY RELEASE RATE DISTRIBUTION FOR LAMINATES WITH MODE III

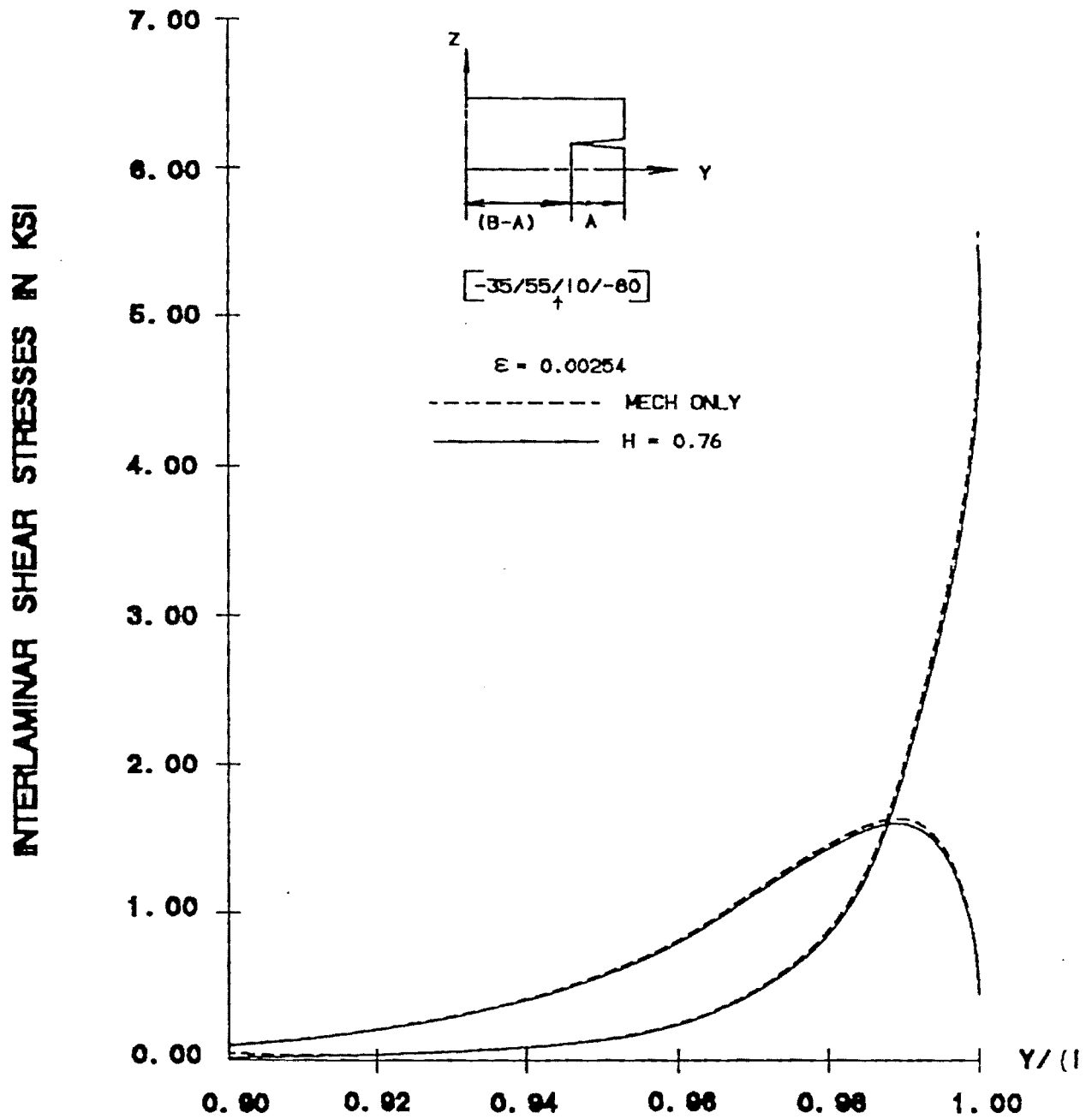


FIGURE 16 - TOTAL ALLEVATED STATE STRESS DISTRIBUTION

APPENDIX I

Derivation of the Governing Equations

In this Appendix the governing equations for the sublaminates shown in Figure 7 are derived using the principle of virtual work.

Consider a sublaminate of thickness h . The origin of a cartesian coordinate system is located within the central plane (x - y) with the z -axis being normal to this plane. The material of each ply is assumed to possess a plane of elastic symmetry parallel to xy as shown in Figure 6.

Stress and moment resultants are given below.

$$(N_x, N_y, N_{xy}, Q_x, Q_y) = \int_{-h/2}^{h/2} (\sigma_x, \sigma_y, \tau_{xy}, \tau_{xz}, \tau_{yz}) dz$$

$$(M_x, M_y, M_{xy}) = \int_{-h/2}^{h/2} (\sigma_x, \sigma_y, \tau_{xy}) z dz \quad (I-1)$$

Because of the existence of a plane of elastic symmetry, the constitutive relations are given by

$$\begin{bmatrix} \sigma_x \\ \sigma_y \\ \sigma_z \\ \tau_{xy} \end{bmatrix} = \begin{bmatrix} C_{11} & & & \\ C_{12} & C_{22} & & \text{SYM} \\ C_{13} & C_{23} & C_{33} & \\ C_{16} & C_{26} & C_{36} & C_{66} \end{bmatrix} \begin{bmatrix} \epsilon_x \\ \epsilon_y \\ \epsilon_z \\ \gamma_{xy} \end{bmatrix}_M$$

$$\begin{bmatrix} \tau_{yz} \\ \tau_{xz} \end{bmatrix} = \begin{bmatrix} C_{44} & \text{SYM} \\ C_{45} & C_{55} \end{bmatrix} \begin{bmatrix} \gamma_{yz} \\ \gamma_{xz} \end{bmatrix}_M \quad (I-2)$$

where C_{ij} are components of the anisotropic stiffness matrix and γ_{xy} , γ_{yz} and γ_{xz} are engineering shear strains.

The displacements are assumed to be of the form

$$\begin{aligned} u &= U(x, y) + z\beta_x(x, y) \\ v &= V(y) + z\beta_y(x, y) \\ w &= W(x, y) \end{aligned} \quad (I-3)$$

where u, v and w are the displacement components in the x, y and z directions, respectively. Equation (I-3) in conjunction with the strain-displacement relations of classical theory of elasticity leads to the following kinematic relations

$$\begin{aligned}
 \epsilon_{xx} &= U_{,x} + z\beta_{x,x} \\
 \epsilon_{yy} &= V_{,y} + z\beta_{y,y} \\
 \epsilon_{zz} &= 0 \\
 \gamma_{xy} &= U_{,y} + V_{,x} + z(\beta_{x,y} + \beta_{y,x}) \\
 \gamma_{xz} &= \beta_x + W_{,x} \\
 \gamma_{yz} &= \beta_y + W_{,y}
 \end{aligned} \tag{I-4}$$

Substitute Equation (I-4) into Equation (I-2) and put the results into Equation (I-1). This yields the following constitutive relations:

$$\begin{bmatrix} N_x \\ N_y \\ N_{xy} \\ M_x \\ M_y \\ M_{xy} \end{bmatrix} = \begin{bmatrix} A_{11} & A_{12} & A_{16} & B_{11} & B_{12} & B_{16} \\ A_{12} & A_{22} & A_{26} & B_{12} & B_{22} & B_{26} \\ A_{16} & A_{26} & A_{66} & B_{16} & B_{26} & B_{66} \\ B_{11} & B_{12} & B_{16} & D_{11} & D_{12} & D_{16} \\ B_{12} & B_{12} & B_{26} & D_{11} & D_{12} & D_{26} \\ B_{16} & B_{26} & B_{66} & D_{16} & D_{26} & D_{66} \end{bmatrix} \begin{bmatrix} U_{,x} \\ V_{,y} \\ U_{,y} + V_{,x} \\ \beta_{x,x} \\ \beta_{y,y} \\ \beta_{x,y} + \beta_{y,x} \end{bmatrix} + \begin{bmatrix} N_x \\ N_y \\ N_{xy} \\ M_x \\ M_y \\ M_{xy} \end{bmatrix}^{NM}$$

$$\begin{bmatrix} Q_y \\ Q_x \end{bmatrix} = \begin{bmatrix} A_{44} & A_{45} \\ A_{45} & A_{55} \end{bmatrix} \begin{bmatrix} \beta_y + W_{,y} \\ \beta_x + W_{,x} \end{bmatrix}$$

where

$$(A_{ij}, B_{ij}, D_{ij}) = \int_{-h/2}^{h/2} C_{ij} (1, z, z^2) dz \tag{I-5}$$

and the non-mechanical terms are defined in Appendix II.

The variation of the strain energy due to virtual displacements δu , δv and δw is

$$\delta\bar{V} = \int_V (\sigma_x \delta\epsilon_x + \sigma_y \delta\epsilon_y + \sigma_z \delta\epsilon_z + \tau_{xy} \delta\gamma_{xy} + \tau_{yz} \delta\gamma_{yz} + \tau_{xz} \delta\gamma_{xz}) dV \quad (I-6)$$

where $\delta\epsilon_x$, $\delta\epsilon_y$, $\delta\epsilon_z$, $\delta\gamma_{xy}$, $\delta\gamma_{xz}$ are the strains associated with the virtual displacements. Using Equations (I-3) and (I-1) then integrating through the thickness gives

$$\delta\bar{V} = \int_A [N_x \delta U_{,x} + N_y \delta V_{,y} + N_{xy} \delta U_{,y} + Q_x \delta\beta_x + Q_y (\delta\beta_y + \delta W_{,y}) + M_x \delta\beta_{x,x} + M_y \delta\beta_{y,y} + M_{xy} \delta\beta_{x,y}] dA \quad (I-7)$$

The variation of the work done by the external forces and by the surface tractions is

$$\begin{aligned} \delta\bar{W} = & \int_A (n_x \delta U + n_y \delta V + q \delta W + m_x \delta\beta_x + m_y \delta\beta_y) dA \\ & + \int_S (\bar{N}_n \delta\bar{U}_n + \bar{N}_{ns} \delta\bar{U}_s + \bar{M}_n \delta\bar{\beta}_n + \bar{M}_{ns} \delta\bar{\beta}_s) ds \end{aligned} \quad (I-8)$$

where a bar denotes values on the boundary. Variables n and s are coordinates normal and tangential to the edge, and

$$\begin{aligned} n_x &= t_{2x} - t_{1x} \\ n_y &= t_{2y} - t_{1y} \\ q &= p_2 - p_1 \\ m_x &= \frac{h}{2} (t_{2x} + t_{1x}) \\ m_y &= \frac{h}{2} (t_{2y} + t_{1y}) \end{aligned} \quad (I-9)$$

where n_x and n_y can be regarded as effective distributed axial forces. Terms m_x and m_y are effective distributed moments and q is an effective lateral pressure.

From the principle of virtual work the equations of equilibrium and boundary conditions are determined from the Euler equations and boundary conditions of the variational equation.

$$\delta\bar{V} = \delta\bar{W} \quad (I-10)$$

Substitution of Equations (I-7) and (I-8) into Equation (I-10) leads the following equations of equilibrium:

$$\begin{aligned}
 N_{x,x} + N_{xy,y} + n_x &= 0 \\
 N_{xy,x} + N_{y,y} + n_y &= 0 \\
 Q_{x,x} + Q_{y,y} + q &= 0 \\
 M_{x,x} + M_{xy,y} - Q_x + m_x &= 0 \\
 M_{xy,x} + M_{y,y} - Q_y + m_y &= 0
 \end{aligned} \tag{I-11}$$

and one member of the following five products must be prescribed on the sublamine edges

$$N_n U_n, N_{ns} U_s, M_n \beta_n, M_{ns} \beta_s \text{ and } Q_n W \tag{I-12}$$

For the ED specimen under uniform extension, $U(x,y)$ in Equation (I-3) is given by

$$U(x,y) = U^*(y) + x\epsilon \tag{I-13}$$

and the response is a function of y and z coordinates only. For this case the equilibrium equations (I-11) take the form

$$\begin{aligned}
 N_{xy,y} + n_x &= 0 \\
 N_{y,y} + n_y &= 0 \\
 Q_{y,y} + q &= 0 \\
 M_{xy,y} - Q_x + m_x &= 0 \\
 M_{y,y} - Q_y + m_y &= 0
 \end{aligned} \tag{I-14}$$

Substitution of the constitutive relations in Equation (I-5) into Equation (I-14) yields the following equilibrium equations in terms of kinematic variables.

APPENDIX II

Hygrothermal Effects on Edge Delamination

The displacement field and constitutive relations governing the free edge ply separation were presented in Appendix I. The hygrothermal expressions, represented with the superscript NM for non-mechanical, are defined as follows

$$\begin{pmatrix} N_1^{NM} \\ M_1^{NM} \end{pmatrix} = \int_{h/2}^{h/2} (1, z) \bar{Q}_{1j} \{ \bar{\alpha}_j (T - T_r) + \bar{\beta}_j C \} dz \quad (II-1)$$

where

$\bar{\alpha}_j$ - Coefficient of thermal expansion

$\bar{\beta}_j$ - Swelling coefficient

T - Local temperature

T_r - Reference temperature

C - Specific moisture concentration

\bar{Q}_{1j} - Reduced stiffness coefficient

The terms $\bar{\alpha}_j$ and $\bar{\beta}_j$ are transformed as second order tensors with the assumption of no thermal or swelling shear strain.

The concept of sublaminates is used when enforcing the boundary conditions.

Cracked Sublaminates

Sublaminates 2:

The boundary conditions for this sublaminate are expressed as:

$$N_{y2} - N_{xy2} - M_{y2} - Q_{y2} = 0 \quad (II-2)$$

$$M_{xy2,y} - Q_{x2} = 0$$

Using the first three conditions in the governing equations, one can express V_2 , U_2 and β_{2y} in terms of β_{2x} to obtain:

$$\begin{bmatrix} A_{12}^1 & B_{26}^1 \\ A_{16}^1 & B_{66}^1 \\ B_{12}^1 & D_{26}^1 \end{bmatrix} \begin{bmatrix} \epsilon \\ \beta_{2x,y} \end{bmatrix} + \begin{bmatrix} A_{22}^1 & A_{26}^1 & B_{22}^1 \\ A_{26}^1 & A_{66}^1 & A_{26}^1 \\ B_{22}^1 & B_{26}^1 & D_{22}^1 \end{bmatrix} \begin{bmatrix} v_{2,y} \\ v_{2,y} \\ \beta_{2y,y} \end{bmatrix} - \begin{bmatrix} N_{y1} \\ N_{xy1} \\ M_{y1} \end{bmatrix}^{NM} = 0 \quad (II-3)$$

Sublaminates 3:

The boundary conditions for this sublaminates are given as:

$$N_{y3} - N_{xy3} = 0$$

$$M_{y3,y} - Q_{y3} = 0$$

$$M_{xy3,y} - Q_{x3} = 0$$

(II-4)

These are used in a similar manner (as in sublaminates 2) to obtain

$$\begin{bmatrix} A_{22}^0 \\ A_{26}^0 \end{bmatrix} \begin{bmatrix} v_{3,y} \\ u_{3,y} \end{bmatrix} + \begin{bmatrix} A_{12}^0 & B_{22}^0 & B_{26}^0 \\ A_{16}^0 & B_{26}^0 & B_{66}^0 \end{bmatrix} \begin{bmatrix} \epsilon \\ \beta_{3,y} \\ \beta_{3x,y} \end{bmatrix} - \begin{bmatrix} N_{y0} \\ N_{xy0} \end{bmatrix} = 0 \quad (II-5)$$

These equations are then substituted back into the governing equations to obtain expressions for the force and moment resultants. They can be expressed in terms of the strain plus non-mechanical effects.

UNCRAKED SUBLAMINATES

Sublaminates 0 and 1:

The boundary conditions of continuity at the interfaces must be satisfied.

$$N_{y1}(0) - N_{xy1}(0) - N_{y0}(0) - N_{xy0}(0) = 0 \quad (II-6)$$

$$M_{xy1}(0) - M_{xy2}(0)$$

$$M_{y0}(0) - M_{y3}(0)$$

$$M_{xy0}(0) - M_{xy3}(0) \quad (II-7)$$

and

$$M_{xy1}(0) - M_{xy2}(0)$$

$$\beta_{1x}(0) - \beta_{2x}(0)$$

$$M_{y0}(0) - M_{y3}(0) \quad (II-8)$$

$$\beta_{0y}(0) - \beta_{3y}(0)$$

$$M_{xy0}(0) - M_{xy3}(0)$$

$$\beta_{0x}(0) - \beta_{3x}(0)$$

Enforcing equations (II-6) and (II-7) in the governing equations yields the following:

$$\begin{bmatrix} A_{12}^1 & A_{22}^1 & A_{26}^1 \\ A_{16}^1 & A_{26}^1 & A_{66}^1 \\ A_{12}^0 & A_{22}^0 & A_{26}^0 \\ A_{16}^0 & A_{26}^0 & A_{66}^0 \end{bmatrix} \begin{bmatrix} \epsilon \\ \epsilon_y \\ \gamma_{xy} \end{bmatrix} - \begin{bmatrix} N_{y1} \\ N_{xy1} \\ N_{y0} \\ N_{xy0} \end{bmatrix}^{NM} + \begin{bmatrix} -N_{y1j} \\ -N_{xy1j} \\ N_{y1j} \\ N_{xy1j} \end{bmatrix} s_j G_j - 0 \quad (II-9)$$

$$\begin{bmatrix} B_{12}^1 & B_{22}^1 & B_{26}^1 \\ -A_1 & B_{26}^1 & B_{66}^1 \end{bmatrix} \begin{bmatrix} \epsilon \\ \epsilon_y \\ \gamma_{xy} \end{bmatrix} - \begin{bmatrix} M_{y1}^{NM} \\ A_1^{NM} \end{bmatrix} - \begin{bmatrix} M_{y1j} s_j \\ M_{xy1j} s_j + B_1 s_c \alpha_j \end{bmatrix} \quad (II-10)$$

$$(j=1-4)$$

The expressions in (II-9) and (II-10) are defined below

$$\begin{bmatrix} \epsilon_y \\ \gamma_{xy} \end{bmatrix} = \begin{bmatrix} C_v \\ C_u \end{bmatrix} \epsilon + \begin{bmatrix} C_v \\ C_u \end{bmatrix}^{NM} \quad (II-11)$$

$$\Delta = A_{22}^* A_{66}^* - (A_{26}^*)^2 \quad (II-12)$$

$$\begin{bmatrix} C_v \\ C_u \end{bmatrix} = \frac{1}{\Delta} \begin{bmatrix} A_{26}^* & A_{16}^* - A_{66}^* & A_{12}^* \\ A_{26}^* & A_{12}^* - A_{22}^* & A_{16}^* \end{bmatrix} \quad (II-13)$$

$$\begin{bmatrix} C_v \\ C_u \end{bmatrix}^{NM} = \frac{1}{\Delta} \begin{bmatrix} A_{66}^* (N_{y1} + N_{yo})^{NM} - A_{26}^* (N_{xy1} + N_{xyo})^{NM} \\ -A_{26}^* (N_{y1} + N_{yo})^{NM} + A_{22}^* (N_{xy1} + N_{xyo})^{NM} \end{bmatrix} \quad (II-14)$$

A_1 and A_1^{NM} are functions of A_{ij} , B_{ij} and D_{ij} . The superscripts * implies a summation of the upper and lower sublaminates.

Continuing with the derivation one can substitute the expressions set forth into equation (I-7) as well as 10 and 11 in the report. This gives the following expression for the total energy release rate.

$$G = \frac{1}{2} \frac{d}{da} \int_0^b \left[\int_{h/2}^{h/2} N_x \epsilon_m dz \right] dy \quad (II-15)$$

The concept of free-expansion in the x-direction is implemented to find the strain induced by the non-mechanical effects on the structure. Setting $N_x = 0$ for each ply in Equation (I-5) and using the boundary conditions of (II-2), (II-4) and (II-6) allows the following.

$$\epsilon_u^k = -T_u^k / E_u^k$$

$$\epsilon_c^k = -T_c^k / E_c^k \quad (II-16)$$

where

$$\begin{aligned}
 T_u^k &= h^k C_v^{NM} \bar{Q}_{12}^k + h^k C_u^{NM} \bar{Q}_{16}^k - (N_x^{NM})^k \\
 E_u^k &= h^k (\bar{Q}_{11}^k + C_v \bar{Q}_{12}^k + C_u \bar{Q}_{16}^k) \\
 T_c^k &= \bar{Q}_{12}^k F_1^{NM} h^k + \bar{Q}_{16}^k F_2^{NM} h^k + B_{12}^k F_3^{NM} - (N_x^{NM})^k \\
 E_c^k &= \bar{Q}_{11}^k h^k + \bar{Q}_{12}^k h^k C_{d11} + \bar{Q}_{16}^k h^k C_{d12} + B_{12}^k C_{d31}
 \end{aligned} \tag{II-17}$$

Superscript k represents the ply. Expressions C_{dij} and F_i^{NM} are found by substituting the conditions of (II-2) into (II-3).

$$\left[C_d \right]_{3 \times 2} = \begin{bmatrix} A_{22}^1 & A_{26}^1 & B_{22}^1 \\ A_{26}^1 & A_{66}^1 & B_{26}^1 \\ B_{22}^1 & B_{26}^1 & D_{22}^1 \end{bmatrix}^{-1} \begin{bmatrix} A_{12}^1 & B_{26}^1 \\ A_{16}^1 & B_{66}^1 \\ B_{12}^1 & D_{26}^1 \end{bmatrix} \tag{II-18}$$

$$\left\{ F^{NM} \right\}_{3 \times 1} = \begin{bmatrix} A_{22}^1 & A_{26}^1 & B_{22}^1 \\ A_{26}^1 & A_{66}^1 & D_{22}^1 \\ B_{22}^1 & B_{26}^1 & D_{22}^1 \end{bmatrix}^{-1} \begin{bmatrix} N_y \\ N_{xy1} \\ M_{y1} \end{bmatrix}^{NM} \tag{II-19}$$

Sublaminates 3 has $B_{ij} = 0$ due to symmetry of the structure. When considering these plies, the term F_1^{NM} and F_2^{NM} are found by substituting the boundary conditions (II-4) into (II-5).

This gives a second expression of F^{NM} for this sublaminate

$$\begin{pmatrix} F^{NM} \\ \end{pmatrix}_{2 \times 1} = \begin{bmatrix} A_{22}^0 & A_{26}^0 \\ A_{26}^0 & A_{66}^0 \end{bmatrix}^{-1} \begin{pmatrix} N_{y0} \\ N_{xy0} \end{pmatrix}^{NM} \quad (II-20)$$

To find the total strain associated with the non-mechanical effects, it is necessary to sum the force over the entire structure and set it to zero. These are used in order to obtain Equation (16), (17) and (18) in the report on page 17. Substituting this in Equation (II-15) gives the total strain energy release rate expression per unit length

$$G = \frac{1}{2} \sum_K - (E_c^k \epsilon^T + T_c^k) (\epsilon^T - \epsilon_c^k) + (E_u^k \epsilon^T + T_u^k) (\epsilon^T - \epsilon_u^k)$$

The expression $\epsilon^T - \epsilon_{c,u}^k$ is in essence the total mechanical strain of that ply.

INTERLAMINAR STRESSES

The interlaminar stresses of the structure are defined in Equations (8) and (9)

$$\begin{aligned} \tau_x &= N_{xy,y}^1 - N_{xy1j} s_j^2 G_j e^{-s_j y} \\ \tau_y &= N_{y,y}^1 - N_{y1j} s_j^2 G_j e^{-s_j y} \quad (j=1-4) \end{aligned} \quad (II-21)$$

While s_j , the positive roots resulting from the polynomial

$$E_8 s^8 + E_6 s^6 + E_4 s^4 + E_2 s^2 + E_0 = 0, \quad (II-22)$$

are independent of the hygrothermal effects, the rest of the terms are not.

Solving Equations (II-9) and (II-10) gives the term G_j while N_{xy1j} and N_{y1j} are found from

$$\begin{pmatrix} N_{y1j} \\ N_{xyj} \end{pmatrix} = \begin{bmatrix} A_{22}^1 & A_{26}^1 & B_{22}^1 & B_{26}^1 \\ A_{26}^1 & A_{66}^1 & B_{26}^1 & B_{66}^1 \end{bmatrix} \begin{pmatrix} v_j \\ u_j \\ \alpha_j \end{pmatrix} \quad (j = 1, 2, 3, 4) \quad (\text{II-23})$$

where v_j , u_j and α_j are found by imposing the boundary conditions on the mode shapes. They are dependent on the four values of s_j as well as the sublamine stiffness matrices.

APPENDIX III

PROGRAM START (INPUT, OUTPUT, TAPE5=INPUT, TAPE6=OUTPUT)

THIS PROGRAM IS FOR THE FINAL PAPER 8-16-87
DIMENSION STATEMENTS

```

REAL BG(4),E(9),GG(4,4),MATR32(3,2),MATR33(3,3),MATR3(3),
C STRAIN(25),SAVE3(3),SAVE33(3,3),WKAREA(99),ZR
COMPLEX SJ(8)
DOUBLE PRECISION BNEG,A,C,DIFF1,DIFF2,UNSY(2),UNSX(2),
C SSSS,SSSC,SSCC,SCCC,ZZZO(0:50),J22,J26,FNM(3),S1NM,S2NM,
C MEMSX,MEMSX,F11M,F22M,SS1,SS2,SSY,SSX,ZZZ1(0:50),
C THICK(40),THETA(50),E1(50),E2(50),CCCC,HSS(5),HSN1,HSN2,
C Q(6,6,50),ZO(0:40),AO(6,6),A1(6,6),U13,U14,BG1,BG2,
C NXO(4),E15,E16,E17,E18,E19,ZTT(0:40),
C NY1(4),X(2),Y(3),CV,CU,W(2),ZZ(3),VV11,VV12
DOUBLE PRECISION ALPHA(4),PHI(4),GAMMA(4),NX1(4),
C B1(6,6),BO(6,6),DO(6,6),D1(6,6),F(4,4),VV13,VV14,J66,
C RDLT,RTA1,RTA2,RSB1,RSB2,U12,U11,A1NM,
C NXY1(4),MY1(4),MXY1(4),WD(2,3),CD(3,2),WIDTH,
C V12(50),V21(50),SS,CC,K66,K26,K22,
C Z1(0:40),FX,FY,G1(2,35),K16,K12,H66
DOUBLE PRECISION SV(5),SU(5),AL,SC,S(8),DY,
C G12(50),G31(50),C2,C1,THETV,THETU,G111(2,35),CS,
C DEL,HO,H1,H22,HE,HG,HNY(50),HNXY(50),HM3,CVNM,
C C11,C12,C22,C26,C44,D,C55,C66,H26,SQ,DUM,CUNM,
C CONY,CONXY,SMNY,SMNXY,
C SB1,SB2,TA1,TA2,ATHM1(40),ATHM2(40),ATHM6(40),BSW2(40),
C NMNYO,NMNXYO,G11(2,35),
C DVV11,DVV12,DU13,DU14,DF(4,4),DX,ATH,CCONY,CCONXY,
C BSW6(40),DELTEMP,BSW1(40),CMOIST(35),
C SIGX(0:40,79:120),
C NMNY1,NMNXY1,NMMX1,NMMY1,SIGY(0:40,79:120)
DOUBLE PRECISION NMSTO(50),NMST2(50),NMST3(50),TNC,UNCL,
C T1(50),T12(50),T13(50),EX(50),EXX(50),EX3(50),JY,
C EXNC,ESTAR,TSTAR,TMST,GLC(0:50),NXNM(50),B12(50)
DATA Q/1800*0.0/, ZR/0.00/

```


DATE OF PROGRAM : SEPT. 1, 1987

THIS IS THE FINAL PROGRAM FOR PREDICTING THE ENERGY RELEASE RATE OF
COMPOSITE LAMINATES INCLUDING HYGROTHERMAL EFFECTS
HOWEVER, IT ONLY CONSIDERS EXTENSION EFFECTS OF STRAIN WHEN DEALING
WITH HYGRAL THERMAL EFFECTS.... LIKE WHITTNEY'S PAPER.....
EXCEPT ON A PLY BY PLY ANALYSIS BASIS OF THE HYGRAL THERMAL EFFECTS

THE INPUT ALLOWS FOR: THE LAMINATE LAY-UP TO CHANGE AND POSITION
OF THE CRACK, DIFFERENT STRAIN VALUES TO BE EVALUATED,
(UP TO 40 LAMINATES AND 25 DIFFERENT STRAIN VALUES)
AND FOR THE EVALUATION OF ONE MOISTURE CONSTANT OR A
RANGE OF THE MOISTURE CONSTANT FROM 0 TO 1.2.

THIS PROGRAM IS FOR THE GIVEN DATA TO BE IN ENGLISH UNITS.

ALL LAMINATES ARE EVALUATED WITHOUT THERMAL EFFECTS AUTOMATICALLY

LZQ IS THE NUMBER OF DIFFERENT LAMINATE (OR CRACK POSITIONS)
TO BE EVALUATED.

```

READ(5,*) LZQ
DO 400 LZZ = 1,LZQ

```

```

READ(5,*) WIDTH, NPLYO, NPLY1, AL
NEXTPL = NPLYO + 1.
TPLY = NPLYO + NPLY1

```

FOR EACH PLY IN THE SUBLAMINATE, THE MATERIAL CHARACTERISTICS MUST BE READ IN.

```

3      PI = 4. * ATAN(1.)
      HO = 0.0
      ATH = 0.0
      H1=0.0
      DO 3 LK = 1, TPLY
      ZO(LK) = 0.0
      Z1(LK) = 0.0

```

```

5      DO 5 I = 1,NPLYO
      READ(5,*) THICK(I), THETA(I), E1(I), E2(I)
      READ(5,*) V12(I)
      READ(5,*) G12(I), G31(I)
      THETA(I) = THETA(I) * PI / 180.
      HO = HO + THICK(I)

```

```

10     DO 10 I = NEXTPL, TPLY
      READ(5,*) THICK(I), THETA(I), E1(I), E2(I)
      READ(5,*) V12(I)
      READ(5,*) G12(I), G31(I)
      THETA(I) = THETA(I) * PI / 180.
      H1 = H1 + THICK(I)

```

```

*****
*****
      THESE ARE WRITE STATEMENTS TO CHECK THE INITIAL CONDITIONS OF THE
      SUBLAMINATE AND VALUES READ IN
*****
*****

```

EACH PLY MAY HAVE DIFFERNT PROPERTIES SO THE PROPERTY OF EACH

```

CC      WRITE(6,289)
      WRITE(6,201) WIDTH
      WRITE(6,202) NPLY1, NPLYO

      WRITE(6,204)
      DO 15 J = 1, TPLY
      JJ = TPLY + 1 - J
      WRITE(6,206) J
      WRITE(6,207) THICK(JJ), THETA(JJ)*180/PI
      WRITE(6,208) E1(JJ)/1E+06 , E2(JJ)/1E+06
      WRITE(6,209) V12(JJ)
15     WRITE(6,214) G12(JJ)/1E+06, G31(JJ)/1E+06

```

```

*****
*****
      DETERMINE THE Z COMPONENT OF ALL LAMINATES

```

```

      CHECK = 0.00000001
      ZTT(0) = 0.0
      ZO(0) = -HO / 2.0
      DO 20 I = 1, NPLYO
20     ZTT(I) = THICK(I) + ZTT(I-1)
      ZO(I) = THICK(I) + ZO(I-1)

      Z1(NPLYO) = -H1 / 2.0

```

```

DO 25 I = NEXTPL,TPLY
  ZTT(I) = THICK(I) + ZTT(I-1)
  Z1(I) = THICK(I) + Z1(I-1)

```

```

*****
FIRST READ IN THE NUMBER OF STRAINS TO BE EVALUATED AND THEIR VALUE
THEN READ IN IF THE MOISTURE CONTENT SHOULD VARY OVER 0 TO 1.2 OR
BE A CONSTANT.

```

```

  NSTRA = ..... NUMBER OF VARIOUS STRAIN VALUES
  IF MOISTV = 1 ... CMOIST VARIES OVER 0 TO 1.2
  IF MOISTV = 0 ... CMOIST IS A SPECIFIC VALUE

```

```

*****

```

```

  READ(5,*) NSTRA
  DO 27 J=1,NSTRA
  READ(5,*) STRAIN(J)

```

```

  DO 400 LST = 1,NSTRA
  READ(5,*) RDLT,RSB1,RSB2,RTA1,RTA2
  WRITE(6,231) STRAIN(LST),RDLT,RSB1,RSB2,RTA1,RTA2

```

```

  READ(5,*) MOISTV
  IF (MOISTV.EQ.0) READ(5,*) CM
  IF (MOISTV.EQ.0) MMC = 1
  IF (MOISTV.EQ.0) WRITE(6,232) CM
  IF (MOISTV.EQ.1) MMC = 25
  IF (MOISTV.EQ.1) WRITE(6,233)

```

```

*****

```

```

  DO 300 JM = 1,MMC +1

```

```

  FIND Q'S AS WELL AS Q-BAR , SAVING Q-BAR
  AND READ AND CALCULATE THE HYGRO THERMO EFFECTS

```

```

*****

```

```

  DO 200 IZZ = 1,2
  LIL = 0
  IF (IZZ.EQ.1) JMM = JM
  IF (IZZ.EQ.2) JMM = 0
  IF (JM.EQ.1 .AND. IZZ.EQ.1) LIL = 1
  IF (JM.GT.1 .AND. IZZ.EQ.2) GO TO 200

```

```

  NMNY1 = ZR
  NMNXY1 = ZR
  NMMX1 = ZR
  NMMY1 = ZR

```

```

  NMNYO = ZR
  NMNXYO = ZR
  HM3 = ZR
  SMNY = ZR
  SMNXY = ZR

```

```

  DO 24 I=1,5
  E(I) = ZR
  E(I+4) = ZR
  HSS(I) = ZR
  DO 26 I=1,6
  DO 26 J= 1,6
  NXNM(I) = ZR
  DF(I,J) = ZR
  AO(I,J) = ZR
  BO(I,J) = ZR
  DO(I,J) = ZR
  A1(I,J) = ZR
  B1(I,J) = ZR
  D1(I,J) = ZR

```

```

DO 28 MM = 1, TPLY
28   IF ( THICK (MM) .GT. ATH ) ATH = THICK (MM)

   IZZ = 2 IS FOR LAMINATE WITHOUT ANY HYGROTHERMAL EFFECTS
   IZZ = 1 IS FOR HYGROTHERMAL EFFECTS CONSIDERED

   DO 30 I = 1, TPLY

   READ THE HYGROTHERMO EFFECTS, BOTTOM PLY IS FIRST AND UPWARD

   IF ( IZZ.EQ.2 ) GO TO 35
     IF ( MOISTV.EQ.0 ) CMOIST (JM) = CM
     IF ( MOISTV.EQ.1 ) CMOIST (JM) = 0.05 * (JM-1)
     DELTEMP = RDLT
     SB1 = RSB1
     SB2 = RSB2
     TA1 = RTA1
     TA2 = RTA2
     GO TO 40
35   DELTEMP = ZR
     CMOIST (JM) = ZR
     SB1 = ZR
     SB2 = ZR
     TA1 = ZR
     TA2 = ZR

40   V21 (1) = V12 (1) * E2 (1) / E1 (1)
     C11 = E1 (1) / ( 1 - V12 (1) * V21 (1) )
     C12 = E2 (1) * V12 (1) / ( 1 - V12 (1) * V21 (1) )
     C22 = E2 (1) / ( 1 - V12 (1) * V21 (1) )
     C44 = G31 (1)
     C55 = G31 (1)
     C66 = G12 (1)

     SS = DSIN (THETA (1)) * DSIN (THETA (1))
     CC = 1 - SS
     CS = 0.5 * DSIN (2*THETA (1))

     SSSS = SS * SS
     SSSC = SS * CS
     SSCC = SS * CC
     SCCC = CC * CS
     CCCC = CC * CC

     Q (1,1,1) = C11 * CCCC + 2 * ( C12 + 2 * C66 ) * SSCC
C     + C22 * SSSS
     Q (1,2,1) = ( C11 + C22 - 4 * C66 ) * SSCC + C12 * ( SSSS
C     + CCCC )
     Q (2,2,1) = C11 * SSSS + 2 * ( C12 + 2 * C66 ) * SSCC
C     + C22 * CCCC
     Q (1,6,1) = ( C11 - C12 - 2 * C66 ) * SCCC
C     + ( C12 - C22 + 2 * C66 ) * SSSC
     Q (2,6,1) = ( C11 - C12 - 2 * C66 ) * SSSC
C     + ( C12 - C22 + 2 * C66 ) * SCCC
     Q (6,6,1) = ( C11 + C22 - 2 * C12 - 2 * C66 ) * SCCC
C     + C66 * ( SSSS + CCCC )
     Q (4,4,1) = C44 * CC + C55 * SS
     Q (5,5,1) = C44 * SS + C55 * CC
     Q (4,5,1) = CS * ( C44 - C55 )
     Q (6,2,1) = Q (2,6,1)
     Q (6,1,1) = Q (1,6,1)
     Q (2,1,1) = Q (1,2,1)

     HSS (1) = HSS (1) + Q (1,2,1)

```

```

HSS (2) = HSS (2) + Q (2,2,1)
HSS (3) = HSS (3) + Q (2,6,1)
HSS (4) = HSS (4) + Q (1,6,1)
HSS (5) = HSS (5) + Q (6,6,1)

```

```

ATHM1 (1) = TA1 * CC + TA2 * SS
ATHM2 (1) = TA1 * SS + TA2 * CC
ATHM6 (1) = CS * ( TA2 - TA1 )
BSW1 (1) = SB1 * CC + SB2 * SS
BSW2 (1) = SB1 * SS + SB2 * CC
BSW6 (1) = CS * ( SB2 - SB1 )

```

30 CONTINUE

FIND THE A, B, AND D MATRICES FOR THE LOWER AND UPPER SUBLAMINATE.
ALSO FINDS HYGRAL THERMAL EXPRESSIONS ON A PER LAMINA AND PER
SUBLAMINATE BASIS.

```

ZZZO (0) = ZO (0) * ZO (0) * ZO (0)
DO 45 I = 1, NPLYO

```

```

NXNM (1) = ( Q (1,1,1) * ( ATHM1 (1) * DELTEMP + BSW1 (1) * CMOIST (JM) )
C          + Q (1,2,1) * ( ATHM2 (1) * DELTEMP + BSW2 (1) * CMOIST (JM) )
C + Q (1,6,1) * ( ATHM6 (1) * DELTEMP + BSW6 (1) * CMOIST (JM) ) ) * THICK (1)

```

```

NMNYO = NMNYO + ( Q (1,2,1) * ( ATHM1 (1) * DELTEMP + BSW1 (1) * CMOIST (JM) )
C          + Q (2,2,1) * ( ATHM2 (1) * DELTEMP + BSW2 (1) * CMOIST (JM) )
C + Q (2,6,1) * ( ATHM6 (1) * DELTEMP + BSW6 (1) * CMOIST (JM) ) ) * THICK (1)

```

```

NMNXYO = NMNXYO + ( Q (1,6,1) * ( ATHM1 (1) * DELTEMP + BSW1 (1) * CMOIST (JM) )
C          + Q (2,6,1) * ( ATHM2 (1) * DELTEMP + BSW2 (1) * CMOIST (JM) )
C + Q (6,6,1) * ( ATHM6 (1) * DELTEMP + BSW6 (1) * CMOIST (JM) ) ) * THICK (1)

```

C

```

ZZZO (1) = ZO (1) * ZO (1) * ZO (1)
B12 (1) = Q (1,2,1) * 0.5 * ( ( ZO (1) * ZO (1) ) - ( ZO (1-1) * ZO (1-1) ) )
DO 45 L = 1,6
DO 45 J = 1,6
IF ( REAL ( Q (J,L,1) ) .EQ. ZR) GO TO 45
AO (J,L) = AO (J,L) + Q (J,L,1) * THICK (1)
BO (J,L) = BO (J,L) + Q (J,L,1) * 0.5 * ( ( ZO (1) * ZO (1) ) - ( ZO (1-1) * ZO (1-1) ) )
DO (J,L) = DO (J,L) + Q (J,L,1) / 3.0 * ( ZZZO (1) - ZZZO (1-1) )
45 CONTINUE

```

```

ZZZ1 (NPLYO) = Z1 (NPLYO) * Z1 (NPLYO) * Z1 (NPLYO)

```

```

DO 50 I = NEXTPL, TPLY
ZZZ1 (I) = Z1 (I) * Z1 (I) * Z1 (I)

```

```

NXNM (I) = ( Q (1,1,1) * ( ATHM1 (I) * DELTEMP + BSW1 (I) * CMOIST (JM) )
C          + Q (1,2,1) * ( ATHM2 (I) * DELTEMP + BSW2 (I) * CMOIST (JM) )
C + Q (1,6,1) * ( ATHM6 (I) * DELTEMP + BSW6 (I) * CMOIST (JM) ) ) * THICK (I)

```

```

NMNY1 = NMNY1 + ( Q (1,2,1) * ( ATHM1 (I) * DELTEMP + BSW1 (I) * CMOIST (JM) )
C          + Q (2,2,1) * ( ATHM2 (I) * DELTEMP + BSW2 (I) * CMOIST (JM) )
C + Q (2,6,1) * ( ATHM6 (I) * DELTEMP + BSW6 (I) * CMOIST (JM) ) ) * THICK (I)

```



```

NMNXY1= NMNXY1+( Q(1,6,1)*( ATHM1(1)*DELTEMP + BSW1(1)*CMOIST(JM) )
C      + Q(2,6,1)*( ATHM2(1)*DELTEMP + BSW2(1)*CMOIST(JM) )
C      + Q(6,6,1)*( ATHM6(1)*DELTEMP + BSW6(1)*CMOIST(JM) ) ) * THICK(1)

```

```

NMMX1= NMMX1 + 0.5 * ( Z1(1)*Z1(1) - Z1(1-1)*Z1(1-1) ) *
C      ( Q(1,1,1)*( ATHM1(1)*DELTEMP + BSW1(1)*CMOIST(JM) )
C      + Q(1,2,1)*( ATHM2(1)*DELTEMP + BSW2(1)*CMOIST(JM) )
C      + Q(1,6,1)*( ATHM6(1)*DELTEMP + BSW6(1)*CMOIST(JM) ) )

```

```

NMMY1= NMMY1 + 0.5 * ( Z1(1)*Z1(1) - Z1(1-1)*Z1(1-1) ) *
C      ( Q(1,2,1)*( ATHM1(1)*DELTEMP + BSW1(1)*CMOIST(JM) )
C      + Q(2,2,1)*( ATHM2(1)*DELTEMP + BSW2(1)*CMOIST(JM) )
C      + Q(2,6,1)*( ATHM6(1)*DELTEMP + BSW6(1)*CMOIST(JM) ) )

```

```

B12(1) = Q(1,2,1)*0.5*((Z1(1)*Z1(1)) - (Z1(1-1)*Z1(1-1)))
DO 50 L=1,6
DO 50 J=1,6
      IF ( REAL( Q(J,L,1) ) .EQ.0 ) GO TO 50
A1(J,L) = A1(J,L) + Q(J,L,1) * THICK(1)
B1(J,L) = B1(J,L)+Q(J,L,1)*0.5*((Z1(1)*Z1(1)) - (Z1(1-1)*Z1(1-1)))
D1(J,L) = D1(J,L)+Q(J,L,1)/3.0*( ZZZ1(1) - ZZZ1(1-1) )

```

50 CONTINUE

SEE IF COUPLING IS TAKING PLACE

```

      COUPL = 2
DO 60 I=1,6
DO 60 J=1,6
60  IF ( REAL(B0(I,J)) .GT.CHECK ) COUPL=1
      IF ( REAL(B1(I,J)) .GT.CHECK ) COUPL=1
      IF ( REAL(D1(2,6)) .GT. CHECK ) COUPL=1
      IF ( REAL(D0(2,6)) .GT. CHECK ) COUPL=1

```

```

      IF ( COUPL.EQ.1 .AND. LIL.EQ.1 ) WRITE(6,205)
      IF ( COUPL.EQ.2 .AND. LIL.EQ.1 ) WRITE(6,210)

```

CHECK THE SIGN OF THE PEEL STRESS *****

```

      HSN1 = NMNY1 + NMNYO
      HSN2 = NMNXY1 + NMNXYO

```

```

      HDD= HSS(2) * HSS(5) - HSS(3) * HSS(3)
      HE = HSS(3) * HSS(4) - HSS(1) * HSS(5)
      HE = HE /HDD
      HG = HSS(1) * HSS(3) - HSS(2) * HSS(4)
      HG = HG / HDD
DO 65 I=1,TPLY

```

```

      HNY(1) = ATH * STRAIN(LST) * ( Q(1,2,1) + Q(2,2,1) * HE +
C      Q(2,6,1) * HG )
      HNX(1) = ATH * STRAIN(LST) * ( Q(1,6,1) + Q(2,6,1) * HE +
C      Q(6,6,1) * HG )

```

65 CONTINUE

```

DO 70 I = 1,NPLY1

```

```

HM3 = HM3 + ATH * HNY(1) * ( NPLY1 - 1 + .5 )
SMNY = SMNY + HNY(1)
SMNXY = SMNXY + HNX(1)

```

```

IF ( HM3.GT.ZR) GO TO 85

```

```

C
C IF (LIL.EQ.1) WRITE(6,*) ' CASE OF COMPRESSIVE PEEL STRESS
C WRITE(6,218)
C DO 75 I=1,TPLY
75 WRITE(6,220) THETA(1),HNY(1),HNXY(1)
C WRITE(6,*) ' THE MOMENT CALCULATED WAS = ',HM3
C

```

```

85 DO 80 I=1,6
DO 80 J=1,6

```

```

IF ( ABS( REAL(BO(I,J)) ) .LT.CHECK) BO(I,J) = ZR
80 IF ( ABS( REAL(B1(I,J)) ) .LT.CHECK) B1(I,J) = ZR

```

```

*****
*****

```

DEFINE SOME PARAMETERS NEEDED IN THE PROGRAM

```

*****

```

```

H22 = B1(2,2) + H1 / 2.00 * A1(2,2)
H26 = B1(2,6) + H1 / 2.00 * A1(2,6)
H66 = B1(6,6) + H1 / 2.00 * A1(6,6)

```

```

C22 = BO(2,2) + HO / 2.00 * A1(2,2)
C26 = BO(2,6) + HO / 2.00 * A1(2,6)
C66 = BO(6,6) + HO / 2.00 * A1(6,6)

```

```

K22 = A1(2,2) + AO(2,2)
K26 = A1(2,6) + AO(2,6)
K66 = A1(6,6) + AO(6,6)
K12 = A1(1,2) + AO(1,2)
K16 = A1(1,6) + AO(1,6)

```

```

D = K22 * K66 - ( K26 * K26)

```

```

E15 = DO(2,2) - HO/2*BO(2,2)
E16 = DO(2,6) - HO/2*BO(2,6)
E17 = DO(6,6) - HO/2*BO(6,6)
E18 = BO(1,2) - HO/2*AO(1,2)
E19 = BO(1,6) - HO/2*AO(1,6)

```

```

VV11 = ( K26 * H26 - K66 * H22 ) / D + ( H1 / 2.00 )
VV12 = ( K26 * C26 - K66 * C22 ) / D + ( HO / 2.00 )
VV13 = ( K26 * H66 - K66 * H26 ) / D
VV14 = ( K26 * C66 - K66 * C26 ) / D

```

```

U11 = ( K26 * H22 - K22 * H26 ) / D
U12 = ( K26 * C22 - K22 * C26 ) / D
U13 = ( K26 * H26 - K22 * H66 ) / D + ( H1 / 2.00 )
U14 = ( K26 * C26 - K22 * C66 ) / D + ( HO / 2.00 )

```

```

F(1,1) = D1(2,2) + B1(2,2) * H1 / 2.0 + H22*VV11 + H26 * U11
F(2,1) = H22 * VV12 + H26 * U12
F(3,1) = D1(2,6) + B1(2,6) * H1 / 2.0 + H22*VV13 + H26 * U13
F(4,1) = H22 * VV14 + H26 * U14

```

```

F(2,2) = DO(2,2) - BO(2,2) * HO / 2.0 + C22 * VV12 + C26*U12
F(3,2) = H26 * VV12 + H66 * U12
F(4,3) = H26 * VV14 + H66 * U14

```

```

F(3,3) = D1(6,6) + B1(6,6) * H1 / 2.0 + H26*VV13 + H66 * U13
F(4,2) = DO(2,6) - BO(2,6) * HO / 2.0 + C22*VV14 + C26 * U14

```

$$F(4,4) = DO(6,6) - BO(6,6) * HO / 2.0 + C26*VV14 + C66 * U14$$

$$DX = K22 * K66$$

$$DVV11 = - K66 * H22 / DX + (H1 / 2.00)$$

$$DVV12 = - K66 * C22 / DX + (HO / 2.00)$$

$$DU13 = - K22 * H66 / DX + (H1 / 2.00)$$

$$DU14 = - K22 * C66 / DX + (HO / 2.00)$$

$$DF(1,1) = D1(2,2) + B1(2,2) * H1 / 2.0 + H22*DVV11$$

$$DF(2,1) = H22 * DVV12$$

$$DF(2,2) = DO(2,2) - BO(2,2) * HO / 2.0 + C22 * DVV12$$

$$DF(4,3) = H66 * DU14$$

$$DF(3,3) = D1(6,6) + B1(6,6) * H1 / 2.0 + H66 * DU13$$

$$DF(4,4) = DO(6,6) - BO(6,6) * HO / 2.0 + C66 * DU14$$

$$C \quad W(1) = F(3,3) * (F(2,2) * F(4,4) - F(4,2) * F(4,2)) - F(3,2) * F(3,2) * F(4,4) + 2 * F(4,3) * F(4,2) * F(3,2) - F(2,2) * F(4,3) * F(4,3)$$

$$C \quad W(2) = - F(3,3) * (F(2,2) * AO(5,5) + F(4,4) * AO(4,4) - 2 * F(4,2) * AO(4,5)) - A1(5,5) * (F(2,2) * F(4,4) - F(4,2) * F(4,2)) + F(3,2) * F(3,2) * AO(5,5) - 2.0 * F(4,3) * F(3,2) * AO(4,5) + F(4,3) * F(4,3) * AO(4,4)$$

$$C \quad X(1) = F(3,1) * (F(2,2) * F(4,4) - F(4,2) * F(4,2)) - F(3,2) * (F(2,1) * F(4,4) - F(4,1) * F(4,2)) + F(4,3) * (F(2,1) * F(4,2) - F(4,1) * F(2,2))$$

$$C \quad X(2) = - F(3,1) * (F(2,2) * AO(5,5) + F(4,4) * AO(4,4) - 2 * F(4,2) * AO(4,5)) - A1(4,5) * (F(2,2) * F(4,4) - F(4,2) * F(4,2)) + F(3,2) * (AO(5,5) * F(2,1) - F(4,1) * AO(4,5)) - F(4,3) * (F(2,1) * AO(4,5) - F(4,1) * AO(4,4))$$

$$C \quad Y(1) = F(3,1) * (F(3,2) * F(4,4) - F(4,3) * F(4,2)) - F(3,3) * (F(2,1) * F(4,4) - F(4,1) * F(4,2)) + F(4,3) * (F(2,1) * F(4,3) - F(4,1) * F(3,2))$$

$$C \quad Y(2) = 0 - A1(4,5) * (F(3,2) * F(4,4) - F(4,2) * F(4,3)) - F(3,1) * (F(3,2) * AO(5,5) - F(4,3) * AO(4,5)) + A1(5,5) * (F(2,1) * F(4,4) - F(4,1) * F(4,2)) + F(3,3) * (F(2,1) * AO(5,5) - F(4,1) * AO(4,5))$$

$$C \quad Y(3) = A1(4,5) * (F(3,2) * AO(5,5) - F(4,3) * AO(4,5)) - A1(5,5) * (F(2,1) * AO(5,5) - F(4,1) * AO(4,5))$$

$$C \quad ZZ(1) = F(3,1) * (F(3,2) * F(4,2) - F(4,3) * F(2,2)) - F(3,3) * (F(2,1) * F(4,2) - F(4,1) * F(2,2)) + F(3,2) * (F(2,1) * F(4,3) - F(4,1) * F(3,2))$$

$$C \quad ZZ(2) = F(3,1) * (F(4,3) * AO(4,4) - F(3,2) * AO(4,5)) - A1(4,5) * (F(3,2) * F(4,2) - F(4,3) * F(2,2)) + A1(5,5) * (F(2,1) * F(4,2) - F(4,1) * F(2,2)) - F(3,3) * (F(4,1) * AO(4,4) - F(2,1) * AO(4,5))$$

$$C \quad ZZ(3) = 0 - A1(4,5) * (F(4,3) * AO(4,4) - F(3,2) * AO(4,5)) + A1(5,5) * (F(4,1) * AO(4,4) - F(2,1) * AO(4,5))$$

NOW OBTAIN THE VALUES OF E SO THAT THE 8TH ORDER POLYNOMIAL MAY BE SOLVED

$$E(1) = F(1,1) * W(1) - F(3,1) * X(1) + F(2,1) * Y(1) - F(4,1) * ZZ(1)$$

$$C \quad E(3) = F(1,1) * W(2) - A1(4,4) * W(1) - F(3,1) * X(2) + A1(4,5) * X(1) + F(2,1) * Y(2) - F(4,1) * ZZ(2)$$

$$C \quad E(5) = (AO(4,4) * AO(5,5) - AO(4,5) * AO(4,5)) * (F(1,1) * F(3,3)$$

$$C \quad - F(3,1) * F(3,1)) + (F(2,2) * AO(5,5) + F(4,4) * AO(4,4) -$$

$$C \quad 2 * F(4,2) * AO(4,5)) * (F(1,1) * A1(5,5) - F(3,1) * A1(4,5))$$

```

C      - A1(4,4)*W(2) + A1(4,5)*X(2) + F(2,1)*Y(3) - F(4,1)*ZZ(3)
E(7) = - (AO(4,4)*AO(5,5) - AO(4,5)*AO(4,5)) * (F(1,1)*A1(5,5)
C      + F(3,3)*A1(4,4) - 2*F(3,1)*A1(4,5)) - (A1(4,4)*A1(5,5) -
C      A1(4,5)*A1(4,5)) * (F(2,2)*AO(5,5) + F(4,4)*AO(4,4)
C      - 2 * AO(4,5) * F(4,2) )

E(9) = (AO(4,4)*AO(5,5) - AO(4,5)*AO(4,5) ) *
C      (A1(4,4) * A1(5,5) - A1(4,5) * A1(4,5) )

CALL UP SUBROUTINE TO SOLVE 8TH ORDER POLYNOMIAL

NDEG = 8
IER = 0
CALL ZPOLR (E,NDEG,SJ,IER)

KK = 0
*****
*****

IF (LIL.EQ.1) WRITE(6,217)
DO 90 L = 1, 8
S(L) = REAL(SJ(L))
IF (REAL(SJ(L)).GT.0) KK = KK + 1
90  IF (REAL(SJ(L)).GT.0) S(KK) = S(L)
DO 95 KK = 1,4
95  IF (LIL.EQ.1) WRITE(6,221) KK, S(KK)

*****
*****

NOW FIND THE UNCOUPLED S VALUES AND THOSE OF THE MEMBRANE

BNEG= DF(1,1) * AO(4,4) + DF(2,2) * A1(4,4)
A = DF(1,1) * DF(2,2) - DF(2,1) * DF(2,1)
C = AO(4,4) * A1(4,4)
SQ = DSQRT (BNEG * BNEG - ( 4.0 * A * C))
DIFF1 = DABS ( BNEG - SQ )
DIFF2 = DABS ( BNEG + SQ )
IF (DIFF1.GT.DIFF2) GO TO 100
UNSY(1) = DSQRT ( (BNEG+SQ) / 2.0 / A )
GO TO 105
100  UNSY(1) = DSQRT ( (BNEG-SQ) / 2.0 / A )
105  UNSY(2) = DSQRT( (BNEG/A) - UNSY(1) * UNSY(1) )

BNEG= DF(3,3) * AO(5,5) + DF(4,4) * A1(5,5)
A = DF(3,3) * DF(4,4) - DF(4,3) * DF(4,3)
C = AO(5,5) * A1(5,5)
SQ = DSQRT (BNEG * BNEG - ( 4.0 * A * C) )
DIFF1 = DABS ( BNEG - SQ )
DIFF2 = DABS ( BNEG + SQ )
IF (DIFF1.GT.DIFF2) GO TO 110
UNSX(1) = DSQRT ( (BNEG+SQ) / 2.0 / A )
GO TO 115
110  UNSX(1) = DSQRT ( (BNEG-SQ) / 2.0 / A )
115  UNSX(2) = DSQRT ( (BNEG/A) - UNSX(1) * UNSX(1) )

*****
*****

IF (LIL.EQ.1) WRITE(6,224) UNSX(1), UNSX(2)
IF (LIL.EQ.1) WRITE(6,223) UNSY(1), UNSY(2)

*****
*****

```

NOW THE S FOR THE MEMBRANE ONLY

```

C      F11M = H1/2. * ( A1(2,2) * (DVV11 + DVV12*H0/H1*A1(4,4)/AO(4,4))
      + B1(2,2) )

```

```

C      F22M = H1/2. * ( A1(6,6) * (U13 + U14*H0/H1*A1(5,5)/AO(5,5))
      + B1(6,6) )

```

```

      MEMSY = DSQRT ( A1(4,4) / F11M )
      MEMSX = DSQRT ( A1(5,5) / F22M )

```

```

*****

```

```

      IF (LIL.EQ.1) WRITE(6,219) MEMSX, MEMSY

```

```

*****

```

```

      DUM = AO(2,2) * AO(6,6) - AO(2,6) * AO(2,6)
      S1NM = ( AO(6,6)*NMNYO - AO(2,6)*NMNXYO ) / DUM
      S2NM = ( AO(2,2)*NMNXYO - AO(2,6)*NMNYO ) / DUM
      IF (LIL.EQ.1) WRITE(6,288) S1NM, S2NM

```

```

      IF ( COUPL.EQ.2) GO TO 130

```

```

      SOLVE FOR WD, CD, CU AND CV

```

```

      WD(1,1) = (AO(2,6) * AO(1,6) - AO(6,6) * AO(1,2) ) / DUM
      WD(1,2) = (AO(2,6) * BO(2,6) - AO(6,6)*BO(2,2) ) / DUM
      WD(1,3) = (AO(2,6)*BO(6,6) - AO(6,6)*BO(2,6) ) / DUM
      WD(2,1) = (AO(2,6) * AO(1,2) - AO(2,2) * AO(1,6) ) / DUM
      WD(2,2) = (AO(2,6)*BO(2,2) - AO(2,2)* BO(2,6) ) / DUM
      WD(2,3) = (AO(2,6) * BO(2,6) - AO(2,2)*BO(6,6) ) / DUM

```

```

      MATR33(1,1) = A1(2,2)
      MATR33(1,2) = A1(2,6)
      MATR33(1,3) = B1(2,2)

```

```

      MATR33(2,1) = MATR33(1,2)
      MATR33(2,2) = A1(6,6)
      MATR33(2,3) = B1(2,6)

```

```

      MATR33(3,1) = MATR33(1,3)
      MATR33(3,2) = MATR33(2,3)
      MATR33(3,3) = D1(2,2)

```

```

      MATR32(1,1) = - A1(1,2)
      MATR32(1,2) = - B1(2,6)

```

```

      MATR32(2,1) = - A1(1,6)
      MATR32(2,2) = - B1(6,6)

```

```

      MATR32(3,1) = - B1(1,2)
      MATR32(3,2) = - D1(2,6)
      IF (IZZ.EQ.2) GO TO 122

```

```

      DO 120 I=1,3
      DO 120 K=1,3
120    SAVE33(I,K) = MATR33(I,K)
      SAVE3(1) = NMNY1
      SAVE3(2) = NMNXY1
      SAVE3(3) = NMMY1
      IRR = 0
      CALL LEQT2F(SAVE33,1,3,3,SAVE3,0,WKAREA,IRR)

```

N=3
 IA=3
 IRR=0
 IDD=0

CALL LEQT2F (MATR33,M,N,IA,MATR32,IDD,WKAREA,IRR)

DO 125 I=1,3
 IF (IZZ.EQ.2) SAVE3(I) = ZR
 FNM(I) = SAVE3(I)
 DO 125 L=1,2
 125 CD(I,L) = MATR32(I,L)

SC = DSQRT((A1(5,5) - A1(4,5) * A1(4,5) / A1(4,4))
 / (D1(6,6) + B1(2,6)*CD(1,2) + B1(6,6)*CD(2,2)
 + D1(2,6) * CD(3,2)))

GO TO 135

IN CASE THE LAYERS ARE UNCOUPLED

130 DY = -1 / (A1(2,2)*A1(6,6) - A1(2,6) * A1(2,6))
 CD(1,1) = (A1(6,6)*A1(1,2) - A1(2,6)*A1(1,6)) / DY
 CD(2,1) = (A1(2,2)*A1(1,6) - A1(2,6) * A1(1,2)) / DY
 CD(3,2) = (A1(2,2)*A1(6,6) + A1(2,6)*A1(2,6)) *
 D1(2,6) / D1(2,2) / DY
 C CD(1,2) = ZR
 CD(2,2) = ZR
 CD(3,1) = ZR

DR = -1 / (AO(2,2)*AO(6,6) - AO(2,6)*AO(2,6))
 WD(1,1) = (AO(6,6)*AO(1,2) - AO(2,6)*AO(1,6)) / DR
 WD(2,1) = (AO(2,2)*AO(1,6) - AO(2,6)*AO(1,2)) / DR
 WD(1,2) = ZR
 WD(1,3) = ZR
 WD(2,2) = ZR
 WD(2,3) = ZR
 SSY = DSQRT(AO(5,5) / DO(6,6))
 SSX = DSQRT(AO(4,4) / DO(2,2))

FNM(1) = (A1(2,6)*NMNXY1 - A1(6,6)*NMNY1) / DY
 FNM(2) = (A1(2,6)*NMNY1 - A1(2,2)*NMNXY1) / DY
 FNM(3) = (A1(2,6)*A1(2,6) - A1(2,2)*A1(6,6)) / DY * NMMY1 / D1(2,2)

C SC = DSQRT((A1(5,5)*A1(6,6)) / (A1(6,6)*D1(6,6)
 - (B1(6,6)*B1(6,6))))

135 C1 = B1(1,6) + CD(1,1)*B1(2,6) + CD(2,1)*B1(6,6)
 C + CD(3,1) * D1(2,6)
 C2 = D1(6,6) + CD(1,2)*B1(2,6) + CD(2,2)*B1(6,6) +
 C CD(3,2) * D1(2,6)

J22 = DO(2,2) + BO(2,2) * WD(1,2) + BO(2,6) * WD(2,2)
 J66 = DO(6,6) + BO(2,6) * WD(1,3) + BO(6,6) * WD(2,3)
 J26 = DO(2,6) + BO(2,2) * WD(1,3) + BO(2,6) * WD(2,3)

BNEG = J22 * AO(5,5) + J66 * AO(4,4) - 2. * J26 * AO(4,5)
 A = J22 * J66 - J26 * J26

C = AO(4,4) * AO(5,5) - AO(4,5) * AO(4,5)

SQ = DSQRT ((BNEG * BNEG) - 4.0 * C * A)

DIFF1 = DABS(BNEG + SQ)

DIFF2 = DABS(BNEG - SQ)

IF (DIFF1.GT.DIFF2) GO TO 140

SS1 = DSQRT ((BNEG + SQ) / 2. / A)

GO TO 145

140 SS1 = DSQRT ((BNEG-SQ) / 2. / A)

145 SS2 = DSQRT ((BNEG/A) - SS1 * SS1)

SSY = DSQRT (AO(4,4) * J22)

SSX = DSQRT (AO(5,5) * J66)

IF (LIL.EQ.1) WRITE(6,*) ' S1 AND S2 = ',SS1, SS2

IF (LIL.EQ.1) WRITE(6,*) ' SX AND SY = ',SSX, SSY

CVNM = (K66 * (NMNY1 + NMNYO) - K26 * (NMNXY1 + NMNXYO)) / D
CUNM = (K22 * (NMNXY1 + NMNXYO) - K26 * (NMNY1 + NMNYO)) / D

CV = STRAIN(LST) / D * (K26 * K16 - K66 * K12) + CVNM

CU = STRAIN(LST) / D * (K26 * K12 - K22 * K16) + CUNM

NOW FIND SOME OF THE NEEDED CONSTANTS.....

FIRST DO LOOP IS TO VARY THE VALUES OF S

DO 150 I = 1,4

FORM THE A MATRIX (MATR32) AND ITS B (MATR3)

MATR33(1,1) = - (F(3,1) * S(I) * S(I) - A1(4,5))

MATR33(1,2) = - (F(2,1) * S(I) * S(I))

MATR33(1,3) = - (F(4,1) * S(I) * S(I))

MATR33(2,1) = - (F(3,3) * S(I) * S(I) - A1(5,5))

MATR33(2,2) = - (F(3,2) * S(I) * S(I))

MATR33(2,3) = - (F(4,3) * S(I) * S(I))

MATR33(3,1) = - (F(3,2) * S(I) * S(I))

MATR33(3,2) = - (F(2,2) * S(I) * S(I) - AO(4,4))

MATR33(3,3) = - (F(4,2) * S(I) * S(I) - AO(4,5))

MATR3(1) = (F(1,1) * S(I) * S(I)) - A1(4,4)

MATR3(2) = F(3,1) * S(I) * S(I) - A1(4,5)

MATR3(3) = F(2,1) * S(I) * S(I)

CALL UP ROUTINE TO FIND THE VALUES OF ALPHA, PHI AND GAMMA

M=1

N=3

IRR=0

IDD=0

IA=3

CALL LEQT2F(MATR33,M,N,IA,MATR3,IDD,WKAREA,IRR)

ALPHA(1) = MATR3(1)

PHI(1) = MATR3(2)

GAMMA(1) = MATR3(3)

SV(I) = VV11 + ALPHA(I)*VV13 + PHI(I)*VV12 + GAMMA(I)*VV14

50 SU(I) = U11 + ALPHA(I)*U13 + PHI(I)*U12 + GAMMA(I)*U14

```

NX1(1) = A1(1,2)*SV(1) + A1(1,6)*SU(1) + B1(1,2) + B1(1,6)*ALPHA(1)
NY1(1) = A1(2,2)*SV(1) + A1(2,6)*SU(1) + B1(2,2) + B1(2,6)*ALPHA(1)
NXY1(1) = A1(2,6)*SV(1) + A1(6,6)*SU(1) + B1(2,6) + B1(6,6)*ALPHA(1)
MY1(1) = B1(2,2)*SV(1) + B1(2,6)*SU(1) + D1(2,2) + D1(2,6)*ALPHA(1)
MXY1(1) = B1(2,6)*SV(1) + B1(6,6)*SU(1) + D1(2,6) + D1(6,6)*ALPHA(1)
NXO(1) = AO(1,2)*SV(1) + AO(1,6)*SU(1) + E18*PHI(1) + E19*GAMMA(1)
  GG(1,1) = NY1(1)
  GG(2,1) = NXY1(1)
  GG(3,1) = MY1(1)
  FTH = C2 * SC
155  GG(4,1) = MXY1(1) + FTH * ALPHA(1) / S(1)

```

```
AINM = B1(2,6)*FNM(1) + B1(6,6)*FNM(2) + D1(2,6)*FNM(3)
```

```

**
BG(1) = A1(1,2)*STRAIN(LST) + CV * A1(2,2) + A1(2,6) * CU-NMNY1
BG(2) = A1(1,6)*STRAIN(LST) + CV * A1(2,6) + A1(6,6) * CU-NMNXY1
BG(3) = B1(1,2)*STRAIN(LST) + B1(2,2) * CV + B1(2,6) * CU-NMMY1
BG(4) = B1(1,6)*STRAIN(LST) + B1(2,6) * CV + B1(6,6) * CU-AINM
C   - C1 * STRAIN(LST)

```

```

BG1 = BG(1)
BG2 = BG(2)

```

```

M=1
N=4
IA=4
IDD=0
IRR=0

```

```
CALL LEQT2F(GG,M,N,IA,BG,IDD,WKAREA,IRR)
```

```
*****
```

```

TVNM = SINM - FNM(1) + H1 / 2.0 * FNM(3)
TUNM = S2NM - FNM(2)

```

```

THETV = -CD(1,1) + WD(1,1) + H1/2.0*CD(3,1)
THETU = -CD(2,1) + WD(2,1)
  THETV = THETV + TVNM
  THETU = THETU + TUNM

```

```

IF (LIL.EQ.1) WRITE(6,215) THETV, THETU
IF (LIL.EQ.1) WRITE(6,216) SMNY, SMNXY

```

```
*****
```

THE STEPS USED TO FIND THE TOTAL ENERGY RELEASE FROM USING A PURE EXTENSION ANALYSIS FOR THE HYGRAL THERMAL EFFECTS. (SIMILAR TO WHITNEY'S). ANALYSIS IS CARRIED OUT ON A PLY BY PLY BASIS

```

ZV = ( K26 * K16 - K66 * K12 ) / D
ZU = ( K26 * K12 - K22 * K16 ) / D

```

C
C
C

```
DO 162 LL = 1,TPLY
```

```

EX(LL) = THICK(LL) * ( Q(1,1,LL) + ZV*Q(1,2,LL) +
C   ZU*Q(1,6,LL) )
C   T1(LL) = NXNM(LL) - CVNM*THICK(LL)*Q(1,2,LL) -
C   CUNM * THICK(LL) * Q(1,6,LL)
C   EXX(LL) = Q(1,1,LL)*THICK(LL) + Q(1,2,LL)*THICK(LL)*CD(1,1)

```



```

C      + Q(1,6,LL)*THICK(LL)*CD(2,1) + B12(LL)*CD(3,1)
T12(LL) = NXNM(LL) - FNM(1)*Q(1,2,LL)*THICK(LL) -
C      FNM(2)*Q(1,6,LL)*THICK(LL) - FNM(3)*B12(LL)
EX3(LL) = Q(1,1,LL)*THICK(LL) + WD(1,1)*Q(1,2,LL)*THICK(LL)
C      + WD(2,1)*Q(1,6,LL)*THICK(LL)
T13(LL) = NXNM(LL) - Q(1,2,LL)*THICK(LL)*S1NM - Q(1,6,LL)
C      * THICK(LL) * S2NM

```

```

IF (IZZ.EQ.2) NMSTO(LL) = 0.0
IF (IZZ.EQ.2) NMST2(LL) = 0.0
IF (IZZ.EQ.2) NMST3(LL) = 0.0
IF (IZZ.EQ.2) GO TO 162

```

```

NMSTO(LL) = T1(LL) / EX(LL)
NMST2(LL) = T12(LL) / EXX(LL)
NMST3(LL) = T13(LL) / EX3(LL)

```

162 CONTINUE

```

C      WRITE(6,*) ' JMM, NMSTO,2,3 OF ALL PLYS ', ( NMSTO(JP),
NMST2(JP), NMST3(JP), ' --- ', JP=1, TPLY)

```

```

C      WRITE(6,*) ' EX, EXX EX3 OF ALL PLYS ', ( EX(JP),
EXX(JP), EX3(JP), ' --- ', JP=1, TPLY)

```

```

TNC = 0.0
EXNC = 0.0
TSTAR = 0.0
ESTAR = 0.0
DO 163 LK = 1, TPLY
  TNC = TNC + T1(LK)
  EXNC = EXNC + EX(LK)
  IF (LK.LE.NPLYO) TSTAR = TSTAR + T13(LK)
  IF (LK.GT.NPLYO) TSTAR = TSTAR + T12(LK)

```

163

```

  IF (LK.LE.NPLYO) ESTAR = ESTAR + EX3(LK)
  IF (LK.GT.NPLYO) ESTAR = ESTAR + EXX(LK)

```

```

IF (IZZ.EQ.2) TNMST = 0.0
IF (IZZ.EQ.2) GO TO 89

```

```

TNMST = ( TNC - (TNC-TSTAR)*2*AL/WIDTH ) / ( EXNC -
C      (EXNC-ESTAR)*2*AL/WIDTH )

```

89 WRITE(6,*) ' TNMST EQUALS ', TNMST

DO 164 LL = 1, TPLY

```

C      IF (LL.LE.NPLYO) WWC = (EX3(LL) *
C      (STRAIN(LST) + TNMST) - T13(LL) )
C * ( STRAIN(LST) - NMST3(LL) + TNMST )

```

```

C      IF (LL.GT.NPLYO) WWC = (EXX(LL) *
C      (STRAIN(LST) + TNMST) - T12(LL) )
C * ( STRAIN(LST) - NMST2(LL) + TNMST )

```

```

C      WWO = ( EX(LL) * (STRAIN(LST) + TNMST) - T1(LL) )
C      * ( STRAIN(LST) - NMSTO(LL) + TNMST )

```

54 GLC(JMM) = GLC(JMM) + WWO - WWC

GLC(JMM) = GLC(JMM) / 2.0

THIS IS TO CALCULATE THE INTERLAMINAR SHEAR STRESSES.

76

```
UNCL = (WIDTH / 2.0) - AL
DO 180 JX = 80,100
  JY = ( 1.0 - JX /100.0) * UNCL
  SIGX(JMM,JX) = 0
  SIGY(JMM,JX) = 0
  DO 180 JS = 1,4
    SIGX(JMM,JX) = BG(JS) * S(JS) * DEXP ( -S(JS) * JY )
    * NXY1(JS) + SIGX(JMM,JX)
C
    SIGY(JMM,JX) = BG(JS) * S(JS) * DEXP ( -S(JS) * JY )
    * NY1(JS) + SIGY(JMM,JX)
C
180 CONTINUE
```

THE PROGRAM CONTINUES AND FINDS THE VARIOUS STRAIN ENERGY RELEASE COMPONENTS

IF (COUPL.EQ.1) GO TO 165

THIS IS FOR A SYSTEM THAT IS COUPLED, THE CRACK LENGTH IS

```
DEL = S(4) * S(2) * ATH * ATH
DEL = DEL * DEL * 0.6144
GO TO 170
```

THIS IS FOR AN UNCOUPLED SYSTEM.....

```
165 SSW = .65 * ( S(1) + S(2) + S(3) )
DEL = 18.7 * S(4) * SSW * ATH * ATH
DEL = DEL * DEL / 571.00
170 DEL = 135.7 * DEL * ATH
```

C IF (LIL.EQ.1) WRITE(6,211) DEL

```
FY = ZR
FX = ZR
```

DO 175 JP=1,4

```
CONY= NY1(JP)*BG(JP)*( DEXP ( -S(JP) * DEL ) - 1 )
CONXY= NXY1(JP) * BG(JP)*( DEXP ( -S(JP) *DEL) - 1 )
CCONXY = CCONXY + CONXY/S(JP)
175 CCONY = CCONY + CONY/S(JP)
```

```
FY = BG1 + CCONY / DEL
FX = BG2 + CCONXY / DEL
```

```
GII(IZZ,JM) = FY / 2.0 * THETV *STRAIN(LST)
GIII(IZZ,JM) = FX / 2.0 * THETU * STRAIN(LST)
```

```
DIFFG= GII(IZZ,JM) - GIII(IZZ,JM)
CON = 2
```

```
IF (DIFFG.GT.REAL(GLC(JMM))) CON=1
IF (DIFFG.GT.REAL(GLC(JMM))) DEL = DEL * .9
IF (DIFFG.GT.REAL(GLC(JMM))) WRITE(6,*) ' IT EXPLODES
```

```
GI(IZZ,JM) = GLC(JMM) -GII(IZZ,JM) -GIII(IZZ,JM)
```

RESULTS ARE PRINTED FOR EACH RUN.

```

300      CONTINUE
        WRITE (6,266) STRAIN(LST)
        WRITE (6,267)
        WRITE (6,269) GLC(0) , GI(2,1) , GII(2,1) , GIII(2,1) ,
C      GI(2,1)/GLC(0)

        DO 350 I=1,MMC +1
        WRITE (6,268) CMOIST(I),GLC(I) , GI(1,1) , GII(1,1) ,
C      GIII(1,1) , GI(1,1)/GLC(I)
350      CONTINUE

        WRITE (6,287)

        DO 360 NS = 80,90,2
360      WRITE (6,285) NS/100. , SIGX(0,NS) , ( SIGX(KL,NS) , KL=1,22,4)

        DO 365 NS = 91,100
365      WRITE (6,285) NS/100. , SIGX(0,NS) , ( SIGX(KL,NS) , KL=1,22,4)

        WRITE (6,286)
        DO 370 NS = 80,90,2
370      WRITE (6,285) NS/100. , SIGY(0,NS) , ( SIGY(KL,NS) , KL=1,22,4)

        DO 375 NS = 91,100
375      WRITE (6,285) NS/100. , SIGY(0,NS) , ( SIGY(KL,NS) , KL=1,22,4)

400      CONTINUE

201     FORMAT(//,' THE WIDTH OF THE LAMINATE IS ',F8.5)
287     FORMAT(/////,' THESE ARE THE IN-PLANE INTERLAMINAR SHEAR ',
C      'STRESSES -- SIGMA XY ',/, ' THEY ARE FOUND AT VARIOUS',
C      ' MOISTURE CONTENTS ',//,' Y LOCATION',7X,' MECH ONLY',8X,
C      'H=0.0',10X,'H=0.2',10X,'H=0.4',10X,
C      'H=0.6',10X,'H=0.8',10X,'H=1.0',//)
285     FORMAT(3X,F7.2,4X,7F15.8)
202     FORMAT(' THE NUMBER OF LAMINATES ABOVE AND BELOW THE CRACK IS'
C      ',13,5X,13)
204     FORMAT(///,' THE PLYS ARE INPUTTED FROM BOTTOM TO TOP',/,
C      ' BUT THE PLY CHARACTERISTICS FROM TOP TO BOTTOM ARE ')
206     FORMAT(//,' FOR PLY',15,' THE SUBLAMINATE HAS THESE PROPERTIES')
205     FORMAT(//,' WITH THIS LAYUP, THE PLYS ARE COUPLED ',//)
210     FORMAT(//,' WITH THIS LAYUP, THE PLYS ARE DECOUPLED ',//)
286     FORMAT(//,' THESE ARE THE OUT-OF-PLANE INTERLAMINAR SHEAR ',
C      'STRESSES -- SIGMA YZ ',/, ' THEY ARE FOUND AT VARIOUS',
C      ' MOISTURE CONTENTS ',//,' Y LOCATION',8X,' MECH ONLY',8X,
C      'H=0.0',10X,'H=0.2',10X,'H=0.4',10X,
C      'H=0.6',10X,'H=0.8',10X,'H=1.0',//)
208     FORMAT(' E1 AND E2 ARE (MSI) ',F8.4,10X,F8.4)
289     FORMAT(//,' THE LAMINA PLY CHARACTERISTICS INITIALLY ARE ',/)
288     FORMAT(/,' S1NM AND S2NM ARE EQUAL TO ',F14.10,4X,F14.10)
211     FORMAT(//,' THE CRACK LENGTH STEP SIZE IS ',F12.8)
266     FORMAT('0',1,' THE STRAIN IS EQUAL TO ',F12.7,/,
C      ' THE VALUES OF GT, GI, GII, AND GIII ARE IN IN-LB/IN/IN
C      ')
267     FORMAT (/,3X,'% CMOIST',8X,'GGG (WHITNEY)',6X,'GI',9X,
C      ' GII',8X,'GIII',6X,' GI/G(W-T)',//)
269     FORMAT(/,' MECH. ONLY ',3X,F12.9,4(2X,F11.7),/)
268     FORMAT(5X,F8.3,3X,F12.9,4(2X,F11.7) )
215     FORMAT(/////,' THETA V IS ',F15.10,' THETA U IS ',F24.19)
216     FORMAT(//,' NY IS ',F23.11,' NXY IS ',F23.18)

```

207 FORMAT(/,' THE THICKNESS AND THETA VALUES ARE ',F9.6,5X,F8.3)
209 FORMAT(' THE POISSON RATIO (1,2) IS ',F10.5)
214 FORMAT(' G OF (1-2), AND (3-1) ARE -MSI ', 2(F9.4,2X))
217 FORMAT('O',////,8X,'THE FOUR CHARACTERISTIC VALUES ASSOCIATED'
C ./,8X,' WITH THE 8 DEGREE POLYNOMIAL FOR THE COUPLED CASE ARE')
218 FORMAT(//,5X,' THETA ',6X,' NY ',8X,' NXY ',//)
219 FORMAT(///,' THE S VALUES OF THE MEMBRANE ARE ',F15.5,3X,F15.5)
220 FORMAT(/,4X,F9.4,3X,F9.2,3X,F9.2)
221 FORMAT(/,' S OF ',12,' IS EQUAL TO ',F20.10)
223 FORMAT(/,' THE UNCOUPLED SY (1,2) VALUES ARE ',F15.5,3X,F15.5)
224 FORMAT(/,' THE UNCOUPLED SX (1,2) VALUES ARE ',F15.5,3X,F15.5)
231 FORMAT(//,' THE STRAIN IS EQUAL TO ',F12.8,/,
C ' THE CHANGE IN TEMPERATURE IS ',F12.5,/,
C ' THE COEFFICIENTS SWELLING DUE TO MOISTURE ARE ',2(2X,F12.8)
C ./,' THE COEFFICIENTS OF THERMAL EXPANSION ARE ',2(2X,F15.9))

232 FORMAT(/,' THE MOISTURE COEFFICIENT IS ',F15.8)
233 FORMAT(/,' THE MOISTURE COEFFICIENT VARIES FROM 0 TO 1.2 ')

78

STOP
END

THE LAMINA PLY CHARACTERISTICS INITIALLY ARE

79

THE WIDTH OF THE LAMINATE IS 1.51200
THE NUMBER OF LAMINATES ABOVE AND BELOW THE CRACK IS 3 1

FOR PLY 1 THE SUBLAMINATE HAS THESE PROPERTIES
THE THICKNESS AND THETA VALUES ARE .005400 35.000
E1 AND E2 ARE (MSI) 18.7000 1.2300
THE POISSON RATIO (1,2) IS .29200
G OF (1-2), AND (3-1) ARE -MSI .8320 .8320

FOR PLY 2 THE SUBLAMINATE HAS THESE PROPERTIES
THE THICKNESS AND THETA VALUES ARE .005400 -35.000
E1 AND E2 ARE (MSI) 18.7000 1.2300
THE POISSON RATIO (1,2) IS .29200
G OF (1-2), AND (3-1) ARE -MSI .8320 .8320

FOR PLY 3 THE SUBLAMINATE HAS THESE PROPERTIES
THE THICKNESS AND THETA VALUES ARE .005400 .000
E1 AND E2 ARE (MSI) 18.7000 1.2300
THE POISSON RATIO (1,2) IS .29200
G OF (1-2), AND (3-1) ARE -MSI .8320 .8320

FOR PLY 4 THE SUBLAMINATE HAS THESE PROPERTIES
THE THICKNESS AND THETA VALUES ARE .005400 90.000
E1 AND E2 ARE (MSI) 18.7000 1.2300
THE POISSON RATIO (1,2) IS .29200
G OF (1-2), AND (3-1) ARE -MSI .8320 .8320

THE STRAIN IS EQUAL TO .00254000
THE CHANGE IN TEMPERATURE IS -280.00000
THE COEFFICIENTS SWELLING DUE TO MOISTURE ARE .00000000 .00556000
THE COEFFICIENTS OF THERMAL EXPANSION ARE -.000000230 .000014900

THE MOISTURE COEFFICIENT VARIES FROM 0 TO 1.2

WITH THIS LAYUP, THE PLYS ARE COUPLED

THE FOUR CHARACTERISTIC VALUES ASSOCIATED
WITH THE 8 DEGREE POLYNOMIAL FOR THE COUPLED CASE ARE

S OF 1 IS EQUAL TO 407.0573682744

S OF 2 IS EQUAL TO 141.1197780418

S OF 3 IS EQUAL TO 116.7332723860

S OF 4 IS EQUAL TO 55.5544207729

THE UNCOUPLED SX (1,2) VALUES ARE 392.22478 106.21737

THE UNCOUPLED SY (1,2) VALUES ARE 134.68589 56.25754

THE S VALUES OF THE MEMBRANE ARE 177.38945 66.26466

S1NM AND S2NM ARE EQUAL TO -.0000157292 .0000000000
 S1 AND S2 = 134.932471163957803943120257 641.500299099584182787943089
 SX AND SY = 7.00358208142090671392409983 33.2966554398959572557143052

THETA V IS .3932559441 THETA U IS -.0981017742335529623

NY IS -38.32041690358 NXY IS -61.959633961712929972

THE STRAIN IS EQUAL TO .0025400
 THE VALUES OF GT, GI, GII, AND GIII ARE IN IN-LB/IN/IN

% CMOIST	GGG (WHITNEY)	GI	GII	GIII	GI/G (W-T)
MECH. ONLY	.101653935	.0670191	.0346174	.0000174	.6592868
.000	.522939955	.4084740	.1144151	.0000509	.7811106
.050	.488576635	.3794622	.1090658	.0000486	.7766688
.100	.455156902	.3513864	.1037241	.0000464	.7720115
.150	.422680755	.3242463	.0983903	.0000442	.7671187
.200	.397148194	.2980421	.0930641	.0000420	.7619672
.250	.360559220	.2727737	.0877458	.0000397	.7565296
.300	.330913832	.2484412	.0824351	.0000375	.7507731
.350	.302212031	.2250445	.0771323	.0000353	.7446576
.400	.274453816	.2025836	.0718371	.0000331	.7381338
.450	.247639187	.1810586	.0665497	.0000308	.7311387
.500	.221768145	.1604694	.0612701	.0000286	.7235909
.550	.196840689	.1408161	.0559982	.0000264	.7153809
.600	.172856820	.1220986	.0507341	.0000242	.7063566
.650	.149816537	.1043169	.0454777	.0000220	.6962975
.700	.127719840	.0874710	.0402291	.0000197	.6848665
.750	.106566730	.0715610	.0349882	.0000175	.6715139
.800	.086357206	.0565869	.0297550	.0000153	.6552653
.850	.067091269	.0425486	.0245296	.0000131	.6341891
.900	.048768918	.0294461	.0193120	.0000109	.6037875
.950	.031390154	.0172794	.0141021	.0000087	.5504724
1.000	.014954976	.0060486	.0088999	.0000064	.4044538
1.050	-.000536616	-.0042464	.0037055	.0000042	7.9132595
1.100	-.015084621	-.0136055	-.0014811	.0000020	.9019465
1.150	-.028689040	-.0220288	-.0066600	-.0000002	.7678481
1.200	-.041349872	-.0295163	-.0118312	-.0000024	.7138182

THESE ARE THE IN-PLANE INTERLAMINAR SHEAR STRESSES -- SIGMA XZ
 THEY ARE FOUND AT VARIOUS MOISTURE CONTENTS

Y LOCATION	MECH ONLY	H=0.0	H=0.2	H=0.4	H=0.6	H=0.8	H=1.0
.80	.06513504	.21416031	.17460962	.13505894	.09550826	.05595758	.01640689
.82	.14545604	.47814372	.38984949	.30155526	.21326102	.12496679	.03667255
.84	.32456173	1.06633353	.86946804	.67260256	.47573707	.27887159	.08200610
.86	.72279559	2.37175315	1.93411286	1.49647257	1.05883228	.62119200	.18355171
.88	1.60209840	5.24186753	4.27581313	3.30975873	2.34370433	1.37764993	.41159552
.90	3.51076178	11.41070230	9.31370571	7.21670913	5.11971255	3.02271596	.92571938
.91	5.15145827	16.64239220	13.59188733	10.54138246	7.49087759	4.44037273	1.38986786
.92	7.47883378	23.94089980	19.57004819	15.19919658	10.82834496	6.45749335	2.08664173
.93	10.67162145	33.68618367	27.57413829	21.46209291	15.35004753	9.23800215	3.12595677
.94	14.79223282	45.68179330	37.47523970	29.26868609	21.06213248	12.85557888	4.64902527
.95	19.47341229	58.01265161	47.76700252	37.52135343	27.27570433	17.03005524	6.78440615
.96	23.13934536	64.48280475	53.47668684	42.47056893	31.46445102	20.45833311	9.45221520
.97	21.18134698	49.34714597	41.81302367	34.27890137	26.74477908	19.21065678	11.67653448
.98	2.06849051	-21.49262058	-15.32190098	-9.15118139	-2.98046180	3.19025779	9.36097738
.99	-56.33255229	-192.21483366	-156.17259550	-120.13035734	-84.08811918	-48.04588102	-12.00364285
1.00	-101.55665215	-68.23277131	-76.30397933	-84.37518734	-92.44639536	-100.51760338	-108.58881140

THESE ARE THE OUT-OF-PLANE INTERLAMINAR SHEAR STRESSES -- SIGMA YZ
 THEY ARE FOUND AT VARIOUS MOISTURE CONTENTS

Y LOCATION	MECH ONLY	H=0.0	H=0.2	H=0.4	H=0.6	H=0.8	H=1.0
.80	1.32976655	4.37292262	3.56528382	2.75764502	1.95000623	1.14236743	.33472863
.82	2.97130973	9.77117861	7.96652670	6.16187479	4.35722288	2.55257097	.74791906
.84	6.63941979	21.83410057	17.80150758	13.76891460	9.73632161	5.70372862	1.67113564
.86	14.83663802	48.79268635	39.78092397	30.76916159	21.75739921	12.74563683	3.73387445
.88	33.15858378	109.05518007	88.91263246	68.77008485	48.62753723	28.48498962	8.34244201
.90	74.12869062	243.83823352	198.79834182	153.75845013	108.71855844	63.67866674	18.63877505
.91	110.86070837	364.70855904	297.33899561	229.96943219	162.59986876	95.23030534	27.86074191
.92	165.83595666	545.65327849	444.85249399	344.05170949	243.25092499	142.45014049	41.64935600
.93	248.16757475	816.71124591	665.82431294	514.93737997	364.05044699	213.16351402	62.27658105
.94	371.58510425	1223.12780736	997.13593640	771.14406544	545.15219448	319.16032352	93.16845256
.95	556.84776170	1833.20386401	1494.47103417	1155.73820433	817.00537449	478.27254465	139.53971481
.96	835.49958063	2750.22755443	2242.07591738	1733.92428033	1225.77264328	717.62100623	209.46936917
.97	1255.78433442	4130.35826748	3367.46245574	2604.56664400	1841.67083225	1078.77502051	315.87920877
.98	1892.06540014	6208.29180153	5062.74636672	3917.20093190	2771.65549709	1626.11006228	480.56462747
.99	2859.77789575	9329.28302912	7612.08957918	5894.89612924	4177.70267929	2460.50922935	743.31577941
1.00	4336.01416454	13960.55352851	11405.37993197	8850.20633544	6295.03273890	3739.85914236	1184.68554582

THE LAMINA PLY CHARACTERISTICS INITIALLY ARE

THE WIDTH OF THE LAMINATE IS 1.51200
THE NUMBER OF LAMINATES ABOVE AND BELOW THE CRACK IS 3 1

THE PLYS ARE INPUTTED FROM BOTTOM TO TOP
BUT THE PLY CHARACTERISTICS FROM TOP TO BOTTOM ARE

FOR PLY 1 THE SUBLAMINATE HAS THESE PROPERTIES
THE THICKNESS AND THETA VALUES ARE .005400 35.000
E1 AND E2 ARE (MSI) 18.7000 1.2300
THE POISSON RATIO (1,2) IS .29200
G OF (1-2), AND (3-1) ARE -MSI .8320 .8320

FOR PLY 2 THE SUBLAMINATE HAS THESE PROPERTIES
THE THICKNESS AND THETA VALUES ARE .005400 .000
E1 AND E2 ARE (MSI) 18.7000 1.2300
THE POISSON RATIO (1,2) IS .29200
G OF (1-2), AND (3-1) ARE -MSI .8320 .8320

FOR PLY 3 THE SUBLAMINATE HAS THESE PROPERTIES
THE THICKNESS AND THETA VALUES ARE .005400 -35.000
E1 AND E2 ARE (MSI) 18.7000 1.2300
THE POISSON RATIO (1,2) IS .29200
G OF (1-2), AND (3-1) ARE -MSI .8320 .8320

FOR PLY 4 THE SUBLAMINATE HAS THESE PROPERTIES
THE THICKNESS AND THETA VALUES ARE .005400 90.000
E1 AND E2 ARE (MSI) 18.7000 1.2300
THE POISSON RATIO (1,2) IS .29200
G OF (1-2), AND (3-1) ARE -MSI .8320 .8320

THE STRAIN IS EQUAL TO .00254000
THE CHANGE IN TEMPERATURE IS -280.00000
THE COEFFICIENTS SWELLING DUE TO MOISTURE ARE .00000000 .00556000
THE COEFFICIENTS OF THERMAL EXPANSION ARE -.000000230 .000014900

THE MOISTURE COEFFICIENT VARIES FROM 0 TO 1.2

WITH THIS LAYUP, THE PLYS ARE COUPLED

THE FOUR CHARACTERISTIC VALUES ASSOCIATED
WITH THE 8 DEGREE POLYNOMIAL FOR THE COUPLED CASE ARE

- S OF 1 IS EQUAL TO 360.7162423543
- S OF 2 IS EQUAL TO 136.3961604492
- S OF 3 IS EQUAL TO 113.9856584772
- S OF 4 IS EQUAL TO 58.0801738692

THE UNCOUPLED SX (1,2) VALUES ARE 352.62874 86.89277

THE UNCOUPLED SY (1,2) VALUES ARE 126.45615 59.53405

THE S VALUES OF THE MEMBRANE ARE 193.07807 70.65819

S1NM AND S2NM ARE EQUAL TO -.0000157292 .0000000000
S1 AND S2 = 134.932471163957803943120257 641.500299099584182787943089
SX AND SY = 7.00358208142090671392409983 33.2966554398959572557143052

THETA V IS .9784024562 THETA U IS .0000000000000009718

NY IS -38.32041690358 NXY IS -61.959633961712929972

THE STRAIN IS EQUAL TO .0025400
THE VALUES OF GT, GI, GII, AND GIII ARE IN IN-LB/IN/IN

% CMOIST	GGG (WHITNEY)	GI	GII	GIII	GI/G (W-T)
MECH. ONLY	.094207177	.0078275	.0863797	.0000000	.0830882
.000	.510289070	.2262277	.2840614	.0000000	.4433324
.050	.476405835	.2055316	.2708742	.0000000	.4314212
.100	.443446720	.1857497	.2576970	.0000000	.4188771
.150	.411411727	.1668819	.2445298	.0000000	.4056324
.200	.380300856	.1489284	.2313725	.0000000	.3916067
.250	.350114106	.1318890	.2182251	.0000000	.3767028
.300	.320851477	.1157637	.2050878	.0000000	.3608016
.350	.292512969	.1005526	.1919603	.0000000	.3437545
.400	.265098582	.0862557	.1788428	.0000000	.3253723
.450	.238608317	.0728730	.1657353	.0000000	.3054085
.500	.213042173	.0604044	.1526377	.0000000	.2835328
.550	.188400151	.0488500	.1395501	.0000000	.2592888
.600	.164682250	.0382098	.1264724	.0000000	.2320215
.650	.141888470	.0284838	.1134047	.0000000	.2007475
.700	.120018811	.0196719	.1003469	.0000000	.1639065
.750	.099073274	.0117741	.0872991	.0000000	.1188427
.800	.079051858	.0047906	.0742613	.0000000	.0606005
.850	.059954563	-.0012788	.0612334	.0000000	-.0213295
.900	.041781389	-.0064340	.0482154	.0000000	-.1539925
.950	.024532337	-.0106751	.0352074	.0000000	-.4351429
1.000	.008207406	-.0140020	.0222094	.0000000	-1.7060144
1.050	-.007193403	-.0164147	.0092213	.0000000	2.2819054
1.100	-.021670092	-.0179132	-.0037569	.0000000	.8266329
1.150	-.035222659	-.0184976	-.0167251	.0000000	.5251615
1.200	-.047851104	-.0181678	-.0296833	.0000000	.3796734

THESE ARE THE IN-PLANE INTERLAMINAR SHEAR STRESSES -- SIGMA XZ
THEY ARE FOUND AT VARIOUS MOISTURE CONTENTS

Y LOCATION	MECH ONLY	H=0.0	H=0.2	H=0.4	H=0.6	H=0.8	H=1.0
.80	.07771543	.25410395	.20728704	.16047014	.11365323	.06683632	.02001942
.82	.17995738	.58840154	.47999260	.37158366	.26317472	.15476578	.04635684
.84	.41625242	1.36100874	1.11025224	.85949573	.60873922	.35798272	.10722621
.86	.96042737	3.14028217	2.56170677	1.98313136	1.40455595	.82598055	.24740514
.88	2.20343709	7.20451590	5.87713337	4.54975083	3.22236829	1.89498576	.56760322
.90	4.98862540	16.31116726	13.30594680	10.30072635	7.29550589	4.29028544	1.28506498
.91	7.43148427	24.29851376	19.82167961	15.34484547	10.86801132	6.39117717	1.91434302
.92	10.93853873	35.76543047	29.17589574	22.58636100	15.99682627	9.40729153	2.81775680
.93	15.78922990	51.62559809	42.11393649	32.60227488	23.09061327	13.57895167	4.06729006
.94	22.04642211	72.08456237	58.80347722	45.52239206	32.24130691	18.96022176	5.67913661
.95	28.96545539	94.70752965	77.25831827	59.80910689	42.35989552	24.91068414	7.46147276
.96	33.46881767	109.43204584	89.26994356	69.10784128	48.94573900	28.78363672	8.62153445
.97	26.48582400	86.59994907	70.64450369	54.68905831	38.73361292	22.77816754	6.82272216
.98	-14.02438527	-45.85513558	-37.40664203	-28.95814848	-20.50965493	-12.06116138	-3.61266782
.99	-113.31362224	-370.49834340	-302.23657021	-233.97479701	-165.71302381	-97.45125061	-29.18947741
1.00	85.42214908	279.30238304	227.84283872	176.38329439	124.922375006	73.46420574	22.00466141

THESE ARE THE OUT-OF-PLANE INTERLAMINAR SHEAR STRESSES -- SIGMA YZ
THEY ARE FOUND AT VARIOUS MOISTURE CONTENTS

Y LOCATION	MECH ONLY	H=0.0	H=0.2	H=0.4	H=0.6	H=0.8	H=1.0
.80	.94069588	3.07576670	2.50907783	1.94238895	1.37570008	.80901121	.24232233
.82	2.18029521	7.12884953	5.81540800	4.50196647	3.18852495	1.87508342	.56164190
.84	5.05374241	16.52407852	13.47963063	10.43518274	7.39073485	4.34628695	1.30183906
.86	11.71605439	38.30765144	31.24972996	24.19180849	17.13388701	10.07596554	3.01804406
.88	27.17098279	88.84019338	72.47199838	56.10380339	39.73560839	23.36741339	6.99921839
.90	63.06243899	206.19347184	168.20374189	130.21401195	92.22428201	54.23455207	16.24482213
.91	96.12643272	314.30187627	256.39391588	198.48595549	140.57799510	82.67003472	24.76207433
.92	146.61442086	479.38102208	391.05836372	302.73570537	214.41304702	126.09038866	37.76773031
.93	223.81654951	731.80663700	596.97629411	462.14595122	327.31560833	192.48526545	57.65492256
.94	342.10566992	1118.57322594	912.48379743	706.39436892	500.30494041	294.21551190	88.12608339
.95	523.86709173	1712.87340224	1397.28825109	1081.70309995	766.11794880	450.53279765	134.94764651
.96	804.27369732	2629.71094384	2145.20477742	1660.69861100	1176.19244458	691.68627816	207.18011174
.97	1239.16420856	4051.66013925	3305.16960716	2558.67907507	1812.18854298	1065.69801089	319.20747880
.98	1917.53432739	6269.70771612	5114.55716346	3959.40661080	2804.25605814	1649.10550548	493.95495282
.99	2971.17774803	9714.77578612	7924.89512080	6135.01445547	4345.13379015	2555.25312483	765.37245950
1.00	4429.35526207	14482.53753133	11814.22953505	9145.92153878	6477.61354250	3809.30554622	1140.99754994

THE LAMINA PLY CHARACTERISTICS INITIALLY ARE

THE WIDTH OF THE LAMINATE IS 1.51200
THE NUMBER OF LAMINATES ABOVE AND BELOW THE CRACK IS 2 2

FOR PLY 1 THE SUBLAMINATE HAS THESE PROPERTIES
THE THICKNESS AND THETA VALUES ARE .005400 30.000
E1 AND E2 ARE (MSI) 18.7000 1.2300
THE POISSON RATIO (1,2) IS .29200
G OF (1-2), AND (3-1) ARE -MSI .8320 .8320

FOR PLY 2 THE SUBLAMINATE HAS THESE PROPERTIES
THE THICKNESS AND THETA VALUES ARE .005400 -60.000
E1 AND E2 ARE (MSI) 18.7000 1.2300
THE POISSON RATIO (1,2) IS .29200
G OF (1-2), AND (3-1) ARE -MSI .8320 .8320

FOR PLY 3 THE SUBLAMINATE HAS THESE PROPERTIES
THE THICKNESS AND THETA VALUES ARE .005400 75.000
E1 AND E2 ARE (MSI) 18.7000 1.2300
THE POISSON RATIO (1,2) IS .29200
G OF (1-2), AND (3-1) ARE -MSI .8320 .8320

FOR PLY 4 THE SUBLAMINATE HAS THESE PROPERTIES
THE THICKNESS AND THETA VALUES ARE .005400 -15.000
E1 AND E2 ARE (MSI) 18.7000 1.2300
THE POISSON RATIO (1,2) IS .29200
G OF (1-2), AND (3-1) ARE -MSI .8320 .8320

THE STRAIN IS EQUAL TO .00254000
THE CHANGE IN TEMPERATURE IS -280.00000
THE COEFFICIENTS SWELLING DUE TO MOISTURE ARE .00000000 .00556000
THE COEFFICIENTS OF THERMAL EXPANSION ARE -.000000230 .000014900

THE MOISTURE COEFFICIENT VARIES FROM 0 TO 1.2

WITH THIS LAYUP, THE PLYS ARE COUPLED

THE FOUR CHARACTERISTIC VALUES ASSOCIATED
WITH THE 8 DEGREE POLYNOMIAL FOR THE COUPLED CASE ARE

- S OF 1 IS EQUAL TO 202.3666962066
- S OF 2 IS EQUAL TO 150.2447234209
- S OF 3 IS EQUAL TO 96.3990023366
- S OF 4 IS EQUAL TO 72.1855545293

THE UNCOUPLED SX (1,2) VALUES ARE 178.08581 90.73315

THE UNCOUPLED SY (1,2) VALUES ARE 137.79324 77.57481

THE S VALUES OF THE MEMBRANE ARE 107.30164 75.55664

S1NM AND S2NM ARE EQUAL TO -.0013126127 .0012407192
 S1 AND S2 = 145.712738394363145201234304 261.712596265395612237542175
 SX AND SY = 35.5756851167439115190147879 60.9585549677314312319553312

THETA V IS .2402517909 THETA U IS 2.0734384470218017861

NY IS -35.48501616832 NXY IS -61.461850910940726086

THE STRAIN IS EQUAL TO .0025400
 THE VALUES OF GT, GI, GII, AND GIII ARE IN IN-LB/IN/IN

% CMOIST	GGG (WHITNEY)	GI	GII	GIII	GI/G (W-T)
MECH. ONLY	.174065036	.0136734	.0093651	.1510265	.0785535
.000	.288599244	.0062276	.0365562	.2458155	.0215787
.050	.277169512	.0030909	.0347433	.2393353	.0111516
.100	.266289514	.0005010	.0329323	.2328563	.0018813
.150	.255959252	-.0015422	.0311230	.2263784	-.0060250
.200	.246178724	-.0030385	.0293156	.2199016	-.0123427
.250	.236947932	-.0039880	.0275100	.2134260	-.0168309
.300	.228266874	-.0043908	.0257062	.2069515	-.0192354
.350	.220135552	-.0042468	.0239042	.2004781	-.0192916
.400	.212553964	-.0035559	.0221040	.1940059	-.0167296
.450	.205522112	-.0023183	.0203057	.1875347	-.0112801
.500	.199039994	-.0005339	.0185092	.1810647	-.0026824
.550	.193107612	.0017973	.0167144	.1745959	.0093072
.600	.187724965	.0046753	.0149215	.1681281	.0249050
.650	.182892052	.0081001	.0131304	.1616615	.0442888
.700	.178608875	.0120716	.0113412	.1551961	.0675870
.750	.174875432	.0165900	.0095537	.1487317	.0948676
.800	.171691725	.0216552	.0077681	.1422685	.1261282
.850	.169057753	.0272671	.0059842	.1358064	.1612888
.900	.166973515	.0334259	.0042022	.1293454	.2001866
.950	.165439013	.0401314	.0024220	.1228856	.2425751
1.000	.164454245	.0473837	.0006436	.1164269	.2881270
1.050	.164019213	.0551828	-.0011329	.1099693	.3364412
1.100	.164133916	.0635287	-.0029077	.1035129	.3870542
1.150	.164798353	.0724214	-.0046806	.0970576	.4394548
1.200	.166012526	.0818609	-.0064517	.0906034	.4931008

THESE ARE THE IN-PLANE INTERLAMINAR SHEAR STRESSES -- SIGMA XZ
 THEY ARE FOUND AT VARIOUS MOISTURE CONTENTS

Y LOCATION	MECH ONLY	H=0.0	H=0.2	H=0.4	H=0.6	H=0.8	H=1.0
.80	.05676172	.13383978	.11323003	.09262028	.07201053	.05140078	.03079103
.82	.16404039	.38262997	.32416132	.26569268	.20722403	.14875538	.09028674
.84	.47716558	1.09647535	.93073896	.76500256	.59926616	.43352976	.26779336
.86	1.40027761	3.15249905	2.68324457	2.21399008	1.74473560	1.27548112	.80622663
.88	4.15778238	9.10572208	7.77928135	6.45284061	5.12639987	3.79995914	2.47351840
.90	12.53662711	26.47078249	22.72981406	18.98884564	15.24787721	11.50690879	7.76594036
.91	21.92391761	45.27705638	39.00125296	32.72544955	26.44964613	20.17384271	13.89803930
.92	38.55372890	77.65399817	67.13410301	56.61420784	46.09431268	35.57441752	25.05452235
.93	68.22669529	133.62809212	116.00701342	98.38593472	80.76485602	63.14377733	45.52269863
.94	121.62386648	230.94006045	201.43654971	171.93303897	142.42952823	112.92601749	83.42250675
.95	218.74381651	401.50598451	352.07750811	302.64903171	253.22055531	203.79207891	154.36360251
.96	398.03248718	704.47704597	621.39034887	538.30365177	455.21695468	372.13025758	289.04356048
.97	736.82244009	1255.70230253	1114.59938720	973.49647187	832.39355653	691.29064120	550.18772587
.98	1403.24313766	2305.35974007	2059.22700449	1813.09426892	1566.96153334	1320.82879776	1074.69606219
.99	2809.86570653	4480.13776195	4023.01286260	3565.88796325	3108.76306390	2651.63816455	2194.51326520
1.00	6138.30786283	9650.30926292	8687.60293079	7724.89659866	6762.19026652	5799.48393439	4836.77760226

THESE ARE THE OUT-OF-PLANE INTERLAMINAR SHEAR STRESSES -- SIGMA YZ
 THEY ARE FOUND AT VARIOUS MOISTURE CONTENTS

Y LOCATION	MECH ONLY	H=0.0	H=0.2	H=0.4	H=0.6	H=0.8	H=1.0
.80	.16585980	.40442354	.34069983	.27697611	.21325240	.14952869	.08580498
.82	.46943498	1.14791593	.96669931	.78548269	.60426608	.42304946	.24183285
.84	1.32621331	3.25626779	2.74082736	2.22538692	1.70994649	1.19450605	.67906562
.86	3.73681543	9.22891300	7.76243950	6.29596600	4.82949250	3.36301900	1.89654550
.88	10.48846496	26.12319742	21.94948048	17.77576354	13.60204660	9.42832966	5.25461272
.90	29.26971559	73.80117525	61.91744992	50.03372460	38.14999927	26.26627395	14.38254862
.91	48.74474315	123.91308072	103.85796283	83.80284494	63.74772705	43.69260916	23.63749127
.92	80.94539936	207.83462309	173.98914281	140.14366253	106.29818225	72.45270198	38.60722170
.93	133.89723658	348.06735925	290.95937200	233.85138474	176.74339749	119.63541023	62.52742298
.94	220.24445378	581.52733260	485.22950028	388.93166795	292.63383563	196.33600331	100.03817099
.95	359.01194536	967.47546061	805.37239730	643.26933399	481.16627068	319.06320737	156.96014406
.96	575.60439987	1596.12349454	1324.41972889	1052.71596324	781.01219759	509.30843195	237.60466630
.97	890.96357501	2584.87680021	2134.31704487	1683.75728954	1233.19753421	782.63777888	332.07802355
.98	1261.01507117	3998.83788332	3271.80265391	2544.76742450	1817.73219508	1090.69696567	363.66173626
.99	1302.72815835	5415.47562712	4327.26291739	3239.05020766	2150.83749794	1062.62478821	-25.58792151
1.00	-883.85251960	3927.98882475	2670.82514260	1413.66146045	156.49777830	-1100.66590385	-2357.82958600

THE LAMINA PLY CHARACTERISTICS INITIALLY ARE

THE WIDTH OF THE LAMINATE IS 1.51200
THE NUMBER OF LAMINATES ABOVE AND BELOW THE CRACK IS 2 2

88

FOR PLY 1 THE SUBLAMINATE HAS THESE PROPERTIES
THE THICKNESS AND THETA VALUES ARE .005400 -35.000
E1 AND E2 ARE (MSI) 18.7000 1.2300
THE POISSON RATIO (1,2) IS .29200
G OF (1-2), AND (3-1) ARE -MSI .8320 .8320

FOR PLY 2 THE SUBLAMINATE HAS THESE PROPERTIES
THE THICKNESS AND THETA VALUES ARE .005400 55.000
E1 AND E2 ARE (MSI) 18.7000 1.2300
THE POISSON RATIO (1,2) IS .29200
G OF (1-2), AND (3-1) ARE -MSI .8320 .8320

FOR PLY 3 THE SUBLAMINATE HAS THESE PROPERTIES
THE THICKNESS AND THETA VALUES ARE .005400 10.000
E1 AND E2 ARE (MSI) 18.7000 1.2300
THE POISSON RATIO (1,2) IS .29200
G OF (1-2), AND (3-1) ARE -MSI .8320 .8320

FOR PLY 4 THE SUBLAMINATE HAS THESE PROPERTIES
THE THICKNESS AND THETA VALUES ARE .005400 -80.000
E1 AND E2 ARE (MSI) 18.7000 1.2300
THE POISSON RATIO (1,2) IS .29200
G OF (1-2), AND (3-1) ARE -MSI .8320 .8320

THE STRAIN IS EQUAL TO .00254000
THE CHANGE IN TEMPERATURE IS -280.00000
THE COEFFICIENTS SWELLING DUE TO MOISTURE ARE .00000000 .00556000
THE COEFFICIENTS OF THERMAL EXPANSION ARE -.000000230 .000014900

THE MOISTURE COEFFICIENT VARIES FROM 0 TO 1.2

WITH THIS LAYUP, THE PLYS ARE COUPLED

THE FOUR CHARACTERISTIC VALUES ASSOCIATED
WITH THE 8 DEGREE POLYNOMIAL FOR THE COUPLED CASE ARE

S OF 1 IS EQUAL TO 233.9388572236
S OF 2 IS EQUAL TO 156.9014619788
S OF 3 IS EQUAL TO 115.2992565645
S OF 4 IS EQUAL TO 48.0575100718

THE UNCOUPLED SX (1,2) VALUES ARE 186.41344 96.42124

THE UNCOUPLED SY (1,2) VALUES ARE 128.78572 49.37034

THE S VALUES OF THE MEMBRANE ARE

119.36060

57.91987

S1NM AND S2NM ARE EQUAL TO -.0007221149 -.0007139234
 S1 AND S2 = 143.691863396728751259452089 285.264127104852281159045526
 SX AND SY = 32.1436979546791447820272102 62.2049978939766992050711339

THETA V IS .4347536621 THETA U IS -1.7344415408201789576

NY IS -54.36619889946 NXY IS 45.618657445050692111

THE STRAIN IS EQUAL TO .0025400
 THE VALUES OF GT, GI, GII, AND GIII ARE IN IN-LB/IN/IN

% CMOIST	GGG (WHITNEY)	GI	GII	GIII	GI/G (W-T)
MECH. ONLY	.131525889	.0207693	.0219689	.0887877	.1579102
.000	.394637005	.1683076	.0866210	.1397084	.4264871
.050	.369347077	.1508205	.0823114	.1362152	.4083435
.100	.345184223	.1344556	.0780061	.1327225	.3895185
.150	.322148443	.1192131	.0737050	.1292304	.3700564
.200	.300239735	.1050929	.0694082	.1257387	.3500298
.250	.279458102	.0920949	.0651156	.1222475	.3295483
.300	.259803542	.0802193	.0608274	.1187569	.3087691
.350	.241276055	.0694660	.0565434	.1152667	.2879108
.400	.223875642	.0598350	.0522636	.1117771	.2672688
.450	.207602302	.0513262	.0479882	.1082879	.2472335
.500	.192456036	.0439398	.0437170	.1047992	.2283110
.550	.178436843	.0376757	.0394500	.1013111	.2111431
.600	.165544724	.0325339	.0351874	.0978235	.1965264
.650	.153779678	.0285144	.0309290	.0943363	.1854237
.700	.143141706	.0256172	.0266748	.0908497	.1789638
.750	.133630807	.0238423	.0224250	.0873635	.1784190
.800	.125246982	.0231897	.0181794	.0838779	.1851516
.850	.117990230	.0236594	.0139381	.0803928	.2005198
.900	.111860552	.0252514	.0097010	.0769081	.2257398
.950	.106857947	.0279657	.0054683	.0734240	.2617089
1.000	.102982416	.0318023	.0012397	.0699404	.3088128
1.050	.100233958	.0367612	-.0029845	.0664573	.3667539
1.100	.098612573	.0428424	-.0072045	.0629747	.4344517
1.150	.098118262	.0500459	-.0114202	.0594925	.5100571
1.200	.098751025	.0583717	-.0156316	.0560109	.5910999

THESE ARE THE IN-PLANE INTERLAMINAR SHEAR STRESSES -- SIGMA XZ
 THEY ARE FOUND AT VARIOUS MOISTURE CONTENTS

Y LOCATION	MECH ONLY	H=0.0	H=0.2	H=0.4	H=0.6	H=0.8	H=1.0
.80	-.57590259	-1.81324378	-1.48462505	-1.15600631	-.82738757	-.49876884	-.17015010
.82	-1.15500766	-3.63542168	-2.97665842	-2.31789515	-1.65913188	-1.00036862	-.34160535
.84	-2.31809701	-7.29018842	-5.96965162	-4.64911482	-3.32857801	-2.00804121	-.68750441
.86	-4.66121070	-14.62677009	-11.97991892	-9.33306775	-6.68621658	-4.03936541	-1.39251424
.88	-9.41933953	-29.38693329	-24.08301174	-18.77909019	-13.47516863	-8.17124708	-2.86732552
.90	-19.28114635	-59.25567119	-48.63455785	-38.01344451	-27.39233116	-16.77121782	-6.15010448
.91	-27.86803356	-84.38953087	-69.36790478	-54.34627868	-39.32465259	-24.30302649	-9.28140039
.92	-40.76807828	-120.61801802	-99.38712650	-78.15623498	-56.92534347	-35.69445195	-14.46356043
.93	-60.74791755	-173.40082769	-143.42661283	-113.45239797	-83.47818312	-53.50396826	-23.52975340
.94	-93.01797598	-251.60892083	-209.36180513	-167.11468943	-124.86757373	-82.62045803	-40.37334233
.95	-148.04567478	-370.59922298	-311.19653492	-251.79384686	-192.39115881	-132.98847075	-73.58578269
.96	-248.37373255	-559.47456937	-476.16166609	-392.84876280	-309.53585952	-226.22295624	-142.91005296
.97	-446.98922674	-881.36980878	-764.37575049	-647.38169221	-530.38763392	-413.39357564	-296.39951735
.98	-885.27484698	-1503.21141125	-1335.11941983	-1167.02742841	-998.93543699	-830.84344557	-662.75145415
.99	-2013.12212234	-2986.72662307	-2717.77038626	-2448.81414945	-2179.85791263	-1910.90167582	-1641.94543901
1.00	-5568.98832566	-7674.18805110	-7084.53781995	-6494.88758880	-5905.23735765	-5315.58712650	-4725.93689534

THESE ARE THE OUT-OF-PLANE INTERLAMINAR SHEAR STRESSES -- SIGMA YZ
 THEY ARE FOUND AT VARIOUS MOISTURE CONTENTS

Y LOCATION	MECH ONLY	H=0.0	H=0.2	H=0.4	H=0.6	H=0.8	H=1.0
.80	3.27617888	10.31723571	8.44724614	6.57725656	4.70726699	2.83727741	.96728784
.82	6.56753777	20.68268192	16.93393167	13.18518142	9.43643117	5.68768092	1.93893067
.84	13.16491904	41.46150260	33.94640184	26.43130108	18.91620032	11.40109956	3.88599881
.86	26.38654493	83.11303161	68.04745804	52.98188448	37.91631091	22.85073735	7.78516379
.88	52.87019183	166.59261716	136.39009616	106.18757515	75.98505414	45.78253314	15.58001213
.90	105.84680471	333.84310700	273.29260785	212.74210869	152.19160953	91.64111038	31.09061122
.91	149.66289213	472.50148909	386.76451483	301.02754057	215.29056630	129.55359204	43.81661778
.92	211.43474532	668.58894580	547.18476643	425.78058706	304.37640769	182.97222833	61.56804896
.93	298.27565716	945.66979161	773.75215728	601.83452295	429.91688862	257.99925428	86.08161995
.94	419.76910709	1336.64857623	1093.18597910	849.72338197	606.26078483	362.79818770	119.33559056
.95	588.25330316	1886.88626457	1542.09703881	1197.30781306	852.51858731	507.72936156	162.94013580
.96	817.80756656	2656.91555150	2168.73092336	1680.54629522	1192.36166707	704.17703893	215.99241079
.97	1117.61798402	3719.40898556	3029.03467417	2338.66036279	1648.28605140	957.91174002	267.53742864
.98	1460.19459243	5123.16377041	4151.96405479	3180.76433917	2209.56462355	1238.36490793	267.16519231
.99	1628.54905698	6683.48801754	5345.79387584	4008.09973414	2670.40559244	1332.71145074	-4.98269096
1.00	446.83474448	6857.50214542	5171.81141375	3486.12068207	1800.42995039	114.73921872	-1570.95151296



APPENDIX II

FRACTURE ANALYSIS OF LOCAL DELAMINATIONS IN LAMINATED COMPOSITES

P. Sriram and E. A. Armanios
School of Aerospace Engineering
Georgia Institute of Technology
Atlanta, Georgia 30332

Abstract

Delamination is a predominant failure mode in continuous fiber reinforced laminated composite structures. One type of delamination is the transverse crack tip delamination which originates at the tip of transverse matrix cracks. An analytical model based on the sublaminar approach and fracture mechanics is developed in this paper to study the growth of such delaminations. Plane strain conditions are assumed and estimates are provided for the total strain energy release rate as well as the mode I and mode II contributions. The energy release rate estimates are used to predict critical delamination growth strains and stresses by assuming a critical energy release rate. These predictions are compared with experimental data on T300/934 Graphite Epoxy $[\pm 25/90_n]_s$ laminates in the range $n=5$ to 8. A good agreement is demonstrated for the range of n where the experimental observations indicate transverse crack tip delamination to be the predominant failure mode.

Introduction

Fiber reinforced composites are now being used in a wide variety of engineering structures. The concept of directional strength and stiffness has been, for the most part, understood sufficiently to enable efficient load bearing designs. One of the current major issues in composite structures is the understanding and prediction of damage modes and failure mechanisms. A thorough knowledge of the failure mechanisms is bound to lead to the design of efficient and durable structures. Failures in these materials often initiate in the form of matrix cracks or delaminations.

Matrix cracks refer to intralaminar failures whereas delaminations refer to interlaminar failures.

Matrix cracks usually occur within laminates where the fibers run at an angle to the primary load direction. Hence, such matrix cracks are also called transverse cracks. Based on the location and direction of growth, two distinct types of delamination can be discerned. These two types are called edge delamination and local or transverse crack tip delamination. Edge delaminations initiate at the load free edges of the structure whereas local delaminations start from a transverse matrix crack. In many cases, both types occur concurrently with varying levels of interaction. It has been observed in simple tension tests of uniform rectangular cross section specimen (Edge Delamination test) that delaminations initiate along the load free edges and propagate normal to the load direction. Transverse matrix cracks running parallel to the fibers have also been observed in off axis plies such as 90° plies. Such transverse cracks terminate where the ply orientation changes. Delaminations can originate at the interface where transverse cracks terminate. These delaminations, called transverse crack delaminations or local delaminations, grow normal to the transverse crack from which they originate. In the case of 90° plies, the growth direction is parallel to the load.

The growth process of edge delaminations and local delaminations is often modelled using a fracture mechanics approach leading to the calculation of a strain energy release rate. This is because the strain energy release rate can correlate delamination behavior from different loading conditions and can account for geometric dependencies. The strain energy release rate associated with a particular growth configuration is a measure of the driving force behind that failure mode. In combination with

appropriate failure criteria, the strain energy release rate provides a means of predicting the failure loads of the structure.

Several methods are available in the literature for analyzing edge delaminations. These include finite element modelling¹⁻³, complex variable stress potential approach⁴, simple classical laminate theory based technique⁵ and higher order laminate theory including shear deformations⁶. Finite element models provide accurate solutions but involve intensive computational effort. Classical laminate theory (CLT) based techniques provide simple closed form solutions and are thus well suited for preliminary design evaluation. Classical laminate theory based techniques provide only the total energy release rate, and thus in a mixed mode situation, there is insufficient information to completely assess the delamination growth tendency. A higher order laminate theory including shear deformations has the ability to provide the individual contributions of the three fracture modes while retaining the simplicity of a closed form solution. A shear deformation model is available for edge delamination and has been shown to agree well with finite element predictions⁶.

Crossman and Wang⁷ have tested T300/934 Graphite epoxy $[\pm 25/90_n]_s$ specimens in simple tension and reported a range of behavior including transverse cracking, edge delamination and local delamination. O'Brien⁸ has presented classical laminate theory solutions for these specimen, demonstrating reasonable agreement in the case of edge delamination but with some discrepancies in the local delamination predictions. An empirical finite element based combined edge and local delamination formulation has also been proposed⁹. Its predictions, however, do not fully explain the dependency of the critical strain on the number of 90° plies.

In this paper, a shear deformation model is developed for the analysis of local delaminations originating from transverse cracks in 90° plies

located in and around the specimen midplane. Plane strain conditions are assumed and thickness strain is neglected. Delaminations are assumed to grow from both ends of the transverse crack tip. The transverse crack is treated as a free boundary and the delamination is considered to be the crack whose growth behavior is to be modelled. The sublamine approach^{10,11} is used to model different regions of the specimen. The resulting boundary value problem is solved to obtain the interlaminar stresses, total strain energy release rate and energy release rate components. Critical local delamination growth loads are predicted for the $[\pm 25/90_n]_s$ specimen.

Analytical Model

The formulation is based on the sublamine approach detailed in ref. 10. A longitudinal section illustrating the geometry of a generic configuration is shown in fig. 1. The central region is assumed to be made of 90° plies with an isolated transverse crack in the middle. Delaminations are assumed to grow from both ends of the transverse crack, and towards both ends as shown. From symmetry considerations, only one quarter of the configuration is modelled. The modelled portion is divided into four sublaminates as shown in fig. 2. The top surface (sublaminates 1 and 4) is stress free. In order to simplify the analysis, plane strain conditions are assumed and the thickness strain (ϵ_z) is set to zero. The consequence of this combined with the fact that the w displacement is zero along the center line is that w is zero in sublaminates 1,2 and 3. Further, this approximation does not allow for the enforcement of boundary conditions on the shear stress resultants, leading to incorrect estimates of the interlaminar normal stresses. The interlaminar shear stresses, however, are not affected by this assumption^{6,10}. The assumptions lead to considerable simplifications in the analysis. In spite of the simplifications, reliable

energy release rate components can be estimated based on the interlaminar shear stress distributions^{6,10}.

A generic sublaminar is shown in fig. 3 along with the notations and sign conventions. The peel and interlaminar shear stresses are denoted by P and T respectively with t and b subscripts for the top and bottom surface respectively. The axial stress resultant, shear stress resultant and bending moment resultant are denoted by N , Q and M respectively. A summary of the governing equations is presented here for convenience. These are derived for a generic sublaminar using the principle of virtual work in Reference 12.

The x and z displacements within the sublaminar are assumed to be of the form

$$u(x,z)=U(x)+z\beta(z) \quad (1)$$

$$w(x,z)=W(x). \quad (2)$$

Here U represents the axial midplane stretching and W is the transverse displacement. The shear deformation is recognized through the rotation β . The origin of the coordinate axes for the sublaminar is taken at the delamination tip as shown in fig. 4. The equilibrium equations take the form

$$N_{,x}+T_t-T_b=0 \quad (3)$$

$$Q_{,x}+P_t-P_b=0 \quad (4)$$

$$M_{,x}-Q+(h/2)(T_t+T_b)=0. \quad (5)$$

where h is the thickness of the sublaminar. The constitutive relations in terms of the force and moment resultants are

$$N=A_{11}U_{,x}+B_{11}\beta_{,x} \quad (6)$$

$$Q=A_{55}(\beta+W_{,x}) \quad (7)$$

$$M=B_{11}U_{,x}+D_{11}\beta_{,x} \quad (8)$$

where the A_{ij} , B_{ij} and D_{ij} are the classical laminate theory axial, coupling and bending stiffnesses. The boundary variables to be prescribed at the sublaminar edges are

N or U

M or β

Q or W.

Additionally, at the interfaces between sublaminates, reciprocal traction and displacement matching boundary conditions have to be specified.

Solution Procedure

A detailed solution is provided in the Appendix. A brief summary is provided here for convenience. The variables in sublaminates 1 and 2 are coupled by their reciprocal interlaminar stresses denoted T_1 and P_1 and by displacement continuity at their common interface. Assuming exponential solutions for the axial force and bending moment resultants ($N_1 = Ae^{sx}$, $M_1 = Be^{sx}$ etc.) leads to an eigen value problem involving the parameter s . The eigen values turn out to be 0 and two nonzero values (say s_1 and s_2) occurring in positive and negative pairs. Since the resultants maintain finite values as x tends to large negative values (left end of sublaminates 1 and 2), the negative roots are dropped out of the solution.

The following boundary conditions from the ends of the modelled region are enforced.

$$N_2(0) = 0 \quad (9)$$

$$Q_4(a) = 0 \quad (10)$$

$$\beta_4(a) = 0 \quad (11)$$

$$N_1 + N_2 = \text{Applied Load} \quad (12)$$

Further, the following displacement matching conditions are applied.

$$u_1(x, -.5h_1) = u_2(x, .5h_2) \quad (13)$$

$$U_1(0) = U_4(0) \quad (14)$$

$$U_2(0)=U_3(0) \quad (15)$$

$$\beta_1(0)=\beta_4(0) \quad (16)$$

It should be noted that a β_2 and β_3 matching condition cannot be applied at this level of modeling since it would amount to specifying both W and $Q^{6,12}$. Consequently, there is a displacement discontinuity at the delamination tip. The effect of this will be discussed subsequently. To eliminate rigid body displacements, U_1 is set to zero at the left end. The following solutions can then be obtained for the resultants in sublaminates 1 and 2.

$$N_1=a_1e^{s_1x}+a_2e^{s_2x}+\epsilon A_{11}(1) \quad (17)$$

$$N_2=-a_1e^{s_1x}-a_2e^{s_2x}+\epsilon A_{11}(2) \quad (18)$$

$$M_1=a_1k_1e^{s_1x}+a_2k_2e^{s_2x} \quad (19)$$

$$M_2=a_1k_3e^{s_1x}+a_2k_4e^{s_2x} \quad (20)$$

The interlaminar shear and peel stresses between sublaminates 1 and 2 can be obtained as

$$T_1=a_1s_1e^{s_1x}+a_2s_2e^{s_2x} \quad (21)$$

$$P_1=(k_1+.5h_1)(a_1s_1^2e^{s_1x})+(k_2+.5h_1)(a_2s_2^2e^{s_2x}) \quad (22)$$

In the above solutions, the k parameters are dependent on the eigen values and the stiffness of sublaminates 1 and 2, the a parameters depend on the k parameters and the initial crack length a , and ϵ is defined as

$$\epsilon=\sigma(h_1+h_2)/(A_{11}(1)+A_{11}(2)) \quad (23)$$

where σ is the applied uniform axial stress. Complete expressions for the eigen values and the a and k parameters can be found in the Appendix.

Proceeding on to sublaminates 3 and 4, the following solutions can be written.

$$N_3=0 \quad (24)$$

$$M_3=\phi_1 \sinh \omega_3x+\phi_2 \cosh \omega_3x \quad (25)$$

where
$$\phi_2=a_1k_3+a_2k_4, \quad (26)$$

$$\phi_1 = -\phi_2 \coth \omega_3 a \quad (27)$$

and
$$\omega_3 = (A_{55}(2)/D_{11}(2))^{0.5} \quad (28)$$

$$N_4 = \epsilon(A_{11}(1) + A_{11}(2)) \quad (29)$$

$$M_4 = a_1 k_1 + a_2 k_2 \quad (30)$$

The corresponding displacement solutions are provided in the Appendix. The compliance of the specimen can be evaluated as

$$C = 2U_4(a)/P \quad (31)$$

where $P/2$ is the load applied to the modelled section. The total energy release rate for the modelled section i.e. the total energy release rate G_T per crack is then given by

$$G_T = P^2/2 w (dC/da) \quad (32)$$

where w is the specimen width. Use of the previously described solutions leads to the following expression.

$$G_T = \frac{P^2}{2w^2} \left(\frac{1}{A_{11}(1)} - \frac{1}{A_{11}(1) + A_{11}(2)} + I_1 - I_2 \right) \quad (33)$$

where the quantities I_1 and I_2 contain exponential terms dependent on the initial delamination length. Using the virtual crack closure technique, from the relative displacements in the cracked portion and the interlaminar stresses ahead of the crack tip, the mode I and mode II energy release rate contributions can be obtained. The mode III energy release rate is zero from the assumption of plane strain. The mode II energy release rate is given by

$$G_{II} = \lim_{\delta \rightarrow 0} \frac{1}{2\delta} \int_0^\delta T_1(x - \delta) \Delta u(x) dx \quad (34)$$

where δ is the virtual crack step size. The result of the limiting process is zero if there is no singularity in the stress field¹⁰. So, the limit is usually taken as the crack step size δ tends to a small value, say Δ , based on the decay length or the length required to capture the essential features of the stress and displacement fields near the crack tip. The decay

length is dependent on the eigen values s_1 and s_2 . In this study, the value of Δ has been set to

$$\Delta_0 = .25(1/s_1 + 1/s_2) \quad (35)$$

since it reasonably fulfills the criterion given above. In a similar fashion, the mode I energy release rate can be obtained based on the normal stress (P) and the w displacements near the crack front. The normal (peel) stress estimate is inaccurate due to the absence of thickness strain. Hence, an alternate approach was used to estimate G_I , the mode I energy release rate. The total energy release rate for this problem is made up entirely of G_I and G_{II} ($G_{III}=0$). From an estimate of G_T and G_{II} , an estimate for G_I can be obtained simply as

$$G_I = G_T - G_{II} \quad (36)$$

The critical load for a given specimen can then be evaluated based on an appropriate fracture law. This is illustrated in the following section.

Results and Discussion

The solutions derived in the previous section have been used to model the behavior of $[\pm 25/90_n]_s$ T300/934 Graphite Epoxy specimen for n values of .5, 1, 2, 3, 4, 6, and 8. These correspond to the specimen tested by Crossman and Wang⁷. The specimen width and length were fixed at .0381 m and .015m respectively, as in the tests. The solutions were generated using a simple computer program based on the closed form expressions for the interlaminar stress and energy release rates. The applied load was set to 100 MPa, of the same order as in the tests.

An example of the total energy release rate variation with the crack length is presented in fig. 5. The asymptotic value of G_T is denoted by G_{T0} in the figure. It can be observed that after a certain crack length, the G_T is independent of the crack length. On the basis of curves like the one shown in fig. 5, the crack length was fixed at 10 ply thicknesses for

the remainder of the study. The dependence of the mode II contribution of the energy release rate on initial crack length (a) is depicted in fig. 6. Typical interlaminar shear and normal stress profiles are presented in figs. 7 and 8 respectively. The corresponding energy release rates have also been calculated and are presented in Table 1 and fig. 9.

In order to evaluate the critical loads, an appropriate mixed mode fracture law has to be applied, based on the calculated energy release components. Since the calculated mode split shows only a small variation with n , the simple Griffith criterion $G_T = G_{TC}$ has been used to scale the stresses to obtain the critical delamination growth stress (σ_c) and strain (ϵ_c) values. The critical energy release rate G_{TC} was chosen as 415 J/m^2 to obtain the critical stresses and strains listed in Table 1. This value of G_{TC} is larger than G_{IC} to account for the presence of mode II and the fact that G_{IIC} is about four times G_{IC} for the material system under consideration. The critical strains are plotted against n , the number of 90° plies in fig. 10. The experimental results of ref. 7 and the predictions of refs. 8 and 9 are also presented in the figure for comparison. The predictions of the model developed in this paper are represented by the solid line while the experimental results are shown as filled squares. The classical laminate theory and finite element critical strain predictions of refs. 8 and 9 are represented by triangles with a connecting line and a dotted line respectively.

In the experiments, the local delamination phenomenon was observed as the predominant failure mode only for the $n=4,6$ and 8 specimens. The shear deformation model presented in this paper provides good agreement with the experimental data in this range. For $n < 4$, edge delamination either in the mid plane or in the $25/90$ interface was observed in the tests. Hence, the predictions of the local delamination models in this region are not of

consequence as long as they do not predict critical loads lower than those predicted by edge delamination models. Thus, it can be seen that the shear deformation model predicts the observed behavior with reasonable accuracy and can be used in conjunction with an appropriate edge delamination model to predict critical loads accurately for the complete range of n values. The edge delamination model presented in References 6 and 12 can be used for this purpose. However, a separate model is required to account for the mid-plane (Mode I) edge delamination behavior.

Conclusions

A shear deformation model has been developed to analyze local delaminations growing from transverse cracks in 90° plies located around the mid plane of symmetric laminates. The predictions of the model agree reasonably with experimental data from $[\pm 25/90_n]_s$ T300/934 Graphite Epoxy laminates. The predicted behavior is such that, in combination with an edge delamination model, the critical loads can be predicted accurately in the range of n from .5 to 8.

Acknowledgements

The authors gratefully acknowledge the financial support provided by NASA under grant NAG-1-637 for performing the research reported in this paper. The authors also wish to thank Mr. A. Badir for help in verifying the analytical model.

References

- [1] Wilkins, D.J., Eisemann, J.R., Camin, R.A., Margolis, W.S. and Benson, R.A., "Characterizing Delamination Growth in Graphite-Epoxy," in Damage in Composite Materials, ASTM STP 775, K.L. Reifsnider, Ed., pp. 168-183 (1982).

- [2] O'Brien, T.K., "Mixed-Mode Strain Energy Release Rate Effects on Edge Delamination of Composites," in Effects of Defects in Composite Materials, ASTM STP 836, pp. 125-142 (1984).
- [3] Wang, S.S. and Choi, I., "The Mechanics of Delamination in Fiber Reinforced Composite Materials. Part II - Delamination Behavior and Fracture Mechanics Parameters," NASA CR-172270 (1983).
- [4] Wang, S.S., "Edge Delamination in Angle Ply Composite Laminates," Proceedings of the 22nd AIAA/ASME/ASCE/AHS Structures, Structural Dynamics and Materials (SDM) Conference, Atlanta, Georgia, 6-8 April, 1981, pp. 473-484.
- [5] O'Brien, T.K., "Characterization of Delamination Onset and Growth in a Composite Laminate," in Damage in Composite Materials, ASTM STP 775, K.L. Reifsnider, Ed., pp. 140-167 (1982).
- [6] Armanios, E.A., and Rehfield, L.W., "Interlaminar Analysis of Laminated Composites using a Sublaminar Approach," Proceedings of the 27th AIAA/ASME/ASCE/AHS Structures, Structural Dynamics and Materials (SDM) Conference, San Antonio, Texas, 19-21 May, 1986, Part 1, pp. 442-452. AIAA Paper 86-0969CP.
- [7] Crossman, F.W., and Wang, A.S.D., "The Dependence of Transverse Cracking and Delamination on Ply Thickness in Graphite/Epoxy Laminates," in Damage in Composite Materials, ASTM STP 775, K.L. Reifsnider, Ed., pp. 118-139 (1982).
- [8] O'Brien, T.K., "Analysis of Local Delaminations and Their Influence on Composite Laminate Behavior," in Delamination and Debonding of Materials, ASTM STP 876, Johnson, W.S., Ed., pp. 282-297 (1985).
- [9] Law, G.E., "A Mixed Mode Fracture Analysis of $(\pm 25/90)_n$ Graphite/Epoxy Composite Laminates," in Effects of Defects in Composite Materials, ASTM STP 836, pp. 143-160 (1984).

[10] Armanios, E.A., "New Methods of Sublaminar Analysis for Composite Structures and Applications to Fracture Processes," Ph.D. Thesis, Georgia Institute of Technology (1984).

[11] Armanios, E.A., Rehfield, L.W., and Reddy, A.D., "Design Analysis and Testing for Mixed-Mode and Mode II Interlaminar Fracture of Composites," in Composite Materials: Testing and Design (Seventh Conference), ASTM STP 893, J.M. Whitney, Ed., pp. 232-255 (1986).

[12] Armanios, E.A., and Rehfield, L.W., "Sublaminar Analysis of Interlaminar Fracture in Composites: Part I - Analytical Model", submitted for publication in the Journal of Composites Technology and Research (July, 1988).

Appendix A

Sublaminar Analysis for Local Delaminations

Interlaminar Stresses and Energy Release Rates

A generic sublaminar is shown in figure 3 along with the notations and sign conventions. The interlaminar normal (peel) and shear stresses are denoted by P and T respectively with the t and b subscripts for the top and bottom surfaces respectively. The axial force resultant, shear force resultant and bending moment resultant are denoted by N , Q and M respectively. Plane strain conditions are assumed to prevail in the $x-z$ plane and the thickness strain ϵ_{zz} is neglected. These assumptions lead to considerable simplification in the analysis. The displacements in the x and z directions are assumed to be of the form

$$u = U(x) + z\beta(x) \quad (\text{A.1})$$

$$w = W(x) \quad (\text{A.2})$$

Here U represents the axial stretching and W is the transverse (thickness direction) displacement. This formulation recognizes shear deformation through the rotation β . The equilibrium equations take the form

$$N_{,x} + T_t - T_b = 0 \quad (\text{A.3})$$

$$Q_{,x} + P_t - P_b = 0 \quad (\text{A.4})$$

$$M_{,x} - Q + \frac{h}{2}(T_t + T_b) = 0 \quad (\text{A.5})$$

where h is the thickness of the sublaminates. The constitutive equations in terms of the force and moment resultants are

$$N = A_{11}U_{,x} + B_{11}\beta_{,x} \quad (\text{A.6})$$

$$Q = A_{55}(\beta + W_{,x}) \quad (\text{A.7})$$

$$M = B_{11}U_{,x} + D_{11}\beta_{,x} \quad (\text{A.8})$$

where A, B and D are the classical laminate theory axial, coupling and bending stiffnesses defined in the customary manner as

$$\begin{aligned} A_{11} &= \int_{-\frac{h}{2}}^{\frac{h}{2}} C_{11} dz \\ B_{11} &= \int_{-\frac{h}{2}}^{\frac{h}{2}} C_{11} z dz \\ D_{11} &= \int_{-\frac{h}{2}}^{\frac{h}{2}} C_{11} z^2 dz \\ A_{55} &= \int_{-\frac{h}{2}}^{\frac{h}{2}} C_{55} dz \end{aligned}$$

Here, the C s are the material moduli. For the case of plane strain in the $x - z$ plane, the C s are defined as follows.

$$\begin{Bmatrix} \sigma_{xx} \\ \sigma_{zz} \\ \tau_{xz} \end{Bmatrix} = \begin{bmatrix} C_{11} & C_{13} & 0 \\ C_{13} & C_{22} & 0 \\ 0 & 0 & C_{55} \end{bmatrix} \begin{Bmatrix} \epsilon_{xx} \\ \epsilon_{zz} \\ \gamma_{xz} \end{Bmatrix} \quad (\text{A.9})$$

The boundary quantities to be prescribed at the sublaminates edges are

$$N \quad \text{or} \quad U$$

$$M \quad \text{or} \quad \beta$$

$$Q \quad \text{or} \quad W$$

Further, at the interfaces between sublaminates, appropriate reciprocal traction and displacement matching boundary conditions have to be used.

The four sublaminates along with the loads acting on each are shown in figure 4. Setting P_1 and T_1 as shown automatically satisfies the traction matching boundary condition at the 1-2 interface. From symmetry, we get $w = 0$ and zero shear stress along the bottom faces of sublaminates 2 and 3. This leads to $w = 0$ in sublaminates 1,2 and 3. Thus, W has been prescribed in these sublaminates and the vertical shear force resultant Q cannot be prescribed at both ends of the sublaminates. Consequently, the calculated peel stress distribution will not be correct. In addition, at the 2-3 interface, the β s cannot be matched, since in these sublaminates, specifying β is equivalent to specifying Q (through eq. A.7). In spite of these simplifications, reliable energy release rate components can be estimated based on the interlaminar shear stress distributions. The mode I contribution can then be evaluated using the total energy release rate, which is not affected significantly by these simplifications.

For the $(\pm 25/90_n)_s$ laminates under consideration, B_{11} is zero in all the four sublaminates. For sublaminates 1 and 2, the equilibrium equations and constitutive relationships can be written as

$$N_{1,x} - T_1 = 0 \quad (\text{A.10})$$

$$N_{2,x} + T_1 = 0 \quad (\text{A.11})$$

$$Q_{1,x} - P_1 = 0 \quad (\text{A.12})$$

$$Q_{2,x} + P_1 - P_2 = 0 \quad (\text{A.13})$$

$$M_{1,x} + \frac{h_1}{2}T_1 - Q_1 = 0 \quad (\text{A.14})$$

$$M_{2,x} + \frac{h_2}{2}T_1 - Q_2 = 0 \quad (\text{A.15})$$

$$N_1 = A_{11(1)}U_{1,x} \quad (\text{A.16})$$

$$N_2 = A_{11(2)}U_{2,x} \quad (\text{A.17})$$

$$Q_1 = A_{55(1)}\beta_1 \quad (\text{A.18})$$

$$Q_2 = A_{55(2)}\beta_2 \quad (\text{A.19})$$

$$M_1 = D_{11(1)}\beta_{1,x} \quad (\text{A.20})$$

$$M_2 = D_{11(2)}\beta_{2,x} \quad (\text{A.21})$$

The subscripts in brackets refer to the sublaminates to which the stiffness coefficients correspond. Equations A.14, A.15 and A.12 can be rewritten in a modified form as

$$M_{1,x} + \frac{h_1}{2}N_{1,x} = A_{55(1)}\beta_1 \quad (\text{A.22})$$

$$M_{2,x} - \frac{h_2}{2}N_{2,x} = A_{55(2)}\beta_2 \quad (\text{A.23})$$

$$\begin{aligned} P_1 &= Q_{1,x} \\ &= M_{1,xx} + \frac{h_1}{2}T_{1,x} \end{aligned} \quad (\text{A.24})$$

Matching the u displacement along the 1-2 interface implies

$$\begin{aligned} u_1\left(-\frac{h_1}{2}, x\right) &= u_2\left(\frac{h_2}{2}, x\right) \\ \text{or } U_1 - \frac{h_1}{2}\beta_1 &= U_2 + \frac{h_2}{2}\beta_2 \end{aligned} \quad (\text{A.25})$$

Combining the equations to eliminate the displacement and interlaminar stress terms leads to the following homogeneous coupled system of ordinary differential equations.

$$N_{1,x} + N_{2,x} = 0 \quad (\text{A.26})$$

$$M_{1,xx} + \frac{h_1}{2}N_{1,xx} - \frac{A_{55(1)}}{D_{11(1)}}M_1 = 0 \quad (\text{A.27})$$

$$M_{2,xx} - \frac{h_2}{2}N_{2,xx} - \frac{A_{55(2)}}{D_{11(2)}}M_2 = 0 \quad (\text{A.28})$$

$$\frac{N_1}{A_{11(1)}} - \frac{h_1}{2} \frac{M_1}{D_{11(1)}} - \frac{N_2}{A_{11(2)}} - \frac{h_2}{2} \frac{M_2}{D_{11(2)}} = 0 \quad (\text{A.29})$$

The solution is assumed of the form

$$\begin{pmatrix} N_1 \\ N_2 \\ M_1 \\ M_2 \end{pmatrix} = \begin{pmatrix} A_1 \\ A_2 \\ A_3 \\ A_4 \end{pmatrix} e^{sx} \quad (\text{A.30})$$

Substitution of this solution into the governing equations results in the following system of algebraic equations.

$$\begin{bmatrix} s & s & 0 & 0 \\ s^2 \frac{h_1}{2} & 0 & s^2 - \frac{A_{55(1)}}{D_{11(1)}} & 0 \\ 0 & -s^2 \frac{h_2}{2} & 0 & s^2 - \frac{A_{55(2)}}{D_{11(2)}} \\ \frac{1}{A_{11(1)}} & -\frac{1}{A_{11(2)}} & -\frac{h_1}{2} \frac{1}{D_{11(1)}} & -\frac{h_2}{2} \frac{1}{D_{11(2)}} \end{bmatrix} \begin{pmatrix} A_1 \\ A_2 \\ A_3 \\ A_4 \end{pmatrix} e^{sx} = \begin{pmatrix} 0 \\ 0 \\ 0 \\ 0 \end{pmatrix} \quad (\text{A.31})$$

The corresponding eigenvalue problem has to be solved in order to obtain non trivial solutions. The eigenvalues turn out to be the roots of the following characteristic equation.

$$s [B_1 s^4 + B_2 s^2 + B_3] = 0 \quad (\text{A.32})$$

where

$$\begin{aligned} B_1 &= -\frac{1}{A_{11(2)}} - \frac{1}{A_{11(1)}} - \frac{1}{D_{11(2)}} \left(\frac{h_2}{2}\right)^2 - \frac{1}{D_{11(1)}} \left(\frac{h_1}{2}\right)^2 \\ B_2 &= \frac{1}{A_{11(2)} D_{11(2)}} + \frac{1}{A_{11(2)} D_{11(1)}} + \frac{A_{55(1)}}{D_{11(1)} D_{11(2)}} \left(\frac{h_2}{2}\right)^2 \\ &\quad + \frac{1}{A_{11(1)} D_{11(1)}} + \frac{1}{A_{11(1)} D_{11(2)}} + \frac{A_{55(2)}}{D_{11(2)} D_{11(1)}} \left(\frac{h_1}{2}\right)^2 \\ B_3 &= -\frac{1}{A_{11(2)} D_{11(1)} D_{11(2)}} - \frac{1}{A_{11(1)} D_{11(1)} D_{11(2)}} \end{aligned}$$

For the material system and ply stacking sequence considered, $B_2^2 > 4B_1B_3$. Hence, the roots can be written as

$$s = 0, \pm \sqrt{\frac{-B_2 \pm \sqrt{B_2^2 - 4B_1B_3}}{2B_1}} \quad (\text{A.33})$$

Only the zero and positive roots of eq. A.33 are considered as they give exponentially decaying solutions, leading to finite values for the resultants at the sublaminates ends. Hence, the solution for N_1 can be written as

$$N_1 = a_1 e^{s_1 x} + a_2 e^{s_2 x} + \alpha_1 \quad (\text{A.34})$$

Using this in eq. A.26 yields

$$N_2 = -a_1 e^{s_1 x} - a_2 e^{s_2 x} + \alpha_2 \quad (\text{A.35})$$

Substituting N_1 and N_2 in eqs. A.27 and A.28 provides the solutions for the bending moments as

$$M_1 = a_1 k_1 e^{s_1 x} + a_2 k_2 e^{s_2 x} \quad (\text{A.36})$$

$$M_2 = a_1 k_3 e^{s_1 x} + a_2 k_4 e^{s_2 x} \quad (\text{A.37})$$

The k parameters in the above solutions are defined as follows.

$$k_1 = \frac{\frac{h_1}{2} s_1^2}{\frac{A_{55(1)}}{D_{11(1)}} - s_1^2} \quad (\text{A.38})$$

$$k_2 = \frac{\frac{h_1}{2} s_2^2}{\frac{A_{55(1)}}{D_{11(1)}} - s_2^2} \quad (\text{A.39})$$

$$k_3 = \frac{\frac{h_2}{2} s_1^2}{\frac{A_{55(2)}}{D_{11(2)}} - s_1^2} \quad (\text{A.40})$$

$$k_4 = \frac{\frac{h_2}{2} s_2^2}{\frac{A_{55(2)}}{D_{11(2)}} - s_2^2} \quad (\text{A.41})$$

If P is the applied force and w represents the specimen width,

$$N_1 + N_2 = \frac{P}{2w} \quad (\text{A.42})$$

Using this in conjunction with eq. A.29 allows determination of the constants α_1 and α_2 . The following solutions for the stresses and the resultants can then be obtained.

$$N_1 = a_1 e^{s_1 x} + a_2 e^{s_2 x} + \frac{P}{2w} \frac{A_{11(1)}}{A_{11(1)} + A_{11(2)}} \quad (\text{A.43})$$

$$N_2 = -a_1 e^{s_1 x} - a_2 e^{s_2 x} + \frac{P}{2w} \frac{A_{11(2)}}{A_{11(1)} + A_{11(2)}} \quad (\text{A.44})$$

$$\begin{aligned} T_1 &= N_{1,x} \\ &= a_1 s_1 e^{s_1 x} + a_2 s_2 e^{s_2 x} \end{aligned} \quad (\text{A.45})$$

$$\begin{aligned} P_1 &= M_{1,xx} + \frac{h_1}{2} T_{1,x} \\ &= (k_1 + \frac{h_1}{2}) a_1 s_1^2 e^{s_1 x} + (k_2 + \frac{h_1}{2}) a_2 s_2^2 e^{s_2 x} \end{aligned} \quad (\text{A.46})$$

The constitutive equations are used to write down the displacement solutions. The rigid body displacements of sublaminates 1 and 2 are matched (in order to satisfy the displacement continuity condition) to obtain

$$U_1 = \frac{a_1}{A_{11(1)} s_1} e^{s_1 x} + \frac{a_2}{A_{11(1)} s_2} e^{s_2 x} + \frac{P}{2w} \frac{1}{A_{11(1)} + A_{11(2)}} x + a_3 \quad (\text{A.47})$$

$$U_2 = -\frac{a_1}{A_{11(1)} s_1} e^{s_1 x} - \frac{a_2}{A_{11(1)} s_2} e^{s_2 x} + \frac{P}{2w} \frac{1}{A_{11(1)} + A_{11(2)}} x + a_3 \quad (\text{A.48})$$

$$\beta_1 = \frac{1}{A_{55(1)}} [a_1 k_1 s_1 e^{s_1 x} + a_2 k_2 s_2 e^{s_2 x} + \frac{h_1}{2} (a_1 s_1 e^{s_1 x} + a_2 s_2 e^{s_2 x})] \quad (\text{A.49})$$

$$\beta_2 = \frac{1}{A_{55(2)}} [a_1 k_3 s_1 e^{s_1 x} + a_2 k_4 s_2 e^{s_2 x} + \frac{h_2}{2} (a_1 s_1 e^{s_1 x} + a_2 s_2 e^{s_2 x})] \quad (\text{A.50})$$

The constants a_1 , a_2 and a_3 occurring in the solutions are determined using the boundary conditions. For sublaminate 3 the governing equations are

$$N_{3,x} = 0 \quad (\text{A.51})$$

$$Q_{3,x} + P_3 = 0 \quad (\text{A.52})$$

$$M_{3,x} - Q_3 = 0 \quad (\text{A.53})$$

$$N_3 = A_{11(2)}U_{3,x} \quad (\text{A.54})$$

$$Q_3 = A_{55(2)}\beta_3 \quad (\text{A.55})$$

$$M_3 = D_{11(2)}\beta_{3,x} \quad (\text{A.56})$$

Matching U at the 2-3 interface and applying $N_3(a) = 0$ gives

$$N_3 = 0 \quad (\text{A.57})$$

$$U_3 = U_2(0) \quad (\text{A.58})$$

$$= -\frac{a_1}{s_1 A_{11(2)}} - \frac{a_2}{s_2 A_{11(2)}} + a_3 \quad (\text{A.59})$$

In order to solve for the bending moment, eqs. A.53, A.55 and A.56 are combined to obtain

$$M_{3,xx} - \frac{A_{55(2)}}{D_{11(2)}}M_3 = 0 \quad (\text{A.60})$$

The solution of eq. A.60 can be written as

$$M_3 = \phi_1 \sinh \omega_3 x + \phi_2 \cosh \omega_3 x \quad (\text{A.61})$$

where the quantity ω_3 is defined by

$$\omega_3^2 = \frac{A_{55(2)}}{D_{11(2)}} \quad (\text{A.62})$$

Since the β matching condition cannot be used at the 2-3 interface, the (remaining) boundary conditions are

$$\left. \begin{aligned} M_3(a) &= 0 \\ M_3(0) &= M_2(0) \end{aligned} \right\} \quad (\text{A.63})$$

The ϕ s can be solved using the boundary conditions A.63 as

$$\phi_2 = a_1 k_3 + a_2 k_4 \quad (\text{A.64})$$

$$\phi_1 = -\phi_2 \coth \omega_3 a \quad (\text{A.65})$$

The solution for sublaminates 3 can be completed by writing the following expressions.

$$Q_3 = \phi_1 \omega_3 \cosh \omega_3 x + \phi_2 \omega_3 \sinh \omega_3 x \quad (\text{A.66})$$

$$\beta_3 = \frac{1}{A_{55(2)}} [\phi_1 \omega_3 \cosh \omega_3 x + \phi_2 \omega_3 \sinh \omega_3 x] \quad (\text{A.67})$$

$$P_3 = \frac{A_{55(2)}}{D_{11(2)}} [\phi_1 \sinh \omega_3 x + \phi_2 \cosh \omega_3 x] \quad (\text{A.68})$$

The equilibrium equations for sublaminates 4 are

$$N_{4,x} = 0 \quad (\text{A.69})$$

$$Q_{4,x} = 0 \quad (\text{A.70})$$

$$M_{4,x} - Q_4 = 0 \quad (\text{A.71})$$

The constitutive relations take the form

$$N_4 = A_{11(1)} U_{4,x} \quad (\text{A.72})$$

$$Q_4 = A_{55(1)} (\beta_4 + W_{4,x}) \quad (\text{A.73})$$

$$M_4 = D_{11(1)} \beta_{4,x} \quad (\text{A.74})$$

Using eq. A.69 with the boundary condition $N_4(a) = \frac{P}{2w}$ yields

$$N_4 = \frac{P}{2w} \quad (\text{A.75})$$

Similarly, using eq. A.70 with $Q_4(a) = 0$ results in

$$Q_4 = 0 \quad (\text{A.76})$$

Matching M_1 and M_4 at the 1-4 interface and using eq. A.71 gives

$$M_4 = a_1 k_1 + a_2 k_2 \quad (\text{A.77})$$

The U_4 displacement is obtained by integrating eq. A.72 and using the displacement matching boundary condition $U_4(0) = U_1(0)$.

$$U_4 = \frac{P}{2w} \frac{1}{A_{11(1)}} x + \frac{a_1}{s_1 A_{11(1)}} + \frac{a_2}{s_2 A_{11(1)}} + a_3 \quad (\text{A.78})$$

Similarly, integrating eq. A.74 and setting $\beta_4(a) = 0$ gives

$$\beta_4 = \frac{1}{D_{11(1)}} [a_1 k_1 + a_2 k_2] (x - a) \quad (\text{A.79})$$

Using the solutions for Q_4 and β_4 and the boundary condition $W_4(0) = 0$ in eq. A.73 yields the following solution for W_4 .

$$W_4 = \frac{A_{55(1)}}{D_{11(1)}} [a_1 k_1 + a_2 k_2] \left(\frac{x^2}{2} - ax \right) \quad (\text{A.80})$$

In order to determine a_1 , a_2 and a_3 , the following boundary conditions are used.

$$N_1(0) = \frac{P}{2w}$$

$$\beta_1(0) = \beta_4(0)$$

$$U_1(-l + a) = 0$$

It is convenient to define the following parameters.

$$\theta_1 = \frac{s_1}{A_{55(1)}} \left(k_1 + \frac{h_1}{2} \right) \quad (\text{A.81})$$

$$\theta_2 = \frac{k_1}{D_{11(1)}} \quad (\text{A.82})$$

$$\theta_3 = \frac{s_2}{A_{55(1)}} \left(k_2 + \frac{h_1}{2} \right) \quad (\text{A.83})$$

$$\theta_4 = \frac{k_2}{D_{11(1)}} \quad (\text{A.84})$$

$$\theta_d = \theta_3 - \theta_1 + (\theta_4 - \theta_2)a \quad (\text{A.85})$$

The nominal (far field) strain is given by

$$\epsilon = \frac{P}{2w} \frac{1}{A_{11(1)} + A_{11(2)}} \quad (\text{A.86})$$

The a parameters are obtained as

$$a_1 = A_{11(2)} \epsilon \frac{\theta_3 + \theta_4 a}{\theta_d} \quad (\text{A.87})$$

$$a_2 = -A_{11(2)} \epsilon \frac{\theta_1 + \theta_2 a}{\theta_d} \quad (\text{A.88})$$

$$a_3 = \epsilon(l - a) - \frac{a_1}{s_1 A_{11(1)}} e^{-s_1(l-a)} - \frac{a_2}{s_2 A_{11(1)}} e^{-s_2(l-a)} \quad (\text{A.89})$$

The specimen compliance C is defined as the ratio of specimen extension to applied load. This is obtained as

$$\begin{aligned} C &= \frac{2U_4(a)}{P} \\ &= \frac{2}{P} \left\{ \frac{Pa}{2wA_{11(1)}} + \frac{a_1}{s_1 A_{11(1)}} + \frac{a_2}{s_2 A_{11(1)}} + a_3 \right\} \end{aligned} \quad (\text{A.90})$$

The total energy release rate associated with the crack (delamination) growth under a constant load P is given by

$$G_T = \frac{P^2}{2w} \frac{dC}{da} \quad (\text{A.91})$$

Using the compliance expression from eq. A.90 in eq. A.91 yields the following expression for G_T .

$$G_T = \frac{P^2}{2w^2} \left(\frac{1}{A_{11(1)}} - \frac{1}{A_{11(1)} + A_{11(2)}} + I_1 - I_2 \right) \quad (\text{A.92})$$

where

$$I_1 = \frac{1}{A_{11(1)} + A_{11(2)}} \frac{A_{11(2)} \theta_2 \theta_3 - \theta_1 \theta_4}{\theta_d^2} \left(\frac{1 - e^{-s_1(l-a)}}{s_1} - \frac{1 - e^{-s_2(l-a)}}{s_2} \right) \quad (\text{A.93})$$

$$I_2 = \frac{1}{A_{11(1)} + A_{11(2)}} \frac{A_{11(2)} (\theta_3 + \theta_4 a) e^{-s_1(l-a)} - (\theta_1 + \theta_2 a) e^{-s_2(l-a)}}{\theta_d} \quad (\text{A.94})$$

The individual fracture mode contributions to the energy release rate can be calculated using the virtual crack closure method, based on the interlaminar stresses and displacements in the vicinity of the crack tip. From the assumed plane strain

condition, the mode III contribution is zero ($G_{III} = 0$). The mode II energy release rate, G_{II} , is calculated using the virtual crack closure technique while G_I is evaluated using

$$G_I = G_T - G_{II} \quad (\text{A.95})$$

G_{II} is calculated from the interlaminar shear stress and relative sliding displacement as

$$G_{II} = \lim_{\delta \rightarrow 0} \frac{1}{2\delta} \int_0^\delta T_1(x - \delta) \Delta u(x) dx \quad (\text{A.96})$$

In the absence of a singularity in the stress field, the result of the limiting process leads to the trivial result $G_{II} = 0$. Hence, the limit is calculated as δ tends to some finite value, say Δ . The value of Δ is chosen depending on the decay length associated with the problem i.e. the length within which the presence of the crack significantly alters the specimen response in comparison with the corresponding far field values. Evidently, the decay length in this problem is dependent on the eigenvalues s_1 and s_2 . The following value of Δ has been chosen in order to reasonably fulfil the decay length criterion.

$$\Delta = \frac{1}{4} \left(\frac{1}{s_1} + \frac{1}{s_2} \right) \quad (\text{A.97})$$

The relative sliding displacement Δu is based only on the difference $U_4 - U_3$ so that the kinematic condition of zero relative displacement at the crack tip is fulfilled. This also simplifies the calculations. The mode II energy release rate component is obtained as

$$G_{II} = \frac{I_3 + I_4}{2\Delta} \quad (\text{A.98})$$

where I_3 and I_4 are defined as

$$I_3 = \left(\frac{1}{A_{11(1)}} + \frac{1}{A_{11(2)}} \right) \left(\frac{a_1}{s_1} + \frac{a_2}{s_2} \right) \left[a_1(1 - e^{-s_1\Delta}) + a_2(1 - e^{-s_2\Delta}) \right] \quad (\text{A.99})$$

$$I_4 = \left(\frac{s_1 \Delta - 1 + e^{-s_1 \Delta}}{s_1} a_1 + \frac{s_2 \Delta - 1 + e^{-s_2 \Delta}}{s_2} a_2 \right) \epsilon \frac{A_{11(1)} + A_{11(2)}}{A_{11(1)}} \quad (\text{A.100})$$

Transverse Crack Spacing

Shear Deformation Model

The model presented so far has dealt with delaminations growing from a transverse crack. The same model can be modified to predict the spacing of these transverse cracks. In order to accomplish this, the delamination effect has to be isolated from the model. This can be achieved approximately by letting the crack length a tend to zero. This yields an approximation since the boundary conditions are not accounted for properly by this limiting process. To get an accurate shear deformation model, we consider only sublaminates 1 and 2 and apply the following boundary conditions for sublaminates 1 and 2.

$$N_2(0) = 0 \quad (\text{A.101})$$

$$M_2(0) = 0 \quad (\text{A.102})$$

Using these boundary conditions in eqs. A.37 and A.44 yields two equations in a_1 and a_2 which can be solved to obtain

$$a_1 = \frac{k_4}{k_4 - k_3} \frac{P}{2w} \frac{A_{11(2)}}{A_{11(1)} + A_{11(2)}} \quad (\text{A.103})$$

$$a_2 = \frac{k_3}{k_3 - k_4} \frac{P}{2w} \frac{A_{11(2)}}{A_{11(1)} + A_{11(2)}} \quad (\text{A.104})$$

The interlaminar shear stress can now be obtained using eq. A.45. The saturation crack spacing corresponds to the distance from the crack where the broken plies regain their uniform stress/strain state i.e. where the interlaminar shear stress has decayed down to its far field (uniform) value. Practically, this distance is calculated by looking for the x where the interlaminar shear stress is some small fraction (say

.001) of its maximum value. The maximum shear stress evidently occurs at $x = 0$ and is given by

$$T_1^{(max)} = a_1 s_1 + a_2 s_2 \quad (\text{A.105})$$

The crack spacing λ can then be determined by solving the following transcendental equation.

$$\frac{a_1 s_1 e^{s_1 \lambda} + a_2 s_2 e^{s_2 \lambda}}{a_1 s_1 + a_2 s_2} = 0.001 \quad (\text{A.106})$$

Membrane Model

A simpler model can be used to estimate the saturation spacing of the transverse cracks. This model treats the sublaminates as membranes i.e. the bending effects are ignored. The equilibrium equations for a generic membrane sublaminate are

$$N_{,x} + T_t - T_b = 0 \quad (\text{A.107})$$

$$\frac{h}{2}(T_t - T_b) - Q = 0 \quad (\text{A.108})$$

The constitutive equations take the form

$$N = \left(A_{11} - \frac{B_{11}^2}{D_{11}} \right) U_{,x} \quad (\text{A.109})$$

$$Q = A_{55} \beta \quad (\text{A.110})$$

The displacements are assumed to be of the following form.

$$u = U(x) + z\beta(x) \quad (\text{A.111})$$

$$w = 0 \quad (\text{A.112})$$

The following governing equations can now be written

$$N_{1,x} - T_1 = 0 \quad (\text{A.113})$$

$$N_{2,x} + T_1 = 0 \quad (\text{A.114})$$

$$\frac{h_1}{2}T_1 - Q_1 = 0 \quad (\text{A.115})$$

$$\frac{h_2}{2}T_1 - Q_2 = 0 \quad (\text{A.116})$$

$$N_1 = \gamma_1 U_{1,x} \quad (\text{A.117})$$

$$N_2 = \gamma_2 U_{2,x} \quad (\text{A.118})$$

$$Q_1 = A_{55(1)}\beta_1 \quad (\text{A.119})$$

$$Q_2 = A_{55(2)}\beta_2 \quad (\text{A.120})$$

$$U_1 - \frac{h_1}{2}\beta_1 = U_2 + \frac{h_2}{2}\beta_2 \quad (\text{A.121})$$

where the γ s are defined as

$$\gamma_1 = A_{11(1)} - \frac{B_{11(1)}^2}{D_{11(1)}} \quad (\text{A.122})$$

$$\gamma_2 = A_{11(2)} - \frac{B_{11(2)}^2}{D_{11(2)}} \quad (\text{A.123})$$

Eqs. A.113 and A.115 can be combined as

$$Q_1 = \frac{h_1}{2}N_{1,x} \quad (\text{A.124})$$

Using eqs. A.119 and A.117 in this leads to

$$\beta_1 = \frac{h_1}{2} \frac{1}{A_{55(1)}} \gamma_1 U_{1,xx} \quad (\text{A.125})$$

Following a similar procedure for β_2 yields

$$\beta_2 = \frac{h_2}{2} \frac{1}{A_{55(2)}} \gamma_1 U_{1,xx} \quad (\text{A.126})$$

Using these two relations in eq. A.121 leads to

$$U_1 - \left(\frac{h_1}{2}\right)^2 \frac{\gamma_1}{A_{55(1)}} U_{1,xx} = U_2 - \left(\frac{h_2}{2}\right)^2 \frac{\gamma_1}{A_{55(2)}} U_{1,xx} \quad (\text{A.127})$$

Combining eqs. A.113, A.114, A.117 and A.118 gives

$$\gamma_1 U_{1,xx} + \gamma_2 U_{2,xx} = 0 \quad (\text{A.128})$$

Substituting this into eq. A.127 results in

$$U_{1,xx} - \left[\left(\frac{h_1}{2} \right)^2 \frac{\gamma_1}{A_{55(1)}} + \left(\frac{h_2}{2} \right)^2 \frac{\gamma_1}{A_{55(2)}} \right] U_{1,xxxx} + \frac{\gamma_1}{\gamma_2} U_{1,xx} = 0 \quad (\text{A.129})$$

The characteristic roots of this differential equation are

$$s = 0, 0, \pm \sqrt{\frac{\gamma_1 + \gamma_2}{\gamma_1 \gamma_2 \left[\left(\frac{h_1}{2} \right)^2 \frac{1}{A_{55(1)}} + \left(\frac{h_2}{2} \right)^2 \frac{1}{A_{55(2)}} \right]}} \quad (\text{A.130})$$

The solution for U_1 can then be written as

$$U_1 = A_1 e^{s_1 x} + A_2 x + A_3 \quad (\text{A.131})$$

where the A s are arbitrary constants to be determined from the boundary conditions. The root s_1 is the positive root such that a decaying solution is obtained in the negative x region. For the special case of $B_{11(1)} = B_{11(2)} = 0$, the nonzero roots can be written in a simpler form as

$$s^2 = \frac{4(A_{11(1)} + A_{11(2)})}{A_{11(1)} A_{11(2)}} \frac{1}{\frac{h_1^2}{A_{55(1)}} + \frac{h_2^2}{A_{55(2)}}} \quad (\text{A.132})$$

The interlaminar shear stress can be obtained as follows.

$$\begin{aligned} T_1 &= N_{1,x} \\ &= \gamma_1 U_{1,xx} \\ &= \gamma_1 A_1 s_1^2 e^{s_1 x} \end{aligned} \quad (\text{A.133})$$

The maximum shear stress is

$$T_1^{(max)} = \gamma_1 A_1 s_1^2 \quad (\text{A.134})$$

Then, the saturation crack spacing λ corresponds to

$$e^{s_1 \lambda} = 0.001 \quad (\text{A.135})$$

Shear Lag Model

This model allows for a nonlinear displacement field through the thickness of the sublaminates. Its fundamental assumption is that the shear deformation neglected in the classical theory of bending can be estimated using the shear stress. The sublaminate axial force equilibrium condition can be written as

$$N_{,x} + (T_t - T_b) = 0 \quad (\text{A.136})$$

The axial stress is assumed to be uniform and is given by

$$\sigma_{xx} = \frac{N}{h} \quad (\text{A.137})$$

The shear stress is estimated as follows

$$\begin{aligned} \sigma_{xz,z} &= -\sigma_{xx,x} \\ &= \frac{-N_{,x}}{h} \\ &= \frac{T_t - T_b}{h} \end{aligned} \quad (\text{A.138})$$

This can be integrated to obtain

$$\sigma_{xz} = \frac{T_t - T_b}{h} z + \frac{T_t + T_b}{2} \quad (\text{A.139})$$

Neglecting transverse displacement, the axial displacement can be obtained by integrating the shear strain, which in turn is obtained from the shear stress.

$$\begin{aligned} u_{,z} &= \frac{\sigma_{xz}}{C_{55}^r} \\ &= \frac{1}{C_{55}^r} \left[(T_t - T_b) \frac{z}{h} + \frac{T_t + T_b}{2} \right] \end{aligned} \quad (\text{A.140})$$

$$u = U(x) + \frac{1}{2C_{55}^r} \left[(T_t - T_b) \frac{z^2}{h} + (T_t + T_b) z \right] \quad (\text{A.141})$$

where $U(x)$ is the mid-plane axial displacement. This displacement expression can be used to obtain an improved axial stress estimate as follows.

$$\sigma_{xx} = C_{11} u_{,x}$$

$$= C_{11} \left[U_{,x} + \frac{1}{2C_{55}} (T_t - T_b)_{,x} \frac{z^2}{h} + (T_t + T_b)_{,x} z \right] \quad (\text{A.142})$$

The corresponding axial stress resultant can be written as

$$\begin{aligned} N &= \int_{-\frac{h}{2}}^{\frac{h}{2}} \sigma_{zz} dz \\ &= C_{11} \left[hU_{,x} + \frac{h^2}{24C_{55}} (T_t - T_b)_{,x} \right] \end{aligned} \quad (\text{A.143})$$

The governing equations for the sublaminates are thus eqs. A.136 (equilibrium), A.141 (displacement field) and A.143 (constitutive relationship). Using these to model sublaminates 1 and 2 results in the following governing equations.

$$N_{1,x} - T_1 = 0 \quad (\text{A.144})$$

$$N_{2,x} + T_2 = 0 \quad (\text{A.145})$$

$$N_1 = C_{11(1)} \left[h_1 U_{1,x} - \frac{h_1^2}{24C_{55(1)}} T_{1,x} \right] \quad (\text{A.146})$$

$$N_2 = C_{11(2)} \left[h_2 U_{2,x} + \frac{h_2^2}{24C_{55(2)}} T_{1,x} \right] \quad (\text{A.147})$$

$$u_1 = U_1 + \frac{1}{2C_{55(1)}} \left[-T_1 \frac{z^2}{h_1} + T_1 z \right] \quad (\text{A.148})$$

$$u_2 = U_2 + \frac{1}{2C_{55(2)}} \left[T_1 \frac{z^2}{h_2} + T_1 z \right] \quad (\text{A.149})$$

Displacement continuity at the 1-2 interface implies

$$u_1(x, -\frac{h_1}{2}) = u_2(x, \frac{h_2}{2}) \quad (\text{A.150})$$

$$\text{or} \quad U_2 = U_1 - \frac{3T_1}{8} \left[\frac{h_1}{C_{55(1)}} + \frac{h_2}{C_{55(2)}} \right] \quad (\text{A.151})$$

Equation A.146 can be rewritten as

$$U_{1,x} = \frac{N_1}{C_{11(1)} h_1} + \frac{h_1}{24C_{55(1)}} T_{1,x} \quad (\text{A.152})$$

Combining eqs. A.147, A.151 and A.152 results in

$$N_2 = C_{11(2)} \left\{ \frac{h_2 N_1}{h_1 C_{11(1)}} - \frac{h_2 T_{1,x}}{3} \left[\frac{h_1}{C_{55(1)}} + \frac{h_2}{C_{55(2)}} \right] \right\} \quad (\text{A.153})$$

But from eqs. A.144 and A.145, we have

$$N_{2,x} = -T_1 = -N_{1,x} \quad (\text{A.154})$$

Using this in the differentiated form of eq. A.153 leads to

$$\left[\frac{1}{h_2 C_{11(2)}} + \frac{1}{h_1 C_{11(1)}} \right] N_{1,x} = \frac{1}{3} \left[\frac{h_1}{C_{55(1)}} + \frac{h_2}{C_{55(2)}} \right] N_{1,xxx} \quad (\text{A.155})$$

The nonzero characteristic roots of this equation are given by

$$s^2 = 3 \left(\frac{C_{55(1)}}{h_1 C_{11(1)}} \right) \left(\frac{C_{55(2)}}{h_2 C_{11(2)}} \right) \left(\frac{h_1 C_{11(1)} + h_2 C_{11(2)}}{h_2 C_{55(1)} + h_1 C_{55(2)}} \right) \quad (\text{A.156})$$

This is the same as in the membrane model except for the factor 3 which is 4 in the membrane model. This difference is related to the fact that the axial displacement distribution through the thickness is parabolic in the shear lag model and linear in the membrane model. The crack spacing λ for the shear lag model is determined as in the case of the membrane model but using the modified characteristic root.

Table 1 Summary of Results

number of 90° plies	G_T J/m ²	G_{II}/G_T	σ_c MPa	ϵ_c %
1/2	2.404	0.276	1313.9	1.6747
1	6.752	0.275	784.0	1.1685
2	22.849	0.267	426.2	0.8058
3	51.049	0.261	285.1	0.6427
4	93.603	0.256	210.6	0.5444
6	228.871	0.250	134.7	0.4264
8	440.065	0.247	97.1	0.3555

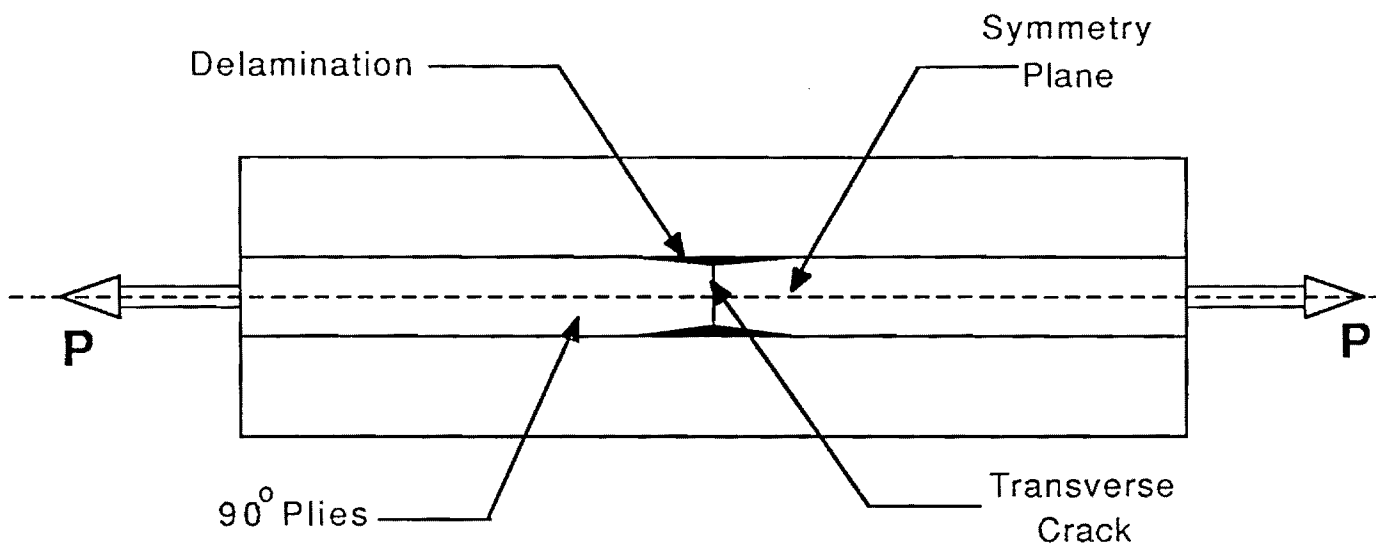


Fig. 1 Specimen Cross Section

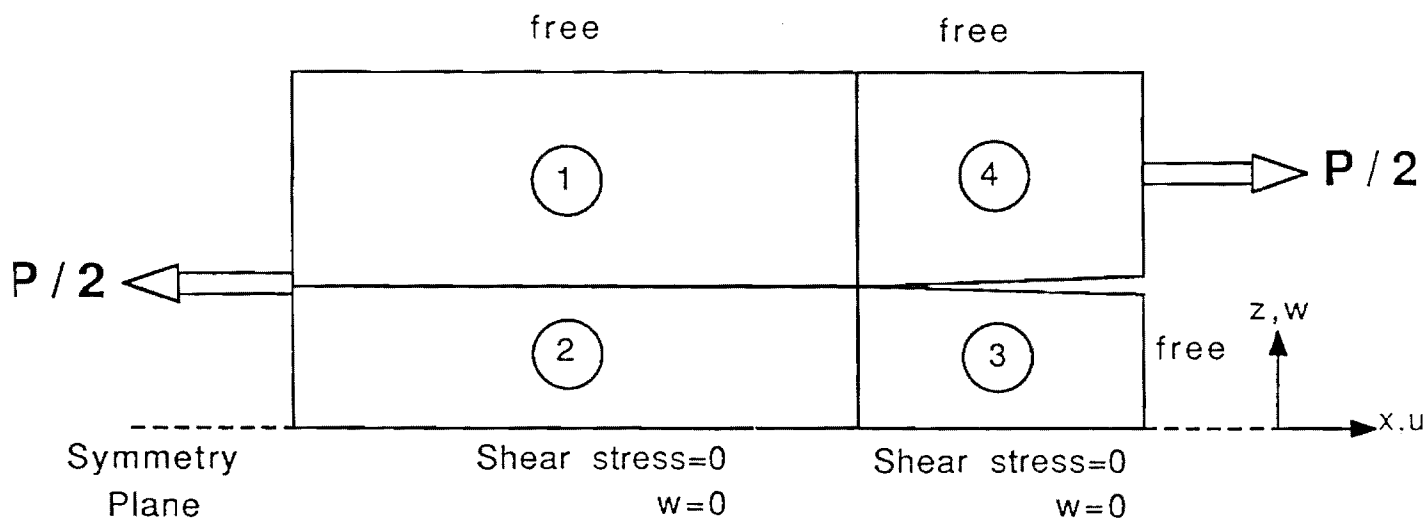


Fig. 2 Modelled Region and Sublaminates Scheme

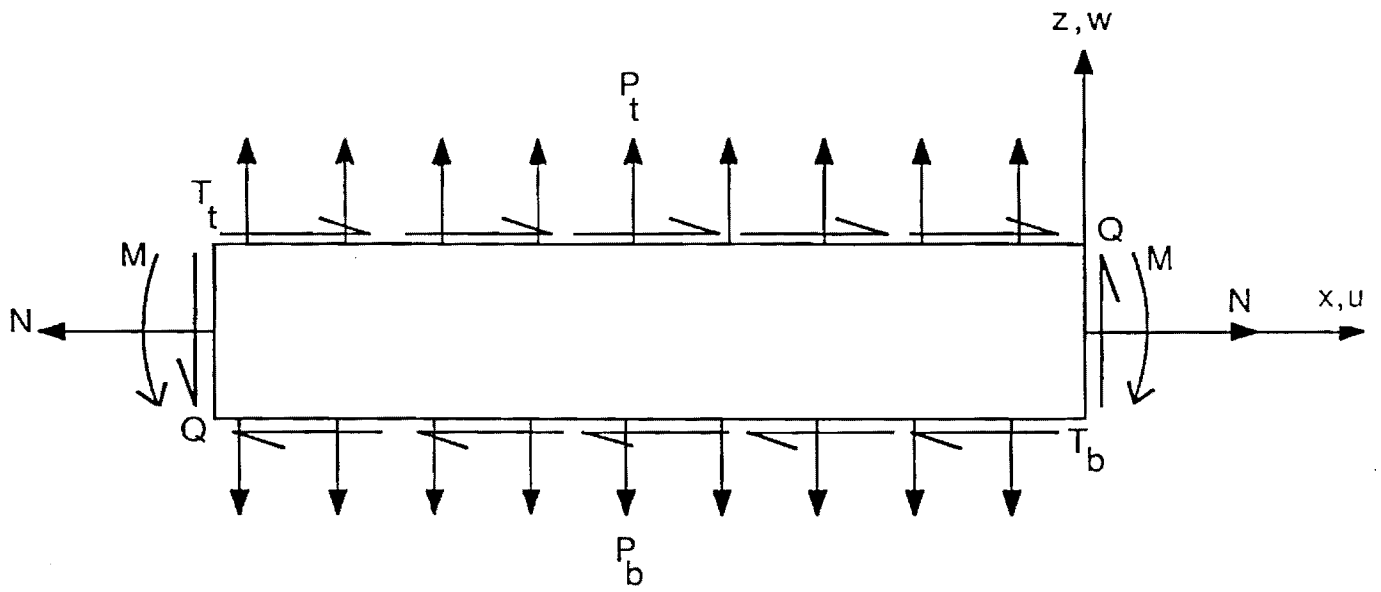


Fig. 3 Generic Sublaminated

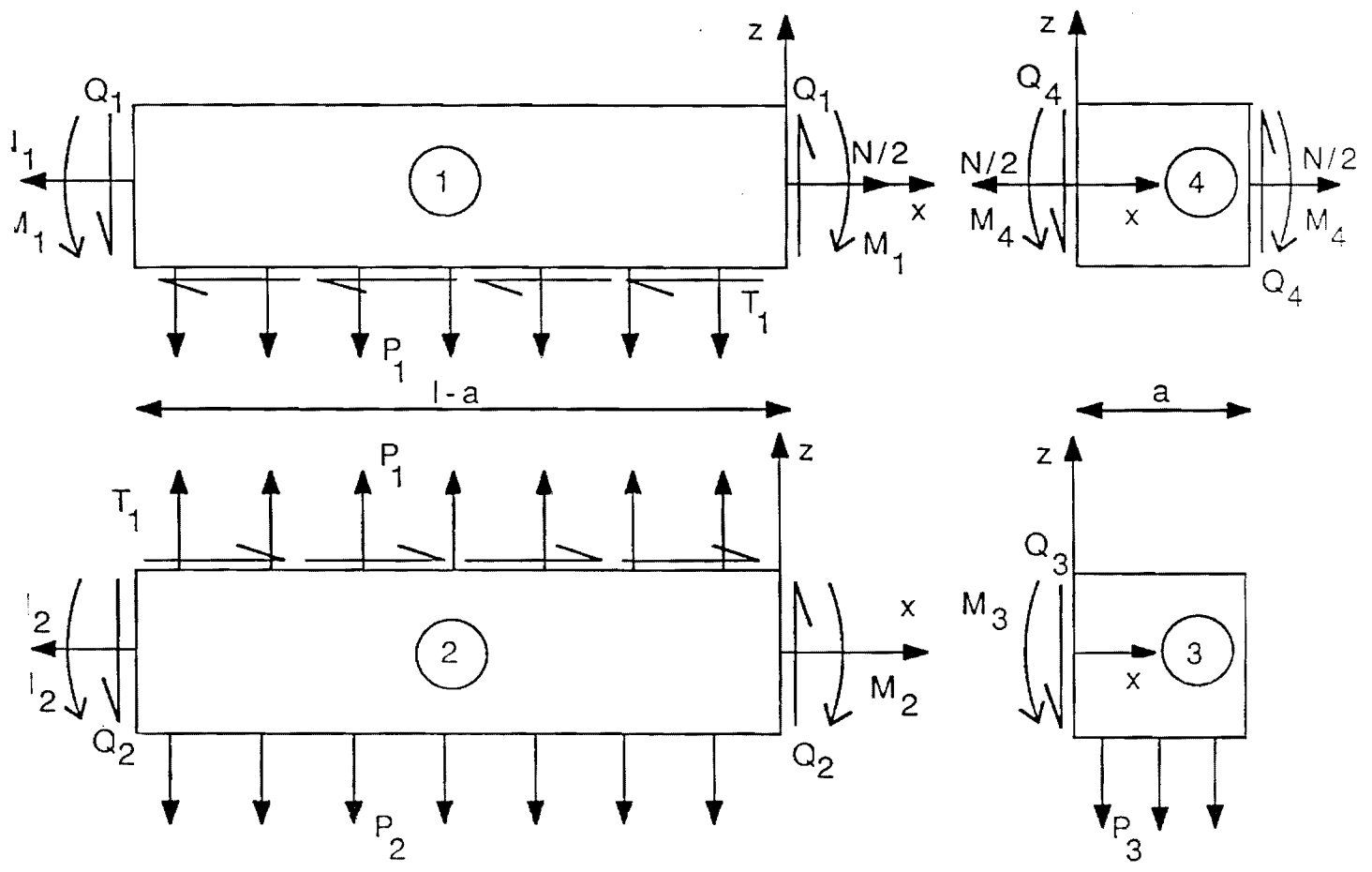


Fig. 4 Sublaminated Forces and Coordinate Systems

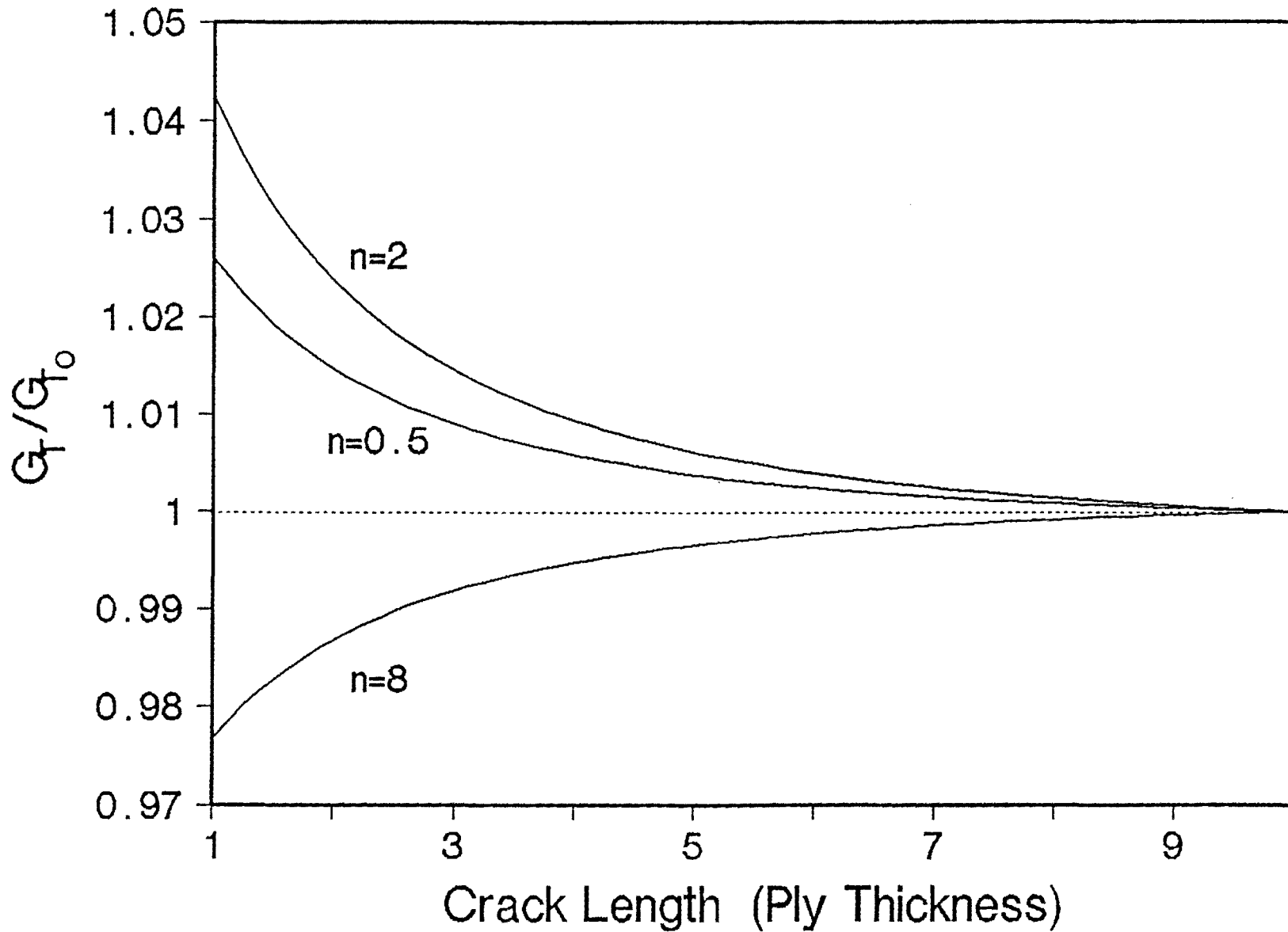


Fig. 5 Total Energy Release Rate Variation with Initial Crack Size

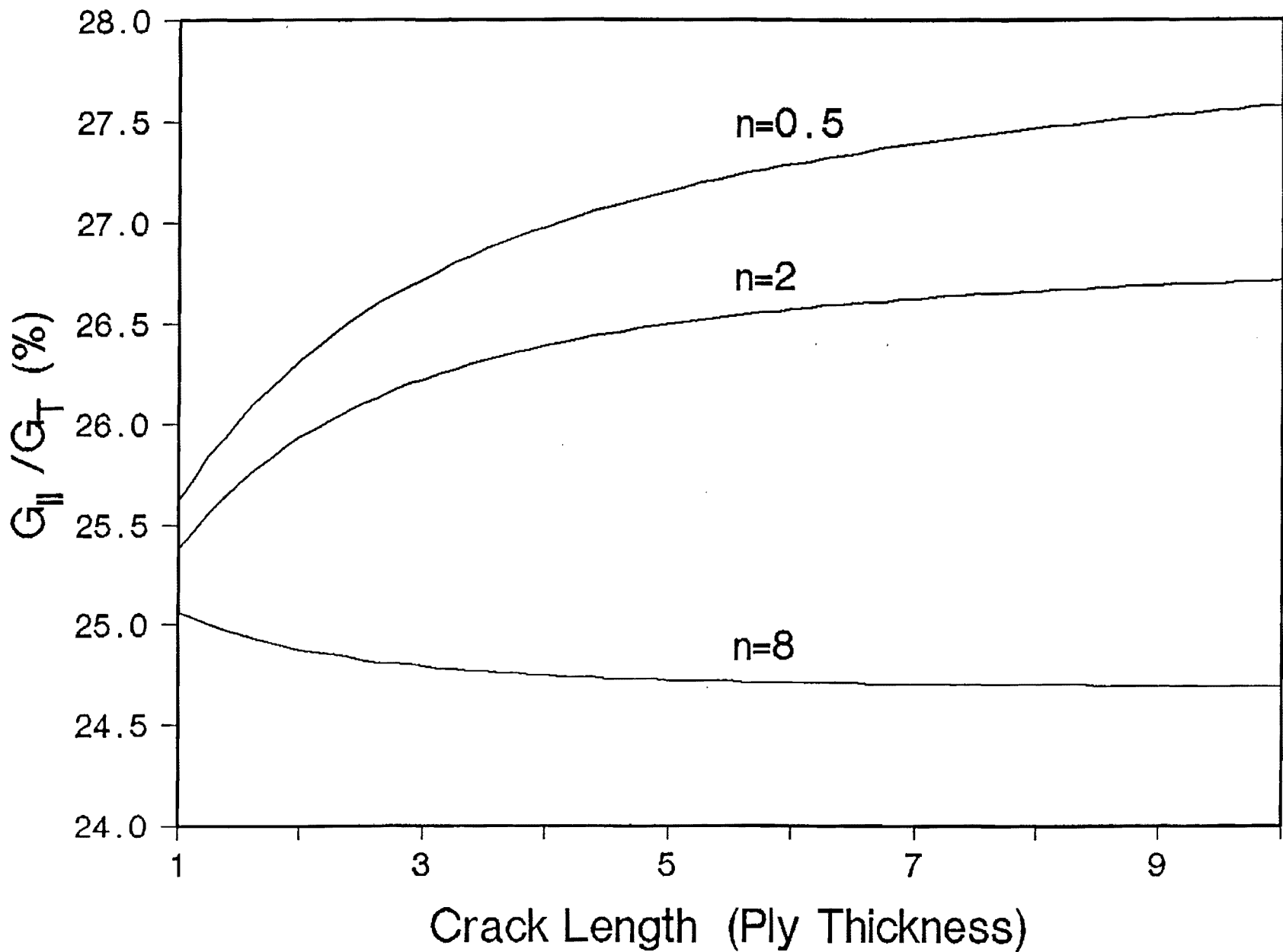


Fig. 6 Mode II Energy Release Rate Dependence on Crack Size

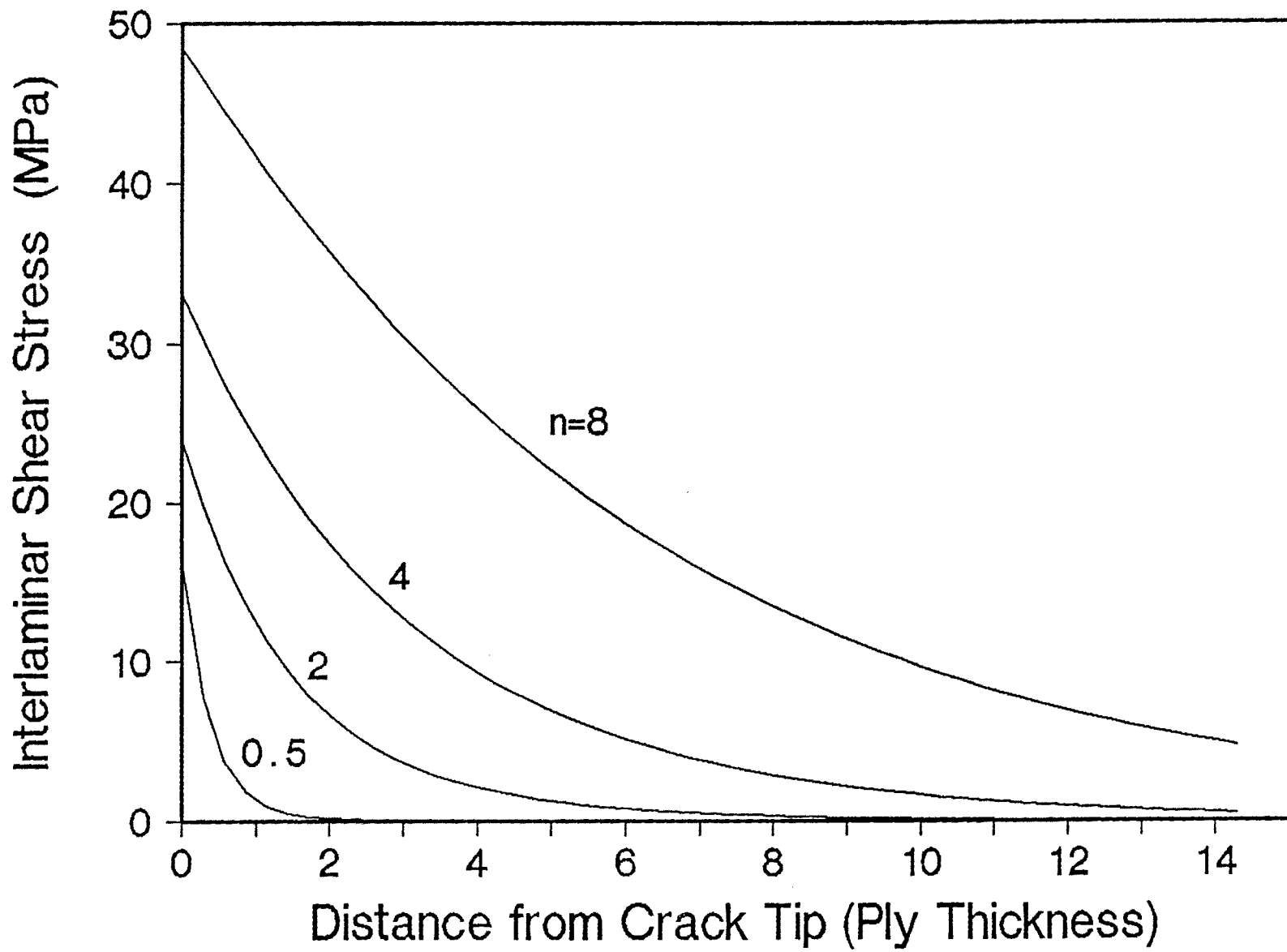


Fig. 7 Interlaminar Shear Stress Distribution

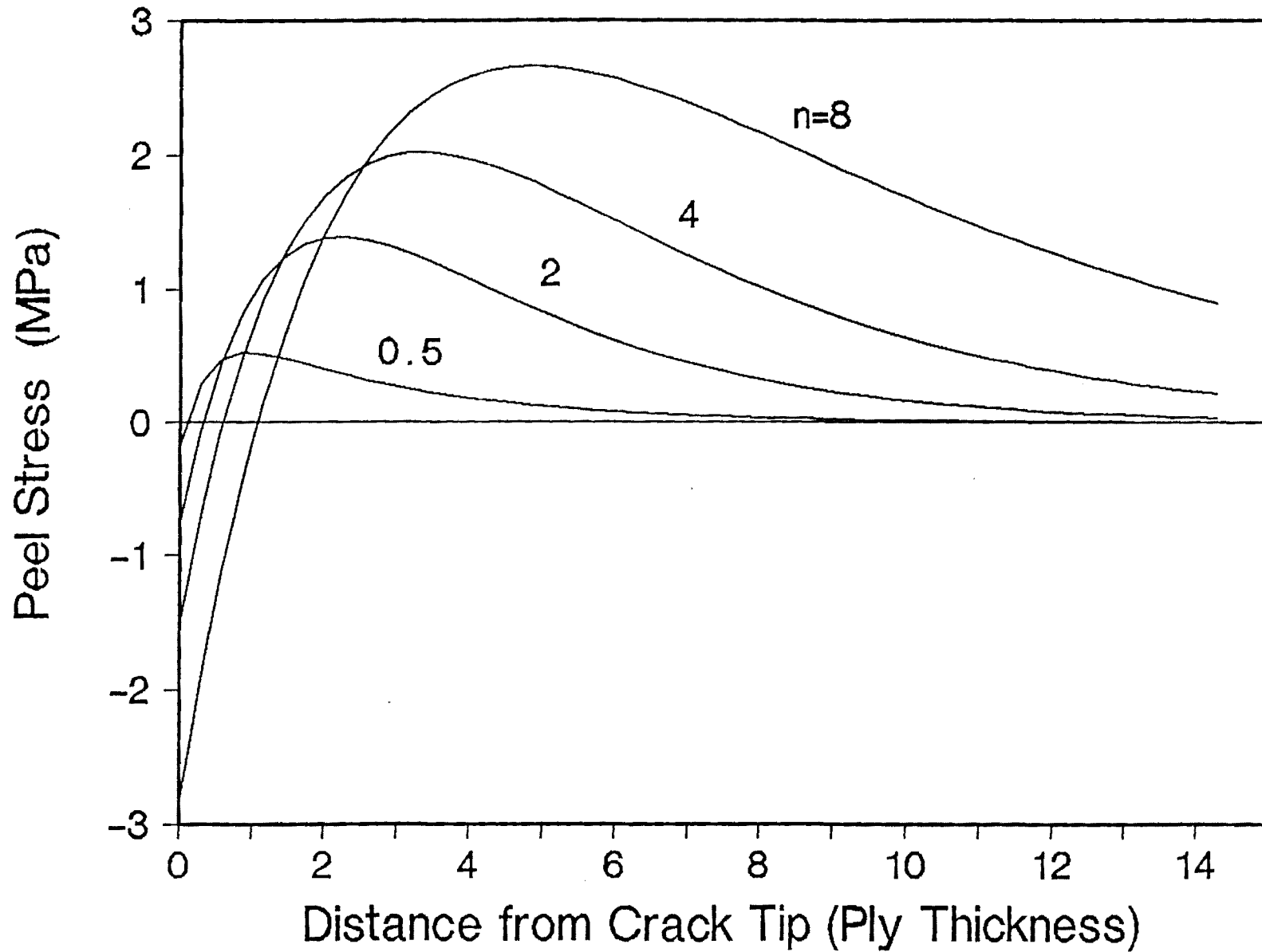


Fig. 8 Interlaminar Normal Stress (Peel Stress) Distribution

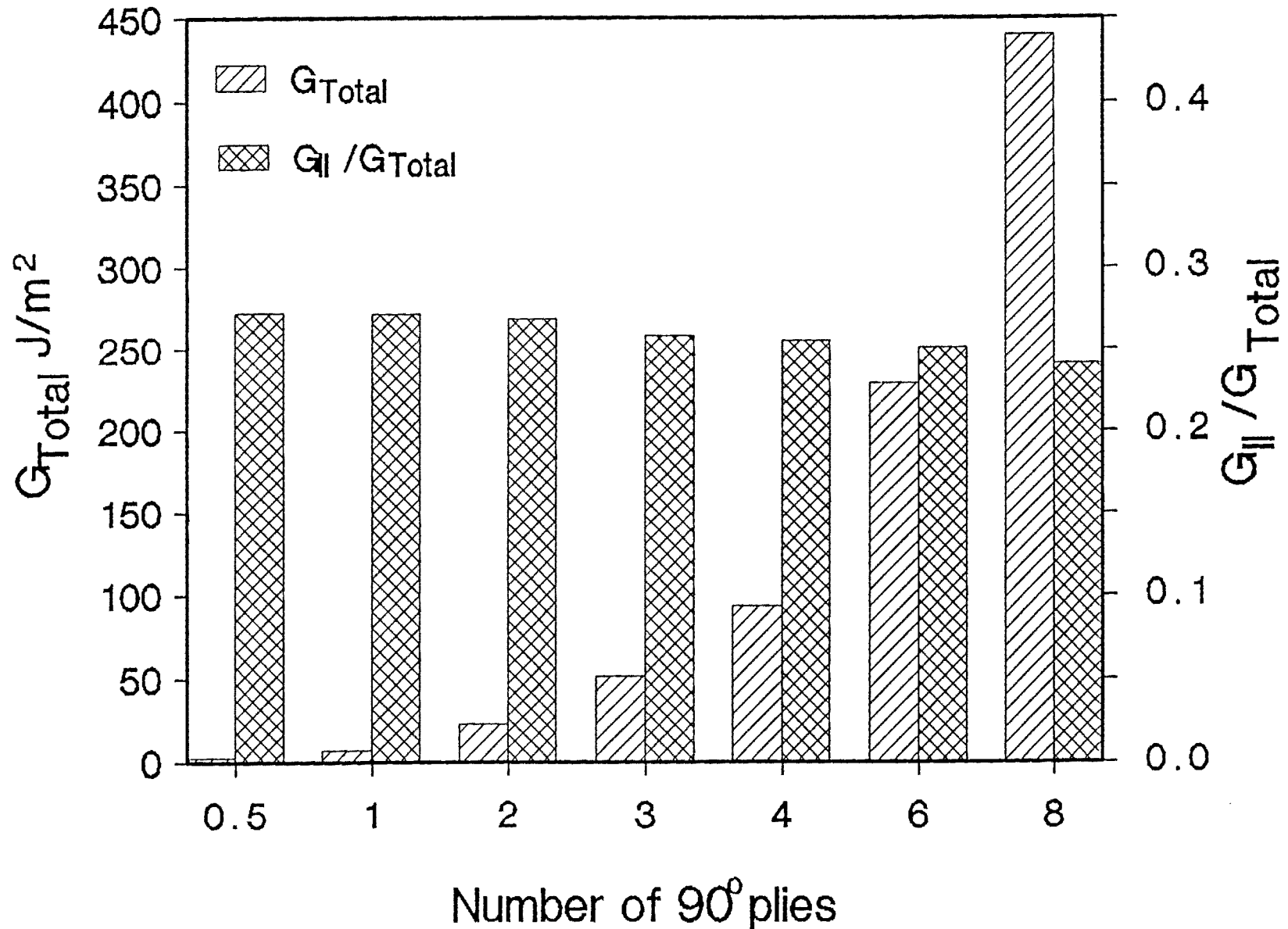


Fig. 9 Energy Release Rate Comparison

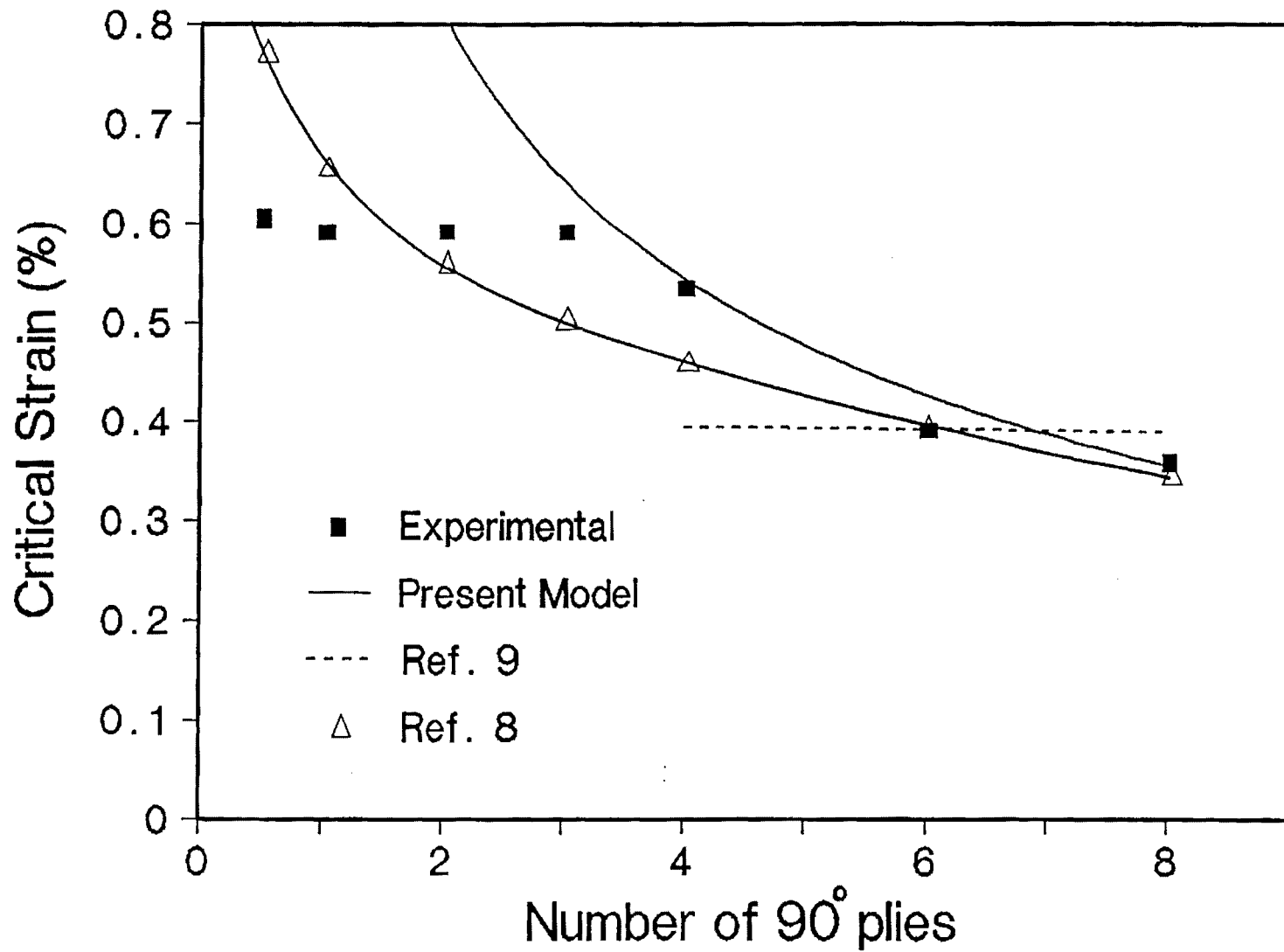


Fig. 10 Critical Delamination Growth Strain Variation



APPENDIX III

Appendix III

III.1 Strain Energy Release Rate

In this analysis, a delamination between belt and core sections is assumed to grow parallel to the belt direction in the tapered and uniform sections. These delaminations in each section are denoted by a and b respectively. The core section in the taper portion is modelled by two equivalent sublaminates. The stiffness properties are smeared to obtain the effective cracked and uncracked stiffnesses which are designated by A_u and A_c as shown in Figure III.1. These stiffnesses change from one ply drop group to another with crack growth a by experiencing a sudden change at discrete locations. Therefore A_u and A_c can be represented in three consecutive regions as follows,

- Region 1: $0 < a < l$

$$A_u = \frac{d + 3l - a}{\frac{d}{A_{BD}} + \frac{l}{A_1} + \frac{l}{A_2} + \frac{l-a}{A_3}} \quad (\text{III.1})$$

$$A_c = A_3 \quad (\text{III.2})$$

- Region 2: $l < a < 2l$

$$A_u = \frac{d + 3l - a}{\frac{d}{A_{BD}} + \frac{l}{A_1} + \frac{2l-a}{A_2}} \quad (\text{III.3})$$

$$A_c = \frac{a + b}{\frac{a-l}{A_2} + \frac{l+b}{A_3}} \quad (\text{III.4})$$

- Region 3: $2l < a < 3l$

$$A_u = \frac{d + 3l - a}{\frac{d}{A_{BD}} + \frac{l}{A_1}} \quad (\text{III.5})$$

$$A_c = \frac{a + b}{\frac{a-2l}{A_1} + \frac{l}{A_2} + \frac{l+b}{A_3}} \quad (\text{III.6})$$

where

h = ply thickness

d = length of uniform thick portion

l = distance between two consecutive ply drop locations

$$A_1 = 6hQ^{45} + 2hQ^0$$

$$A_2 = 4hQ^{45} + 2hQ^0$$

$$A_3 = 2hQ^{45} + 2hQ^0$$

$$A_{BD} = 7hQ^0 + 2hQ^{45}$$

$Q^0 = Q_{11}$ of a 0 degree ply

$Q^{45} = Q_{11}$ of a ± 45 degree ply

Geometry of the sublaminates model is shown in Figure (III.1)

Also axial stiffnesses A_B , A_s , and A_F are given by

$$A_B = \frac{d + 3l - a}{\frac{d}{A_{BD}} + \frac{3l-a}{A_{BT}}} \quad (\text{III.7})$$

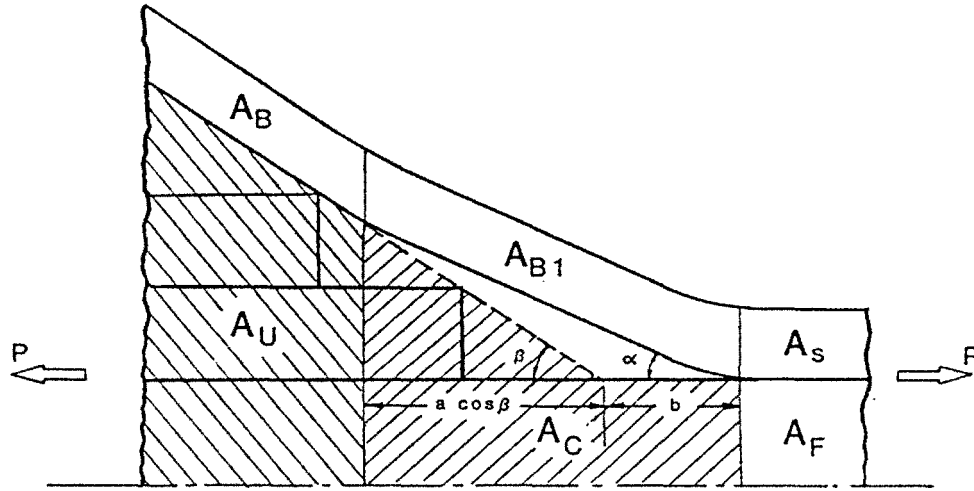


Figure III.1: Geometry of the Sublaminar Model

$$A_F = A_3 \quad (III.8)$$

$$A_s = A_{BD} \quad (III.9)$$

where

A_{BT} = Taper belt stiffness

For a membrane behavior, equilibrium equations are reduced to

$$N_{,x} = 0 \quad (III.10)$$

and the displacement field is assumed to be

$$u(x, z) = U(x) \quad (III.11)$$

and

$$w = 0 \quad (III.12)$$

The constitutive relations are represented by

$$N = A_{11}U_{,x} \quad (\text{III.13})$$

The stress and displacement fields, are determined based on the stiffnesses derived in Equations(III.1-III.9). In this model, load is shared by the core and the belt portions according to their respective stiffness ratios

$$P_1 = \frac{PA_B}{A_B + A_u} \quad (\text{III.14})$$

$$P_2 = \frac{PA_u}{A_B + A_u} \quad (\text{III.15})$$

where P is half of the total axial load applied at the ends.

Using the Equations (III.10), (III.13), and the expressions for P_1 and P_2 from Equations (III.14), (III.15) the axial displacement at $x = c$ can be written as

$$\begin{aligned} U_5 = & \frac{PA_Bc}{A_s(A_B + A_u)} + \frac{P(d + 3l + b)}{(A_B + Au)} \left(\frac{A_B}{A_{B1}} - \frac{A_B}{A_s} \right) \\ & + \frac{P(d + 3l - a)}{(A_B + Au)} \left(1 - \frac{A_B}{A_{B1}} \right) \end{aligned} \quad (\text{III.16})$$

$$\begin{aligned} U_6 = & \frac{PA_uc}{A_3(A_B + A_u)} + \frac{P(d + 3l + b)}{(A_B + Au)} \left(\frac{A_u}{A_c} - \frac{A_u}{A_F} \right) \\ & + \frac{P(d + 3l - a)}{(A_B + Au)} \left(1 - \frac{A_u}{A_c} \right) \end{aligned} \quad (\text{III.17})$$

where A_{B1} is the belt stiffness in the pop-off region as shown in Figure III.1.

A three-dimensional transformation is required in order to estimate the effective axial stiffness of the belt region A_B and A_{B1} . This is due to the belt layup and

the orientation of the different belt portions to the loading axis as shown in Figure III.1. The three-dimensional transformation is presented in section III.3.

The tapered laminate is assumed to be fixed at $x = 0$. Therefore the external work done is given by

$$W = P_1 U_5 + P_2 U_6 \quad (\text{III.18})$$

Substitute from Equations (III.14) through (III.17) into Equation (III.18) to get

$$\begin{aligned} \frac{W}{P^2} = \frac{1}{(A_B + A_u)^2} & \left[(c - d - 3l - b) \left(\frac{A_B^2}{A_s} + \frac{A_u^2}{A_f} \right) + (d + 3l - a)(A_B + A_u) \right. \\ & \left. + (a + b) \left(\frac{A_B^2}{A_{B1}} + \frac{A_u^2}{A_c} \right) \right] \end{aligned} \quad (\text{III.19})$$

The strain energy release rate G due to the external work done is determined by

$$G = \frac{1}{2P^2} \frac{dW}{dA} \quad (\text{III.20})$$

where A is the delamination surface area. G is calculated for delamination lengths ranging from 0 to $60h$. In the analysis, S2/SP250 Glass-Epoxy is used. Its properties are given in Table III.1.

Table III.1: Material Properties of S2/SP250 Glass-Epoxy

E_{11} (MSI)	E_{22} (MSI)	G_{12} (MSI)	G_{13} (MSI)	G_{23} (MSI)	ν_{12}
7.3	2.1	0.87	0.5	0.5	0.275

III.2 Interlaminar Stresses

In this part, an analysis for the interlaminar stresses in the belt-core interface in the tapered section will be developed.

The simple analytical model assumes a beam model for the belt in the tapered section which is shown in Figure III.2. Material and geometric discontinuities are modelled as extensional k_i and concentrated shear springs g_i ($i=1-4$) as shown in Figure III.3. The resin pockets are assumed to be subjected primarily to shear stress and they are represented by a distributed shear spring with a constant stiffness G . The effect of the core is incorporated as elastic supports on the beam-belt model.

A minimum complementary potential energy formulation is used to estimate the interlaminar stresses. The total complementary potential energy consists of bending, shear and extensional energy contributions,

$$\Pi^c = \Pi_b + \Pi_s + \Pi_e + \Pi_k \quad (\text{III.21})$$

where Π_b , Π_s , Π_e , Π_k represent bending, shear and extensional energy components and energy stored in elastic springs, respectively. These are given as,

$$\Pi_b = \frac{1}{2} \int_0^{3l} \frac{M^2(s)}{D_{11}} ds \quad (\text{III.22})$$

$$\Pi_s = \frac{1}{2} \int_0^{3l} \frac{\alpha V^2(s)}{G_1} ds \quad (\text{III.23})$$

$$\Pi_e = \frac{1}{2} \int_0^{3l} \frac{N^2(s)}{A_{11}} ds \quad (\text{III.24})$$

$$\Pi_k = \frac{1}{2} \int_0^{3l} \frac{\tau^2(s)}{G_2} ds + \frac{R_1^2}{2k_1} + \frac{R_2^2}{2k_2} + \frac{R_3^2}{2k_3} + \frac{R_4^2}{2k_4} + \frac{T_1^2}{2g_1} + \frac{T_2^2}{2g_2} + \frac{T_3^2}{2g_3} + \frac{T_4^2}{2g_4} \quad (\text{III.25})$$

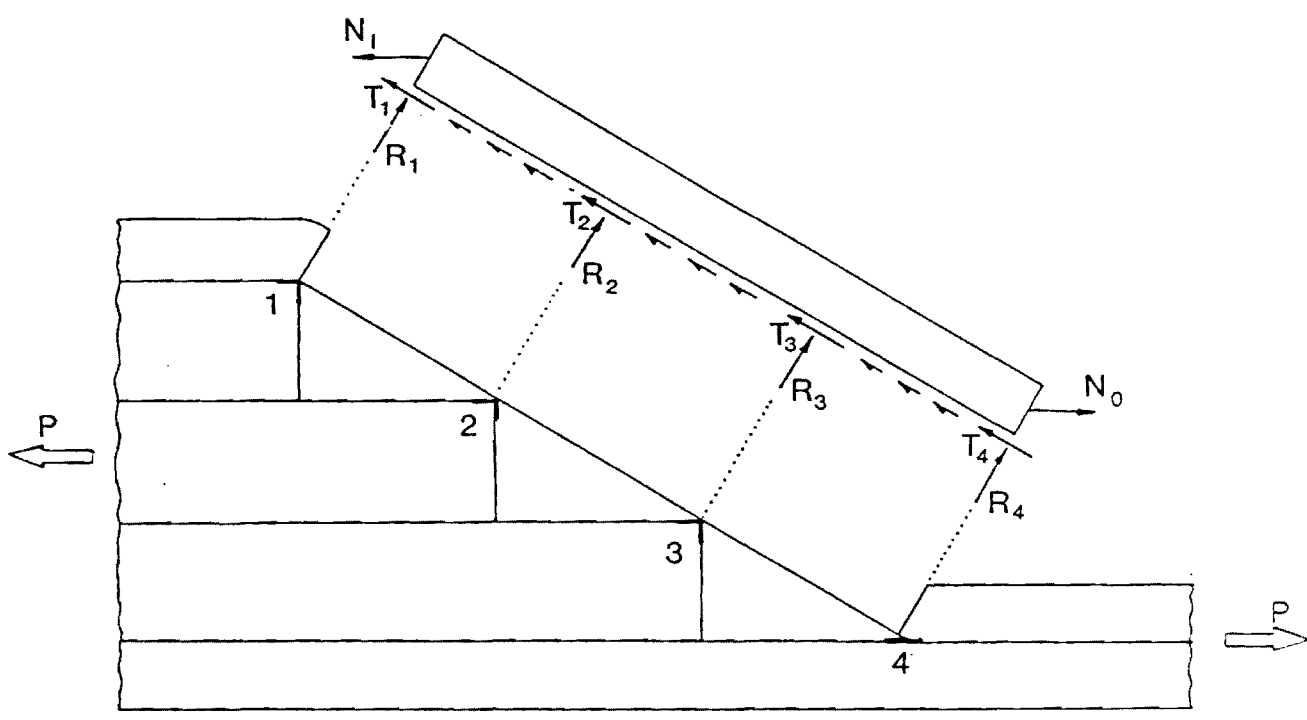


Figure III.2: Geometry of the Model

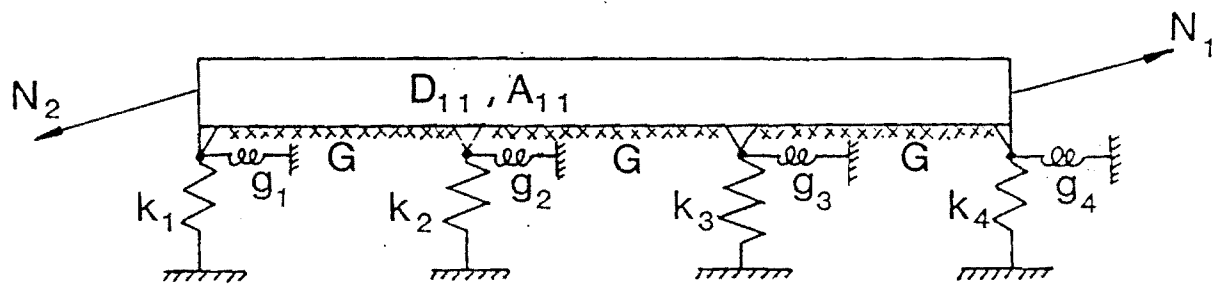


Figure III.3: Modelling of the Beam-Belt

where R_i, T_i ($i=1,2,3,4$) are unknowns. The constant shear stress, c , due to resin filler is an additional unknown. The total number of unknowns in this formulation is nine. These unknowns are constrained by following equilibrium equations.

$$R_1 = -R_3 - 2R_4 + 2N_{12} + N_{22} - \frac{t}{2l}(N_{11} - N_{21}) \quad (\text{III.26})$$

$$R_2 = 2R_3 + 3R_4 - 3N_{12} + \frac{t}{2l}(N_{11} - N_{21}) \quad (\text{III.27})$$

$$T_1 = -T_2 - T_3 - T_4 - 3cl - N_{12} + N_{11} \quad (\text{III.28})$$

where N_{11}, N_{12}, N_{21} and N_{22} denote the components of the extensional load at two ends of the belt section.

The bending moment, shear force and axial force in each of the three ply drop regions are written as

- Region 1: $0 < s < l$

$$M(s) = -N_{12}s + \frac{ct}{2}s + R_4s + T_4\frac{t}{2} \quad (\text{III.29})$$

$$V(s) = N_{12} - R_4 \quad (\text{III.30})$$

$$N(s) = N_{11} - cs - T_4 \quad (\text{III.31})$$

- Region 2: $l < s < 2l$

$$M(s) = -N_{12}s + \frac{ct}{2}s + (R_3 + R_4)s - R_3l + (T_3 + T_4)\frac{t}{2} \quad (\text{III.32})$$

$$V(s) = N_{12} - R_3 - R_4 \quad (\text{III.33})$$

$$N(s) = N_{11} - cs - T_3 - T_4 \quad (\text{III.34})$$

- Region 3: $2l < s < 3l$

$$M(s) = -N_{12}s + \frac{ct}{2}s + (-R_2 + R_3 + R_4)s + (2R_2 - R_3)l + (T_2 + T_3 + T_4)\frac{t}{2} \quad (\text{III.35})$$

$$V(s) = N_{12} - R_2 - R_3 - R_4 \quad (\text{III.36})$$

$$N(s) = N_{11} - cs - T_2 - T_3 - T_4 \quad (\text{III.37})$$

Therefore the bending energy in Equation (III.22) can be written as

$$\begin{aligned} \Pi_b &= \frac{1}{2D_{11}} \int_0^l \left[-N_{12}s + \frac{ct}{2}s + R_4s + T_4\frac{t}{2} \right]^2 ds \\ &+ \frac{1}{2D_{11}} \int_l^{2l} \left[-N_{12}s + \frac{ct}{2}s + (R_3 + R_4)s - R_3l + (T_3 + T_4)\frac{t}{2} \right]^2 ds \\ &+ \frac{1}{2D_{11}} \int_{2l}^{3l} \left\{ -N_{12}s + \frac{ct}{2}s + \left[-R_3 - 2R_4 + N_{12} - \frac{t}{2l}(N_{11} - N_{21}) \right] s \right\}^2 ds \end{aligned}$$

$$\begin{aligned}
& + \left[3R_3 + 6R_4 - 6N_{12} + \frac{t}{2l}(N_{11} - N_{21}) \right] l \\
& + (T_2 + T_3 + T_4) \frac{t}{2} \Big\}^2 ds \quad (III.38)
\end{aligned}$$

Similarly for the shear energy

$$\begin{aligned}
\Pi_s = & r \int_0^l (N_{12} - R_4)^2 ds + r \int_l^{2l} (N_{12} - R_3 - R_4)^2 ds \\
& + r \int_{2l}^{3l} \left[-2N_{12} + R_3 + 2R_4 + \frac{t}{2l}(N_{11} - N_{21}) \right]^2 ds \quad (III.39)
\end{aligned}$$

where

$$r = \frac{3}{5G_2A}$$

The energy of extensional loads can be expressed by

$$\begin{aligned}
\Pi_e = & \frac{1}{2A_{11}} \int_0^l (N_{11} - cs - T_4)^2 ds + \frac{1}{2A_{11}} \int_l^{2l} (N_{11} - cs - T_3 - T_4)^2 ds \\
& + \frac{1}{2A_{11}} \int_{2l}^{3l} (N_{11} - cs - T_2 - T_3 - T_4)^2 ds \quad (III.40)
\end{aligned}$$

The energy stored in the elastic springs is written as

$$\begin{aligned}
\Pi_k = & \frac{3c^2}{2G_2} l + \frac{1}{2k_1} \left[-R_3 - 2R_4 + 2N_{12} + N_{22} - \frac{t}{2l}(N_{11} - N_{21}) \right]^2 \\
& + \frac{1}{2k_2} \left[2R_3 + 3R_4 - \frac{1}{l}M_1 + \frac{1}{l}M_2 - 3N_{12} + \frac{t}{2l}(N_{11} - N_{21}) \right]^2
\end{aligned}$$

$$\begin{aligned}
& + \frac{R_3^2}{2k_3} + \frac{R_4^2}{2k_4} + \frac{T_1^2}{2g_1} + \frac{T_2^2}{2g_2} + \frac{1}{2g_1} [-T_2 - T_3 - T_4 - 3cl - N_{12} + N_{11}]^2 \\
& + \frac{T_2^2}{2g_2} + \frac{T_3^2}{2g_3} + \frac{T_4^2}{2g_4}
\end{aligned} \tag{III.41}$$

The complementary potential energy in Equations (III.38) through (III.41) is expressed in terms of 6 unknowns, namely R_3 , R_4 , T_i ($i=2,3,4$) and c . By minimizing these expressions the following system of linear equations is obtained

$$\begin{aligned}
& \left(\frac{27t^2l^3}{12D} + \frac{3l}{G_2} + \frac{9l^2}{g_1} \right) c + \frac{tl^3}{D} R_3 + \frac{5tl^3}{2D} R_4 + \left(\frac{5t^2l^2}{8D} + \frac{3l}{g_1} \right) T_2 + \left(\frac{t^2l^2}{D} + \frac{3l}{g_1} \right) T_3 \\
& + \left(\frac{9t^2l^2}{8D} + \frac{3l}{g_1} \right) T_4 = \frac{5tl^3}{2D} N_{12} + \frac{3l}{g_1} (N_{11} - N_{21}) + \frac{t^2l^2}{3D} (N_{11} - N_{21})
\end{aligned} \tag{III.42}$$

$$\begin{aligned}
& \frac{tl^3}{D} c + \left(\frac{2l^3}{3D} + \frac{1}{k_1} + \frac{4}{k_2} + \frac{1}{k_3} \right) R_3 + \left(\frac{3l^3}{2D} + \frac{2}{k_1} + \frac{6}{k_2} \right) R_4 + \frac{tl^2}{4D} T_2 \\
& + \frac{tl^2}{2D} T_3 + \frac{tl^2}{2D} T_4 = \left(\frac{3l^3}{2D} + \frac{2}{k_1} + \frac{6}{k_2} \right) N_{12} + \frac{2N_{22}}{k_1} \\
& + \left(\frac{tl^3}{12D} - \frac{t}{2k_1l} - \frac{t}{k_2l} \right) (N_{11} - N_{21})
\end{aligned} \tag{III.43}$$

$$\begin{aligned}
& \frac{5tl^3}{2D} c + \left(\frac{3l^3}{2D} + \frac{2}{k_1} + \frac{6}{k_2} \right) R_3 + \left(\frac{4l^3}{D} + \frac{4}{k_1} + \frac{9}{k_2} + \frac{1}{k_4} \right) R_4 + \frac{tl^2}{2D} T_2 + \frac{5tl^2}{4D} T_3 \\
& + \frac{3tl^2}{2D} T_4 = \left(\frac{4l^3}{D} + \frac{4}{k_1} + \frac{9}{k_2} \right) N_{12} + \frac{2N_{22}}{k_1} + \frac{tl^2}{6D} (N_{11} - N_{21})
\end{aligned} \tag{III.44}$$

$$\begin{aligned}
& \left(\frac{5t^2l^2}{8D} + \frac{3l}{g_1} \right) c + \frac{tl^2}{4D} R_3 + \frac{tl^2}{2D} R_4 + \left(\frac{t^2l}{4D} + \frac{1}{g_1} + \frac{1}{g_2} \right) T_2 + \left(\frac{t^2l}{4D} + \frac{1}{g_1} \right) T_3 \\
& + \left(\frac{t^2l}{4D} + \frac{1}{g_1} \right) T_4 = \frac{tl^2}{2D} N_{12} + \frac{1}{g_1} (N_{11} - N_{21}) + \frac{t^2l}{8D} (N_{11} - N_{21}) \quad (\text{III.45})
\end{aligned}$$

$$\begin{aligned}
& \left(\frac{t^2l^2}{D} + \frac{3l}{g_1} \right) c + \frac{tl^2}{2D} R_3 + \frac{5tl^2}{4D} R_4 + \left(\frac{t^2l}{4D} + \frac{1}{g_1} \right) T_2 + \left(\frac{t^2l}{2D} + \frac{1}{g_1} + \frac{1}{g_3} \right) T_3 \\
& + \left(\frac{t^2l}{2D} + \frac{1}{g_1} \right) T_4 = \frac{5tl^2}{4D} N_{12} + \frac{1}{g_1} (N_{11} - N_{21}) + \frac{t^2l}{8D} (N_{11} - N_{21}) \quad (\text{III.46})
\end{aligned}$$

$$\begin{aligned}
& \left(\frac{9t^2l^2}{8D} + \frac{3l}{g_1} \right) c + \frac{tl^2}{2D} R_3 + \frac{3tl^2}{2D} R_4 + \left(\frac{t^2l}{4D} + \frac{1}{g_1} \right) T_2 + \left(\frac{t^2l}{2D} + \frac{1}{g_1} \right) T_3 \\
& + \left(\frac{3t^2l}{4D} + \frac{1}{g_1} + \frac{1}{g_4} \right) T_4 = \frac{3tl^2}{2D} N_{12} + \frac{1}{g_1} (N_{11} - N_{21}) \\
& + \frac{t^2l}{16D} (N_{11} - N_{21}) \quad (\text{III.47})
\end{aligned}$$

The concentrated normal and shear forces at the ply drop regions and the inter-laminar shear in the resin filler are estimated by solving the simultaneous system of equations in (III.42) through (III.47) and using Equation (III.26) through (III.28).

III.3 3-D Transformation of Stiffnesses

It has been determined that a three dimensional transformation of stiffnesses is required in order to estimate the effective axial stiffness of the belt regions, A_B and A_{B1} . This is due to the belt layup and the orientation of the different belt portions to the loading axis as shown in Figure III.4.

The loading axis corresponds to axis 1 in the 123 coordinate system which is the transformed system. The principal material coordinates are denoted by 1', 2' and 3'.

The stress-strain relationships in the principal material coordinates for an orthotropic laminate are given by

$$\{\bar{\sigma}\}_{6 \times 1} = [Q]_{6 \times 6} \{\bar{\epsilon}\}_{6 \times 1} \quad (\text{III.48})$$

where

$$Q_{11} = (1 - \nu_{23}\nu_{32})V E_{11} \quad (\text{III.49})$$

$$Q_{22} = (1 - \nu_{31}\nu_{13})V E_{22} \quad (\text{III.50})$$

$$Q_{33} = (1 - \nu_{12}\nu_{21})V E_{33} \quad (\text{III.51})$$

$$Q_{12} = (\nu_{21} + \nu_{23}\nu_{31})V E_{11} = (\nu_{12} + \nu_{13}\nu_{32})V E_{22} \quad (\text{III.52})$$

$$Q_{13} = (\nu_{31} + \nu_{21}\nu_{32})V E_{11} = (\nu_{13} + \nu_{23}\nu_{12})V E_{33} \quad (\text{III.53})$$

$$Q_{23} = (\nu_{32} + \nu_{12}\nu_{31})V E_{22} = (\nu_{23} + \nu_{21}\nu_{13})V E_{33} \quad (\text{III.54})$$

$$Q_{44} = G_{23} \quad (\text{III.55})$$

$$Q_{55} = G_{31} \quad (\text{III.56})$$

$$Q_{66} = G_{12} \quad (\text{III.57})$$

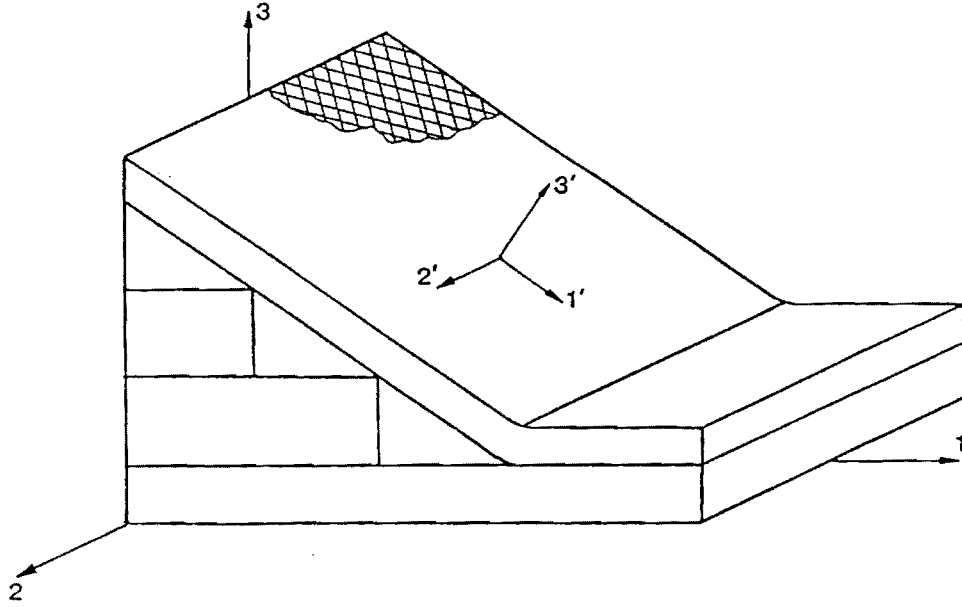


Figure III.4:

$$V = (1 - \nu_{12}\nu_{21} - \nu_{23}\nu_{32} - \nu_{31}\nu_{13} - 2\nu_{12}\nu_{23}\nu_{31})^{-1} \quad (\text{III.58})$$

The presence of angle plies in the belt region making an angle θ in the $1'2'$ -plane results in the following constitutive relationship

$$\{\sigma'\} = [\bar{Q}] \{\epsilon'\} \quad (\text{III.59})$$

where the transformed reduced stiffnesses \bar{Q}_{ij} are given in terms of reduced stiffnesses Q_{ij} as

$$\bar{Q}_{11} = c^4 Q_{11} + 2c^2 s^2 Q_{12} + s^4 Q_{22} + 4c^2 s^2 Q_{66} \quad (\text{III.60})$$

$$\bar{Q}_{22} = s^4 Q_{11} + 2c^2 s^2 Q_{12} + c^4 Q_{22} + 4c^2 s^2 Q_{66} \quad (\text{III.61})$$

$$\bar{Q}_{12} = c^2 s^2 Q_{11} + (c^4 + s^4) Q_{12} + c^2 s^2 Q_{22} - 4c^2 s^2 Q_{66} \quad (\text{III.62})$$

$$\bar{Q}_{66} = 4c^2 s^2 Q_{11} - 8c^2 s^2 Q_{12} + 4c^2 s^2 Q_{22} + 4(c^2 - s^2)^2 Q_{66} \quad (\text{III.63})$$

$$\bar{Q}_{33} = Q_{33} \quad (\text{III.64})$$

$$\bar{Q}_{13} = c^2 Q_{13} + s^2 Q_{23} \quad (\text{III.65})$$

$$\bar{Q}_{23} = s^2 Q_{13} + c^2 Q_{23} \quad (\text{III.66})$$

$$c = \cos\theta$$

$$s = \sin\theta$$

Any ply in the belt portion of the taper makes an angle β with the loading axis if it is in the uncracked belt portion and an angle α if it is in the cracked belt portion. By performing a rotation about the 2-axis, the stiffness along the loading axis, takes the form

$$\{\sigma\} = [C]\{\epsilon\} \quad (\text{III.67})$$

where σ_{ij} and ϵ_{ij} are in 123-axis system and C_{ij} represent the elements of transformed stiffness matrix in this coordinate system.

Since we have assumed

$$u(x, z) = U(x) \quad (\text{III.68})$$

and

$$w = 0 \quad (\text{III.69})$$

For plane stress condition in 1-3 plane (i.e. $\sigma_{i2} = 0$; $i = 1,2,3$) stress strain relations reduce to

$$\sigma_{11} = \left(C_{11} - C_{12}^2/C_{22} \right) \epsilon_{11} \quad (\text{III.70})$$

where

$$C_{11} = \bar{c}^4 \bar{Q}_{11} + 2\bar{c}^2 \bar{s}^2 \bar{Q}_{13} + \bar{s}^4 \bar{Q}_{33} + \bar{c}^2 \bar{s}^2 \bar{Q}_{55} \quad (\text{III.71})$$

$$C_{12} = \bar{c}^2 \bar{Q}_{12} + \bar{s}^2 \bar{Q}_{23} \quad (\text{III.72})$$

$$C_{22} = \bar{Q}_{22} \quad (\text{III.73})$$

where \bar{c} and \bar{s} are cosine and sine of the angle which the cracked and uncracked belt portions makes with the loading axis.

The coefficient of ϵ_{11} in Equation (III.70) represents the transformed axial stiffness. This value is used in the derivation of A_B and A_{B1} .

A-10-1-100

FINAL REPORT

**ANALYSIS OF DELAMINATION RELATED
FRACTURE PROCESSES IN COMPOSITES**

**NASA GRANT NAG-1-637
GEORGIA TECH PROJECT E16-654**

**PRINCIPAL INVESTIGATOR
Erian A. Armanios**

FINAL REPORT

ANALYSIS OF DELAMINATION RELATED FRACTURE PROCESSES IN COMPOSITES

NASA GRANT NAG-1-637
GEORGIA TECH PROJECT E16-654

PRINCIPAL INVESTIGATOR
Erian A. Armanios

This is a final report that summarizes the results achieved under this grant. The first major accomplishment is the development of the sublaminar modeling approach and shear deformation theory. The sublaminar approach allows the flexibility of considering one ply or groups of plies as a single laminated unit with effective properties. This approach is valid when the characteristic length of the response is small compared to the sublaminar thickness. The sublaminar approach was validated comparing its predictions with a finite element solution [1]. A shear deformation theory represents an optimum compromise between accuracy and computational effort in delamination analysis of laminated composites [2]. This conclusion was reached by applying several theories with increasing level of complexity to the prediction of interlaminar stresses and strain energy release rate in a double cracked-lap-shear configuration.

The shear deformation theory and sublaminar approach was applied to the free-edge delamination [1,3] and internal delamination analysis [4] of laminated plates including the influence of hygrothermal stresses [5,6] and combined loading [7]. The analysis was also applied to tapered laminates subjected to tensile loading [8,9].

The second accomplishment is the development of the variationally asymptotical analysis for thin-walled anisotropic beams with closed cross sections [10-12]. The theory is a prerequisite for isolating the influence of damage by comparing predictions with an reference undamaged configuration. Existing composite beam theories have significant differences in the derived expressions for the stiffness coefficients. The variationally asymptotical analysis was developed in order to isolate the effects contributing to these differences. The major advantage of this approach lies in the fact that the displacement field is not assumed *a priori* as is the case for the existing theories and emerges as a result of the analysis. Moreover, the assumed displacement fields in the existing theories follow the classical isotropic formulation. However, no proof is provided with regard to the validity of such a displacement field for anisotropic materials.

The displacement field which resulted from the theory showed two new contributions which were identified as out-of-plane warping due to axial strain and bending. These contributions emerge in addition to the classical out-of-plane torsional warping and are significantly influenced by the material's anisotropy. However, they vanish for materials that are orthotropic or whose properties are antisymmetric relative to the beam middle surface. These configurations coincide with the cases where the predictions of the existing theories are in agreement with test results and numerical simulations. For generally anisotropic materials the error associated with the existing theory predictions correspond to the neglect axial strain and bending related out-of-plane warping.

In addition to providing a definitive answer to the reasons for the disparity in existing theories predictions, the variationally asymptotical theory provides a consistent approach to deriving the displacement field in anisotropic structures. A number of investigators have now adopted this approach for the modeling of initially curved and twisted composite beams and laminated composite plates [13, 14]. Moreover, the closed

form expressions indicate that the new contributions are proportional to the extensional strain and bending curvature. This provides a proof for the work of Kosmatka [15] where an improvement to the displacement field was proposed by adding two terms which are proportional to the extensional strain and bending curvatures. However, their contributions were determined using a finite element simulation.

The details of the sublaminar and Variationally asymptotical analyses are provided by the work of Ref. 12 which is provided in Appendix A for convenience. A list of the publications and presentations related to the Grant is provided in Appendix B.

REFERENCES

- [1]. Armanios, E. A. Rehfield, L. W., Raju, I. S., and O'Brien, T. K. "Sublaminar Analysis of Interlaminar Fracture in Composites: Part II--Applications," *Journal of Composites Technology & Research*, Vol. 11, No. 4, Winter 1989, pp. 147-153.
- [2]. Rehfield, L. W., Armanios, E. A. and Weinstein, F., "Analytical Modeling of Interlaminar Fracture in Laminated Composites," *Composites '86: Recent Advances in Japan and the United States, Proceedings of the Third Japan-U.S. Conference on Composite Materials*, K. Kawata, S. Umekawa, and A. Kobayashi, Eds., pp. 331-340, 1986.
- [3]. Armanios, E. A. and Rehfield, L. W., "Sublaminar Analysis of Interlaminar Fracture in Composites: Part I - Analytical Model," *Journal of Composites Technology & Research*, Vol. 11, No. 4, Winter 1989, pp. 135-146.
- [4]. Armanios, E. A., Sriram, P., and Badir, A.M., "Fracture Analysis of Transverse Crack-Tip and Free Edge Delamination in Laminated Composites," *Composite Materials: Fatigue and Fracture (Third Volume)*, ASTM STP 1110, T. K. O'Brien, Ed., American Society for Testing and Materials, Philadelphia, 1991, pp. 269-286.
- [5]. Armanios, E.A. and Mahler, M.A., "Residual Thermal and Moisture Influences on the Free-Edge Delamination of Laminated Composites," *Proceedings of the AIAA/ASME/ASCE/AHS 19th Structures, Structural Dynamics and Materials (SDM) Conference*, Part 1, pp. 371-381, 1988.
- [6]. Armanios, E.A. and Badir, A.M., "Hygrothermal Influence on Mode I Edge Delamination in Composites," *Journal of Composite Structures*, Vol. 15, No. 4, 1990, pp. 323-342.
- [7]. Armanios, E.A. and Rehfield, L.W., "Interlaminar Fracture Analysis of Composite Laminates Under Bending and Combined Bending and Extension," *Composite Materials: Testing and Design (Eight Conference)*, ASTM STP 972, J.D. Whitcomb, Ed., American Society for Testing and Materials, Philadelphia, 1988, pp. 81-94.
- [8]. Armanios, E.A., and Parnas, L., "Delamination Analysis of Tapered Laminated Composites Under Tensile Loading," *Composite Materials: Fatigue and Fracture (Third Volume)*, ASTM STP 1110, T. K. O'Brien, Ed., American Society for Testing and Materials, Philadelphia, 1991, pp. 340-358.
- [9]. Parnas, L., "Failure Mechanisms and Prediction in Advanced Composite Materials," Ph.D Thesis, School of Aerospace Engineering, Georgia Institute of Technology, March 1991.

[10] Armanios, E.A., Badir, A. and Berdichevsky, V., "Effect of Damage on Elastically Tailored Composite Laminates," Proceedings of the AHS International Technical Specialists' Meeting on Rotorcraft Basic Research, Atlanta, Georgia, March 25-27, 1991, pp. (48-1)-(48-11).

[11]. Berdichevsky, V., Armanios, E. A. and Badir, A., "Theory of Anisotropic Thin-walled Closed-cross-section Beams," *Composites Engineering*, Vol. 2, Nos. 5-7, pp. 411-432, 1992.

[12] Badir, A. M., "Analysis of Advanced Thin-Walled Composite Structures". Ph.D. Thesis, Georgia Institute of Technology, February 1992.

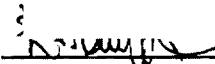
[13] Hodges, D. W., Lee, B. K. and Atilgan, A. R., " Application of the Variational-Asymptotical Method to Laminated Composite Plates," AIAA Paper 92-2357, *Proceedings of the 33rd Structures, Structural Dynamics, and Materials Conference*, Dallas, Texas, April 13-15, 1992, pp. 514 - 524.

[14] Cesnik, C. E., Hodges, D. W. and Atilgan, A. R., " Variational-Asymptotical Analysis of Initially Twisted and Curved Composite Beams," *Developments in Theoretical and Applied Mechanics*, vol. 16, Proceedings of the Sixteenth Southeastern Conference on Theoretical and Applied Mechanics, Nashville, Tennessee, April 12-14, 1992, pp. II.3.29-II.3.36.

[15] Kosmatka, J. B., "Extension-bend-Twist Coupling Behavior of Thin-walled Advanced Composite Beams with Initial Twist," *Proceedings of the 32nd AIAA/ASME/AHS/ASC Structures, Structural Dynamics and Materials Conference*, 1991, pp. 1037-1049.

APPENDIX A

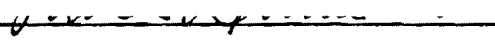
ANALYSIS OF ADVANCED THIN-WALLED
COMPOSITE STRUCTURES


Erian A. Armanios, Chairman


Victor L. Berdichevsky


George A. Kardomateas


Dewey H. Hodges


James T. Wang

Date Approved by Chairman 2/13/92

ANALYSIS OF ADVANCED THIN-WALLED
COMPOSITE STRUCTURES

A THESIS
Presented to
The Academic Faculty

by

Ashraf M. Badir

In Partial Fulfillment
of the Requirements for the Degree
Doctor of Philosophy in Aerospace Engineering

Georgia Institute of Technology
February, 1992

ACKNOWLEDGEMENTS

I wish to express my sincere appreciation to my thesis advisor, Dr. Erian A. Armanios, for the guidance, assistance, and encouragement which he has generously provided throughout the preparation of this work and his high confidence in me.

I also wish to express my sincere gratitude to Dr. Victor L. Berdichevsky for his advise, assistance and patience throughout the last two years. I am indebted to him for many enlightening discussions.

I wish to thank Drs. G. Kardomateas, D. Hodges, and J. Wang for serving on the thesis committee and for their useful comments.

I wish to extend my special thanks to the members of the advanced structures group and my colleagues, Dr. P. Sriram, Dr. Ali Atilgan, Dr. Levend Parnas, Dr. Brian Fortson, Dr. Y. Song, Jian Li, Carlos Bezzeril, Dr. Bob Bless, Mahera Philobos, David Palmer, and Allen Siu.

My profound appreciation goes to my parents for their constant encouragement and lifelong care and devotion.

The author gratefully acknowledges the financial support provided by NASA under Grant NAG-1-637 and the U.S. Army Research Office under Grant DAAL03-88-C-0003 for performing this research.

TABLE OF CONTENTS

ACKNOWLEDGEMENTS	ii
TABLE OF CONTENTS	iii
LIST OF TABLES	vi
LIST OF ILLUSTRATIONS	vii
Chapter	1
I INTRODUCTION	1
1.1 Background	1
II DELAMINATION ANALYSIS	4
2.1 Review of Previous Work	4
2.2 Mid-Plane Edge Delamination	9
2.2.1 Uncracked Region (Sublaminates 1)	14
2.2.2 Cracked Region (Sublaminates 2)	16
2.3 Local Delamination	23
III APPLICATIONS OF DELAMINATION MODELS	33
3.1 Mode I Edge Delamination	33
3.2 Edge and Local Delamination	36
3.2.1 Local Delamination	36

3.2.2	Edge Delamination	37
3.2.3	Failure Loads and Modes	37
3.3	Conclusions	39
IV THEORY OF ANISOTROPIC THIN-WALLED BEAMS		60
4.1	Review of Previous Work	60
4.2	Coordinate Systems	63
4.3	Shell Energy Functional	67
4.4	Asymptotical Analysis of the Shell Energy Functional	70
4.4.1	Zeroth-Order Approximation	70
4.4.2	First-Order Approximation	74
4.4.3	Second-Order Approximation	81
4.4.4	Convergence of Displacement Field	85
4.4.5	Strain Field	86
4.4.6	Constitutive Relationships	88
4.4.7	Equilibrium Equations	92
4.5	Summary of governing equations	93
4.6	Analytical comparison with previous results	93
4.7	Closing Remarks	96
V APPLICATIONS OF ANISOTROPIC THIN-WALLED BEAM THEORY		97
5.1	Effect of Out-of-Plane Warping due to Extension and Bending	98
5.1.1	CUS Configuration	98
5.1.2	CAS Configuration	99
5.2	Comparison of Flexibility Coefficients	100
5.3	Comparison of Deformation	102

	v
5.4 Shear Deformation Contribution	105
5.5 Conclusion	107
5.6 Closing Remarks	107
VI CONCLUSIONS AND RECOMMENDATIONS	119
APPENDIX	120
A Convergence of Displacement Field	121
1.1 Third-Order Approximation	121
BIBLIOGRAPHY	126
VITA	135

To my parents...

LIST OF TABLES

3.1	ED Specimen Geometry and Material Properties	33
3.2	ED Specimen Geometry and Material Properties, Ref. [18]	35
5.1	Properties of T300/5208 Graphite/Epoxy	101
5.2	Comparison of Flexibility Coefficients of NABSA, TAIL and Present (lb, in units)	102
5.3	Geometry and Mechanical Properties of Thin-Walled Beam with $[+12]_4$ CUS square cross-section	103
5.4	MSC/NASTRAN and Present Solutions for a CUS Cantilevered Beam with $[+12]_4$ Layups Subjected to Various Tip Load Cases	104
5.5	Cantilever Geometry and Properties	105
5.6	Cantilever Geometry and Properties	106

LIST OF ILLUSTRATIONS

2.1	Damage Modes	5
2.2	Mid-Plane Edge Delamination	10
2.3	Sublaminde Modeling Scheme (Mid-Plane Edge Delamination)	10
2.4	Notation and Sign Convention for a Generic Sublaminde	12
2.5	Effective non-mechanical free expansion strain across the entire width of the laminate	19
2.6	Local Delamination Specimen Cross Section	23
2.7	Sublaminde Scheme for Local Delamination	24
2.8	Generic Sublaminde for Local Delamination	25
2.9	Sublaminde Forces and Coordinate Systems	26
3.1	Mode I Strain Energy Release Rate in a $[15/ - 15_2/15/90_2]_s$ Laminate	41
3.2	Mode I Strain Energy Release Rate in a $[60/ - 60_2/60/90_2]_s$ Laminate	42
3.3	Mode I Strain Energy Release Rate in a $[0_3/90_3]_s$ Laminate	43
3.4	Influence of Residual Thermal and Moisture Stresses on Mode I Strain Energy Release Rate in a $[15/ - 15_2/15/90_2]_s$ Laminate	44
3.5	Influence of Residual Thermal and Moisture Stresses on Mode I Strain Energy Release Rate in a $[60/ - 60_2/60/90_2]_s$ Laminate	45
3.6	Influence of Residual Thermal and Moisture Stresses on Mode I Strain Energy Release Rate in a $[0_3/90_3]_s$ Laminate	46
3.7	Peel Stress Distribution ahead of the Crack in a $[15/ - 15_2/15/90_2]_s$ Laminate	47

3.8 Peel Stress Distribution ahead of the Crack in a $[60/ - 60_2/60/90_2]_s$ Laminate	48
3.9 Peel Stress Distribution ahead of the Crack in a $[0_3/90_3]_s$ Laminate	49
3.10 Mode I Strain Energy Release Rate in a $[45/ - 45_2/45/90_2]_s$ Laminate	50
3.11 Mode I Strain Energy Release Rate in a $[0_3/90_3]_s$ Laminate	51
3.12 Peel Stress Distribution ahead of the Crack in a $[0_3/90_3]_s$ Laminate	52
3.13 Peel Stress Distribution ahead of the Crack in a $[30/ - 30_2/30/90_2]_s$ Laminate	53
3.14 Total Local Delamination Energy Release Rate Variation	54
3.15 Interlaminar Shear Stress Distribution (Local Delamination)	55
3.16 Total Energy Release Rate for $[\pm 25/90_n]_s$ Graphite/Epoxy Specimen	56
3.17 Interlaminar Normal Stress (Mid Plane Delamination)	57
3.18 Total Energy Release Rate (Mid Plane Delamination) for $[\pm 25/90_2]_s$	58
3.19 Critical Delamination Strain Variation	59
4.1 Cartesian Coordinate System	64
4.2 Curvilinear Coordinate System	65
5.1 Beam Cross Section	109
5.2 Significance of out-of-plane bending related warping on the bending slope of an antisymmetric $[15]_6$ cantilever under 1 lb transverse tip Load	109
5.3 Significance of out-of-plane bending related warping on the bending slope of a symmetric $[30]_6$ cantilever under 1 lb transverse tip Load	110
5.4 Bending Slope of an Anti-Symmetric $[15]_6$ Cantilever Under 1 lb Trans- verse Tip Load	111

5.5	Bending Slope of a Symmetric $[30]_6$ Cantilever Under 1 lb Transverse Tip Load	112
5.6	Twist of a Symmetric $[30]_6$ Cantilever Under 1 lb Transverse Tip Load	113
5.7	Twist of a Symmetric $[45]_6$ Cantilever Under 1 lb Transverse Tip Load	114
5.8	Bending Slope at Mid-Span Under Unit Tip Torque of Symmetric Lay-up Cantilever Beams	115
5.9	Twist at Mid-Span Under Unit Tip Torque of Symmetric Lay-up Cantilever Beams	116
5.10	Deflection of an Antisymmetric $[15]_6$ Cantilever under 1 lb transverse tip load	117
5.11	Shear Deformation γ_{xy} of an Antisymmetric $[15]_6$ Cantilever under 1 lb transverse tip load	118

CHAPTER I

INTRODUCTION

1.1 Background

The use of fiber reinforced composites is increasing in engineering applications. One of the major issues in composite structures is the understanding of the role of the material's anisotropy on the deformation modes, damage modes and failure mechanisms. This research work addresses these stiffness and strength related issues by developing analytical models for the prediction of deformation modes and their coupling effects and damage onset and growth in laminated composites. Accurate prediction of stiffness, response, damage modes and failure mechanisms is bound to lead to the design of efficient and damage tolerant composite structures.

Delamination is a predominant failure mode in continuous fiber reinforced laminated composite structures. Based on the location and direction of growth, there are two distinct types of delamination, namely, free edge delamination and local or transverse crack tip delamination. In many cases, both types occur concurrently with varying levels of interaction.

In the first part of this work shear deformation models including hygrothermal effects are developed for the analysis of mid-plane edge delamination and local delamination originating from transverse cracks in 90° plies. The results of these models are combined with a previously developed shear deformation model for mixed-mode edge delamination to yield a unified analysis of delamination and the ability to iden-

tify the critical failure modes and loads.

Elastically tailored composite design are being used to achieve favorable deformation modes under a given loading environment. Coupling between deformation modes such as extension-twist or bending-twist is created by an appropriate selection of fiber orientation, stacking sequence and materials. An example is the X-29 swept forward wing aircraft where a laminated composite skin is used to create the bending-twist coupling required to handle divergence. This design uses AS-1/3501-5A graphite/epoxy wing covers with -45° outboard plies 9° forward of the wing's 40 % chord line. Elastically tailored composite rotor blades have the potential to be used in rotorcraft structures in order to control flapping and twisting motions at different rotor speeds. This concept can be utilized in tilt rotor aircraft in order to achieve a compromise between hover performance and forward flight propulsive efficiency. A change in the blade twist between flight modes can be developed through the use of extension-twist coupling as implemented in the XV-15 tilt rotor aircraft. Twist control is achieved by assuming a 15 percent change in operating rpm between hover and forward flight regimes.

The coupling of deformation modes provides a flexibility to meet design requirements on the aeroelastic behavior, dynamic response and stability of structures and results in improved fatigue life and durability.

A prerequisite for the implementation of an elastically tailored concept, is the development of an analytical model which accurately predicts the various stiffness components and isolate the material and geometrical parameters controlling the behavior.

In the second part, a variationally and asymptotically consistent theory for thin-walled beams that incorporates the anisotropy associated with laminated composites is developed. The theory is based on an asymptotical analysis of 2D shell energy.

The major advantage of this approach lies in the fact that the displacement function is not assumed a priori and is determined as a result of the minimization of the energy functional. As a result, two nonclassical contributions to the warping emerge. While these new contributions vanish for isotropic and orthotropic materials, they have a significant influence on the response of generally anisotropic materials. The accuracy of previously developed theories is assessed by comparing the resulting displacement fields and an assessment of the significance of shear deformation is presented. Comparison of predictions with finite element simulation and test results illustrate the consistency and accuracy of the developed theory.

The delamination analysis model is presented in the first part of this work. This is followed by the development of the thin-walled anisotropic beam theory. Each part includes a literature survey in order to place the present work in proper perspective. A comparison of prediction is presented in order to validate the developed theories and assess their accuracy.

CHAPTER II

DELAMINATION ANALYSIS

This chapter addresses damage modeling in laminated composite plates. A review of previous work is presented first, this is followed by a development of the analytical model.

2.1 Review of Previous Work

Failure in laminated composite materials often initiates in the form of matrix fractures, namely, transverse matrix cracks and delaminations. Based on the location and direction of growth, two distinct types of delamination can be discerned. These two types are called edge delamination and local or transverse crack tip delamination, as shown in Fig. 2.1. Edge delaminations initiate at the load free edges of the laminate whereas local delaminations start from a transverse matrix crack. Transverse matrix cracks refer to intralaminar failures whereas delaminations refer to interlaminar failures. Transverse cracks usually occur within laminates where the fibers run at an angle to the primary load direction and hence the name. In many cases, both types occur concurrently with varying levels of interaction.

It has been observed [1] in simple tension tests of uniform rectangular cross section specimen (Edge Delamination tests) that delaminations initiate along the load free edges and propagate normal to the load direction as shown in Fig. 2.1. Transverse matrix cracks running parallel to the fibers have also been observed in off-axis and 90° plies. Such transverse cracks extend through the thickness of similarly oriented

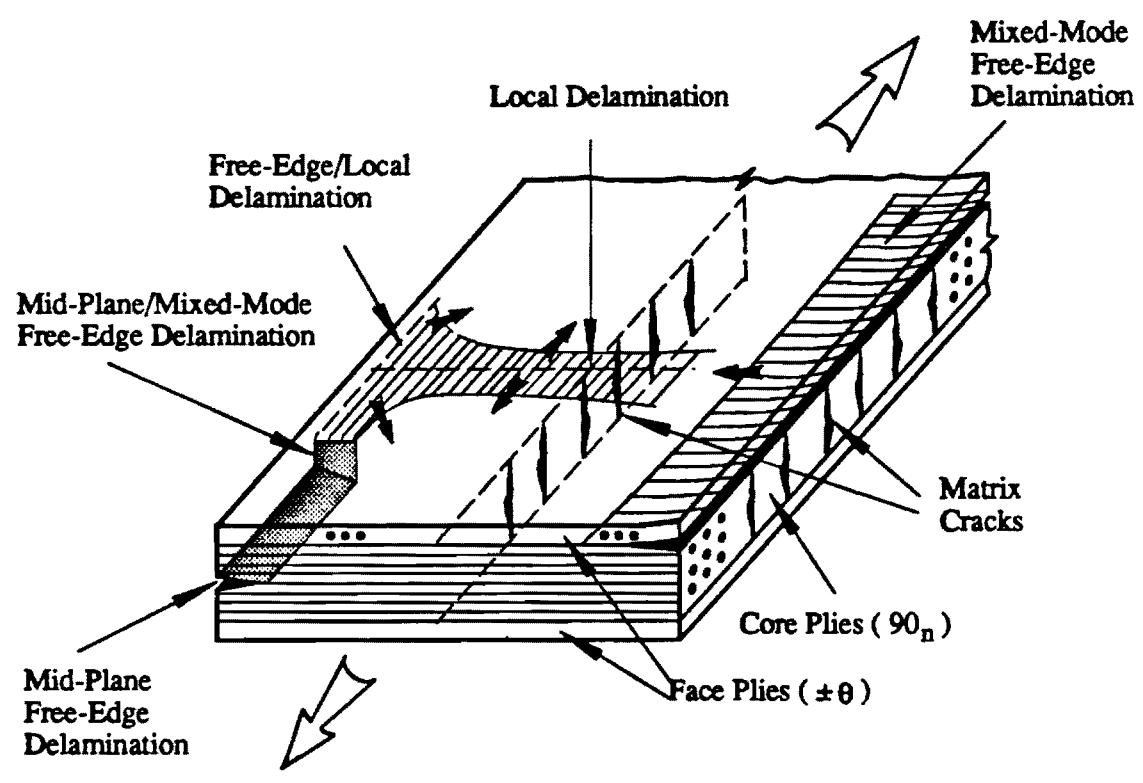


Figure 2.1: Damage Modes

plies and terminate where the ply orientation changes. Delaminations can also originate at the interfaces where transverse cracks terminate. These transverse crack tip delaminations or local delaminations, grow normal to the transverse crack from which they originate. In the case of 90° plies, the growth direction is parallel to the load.

The growth process of edge delaminations and local delaminations is often modeled using a fracture mechanics approach leading to the calculation of a strain energy release rate. This is because the strain energy release rate can correlate delamination behavior from different loading conditions and can account for geometric dependencies. The strain energy release rate associated with a particular growth configuration is a measure of the driving force behind that failure mode. In combination with appropriate failure criteria, the strain energy release rate provides a means of predicting the failure loads of the structure.

Several methods are available in the literature for analyzing edge delaminations. These include finite element modeling as in [2], [3], and [4], the complex variable stress potential approach [5], a simple technique based on classical laminate theory [1] and a higher order laminate theory including shear deformations [6]. Finite element models provide accurate solutions but involve intensive computational effort. Classical laminate theory (CLT) provides simple closed form solutions and is thus well suited for preliminary design evaluation. However, CLT provides only the total energy release rate, and thus, in a mixed mode situation, there is insufficient information to completely assess the delamination growth tendency. A higher order laminate theory including shear deformations has the ability to provide the individual contributions of the three fracture modes while retaining the simplicity of a closed form solution. A shear deformation model is available for off-mid-plane edge delamination and has been shown to agree well with finite element predictions [7].

Crossman and Wang [8] have tested T300/934 graphite/epoxy $\{\pm 25/90_n\}$, speci-

mens in simple tension and reported a range of behavior including transverse cracking, edge delamination and local delamination. O'Brien [9] has presented classical laminate theory solutions for these specimens, demonstrating reasonable agreement in the case of edge delamination but with some discrepancies in the local delamination predictions. The local delamination model overestimates the failure strains for $[\pm 25/90_n]_s$ specimens for small values of n mainly due to the implicit critical strain energy matching used.

A finite element model combining edge and local delaminations has been proposed by Law [10]. His predictions, however, do not fully explain the dependency of the critical strain on the number of 90° plies. A similar three-dimensional finite element analysis including hygrothermal effects has been performed by Wang *et al.* [11] to determine the delamination onset load for combined delamination, qualitatively demonstrating stable crack growth.

A three-dimensional finite element analysis of delamination from matrix cracks has been developed by Fish and O'Brien[12]. They conducted an experimental and analytical study on the influence of matrix cracking on delamination in $[+15/-90_n/-15]_s$ glass-epoxy laminates subjected to monotonically increasing tension loads. Experimental results showed that local delaminations form at the intersection of matrix cracks in the $+15^\circ$ plies and the free-edge. Comparison of a Quasi-three-dimensional (Q3D) finite element results with a three-dimensional (3D) finite element analysis showed significant differences in the relative and absolute magnitudes of the interlaminar stress components. Thus, discrepancies in failure predictions may exist between Q3D and 3D analysis. The results of this study emphasized the importance of incorporating the various damage mechanisms that influence subsequent damage development in the failure analysis.

Thermal and moisture effects on the strain energy release rates for interlaminar

fracture of unidirectional graphite/epoxy have been investigated by Russell and Street [13]. This investigation also included a study of the effects of shear loading through the use of various test configurations (Double Cantilever Beam, Cracked Lap Shear etc.). Initiation energies for delamination were found to increase as the proportion of shear loading increased and as the temperature was lowered, but no significant moisture influence was observed. The fracture resistance to crack extension was found to increase under tensile dominated loadings with both temperature and moisture content, but for high shear loading, the resistance was insensitive to the hygrothermal conditions.

O'Brien, Raju and Garber have presented a CLT based analysis of mixed mode edge delamination specimens including hygrothermal effects [14]. They have used finite element modeling to determine the strain energy release rate components. Their results indicate total strain energy release rate increases of as much as 170% due to thermal effects for some T300/5208 graphite/epoxy laminates. However, a moisture content of 0.75% has been shown to totally alleviate this increase. According to this analysis, in general, the consideration of thermal effects increases the energy release rate whereas moisture effects have the opposite influence. These results have been confirmed using shear deformation models in the case of off-mid-plane edge delaminations [15]. It was found that the interlaminar stresses follow the same trend as the energy release rate, with increase due to thermal effects and alleviation due to hygroscopic effects.

Aoki and Kondo calculated the strain energy release rate under thermal loading for mixed mode edge delamination. They used conventional finite element method [16] and a simplified method [16, 17] based on the classical lamination theory in combination with the J-integral for mechanical loading. Two types of axial constraint conditions were considered : (1) constant strain or fixed-grip and (2) constant load.

Numerical examples for cross-ply and angle-ply laminates showed that in angle-ply laminate, the energy release rate under free axial elongation increased constantly with delamination growth, while it remained constant under fixed-grip conditions. A higher order plate theory including transverse normal strain and thermal effects has been developed by Whitney [18] for the analysis of mid-plane edge delaminations. This approach provides the interlaminar stresses also, in addition to the strain energy release rate. A $[0_3/90_3]_s$ graphite/epoxy mode I specimen was analyzed and the maximum interlaminar normal stress was shown to increase by a factor of 2.7 due to thermal effects, when compared with the pure mechanical strain reference configuration.

From this summary it is found that there is a need for a unified approach that includes the analysis of free edge as well as local delamination and their interaction. In practical composite configuration free edge delamination does not occur in isolation, it is accompanied by other damage modes. Developing an analysis methodology that includes the interaction of delamination with other damage modes is essential for designing damage tolerant structures.

The study of delamination consists of two main sections. These are the analysis of mid-plane edge delamination and local delamination in laminated composite plates.

2.2 Mid-Plane Edge Delamination

A mid-plane edge delamination specimen is shown in Fig. 2.2. A uniform axial strain ϵ is applied in the x direction. From symmetry only one quarter of the specimen is considered. The sublaminates scheme and the choice of coordinate axes are illustrated in Fig. 2.3.

Sublaminates 1 and 2 in Fig. 2.3 represent the uncracked and the cracked regions,

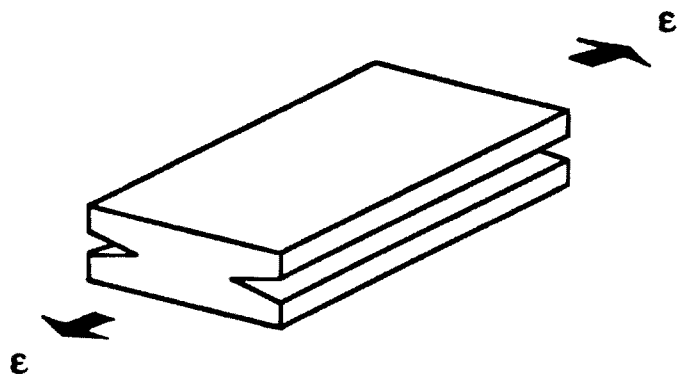


Figure 2.2: Mid-Plane Edge Delamination

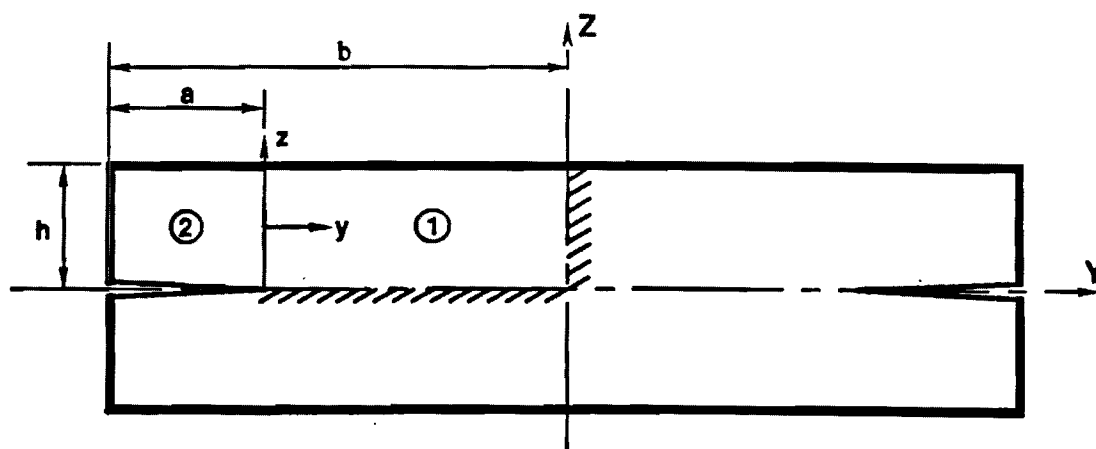


Figure 2.3: Sublaminates Modeling Scheme (Mid-Plane Edge Delamination)

respectively. The analysis is based on the following displacement fields within each sublaminar

$$\begin{aligned} u &= x\varepsilon + U(y) + z\beta_x(y) \\ v &= V(y) + z\beta_y(y) \\ w &= W(y) \end{aligned} \quad (2.1)$$

where u , v , and w denote the displacements relative to the x , y , and z axes, respectively. Shear deformation is recognized through the rotations β_x and β_y . In the present formulation thickness strain is neglected, and consequently inaccurate values of interlaminar peel stress, σ_{zz} , are expected. However, the peel stress can be modified by enforcing the free edge boundary condition associated with the transverse shear stress resultant.

A generic sublaminar along with the applied forces and moments is shown in Fig. 2.4. The force and moment resultants are denoted by N_i , Q_i , and M_i , respectively. The constitutive relationships in terms of these force and moment resultants can be written as

$$\begin{aligned} N_i &= A_{ij}\varepsilon_j + B_{ik}\kappa_k - N_i^{nm} & (i, j, k = 1, 2, 6) \\ M_i &= B_{ij}\varepsilon_j + D_{ik}\kappa_k - M_i^{nm} & (i, j, k = 1, 2, 6) \\ Q_i &= A_{ij}\varepsilon_j & (i, j = 4, 5) \end{aligned} \quad (2.2)$$

The subscripts x, y, z, yz, xz , and xy are replaced by the subscripts 1-6, respectively. The non-mechanical forces and moments resulting from hygrothermal effects are labeled with superscript nm for non-mechanical. They are defined as

$$(N_i^{nm}, M_i^{nm}) = \int_{-\frac{h}{2}}^{+\frac{h}{2}} \{ \Delta T \bar{\alpha}_j + \Delta H \bar{\beta}_j \} \bar{Q}_{ij}(1, z) dz \quad (2.3)$$

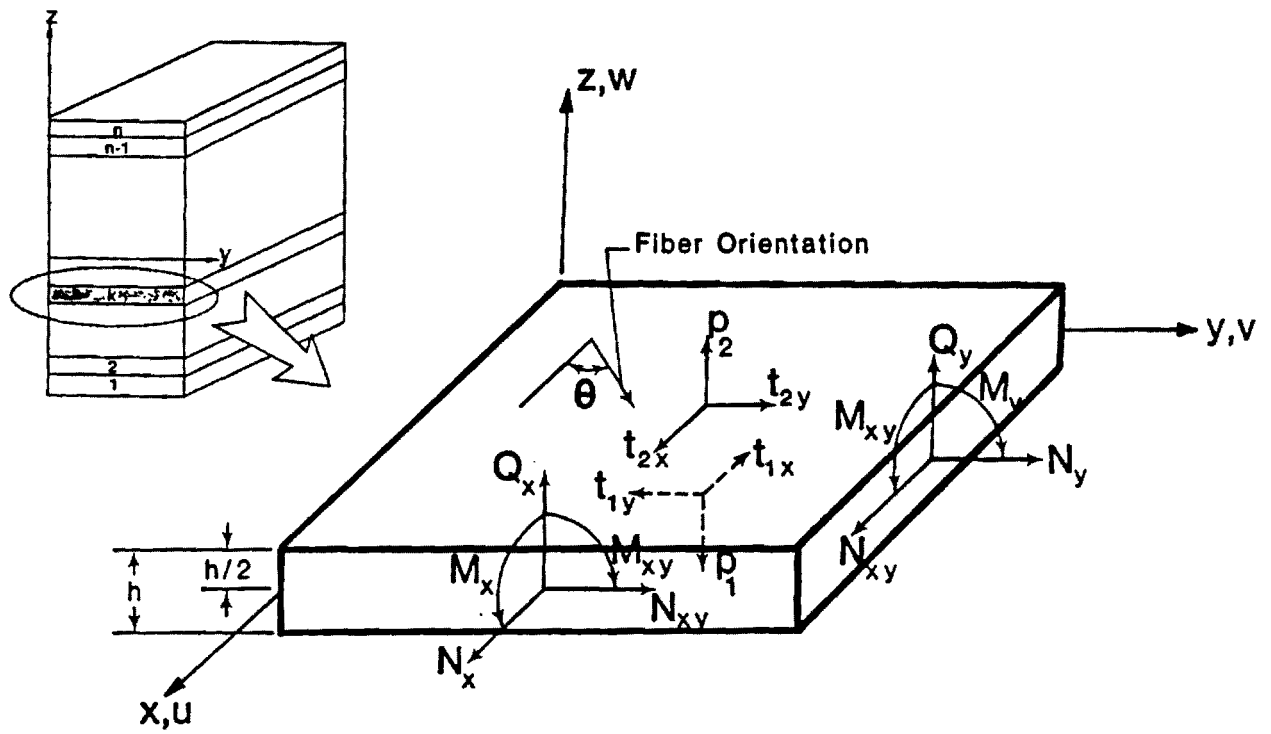


Figure 2.4: Notation and Sign Convention for a Generic Sublaminate

The thermal coefficient is denoted by $\bar{\alpha}_j$ in Eq. (2.3), while the swelling coefficient by $\bar{\beta}_j$. The \bar{Q}_{ij} are the plane stress sublaminar reduced stiffnesses [19]. The bars on α_j, β_j and Q_{ij} indicate that these quantities are to be obtained through appropriate coordinate transformations. The change in temperature between the ambient and the stress free temperature is denoted by ΔT . The percentage moisture weight gain is represented by ΔH .

For a sublaminar of thickness h , the elastic stiffnesses A_{ij}, B_{ij} , and D_{ij} in Eqs. (2.2) are defined as

$$(A_{ij}, B_{ij}, D_{ij}) = \int_{-\frac{h}{2}}^{+\frac{h}{2}} \bar{Q}_{ij}(1, z, z^2) dz \quad (2.4)$$

The equilibrium equations can be written as follows

$$\begin{aligned} N_{x,y,y} + t_{2x} - t_{1x} &= 0 \\ N_{y,y} + t_{2y} - t_{1y} &= 0 \\ Q_{y,y} + p_2 - p_1 &= 0 \\ M_{x,y,y} - Q_x + \frac{h}{2}(t_{2x} + t_{1x}) &= 0 \\ M_{y,y} - Q_y + \frac{h}{2}(t_{2y} + t_{1y}) &= 0 \end{aligned} \quad (2.5)$$

where t_{2x}, t_{2y}, p_2 and t_{1x}, t_{1y}, p_1 denote the interlaminar stress components at the sublaminar upper and lower surfaces, respectively. These stress components appear in Fig. 2.4. Partial differentiation is denoted by a comma in Eqs. (2.5). Application of the boundary conditions and the governing equations to each of the sublaminates results in a system of differential equations which are solved to obtain the stresses and strain energy release rate. The boundary conditions to be prescribed at constant values of y , the sublaminar sections, are N_{xy} or U, N_y or V, Q_y or W, M_y or β_y and M_{xy} or β_x .

2.2.1 Uncracked Region (Sublaminates 1)

From symmetry conditions at the sublaminates bottom surface, both w and the shearing stresses are zero. Since thickness strain is neglected, this leads to w being zero everywhere in this sublaminates. The equilibrium equations can be written as

$$\begin{aligned}
 N_{x_{y_1},y} &= 0 \\
 N_{y_1,y} &= 0 \\
 Q_{y_1,y} - p_1 &= 0 \\
 M_{x_{y_1},y} - Q_{x_1} &= 0 \\
 M_{y_1,y} - Q_{y_1} &= 0
 \end{aligned} \tag{2.6}$$

where subscript 1 refers to sublaminates 1. From Eqs. (2.6) and the continuity of axial and in-plane shear stress resultants between sublaminates 1 and 2, we get

$$N_{y_1} = N_{x_{y_1}} = 0 \tag{2.7}$$

By substituting from the constitutive relations into Eqs (2.6) and Eq. (2.7), and assuming an exponential form for the rotations β_{1y} and β_{1x} . we get the following characteristic equation

$$E_4 s^4 - E_2 s^2 + E_0 = 0 \tag{2.8}$$

with

$$\begin{aligned}
 E_0 &= A_{44}A_{55} - (A_{45})^2 \\
 E_2 &= \Omega_{21}A_{55} + \Omega_{32}A_{44} - \Omega_{22}A_{45} - \Omega_{31}A_{45} \\
 E_4 &= \Omega_{21}\Omega_{32} - \Omega_{22}\Omega_{31}
 \end{aligned}$$

where

$$[\Omega]_{3 \times 2} = \begin{bmatrix} (A_{12}\xi_{12} + A_{16}\xi_{22} + B_{12}) & (A_{12}\xi_{13} + A_{16}\xi_{23} + B_{16}) \\ (B_{22}\xi_{12} + B_{26}\xi_{22} + D_{22}) & (B_{22}\xi_{13} + B_{26}\xi_{23} + D_{26}) \\ (B_{26}\xi_{12} + B_{66}\xi_{22} + D_{26}) & (B_{26}\xi_{13} + B_{66}\xi_{23} + D_{66}) \end{bmatrix}$$

and

$$[\xi]_{2 \times 3} = - \begin{bmatrix} A_{22} & A_{26} \\ A_{26} & A_{66} \end{bmatrix}^{-1} \begin{bmatrix} A_{12} & B_{22} & B_{26} \\ A_{16} & B_{26} & B_{66} \end{bmatrix}$$

Coefficient E_0 depends solely on the sublaminar axial stiffness, while E_4 is predominantly influenced by the bending and coupling coefficients D_{ij} and B_{ij} . The numerical value of E_4 can be orders of magnitude smaller than E_2 and E_0 . This results in the presence of a boundary zone in the response. For the material and laminate layups considered, the roots of this characteristic equation are real. Only the negative roots of Eq. (2.8) are considered as they give solutions decaying exponentially from the delamination tip. The solution can be written as

$$\begin{Bmatrix} \beta_{1y} \\ \beta_{1x} \end{Bmatrix} = \begin{Bmatrix} 1 \\ \eta_j \end{Bmatrix} I_j e^{-\eta_j y} \quad (0 \leq y \leq b - a) \quad (2.9)$$

where

$$\eta_j = - \frac{\Omega_{21} s_j^2 - A_{44}}{\Omega_{22} s_j^2 - A_{45}} \quad (j = 1, 2)$$

Parameters I_j are arbitrary constants to be determined from the boundary conditions. By substituting Eq. (2.7) into the constitutive relations and using the assumed displacement fields, we obtain

$$\begin{Bmatrix} V_{1,y} \\ U_{1,y} \end{Bmatrix} = \begin{bmatrix} \xi_{11} \\ \xi_{21} \end{bmatrix} \{\varepsilon\} + \begin{Bmatrix} S_1 \\ S_2 \end{Bmatrix}^{nm} + \begin{bmatrix} \xi_{12} & \xi_{13} \\ \xi_{22} & \xi_{23} \end{bmatrix} \begin{Bmatrix} \beta_{1y,y} \\ \beta_{1x,y} \end{Bmatrix} \quad (2.10)$$

where

$$\begin{Bmatrix} S_1 \\ S_2 \end{Bmatrix}^{nm} = \begin{bmatrix} A_{22} & A_{26} \\ A_{26} & A_{66} \end{bmatrix}^{-1} \begin{Bmatrix} N_y \\ N_{xy} \end{Bmatrix}^{nm}$$

Substitute from Eqs. (2.10) into the constitutive relations to get the resultant forces and moments in terms of the total extensional strain

$$\begin{Bmatrix} N_{x1} \\ M_{y1} \\ M_{xy1} \end{Bmatrix} = \begin{bmatrix} A_{11} + A_{12}\xi_{11} + A_{16}\xi_{21} \\ B_{12} + B_{22}\xi_{11} + B_{26}\xi_{21} \\ B_{16} + B_{26}\xi_{11} + B_{66}\xi_{21} \end{bmatrix} \{\varepsilon\}$$

$$+ \begin{bmatrix} A_{12}S_1^{nm} + A_{16}S_2^{nm} - N_x^{nm} \\ B_{22}S_1^{nm} + B_{26}S_2^{nm} - M_y^{nm} \\ B_{26}S_1^{nm} + B_{66}S_2^{nm} - M_{xy}^{nm} \end{bmatrix} + [\Omega]_{3 \times 2} \begin{Bmatrix} \beta_{1y,y} \\ \beta_{1x,y} \end{Bmatrix} \quad (2.11)$$

2.2.2 Cracked Region (Sublaminates 2)

From the stress free boundary conditions at the face $y = -a$ of sublaminates 2 and the equilibrium equations, we get

$$N_{y_2} = N_{xy_2} = Q_{y_2} = M_{y_2} = 0$$

The equilibrium equations reduce to

$$M_{xy_2,y} - Q_{x_2} = 0$$

Following a similar procedure as in sublaminates 1, the rotation can be written as

$$\beta_{2x} = H_1 e^{\lambda y} \quad (-a \leq y \leq 0) \quad (2.12)$$

with

$$\lambda = \sqrt{\frac{A_{44}A_{55} - A_{45}^2}{A_{44}(D_{66} + B_{26}\varphi_{12} + B_{66}\varphi_{22} + D_{26}\varphi_{32})}}$$

where

$$[\varphi]_{3 \times 2} = -[\psi]^{-1} \begin{bmatrix} A_{12} & B_{26} \\ A_{16} & B_{66} \\ B_{12} & D_{26} \end{bmatrix}$$

and

$$[\psi] = \begin{bmatrix} A_{22} & A_{26} & B_{22} \\ A_{26} & A_{66} & B_{26} \\ B_{22} & B_{26} & D_{22} \end{bmatrix}$$

H_1 is an arbitrary constant to be determined from the continuity conditions between sublaminates 1 and 2. The force and moment resultants can be expressed in

terms of the total strain

$$\begin{aligned} \begin{Bmatrix} N_x \\ M_{xy} \end{Bmatrix} &= \begin{bmatrix} A_{11} + A_{12}\varphi_{11} + A_{16}\varphi_{21} + B_{12}\varphi_{31} \\ B_{16} + B_{26}\varphi_{11} + B_{66}\varphi_{21} + D_{26}\varphi_{31} \end{bmatrix} \{\varepsilon\} \\ &+ \begin{bmatrix} A_{12}F_1^{nm} + A_{16}F_2^{nm} + B_{12}F_3^{nm} - N_x^{nm} \\ B_{26}F_1^{nm} + B_{66}F_2^{nm} + D_{26}F_3^{nm} - M_{xy}^{nm} \end{bmatrix} \\ &+ \begin{bmatrix} B_{16} + A_{12}\varphi_{12} + A_{16}\varphi_{22} + B_{12}\varphi_{32} \\ D_{66} + B_{26}\varphi_{12} + B_{66}\varphi_{22} + D_{26}\varphi_{32} \end{bmatrix} \lambda H_1 \varepsilon^{\lambda y} \end{aligned} \quad (2.13)$$

where

$$\begin{Bmatrix} F_1 \\ F_2 \\ F_3 \end{Bmatrix}^{nm} = [\psi]^{-1} \begin{Bmatrix} N_y \\ N_{xy} \\ M_y \end{Bmatrix}^{nm}$$

The response associated with sublaminates 1 and 2 shown in Fig. 2.3 is coupled through the following conditions at $y = 0$,

$$M_{y_1}(0) = M_{y_2}(0) = 0$$

$$M_{xy_1}(0) = M_{xy_2}(0) = 0$$

$$\beta_{1x}(0) = \beta_{2x}(0)$$

The solution for both sublaminates i.e., the values of I_j and H_1 can be obtained by applying these conditions. The final expressions for the sublaminate rotations is given by Eqs. (2.9) and Eq. (2.12) where

$$I_1 = \frac{\left\{ -\Theta_1 + (\Theta_4 + \Theta_5\eta_2)\left(\frac{\Lambda_1}{\Lambda_4}\right) \right\} \varepsilon + \Theta_5\eta_2\left(\frac{\Lambda_2}{\Lambda_4}\right) - \Theta_2 + \Theta_4\left(\frac{\Lambda_2}{\Lambda_4}\right)}{\Theta_3 - (\Theta_4 + \Theta_5\eta_2)\frac{\Lambda_3}{\Lambda_4} + \Theta_5\eta_1}$$

$$I_2 = -\frac{1}{\Lambda_4}(\Lambda_1\varepsilon + \Lambda_2 + \Lambda_3I_1)$$

$$H_1 = \eta_1I_1 + \eta_2I_2$$

with

$$\Lambda_1 = B_{12} + B_{22}\zeta_{11} + B_{26}\zeta_{21}$$

$$\Lambda_2 = B_{22}S_1^{nm} + B_{26}S_2^{nm} - M_y^{nm}$$

$$\Lambda_3 = -(\Omega_{21} + \eta_1 \Omega_{22})s_1$$

$$\Lambda_4 = -(\Omega_{21} + \eta_2 \Omega_{22})s_2$$

and

$$\Theta_1 = B_{26}(\xi_{11} - \varphi_{11}) + B_{66}(\xi_{21} - \varphi_{21}) - D_{26}\varphi_{31}$$

$$\Theta_2 = B_{26}(S_1^{nm} - F_1^{nm}) + B_{66}(S_2^{nm} - F_2^{nm}) - D_{26}F_3^{nm}$$

$$\Theta_3 = -(\Omega_{31} + \eta_1 \Omega_{32})s_1$$

$$\Theta_4 = -(\Omega_{31} + \eta_2 \Omega_{32})s_2$$

$$\Theta_5 = -(D_{66} + B_{26}\varphi_{12} + B_{66}\varphi_{22} + D_{26}\varphi_{32})\lambda$$

The total strain energy release rate can be calculated by considering the work done by the external forces. This is given by

$$G_T = G_I = -\frac{2}{L} \sum_{i=1}^2 \frac{dW_i}{da} \quad (2.14)$$

where W_i = work done by the external force in sublaminates i , L = laminate length, and a = crack length.

The work done by the external forces is written in terms of the mechanical strain, ε_i^m , as

$$W_i = \frac{L}{2} \int_{y_i} \varepsilon_i^m N_{x_i} dy \quad (2.15)$$

with

$$\varepsilon_i^m = \varepsilon - \varepsilon_i^{nm} \quad (2.16)$$

The sublaminates free expansion strains, ε_i^{nm} , are calculated by setting the axial force resultant to zero, i.e.

$$\int_{y_i} N_{x_i} dy = 0 \quad (2.17)$$

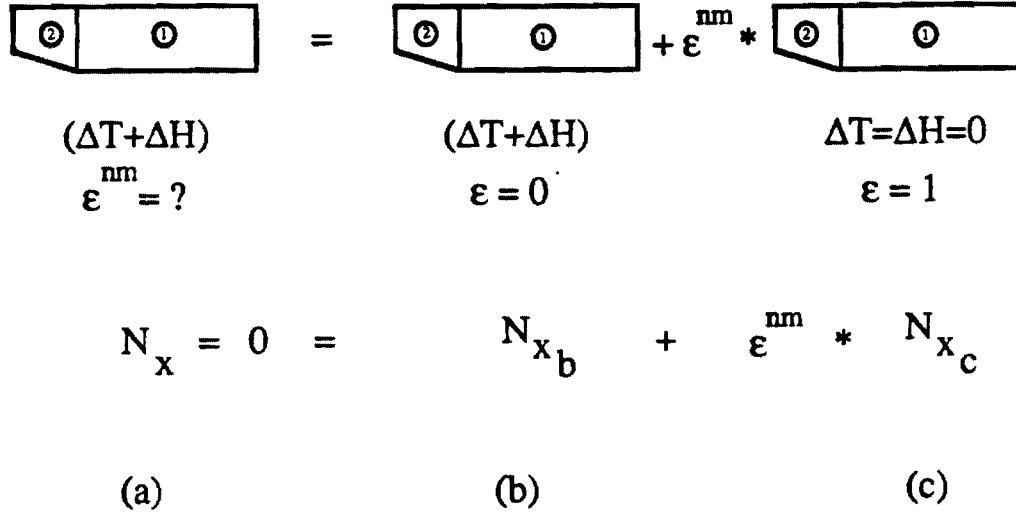


Figure 2.5: Effective non-mechanical free expansion strain across the entire width of the laminate

where N_x is given in Eq. (2.11) and Eq. (2.13). The expression for each sublaminates is

$$\begin{aligned}
 \epsilon_1^{nm} &= -\frac{A_{12}S_1^{nm} + A_{16}S_2^{nm} - N_x^{nm}}{A_{11} + A_{12}\xi_{11} + A_{16}\xi_{21}} \\
 \epsilon_2^{nm} &= -\frac{A_{12}F_1^{nm} + A_{16}F_2^{nm} + B_{12}F_3^{nm} - N_x^{nm}}{A_{11} + A_{12}\varphi_{11} + A_{16}\varphi_{21} + B_{12}\varphi_{31}}
 \end{aligned} \quad (2.18)$$

The total strain, ϵ , is given by

$$\epsilon = \epsilon^m + \epsilon^{nm} \quad (2.19)$$

where ϵ^m is the effective mechanical strain and ϵ^{nm} is the effective free-expansional strain across the entire width of the laminate estimated by decomposing the non-mechanical problem in Fig. 2.5(a) into the superposition of the two cases shown in Fig. 2.5(b) and Fig. 2.5(c). In case (b) the laminate is subjected to a non-mechanical change ($\Delta T + \Delta H$), while the strain is prescribed to be zero. In case (c) a unit axial strain is applied, while no hygrothermal change is considered. Knowing that no axial

force is applied in the main problem, i.e. Fig. 2.5(a), the sum of the axial forces in the two subproblems should be zero, hence

$$N_{x_b} + \epsilon^{nm} N_{x_c} = 0 \quad (2.20)$$

and

$$\epsilon^{nm} = -\frac{N_{x_b}}{N_{x_c}} \quad (2.21)$$

where N_{x_b} and N_{x_c} are the axial forces in case (b) and case (c), respectively. These axial forces are computed by substituting the expressions of N_{x_1} and N_{x_2} from Eq. (2.11) and Eq. (2.13) into the relations

$$\begin{aligned} N_{x_b} &= \left[\int_0^{(b-a)} N_{x_1} dy + \int_{-a}^0 N_{x_2} dy \right]_{\epsilon=0, (\Delta T + \Delta H)} \\ N_{x_c} &= \left[\int_0^{(b-a)} N_{x_1} dy + \int_{-a}^0 N_{x_2} dy \right]_{\epsilon=1, \Delta T = \Delta H = 0} \end{aligned} \quad (2.22)$$

The expressions for N_{x_b} and N_{x_c} are found to be

$$\begin{aligned} N_{x_b} &= (A_{12}S_1^{nm} + A_{16}S_2^{nm} - N_x^{nm})(b-a) \\ &\quad + (A_{12}F_1^{nm} + A_{16}F_2^{nm} + B_{12}F_3^{nm} - N_x^{nm})a \end{aligned} \quad (2.23)$$

and

$$\begin{aligned} N_{x_c} &= (A_{11} + A_{12}\xi_{11} + A_{16}\xi_{21})(b-a) \\ &\quad + (A_{11} + A_{12}\varphi_{11} + A_{16}\varphi_{21} + B_{12}\varphi_{31})a \end{aligned} \quad (2.24)$$

The crack length and half of the total laminate width are denoted by a and b , respectively, as shown in Fig. 2.3.

By combining the expressions of N_{x_i} from Eqs. (2.11) and Eqs. (2.13) with Eqs. (2.14)-(2.24), the total energy release rate for the Mode I case can be written in the form

$$G_I = (G_{IL}) + (G_{IL_o}) + (G_{IR} + G_{IR_o}) \quad (2.25)$$

where

$$\begin{aligned}
G_{IL} &= (\varepsilon - \varepsilon_1^{nm}) [(A_{11} + A_{12}\xi_{11} + A_{16}\xi_{21})\varepsilon + (A_{12}S_1^{nm} + A_{16}S_2^{nm} - N_x^{nm})] \\
&\quad - (\varepsilon - \varepsilon_2^{nm}) [(A_{11} + A_{12}\varphi_{11} + A_{16}\varphi_{21} + B_{12}\varphi_{31})\varepsilon \\
&\quad\quad + (A_{12}F_1^{nm} + A_{16}F_2^{nm} + B_{12}F_3^{nm} - N_x^{nm})] \\
G_{IL_a} &= -\frac{d\varepsilon}{da}(b-a) \{ (A_{11} + A_{12}\xi_{11} + A_{16}\xi_{21}) [(2\varepsilon - \varepsilon_1^{nm}) \\
&\quad\quad + (A_{12}S_1^{nm} + A_{16}S_2^{nm} - N_x^{nm})] \} \\
&\quad - \frac{d\varepsilon}{da}a \{ (A_{11} + A_{12}\varphi_{11} + A_{16}\varphi_{21} + B_{12}\varphi_{31}) (2\varepsilon - \varepsilon_2^{nm}) \\
&\quad\quad + (A_{12}F_1^{nm} + A_{16}F_2^{nm} + B_{12}F_3^{nm} - N_x^{nm}) \} \\
G_{IR} &= -(\varepsilon - \varepsilon_1^{nm}) [(\Omega_{11} + \eta_1\Omega_{12}) I_1 s_1 e^{-s_1(b-a)} + (\Omega_{11} + \eta_2\Omega_{12}) I_2 s_2 e^{-s_2(b-a)}] \\
&\quad - (\varepsilon - \varepsilon_2^{nm}) (B_{16} + A_{12}\varphi_{12} + A_{16}\varphi_{22} + B_{12}\varphi_{32}) H_1 \lambda e^{-\lambda a} \\
G_{IR_a} &= -\frac{d\varepsilon}{da} \{ (\Omega_{11} + \eta_1\Omega_{12}) I_1 [\varepsilon^{-s_1(b-a)} - 1] + (\Omega_{11} + \eta_2\Omega_{12}) I_2 [\varepsilon^{-s_2(b-a)} - 1] \\
&\quad + (B_{16} + A_{12}\varphi_{12} + A_{16}\varphi_{22} + B_{12}\varphi_{32}) H_1 (1 - e^{-\lambda a}) \}
\end{aligned}$$

and

$$\begin{aligned}
\frac{d\varepsilon}{da} &= \frac{d\varepsilon^{nm}}{da} = \frac{A_{12}(S_1^{nm} - F_2^{nm}) + A_{16}(S_2^{nm} - F_2^{nm}) - B_{12}F_3^{nm}}{N_{x_c}} \\
&\quad - \frac{N_{x_b} [A_{12}(\xi_{11} - \varphi_{11}) + A_{16}(\xi_{21} - \varphi_{21}) - B_{12}\varphi_{31}]}{N_{x_c}^2} \quad (2.26)
\end{aligned}$$

The resulting expression for the total energy release rate G_I is composed of three terms. The first term, denoted by G_{IL} is independent of the delamination length while the second, G_{IL_a} , is a linear function of the crack length. The third term denoted by $(G_{IR} + G_{IR_a})$, is an exponentially decaying function of the delamination length.

In computing the non-mechanical strains, the laminate is assumed to be held at the prescribed temperature and moisture levels. This is followed by testing under

fixed-grip condition, i.e., the constant strain measured in the lab is the mechanical strain ϵ^m . In Refs.[18] and [20], Whitney considered the strain measured in the tests to be the total strain, i.e. $\epsilon = \epsilon^m + \epsilon^{nm} = \text{constant}$. The difference between the two interpretations is detected by the terms G_{IL} and G_{IR} in Eq. (2.25). These two terms are neglected in Refs. [18] and [20] since the total strain ϵ is assumed to be constant.

As mentioned previously, neglecting the thickness strain leads to inaccurate estimates for the peel stress. The peel stress is given by

$$p = Q_{y_1, y} = -(A_{44} + A_{45}\eta_j)I_j s_j \epsilon^{-s_j y} \quad (j = 1, 2) \quad (2.27)$$

The equilibrium of transverse force requires that

$$\int_0^{(b-a)} p dy = 0 \quad (2.28)$$

or from the equilibrium equations (2.6)

$$Q_{y_1}|_{y_1=(b-a)} - Q_{y_1}|_{y_1=0} = 0$$

While for all practical purpose the resultant shear stress $Q_{y_1}|_{y_1=(b-a)}$ vanishes due to the free edge, the resultant shear stress at the delamination front $Q_{y_1}|_{y_1=0} \neq 0$. That is in order for the peel stress to satisfy transverse force equilibrium, the shear force boundary condition at the sublaminde end should be enforced. This is done by adding to the peel stress distribution an appropriate boundary function expressed in terms of the characteristics roots as

$$a_1 e^{-s_1 y} + a_2 e^{-s_2 y}$$

The coefficients a_1 and a_2 are obtained by enforcing equilibrium of transverse force given in Eq. (2.28) and moment given by

$$\int_0^{(b-a)} p y dy + M_{y_1}|_{y_1=(b-a)} = 0$$

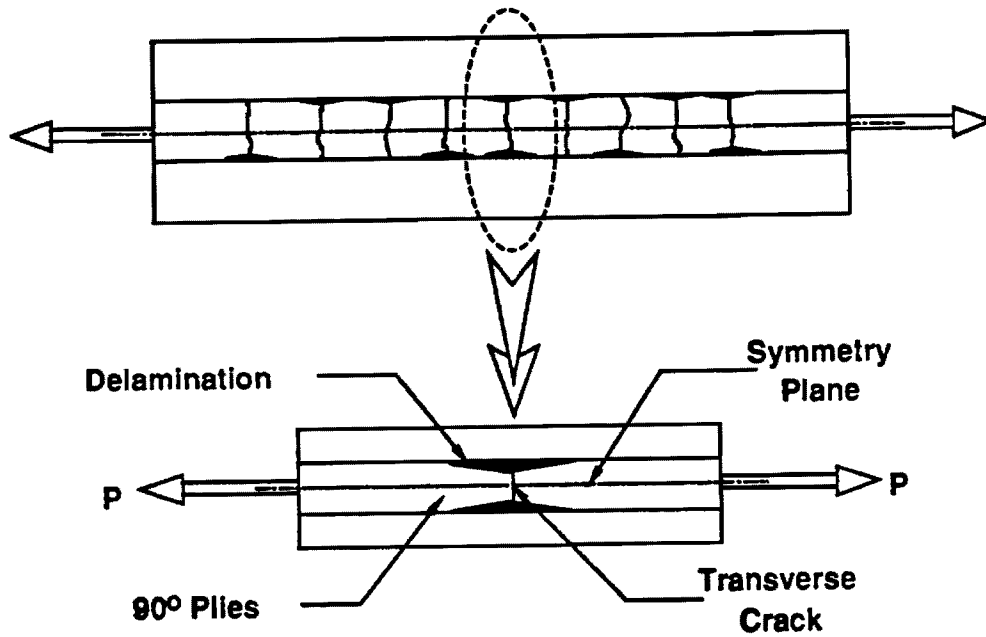


Figure 2.6: Local Delamination Specimen Cross Section

The corrected peel stress distribution is

$$p = \frac{s_1 s_2}{s_1 - s_2} M_{y_1} |_{y_1=(b-a)} [s_1 e^{-s_1 y} - s_2 e^{-s_2 y}]$$

2.3 Local Delamination

A longitudinal section illustrating the geometry of a generic configuration is shown in Fig. 2.6. The central region is assumed to be made of 90° plies with an isolated transverse crack in the middle. Delaminations are assumed to grow from both ends of the transverse crack, and towards both specimen ends as shown. From symmetry considerations, only one quarter of the configuration is modeled. The modeled portion of length L is divided into four sublaminates as shown in Fig. 2.7. The crack length is denoted by a . The top surface (sublaminates 1 and 4) is stress free. In order to

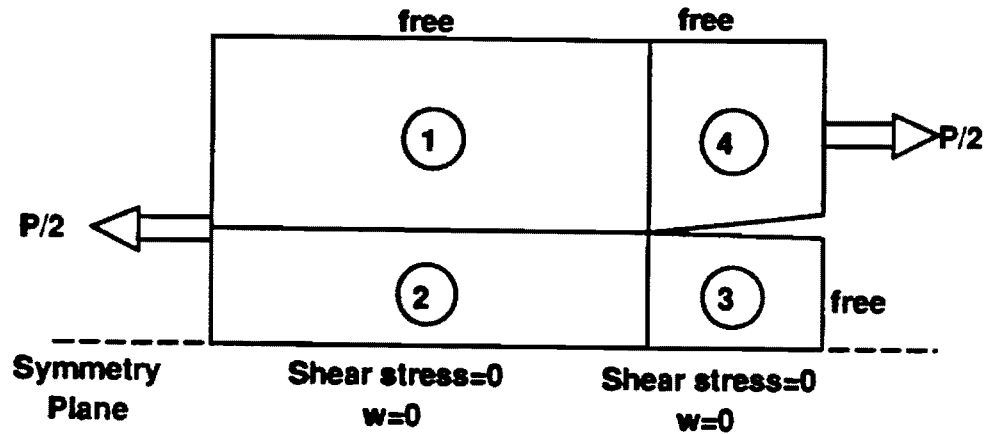


Figure 2.7: Sublaminated Scheme for Local Delamination

simplify the analysis, the thickness strain ϵ_z is neglected. The consequence of this, combined with the fact that the transverse displacement w is zero along the center line, is that w is zero in sublaminates 1, 2, and 3. Also, this approximation does not allow for the enforcement of boundary conditions on the shear stress resultants, leading to incorrect estimates of the interlaminar normal stresses. The interlaminar shear stress estimates, however, are reliable [6]. These assumptions lead to considerable simplifications in the analysis. In spite of the simplifications, reliable energy release rate components can be estimated based on the interlaminar shear stress distributions [7].

A generic sublaminated beam is shown in Fig. 2.8 along with the notations and sign conventions. The peel and interlaminar shear stresses are denoted by P and T , respectively, with t and b subscripts for the top and bottom surfaces, respectively.

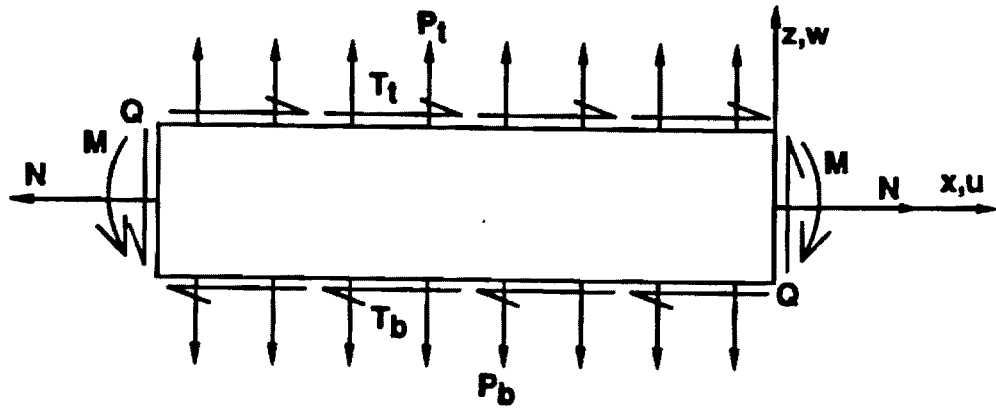


Figure 2.8: Generic Sublaminates for Local Delamination

The axial stress resultant, shear stress resultant, and bending moment resultant are denoted by N , Q , and M , respectively. The governing equations correspond to the one-dimensional form of Eqs. (2.1 - 2.5). These are summarized in the following for convenience.

The x and z displacements within the sublaminates are assumed to be of the form

$$u(x, z) = U(x) + z\beta(x)$$

$$w(x, z) = W(x)$$

Here, U represents the axial mid-plane stretching and W is the transverse displacement. The shear deformation is recognized through the rotation, β . These displacements are the total quantities and include the hygrothermal effects. The origin of the coordinate axes for the sublaminates is taken at the delamination tip as shown in Fig. 2.9 . The equilibrium equations take the form

$$N_{,x} + T_t - T_b = 0$$

$$Q_{,x} + P_t - P_b = 0 \quad (2.29)$$

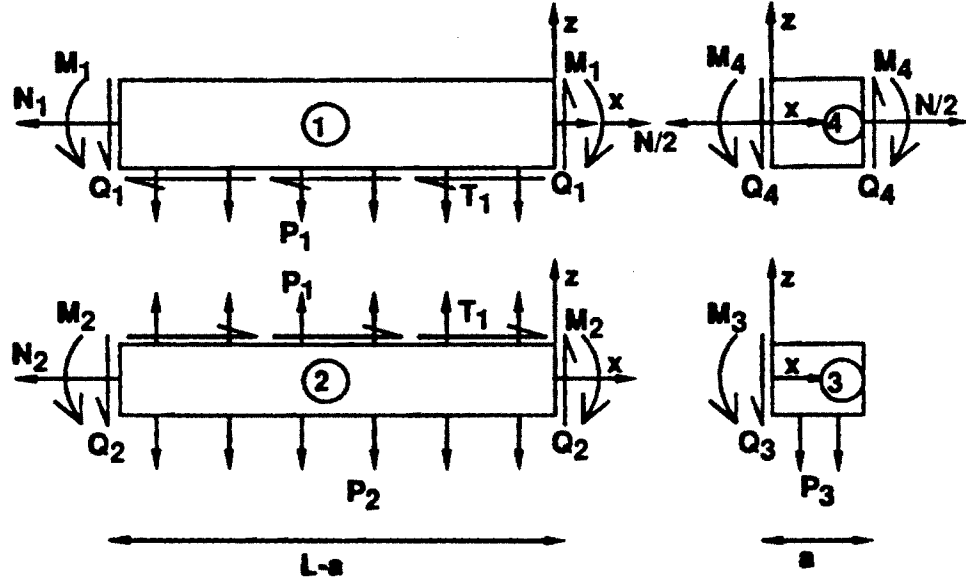


Figure 2.9: Sublaminates Forces and Coordinate Systems

$$M_{,x} - Q + \frac{h}{2}(T_t + T_b) = 0$$

where h is the thickness of the sublaminates. The constitutive relationships in terms of the force and moment resultants are

$$N = A_{11}U_{,x} + B_{11}\beta_{,x}$$

$$Q = A_{55}(\beta + W_{,x})$$

$$M = B_{11}U_{,x} + D_{11}\beta_{,x}$$

The boundary variables to be prescribed at the sublaminates edges are

$$N \text{ or } U$$

$$M \text{ or } \beta$$

$$Q \text{ or } W$$

Additionally, at the interfaces between sublaminates, reciprocal traction, and displacement matching boundary conditions have to be specified. The stress resultants in these equations include the equivalent hygrothermal loads also.

The solutions in sublaminates 1 and 2 are coupled by the reciprocal interlaminar stresses denoted T_1 and P_1 and by displacement continuity at the common interface. Assuming exponential solutions for the axial force and bending moment resultants leads to an eigenvalue problem involving the exponential parameters. The characteristic equation is of the form

$$s[B_1s^4 + B_2s^2 + B_3] = 0$$

where s is the eigenvalue parameter, and the B coefficients are given by

$$B_1 = \left(\frac{1}{A_{11(2)}} + \frac{1}{A_{11(1)}} + \frac{h_1^2}{4D_{11(1)}} + \frac{h_2^2}{4D_{11(2)}} \right) \frac{D_{11(1)} D_{11(2)}}{A_{55(1)} A_{55(2)}}$$

$$B_2 = -\frac{D_{11(2)}}{A_{55(2)}} \left(\frac{1}{A_{11(1)}} + \frac{1}{A_{11(2)}} + \frac{h_2^2}{4D_{11(2)}} \right) - \frac{D_{11(1)}}{A_{55(1)}} \left(\frac{1}{A_{11(1)}} + \frac{1}{A_{11(2)}} + \frac{h_1^2}{4D_{11(1)}} \right)$$

and

$$B_3 = \frac{1}{A_{11(1)}} + \frac{1}{A_{11(2)}}$$

The eigenvalues turn out to be zero and two nonzero values given by

$$s = \pm \left(\frac{-B_2 \pm (B_2^2 - 4B_1B_3)^{1/2}}{2B_1} \right)^{1/2}$$

For the problem under consideration, all the square roots in this expression lead to real quantities and thus the eigenvalues are real. Since the eigenvalues involve only the stiffness parameters, they are not affected by the inclusion of hygrothermal effects. Further, due to the fact that B_1 has D terms in the numerator, it is much smaller

than B_3 . This leads to the boundary layer nature of the solution. Since the response (axial forces, moments) has finite values at large distances from the origin, namely, at the ends of the specimen, only the exponentially decaying and constant solutions are used. Using subscripts to denote the sublaminates of validity, the following boundary conditions from the ends of the modeled region are enforced.

$$N_2(0) = 0$$

$$Q_4(a) = 0$$

$$\beta_4(a) = 0$$

$$N_1 + N_2 = \text{Applied Load}$$

The conditions on N apply only to the mechanical quantities. Further, the following displacement matching conditions are applied.

$$u_1 \left(x, -\frac{h_1}{2} \right) = u_2 \left(x, \frac{h_2}{2} \right)$$

$$U_1(0) = U_4(0)$$

$$U_2(0) = U_3(0)$$

$$\beta_1(0) = \beta_4(0)$$

It should be noted that a β_2 and β_3 matching condition cannot be applied at this level of modeling since it would amount to specifying both W and Q . To eliminate rigid body displacements, U_1 is set to zero at the left end. The following solutions can then be obtained for the stress resultants in sublaminates 1 and 2

$$N_1 = a_1 e^{\epsilon_1 x} + a_2 e^{\epsilon_2 x} + \epsilon A_{11(1)} - N_1^{nm}$$

$$N_2 = -a_1 e^{\epsilon_1 x} - a_2 e^{\epsilon_2 x} + \epsilon A_{11(2)} - N_2^{nm}$$

$$M_1 = a_1 k_1 e^{s_1 x} + a_2 k_2 e^{s_2 x} - M_1^{nm}$$

$$M_2 = a_1 k_3 e^{s_1 x} + a_2 k_4 e^{s_2 x} - M_2^{nm}$$

Here k_1 is defined as

$$k_1 = \frac{\frac{h_1}{2} s_1^2}{\frac{A_{55(1)}}{D_{11(1)}} - s_1^2}$$

The parameter k_2 is defined in a similar manner using the eigenvalue, s_2 . The remaining parameters, k_3 and k_4 , are similar to k_1 and k_2 but based on sublaminates 2 properties. The nominal strain, ε , is defined as

$$\varepsilon = \left(\frac{P}{2b} + N_1^{nm} + N_2^{nm} \right) \frac{1}{A_{11(1)} + A_{11(2)}}$$

where P is the applied uniform axial force and b is the specimen width. The a'_j 's can be derived from the boundary conditions as follows

$$a_1 = \frac{\theta_3 + \theta_4 a}{\theta_d} \frac{1}{A_{11(1)} + A_{11(2)}} \left(\frac{P}{2b} A_{11(2)} + N_1^{nm} A_{11(2)} - N_2^{nm} A_{11(1)} \right)$$

$$a_2 = -\frac{\theta_1 + \theta_2 a}{\theta_d} \frac{1}{A_{11(1)} + A_{11(2)}} \left(\frac{P}{2b} A_{11(2)} + N_1^{nm} A_{11(2)} - N_2^{nm} A_{11(1)} \right)$$

with

$$\theta_1 = \frac{s_1}{A_{55(1)}} \left(k_1 + \frac{h_1}{2} \right)$$

$$\theta_2 = \frac{k_1}{D_{11(1)}}$$

$$\theta_3 = \frac{s_2}{A_{55(1)}} \left(k_2 + \frac{h_1}{2} \right)$$

$$\theta_4 = \frac{k_2}{D_{11(1)}}$$

and

$$\theta_d = \theta_3 - \theta_1 + (\theta_4 - \theta_2)a$$

The interlaminar shear and peel stresses between sublaminae 1 and 2 can be obtained using the equilibrium equations (2.29) as

$$T_1 = a_1 s_1 e^{s_1 x} + a_2 s_2 e^{s_2 x}$$

$$P_1 = \left(k_1 + \frac{h_1}{2}\right) a_1 s_1 e^{s_1 x} + \left(k_2 + \frac{h_1}{2}\right) a_2 s_2 e^{s_2 x}$$

As mentioned previously, this peel stress estimate is not accurate because of the inability to apply boundary conditions on shear. Recognizing the fact that there are no applied shear forces, it can be concluded that the peel stress distribution should be self equilibrating. This assumption can be satisfied by including additional exponential terms in the above peel stress expression and determining these additional terms by setting the net force and moment due to the peel stress to zero as shown in section 2.2. The peel stress estimated through this correction process is referred to as the modified peel stress. Proceeding on to sublaminae 3 and 4, the following solutions can be written.

$$N_3 = 0$$

$$M_3 = \varphi_1 \sinh(\omega_3 x) + \varphi_2 \cosh(\omega_3 x)$$

where

$$\varphi_2 = a_1 k_3 + a_2 k_4$$

$$\varphi_1 = -\varphi_2 \coth(\omega_3 a)$$

and

$$\omega_3^2 = \frac{A_{55(2)}}{D_{11(2)}}$$

$$N_4 = \frac{P}{2b}$$

$$M_4 = a_1 k_1 + a_2 k_2$$

The total energy release rate G_T is calculated using $G_T = dW_e/da$ where W_e is the work done per unit width by the external (constant) loads on the specimen displacements. For the case where hygrothermal effects are included, there are additional terms due to the work done by N_i^{nm} . In reality, these N_i^{nm} quantities are not applied loads but correspond to residual stresses. Thus, the additional terms are due to the work done by the applied mechanical strains on these residual stresses. The total energy release including hygrothermal effects is given by

$$G_T = \frac{P}{2b} \left(\frac{P}{b} + N_1^{nm} \right) \left(\frac{1}{A_{11(1)}} - \frac{1}{A_{11(1)} + A_{11(2)}} + I_1 - I_2 \right) + \frac{P}{2b} N_2^{nm} \left(-\frac{1}{A_{11(1)} + A_{11(2)}} - I_3 + I_2 \right) \quad (2.30)$$

where the I factors are

$$I_1 = \chi \frac{\theta_2 \theta_3 - \theta_1 \theta_4}{\theta_d^2} \left(\frac{1 - e^{-s_1(L-a)}}{s_1} - \frac{1 - e^{-s_2(L-a)}}{s_2} \right) \\ I_2 = \chi \frac{(\theta_3 + \theta_4 a) e^{-s_1(L-a)} - (\theta_1 + \theta_2 a) e^{-s_2(L-a)}}{\theta_d} \quad (2.31)$$

with

$$\chi = \frac{1}{A_{11(1)} + A_{11(2)}} \frac{A_{11(2)}}{A_{11(1)}}$$

Parameter I_3 is the same as I_1 but with the ratio $A_{11(1)}/A_{11(2)}$ instead of unity in Eq. (2.31). Using the virtual crack closure technique [21], from the relative displacements in the cracked portion and the interlaminar stresses ahead of the crack tip, the mode I and mode II energy release rate contributions can be obtained. The mode III energy release rate is zero from the assumption of plane strain. The mode II energy release rate is given by

$$G_{II} = \lim_{\delta \rightarrow 0} \frac{1}{2\delta} \int_0^\delta T_1(x - \delta) \Delta u(x) dx$$

where δ is the virtual crack step size and Δu is the differential axial displacement across the crack surface. This calculation can be simplified using only the linear

part of the differential displacement [7]. In a similar fashion, the mode I energy release rate can be obtained based on the normal stress (P) and the differential w displacements near the crack front. Since the unmodified peel stress estimate is inaccurate, an alternate approach was used to estimate G_I , the mode I energy release rate. The total energy release rate for this problem is made up entirely of G_I and G_{II} ($G_{III} = 0$). From an estimate of G_T and G_{II} , an estimate for G_I can be obtained simply as

$$G_I = G_T - G_{II}$$

The critical load for a given specimen can then be evaluated based on an appropriate fracture law. This is illustrated in the next chapter.

CHAPTER III

APPLICATIONS OF DELAMINATION MODELS

3.1 Mode I Edge Delamination

The analytical model is applied to the mid-plane edge delamination specimen shown in Fig. 2.2. The material considered is T300/5208 graphite epoxy. Its properties are listed in Table 3.1.

The difference between the ambient and cure temperature, ΔT , is $-156^\circ C$. The moisture level was allowed to vary from 0 to 1.2 percent of the laminate weight, which reflects feasible conditions. Laminates of the class $[\theta/-\theta_2/\theta/90_2]_s$ and $[0_3/90_3]_s$ have been analyzed.

Normalized values of strain energy release rate are shown in Figs. 3.1-3.6, where the labels M , $M + T$, and $M + T + H$ stand for mechanical, mechanical and thermal, and mechanical, thermal and moisture, respectively. The strain energy release

Table 3.1: ED Specimen Geometry and Material Properties

$E_{11} = 128 \text{ GPa}$	Thermal Coefficients :	$\alpha_1 = -0.41 \mu\epsilon/^\circ C$
$E_{22} = 8.47 \text{ GPa}$		$\alpha_2 = 26.8 \mu\epsilon/^\circ C$
$G_{12} = 5.73 \text{ GPa}$	Swelling Coefficients :	$\beta_1 = 0$
$G_{31} = 3.27 \text{ GPa}$		$\beta_2 = 5560 \mu\epsilon/\%W$
$G_{23} = 3.27 \text{ GPa}$	Width = $2b = 38.4 \text{ mm}$	
$\nu_{12} = 0.292$	Ply Thickness = 0.14 mm	

rate parameter in the figures is defined as the total energy release rate divided by $E_{22}h(\epsilon^m)^2$.

The strain energy release rate in Figs. 3.1-3.3 is zero at $a = 0$. Residual thermal stresses results in an increase of 275%, 40% and 280% of the energy release rate for the $[15/-15_2/15/90_2]_s$, $[60/-60_2/60/90_2]_s$ and $[0_3/90_3]_s$ laminates, respectively. Residual moisture alleviates this effect as illustrated in Figs. 3.4-3.6. The specific moisture content for total alleviation from the thermal effect is equal to 0.763% irrespective of the layup.

The peel stress distribution, σ_{zz} , appears in Figs. 3.7-3.9. The stress parameter in these figures is defined as the interlaminar stress divided by $E_{22}\epsilon^m$. The inaccurate peel stress distribution given in Eq. (2.27) is plotted for the case where mechanical loading only is considered. The corrected peel stress distribution is self-equilibrating and yields a tensile peel stress at the delamination front.

The magnitude of the peel stresses shows a strong dependency on the thermal and moisture conditions. The stress increases with thermal effect as compared to pure mechanical loading. The addition of moisture alleviates the thermal effect. Moreover, the distance at which the peel stress reverses its sign is not affected by the residual thermal and moisture strains. It is worth noting that at the specific moisture percent (0.763%) producing complete alleviation of the total energy release rate from the thermal effect, the interlaminar peel stress distribution is identical to the case where only mechanical loading is considered. This is shown in Figs. 3.7-3.9. This finding establishes a similarity in behavior between the energy release rate and the interlaminar stresses.

The analytical model presented herein was applied to the laminates presented in Ref. [18]. The Graphite/Epoxy lamina properties from Ref. [18] are listed in Table 3.2. Similar values of strain energy release rate G_I were calculated for the wide range

Table 3.2: ED Specimen Geometry and Material Properties, Ref. [18]

$E_{11}/E_{22} = 14$	Ply Thickness = 0.1267 mm
$E_{33}/E_{22} = 1$	
$G_{12}/E_{22} = 0.533$	Thermal Coefficients : $\alpha_1 = -0.9\mu\epsilon/^\circ C$
$G_{23}/E_{22} = 0.323$	$\alpha_2 = \alpha_3 = 23.0\mu\epsilon/^\circ C$
$\nu_{12} = 0.3$	
$\nu_{23} = 0.55$	width = $2b = 38.0\text{mm}$

of a/h where the G_I remains constant as shown in Figs. 3.10 and 3.11. Negligible change in the G_I value with decreasingly small values of a/h were obtained. This is in contrast with the increase in G_I at small values of a/h reported in Ref. [18]. Although thickness strain is neglected in Eqs. (2.1), the peel stress distribution has been estimated through a modification as described previously, which simplifies considerably the computational effort. A comparison of the peel stress distribution with Ref. [18] is shown in Figs. 3.12 and 3.13.

The peel stress intensity at the delamination front in the $[30/-30_2/30/90_2]_s$ is higher than the $[0_3/90_3]_s$ laminate. This is due to the difference in poisson's ratio between the core plies made of 90° plies and the outer plies. The poisson's ratio mismatch is larger for the case of $[30/-30_2/30/90_2]_s$ compared to the $[0_3/90_3]_s$ layup. The interlaminar peel stress distribution predicted by the present approach is in good agreement with the distribution of Ref. [18] for the case of a $[0_3/90_3]_s$ laminate. This is in contrast with the case of a $[30/-30_2/30/90_2]_s$ where the maximum stress intensity as well as the distribution differ from the predictions of Ref. [18]. This difference may be due to the transverse normal strain influence on the analysis of these laminates.

3.2 Edge and Local Delamination

The delamination models have been used to study the behavior of $[\pm 25/90_n]$, T300/934 Graphite Epoxy specimen for n values of 0.5, 1, 2, 3, 4, 6, and 8. These correspond to the specimen tested by Crossman and Wang [8]. The specimen width and length were fixed at 0.025m and 0.15m, respectively, as in the tests. In computing the non-mechanical strains, the laminate is assumed to be held at the prescribed temperature and moisture levels. In predicting critical strains, the difference between test and stress free temperatures is assumed to be -155°C and specimen is assumed to be dry. It is assumed that local delamination occurs under fixed load conditions whereas edge delamination occurs under fixed grip conditions. This difference is a consequence of the modeling approaches used in the analyses. The applied uniform load was 100 MPa axial stress for the local delamination analysis and 0.5% strain for the edge delamination analysis. The solutions were generated using simple computer programs based on the closed form expressions for the interlaminar stresses and energy release rates.

3.2.1 Local Delamination

An example of the total energy release rate variation associated with local delamination (neglecting hygrothermal effects) with the crack length is presented in Fig. 3.14. The asymptotic value of G_T is denoted by G_{T0} in the figure. It can be observed that after a certain crack length, the G_T is independent of the crack length. On the basis of curves like the one shown in Fig. 3.14, the crack length was fixed at 10 ply thicknesses for the remainder of the studies. Typical interlaminar shear stress profiles including the hygrothermal effect are presented in Fig. 3.15. The corresponding total strain energy release rates appear in Fig. 3.16. The inclusion of thermal effects increases

the stress and the energy release rate while the inclusion of moisture effects has the opposite effect. In fact a moisture level of about 0.75% almost exactly negates the thermal effects. After some initial dependence on crack length, the mode mix tended to stabilize to a constant value. Using the model developed here, the asymptotic mode II component of the local delamination energy release rate was found to be approximately 30 percent for all n values. In the case of off-mid-plane edge delamination, the mode II contribution was less than 10 percent for the $n = 0.5$ specimen and progressively less for the thicker specimen.

3.2.2 Edge Delamination

As in the case of local delaminations, the interlaminar stress increases with thermal effects and the addition of moisture alleviates this as shown in Fig. 3.17 for the case of mid-plane edge delamination. A moisture level of about 0.75% produces a modified peel stress distribution that is indistinguishable from the case of mechanical loading alone. Moreover, the distance at which the modified peel stress reverses its sign is not affected by the residual hygrothermal strains. The hygrothermal influence on mid-plane delamination strain energy release rate is illustrated in Fig. 3.18 where the strain energy release rate is plotted versus moisture content for a $[\pm 25/90_2]$ laminate. The strain energy release rate follows the trend of increasing with residual thermal stress as in the case of peel stress. Further, residual moisture alleviates the thermal effects and a moisture level of about 0.75% results in a total alleviation of thermal effects. Similar behavior is observed in the case of off-mid-plane edge delamination.

3.2.3 Failure Loads and Modes

In order to evaluate the critical loads for local delamination, an appropriate mixed mode fracture law has to be applied, based on the calculated energy release compo-

nents. The following mixed mode criterion [22] has been fitted to the test data of Ref. [23] to calculate the mixed mode G_{Tc} which is then used in the Griffith criterion $G_T = G_{Tc}$ to obtain the critical delamination growth stress σ_c and strain ε_c values.

$$G_{Tc} = \xi^\eta G_{Ic} + (1 - \xi)^\eta G_{IIc}$$

Here ξ is the mode I fraction (G_I/G_T) and G_{Ic} and G_{IIc} are the critical strain energy release rates for the limiting cases of pure mode I and pure mode II, respectively. The exponential parameter η is a material constant and for the T300/934 system, its value is approximately 0.9. In the case of mid-plane delamination, since only mode I is present, G_{Tc} was taken as $G_{Ic}(125J/m^2)$. Based on the mixed mode criterion, G_{Tc} was about $400J/m^2$ for the local delamination case ($\xi = 0.7$). The failure loads for edge delamination at the $-25/90$ interface have also been calculated using a G_{Tc} value of $150 J/m^2$. This G_{Tc} value is different from the value used for mid-plane delamination due to the limited (less than 10 percent) presence of mode II.

In order to consider a worst case situation, thermal stresses were included and the moisture level was set at zero. Though the thermal stresses had a significant effect on the calculated peak stresses, the effect on the energy release rate was not significant except in the case of mid-plane edge delamination for the material system and layup considered. The critical strains are plotted against n , the number of 90° plies in Fig. 3.19. The experimental results of Ref. [8] are also presented in the figure for comparison. The results of the model developed in this paper are represented by the solid and dotted lines while the experimental results are shown as filled squares. The CLT based model of Ref. [9] agrees well with the shear deformation model in terms of the total energy release rate. However, the CLT based model does not provide information on the mode split and thus, the value of $G_c (\approx G_{Ic})$ used can lead to bias in the critical strain estimates. In the experiments, the local delamination phenomenon

was observed as the predominant failure mode only for the $n = 4, 6$ and 8 specimens. The shear deformation model presented in this paper provides good agreement with the experimental data in this range. For $n < 4$, edge delamination either in the mid-plane or in the $25/90$ interface was observed in the tests, in agreement with the edge delamination models. Further, the relative closeness of the calculated critical strains from the mid-plane and off-mid-plane edge delamination models implies that, in practice, one could have interaction between these two modes. In such cases, one can expect the delamination to wander around the mid-plane and the $25/90$ interfaces. This is especially so in the case $n = 0.5$ where mid-plane delamination is not actually between two distinct layers but in the middle of a single layer. Experimental observations [8] are in agreement with this expectation. Thus, it can be seen that the shear deformation models reproduce the observed behavior with reasonable accuracy and can be used to estimate critical loads for a range specimen thicknesses incorporating various delamination modes.

3.3 Conclusions

Shear deformation models including hygrothermal effects have been developed to analyze local delaminations growing from transverse cracks in 90° plies and edge delaminations located around the mid-plane of symmetric laminates. The models have been combined into a unified delamination analysis code in order to predict damage modes and loads in laminated composites. The analytical results of the shear deformation models agree reasonably with critical strain experimental data from $[\pm 25/90_n]$, T300/934 graphite epoxy laminates in the range of n from 0.5 to 8 . Residual thermal and moisture stresses are found to have only minor effects on the critical strains except in the case of mid-plane edge delamination for the geometry

and material considered. The same failure modes as in the tests are reproduced in the analysis. The integrated delamination code is expected to be of use in design evaluation applications.

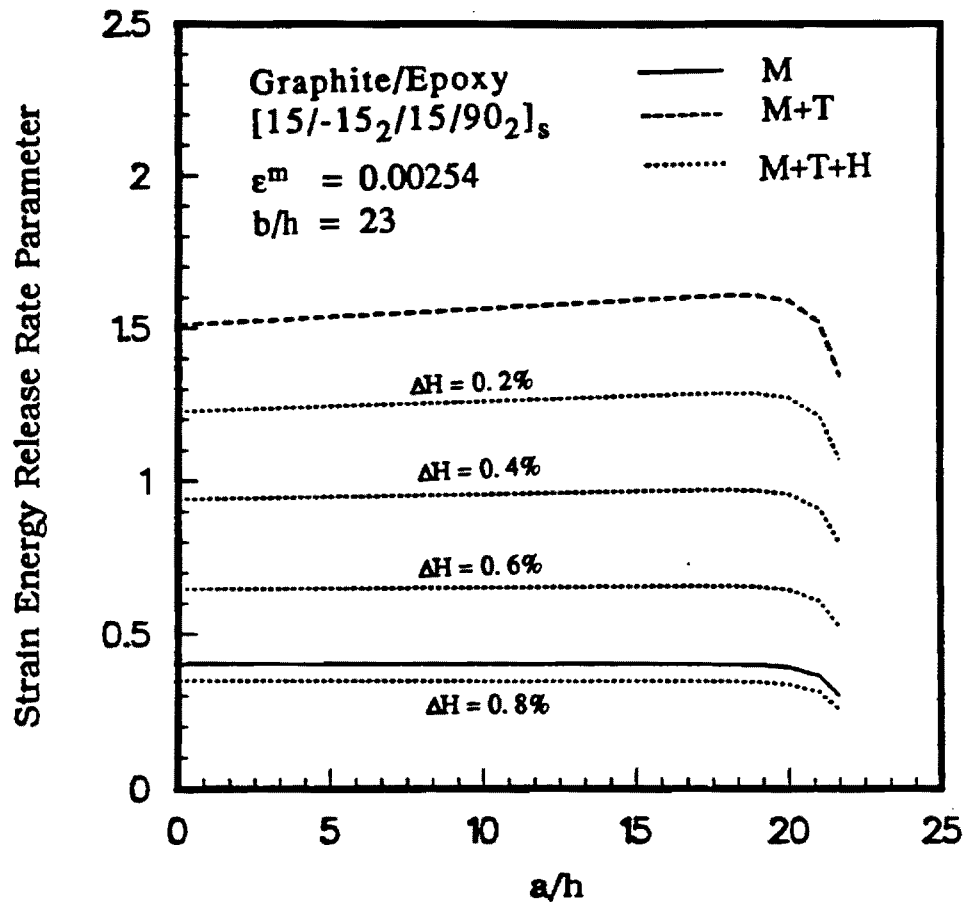


Figure 3.1: Mode I Strain Energy Release Rate in a $[15/-15_2/15/90_2]_s$ Laminate

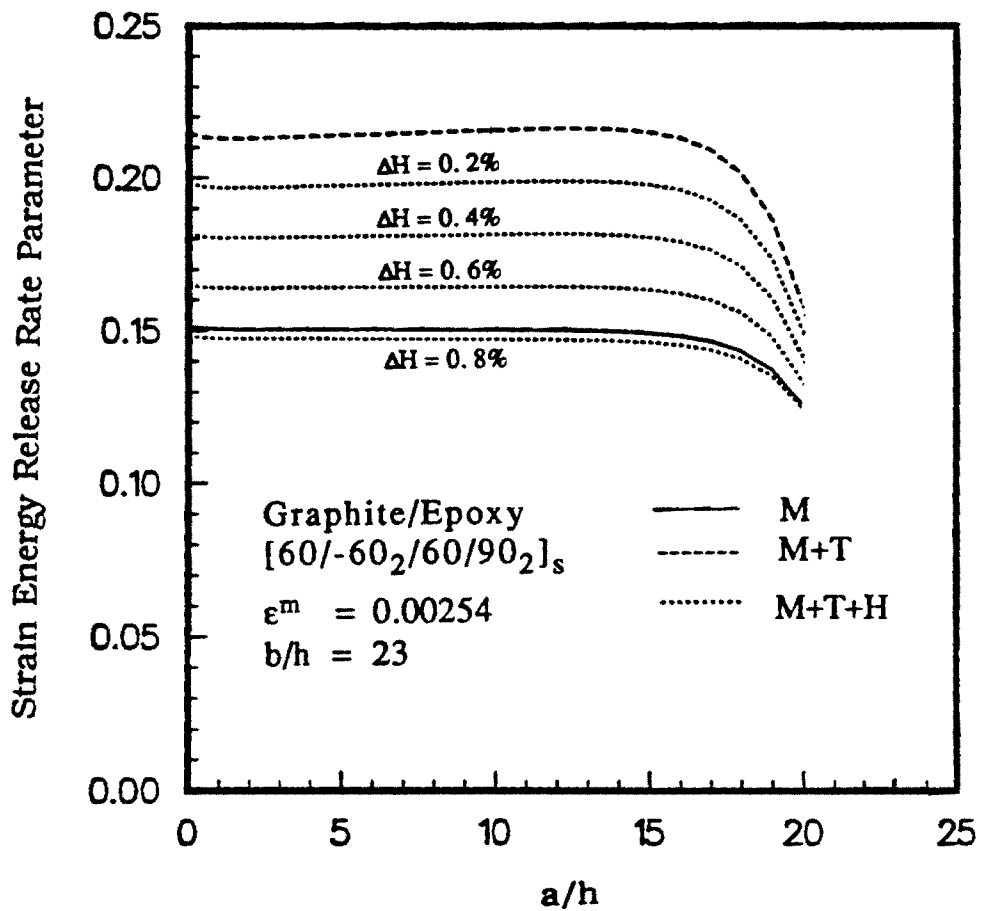


Figure 3.2: Mode I Strain Energy Release Rate in a $[60/-60_2/60/90_2]_s$ Laminate

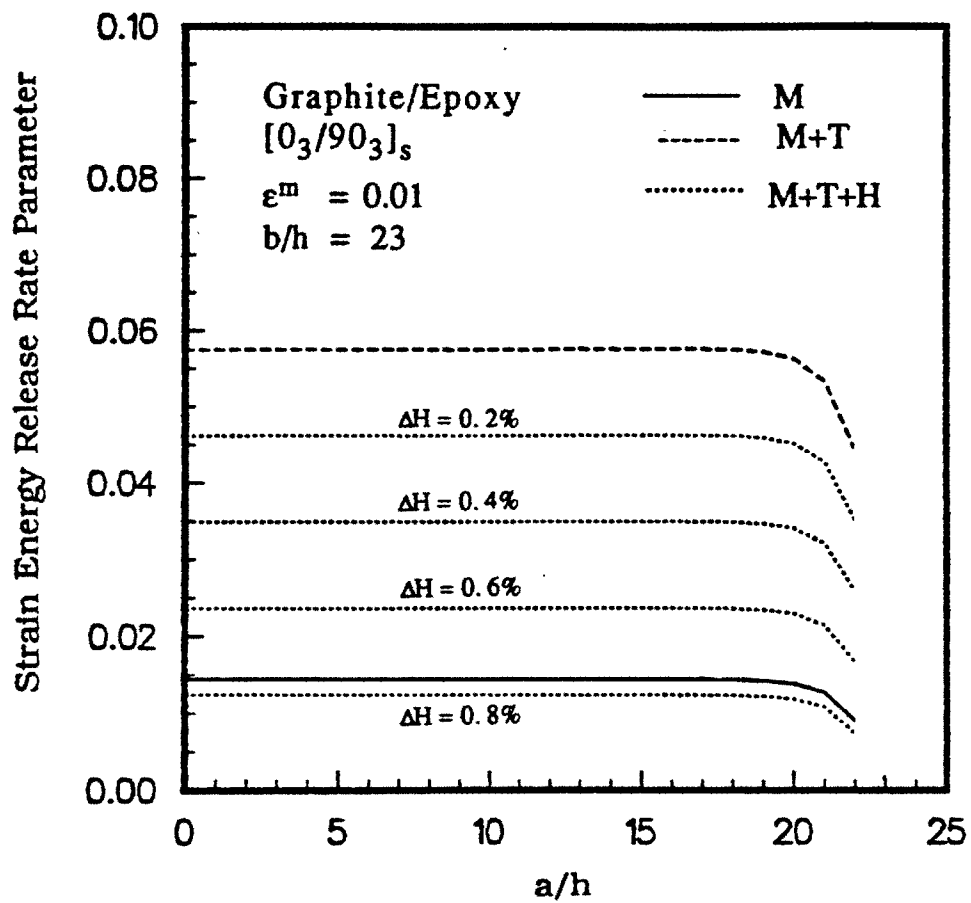


Figure 3.3: Mode I Strain Energy Release Rate in a [0₃/90₃]_s Laminate

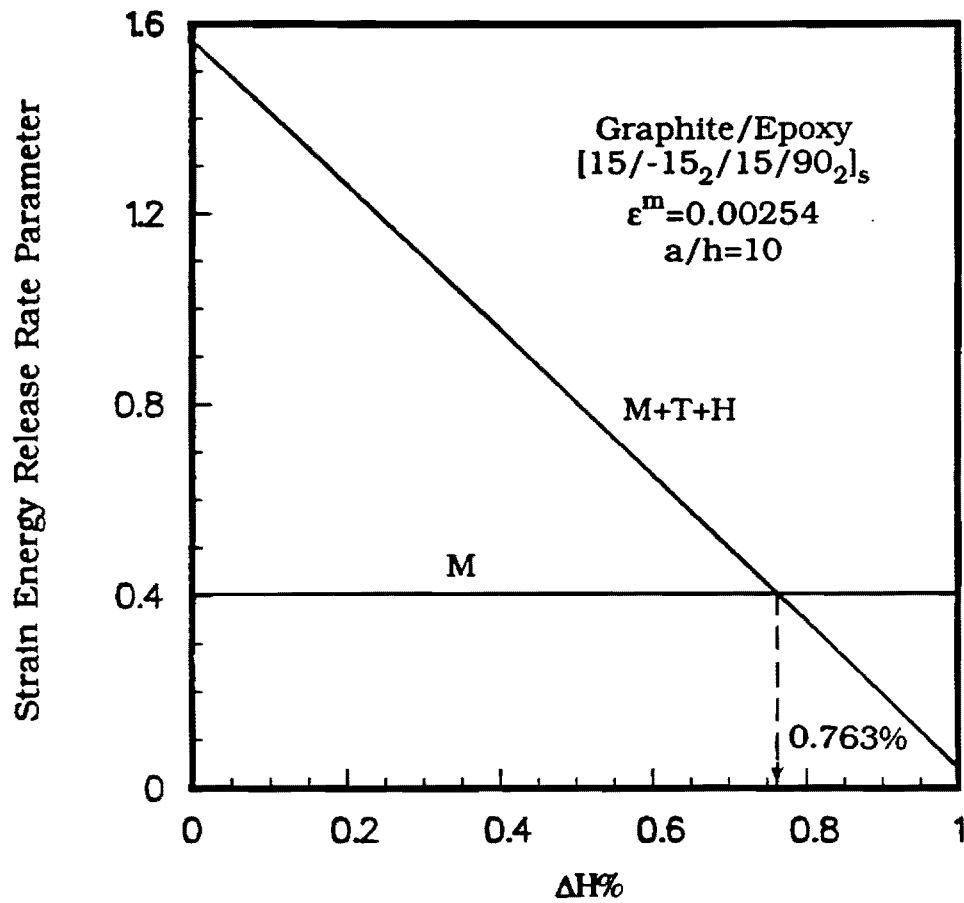


Figure 3.4: Influence of Residual Thermal and Moisture Stresses on Mode I Strain Energy Release Rate in a $[15/-15_2/15/90_2]_s$ Laminate

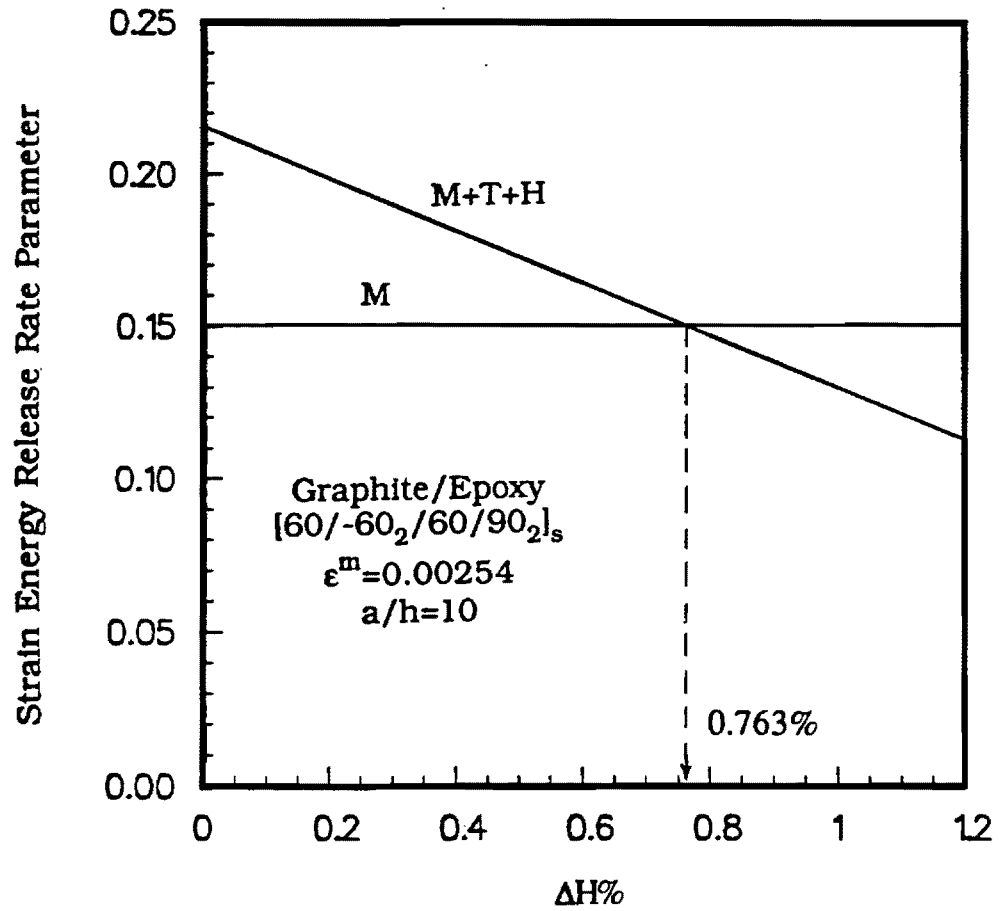


Figure 3.5: Influence of Residual Thermal and Moisture Stresses on Mode I Strain Energy Release Rate in a $[60/-60_2/60/90_2]_s$ Laminate

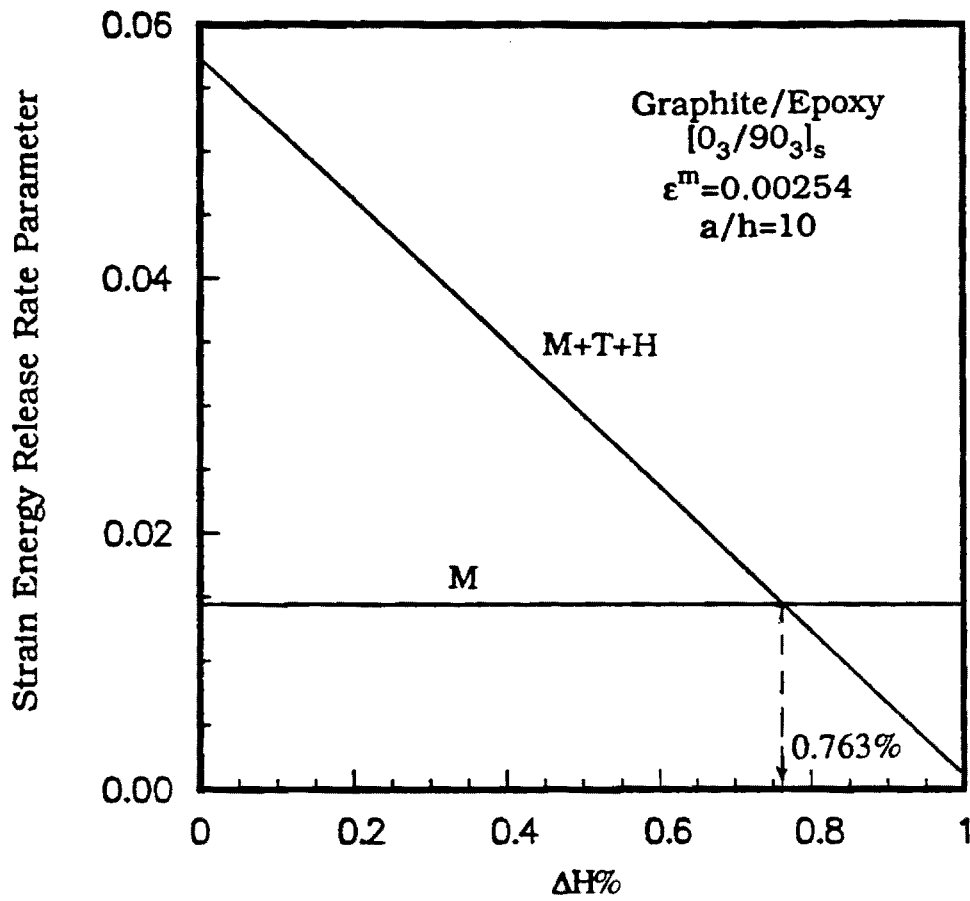


Figure 3.6: Influence of Residual Thermal and Moisture Stresses on Mode I Strain Energy Release Rate in a $[0_3/90_3]_s$ Laminate

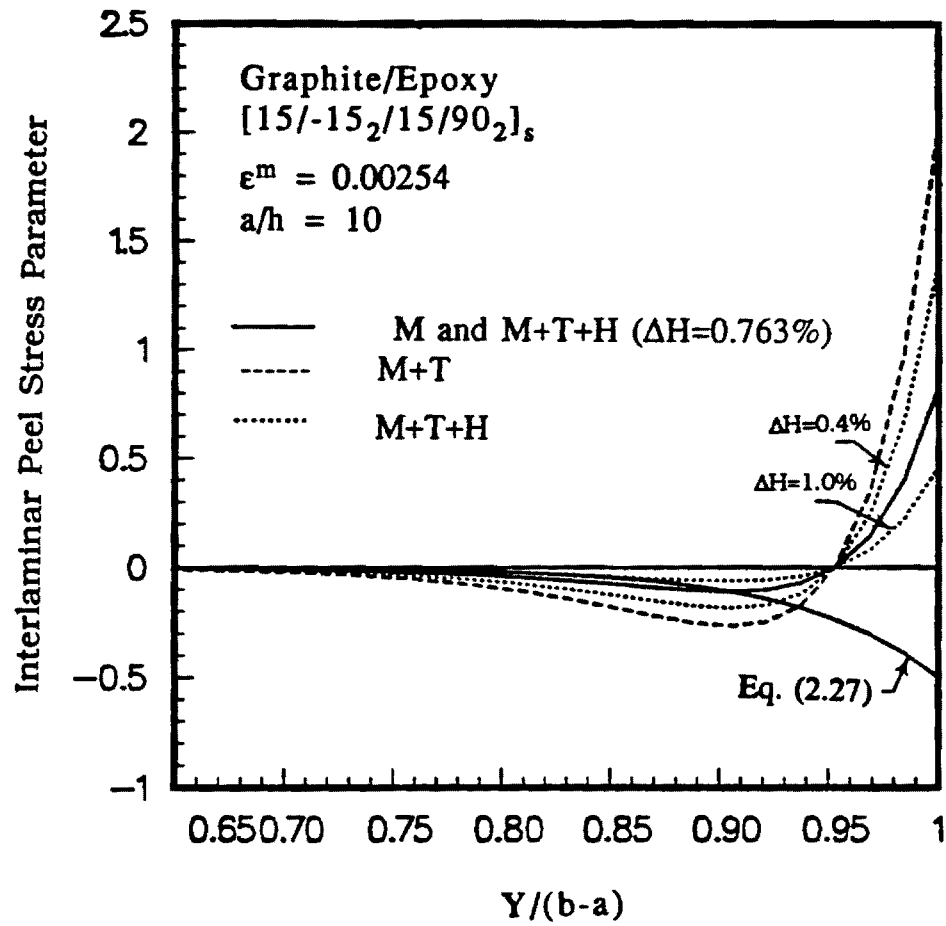


Figure 3.7: Peel Stress Distribution ahead of the Crack in a $[15/-15_2/15/90_2]_s$ Laminate

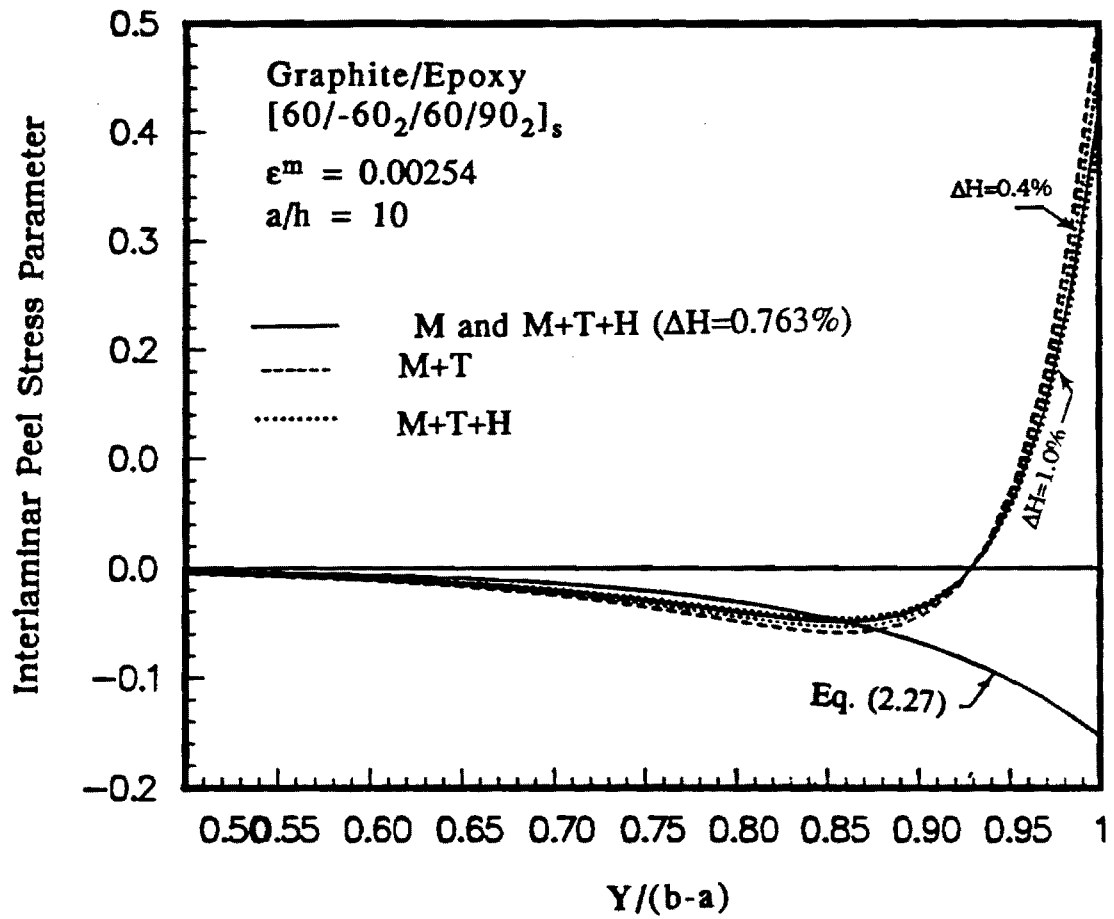


Figure 3.8: Peel Stress Distribution ahead of the Crack in a $[60/-60_2/60/90_2]_s$ Laminate

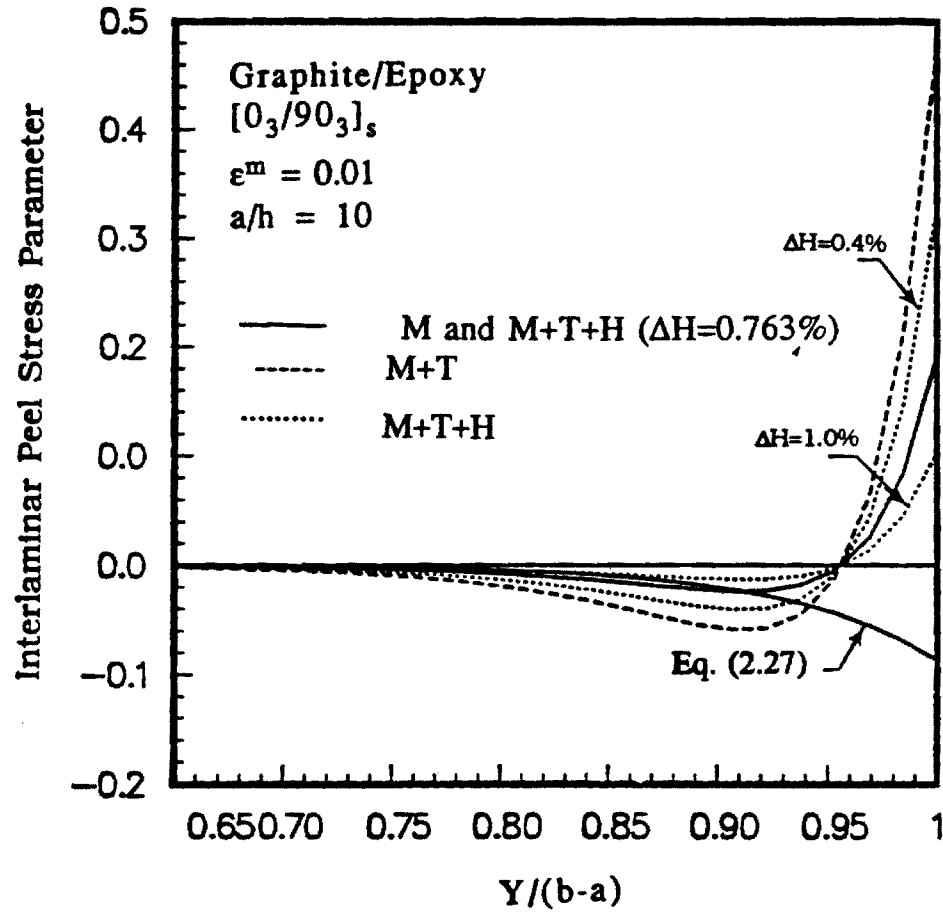


Figure 3.9: Peel Stress Distribution ahead of the Crack in a $[0_3/90_3]_s$ Laminate

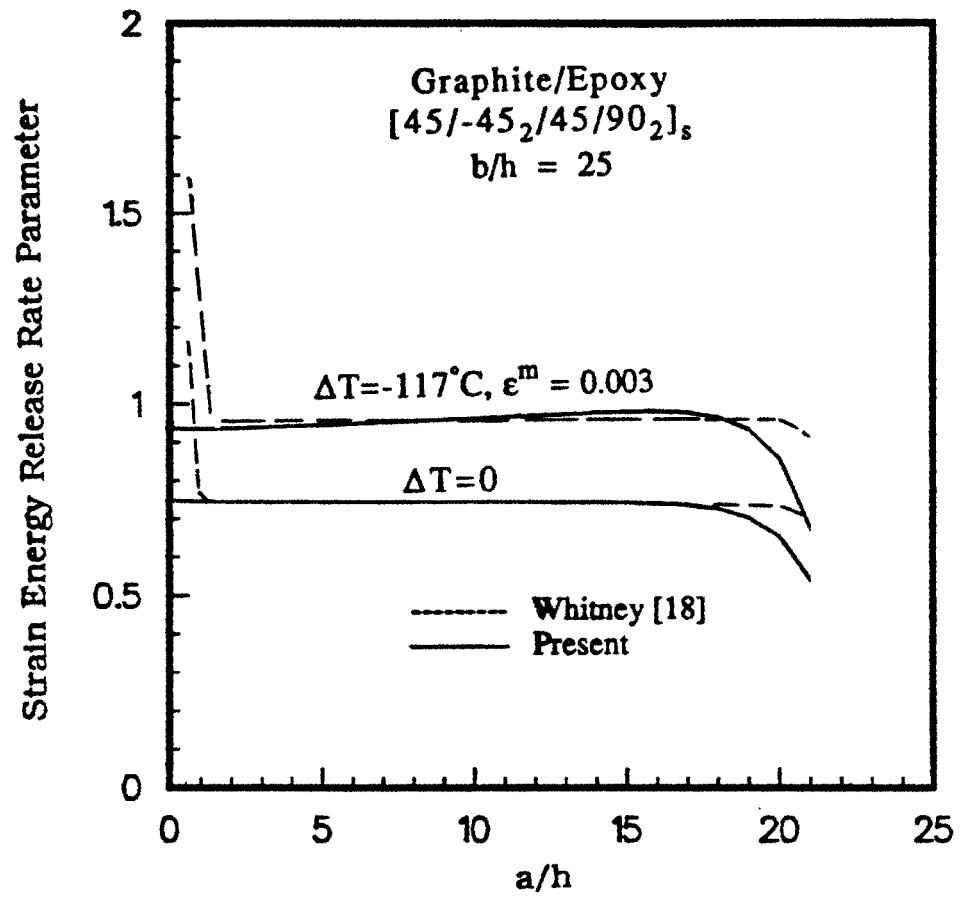


Figure 3.10: Mode I Strain Energy Release Rate in a $[45/-45_2/45/90_2]_s$ Laminate

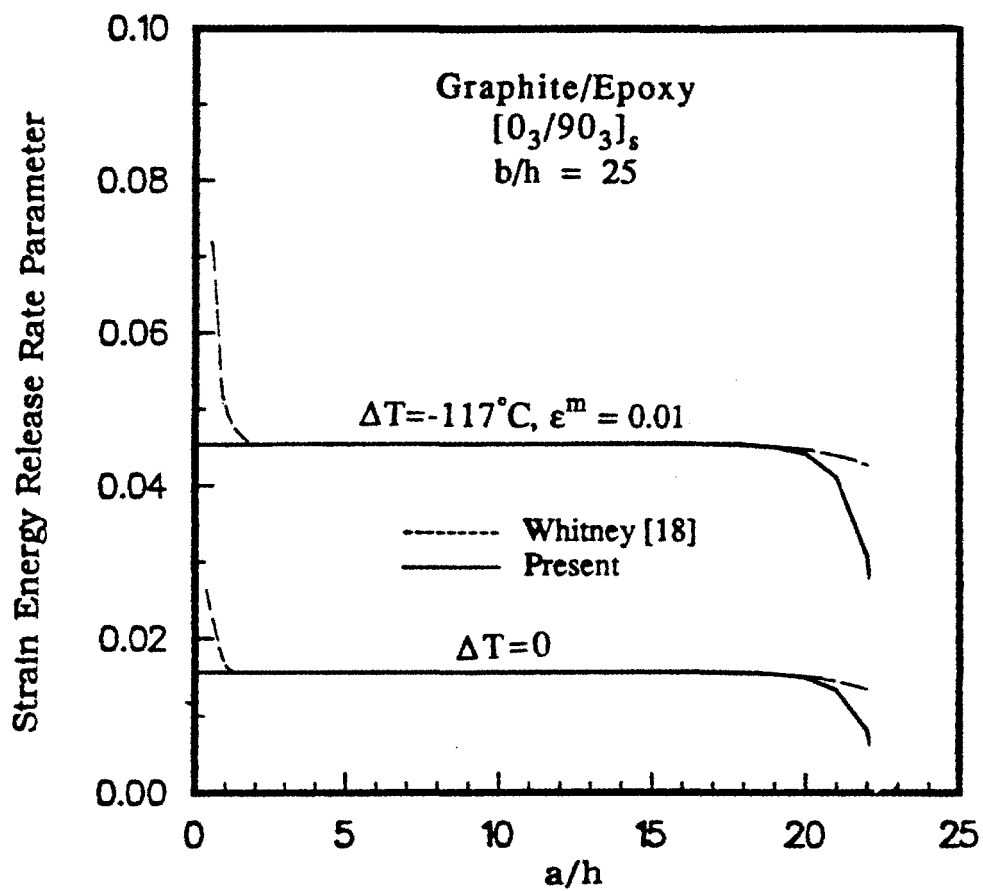


Figure 3.11: Mode I Strain Energy Release Rate in a $[0_3/90_3]_s$ Laminate

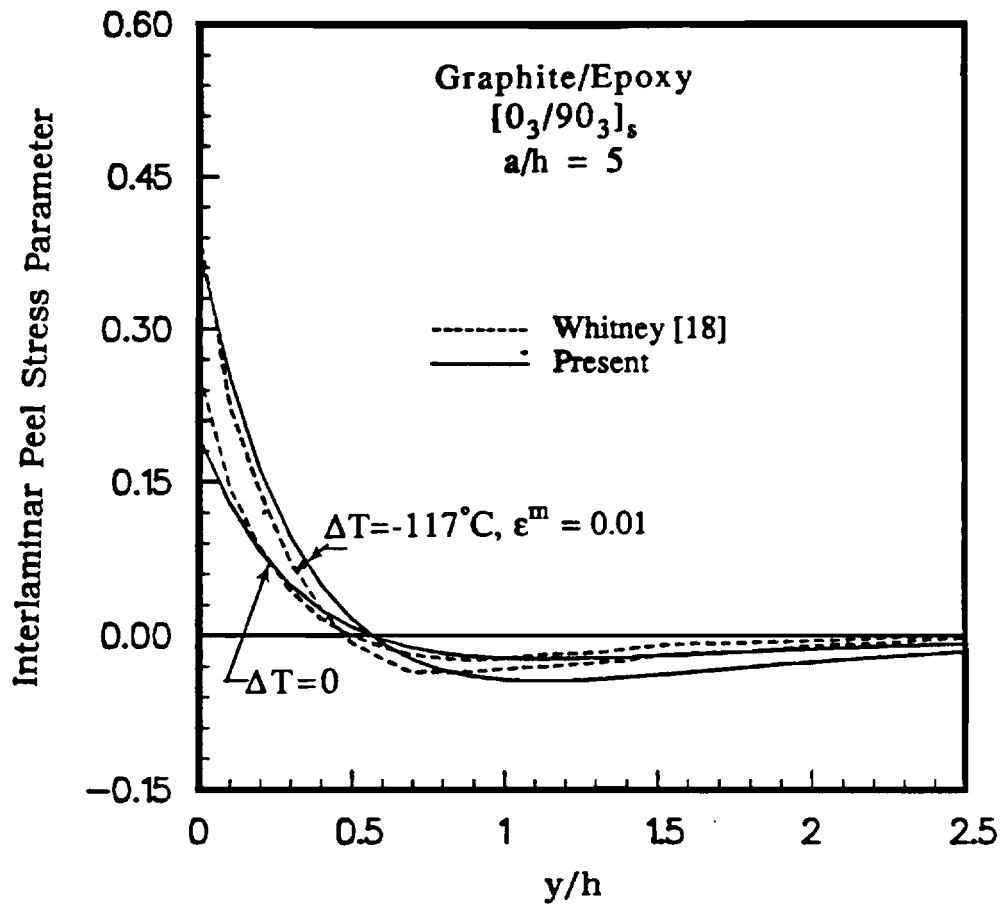


Figure 3.12: Peel Stress Distribution ahead of the Crack in a [0₃/90₃]_s Laminate

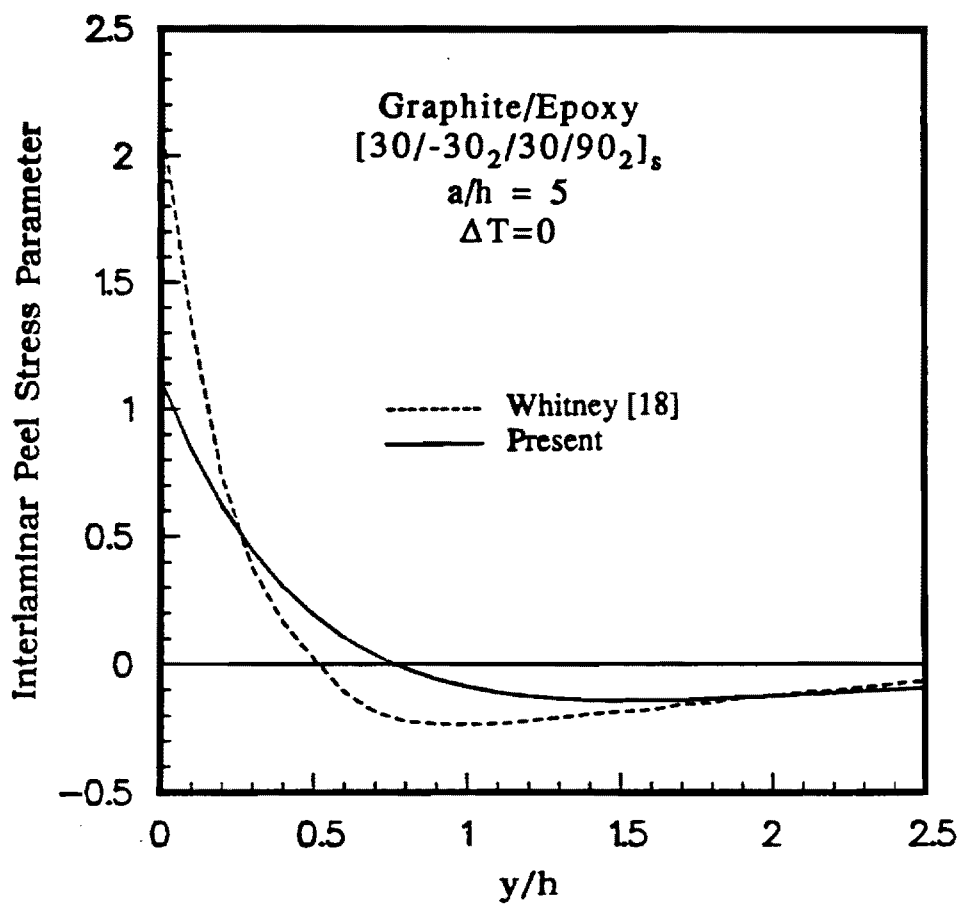


Figure 3.13: Peel Stress Distribution ahead of the Crack in a [30/ - 30₂/30/90₂]_s Laminate

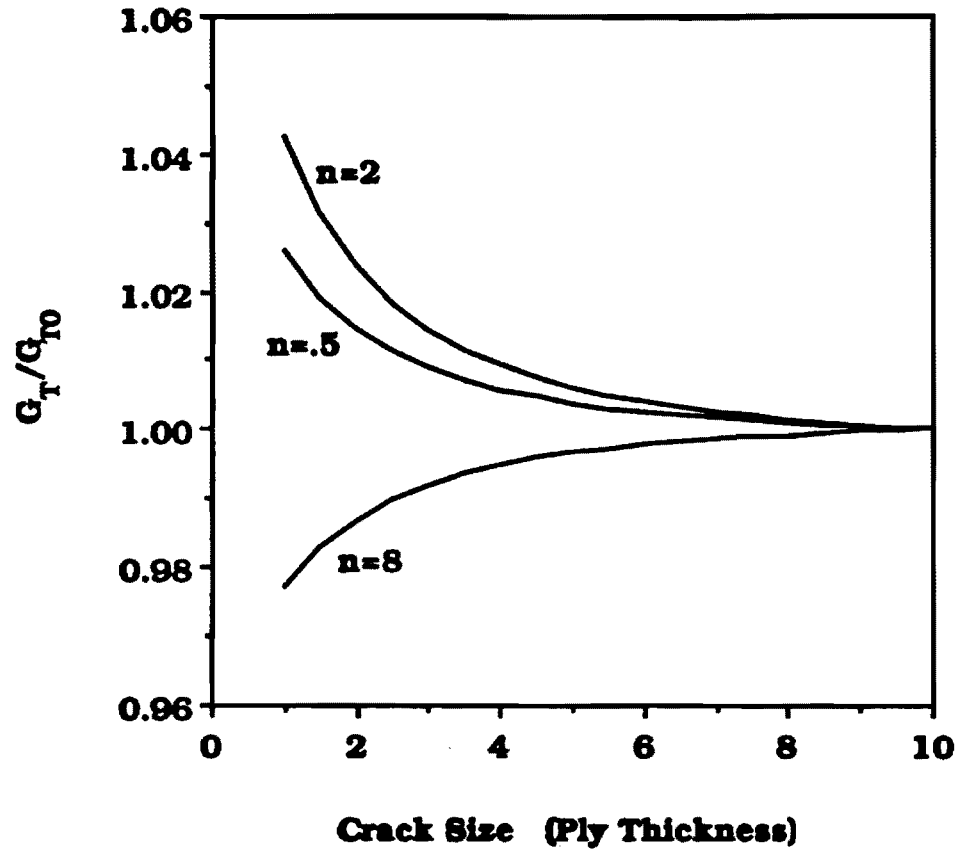


Figure 3.14: Total Local Delamination Energy Release Rate Variation

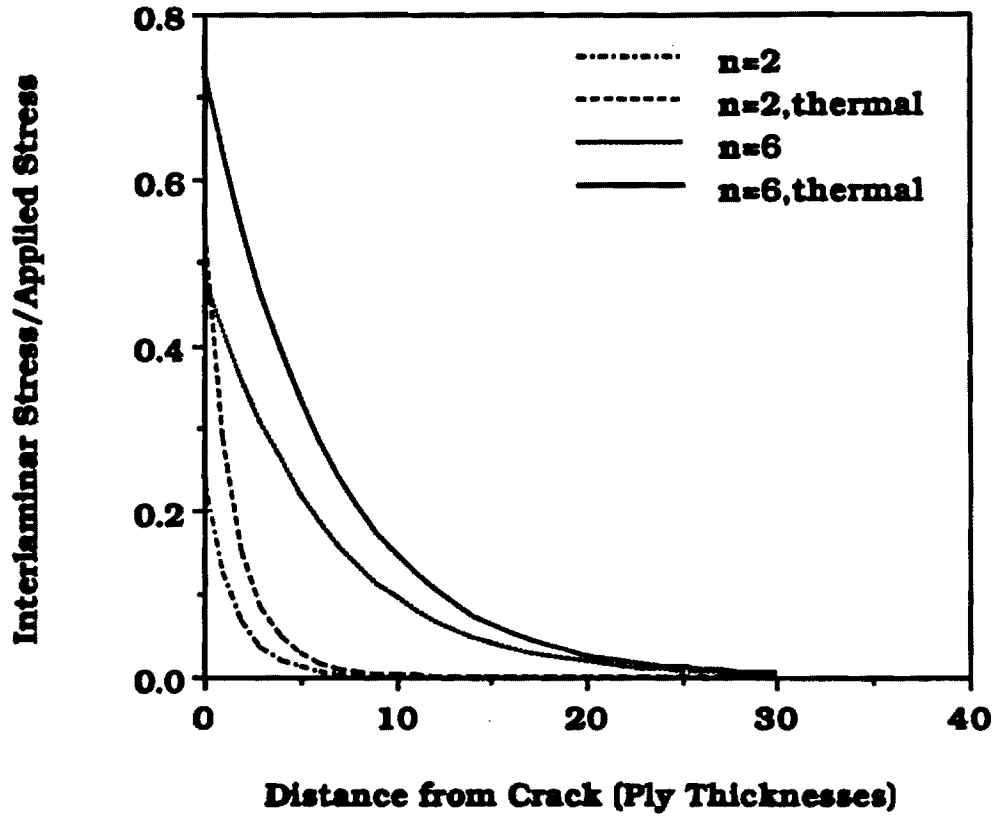


Figure 3.15: Interlaminar Shear Stress Distribution (Local Delamination)

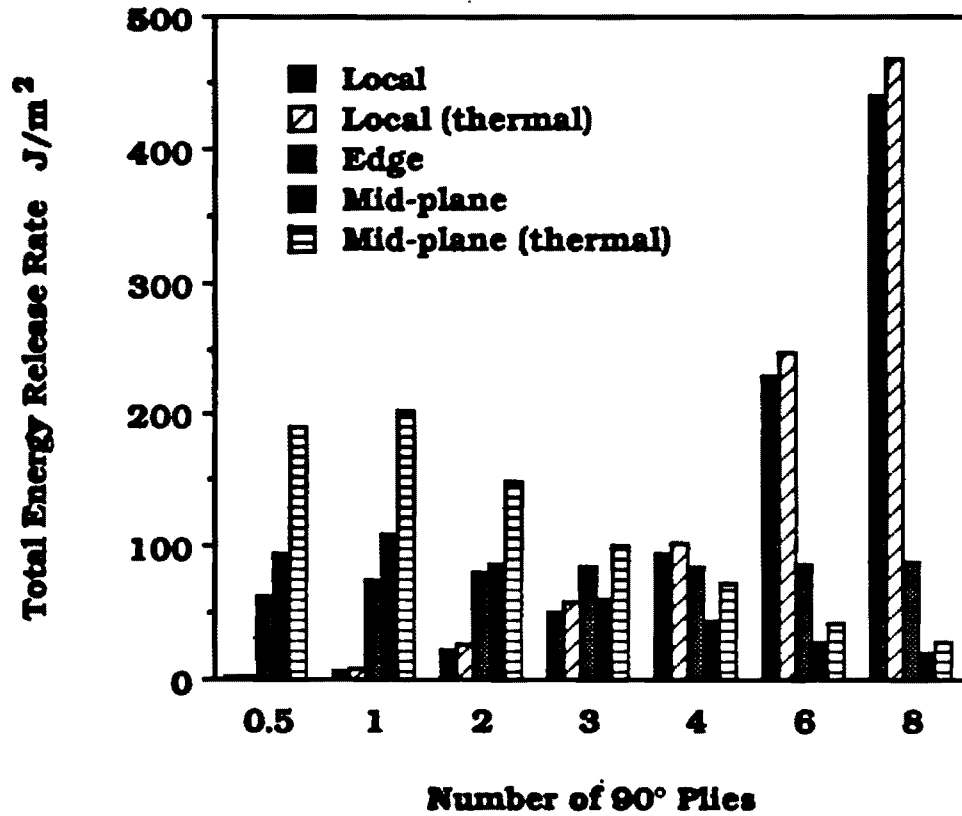


Figure 3.16: Total Energy Release Rate for $[\pm 25/90_n]$, Graphite/Epoxy Specimen

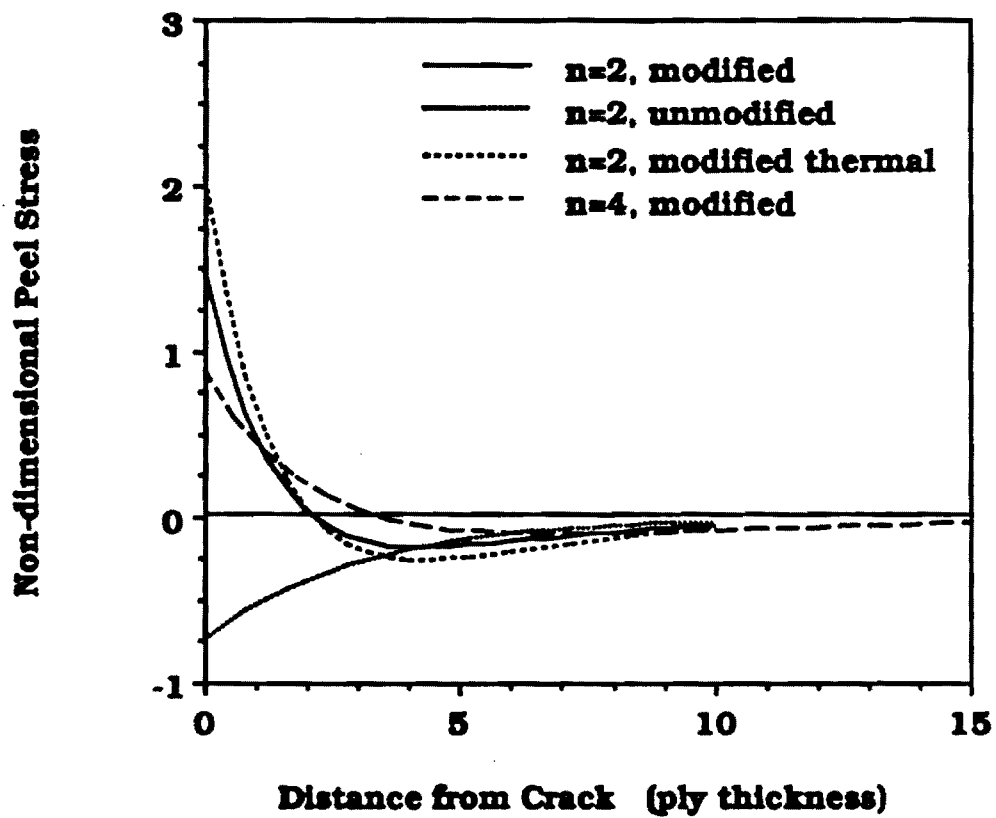


Figure 3.17: Interlaminar Normal Stress (Mid Plane Delamination)

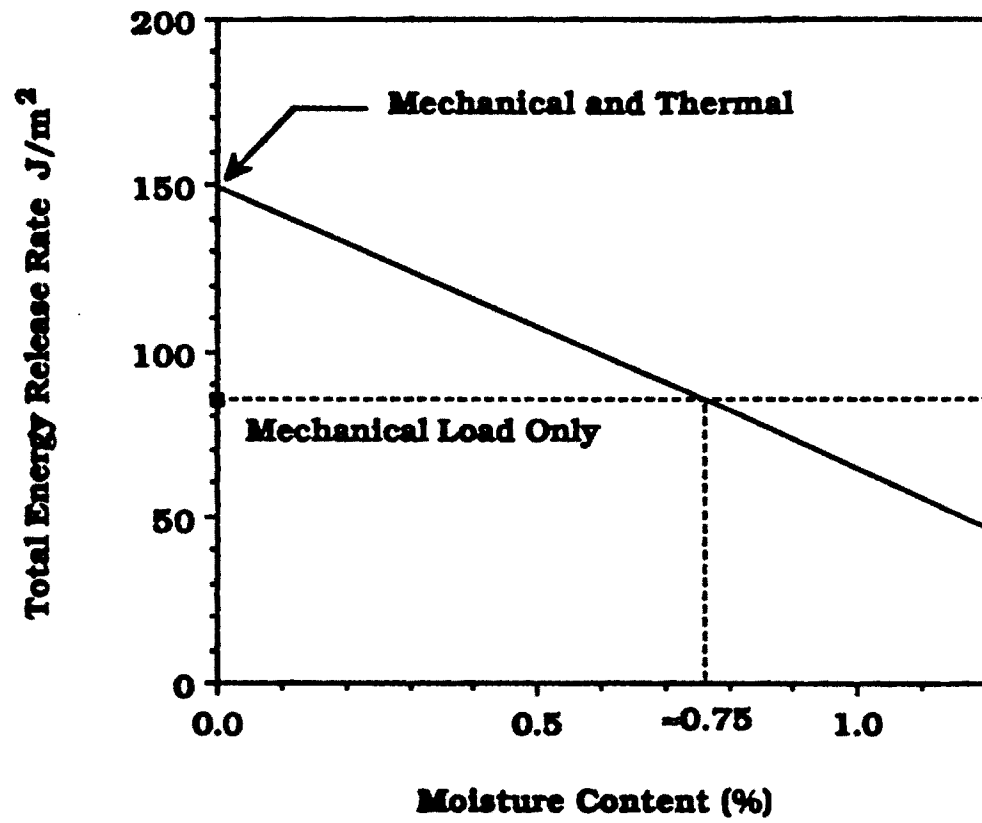


Figure 3.18: Total Energy Release Rate (Mid Plane Delamination) for $[\pm 25/90_2]_s$.

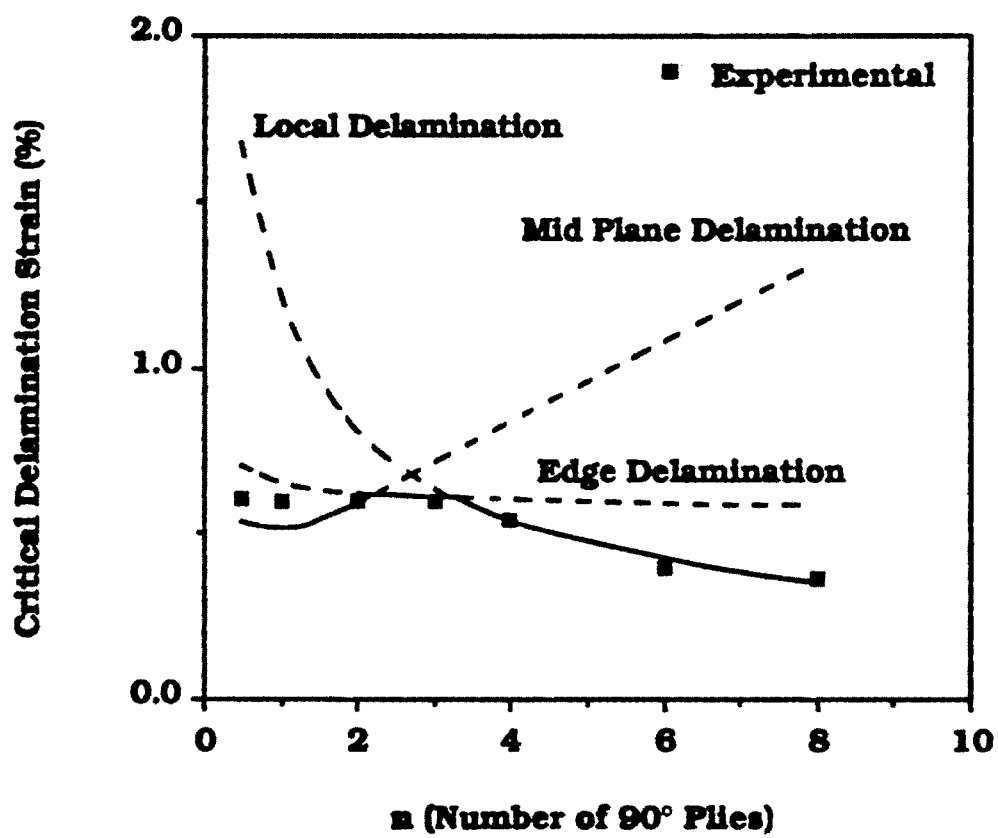


Figure 3.19: Critical Delamination Strain Variation

CHAPTER IV

THEORY OF ANISOTROPIC THIN-WALLED BEAMS

A variationally and asymptotically consistent theory is developed in order to derive the governing equations of anisotropic thin-walled beams with closed cross sections. The theory is based on an asymptotical analysis of two-dimensional shell theory. Closed-form expressions for the beam stiffness coefficients, stress and displacement fields are provided. The influence of material anisotropy on the displacement field is identified. A comparison of results obtained by other analytical developments is performed.

A review of previous work is presented first, this is followed by a detailed development of the theory. Finally an analytical comparison of the displacement field with previously developed theories is provided.

4.1 Review of Previous Work

Elastically tailored composite designs are being used to achieve favorable deformation modes under a given loading environment. Coupling between deformation modes such as extension-twist or bending-twist is created by an appropriate selection of fiber orientation, stacking sequence and materials. The fundamental mechanism producing elastic tailoring in composite beams is a result of their anisotropy. Several theories have been developed for the analysis of thin-walled anisotropic beams. An extensive review is provided in Ref. [26]. A number of issues relevant to the research undertaken in this thesis is highlighted in the following.

A basic element in the analytical modeling development is the derivation of the effective stiffness coefficients and governing equations which allows the three-dimensional ($3D$) state of stress to be recovered from a one-dimensional ($1D$) beam formulation. For isotropic or orthotropic materials this is a classical problem, which is considered in a number of text books such as Refs. [52]-[59].

For generally anisotropic materials, a description of the major approaches is provided in Refs. [24]-[49]. A number of $1D$ theories have been developed in Refs. [27], [28], [30], [42], [43], and [46]. A discussion of the displacement provided in these works is presented in the analytical comparison section of this chapter.

Missing from the review of Ref. [26] and all other current publications is the work of Reissner and Tsai in Ref. [27]. It presents an exact solution to the governing equilibrium, compatibility and constitutive relationships of shell theory. Closed as well as open cross-sections were considered. However, the authors left to the reader the derivation of the explicit expressions for the stiffness coefficients. This may be the reason for their work to have been overlooked. These expressions are important in identifying the parameters controlling the behavior and in performing parametric design studies. Furthermore, the explicit form of the displacement field helps evaluate and understand predictions of other analytical and numerical models.

A number of assumptions were adopted in Reissner and Tsai's development regarding material properties such as neglecting the coupling between in-plane strains and curvature which can be significant in anisotropic materials. It is important to assess the influence of these assumptions on the accuracy. This has been done in the present work by using an asymptotical expansion of the shell energy.

Mansfield and Sobey [28] and Libove [29] obtained the beam flexibilities relating the stretching, twisting and bending deformations to the applied axial load, torsional and bending moments for a special origin and axes orientation. Their analyses are

similar. Although they did not refer to the work of Reissner and Tsai [27], surprisingly when their analyses is applied to the special case outlined in Ref. [27], their stiffnesses coincide. However, one has to carry out details to show this fact. They adopted the assumptions of a negligible hoop stress resultant N_{θ} , and a membrane state in the thin-walled beam section. The special case in Ref. [27] refers to the one where classical assumption of neglecting shear, hoop stress and constant shear flow is adopted.

A pertinent element in the analytical modeling development is the inclusion of section warping. The major difference among the various theories lies in the methodology used to eliminate warping and consequently obtain a one-dimensional theory. The work of Refs. [30], [41], [42], [43], [44], [45], and [46] use the displacement field of thin-walled isotropic beams with shear deformation as the basis of their analytical development. In Refs. [42] and [46] the torsional rigidity is derived in terms of Classical Lamination Theory in what the author described as a “practical manner”. In Refs. [43] and [44] a shear correction factor has been introduced in order to reduce the overestimated bending stiffness. This factor was derived for the case of pure torsion by using the virtual work method and enforcing compatibility. While this approach shows an improvement in predictions, it is problem dependent. Another modification was proposed in the finite element formulation of Ref. [38]. This formulation aims at minimizing the error associated with the neglect of bending-related warping in the theory of Ref. [30]. This modification was based on shear stiffness correction factors determined by numerical comparison of results with an MSC/NASTRAN solution of cantilevered beam configurations loaded transversely at the free end.

This summary points to the necessity of addressing three fundamental issues. The first, is the effect of the material’s anisotropy on the displacement field and how to include its contribution in a consistent manner. No rigorous proof is provided to validate the assumed displacement fields in Refs. [30], [42], [43], [44], [45], and

[46] for beams made of anisotropic material as indicated by the various correction factors introduced. The second, is the significance of the shear deformation relative to the other contributions such as section related warping. The last is the accuracy of the membrane stress state assumption in thin-walled anisotropic beam sections. The present work addresses these issues by using an asymptotical expansion of the $2D$ shell energy to derive the $1D$ beam displacement field. As a consequence, the material's anisotropy is accounted for in a consistent manner and the deformation modes that have a lead contribution to the energy emerge naturally.

4.2 Coordinate Systems

Consider the slender thin-walled elastic cylindrical shell shown in Fig. 4.1. The length of the shell is denoted by L , its thickness by h , the radius of curvature of the middle surface by R and the maximum cross sectional dimension by d . It is assumed that

$$d \ll L \quad h \ll d \quad h \ll R \quad (4.1)$$

The shell is loaded by external forces applied to the lateral surfaces and at the ends. It is assumed that the variation of the external forces and material properties over distances of order d in the axial direction and over distances of order h in the circumferential direction, is small. The material is anisotropic and its properties can vary circumferentially and in the normal direction to the middle surface as well.

It is convenient to consider two coordinate systems for the description of the state of stress in thin-walled beams. The first one is the Cartesian system x, y and z shown in Fig. 4.1. The axial coordinate is x while y and z are associated with the beam cross section. The second coordinate system, is the curvilinear system x, s and ξ shown in Fig. 4.2. The circumferential coordinate s is measured along the tangent to the middle surface in a counter-clockwise direction whereas ξ is measured along

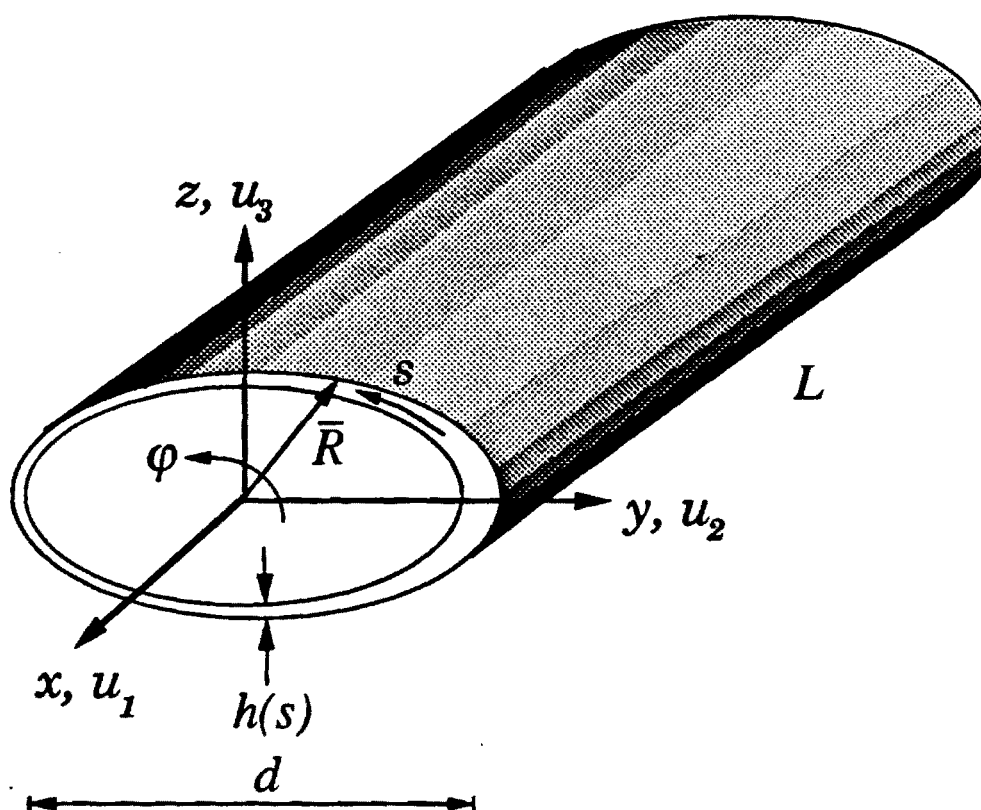


Figure 4.1: Cartesian Coordinate System

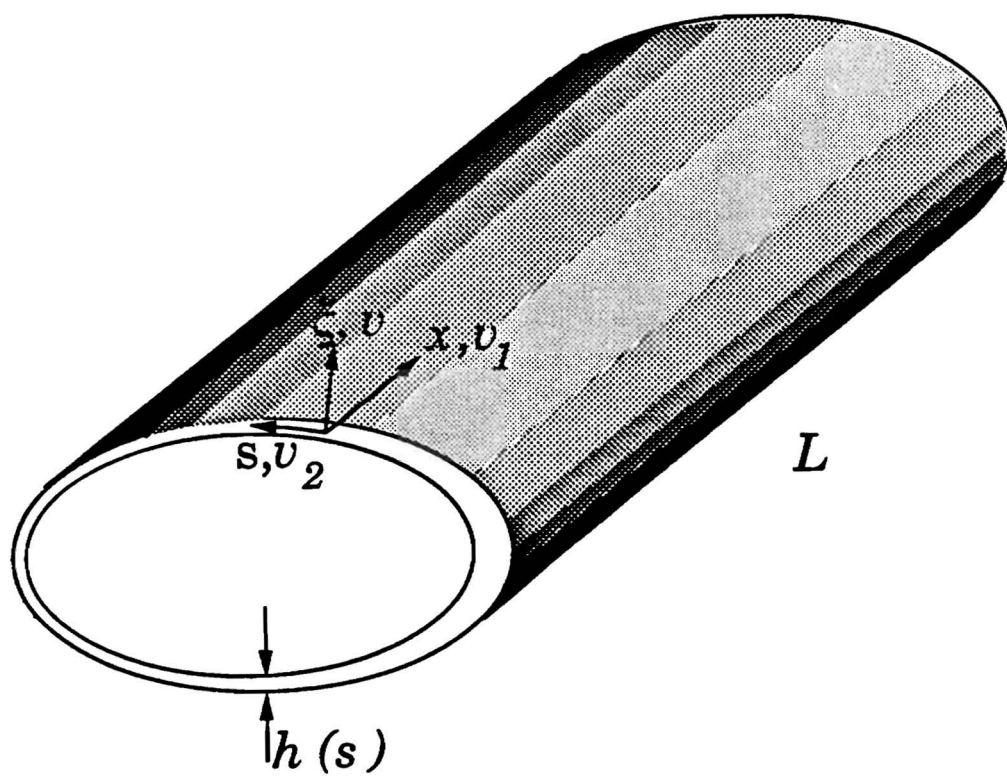


Figure 4.2: Curvilinear Coordinate System

the outward normal to the middle surface. A number of relationships have a simpler form when expressed in terms of curvilinear coordinates. A relationship between the two coordinate systems can be established as follows.

Define the position vector \vec{r} of the shell middle surface as

$$\vec{r} = x\vec{i}_x + y(s)\vec{i}_y + z(s)\vec{i}_z$$

where $\vec{i}_x, \vec{i}_y, \vec{i}_z$ are unit vectors associated with the cartesian coordinate system x, y and z . Equations $y = y(s)$ and $z = z(s)$ define the closed contour Γ in the y, z plane. The normal vector to the middle surface \vec{n} has two nonzero components

$$\vec{n} = n_y(s)\vec{i}_y + n_z(s)\vec{i}_z \quad (4.2)$$

The position vector \vec{R} of an arbitrary material point can be written in the form

$$\vec{R} = \vec{r} + \xi\vec{n} \quad (4.3)$$

Equations (4.2) and (4.3) establish the relations between the cartesian coordinates x, y, z and the curvilinear coordinates x, s, ξ . The coordinate ξ lies within the limits

$$-\frac{h(s)}{2} \leq \xi \leq \frac{h(s)}{2}$$

The shell thickness varies along the circumferential direction and is denoted by $h(s)$.

The tangent vector \vec{t} , the normal vector \vec{n} and the projection of the position vector \vec{r} on \vec{t} and \vec{n} are expressed in terms of the cartesian and curvilinear coordinates as

$$\begin{aligned} \vec{t} &= \frac{d\vec{r}}{ds} = \frac{dy}{ds}\vec{i}_y + \frac{dz}{ds}\vec{i}_z \\ \vec{n} &= \vec{t} \times \vec{i}_x = \frac{dz}{ds}\vec{i}_y - \frac{dy}{ds}\vec{i}_z \\ r_t &= \vec{r} \cdot \vec{t} = y\frac{dy}{ds} + z\frac{dz}{ds} \\ r_n &= \vec{r} \cdot \vec{n} = y\frac{dz}{ds} - z\frac{dy}{ds} \end{aligned} \quad (4.4)$$

An asymptotical analysis is used to model the slender thin-walled shell as a beam with effective stiffnesses. The method follows an iterative process. The displacement function corresponding to the zeroth-order approximation is obtained first by keeping the leading order terms in the energy functional. A set of successive corrections is added and the associated energy functional is determined. The process is terminated when the new cycle does not generate any additional terms of the same order in the energy functional.

4.3 Shell Energy Functional

Consider in a $3D$ space the prismatic shell in Fig. 4.2. A curvilinear frame x , s , and ξ is associated with the undeformed shell configuration. Values 1, 2 and 3 denoting x , s , and ξ , respectively are assigned to the curvilinear frame. Throughout this study, Latin superscripts (or subscripts) run from 1 to 3, while Greek superscripts (or subscripts) run from 1 to 2, unless otherwise stated.

The strain energy density of a $3D$ elastic body is a quadratic form of the strains

$$U = \frac{1}{2} E^{ijkl} \epsilon_{ij} \epsilon_{kl}$$

The material properties are expressed by the Hookean tensor E^{ijkl} . Following the classical shell formulation of [60], [61], and [62] the through-the-thickness stress components σ^{i3} are considerably smaller than the remaining components $\sigma^{\alpha\beta}$. Therefore we can set

$$\sigma^{i3} = 0 \tag{4.5}$$

so that the strains can be written as

$$\epsilon_{\alpha\beta} = \gamma_{\alpha\beta} + \xi \rho_{\alpha\beta} \tag{4.6}$$

where $\gamma_{\alpha\beta}$ and $\rho_{\alpha\beta}$ represent the in-plane strain components and the change in the shell middle surface curvatures, respectively. For a cylindrical shell these are related to the displacement variables by

$$\begin{aligned}
 \gamma_{11} &= \frac{\partial v_1}{\partial x} \\
 2\gamma_{12} &= \frac{\partial v_1}{\partial s} + \frac{\partial v_2}{\partial x} \\
 \gamma_{22} &= \frac{\partial v_2}{\partial s} + \frac{v}{R} \\
 \rho_{11} &= \frac{\partial^2 v}{\partial x^2} \\
 \rho_{12} &= \frac{\partial^2 v}{\partial s \partial x} + \frac{1}{4R} \left(\frac{\partial v_1}{\partial s} - 3 \frac{\partial v_2}{\partial x} \right) \\
 \rho_{22} &= \frac{\partial^2 v}{\partial s^2} - \frac{\partial}{\partial s} \left(\frac{v_2}{R} \right)
 \end{aligned} \tag{4.7}$$

where v_1 , v_2 and v represent the middle surface displacements in the axial, tangential and normal directions, respectively as shown in Fig. 4.2. These are related to the displacement components in Cartesian coordinates by

$$\begin{aligned}
 v_1 &= u_1 \\
 v_2 &= u_2 \frac{dy}{ds} + u_3 \frac{dz}{ds} \\
 v &= u_2 \frac{dz}{ds} - u_3 \frac{dy}{ds}
 \end{aligned} \tag{4.8}$$

where u_1 , u_2 and u_3 denote the displacements along the x , y and z coordinates, respectively.

The energy density of the 2D elastic body is obtained in terms of $\gamma_{\alpha\beta}$ and $\rho_{\alpha\beta}$ by the following procedure.

The 3D energy is first minimized with respect to ϵ_{i3} . This is equivalent to satisfying Eq. (4.5). The result is

$$\hat{U} = \min_{\epsilon_{i3}} U = \frac{1}{2} D^{\alpha\beta\gamma\delta} \epsilon_{\alpha\beta} \epsilon_{\gamma\delta} \tag{4.9}$$

where $D^{\alpha\beta\gamma\delta}$ represent the component of the 2D Young's modulus. The expressions for $D^{\alpha\beta\gamma\delta}$ are given in terms of $E^{\alpha\beta\gamma\delta}$ by

$$D^{\alpha\beta\gamma\delta} = E^{\alpha\beta\gamma\delta} - \frac{E^{\alpha\beta 33} E^{\gamma\delta 33}}{E^{3333}} - H_{\mu\lambda} G^{\alpha\beta\mu} G^{\gamma\delta\lambda} \quad (4.10)$$

where

$$G^{\alpha\beta\mu} = E^{\alpha\beta\mu 3} - \frac{E^{\alpha\beta 33} E^{\mu 333}}{E^{3333}}$$

and $H_{\mu\lambda}$ are components of the inverse of the 2D matrix $\|E^{\mu 3\lambda 3} - \frac{E^{\mu 333} E^{\lambda 333}}{E^{3333}}\|$. The expression for $D^{\alpha\beta\gamma\delta}$ in terms of familiar Classical Lamination Theory (CLT) parameters is provided in Eqs. (4.43) and (4.44).

The strain $\varepsilon_{\alpha\beta}$ from Eq. (4.6) is substituted into Eq. (4.9). After integration of the result over the thickness ξ one obtains the energy of the shell Φ per unit middle surface area

$$2\Phi = h C^{\alpha\beta\gamma\delta} \gamma_{\alpha\beta} \gamma_{\gamma\delta} + h^2 C_1^{\alpha\beta\gamma\delta} \gamma_{\alpha\beta} \rho_{\gamma\delta} + \frac{h^3}{12} C_2^{\alpha\beta\gamma\delta} \rho_{\alpha\beta} \rho_{\gamma\delta} \quad (4.11)$$

where

$$\begin{aligned} C^{\alpha\beta\gamma\delta} &= \frac{1}{h} \langle D^{\alpha\beta\gamma\delta} \rangle \\ C_1^{\alpha\beta\gamma\delta} &= \frac{2}{h^2} \langle D^{\alpha\beta\gamma\delta} \xi \rangle \\ C_2^{\alpha\beta\gamma\delta} &= \frac{12}{h^3} \langle D^{\alpha\beta\gamma\delta} \xi^2 \rangle \end{aligned}$$

and a function of ξ , say $\alpha(\xi)$, between pointed brackets is defined as an integral through the thickness, viz.,

$$\langle \alpha \rangle = \int_{-h(s)/2}^{+h(s)/2} \alpha(\xi) d\xi \quad (4.12)$$

The first term in Eq. (4.11) represents the in-plane contribution, the second the coupling between in-plane and bending, and the third the bending contribution to the shell energy.

For an applied external loading P_i , the displacement field u_i determining the deformed state are the stationary points of the energy functional

$$I = \int \Phi dx ds - \int P_i u_i dx ds \quad (4.13)$$

4.4 Asymptotical Analysis of the Shell Energy Functional

4.4.1 Zeroth-Order Approximation

Let Δ and E be the order of displacements and stiffness coefficients $C^{\alpha\beta\gamma\delta}$, respectively. Assume that the order of the external forces is

$$P \sim O\left(\frac{E\Delta h}{L^2}\right) \quad (4.14)$$

This assumption is shown later to be consistent with the equilibrium equations. An alternative would be to assume the order of the external force as some quantity P and derive the order of the displacements as PL^2/Eh from an asymptotical analysis of the energy functional.

For a thin-walled slender beam whose dimensions satisfy Eq. (4.1) the rate of change of the displacements along the axial direction is much smaller than their rate of change along the circumferential direction. That is, for each displacement component

$$\left|\frac{\partial v_i}{\partial x}\right| \ll \left|\frac{\partial v_i}{\partial s}\right| \quad (4.15)$$

Using Eq. (4.7) and assuming that d is smaller or of the same order as R , the order of magnitude of the in-plane strains and curvatures is

$$\begin{aligned} \gamma_{11} &\sim O\left(\frac{\Delta}{L}\right) \\ 2\gamma_{12} &\sim O\left(\frac{\Delta}{d}\right) \end{aligned}$$

$$\gamma_{22} \sim O\left(\frac{\Delta}{d}\right)$$

$$\rho_{11} \sim O\left(\frac{\Delta}{L^2}\right)$$

$$\rho_{12} \sim O\left(\frac{\Delta}{d^2}\right)$$

$$\rho_{22} \sim O\left(\frac{\Delta}{d^2}\right)$$

Since γ_{11} and ρ_{11} are much smaller than γ_{12} , γ_{22} and ρ_{12} , ρ_{22} , respectively, their contribution to the elastic energy is neglected.

The order of magnitude of the shell energy per unit area and the work done by external forces is

$$\Phi \sim O\left(\frac{E\Delta^2 h}{d^2}\right)$$

$$P_i u_i \sim O\left(\frac{E\Delta^2 h}{L^2}\right)$$

Since $P_i u_i \ll \Phi$, the contribution of external forces is neglected. Therefore the energy functional takes the form

$$\begin{aligned} 2I = \int_0^L \int \{ & 4hC_1^{1212}(\gamma_{12})^2 + 4hC_1^{1222}\gamma_{12}\gamma_{22} + hC_1^{2222}(\gamma_{22})^2 + 4h^2C_1^{1212}\gamma_{12}\rho_{12} \\ & + 2h^2C_1^{1222}\gamma_{12}\rho_{22} + 2h^2C_1^{2212}\gamma_{22}\rho_{12} + h^2C_1^{2222}\gamma_{22}\rho_{22} \\ & + \frac{h^3}{3}C_2^{1212}(\rho_{12})^2 + \frac{h^3}{3}C_2^{1222}\rho_{12}\rho_{22} + \frac{h^3}{12}C_2^{2222}(\rho_{22})^2 \} ds dx \end{aligned} \quad (4.16)$$

Using Eq. (4.15), the strain-displacement relationships in Eq. (4.7) can be written as

$$\begin{aligned} 2\gamma_{12} &= \frac{\partial v_1}{\partial s} \\ \gamma_{22} &= \frac{\partial v_2}{\partial s} + \frac{v}{R} \\ \rho_{12} &= \frac{1}{4R} \frac{\partial v_1}{\partial s} \\ \rho_{22} &= \frac{\partial^2 v}{\partial s^2} - \frac{\partial}{\partial s} \left(\frac{v_2}{R} \right) \end{aligned} \quad (4.17)$$

The integrand in Eq. (4.16) is a positive quadratic form, therefore the minimum of the functional is reached by functions v , v_1 , and v_2 for which $\gamma_{12} = \gamma_{22} = \rho_{12} = \rho_{22} = 0$. From Eq. (4.17) this corresponds to

$$\frac{\partial v_1}{\partial s} = 0 \quad (4.18)$$

$$\frac{\partial v_2}{\partial s} + \frac{v}{R} = 0 \quad (4.19)$$

$$\frac{\partial^2 v}{\partial s^2} - \frac{\partial}{\partial s} \left(\frac{v_2}{R} \right) = 0 \quad (4.20)$$

The function v in Eqs. (4.19) and (4.20) should be single valued, i. e.

$$\overline{\left(\frac{\partial v}{\partial s} \right)} \equiv \frac{1}{l} \oint \frac{\partial v}{\partial s} ds = 0 \quad (4.21)$$

The bar in (4.21) and in the subsequent derivation denotes averaging along the closed contour Γ whose length is denoted by l in Eq. (4.21).

Equation (4.18) implies that v_1 is a function of x only, i.e.

$$v_1 = U_1(x) \quad (4.22)$$

Integrate Eq. (4.20) to get

$$\frac{\partial v}{\partial s} - \frac{v_2}{R} = -\varphi(x) \quad (4.23)$$

where $\varphi(x)$ is an arbitrary function which is shown later to represent the cross-sectional twist. From Eq. (4.21) and (4.23), one obtains the relation between $\varphi(x)$ and v_2 .

$$\varphi(x) = \overline{\left(\frac{v_2}{R} \right)}$$

Substitute v from Eq. (4.19) into Eq. (4.23), to get the following second-order differential equation for v_2

$$\frac{\partial}{\partial s} \left(R \frac{\partial v_2}{\partial s} \right) + \frac{v_2}{R} = \varphi(x) \quad (4.24)$$

To solve this equation, one has to recall the relations between the radius of curvature R and the components $y(s)$ and $z(s)$ of the position vector associated with contour Γ

$$\begin{aligned}\frac{d^2 z}{ds^2} &= \frac{1}{R} \frac{dy}{ds} \\ \frac{d^2 y}{ds^2} &= -\frac{1}{R} \frac{dz}{ds}\end{aligned}\quad (4.25)$$

It follows from Eqs. (4.25) and (4.4) that $\frac{dy}{ds}$ and $\frac{dz}{ds}$ are solutions of the homogeneous form of Eq. (4.24) and $v_2 = \varphi(x)r_n$ is its particular solution. The general solution is therefore given by

$$v_2 = U_2(x) \frac{dy}{ds} + U_3(x) \frac{dz}{ds} + \varphi(x)r_n \quad (4.26)$$

where U_2 and U_3 are arbitrary functions of x . Substitute from Eq. (4.26) into Eq. (4.19) to get

$$v = U_2(x) \frac{dz}{ds} - U_3(x) \frac{dy}{ds} - \varphi(x)r_t \quad (4.27)$$

Eqs. (4.22), (4.26) and (4.27) represent the curvilinear displacement field that minimizes the zeroth-order approximation of the shell energy. Using Eq. (4.8) the curvilinear displacement field is written in Cartesian coordinates as

$$\begin{aligned}u_1 &= U_1(x) \\ u_2 &= U_2(x) - z\varphi(x) \\ u_3 &= U_3(x) + y\varphi(x)\end{aligned}\quad (4.28)$$

The variables $U_1(x)$, $U_2(x)$ and $U_3(x)$ represent the average cross-sectional translation while $\varphi(x)$ the cross-sectional rotation normally referred to in beam theory as the torsional rotation. This displacement field corresponds to the zeroth-order approximation and does not include bending behavior. For a centroidal coordinate system $U_1(x)$, $U_2(x)$, $U_3(x)$ and $\varphi(x)$ can be expressed as

$$U_1(x) = \bar{u}_1$$

$$\begin{aligned}
U_2(x) &= \bar{u}_2 \\
U_3(x) &= \bar{u}_3 \\
\varphi(x) &= \frac{(\bar{u} \cdot \bar{t})}{\bar{r}_n}
\end{aligned} \tag{4.29}$$

4.4.2 First-Order Approximation

A first-order approximation can be constructed by rewriting the displacement field in Eqs. (4.22), (4.26) and (4.27) in the form

$$\begin{aligned}
v_1 &= U_1(x) + w_1(s, x) \\
v_2 &= U_2(x) \frac{dy}{ds} + U_3(x) \frac{dz}{ds} + \varphi(x) r_n + w_2(s, x) \\
v &= U_2(x) \frac{dz}{ds} - U_3(x) \frac{dy}{ds} - \varphi(x) r_t + w(s, x)
\end{aligned} \tag{4.30}$$

where w_1, w_2 and w can be regarded as correction functions to be determined based on their contributions to the energy functional.

Substitute Eq. (4.30) into (4.7) to obtain the strains and curvatures in terms of the displacement corrections

$$\begin{aligned}
\gamma_{11} &= \overset{\circ}{\gamma}_{11} + \frac{\partial w_1}{\partial x} \\
2\gamma_{12} &= 2\overset{\circ}{\gamma}_{12} + \frac{\partial w_2}{\partial x} + 2\hat{\gamma}_{12} \quad , \quad 2\hat{\gamma}_{12} = \frac{\partial w_1}{\partial s} \\
\gamma_{22} &= \overset{\circ}{\gamma}_{22} + \hat{\gamma}_{22} \quad , \quad \hat{\gamma}_{22} = \frac{\partial w_2}{\partial s} + \frac{w}{R} \\
\rho_{11} &= \overset{\circ}{\rho}_{11} + \frac{\partial^2 w}{\partial x^2} \\
\rho_{12} &= \overset{\circ}{\rho}_{12} + \frac{\partial^2 w}{\partial s \partial x} - \frac{3}{4R} \frac{\partial w_2}{\partial x} + \hat{\rho}_{12} \quad , \quad \hat{\rho}_{12} = \frac{1}{4R} \frac{\partial w_1}{\partial s} \\
\rho_{22} &= \overset{\circ}{\rho}_{22} + \hat{\rho}_{22} \quad , \quad \hat{\rho}_{22} = \frac{\partial^2 w}{\partial s^2} - \frac{\partial}{\partial s} \left(\frac{w_2}{R} \right)
\end{aligned} \tag{4.31}$$

where $\gamma^\circ_{\alpha\beta}$ and $\rho^\circ_{\alpha\beta}$ are the strains and curvatures corresponding to the zeroth-order approximation. These are expressed as

$$\begin{aligned}
\hat{\gamma}_{11} &= U_1'(x) \sim O\left(\frac{\Delta}{L}\right) \\
2\hat{\gamma}_{12} &= U_2'(x)\frac{dy}{ds} + U_3'(x)\frac{dz}{ds} + \varphi'(x)r_n \sim O\left(\frac{\Delta}{L}\right) \\
\hat{\gamma}_{22} &= 0 \\
\hat{\rho}_{11} &= U_2''(x)\frac{dz}{ds} - U_3''(x)\frac{dy}{ds} - \varphi''(x)r_t \sim O\left(\frac{\Delta}{L^2}\right) \\
\hat{\rho}_{12} &= \frac{1}{4R} \left[U_2'(x)\frac{dy}{ds} + U_3'(x)\frac{dz}{ds} + \varphi'(x)r_n \right] - \varphi'(x) \sim O\left(\frac{\Delta}{dL}\right) \\
\hat{\rho}_{22} &= 0
\end{aligned} \tag{4.32}$$

The prime in Eq. (4.32) denotes differentiation with respect to x . Among the new terms introduced by the function w_i , the leading ones are denoted by superscript $\hat{\cdot}$ in Eq. (4.31). The order of w_i is $(\frac{\Delta d}{L})$, this is derived from Eqs. (4.31) and (4.32) where it is seen that the leading terms $2\hat{\gamma}_{12}$ and $\hat{\rho}_{12}$ are of the same order of magnitude as $2\gamma^\circ_{12}$ and ρ°_{12} , respectively, i.e.

$$\begin{aligned}
2\hat{\gamma}_{12} &= \frac{\partial w_1}{\partial s} \sim O\left(\frac{\Delta}{L}\right) \\
\hat{\rho}_{12} &= \frac{1}{4R} \frac{\partial w_1}{\partial s} \sim O\left(\frac{\Delta}{dL}\right)
\end{aligned} \tag{4.33}$$

Therefore,

$$w_1 \sim O\left(\frac{\Delta d}{L}\right) \tag{4.34}$$

An alternative approach is to assume the order of w_i as $(\frac{\Delta d}{L})$ and verify this assumption, as shown later, once w_i is determined. The order of magnitude of the remaining leading terms in Eq. (4.31) is as follows

$$\hat{\gamma}_{22} \sim O\left(\frac{\Delta}{L}\right)$$

$$\hat{\rho}_{22} \sim O\left(\frac{\Delta}{dL}\right) \quad (4.35)$$

The energy functional can be represented by $\Phi(\gamma_{11}, 2\gamma_{12}, \gamma_{22}, \rho_{11}, \rho_{12}, \rho_{22})$. By keeping the strains and curvature associated with the zeroth-order approximation and the leading terms contribution over the other terms (i.e., by dropping the terms $\frac{\partial w_1}{\partial x}$, $\frac{\partial w_2}{\partial x}$, $\frac{\partial^2 w}{\partial x^2}$, and $\frac{\partial^2 w}{\partial s \partial x} - \frac{1}{4R} \frac{\partial w_2}{\partial x}$ in Eq. (4.31)) the energy function can be written as

$$\Phi(\overset{\circ}{\gamma}_{11}, 2\overset{\circ}{\gamma}_{12} + 2\hat{\gamma}_{12}, 0 + \hat{\gamma}_{22}, \overset{\circ}{\rho}_{11}, \overset{\circ}{\rho}_{12} + \hat{\rho}_{12}, 0 + \hat{\rho}_{22})$$

The interaction terms associated with ρ°_{11} and ρ°_{12} , namely

$$h\overset{\circ}{\rho}_{11}\hat{\gamma}_{12}, h\overset{\circ}{\rho}_{11}\hat{\gamma}_{22}, h^2\overset{\circ}{\rho}_{11}\hat{\rho}_{12}, h^2\overset{\circ}{\rho}_{11}\hat{\rho}_{22}$$

$$h\overset{\circ}{\rho}_{12}\hat{\gamma}_{12}, h\overset{\circ}{\rho}_{12}\hat{\gamma}_{22}, h^2\overset{\circ}{\rho}_{12}\hat{\rho}_{12}, h^2\overset{\circ}{\rho}_{12}\hat{\rho}_{22}$$

are of order $\left(\frac{\Delta^2 h}{L^2 d}\right)$ or smaller. They are neglected in comparison with the following terms

$$\overset{\circ}{\gamma}_{11}\hat{\gamma}_{12}, \overset{\circ}{\gamma}_{11}\hat{\gamma}_{22}, \overset{\circ}{\gamma}_{12}\hat{\gamma}_{12}, \overset{\circ}{\gamma}_{12}\hat{\gamma}_{22} \quad (4.36)$$

of order $\left(\frac{\Delta^2}{L^2}\right)$. Similarly, the contribution of the work done by external forces, $P_i w_i$, is neglected since its order is $\left(Eh \frac{\Delta^2}{L^2} \left(\frac{d}{L}\right)\right)$ in comparison with the order of the remaining terms in the energy functional $\left(Eh \frac{\Delta^2}{L^2}\right)$. Therefore in order to determine the functions w_i one has to minimize the functional

$$\oint \Phi(\overset{\circ}{\gamma}_{11}, 2\overset{\circ}{\gamma}_{12} + 2\hat{\gamma}_{12}, \hat{\gamma}_{22}, 0, \hat{\rho}_{12}, \hat{\rho}_{22}) ds$$

If the rigid body motion is suppressed the solution is unique. The terms $\hat{\rho}_{12}$, $\hat{\rho}_{22}$ are essential to the uniqueness of the solution; however, their contribution to the energy, expressed by the interaction terms

$$h\hat{\rho}_{12}\overset{\circ}{\gamma}_{11}, h\hat{\rho}_{12}\overset{\circ}{\gamma}_{12}, h\hat{\rho}_{22}\overset{\circ}{\gamma}_{11}, h\hat{\rho}_{22}\overset{\circ}{\gamma}_{12}$$

is of order $\left(\frac{\Delta^2}{L^2}\left(\frac{h}{d}\right)\right)$ or smaller, and is consequently dropped in comparison with the membrane contribution listed in (4.36). This aspect is discussed by Berdichevsky and Misiura [63], with regard to the accuracy of classical shell theory. Therefore, the shell energy can be represented by

$$I = \int_0^L \oint \Phi(\overset{\circ}{\gamma}_{11}, 2\overset{\circ}{\gamma}_{12} + 2\hat{\gamma}_{12}, \hat{\gamma}_{22}, 0, 0, 0) ds dx \quad (4.37)$$

It is worth noting that the bending contribution does not appear in Eq. (4.37). That is, to the first-order approximation the shell energy corresponds to a membrane state.

The first variation of the energy functional is

$$\delta I = \int_0^L \oint \left\{ \frac{\partial \Phi}{\partial (2\gamma_{12})} \delta \left(\frac{\partial w_1}{\partial s} \right) + \frac{\partial \Phi}{\partial \gamma_{22}} \delta \left(\frac{\partial w_2}{\partial s} + \frac{w}{R} \right) \right\} ds dx \quad (4.38)$$

Recall that $\frac{\partial \Phi}{\partial (2\gamma_{12})} = N_{12}$ and $\frac{\partial \Phi}{\partial \gamma_{22}} = N_{22}$, Eq. (4.38) takes the form

$$\delta I = \int_0^L \oint \left\{ N_{12} \frac{\partial(\delta w_1)}{\partial s} + N_{22} \left(\frac{\partial(\delta w_2)}{\partial s} + \frac{1}{R} \delta w \right) \right\} ds dx$$

Set the first variation of the energy to zero, to obtain the following

$$\begin{aligned} \frac{\partial N_{12}}{\partial s} &= 0 \\ \frac{\partial N_{22}}{\partial s} &= 0 \\ \frac{N_{22}}{R} &= 0 \end{aligned}$$

which result in

$$N_{12} = \text{constant} \quad (4.39)$$

and

$$N_{22} = 0 \quad (4.40)$$

This is similar to the classical solution of constant shear flow and vanishing hoop stress resultant. By setting N_{22} to zero the energy density is expressed in terms of

γ_{11} and γ_{12} only

$$2\Phi_1 = \min_{\gamma_{22}} 2\Phi = \min_{\gamma_{22}} h C^{\alpha\beta\gamma\delta} \gamma_{\alpha\beta} \gamma_{\gamma\delta} = A(s)(\gamma_{11})^2 + 2B(s)\gamma_{11}\gamma_{12} + C(s)(\gamma_{12})^2 \quad (4.41)$$

The variables $A(s)$, $B(s)$ and $C(s)$ represent the axial, coupling and shear stiffnesses, respectively. They are defined in terms of the $D^{\alpha\beta\gamma\delta}$ as follows

$$\begin{aligned} A(s) &= \langle D^{1111} \rangle - \frac{(\langle D^{1122} \rangle)^2}{\langle D^{2222} \rangle} \sim O(Eh) \\ B(s) &= 2 \left[\langle D^{1112} \rangle - \frac{\langle D^{1122} \rangle \langle D^{1222} \rangle}{\langle D^{2222} \rangle} \right] \sim O(Eh) \\ C(s) &= 4 \left[\langle D^{1212} \rangle - \frac{(\langle D^{1222} \rangle)^2}{\langle D^{2222} \rangle} \right] \sim O(Eh) \end{aligned} \quad (4.42)$$

where the $2D$ Young's modulus $D^{\alpha\beta\gamma\delta}$ are expressed in terms of the Hookean tensor $E^{\alpha\beta\gamma\delta}$ in Eq. (4.10). The pointed brackets denote integration over the thickness as defined in Eq. (4.12).

For convenience, $D^{\alpha\beta\gamma\delta}$ is given in matrix form as

$$[D] = [Q^1] - 2 [Q^2] [Q^3]^{-1} [Q^4] + [Q^4]^T [Q^3]^{-1} [Q^4] \quad (4.43)$$

where

$$\begin{aligned} [D] &= \begin{bmatrix} D^{1111} & D^{1122} & D^{1112} \\ D^{1122} & D^{2222} & D^{1222} \\ D^{1112} & D^{1222} & D^{1212} \end{bmatrix} \\ [Q^1] &= \begin{bmatrix} \bar{Q}_{11} & \bar{Q}_{12} & \bar{Q}_{16} \\ \bar{Q}_{12} & \bar{Q}_{22} & \bar{Q}_{26} \\ \bar{Q}_{16} & \bar{Q}_{26} & \bar{Q}_{66} \end{bmatrix} \\ [Q^2] &= \begin{bmatrix} \bar{Q}_{13} & \bar{Q}_{15} & \bar{Q}_{14} \\ \bar{Q}_{23} & \bar{Q}_{25} & \bar{Q}_{24} \\ \bar{Q}_{36} & \bar{Q}_{56} & \bar{Q}_{46} \end{bmatrix} \\ [Q^3] &= \begin{bmatrix} \bar{Q}_{33} & \bar{Q}_{35} & \bar{Q}_{36} \\ \bar{Q}_{35} & \bar{Q}_{55} & \bar{Q}_{45} \\ \bar{Q}_{36} & \bar{Q}_{45} & \bar{Q}_{44} \end{bmatrix} \end{aligned} \quad (4.44)$$

$$[Q^4] = \begin{bmatrix} \bar{Q}_{13} & \bar{Q}_{23} & \bar{Q}_{36} \\ \bar{Q}_{15} & \bar{Q}_{25} & \bar{Q}_{56} \\ \bar{Q}_{14} & \bar{Q}_{24} & \bar{Q}_{46} \end{bmatrix}$$

The indices adopted in Eq. (4.44) follow the convention of Ref. [50]. The bars over the reduced stiffness coefficients Q_{ij} of Classical Laminate Theory, Refs. [19] and [50], indicate that these quantities are to be obtained through appropriate coordinate transformations.

Equation (4.41) indicates that, to the first-order, the energy density function is independent of functions w_2 and w . That is, the in-plane warping contribution to the shell energy is negligible. The function w_1 however, can be determined from Eq. (4.39) and (4.41) and by enforcing the condition on w_1 to be single valued as follows

$$N_{12} = \frac{\partial \Phi_1}{\partial (2\gamma_{12})} = \frac{1}{2} (B(s)\gamma_{11} + C(s)\gamma_{12}) = \text{constant} \quad (4.45)$$

Substitute from Eqs. (4.31) and (4.32) into (4.45) to get

$$\begin{aligned} & \frac{1}{2} B \left(U_1'(x) + \frac{\partial w_1}{\partial x} \right) \\ & + \frac{1}{4} C \left(U_2'(x) \frac{dy}{ds} + U_3'(x) \frac{dz}{dx} + \varphi'(x) r_n(s) + \frac{\partial w_2}{\partial x} + \frac{\partial w_1}{\partial s} \right) = \text{constant} \end{aligned} \quad (4.46)$$

Following the relations in Eq. (4.15), the term $\frac{\partial w_2}{\partial x}$ is neglected in comparison with $\frac{\partial w_1}{\partial s}$. Moreover, the term $\frac{1}{2} B \frac{\partial w_1}{\partial x}$ in Eq. (4.46) may be neglected in comparison with $\frac{1}{4} C \frac{\partial w_1}{\partial s}$. This is possible, if $|B|$ is less or of the same order of magnitude as C . For the case when $|B| \gg C$ additional investigation is needed. Since the elastic energy is positive definite, $B^2 \leq AC$, and B could be greater than C only if $A \gg C$. In practical laminated composite designs $|B| < C$ as the shear stiffness is greater than the extension-shear coupling. Therefore, Eq. (4.46) becomes

$$\frac{1}{2} B U_1'(x) + \frac{1}{4} C \left(U_2'(x) \frac{dy}{ds} + U_3'(x) \frac{dz}{dx} + \varphi'(x) r_n(s) + \frac{\partial w_1}{\partial s} \right) = \text{constant} \quad (4.47)$$

Equation (4.47) is a first order ordinary differential equation in w_1 . The value of the constant in the right hand side of (4.47) can be found from the single value condition of the function w_1 :

$$\overline{\left(\frac{\partial w_1}{\partial s}\right)} \equiv \frac{1}{l} \oint \frac{\partial w_1}{\partial s} ds = 0 \quad (4.48)$$

The solution of Eq. (4.47) is determined within an arbitrary function of x . This function can be specified from various conditions. Each one yields a specific interpretation of the variable U_1 . For example if $\overline{w_1} = 0$ the variable $U_1 = \overline{v_1}$ according to Eq. (4.30). The choice of these conditions does not affect the final form of the 1D beam theory and therefore will not be specified in this formulation. The result is the following simple analytical solution of Eq. (4.47)

$$w_1 = -yU_2'(x) - zU_3'(x) + G(s)\varphi'(x) + g_1(s)U_1'(x) \quad (4.49)$$

where

$$\begin{aligned} G(s) &= \int_0^s \left[\frac{2A_\epsilon}{l\bar{c}} c(\tau) - r_n(\tau) \right] d\tau \sim O(d^2) \\ g_1(s) &= \int_0^s \left[b(\tau) - \frac{\bar{b}}{\bar{c}} c(\tau) \right] d\tau \sim O(d) \\ b(s) &= -2\frac{B(s)}{C(s)} \quad c(s) = \frac{1}{C(s)} \quad A_\epsilon = \frac{l}{2r_n} \end{aligned} \quad (4.50)$$

The area enclosed by contour Γ is denoted by A_ϵ in Eq. (4.50). It is seen from expression (4.49) that w_1 is of order $\left(\frac{\Delta d}{L}\right)$ and relation (4.34) is justified. The displacement field corresponding to the first correction is obtained by substituting Eq. (4.49) into Eq. (4.30) and dropping w_2 and w since their contribution to the shell energy is negligible compared to w_1 . The result referred to as the first-order approximation is given by

$$\begin{aligned} v_1 &= U_1(x) - y(s)U_2'(x) - z(s)U_3'(x) + G(s)\varphi'(x) + g_1(s)U_1'(x) \\ v_2 &= U_2(x)\frac{dy}{ds} + U_3(x)\frac{dz}{ds} + \varphi(x)r_n \end{aligned} \quad (4.51)$$

$$v = U_2(x) \frac{dz}{ds} - U_3(x) \frac{dy}{ds} - \varphi(x)r_t$$

4.4.3 Second-Order Approximation

Following a similar procedure to the one described in section 4.4.2, a second-order approximation can be constructed by rewriting the displacement field in Eq. (4.51) in the form

$$\begin{aligned} v_1 &= U_1(x) - yU_2'(x) - zU_3'(x) + G(s)\varphi'(x) + g_1(s)U_1'(x) + \bar{w}_1(s, x) \\ v_2 &= U_2(x) \frac{dy}{ds} + U_3(x) \frac{dz}{ds} + \varphi(x)r_n + \bar{w}_2(s, x) \\ v &= U_2(x) \frac{dz}{ds} - U_3(x) \frac{dy}{ds} - \varphi(x)r_t + \bar{w}(s, x) \end{aligned} \quad (4.52)$$

where \bar{w}_1 , \bar{w}_2 and \bar{w} can be regarded as correction functions to be determined based on their contributions to the energy functional.

Substitute Eq. (4.52) into (4.7) to obtain the strains and curvatures in terms of the displacement corrections

$$\begin{aligned} \gamma_{11} &= \check{\gamma}_{11} + \frac{\partial \bar{w}_1}{\partial x} \\ 2\gamma_{12} &= 2\check{\gamma}_{12} + \frac{\partial \bar{w}_2}{\partial x} + 2\hat{\gamma}_{12} \quad , \quad 2\hat{\gamma}_{12} = \frac{\partial \bar{w}_1}{\partial s} \\ \gamma_{22} &= \check{\gamma}_{22} + \hat{\gamma}_{22} \quad , \quad \hat{\gamma}_{22} = \frac{\partial \bar{w}_2}{\partial s} + \frac{\bar{w}}{R} \\ \rho_{11} &= \check{\rho}_{11} + \frac{\partial^2 \bar{w}}{\partial x^2} \\ \rho_{12} &= \check{\rho}_{12} + \frac{\partial^2 \bar{w}}{\partial s \partial x} - \frac{3}{4R} \frac{\partial \bar{w}_2}{\partial x} + \hat{\rho}_{12} \quad , \quad \hat{\rho}_{12} = \frac{1}{4R} \frac{\partial \bar{w}_1}{\partial s} \\ \rho_{22} &= \check{\rho}_{22} + \hat{\rho}_{22} \quad , \quad \hat{\rho}_{22} = \frac{\partial^2 \bar{w}}{\partial s^2} - \frac{\partial}{\partial s} \left(\frac{\bar{w}_2}{R} \right) \end{aligned} \quad (4.53)$$

where $\check{\gamma}_{\alpha\beta}$ and $\check{\rho}_{\alpha\beta}$ are the strains and curvatures corresponding to the first-order approximation. These are expressed as

$$\check{\gamma}_{11} = \underbrace{\left(\frac{\Delta}{L} \right)}_{U_1'(x)} - \underbrace{\left(\frac{\Delta d}{L^2} \right)}_{yU_2''(x)} - \underbrace{\left(\frac{\Delta d}{L^2} \right)}_{zU_3''(x)} + G(s)\varphi''(x) + g_1(s)U_1''(x)$$

$$\begin{aligned}
2\check{\gamma}_{12} &= \frac{2A_c}{l\bar{c}} c\varphi'(x) + \frac{dg_1}{ds} U_1'(x) \sim O\left(\frac{\Delta}{L}\right) \\
\check{\gamma}_{22} &= 0 \\
\check{\rho}_{11} &= U_2''(x) \frac{dz}{ds} - U_3''(x) \frac{dy}{ds} - \varphi''(x)r_i \sim O\left(\frac{\Delta}{L^2}\right) \\
\check{\rho}_{12} &= \frac{1}{4R} \frac{dg_1}{ds} U_1'(x) + \left(\frac{1}{4R} \frac{2A_c}{l\bar{c}} c - 1\right) \varphi'(x) \sim \left(\frac{\Delta}{dL}\right) \\
\check{\rho}_{22} &= 0
\end{aligned} \tag{4.54}$$

The terms written over the overbraced expressions in Eq. (4.54) denote their order. Among the new terms introduced by the function \tilde{w}_i , the leading ones are denoted by superscript $\hat{\cdot}$ in Eq. (4.53). The order of \tilde{w}_i is assumed to be

$$\tilde{w}_i \sim O\left(\frac{\Delta d^2}{L^2}\right) \tag{4.55}$$

Such an assumption will be justified later. Therefore, the order of magnitude of the leading terms, Eq. (4.53), is as follows

$$\begin{aligned}
\hat{\gamma}_{12} \sim \hat{\gamma}_{22} &\sim O\left(\frac{\Delta d}{L^2}\right) \\
\hat{\rho}_{12} \sim \hat{\rho}_{22} &\sim O\left(\frac{\Delta}{L^2}\right)
\end{aligned} \tag{4.56}$$

The energy functional can be represented by $\Phi(\gamma_{11}, 2\gamma_{12}, \gamma_{22}, \rho_{11}, \rho_{12}, \rho_{22})$. By keeping the strains and curvature associated with the first-order approximation and the leading terms contribution over the other terms (i.e., by dropping the terms $\frac{\partial \tilde{w}_1}{\partial x}$, $\frac{\partial \tilde{w}_2}{\partial x}$, $\frac{\partial^2 \tilde{w}}{\partial x^2}$, and $\frac{\partial^2 \tilde{w}}{\partial s \partial x} - \frac{1}{4R} \frac{\partial \tilde{w}_2}{\partial x}$ in Eq. (4.53)) the energy function can be written as

$$\Phi(\check{\gamma}_{11}, 2\check{\gamma}_{12} + 2\hat{\gamma}_{12}, 0 + \hat{\gamma}_{22}, \check{\rho}_{11}, \check{\rho}_{12} + \hat{\rho}_{12}, 0 + \hat{\rho}_{22}) \tag{4.57}$$

In the following, the order of magnitude of the energy due to bending, i.e. due to $\check{\rho}_{11}$, $\check{\rho}_{12}$, $\hat{\rho}_{12}$, and $\hat{\rho}_{22}$, is investigated.

The interaction terms associated with $\check{\rho}_{11}$, namely

$$h\check{\rho}_{11}\hat{\gamma}_{12}, h\check{\rho}_{11}\hat{\gamma}_{22}, h^2\check{\rho}_{11}\hat{\rho}_{12}, h^2\check{\rho}_{11}\hat{\rho}_{22}$$

are of order $\left(\frac{\Delta^2hd}{L^4}\right)$ or smaller. They are neglected in comparison with the following membrane contribution to the energy

$$\check{\gamma}_{11}\hat{\gamma}_{12}, \check{\gamma}_{11}\hat{\gamma}_{22}, \check{\gamma}_{12}\hat{\gamma}_{12}, \check{\gamma}_{12}\hat{\gamma}_{22} \begin{cases} \sim O\left(\frac{\Delta^2d}{L^3}\right) & \text{associated with } U'_1 \text{ and } \varphi' \\ \sim O\left(\frac{\Delta^2d^2}{L^4}\right) & \text{associated with } U''_2 \text{ and } U''_3 \end{cases} \quad (4.58)$$

The interaction terms due to the bending curvature $\check{\rho}_{12}$ are

$$h\check{\rho}_{12}\hat{\gamma}_{12}, h\check{\rho}_{12}\hat{\gamma}_{22} \sim O\left(\frac{\Delta^2h}{L^3}\right) \text{ associated with } U'_1 \text{ and } \varphi' \quad (4.59)$$

$$h^2\check{\rho}_{12}\hat{\rho}_{12}, h^2\check{\rho}_{12}\hat{\rho}_{22} \sim O\left[\frac{\Delta^2d}{L^3}\left(\frac{h^2}{d^2}\right)\right] \text{ associated with } U'_1 \text{ and } \varphi' \quad (4.60)$$

These terms are of higher order in comparison with the membrane contribution associated with U'_1 and φ' in Eq. (4.58), and may be neglected. The remaining interaction terms associated with $\hat{\rho}_{12}$ and $\hat{\rho}_{22}$, namely

$$h\check{\gamma}_{11}\hat{\rho}_{12}, h\check{\gamma}_{11}\hat{\rho}_{22}, h\check{\gamma}_{12}\hat{\rho}_{12}, h\check{\gamma}_{12}\hat{\rho}_{22} \begin{cases} \sim O\left(\frac{\Delta^2h}{L^3}\right) & \text{associated with } U'_1 \text{ and } \varphi' \\ \sim O\left(\frac{\Delta^2hd}{L^4}\right) & \text{associated with } U''_2 \text{ and } U''_3 \end{cases} \quad (4.61)$$

are of higher order when compared to the corresponding membrane ones, listed in (4.58). Therefore in order to determine the functions \bar{w}_i , one has to minimize the shell energy expressed by

$$I = \int_0^L \oint \Phi(\check{\gamma}_{11}, 2\check{\gamma}_{12} + 2\hat{\gamma}_{12}, \hat{\gamma}_{22}, 0, 0, 0) dsdz \quad (4.62)$$

The contribution of the new corrections in the work done by external forces is negligible compared to the first-order approximation. Consequently its contribution is neglected in Eq. (4.62). It is worth noting that the bending contribution does not appear in Eq. (4.62). That is, to the second order approximation the shell energy corresponds to a membrane state.

The first variation of the energy functional is

$$\delta I = \int_0^L \oint \left\{ \frac{\partial \Phi}{\partial (2\gamma_{12})} \delta \left(\frac{\partial \bar{w}_1}{\partial s} \right) + \frac{\partial \Phi}{\partial \gamma_{22}} \delta \left(\frac{\partial \bar{w}_2}{\partial s} + \frac{\bar{w}}{R} \right) \right\} ds dx \quad (4.63)$$

Recall that $\frac{\partial \Phi}{\partial (2\gamma_{12})} = N_{12}$ and $\frac{\partial \Phi}{\partial \gamma_{22}} = N_{22}$, Eq. (4.63) takes the form

$$\delta I = \int_0^L \oint \left\{ N_{12} \frac{\partial(\delta \bar{w}_1)}{\partial s} + N_{22} \left(\frac{\partial(\delta \bar{w}_2)}{\partial s} + \frac{1}{R} \delta \bar{w} \right) \right\} ds dx$$

Set the first variation of the energy to zero, to obtain Eqs. (4.39) and (4.40). By setting N_{22} to zero, the energy density is expressed in terms of γ_{11} and γ_{12} only as given by Eq. (4.41). The function \bar{w}_1 can be determined from Eq. (4.39) and (4.41) and by enforcing the condition on \bar{w}_1 to be single valued as previously outlined in section 4.4.2. Substitute from Eqs. (4.53) and (4.54) into (4.45) to get

$$\begin{aligned} & \frac{1}{2} \overbrace{B}^{(Eh)} \left[\overbrace{U_1'(x)}^{\left(\frac{\Delta}{L}\right)} - \overbrace{y(s)U_2''}^{\left(\frac{\Delta d}{L^2}\right)} - \overbrace{z(s)U_3''}^{\left(\frac{\Delta d}{L^2}\right)} + \overbrace{G(s)\varphi''(x)}^{\left(\frac{\Delta d}{L^2}\right)} + \overbrace{g_1(s)U_1''(x)}^{\left(\frac{\Delta d}{L^2}\right)} + \overbrace{\frac{\partial \bar{w}_1}{\partial x}}^{\left(\frac{\Delta d^2}{L^3}\right)} \right] \\ & + \frac{1}{4} \overbrace{C'}^{(Eh)} \left[\overbrace{\frac{2A_e}{l\bar{c}} c\varphi'(x)}^{\left(\frac{\Delta}{L}\right)} + \overbrace{\frac{dg_1}{ds} U_1'(x)}^{\left(\frac{\Delta}{L}\right)} + \overbrace{\frac{\partial \bar{w}_2}{\partial x}}^{\left(\frac{\Delta d^2}{L^3}\right)} + \overbrace{\frac{\partial \bar{w}_1}{\partial s}}^{\left(\frac{\Delta d}{L^2}\right)} \right] = \text{constant} \quad (4.64) \end{aligned}$$

Comparing the order of magnitude of each kinematical variable, Eq. (4.64) reduces to

$$\begin{aligned} & \frac{1}{2} B [U_1'(x) - y(s)U_2'' - z(s)U_3''] \\ & + \frac{1}{4} C' \left[\frac{2A_e}{l\bar{c}} c\varphi'(x) + \frac{dg_1}{ds} U_1'(x) + \frac{\partial \bar{w}_1}{\partial s} \right] = \text{constant} \quad (4.65) \end{aligned}$$

Using the single value condition of function \bar{w}_1 , the following simple analytical solution of Eq. (4.65) is obtained

$$\bar{w}_1 = g_2 U_2''(x) + g_3(s) U_3''(x) \quad (4.66)$$

where

$$\begin{aligned} g_2(s) &= - \int_0^s \left[b(\tau)y(\tau) - \frac{\overline{by}}{\bar{c}}c(\tau) \right] d\tau \sim O(d^2) \\ g_3(s) &= - \int_0^s \left[b(\tau)z(\tau) - \frac{\overline{bz}}{\bar{c}}c(\tau) \right] d\tau \sim O(d^2) \end{aligned} \quad (4.67)$$

It is seen from expression (4.50) and (4.67) that $G(s)$, $g_1(s)$, $g_2(s)$ and $g_3(s)$ are single-valued functions, with

$$G(0) = G(l) = g_1(0) = g_1(l) = g_2(0) = g_2(l) = g_3(0) = g_3(l) = 0$$

Using Eqs. (4.66) and (4.67), \bar{w}_1 is found to be of order $\left(\frac{\Delta d^2}{L^2}\right)$ and the assumption in Eq. (4.55) is justified.

4.4.4 Convergence of Displacement Field

The displacement field corresponding to the second correction is obtained by substituting Eq. (4.66) into Eq. (4.52) and dropping \bar{w}_2 and \bar{w} since their contribution to the shell energy is negligible compared to \bar{w}_1 . The result is

$$\begin{aligned} v_1 &= \underline{U_1(x)} - \underline{y(s)U_2'(x)} - \underline{z(s)U_3'(x)} + \underline{G(s)\varphi'(x)} \\ &\quad + g_1(s)U_1'(x) + g_2(s)U_2''(x) + g_3(s)U_3''(x) \\ \underline{v_2} &= U_2(x)\frac{dy}{ds} + U_3(x)\frac{dz}{ds} + \varphi(x)r_n \\ \underline{v_3} &= U_2(x)\frac{dz}{ds} - U_3(x)\frac{dy}{ds} - \varphi(x)r_t \end{aligned} \quad (4.68)$$

A third cycle is carried out, however no additional terms of the same order in the energy functional result as shown in the Appendix, and the final displacement field converges to the expression given in Eq. (4.68).

The underlined terms in Eq. (4.68) correspond to the classical theory of extension, bending and torsion of beams. The additional terms $g_1(s)U_1'$, $g_2(s)U_2''$ and $g_3(s)U_3''$ in Eq. (4.68) represent warping due to axial strain and bending. These new terms

emerge naturally in addition to the classical torsional related warping $G(s)\varphi'$. They are strongly influenced by the material anisotropy, and vanish for materials that are either orthotropic or whose properties are antisymmetric relative to the shell middle surface. For these layups the coupling parameter $b(s)$ defined in Eqs. (4.50) and (4.42) vanishes. The significance of the axial and bending-related warping terms and their effect on the accuracy, is shown in the applications of Chapter V. Moreover, the expression for torsional related warping $G(s)$ differs from the work of Refs. [30] and [42]-[46]. A comparison of these expressions is presented in section 4.6.

4.4.5 Strain Field

We now substitute the displacement field of Eq. (4.68) into the in-plane strain components of Eq. (4.7), while using Eq. (4.50), to obtain

$$\begin{aligned} \gamma_{11} &= \underbrace{\left(\frac{\Delta}{l}\right)}_{U_1'(x)} - \underbrace{\left(\frac{\Delta d}{l^2}\right)}_{yU_2''(x)} - \underbrace{\left(\frac{\Delta d}{l^2}\right)}_{zU_3''(x)} + \underbrace{\left(\frac{\Delta d}{l^2}\right)}_{G(s)\varphi''(x)} \\ &\quad + \underbrace{\left(\frac{\Delta d}{l^2}\right)}_{g_1(s)U_1''(x)} + \underbrace{\left(\frac{\Delta d^2}{l^3}\right)}_{g_2U_2'''(x)} + \underbrace{\left(\frac{\Delta d^2}{l^3}\right)}_{g_3U_3'''(x)} \\ 2\gamma_{12} &= \underbrace{\left(\frac{\Delta}{l}\right)}_{\frac{2A_c}{l\bar{c}}c\varphi'(x)} + \underbrace{\left(\frac{\Delta}{l}\right)}_{\frac{dg_1}{ds}U_1'(x)} + \underbrace{\left(\frac{\Delta d}{l^2}\right)}_{\frac{dg_2}{ds}U_2''(x)} + \underbrace{\left(\frac{\Delta d}{l^2}\right)}_{\frac{dg_3}{ds}U_3''(x)} \\ \gamma_{22} &= 0 \end{aligned} \tag{4.69}$$

The terms g_1U_1'' , g_2U_2''' , and g_3U_3''' can be neglected in comparison with U_1' , yU_2'' , and zU_3'' , respectively. Therefore, the in-plane strain components become

$$\begin{aligned} \gamma_{11} &= U_1'(x) - y(s)U_2''(x) - z(s)U_3''(x) + G\varphi'' \\ 2\gamma_{12} &= \frac{2A_c}{l\bar{c}}c\varphi' + \frac{dg_1}{ds}U_1' + \frac{dg_2}{ds}U_2'' + \frac{dg_3}{ds}U_3'' \\ \gamma_{22} &= 0 \end{aligned} \tag{4.70}$$

Using Eq. (4.70), the shell energy density, Eq. (4.41), can be written as

$$\begin{aligned}
2\Phi_1 = & \underbrace{(Eh)}_A \left[\underbrace{\left(\frac{\Delta^2}{L^2}\right)}_{(U_1')^2} + (yU_2'')^2 + (zU_3'')^2 + \underbrace{\left(\frac{\Delta^2 d^2}{L^4}\right)}_{(G\varphi'')^2} - 2yU_1'U_2'' - 2zU_1'U_3'' \right. \\
& + \left. \underbrace{\left(\frac{\Delta^2 d}{L^3}\right)}_{2GU_1'\varphi''} + 2yzU_2''U_3'' - \underbrace{\left(\frac{\Delta^2 d^2}{L^4}\right)}_{2yGU_2''\varphi''} - \underbrace{\left(\frac{\Delta^2 d^2}{L^4}\right)}_{2zGU_3''\varphi''} \right] \\
& + \underbrace{(Eh)}_B \left[\frac{dg_1}{ds} (U_1'')^2 - y \frac{dg_2}{ds} (U_2'')^2 - z \frac{dg_3}{ds} (U_3'')^2 + \underbrace{\left(\frac{\Delta^2 d}{L^3}\right)}_{G \frac{2A_\epsilon}{l\bar{c}} c\varphi'\varphi''} \right. \\
& + \frac{2A_\epsilon}{l\bar{c}} cU_1'\varphi' + \frac{dg_2}{ds} U_1'U_2'' + \frac{dg_3}{ds} U_1'U_3'' - \frac{2A_\epsilon}{l\bar{c}} cyU_2''\varphi' \\
& - y \frac{dg_1}{ds} U_2''U_1' - y \frac{dg_3}{ds} U_2''U_3'' - \frac{2A_\epsilon}{l\bar{c}} czU_3''\varphi' - z \frac{dg_1}{ds} U_3''U_1' \\
& \left. - z \frac{dg_2}{ds} U_3''U_2'' + \underbrace{\left(\frac{\Delta^2 d}{L^3}\right)}_{G \frac{dg_1}{ds} \varphi''U_1'} + \underbrace{\left(\frac{\Delta^2 d^2}{L^4}\right)}_{G \frac{dg_2}{ds} \varphi''U_2''} + \underbrace{\left(\frac{\Delta^2 d^2}{L^4}\right)}_{G \frac{dg_3}{ds} \varphi''U_3''} \right] \\
& + \frac{1}{4} \underbrace{(Eh)}_C \left[\underbrace{\left(\frac{\Delta^2}{L^2}\right)}_{\left(\frac{2A_\epsilon}{l\bar{c}} c\varphi'\right)^2} + \left(\frac{dg_1}{ds} U_1''\right)^2 + \left(\frac{dg_2}{ds} U_2''\right)^2 + \left(\frac{dg_3}{ds} U_3''\right)^2 \right. \\
& + \underbrace{\left(\frac{\Delta^2}{L^2}\right)}_{\frac{4A_\epsilon}{l\bar{c}} c \frac{dg_1}{ds} U_1'\varphi'} + \underbrace{\left(\frac{\Delta^2 d}{L^3}\right)}_{\frac{4A_\epsilon}{l\bar{c}} c \frac{dg_2}{ds} U_2''\varphi'} + \underbrace{\left(\frac{\Delta^2 d}{L^3}\right)}_{\frac{4A_\epsilon}{l\bar{c}} c \frac{dg_3}{ds} U_3''\varphi'} \\
& \left. + 2 \frac{dg_1}{ds} \frac{dg_2}{ds} U_1'U_2'' + 2 \frac{dg_1}{ds} \frac{dg_3}{ds} U_1'U_3'' + 2 \frac{dg_2}{ds} \frac{dg_3}{ds} U_2''U_3'' \right] \quad (4.71)
\end{aligned}$$

where the underlined terms are associated with the $G\varphi''$ contribution in Eq. (4.70). These terms are of higher order and may be neglected in comparison with the remain-

ing overbraced leading terms, as shown in Eq. (4.71). Therefore, one may drop $G\varphi''$ from Eq. (4.70), and the final expressions for the in-plane strain components, using Eqs. (4.50) and (4.67), become

$$\begin{aligned}\gamma_{11} &= U_1'(x) - y(s)U_2''(x) - z(s)U_3'''(x) \\ 2\gamma_{12} &= \frac{2A_\epsilon}{l\bar{c}}c(s)\varphi' + \left[b(s) - \frac{\bar{b}}{\bar{c}}c(s) \right] U_1' \\ &\quad - \left[b(s)y(s) - \frac{\bar{b}y}{\bar{c}}c(s) \right] U_2'' \\ &\quad - \left[b(s)z(s) - \frac{\bar{b}z}{\bar{c}}c(s) \right] U_3''' \\ \gamma_{22} &= 0\end{aligned}\tag{4.72}$$

It is worth noting that the vanishing of hoop stress resultant in Eq. (4.40) and hoop strain in Eq. (4.72) should be interpreted as negligible contribution relative to other parameters. The longitudinal strain γ_{11} is a linear function of y and z . This result was adopted as an assumption in the work of Ref. [29].

In the present formulation, parameters A , B and C were assumed to be of the same order. However, the results are valid for configurations which satisfy the following inequalities

$$\frac{A}{C} \left(\frac{d}{L} \right) \ll 1 \quad \frac{B}{C} \left(\frac{d}{L} \right) \ll 1$$

4.4.6 Constitutive Relationships

Dropping the underlined terms in Eq. (4.71) and integrating over the shell middle surface to get the energy of 1D beam theory

$$I = \int_0^L \Phi_2 dx - \int \mathcal{P}_i u_i dx ds \tag{4.73}$$

where

$$\begin{aligned}\Phi_2 = & \frac{1}{2} \left[C_{11}(U_1')^2 + C_{22}(\varphi')^2 + C_{33}(U_3'')^2 + C_{44}(U_2'')^2 \right] \\ & + C_{12}U_1'\varphi' + C_{13}U_1'U_3'' + C_{14}U_1'U_2'' \\ & + C_{23}\varphi'U_3'' + C_{24}\varphi'U_2'' + C_{34}U_2''U_3''\end{aligned}\quad (4.74)$$

Explicit expressions for the stiffness coefficients C_{ij} ($i, j = 1, 4$) are given in Eq. (4.78).

The constitutive relationships can be written in terms of stress resultants and kinematic variables by differentiating Eq. (4.74) with respect to the associated kinematic variable or by relating the traction T , torsional moment M_x , and bending moments M_y and M_z to the shear flow and axial stress as follows

$$\begin{aligned}T = \frac{\partial \Phi_2}{\partial U_1'} &= \oint \int \sigma_{11} d\xi ds = \oint N_{11} ds \\ M_x = \frac{\partial \Phi_2}{\partial \varphi'} &= \oint \int \sigma_{12} r_n(s) d\xi ds = \oint N_{12} r_n(s) ds \\ M_y = \frac{\partial \Phi_2}{\partial U_3''} &= - \oint \int \sigma_{11} z d\xi ds = - \oint N_{11} z(s) ds \\ M_z = \frac{\partial \Phi_2}{\partial U_2''} &= - \oint \int \sigma_{11} y d\xi ds = - \oint N_{11} y(s) ds\end{aligned}\quad (4.75)$$

The shear flow N_{12} is derived from the energy density in Eq. (4.45) and the axial stress resultant N_{11} is given by

$$N_{11} = \frac{\partial \Phi_1}{\partial \gamma_{11}} = A(s)\gamma_{11} + B(s)\gamma_{12}\quad (4.76)$$

and the associated axial and shear stresses are uniform through the wall thickness.

Substitute Eq. (4.72) into Eqs. (4.45) and (4.76) and use Eq. (4.75) to get

$$\begin{Bmatrix} T \\ M_x \\ M_y \\ M_z \end{Bmatrix} = \begin{bmatrix} C_{11} & C_{12} & C_{13} & C_{14} \\ C_{12} & C_{22} & C_{23} & C_{24} \\ C_{13} & C_{23} & C_{33} & C_{34} \\ C_{14} & C_{24} & C_{34} & C_{44} \end{bmatrix} \begin{Bmatrix} U_1' \\ \varphi' \\ U_3'' \\ U_2'' \end{Bmatrix}\quad (4.77)$$

where expressions for the stiffness coefficients C_{ij} ($i, j = 1, 4$) in terms of the cross section geometry and materials properties are as follows

$$\begin{aligned}
 C_{11} &= \int \left(A - \frac{B^2}{C} \right) ds + \overbrace{\frac{[\int (B/C) ds]^2}{\int (1/C) ds}}^{\text{due to } g_1 U_1'} \\
 C_{12} &= \frac{\int (B/C) ds}{\int (1/C) ds} A_e \\
 C_{13} &= - \int \left(A - \frac{B^2}{C} \right) z ds - \overbrace{\frac{\int (B/C) ds \int (B/C) z ds}{\int (1/C) ds}}^{\text{due to } g_1 U_1' \text{ and } g_3 U_3''} \\
 C_{14} &= - \int \left(A - \frac{B^2}{C} \right) y ds - \overbrace{\frac{\int (B/C) ds \int (B/C) y ds}{\int (1/C) ds}}^{\text{due to } g_1 U_1' \text{ and } g_2 U_2''} \\
 C_{22} &= \frac{1}{\int (1/C) ds} A_e^2 \\
 C_{23} &= - \frac{\int (B/C) z ds}{\int (1/C) ds} A_e \\
 C_{24} &= - \frac{\int (B/C) y ds}{\int (1/C) ds} A_e \\
 C_{33} &= \int \left(A - \frac{B^2}{C} \right) z^2 ds + \overbrace{\frac{[\int (B/C) z ds]^2}{\int (1/C) ds}}^{\text{due to } g_3 U_3''} \\
 C_{34} &= \int \left(A - \frac{B^2}{C} \right) y z ds + \overbrace{\frac{\int (B/C) y ds \int (B/C) z ds}{\int (1/C) ds}}^{\text{due to } g_2 U_2'' \text{ and } g_3 U_3''} \\
 C_{44} &= \int \left(A - \frac{B^2}{C} \right) y^2 ds + \overbrace{\frac{[\int (B/C) y ds]^2}{\int (1/C) ds}}^{\text{due to } g_2 U_2''}
 \end{aligned} \tag{4.78}$$

The out-of-plane warping contribution to the stiffnesses due to the axial strain (i.e., due to $g_1 U_1'$), bending about y axis (i.e., due to $g_3 U_3''$), and bending about z axis (i.e., due to $g_2 U_2''$) is shown by the overbraces in Eq. (4.78).

The coefficients C_{ij} ($i, j = 1, 4$) can be expressed in terms of the in-plane axial stiffness coefficients A_{ij} of Classical Lamination Theory (CLT) if one neglects the through-the-thickness contribution to the stiffnesses in Eq. (4.78). The result is

$$\begin{aligned}
C_{11} &= \oint \left(K_{11} - \frac{K_{12}^2}{K_{22}} \right) ds + \frac{[\oint (K_{12}/K_{22}) ds]^2}{\oint (1/K_{22}) ds} \\
C_{12} &= 2A_e \frac{\oint (K_{12}/K_{22}) ds}{\oint (1/K_{22}) ds} \\
C_{13} &= - \oint \left(K_{11} - \frac{K_{12}^2}{K_{22}} \right) z ds - \frac{\oint (K_{12}/K_{22}) ds \oint (K_{12}/K_{22}) z ds}{\oint 1/K_{22} ds} \\
C_{14} &= - \oint \left(K_{11} - \frac{K_{12}^2}{K_{22}} \right) y ds - \frac{\oint (K_{12}/K_{22}) ds \oint (K_{12}/K_{22}) y ds}{\oint 1/K_{22} ds} \\
C_{22} &= 4A_e^2 \frac{1}{\oint (1/K_{22}) ds} \\
C_{23} &= -2A_e \frac{\oint (K_{12}/K_{22}) z ds}{\oint (1/K_{22}) ds} \\
C_{24} &= -2A_e \frac{\oint (K_{12}/K_{22}) y ds}{\oint (1/K_{22}) ds} \\
C_{33} &= \oint \left(K_{11} - \frac{K_{12}^2}{K_{22}} \right) z^2 ds + \frac{[\oint (K_{12}/K_{22}) z ds]^2}{\oint (1/K_{22}) ds} \\
C_{34} &= \oint \left(K_{11} - \frac{K_{12}^2}{K_{22}} \right) y z ds + \frac{\oint (K_{12}/K_{22}) y ds \oint (K_{12}/K_{22}) z ds}{\oint 1/K_{22} ds} \\
C_{44} &= \oint \left(K_{11} - \frac{K_{12}^2}{K_{22}} \right) y^2 ds + \frac{[\oint (K_{12}/K_{22}) y ds]^2}{\oint (1/K_{22}) ds}
\end{aligned}$$

where, the stiffnesses K_{ij} are

$$\begin{aligned}
K_{11} &= A_{11} - \frac{(A_{12})^2}{A_{22}} \\
K_{12} &= A_{16} - \frac{A_{12}A_{26}}{A_{22}} \\
K_{22} &= A_{66} - \frac{(A_{26})^2}{A_{22}}
\end{aligned} \tag{4.79}$$

4.4.7 Equilibrium Equations

The equilibrium equations are derived using the principle of virtual work. The variation of the internal strain energy is

$$\delta U = \int_0^L \oint (N_{xx} \delta \gamma_{xx} + 2N_{xs} \delta \gamma_{xs}) ds dx$$

Using the strain displacement relations, one-dimensional stretching, twisting, and bending generalized internal forces are defined as

$$T = \oint N_{xx} ds$$

$$M_x = 2A_c N_{xs}$$

$$M_y = - \oint N_{xx} z ds$$

$$M_z = - \oint N_{xx} y ds$$

Consider a beam subjected to external forces and moment resultants \bar{T} , \bar{M}_x , \bar{M}_y , and \bar{M}_z at both ends. Moreover, surface tractions P_x , P_y , and P_z are applied along the x , y , and z directions, respectively. The variation of the virtual work of the external forces can be written as

$$\begin{aligned} \delta W_e = & \bar{T} \delta U_1|_0^L + \bar{M}_x \delta \varphi|_0^L - \bar{M}_y \delta U_3'|_0^L - \bar{M}_z \delta U_2'|_0^L \\ & + \int_0^L \left[\left(\oint P_x ds \right) \delta U_1 - \left(\oint P_x y ds \right) \delta U_2' - \left(\oint P_x z ds \right) \delta U_3' + \left(\oint P_y ds \right) \delta U_2 \right. \\ & \left. - \left(\oint P_y z ds \right) \delta \varphi - \left(\oint P_z ds \right) \delta U_3' - \left(\oint P_z y ds \right) \delta \varphi \right] dx \end{aligned}$$

Using the principle of virtual work

$$\delta U = \delta W_e$$

one obtains a system of linear equilibrium equations as follows

$$T' + \oint P_x ds = 0$$

$$\begin{aligned}
M_x' + \oint (P_z y - P_y z) ds &= 0 \\
M_y'' + (\oint P_x z ds)' + \oint P_z ds &= 0 \\
M_z'' + (\oint P_x y ds)' + \oint P_y ds &= 0
\end{aligned} \tag{4.80}$$

One of the member of each of the following four pairs must be prescribed at the beam ends :

$$T \text{ or } U_1, M_x \text{ or } \varphi, M_y \text{ or } U_3', \text{ and } M_z \text{ or } U_2' \tag{4.81}$$

4.5 Summary of governing equations

The development presented in this work encompasses five equations. The first, is the displacement field given in Eq. (4.68). Its functional form was determined based on an asymptotical expansion of shell energy. The associated strain field is given in Eq. (4.72) and the stress resultants in Eq. (4.45), (4.75) and (4.76). The fourth, are the constitutive relationships in Eq. (4.77) with the stiffness coefficients expressed as integral of material properties and cross sectional geometry in Eq. (4.78). Finally the equilibrium equations and boundary conditions are given in Eqs. (4.80) and (4.81), respectively.

In the present development the determination of the displacement field is essential in obtaining accurate expressions for the beam stiffnesses. A comparison of the derived displacement field with results obtained by previous investigators is presented in the following section.

4.6 Analytical comparison with previous results

In anisotropic materials the importance of physical effects such as transverse shear strains is influenced by the relative magnitude of elastic moduli. For example in

laminated composites the extensional modulus along the fibers direction is usually large relative to the shear moduli and consequently transverse shear effects can be significant. Several theories have addressed this issue by including transverse shear in the assumed displacement field [30], and [42]-[46]. The displacement function Eq. (4.68) derived from the asymptotical analysis does not include transverse shear strain terms explicitly. This is a consequence of the vanishing of the through-the-thickness stress component σ^{i3} in Eq. (4.5) or (4.9) where the transverse shear strains are expressed in terms of other strain components. Their effect however is implicitly included in the stretching-related warping term $g_1(s)$ and the bending-related warping terms $g_2(s)$ and $g_3(s)$ as illustrated by the applications of Chapter V.

Rehfield's theory [30] recognizes the significance of transverse shear strain in thin-walled composite beams. Its displacement field is given by

$$\begin{aligned} u_1 &= U_1(x) - y(s)[U_2'(x) - 2\gamma_{xy}(x)] - z(s)[U_3'(x) - 2\gamma_{xz}(x)] + g(s, x) \\ u_2 &= U_2(x) - z(s)\varphi(x) \\ u_3 &= U_3(x) + y(s)\varphi(x) \end{aligned} \quad (4.82)$$

where γ_{xy} and γ_{xz} are the transverse shear strains. The warping function $g(s, x)$ is given as

$$g(s, x) = \tilde{G}(s)\varphi'(x) \quad (4.83)$$

with

$$\tilde{G}(s) = 2A_c \frac{s}{l} - \int_0^s \tau_n(\tau) d\tau \quad (4.84)$$

A comparison of the displacement fields in Eq. (4.68) and (4.82) shows that the warping function in Rehfield's formulation includes the torsional-related contribution and does not include explicit terms that express the bending-related warping. The torsional-related warping function $G(s)$ in Eq. (4.50) is different from the function in

Eq. (4.84). The two expressions coincide when $c = \text{constant}$ that is, when the wall stiffness and thickness are uniform along the cross section circumference.

The torsional related warping function in Eq. (4.84) was modified by Atilgan [44], and Rehfield and Atilgan [43] as

$$\hat{G}(s) = \int_0^s \left[\frac{2A_c}{l c_1} c_1 - r_n(\tau) \right] d\tau \quad (4.85)$$

where

$$c_1 = \frac{1}{A'_{66} - \frac{(A'_{16})^2}{A'_{11}}} \quad (4.86)$$

and

$$\begin{bmatrix} A'_{11} & A'_{16} \\ A'_{16} & A'_{66} \end{bmatrix} = \begin{bmatrix} A_{11} - \frac{(A_{12})^2}{A_{22}} & A_{16} - \frac{A_{12}A_{26}}{A_{22}} \\ A_{16} - \frac{A_{12}A_{26}}{A_{22}} & A_{66} - \frac{(A_{26})^2}{A_{22}} \end{bmatrix} \quad (4.87)$$

The A_{ij} in Eq. (4.87) are the in-plane axial stiffnesses of CLT, Refs. [19] and [50], they are related to the modulus tensor by

$$\begin{aligned} A_{11} &= \langle E^{1111} \rangle, & A_{12} &= \langle E^{1122} \rangle, & A_{22} &= \langle E^{2222} \rangle \\ A_{16} &= \langle E^{1112} \rangle, & A_{26} &= \langle E^{1222} \rangle, & A_{66} &= \langle E^{1212} \rangle \end{aligned}$$

A comparison of the modified torsional warping function in Eq. (4.85) and $G(s)$ in Eq. (4.50) shows that they coincide for laminates with no extension-shear coupling ($\langle D^{1112} \rangle = \langle D^{1222} \rangle = 0$, in Eq. (4.10)). For the case where the through-the-thickness contribution is neglected in Eq. (4.10), this reduces to $A_{16} = A_{26} = 0$.

The warping function obtained in Refs. [42] and [46] for composite box beams is identical to the expression of Refs. [43] and [44] in Eqs. (4.83) and (4.85).

An assessment of all the previous warping expressions can be made by checking whether they reduce to the exact expression for isotropic materials (see, for example, Ref. [59])

$$\bar{\bar{G}}(s) = \int_0^s \left[\frac{2A_c}{l c_2} c_2 - r_n(\tau) \right] d\tau \quad (4.88)$$

with

$$c_2 = \frac{1}{\mu h(s)}$$

where μ is the shear modulus.

For isotropic materials the in-plane coupling b is zero and consequently g_1 , g_2 and g_3 in Eqs. (4.50) and (4.67) vanish. That is the warping is torsion-related and reduces to $G(s)\varphi'$. Moreover, the shear parameter c is equal to $\frac{1}{4\mu h(s)}$ and the expressions for $G(s)$ and $\bar{G}(s)$ in Eqs. (4.50) and (4.88) coincide.

Rehfield's warping function in Eq. (4.84) coincides with Eq. (4.88) when the material is isotropic and the wall thickness is constant. Also the works of Refs. [43], [44] and [46] reduce to Eq. (4.88) for isotropic materials.

4.7 Closing Remarks

The major advantage of the approach adopted in this work is the fact that the displacement function emerges as a result of the asymptotical analysis of the shell energy. The influence of the material's anisotropy is accounted for in a consistent manner and the deformation modes are determined on the basis of their contribution to the associated energy. Two new contributions to the warping emerge due to stretching and bending. They are of the same order of the classical torsional-related warping. Their significance is illustrated in the applications provided in the next chapter.

CHAPTER V

APPLICATIONS OF ANISOTROPIC THIN-WALLED BEAM THEORY

An evaluation of the variationally consistent theory developed in chapter IV is provided. The theory is applied to beams with arbitrary closed cross-sections made of laminated composite materials with variable thickness and stiffness subjected to axial load, torsion and bending. A comparison of flexibility coefficients and deformation with finite element predictions, closed form solutions and experimental data is performed to validate predictions and isolate the influence of different contributions to the section warping. In addition to the torsional related warping, two new contributions namely, axial strain and bending related out-of-plane warping were identified in the developed theory. Extension and bending related out-of-plane warping are shown to have a significant effect on the accuracy of predictions. Comparison of predictions provides also a check of the asymptotical analysis result regarding the contribution of shear deformation. Although the resulting displacement field does not include an explicit shear deformation term similar to Timoshenko's theory, shear deformation contribution is shown to be implicitly accounted for through the out-of-plane warping due to extension and bending.

Two special layups: The circumferentially uniform stiffness (CUS) and circumferentially Asymmetric stiffness (CAS) have been considered in Refs. [41]-[46] and [51]. They are associated with different non-classical behaviors. These behaviors are

shown to be influenced by the out-of-plane warping due to extension and bending in the next section.

5.1 Effect of Out-of-Plane Warping due to Extension and Bending

5.1.1 CUS Configuration

This configuration produces both extension-twist and bending-transverse shear couplings. The axial, coupling and in-plane stiffnesses A , B , and C given in Eq. (4.42) are constant throughout the cross section and hence the name circumferentially uniform stiffness (CUS) adopted in Ref. [43], [44], [45] and [51]. Such a configuration is manufactured by wrapping the composite lay-up using a winding technique. For a box-beam, the ply lay-ups on opposite sides are of reversed orientation, and hence the name antisymmetric configuration adopted in Refs. [41], [42], and [46].

Since A , B , and C are constants, the stiffness matrix in Eq. (4.78), for a centroidal coordinate system, reduces to

$$[C_{ij}] = \begin{bmatrix} C_{11} & C_{12} & 0 & 0 \\ C_{12} & C_{22} & 0 & 0 \\ 0 & 0 & C_{33} & 0 \\ 0 & 0 & 0 & C_{44} \end{bmatrix} \quad (5.1)$$

The nonzero stiffness coefficients are given by

$$\begin{aligned} C_{11} &= Al \\ C_{12} &= BA_c \\ C_{22} &= \frac{C}{l} A_c^2 \\ C_{33} &= A \oint z^2 ds - \frac{B^2}{C} \oint z^2 ds \\ C_{44} &= A \oint y^2 ds - \frac{B^2}{C} \oint y^2 ds \end{aligned} \quad (5.2)$$

where l denotes the length of the closed contour Γ . For such a case the out-of-plane warping due to axial strain vanishes and g_1 does not affect the response. This is shown by considering A , B , and C as constants in Eq. (4.78). The influence of the out-of-plane warping due to bending in the x - z and x - y planes are expressed by the underlined terms in the expressions of C_{33} and C_{44} , respectively. These terms are significant in predicting the deflection of antisymmetric configurations.

5.1.2 CAS Configuration

This configuration produces both bending-twist and extension-transverse shear couplings. The stiffness A is constant throughout the cross section. For a box beam, the coupling stiffness, B , vanishes for the vertical members, while its values in the top and bottom members are of opposite signs

$$B_{top} = -B_{bottom}$$

$$B_{vertical\ members} = 0 \quad (5.3)$$

and hence the name circumferentially asymmetric stiffness (CAS) adopted in Ref. [43], [44], [45] and [51]. For a box-beam, the ply lay-ups on opposite sides are mirror images, and hence the name symmetric configuration adopted in Ref. [41],[42], and [46]. The stiffness C along the horizontal and vertical members are equal and expressed by

$$C_{top} = C_{bottom}$$

$$C_{vertical\ left} = C_{vertical\ right} \quad (5.4)$$

The stiffness matrix, for a centroidal system of axes, reduces to

$$[C_{ij}] = \begin{bmatrix} C_{11} & 0 & 0 & 0 \\ 0 & C_{22} & C_{23} & 0 \\ 0 & C_{23} & C_{33} & 0 \\ 0 & 0 & 0 & C_{44} \end{bmatrix} \quad (5.5)$$

The nonzero stiffness coefficients are expressed by

$$\begin{aligned}
 C_{11} &= Al - 2 \frac{B_t^2 d}{C_t} \\
 C_{22} &= \frac{C_t}{2 \left[d + a \left(\frac{C_t}{C_v} \right) \right]} A_e^2 \\
 C_{23} &= \frac{B_t}{2 \left[d + a \left(\frac{C_t}{C_v} \right) \right]} A_e^2 \\
 C_{33} &= A \int z^2 ds - \frac{B_t^2}{2C_t} \left\{ a - \frac{A_e}{\left[d + a \left(\frac{C_t}{C_v} \right) \right]} \right\} A_e \\
 C_{44} &= A \int y^2 ds - \frac{B_t^2 d^3}{6C_t}
 \end{aligned} \tag{5.6}$$

Subscripts t and v denote top and vertical members, respectively. The box width and height are represented by d and a , respectively. Equations (5.6) are derived by substituting Eqs. (5.3) and (5.4) into Eq. (4.78) and considering A to be constant. The underlined term in the expression of the axial stiffness C_{11} represents the extension contribution to the out-of-plane warping. The bending contributions to the out-of-plane warping are represented by the underlined terms in the expressions of C_{33} and C_{44} . For the CAS configuration, bending about the y -axis is coupled with torsion while extension and bending about the z -axis are decoupled.

In order to assess the accuracy of the predictions and isolate the influence of stretching and bending-related warping, the present theory is applied to the box beam given in Ref. [51]. The cross sectional configuration is shown in Fig. 5.1 and the material properties in Table 5.1.

5.2 Comparison of Flexibility Coefficients

A comparison of the flexibility coefficients S_{ij} with the predictions from two models is provided in Table 5.2. The flexibility coefficients S_{ij} are obtained by inverting

Table 5.1: Properties of T300/5208 Graphite/Epoxy

$$E_{11} = 21.3 \text{ Msi}$$

$$E_{22} = E_{33} = 1.6 \text{ Msi}$$

$$G_{12} = G_{13} = 0.9 \text{ Msi}$$

$$G_{23} = 0.7 \text{ Msi}$$

$$\nu_{12} = \nu_{13} = 0.28$$

$$\nu_{23} = 0.5$$

the 4×4 matrix in Eq. (4.77). NABSA (Nonhomogeneous Anisotropic Beam Section Analysis) is a finite element model based on an extension of the work presented in Ref. [32]. In this model all possible types of warping are accounted for. The TAIL model is based on Ref. [30], but neglecting the restrained torsional warping. The predictions of the NABSA and TAIL models are provided in Ref. [51]. The percentage differences appearing in Table 5.2 are relative to the NABSA predictions. The present theory is in good agreement with NABSA. Its predictions show a difference ranging from +0.7 to +3.6 percent while those based on Ref. [30] range from +3.6 to -18.4 percent.

Since the box beam has a CUS configuration, the out-of-plane warping due to bending has a significant effect on the prediction of the bending flexibilities ($\frac{1}{C_{33}}$) and ($\frac{1}{C_{44}}$) as shown in Eq. (5.2). Neglecting g_3 and g_2 in the expressions of C_{33} and C_{44} leads to values of $0.11424 \times 10^{-4} \text{ lb}^{-1}\text{in}^{-2}$ and $0.38410 \times 10^{-4} \text{ lb}^{-1}\text{in}^{-2}$ for S_{33} and S_{44} , respectively. Comparison of these values with the underlined results in Table 5.2 shows a 65 percent increase in the bending flexibilities due to out-of-plane bending

Table 5.2: Comparison of Flexibility Coefficients of NABSA, TAIL and Present (lb, in units)

Flexibility	NABSA	PRESENT	% Diff.	TAIL	% Diff.
$S_{11} \times 10^5$	0.143883	0.14491	+0.7	0.14491	+0.7
$S_{22} \times 10^4$	0.312145	0.32364	+3.6	0.32364	+3.6
$S_{12} \times 10^5$	-0.417841	-0.43010	+2.9	-0.43010	+2.9
$S_{33} \times 10^4$	0.183684	<u>0.1886</u>	+2.6	0.17294	-5.8
$S_{44} \times 10^5$	0.614311	<u>0.63429</u>	+3.2	0.50157	-18.4

related warping.

5.3 Comparison of Deformation

The present theory is applied to the prediction of the tip deformation in a cantilevered beam made of Graphite/Epoxy and subjected to different types of loading. The beam has a CUS square cross section with $[+12]_4$ lay-up. The geometry and mechanical properties are given in Table 5.3. Comparison of results with the MSC/NASTRAN finite element analysis of Ref. [38] is provided in Table 5.4. The applied axial and transverse forces are equal to 100 lb, while the applied torsional moment is 100 lb-in.

The MSC/NASTRAN analysis is based on a 2D plate model accounting for both shear deformation and warping. The predictions of the present theory range from +1.7 to -0.7 percent difference relative to the finite element results.

The deflection due to transverse load neglecting out-of-plane bending related warping is equal to 1.341 inch compared to 1.853 inch (38% difference) in Table 5.4. For a CUS configuration, the extension-torsional response is decoupled from bending as shown in Eq. (5.2). Since C is constant and g_1 does not affect the stiffness coefficients,

Table 5.3: Geometry and Mechanical Properties of Thin-Walled Beam with $[+12]_4$ GUS square cross-section

Length = 24.0 in.	$E_{11} = E_{22} = E_{33} = 11.65$ Msi
Width = depth = 1.17 in.	$G_{12} = G_{13} = 0.82, G_{23} = 0.7$ Msi
Ply thickness = 0.0075 in.	$\nu_{12} = \nu_{13} = 0.05, \nu_{23} = 0.3$

as outlined in section 5.1.1, the flexibility coefficients controlling extension and twist response, S_{11} , S_{12} and S_{22} coincide with those of Refs. [43] and [44]. As a consequence, the axial displacement and twist angle predictions coincide. However, the lateral deflection under transverse load differs. The tip lateral deflection predicted using the theory of Ref. [30], which includes shear deformation, and Refs. [43] and [44], which include a shear deformation correction to Ref. [30], is 1.724 inch resulting in -7.6 percentage difference compared to the NASTRAN result. This is due to the effect of bending-related out-of-plane warping on the bending flexibilities $\frac{1}{C_{33}}$ and $\frac{1}{C_{44}}$, ($C_{33} = C_{44}$ for this case), as shown by the underlined terms in Eq. (5.2).

Figures 5.2 and 5.3 show the bending slope variation along the beam span for antisymmetric and symmetric cantilevers under a 1 lb transverse tip load, respectively. The beam geometry and its material properties are given in Table 5.5. The experimental results are reported in Refs. [41], [42], and [46]. The influence of the out-of-plane warping due to bending is isolated in these figures. The bending related out-of-plane warping, $g_2 U_2''$ and $g_3 U_3''$ terms in Eq. (4.68), results in a 91 and 20 % increase in the bending slope for the antisymmetric and symmetric configurations,

Table 5.4: MSC/NASTRAN and Present Solutions for a CUS Cantilevered Beam with $[+12]_4$ Layups Subjected to Various Tip Load Cases

Tip Load	Tip Deformation		% Diff.
	<u>NASTRAN</u>	<u>Present</u>	
Axial Force	Axial Disp. : 0.002189 in.	0.002202 in.	+0.6 %
Axial Force	Twist : 0.3178 deg.	0.32325 deg.	+1.7 %
Torsional Moment	Twist : 2.959 deg.	2.998 deg.	+1.32 %
Transverse Force	Deflection : 1.866 in.	1.853 in.	-0.7 %

respectively. The analytical predictions reported in Refs. [41], [42], and [46] together with results obtained on the basis of the analyses in Ref. [30], [43], [44] and the present theory are combined in Figs. 5.4 and 5.5. Results show that the present theory is in good agreement with the test data and the closest when compared to the other analytical approaches which include shear deformation, Refs. [30], [42], and [46], and shear deformation corrections, Refs. [43] and [44].

The bending slope in Figs. 5.2-5.5 is defined in terms of the cross section rotation for theories including shear deformation. For the geometry and material properties considered, this effect is negligible as shown in Figs. 5.4 and 5.5 where the spanwise slope at the fixed end from theories with shear deformation, is indistinguishable from zero. The nonzero value shown by the test data may be due to the experimental set up used to achieve clamped end conditions.

The spanwise twist distribution of symmetric cantilevered beam with $[30]_6$ and $[45]_6$ lay-ups is plotted in Figs. 5.6 and 5.7, respectively. The beams are subjected to a transverse tip load of 1 lb. Their dimensions and material properties are given in Table 5.5. Results show that the present theory and those of Refs. [43] and [44] are

Table 5.5: Cantilever Geometry and Properties

Width = 0.953 in.	$E_{11} = 20.59 \text{ Msi}, E_{22} = E_{33} = 1.42 \text{ Msi}$
Depth = 0.53 in.	$G_{12} = G_{13} = 0.87 \text{ Msi}, G_{23} = 0.7 \text{ Msi}$
Ply thickness = 0.005 in.	$\nu_{12} = \nu_{13} = 0.42, \nu_{23} = 0.5$

the closest to the test data. A similar behavior is found for the bending slope and the twist angle at the mid-span of the symmetric cantilevered beams appearing in Figs. 5.8 and 5.9. The beams are subjected to a tip torque of 1 lb-in.

5.4 Shear Deformation Contribution

The significance of the out-of-plane warping due to bending is illustrated in Fig. 5.2. A similar behavior is obtained in Ref. [65] when the shear deformation contribution is neglected. This indicates that the out-of-plane warping due to bending includes implicitly the shear deformation contribution. In order to assess this similarity, the present theory and the numerical work of Ref. [65] are applied to the prediction of the deflection in a cantilevered beam made of graphite/epoxy and subjected to a transverse tip load of 1 lb. The beam has a CUS cross-section with $[+15]_6$ lay-up. The geometry and mechanical property, provided in Ref. [65], are given for convenience in Table 5.6. Figure 5.10 shows a similar behavior suggesting that in the present theory, shear deformation is implicitly accounted through bending-related warping. The prediction of Ref. [65] are referred to Classical when shear deformation is neglected. Further evidence could be provided by estimating the equivalent shear deformation strain. This can be expressed by the slope of the plane that approximates

Table 5.6: Cantilever Geometry and Properties

Width = 0.923 in.	$E_{11} = 20.6 \text{ Msi}, E_{22} = E_{33} = 1.42 \text{ Msi}$
Depth = 0.50 in.	$G_{12} = G_{13} = 0.87 \text{ Msi}, G_{23} = 0.696 \text{ Msi}$
Ply thickness = 0.005 in.	$\nu_{12} = \nu_{13} = 0.3, \nu_{23} = 0.34$

the cross-section warping and is given [66] by

$$2\gamma_{xy} = -\frac{\int y v_1 dA}{I_{zz}} \quad (5.7)$$

where A and I_{zz} represent the cross-sectional area and moment of inertia about the z -axis, respectively.

For a CUS box cross-section subjected to a vertical tip transverse load p_z , the shear strain distribution across the cantilever length is obtained by substituting the axial displacement v_1 from Eq. (4.68) into Eq. (5.7). The result is the following analytical expression

$$2\gamma_{xy} = \frac{(L - x_1) had}{4I_{zz}} \left(\frac{a^2}{3} + ad + \frac{d^2}{3} \right) S_{33} p_z \quad (5.8)$$

where

S_{33} = Bending flexibility

L = Length of cantilever

x_1 = Cross-section position measured from the fixed end

h = Laminate thickness

a = Box height

d = Box width

A comparison of the shear strain γ_{xy} over the length of the cantilever with the prediction of Ref. [65] is shown in Fig. 5.11. The shear strain at the fixed end is 4.5924×10^{-4} based on Eq. (5.8) which is within 2 percent of 4.6857×10^{-4} calculated on the basis of Ref. [65].

5.5 Conclusion

The anisotropic thin-walled closed section has been validated by comparison of response predictions with finite element solutions, other closed form analyses and test data. The influence of the two new nonclassical contributions namely, extensional and bending related out-of-plane warping on the accuracy of the response predictions is shown to be significant. Moreover, the contribution of shear deformation is shown to be implicitly accounted for through the bending related out-of-plane warping, and in-plane warping effect is found to be negligible.

5.6 Closing Remarks

For anisotropic beams, the major reason for the discrepancy in the predictions of the analytical models of Refs. [30] and [41]-[46] and the present theory is due to the a priori assumed displacement fields which neglect the extension and bending-related out-of-plane warping. The influence of the material's anisotropy on the displacement is too complex to cast in a kinematic assumption similar to classical theory of extension-bending and torsion.

A consistent approach to account for the various behavioral modes associated with anisotropic beams was adopted in this work. It is based on an asymptotical analysis of the energy. The influence of the material's anisotropy on the displacement and stiffness coefficients was isolated, and by comparison an assessment of previous

analyses was performed. In particular, this approach accounts implicitly the shear deformation contribution shown to be significant in previous models. The difference being the consistent order of magnitude that this contribution is accounted for and its significance relative to other contributions.

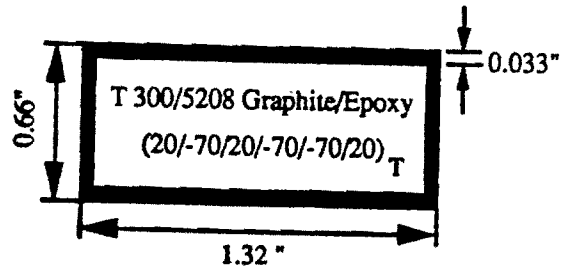
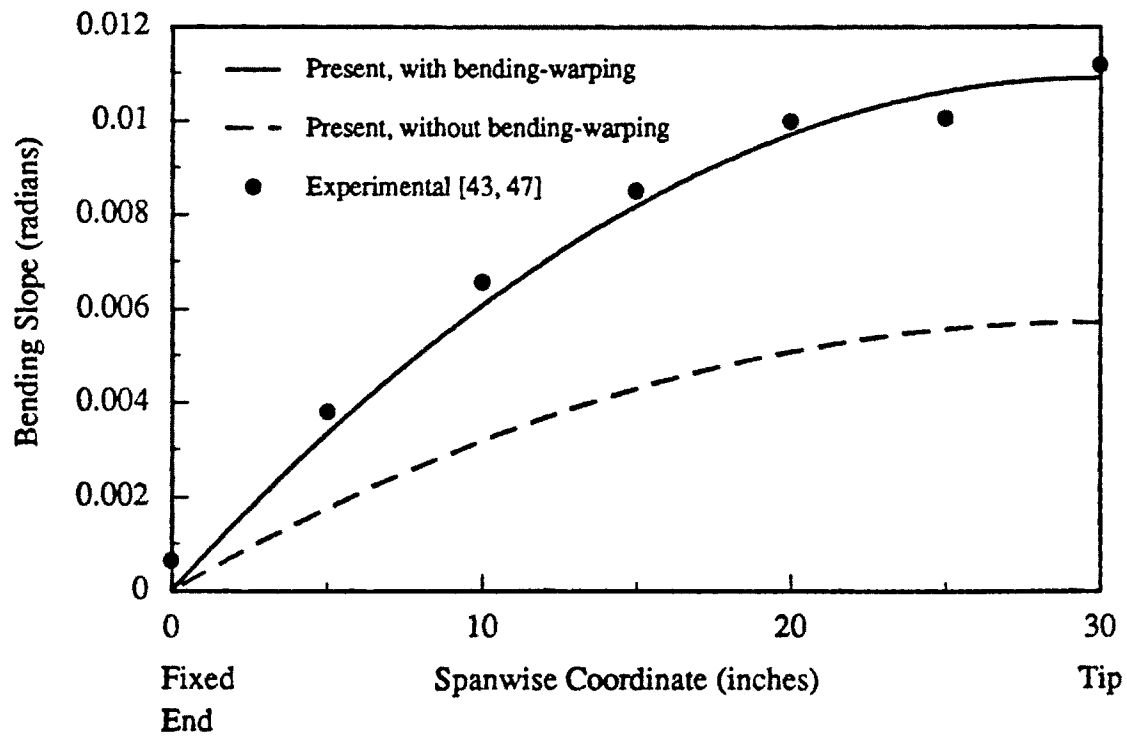


Figure 5.1: Beam Cross Section

Figure 5.2: Significance of out-of-plane bending related warping on the bending slope of an antisymmetric $[15]_6$ cantilever under 1 lb transverse tip Load

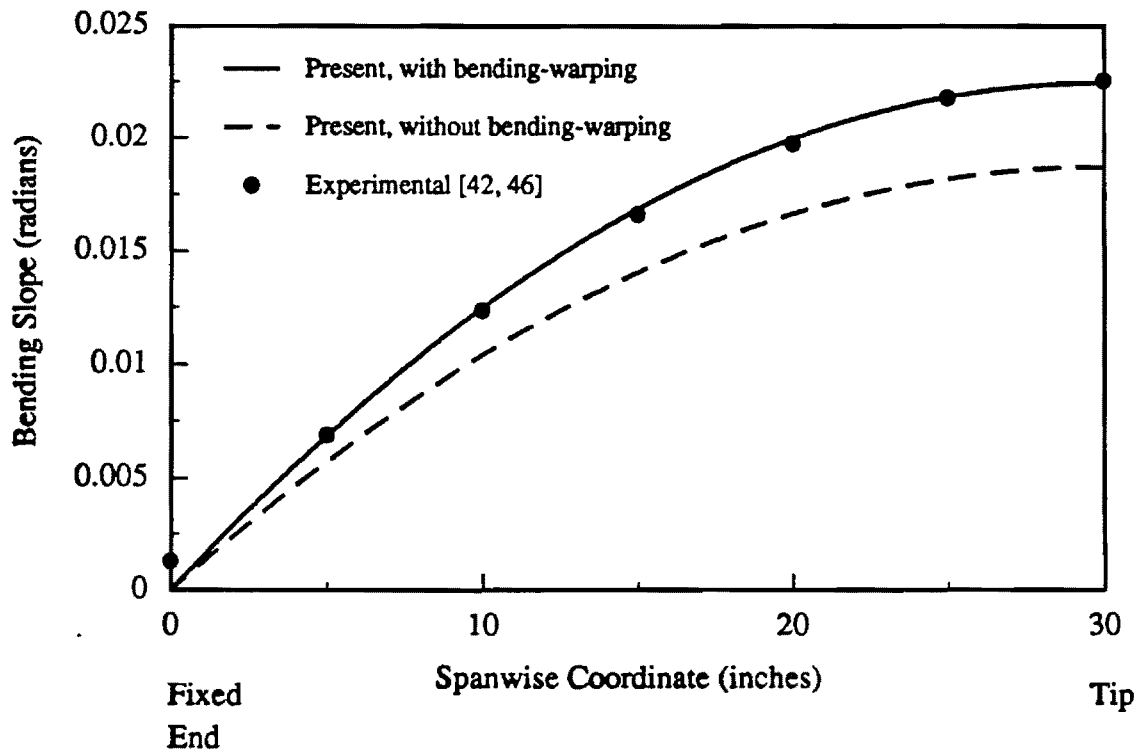


Figure 5.3: Significance of out-of-plane bending related warping on the bending slope of a symmetric $[30]_6$ cantilever under 1 lb transverse tip Load

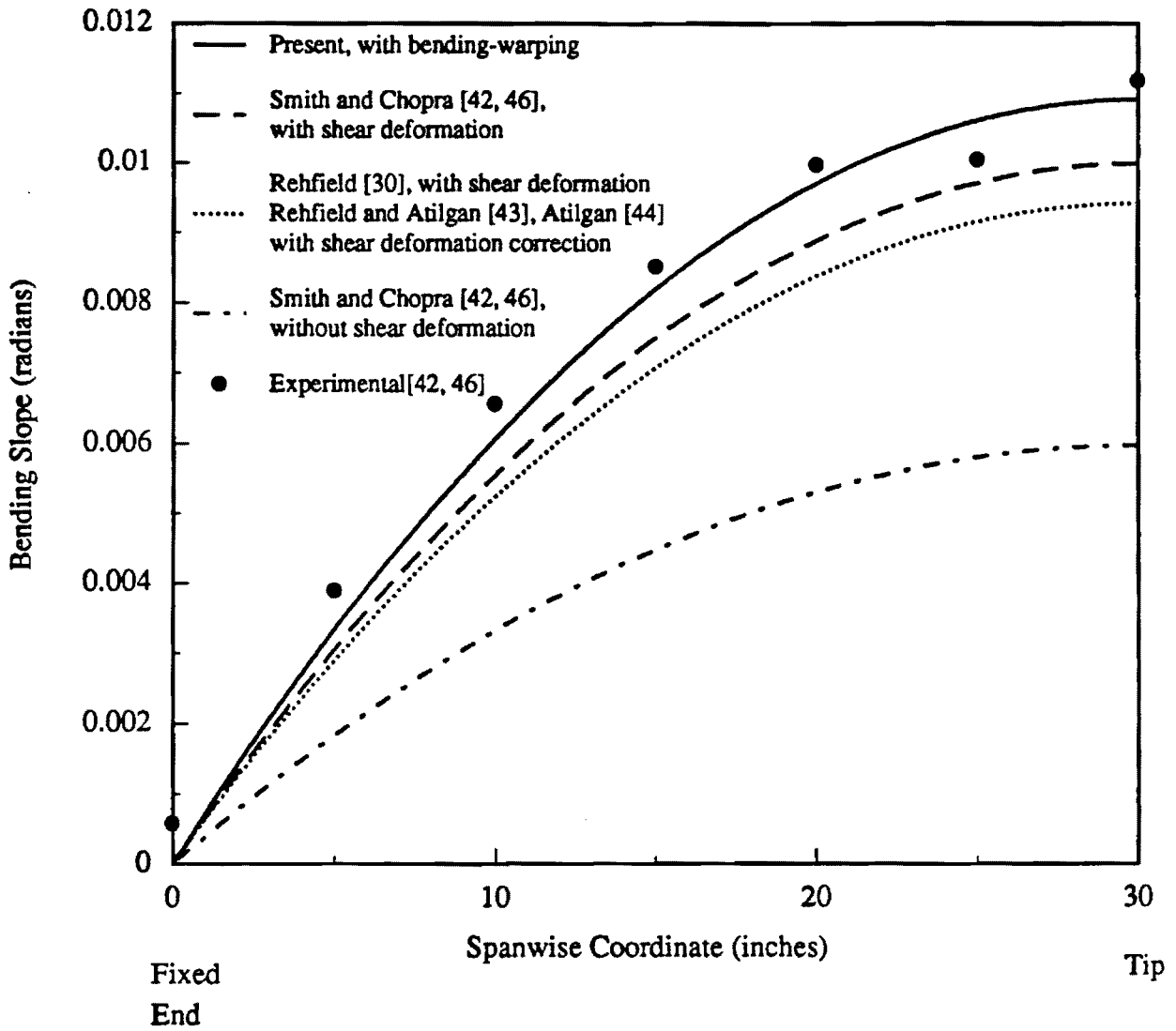


Figure 5.4: Bending Slope of an Anti-Symmetric $[15]_6$ Cantilever Under 1 lb Transverse Tip Load

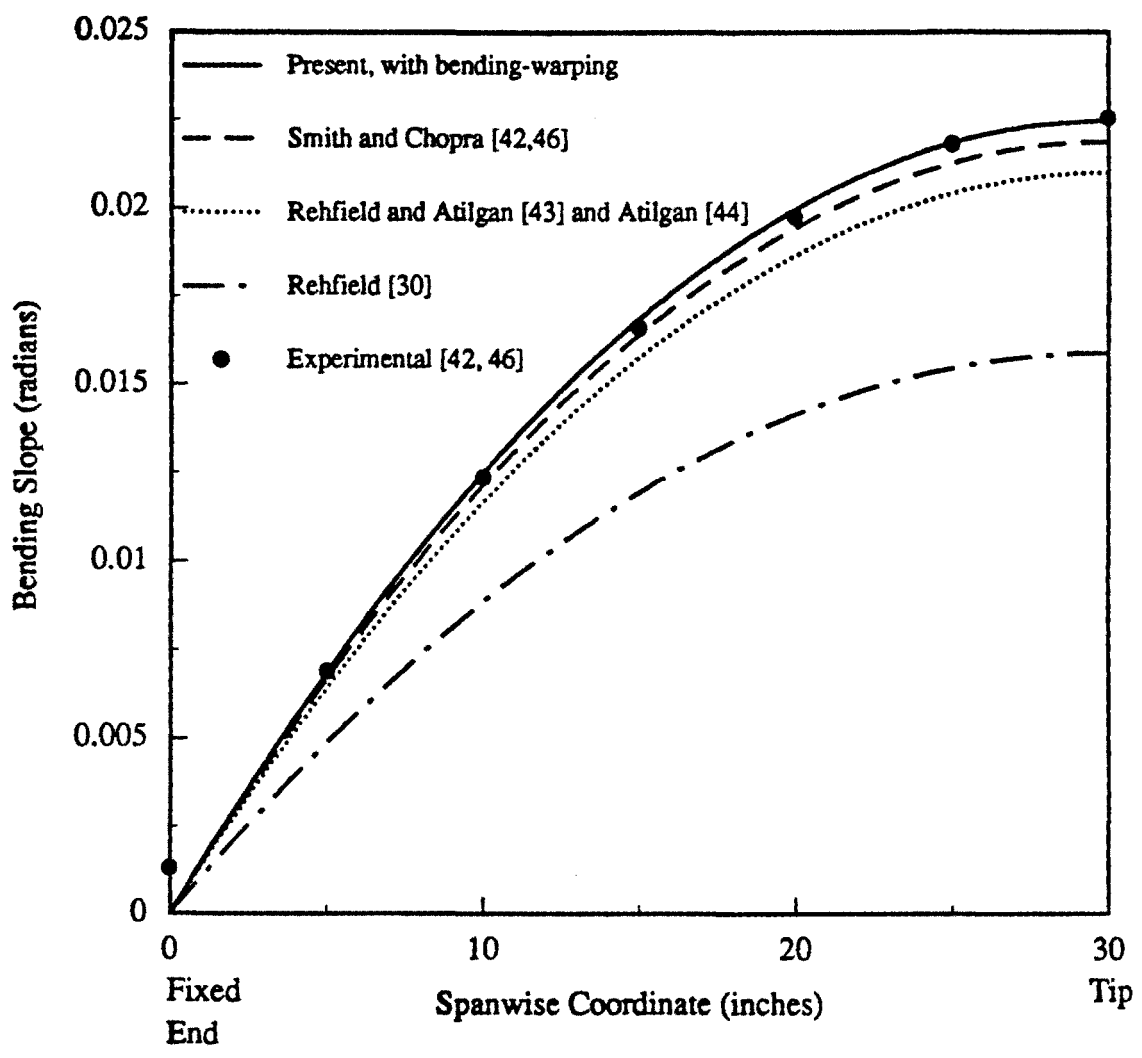


Figure 5.5: Bending Slope of a Symmetric $[30]_6$ Cantilever Under 1 lb Transverse Tip Load

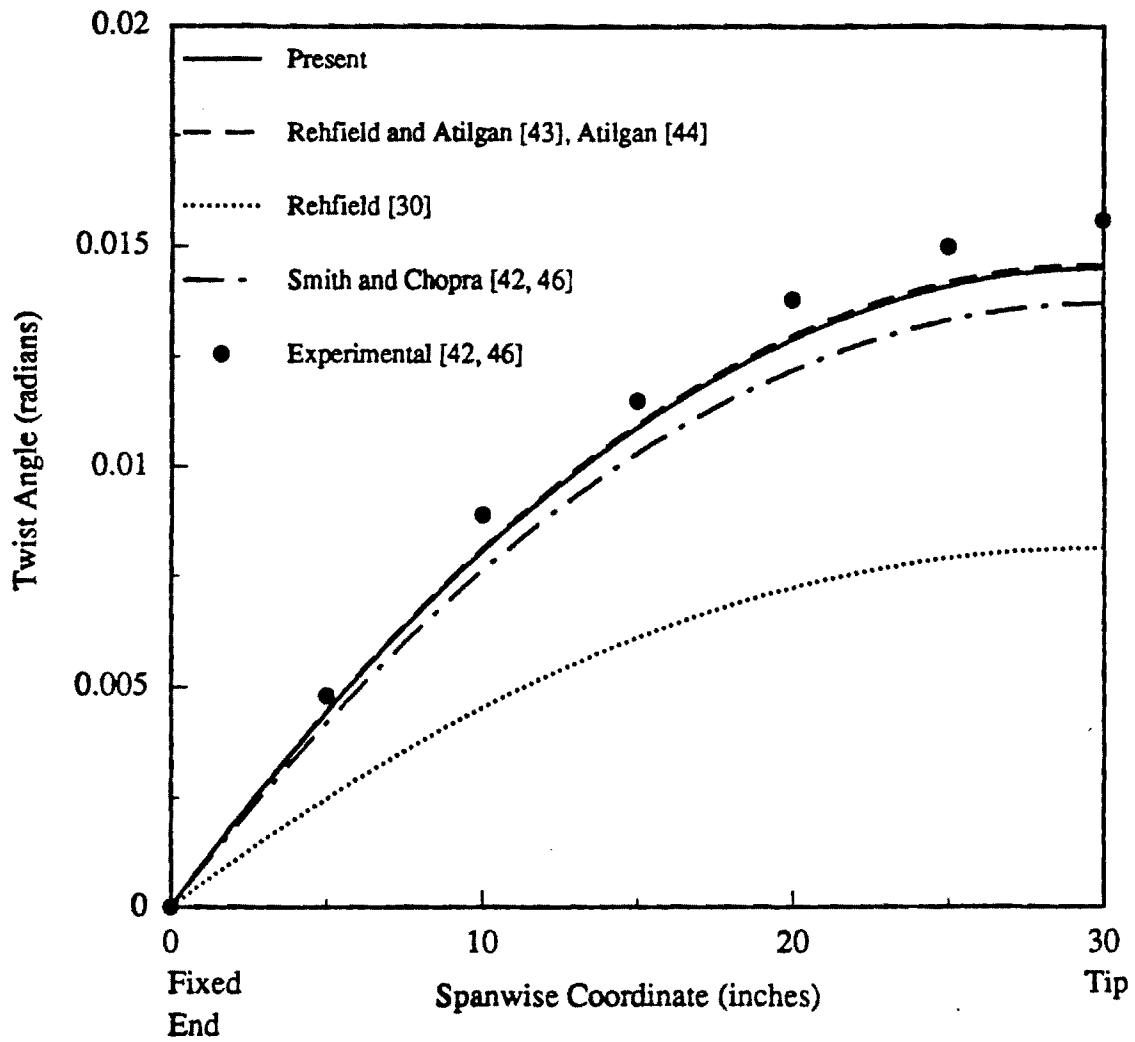


Figure 5.6: Twist of a Symmetric $[30]_6$ Cantilever Under 1 lb Transverse Tip Load

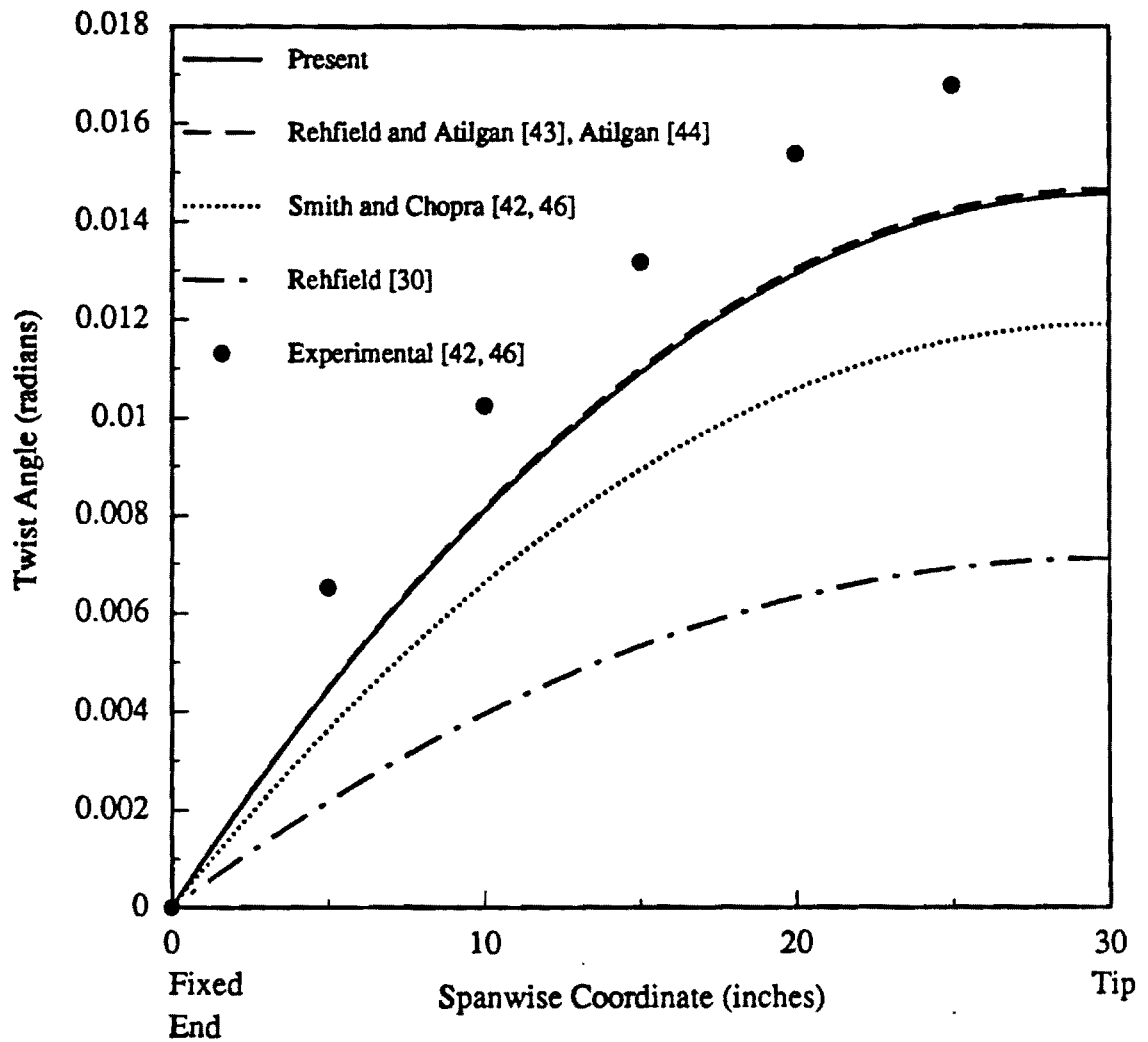


Figure 5.7: Twist of a Symmetric $[45]_6$ Cantilever Under 1 lb Transverse Tip Load

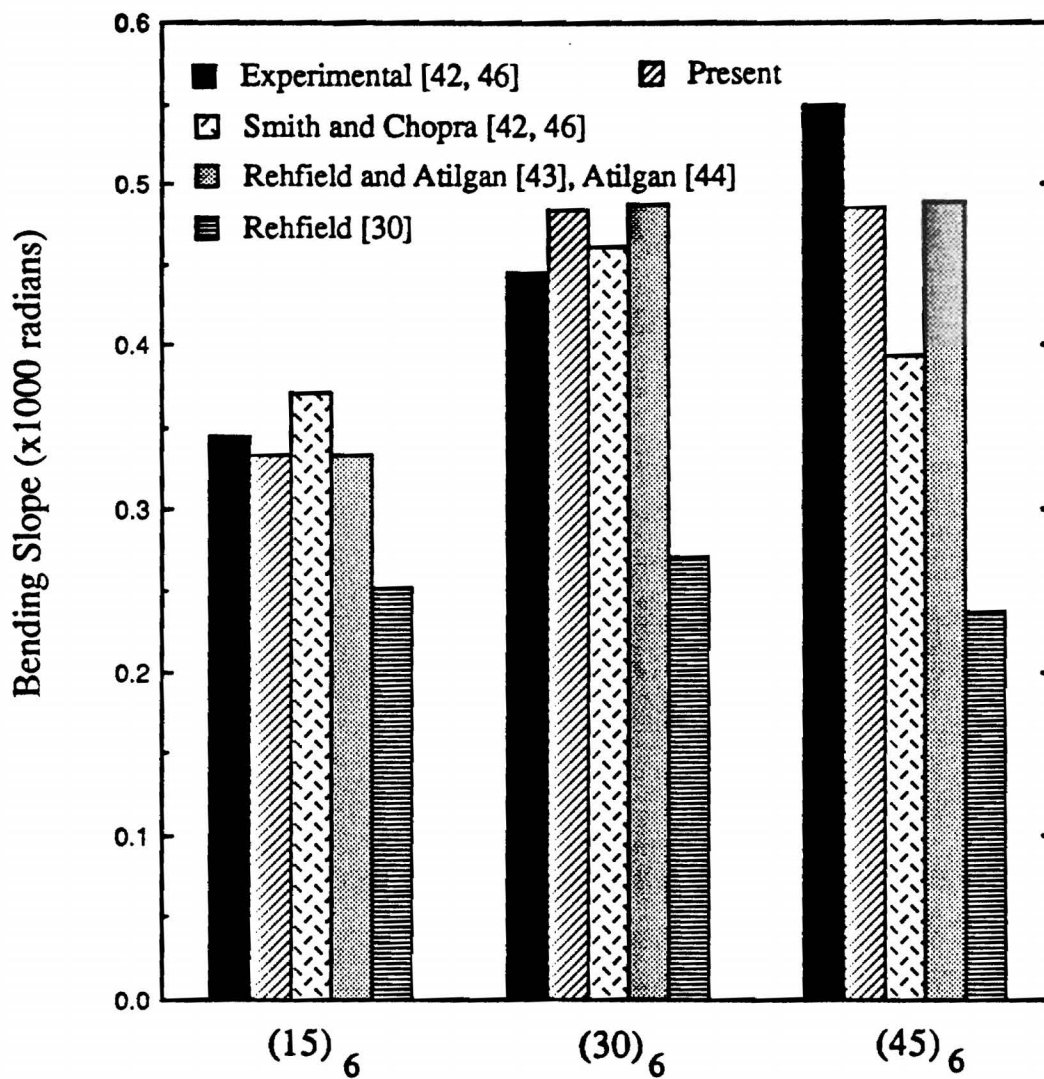


Figure 5.8: Bending Slope at Mid-Span Under Unit Tip Torque of Symmetric Lay-up Cantilever Beams

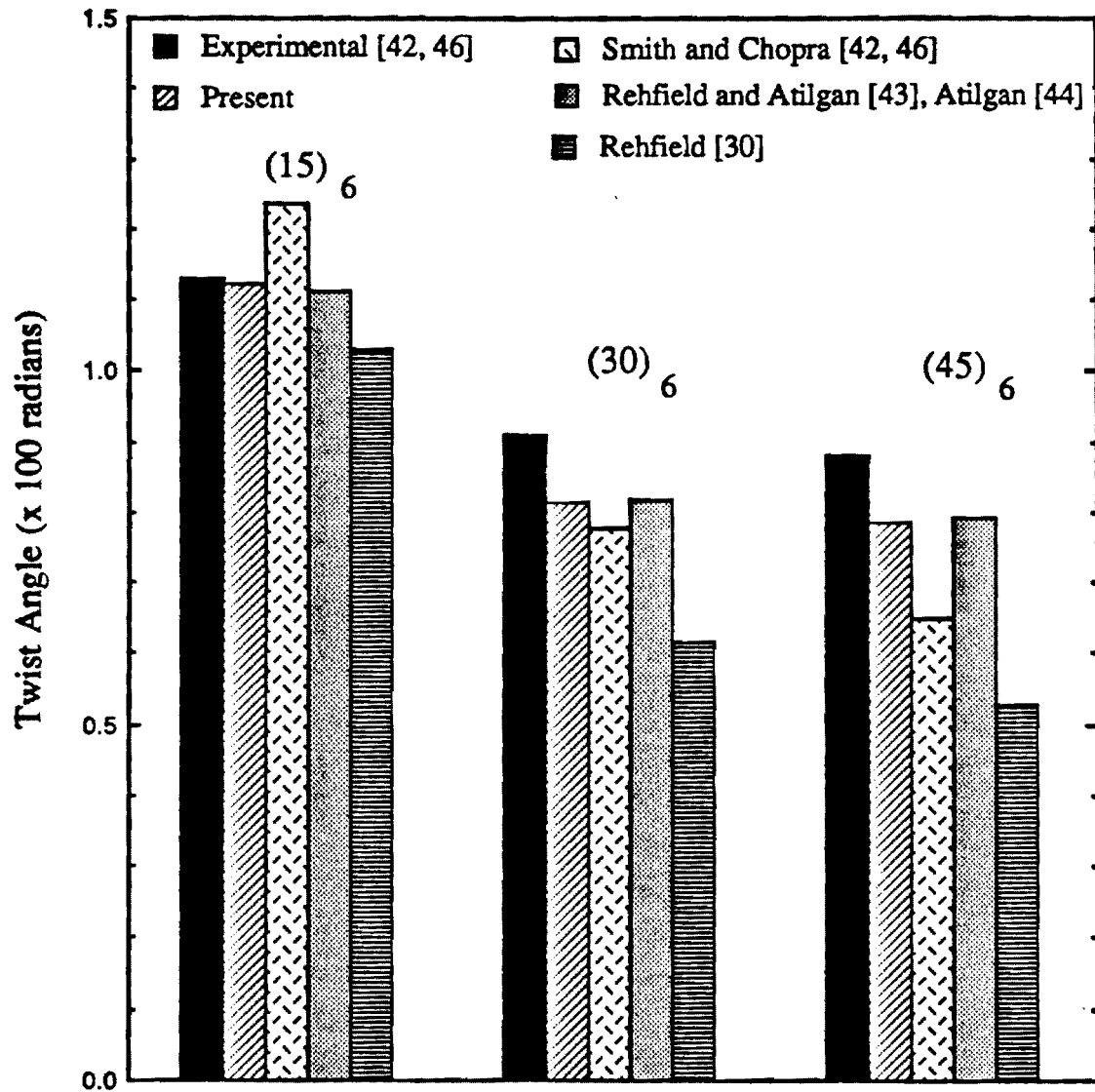


Figure 5.9: Twist at Mid-Span Under Unit Tip Torque of Symmetric Lay-up Cantilever Beams

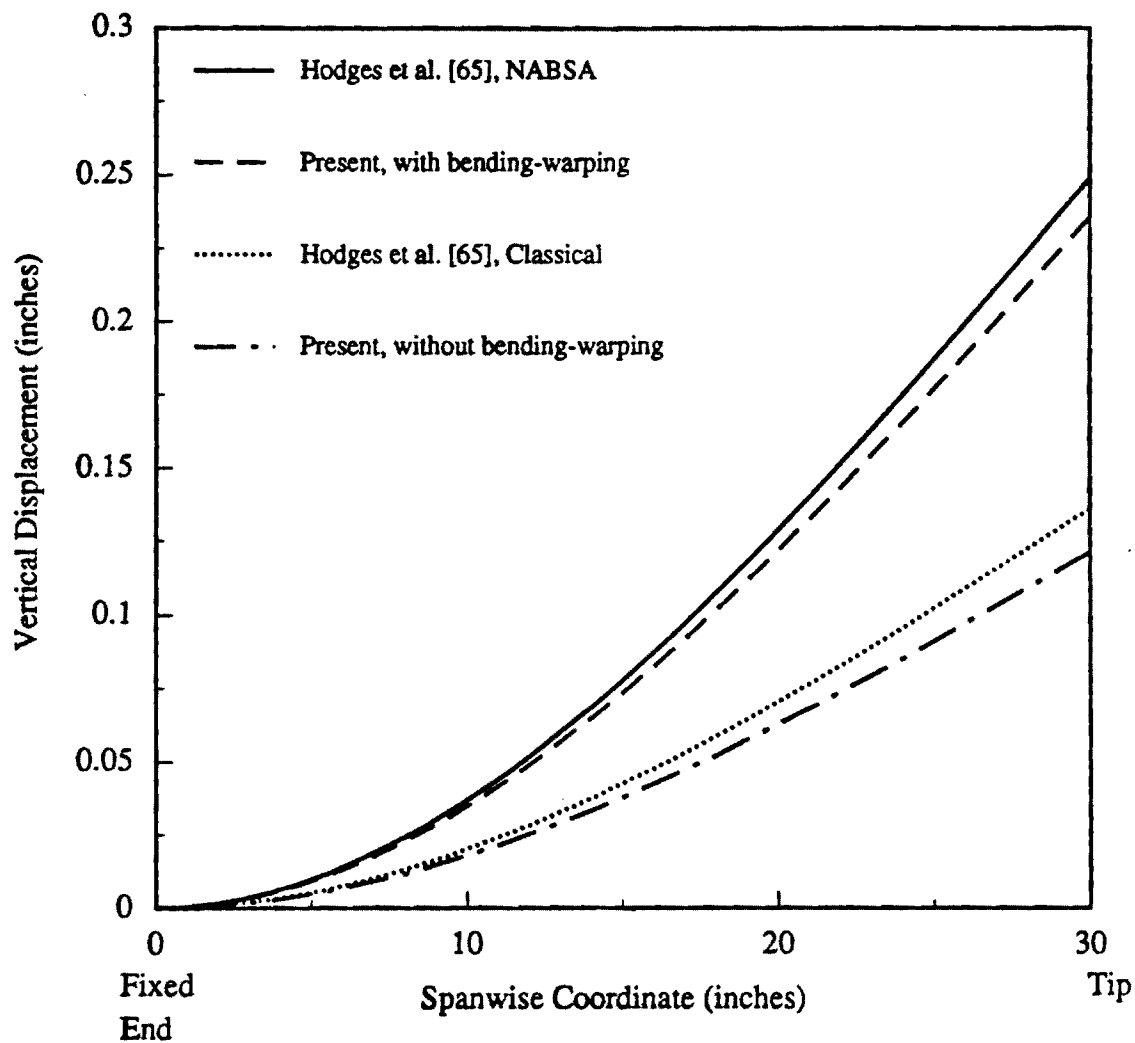


Figure 5.10: Deflection of an Antisymmetric $[15]_6$ Cantilever under 1 lb transverse tip load

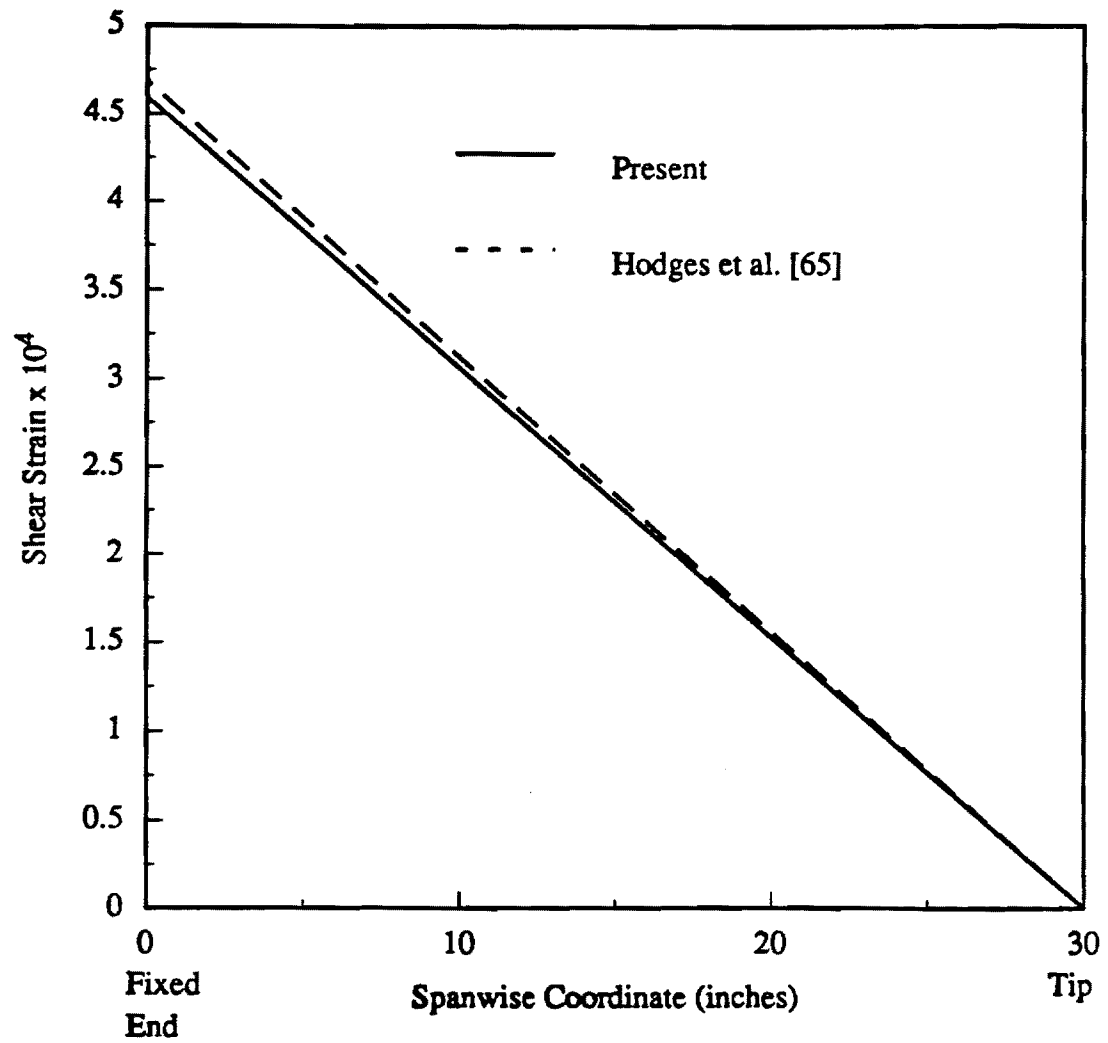


Figure 5.11: Shear Deformation γ_{xy} of an Antisymmetric $[15]_6$ Cantilever under 1 lb transverse tip load

CHAPTER VI

CONCLUSIONS AND RECOMMENDATIONS

This research addresses two key issues for the continuing implementation of composites in advanced structures namely, the understanding of the role of the material's anisotropy on its stiffness behavior and its damage modes. An analytical model based upon a shear deformation theory and a sublaminate approach was developed in order to investigate mid-plane and matrix crack-tip delaminations. This model was combined with an earlier analysis for mixed-mode free-edge delamination to form an integrated code for the prediction of damage onset in laminated composites. The code predictions were validated by comparing its results with test data. Of significance is the ability it provides for the prediction of damage progression sequence and corresponding critical strains. Moreover, the effect of hygrothermal stresses on the strain energy release rate and interlaminar stresses was isolated. The increase in strain energy release rate and interlaminar stresses associated with curing stresses can precipitate failure and should be considered for an accurate prediction of failure.

The findings of this research work point to new research inquiries. The first is characterization and prediction of damage onset and growth under cyclic loading including the effect of hygrothermal stresses. The investigation can lead to the determination of composite components' life and inspection intervals. The second is the study of the effect of damage modes and their interactions on the vibration characteristics and damping of laminated composites. The result of this investigation will assess the effect of damage modes on the natural frequencies and mode shapes and

can lead to the development of Non-Destructive Evaluation methods.

The asymptotical analysis used to develop the thin-walled anisotropic beam theory provides a rigorous basis for the prediction of the beam stiffnesses and associated displacement field. Closed-form expressions for the stiffnesses have been developed and new contributions to the warping have been found. This analysis can be extended to beams with multi-cell type cross sections and pretwisted configurations. Moreover, the previous results on the effects of hygrothermal stresses point to the significance of including their contribution in the thin-walled closed section beam analysis. The consideration of dynamic and aerodynamic loadings using asymptotical analysis will provide a rigorous basis for the investigation of the dynamic and aeroelastic response of composite structures. Finally, the presence of embedded delamination on the response of composite beams is a first step toward studying the effect of damage modes on their stiffness and strength. In this respect, the analysis of composite beams with open cross section can be regarded as the final stage of damage in a closed section beam.

When accomplished, these recommended research tasks will provide an understanding of the effects of damage on the performance of advanced structures made out of composite and will lead to the development of reliable design tools to ensure their damage tolerance.

Appendix A

Convergence of Displacement Field

In this appendix detailed calculation of the third and final cycle is provided. Results show that no additional correction terms of the same order in the energy functional emerge and the displacement field given in Eq. (4.68) is the converged one.

1.1 Third-Order Approximation

A third cycle is carried out by rewriting the displacement field in Eq. (4.68) in the form

$$\begin{aligned}
 v_1 &= U_1(x) - y(s)U_2'(x) - z(s)U_3'(x) + G(s)\varphi'(x) \\
 &\quad + g_1(s)U_1'(x) + g_2(s)U_2''(x) + g_3(s)U_3''(x) + \tilde{w}_1(s, x) \\
 v_2 &= U_2(x)\frac{dy}{ds} + U_3(x)\frac{dz}{ds} + \varphi(x)r_n + \tilde{w}_2(s, x) \\
 v &= U_2(x)\frac{dz}{ds} - U_3(x)\frac{dy}{ds} - \varphi(x)r_t + \tilde{w}(s, x)
 \end{aligned} \tag{A-1}$$

where \tilde{w}_1 , \tilde{w}_2 and \tilde{w} are correction functions to be determined based on their contributions to the energy functional.

Substitute Eq. (A-1) into (4.7) to obtain the strains and curvatures in terms of the displacement corrections

$$\begin{aligned}
 \gamma_{11} &= \check{\gamma}_{11} + \frac{\partial \tilde{w}_1}{\partial x} \\
 2\gamma_{12} &= 2\check{\gamma}_{12} + \frac{\partial \tilde{w}_2}{\partial x} + 2\hat{\gamma}_{12} \quad , \quad 2\hat{\gamma}_{12} = \frac{\partial \tilde{w}_1}{\partial s} \\
 \gamma_{22} &= \check{\gamma}_{22} + \hat{\gamma}_{22} \quad , \quad \hat{\gamma}_{22} = \frac{\partial \tilde{w}_2}{\partial s} + \frac{\tilde{w}}{R}
 \end{aligned}$$

$$\begin{aligned}
\rho_{11} &= \check{\rho}_{11} + \frac{\partial^2 \bar{w}_i}{\partial x^2} \\
\rho_{12} &= \check{\rho}_{12} + \frac{\partial^2 \bar{w}_i}{\partial s \partial x} - \frac{3}{4R} \frac{\partial \bar{w}_2}{\partial x} + \hat{\rho}_{12} \quad , \quad \hat{\rho}_{12} = \frac{1}{4R} \frac{\partial \bar{w}_1}{\partial s} \\
\rho_{22} &= \check{\rho}_{22} + \hat{\rho}_{22} \quad , \quad \hat{\rho}_{22} = \frac{\partial^2 \bar{w}_i}{\partial s^2} - \frac{\partial}{\partial s} \left(\frac{\bar{w}_2}{R} \right)
\end{aligned} \tag{A-2}$$

where $\check{\gamma}_{\alpha\beta}$ and $\check{\rho}_{\alpha\beta}$ are the strains and curvatures corresponding to the second-order approximation. These are expressed as

$$\begin{aligned}
\check{\gamma}_{11} &= \underbrace{\left(\frac{\Delta}{L} \right)}_{U_1'(x)} - \underbrace{\left(\frac{\Delta d}{L^2} \right)}_{yU_2''(x)} - \underbrace{\left(\frac{\Delta d}{L^2} \right)}_{zU_3''(x)} + \underbrace{\left(\frac{\Delta d}{L^2} \right)}_{G(s)\varphi''(x)} \\
&\quad + \underbrace{\left(\frac{\Delta d}{L^2} \right)}_{g_1(s)U_1''(x)} + \underbrace{\left(\frac{\Delta d^2}{L^3} \right)}_{g_2U_2'''(x)} + \underbrace{\left(\frac{\Delta d^2}{L^3} \right)}_{g_3U_3'''(x)} \\
2\check{\gamma}_{12} &= \underbrace{\left(\frac{\Delta}{L} \right)}_{\frac{2A_\epsilon}{l\bar{c}}c\varphi'(x)} + \underbrace{\left(\frac{\Delta}{L} \right)}_{\frac{dg_1}{ds}U_1'(x)} + \underbrace{\left(\frac{\Delta d}{L^2} \right)}_{\frac{dg_2}{ds}U_2''(x)} + \underbrace{\left(\frac{\Delta d}{L^2} \right)}_{\frac{dg_3}{ds}U_3''(x)} \\
\check{\gamma}_{22} &= 0 \\
\check{\rho}_{11} &= U_2''(x) \frac{dz}{ds} - U_3''(x) \frac{dy}{ds} - \varphi''(x)r_t \sim O\left(\frac{\Delta}{L^2}\right) \\
\check{\rho}_{12} &= \frac{1}{4R} \frac{dg_1}{ds} U_1'(x) + \left(\frac{1}{4R} \frac{2A_\epsilon}{l\bar{c}} c - 1 \right) \varphi'(x) \sim O\left(\frac{\Delta}{dL}\right) \\
\check{\rho}_{22} &= 0
\end{aligned} \tag{A-3}$$

An order of magnitude comparison for each strain and curvature measure shows that some terms of higher order in $\check{\gamma}_{11}$ can be cancelled and its expression simplifies to

$$\check{\gamma}_{11} = \underbrace{\left(\frac{\Delta}{L} \right)}_{U_1'(x)} - \underbrace{\left(\frac{\Delta d}{L^2} \right)}_{yU_2''(x)} - \underbrace{\left(\frac{\Delta d}{L^2} \right)}_{zU_3''(x)} + \underbrace{\left(\frac{\Delta d}{L^2} \right)}_{G(s)\varphi''(x)}$$

Among the new terms introduced by the function \bar{w}_i , the leading ones are denoted by superscript $\hat{\cdot}$ in Eq. (A-2). The order of \bar{w}_i is assumed to be

$$\bar{w}_i \sim O\left(\frac{\Delta d^3}{L^3}\right) \tag{A-4}$$

Consequently, the order of magnitude of the leading terms in Eq. (A-2), is as follows

$$\begin{aligned}\hat{\gamma}_{12} \sim \hat{\gamma}_{22} &\sim O\left(\frac{\Delta d^2}{L^3}\right) \\ \hat{\rho}_{12} \sim \hat{\rho}_{22} &\sim O\left(\frac{\Delta d}{L^3}\right)\end{aligned}\quad (\text{A-5})$$

The energy functional can be represented by $\Phi(\gamma_{11}, 2\gamma_{12}, \gamma_{22}, \rho_{11}, \rho_{12}, \rho_{22})$. By keeping the strains and curvature associated with the second-order approximation and the leading terms contribution over the other terms (i.e., by dropping the terms $\frac{\partial \hat{w}_1}{\partial x}$, $\frac{\partial \hat{w}_2}{\partial x}$, $\frac{\partial^2 \hat{w}}{\partial x^2}$, and $\frac{\partial^2 \hat{w}}{\partial s \partial x} - \frac{1}{4R} \frac{\partial \hat{w}_2}{\partial x}$ in Eq. (A-2)) the energy function can be written as

$$\Phi(\check{\gamma}_{11}, 2\check{\gamma}_{12} + 2\hat{\gamma}_{12}, 0 + \hat{\gamma}_{22}, \check{\rho}_{11}, \check{\rho}_{12} + \hat{\rho}_{12}, 0 + \hat{\rho}_{22}) \quad (\text{A-6})$$

In the following, the order of magnitude of the energy due to bending, i.e. due to $\check{\rho}_{11}$, $\check{\rho}_{12}$, $\hat{\rho}_{12}$, and $\hat{\rho}_{22}$, is assessed.

The interaction terms associated with $\check{\rho}_{11}$, namely

$$h\check{\rho}_{11}\hat{\gamma}_{12}, h\check{\rho}_{11}\hat{\gamma}_{22}, h^2\check{\rho}_{11}\hat{\rho}_{12}, h^2\check{\rho}_{11}\hat{\rho}_{22}$$

are of order $\left(\frac{\Delta^2 h d^2}{L^5}\right)$ or smaller. They are neglected in comparison with the following membrane contribution to the energy

$$\check{\gamma}_{11}\hat{\gamma}_{12}, \check{\gamma}_{11}\hat{\gamma}_{22}, \check{\gamma}_{12}\hat{\gamma}_{12}, \check{\gamma}_{12}\hat{\gamma}_{22} \begin{cases} \sim O\left(\frac{\Delta^2 d^2}{L^4}\right) & \text{associated with } U'_1 \text{ and } \varphi' \\ \sim O\left(\frac{\Delta^2 d^3}{L^5}\right) & \text{associated with } U''_2 \text{ and } U''_3 \end{cases} \quad (\text{A-7})$$

The interaction terms due to the bending curvature $\check{\rho}_{12}$ are

$$h\check{\rho}_{12}\hat{\gamma}_{12}, h\check{\rho}_{12}\hat{\gamma}_{22} \sim O\left(\frac{\Delta^2 h d}{L^4}\right) \text{ associated with } U'_1 \text{ and } \varphi'$$

$$h^2\check{\rho}_{12}\hat{\rho}_{12}, h^2\check{\rho}_{12}\hat{\rho}_{22} \sim O\left(\frac{\Delta^2 h^2}{L^4}\right) \text{ associated with } U'_1 \text{ and } \varphi'$$

These terms are of higher order of magnitude in comparison with the corresponding membrane contribution in Eq. (A-7), and may be neglected. The remaining interaction terms associated with $\hat{\rho}_{12}$ and $\hat{\rho}_{22}$, namely

$$h\check{\gamma}_{11}\hat{\rho}_{12}, h\check{\gamma}_{12}\hat{\rho}_{12}, h\check{\gamma}_{11}\hat{\rho}_{22}, h\check{\gamma}_{12}\hat{\rho}_{22} \begin{cases} \sim O\left(\frac{\Delta^2hd}{L^4}\right) & \text{associated with } U_1' \text{ and } \varphi' \\ \sim O\left(\frac{\Delta^2hd^2}{L^5}\right) & \text{associated with } U_2'' \text{ and } U_3'' \end{cases}$$

may also be neglected in comparison with (A-7). Therefore in order to determine the functions \tilde{w}_i , one has to minimize the shell energy expressed by

$$I = \int_0^L \int \Phi(\check{\gamma}_{11}, 2\check{\gamma}_{12} + 2\hat{\gamma}_{12}, \hat{\gamma}_{22}, 0, 0, 0) dsdx \quad (\text{A-8})$$

Setting the first variation of the energy functional to zero to get Eq. (4.45). Substitute from Eq. (A-2) into Eq. (4.45) to obtain

$$\begin{aligned} & \frac{1}{2} \overbrace{B}^{(Eh)} \left[\overbrace{U_1'(x)}^{\left(\frac{\Delta}{L}\right)} - \overbrace{y(s)U_2''}^{\left(\frac{\Delta d}{L^2}\right)} - \overbrace{z(s)U_3''}^{\left(\frac{\Delta d}{L^2}\right)} + \overbrace{G(s)\varphi''(x)}^{\left(\frac{\Delta d}{L^2}\right)} + \overbrace{\frac{\partial \tilde{w}_1}{\partial x}}^{\left(\frac{\Delta d^3}{L^4}\right)} \right] \\ & + \frac{1}{4} \overbrace{C}^{(Eh)} \left[\overbrace{\frac{2A_c}{l\bar{c}}c\varphi'(x)}^{\left(\frac{\Delta}{L}\right)} + \overbrace{\frac{dg_1}{ds}U_1'(x)}^{\left(\frac{\Delta}{L}\right)} + \overbrace{\frac{dg_2}{ds}U_2''(x)}^{\left(\frac{\Delta d}{L^2}\right)} \right. \\ & \left. + \overbrace{\frac{dg_3}{ds}U_3''(x)}^{\left(\frac{\Delta d}{L^2}\right)} + \overbrace{\frac{\partial \tilde{w}_2}{\partial x}}^{\left(\frac{\Delta d^3}{L^4}\right)} + \overbrace{\frac{\partial \tilde{w}_1}{\partial s}}^{\left(\frac{\Delta d^2}{L^3}\right)} \right] = \text{constant} \quad (\text{A-9}) \end{aligned}$$

Equation (A-9) shows that the contribution of \tilde{w} is of higher order in comparison with all other terms and may be cancelled from the left hand side. Therefore no additional corrections to the displacement field emerges, and the displacement field obtained in

Eq. (4.68) is the converged one. An alternative is to neglect the terms of higher order in Eq. (A-9), while keeping the leading \tilde{w}_1 term, to obtain

$$\begin{aligned} & \frac{1}{2}B [U_1'(x) - y(s)U_2'' - z(s)U_3''] \\ & + \frac{1}{4}C \left[\frac{2A_e}{l\bar{c}} c\varphi'(x) + \frac{dg_1}{ds}U_1'(x) + \frac{dg_2}{ds}U_2''(x) + \frac{dg_3}{ds}U_3''(x) + \frac{\partial \tilde{w}_1}{\partial s} \right] = \text{constant} \end{aligned} \quad (\text{A} - 10)$$

Solution of Eq. (A-10) is determined using the single value condition of the axial displacement and \tilde{w}_1 is found to be a function of x only. Such a function has already been considered and no new terms of the same order in the energy functional are generated from the third and therefore final cycle.

Bibliography

- [1] O'Brien, T.K., "Characterization of Delamination Onset and Growth in a Composite Laminate," *Damage in Composite Materials, ASTM STP 775*, K.L. Reifsnider, Ed., 1982, pp. 140-167.
- [2] Wilkins, D.J., Eisemann, J.R., Camin, R.A., Margolis, W.S., and Benson, R.A., "Characterizing Delamination Growth in Graphite-Epoxy," *Damage in Composite Materials, ASTM STP 775*, K.L. Reifsnider, Ed., 1982, pp. 168-183.
- [3] O'Brien, T.K., "Mixed-Mode Strain Energy Release Rate Effects on Edge Delamination of Composites," *Effects of Defects in Composite Materials, ASTM STP 836*, 1984, pp. 125-142.
- [4] Wang, S.S., and Choi, I., "The Mechanics of Delamination in Fiber Reinforced Composite Materials. Part II - Delamination Behavior and Fracture Mechanics Parameters," *NASA CR-172270*, 1983.
- [5] Wang, S.S., "Edge Delamination in Angle Ply Composite Laminates," *Proceedings of the 22nd AIAA/ASME/ASC/AHS Structures, Structural Dynamics and Materials Conference*, Atlanta, Ga, 6-8 April, 1981, pp. 473-484.
- [6] Armanios, E.A., and Rehfield, L.W., "Sublaminar Analysis of Interlaminar Fracture in Composites: Part I - Analytical Model," *Journal of Composites Technology and Research*, Vol. 11, No. 4, 1989, pp. 135-146.

- [7] Armanios, E.A., Rehfield, L.W., Raju, I.S., and O'Brien, T.K., "Sublaminar Analysis of Interlaminar Fracture in Composites: Part II - Applications," *Journal of Composites Technology and Research*, Vol. 11, No. 4, 1989, pp. 147-153.
- [8] Crossman, F.W., and Wang, A.S.D., "The Dependence of Transverse Cracking and Delamination on Ply Thickness in Graphite/Epoxy Laminates," *Damage in Composite Materials*, ASTM STP 775, K.L. Reifsnider, Ed., 1982, pp. 118-139.
- [9] O'Brien, T.K., "Analysis of Local Delaminations and their Influence on Composite Laminate Behavior," *Delamination and Debonding of Materials*, ASTM STP 876, W.S. Johnson, Ed., 1985, pp. 282-297.
- [10] Law, G.E., "A Mixed Mode Fracture Analysis of ($\pm 25/90_n$), Graphite/Epoxy Composite Laminates," *Effects of Defects in Composite Materials*, ASTM STP 836, 1984, pp. 143-160.
- [11] Wang, A.S.D, Kishore, N.N., and Li, C.A., "Crack Development in Graphite Epoxy Cross Ply Laminates under Uniaxial Tension," *Composites Science and Technology*, Vol. 24, No. 1, 1985, pp. 1-31.
- [12] Fish, John C. , and O'Brien, T. Kevin, "Three-Dimensional Finite Element Analysis of Delamination from Matrix Cracks in Glass-Epoxy Laminates," *Testing and Design*, *ASTM 10th Symposium on Composite Materials*, San Francisco, CA., April 24-25, 1990.
- [13] Russell, A.J., and Street, K.N., "Moisture and Temperature Effects on the Mixed Mode Delamination Fracture of Unidirectional Graphite/Epoxy," *Delamination and Debonding of Materials*, ASTM STP 876, W.S. Johnson, Ed., 1985, pp. 349-370.

- [14] O'Brien, T.K., Raju, I.S., and Garber, D.P., "Residual Thermal and Moisture Influences on the Strain Energy Release Rate Analysis of Edge Delamination," *Journal of Composites Technology and Research*, Vol. 8, No. 2, 1986, pp. 37-47.
- [15] Armanios, E.A., and Mahler, M.A., "Residual Thermal and Moisture Influences on the Free-Edge Delamination of Laminated Composites," *Proceedings of the 29th AIAA/ASME/AHS/ASC Structures, Structural Dynamics and Materials Conference*, Williamsburg, Va., 18-20 April, 1988, pp. 371-381. AIAA Paper 88-2259.
- [16] Aoki, Takahira and Kondo, Kyohei, "Delamination Energy Release Rates under Thermal Loading in Fiber-Reinforced Composite Laminates," *Composite Structures*, Vol. 14, 1990, pp. 213-231.
- [17] Kondo, K. and Aoki, T., "An Energy Release Rate Approach for Free-Edge Delamination Problem in Composite Laminates," *Composite Structures*, Vol. 2, No. 4, 1987, pp. 241-257.
- [18] Whitney, J.M., "Stress Analysis of Mode I Edge Delamination Specimen for Composite Materials," *AIAA Journal*, Vol. 24, No. 7, 1986, pp. 1163-1168.
- [19] Jones, R.M., *Mechanics of Composite Materials*, McGraw Hill Book Co., New York, 1975.
- [20] Whitney, J. M. and Knight, M., "A Modified Free-Edge Delamination Specimen," *Delamination and Debonding of Materials*, ASTM STP 876, edited by W. S. Johnson, Philadelphia, 1985, pp. 298-314.
- [21] Irwin, G. R., "Fracture I," *Handbuk der Physik*, Vol. VI, Flugge, Ed., Springer-Verlag, 1958, pp. 558-590.

- [22] Armanios, E.A., Rehfield, L.W., and Weinstein, F., "Understanding and Predicting Sublaminar Damage Mechanisms in Composite Structures," *Composite Materials: Testing and Design (Ninth Volume)*, *ASTM STP 1059*, S.P. Garbo, Ed., 1990, pp. 231-249.
- [23] Wang, A.S.D., Kishore, N.N., and Feng, W.W., "On Mixed Mode Fracture in Off-Axis Unidirectional Graphite-Epoxy Composites," *Progress in Science and Engineering of Composites*, T. Hayashi, K Kawata and S. Umekawa, Eds., ICCM-IV, Tokyo, 1982, pp. 599-606.
- [24] V. L. Berdichevsky, "On the Energy of an Elastic Rod," *Journal of Applied Mathematics and Mechanics (PMM)*, Vol. 45, 1982, pp.518-529.
- [25] Berdichevsky, V. L., "Variational-Asymptotic Method of Constructing a Theory of Shells," *Journal of Applied Mathematics and Mechanics (PMM)* Vol. 43, No. 4, 1979, pp. 664-687
- [26] Hodges, D. H., "Review of Composite Rotor Blade Modeling," *AIAA Journal*, Vol.28, No. 3, 1990. pp. 561-565.
- [27] Reissner E. and Tsai, W. T., "Pure Bending, Stretching, and Twisting of Anisotropic Cylindrical Shells," *Journal of Applied Mechanics*, Vol. 39, March 1972, pp. 148-154.
- [28] Mansfield, E. H., and Sobey, A. J., "The Fibre Composite Helicopter Blade - Part 1: Stiffness Properties - Part 2: Prospect for Aeroelastic Tailoring," *Aeronautical Quarterly*, Vol. 30, May 1979, pp. 413-449.
- [29] Libove, C., "Stresses and Rate of Twist in Single-Cell Thin-Walled Beams with

- Anisotropic Walls," *AIAA Journal*, Vol. 26, No. 9, September 1988, pp. 1107-1118.
- [30] Rehfield, L. W., "Design Analysis Methodology for Composite Rotor Blades," *Proceedings of the Seventh DoD/NASA Conference on Fibrous Composites in Structural Design*, AFWAL-TR-85-3094, June 1985, pp. (V(a)-1)-(V(a)-15).
- [31] Borri, M., and Merlini, T., "A Large Displacement Formulation for Anisotropic Beam Analysis," *Meccanica*, Vol.21, 1986, pp. 30-37.
- [32] Giavotto, V., Borri, M., Mantegazza, P., Ghiringhelli, G., Carmashi, V., Maffioli, G.C., and Mussi, F., "Anisotropic Beam Theory and Applications," *Computers and Structures*, Vol. 16, No. 1-4, 1983, pp. 403-413.
- [33] Bauchau, O.A., and Hong, C.H., "Large Displacement Analysis of Naturally Curved and Twisted Composite Beams," *AIAA Journal*, Vol. 25, No.10, 1987, pp. 1469-1475.
- [34] Bauchau, O.A., and Hong, C.H., "Nonlinear Composite Beam Theory," *Journal of Applied Mechanics*, Vol.55, No.1, 1988, pp. 156-163.
- [35] Librescu, L. and Song, O., "Static Aeroelastic Tailoring of Composite Aircraft Wings Modeled as Thin-Walled Beam Structure," Presented at the *Fifth Japan-US Conference on Composite Materials*, June 24-27, 1990, Tokyo, Japan.
- [36] Kosmatka, J.B., "Structural Dynamic Modeling of Advanced Composite Propellers by the Finite Element Method," *Ph.D. Dissertation*, University of California, Los Angeles, 1986.
- [37] Lee, S.W., and Stemple, A.D., "A Finite Element Model for Composite Beams with Arbitrary Cross-Sectional Warping," *Proceedings of the 28th Structures*,

- Structural Dynamics and Materials Conference*, April 6-8, 1987, Monterey, California, AIAA Paper No. 87-0773, pp. 304-313.
- [38] Nixon, M.W., "Analytical and Experimental Investigations of Extension-Twist-Coupled Structures," *M.Sc. Thesis*, George Washington University, May 1989.
- [39] Nixon, Mark W., "Improvements to Tilt Rotor Performance Through Passive Blade Twist Control," *NASA TM 100583, USAAVSCOM TM 88-B-010*, April 1988.
- [40] Nixon, M.W., "Preliminary Structural Design of Composite Main Rotor Blades for Minimum Weight," *NASA TP 2730, AVSCOM TM 87-B-6*, July 1987.
- [41] Chandra, R., Stemple, A. D., and Chopra, I., "Thin-walled Composite Beams under Bending, Torsional, and Extensional Loads," *Journal of Aircraft*, Vol. 27, No. 7, July 1990, pp. 619-626.
- [42] Smith, Edward C., and Chopra, Inderjit, "Formulation and Evaluation of an Analytical Model for Composite Box-Beams," *Proceedings of the 31st Structures, Structural Dynamics and Materials Conference*, Long Beach, California, April 2-4, 1990, pp. 759-782.
- [43] Rehfield, L.W., and Atilgan, A.R., "Shear Center and Elastic Axis and Their Usefulness for Composite Thin-Walled Beams," *Proceedings of the American Society For Composites, Fourth Technical Conference*, Blacksburg, Virginia, October 3-5, 1989.
- [44] Atilgan, Ali Rana, "Towards A Unified Analysis Methodology For Composite Rotor Blades," *Ph. D. Dissertation*, School of Aerospace Engineering, Georgia Institute of Technology, August 1989.

- [45] Rehfield, L. W., Atilgan, A. R., and Hodges, D. H., "Nonclassical Behavior of Thin-Walled Composite Beams with Closed Cross Sections." *Journal of the American Helicopter Society*, Vol. 35, (2), April 1990, pp. 42-50.
- [46] Smith, Edward C., and Chopra, Inderjit, "Formulation and Evaluation of an Analytical Model for Composite Box-Beams," *Journal of the American Helicopter Society*, July 1991, pp.23-35.
- [47] Hong, C. H., and Chopra, I., "Aeroelastic Stability of a Composite Blade," *Journal of the American Helicopter Society*, Vol. 30, No. 2, 1985, pp. 57-67.
- [48] Stemple, A. D., and Lee, S. W., "A Finite Element Model for Composite Beams with Arbitrary Cross-Sectional Warping," *AIAA Journal*, Vol. 26, No. 12, 1988.
- [49] Berdichevsky, V. L. "Variational-Asymptotic Method of Constructing the Non-linear Shell Theory," *W. T. Koiter and G. K. Mikhailov, Eds., Theory of Shells*, North-Holland Publishing Company , 1980, pp. 137-161.
- [50] Vinson, J. R., and Sierakowski, R. L., *The Behavior of Structures Composed of Composite Materials*, Martinus Nijhoff Publishers, 1987.
- [51] Hodges, D. H., Atilgan A. R., Fulton M. V., and Rehfield L. W., "Dynamic Characteristics of Composite Beam Structures," *Proceedings of the AHS National Specialists' Meeting on Rotorcraft Dynamics*, Fort Worth, Texas, Nov. 13-14, 1989.
- [52] Sokolnikoff, I. S., *Mathematical Theory of Elasticity*, McGraw-Hill, New York, 1956.
- [53] Timoshenko, S., and Goodier, J. N., *Theory of Elasticity*, McGraw-Hill, New York, 1951.

- [54] Washizu, K., *Variational Methods in Elasticity and Plasticity*, Pergamon, New York, 1968.
- [55] Wempner, G., *Mechanics of Solids with Applications to Thin Bodies*, Sijthoff & Noordhoff International Publishers, 1981.
- [56] Crandall, Stephen H., Dahl, Norman C., and Lardner, Thomas J., *An Introduction to the Mechanics of Solids*, McGraw-Hill Book Company, 1978.
- [57] Gjelsvik, Atle, *The Theory of Thin Walled Bars*, John Wiley & Sons, 1981.
- [58] Libai, A., and Simmonds, J. G., *The Nonlinear Theory of Elastic Shells : One Spatial Dimension*, Academic Press, Inc., 1988.
- [59] Megson, T. H. G., *Aircraft Structures for Engineering Students*, Second Edition, Halsted Press, 1990.
- [60] Koiter, W. T., "A Consistent First Approximation in the Theory of Thin Elastic Shells," *Proc. IUTAM Symp.*, Delft, 1959.
- [61] Sanders, J. L., "An Improved First-Approximation Theory for Thin Shells," *NASATR-R24*, 1959.
- [62] Koiter, W. T., "A Consistent First Approximation in the General Theory of Thin Elastic Shells," *Proc. IUTAM Symp on the Theory of Thin Shells*, Delft, August 1969, 12-33, North-Holland Publ. Amsterdam, 1960, Edited by W. T. Koiter.
- [63] Berdichevsky, V. L., and Misiura, V., "Effect of Accuracy Loss in Classical Shell Theory," *Journal of Applied Mechanics*, to appear.
- [64] Berdichevsky, V. L., and Starosel'skii, L. A., "On the Energy of Curvilinear Timoshenko-Type Rods," *Journal of Applied Mathematics and Mechanics*

(*PMM*), Vol. 47, No. 6, pp. 809-817, 1983.

- [65] Hodges, Dewey H., Atilgan, Ali R., Cesnik, Carlos E. S., and Fulton, Mark V., "On a Simplified Strain Energy Function for Geometrically Nonlinear Behavior of Anisotropic Beams," Presented at the Seventeenth European Rotorcraft Forum, September 24-26, 1991, Berlin, Germany. To appear in *Composite Engineering*, 1992.
- [66] Hodges, Dewey H., Private Communication, School of Aerospace Engineering, Georgia Institute of Technology, December 1991.

VITA

Ashraf M. Badir was born on September 11, 1959 in Alexandria, Egypt. He graduated in 1982 from Alexandria University with a Bachelor of Science Degree in Civil Engineering with Honor. He worked as a Research and Teaching Assistant for the Department of Structural Engineering, Alexandria University until he earned a Master of Science Degree in Civil Engineering from Alexandria University in 1985. He also worked as a part-time design engineer for two years starting 1983 in a civil engineering consulting office in Alexandria. He was appointed assistant lecturer of theory of structures in Alexandria University in September 1985. In 1986, he joined the Civil Engineering Department of University of Windsor, Ontario, Canada where he worked as a Graduate Research and Teaching Assistant. He joined the School of Aerospace Engineering at the Georgia Institute of Technology in Winter 1988 and earned a Master's of Science Degree in 1989.

APPENDIX B

PUBLICATIONS AND PRESENTATIONS

Refereed Papers:

1. Armanios, E.A. and Rehfield, L.W., "Sublaminar Analysis of Interlaminar Fracture in Composites: Part I - Analytical Model," *Journal of Composites Technology & Research*, Vol. 11, No. 4, Winter 1989, pp. 135-146.
2. Armanios, E.A. Rehfield, L.W., Raju, I.S., and O'Brien, T.K. "Sublaminar Analysis of Interlaminar Fracture in Composites: Part II--Applications," *Journal of Composites Technology & Research*, Vol. 11, No. 4, Winter 1989, pp. 147-153.
3. Armanios, E.A. and Badir, A.M., "Hygrothermal Influence on Mode I Edge Delamination in Composites," *Journal of Composite Structures*, Vol. 15, No. 4, 1990, pp. 323-342.
4. Armanios, E.A., and Parnas, L., "Delamination Analysis of Tapered Laminated Composites Under Tensile Loading," *Composite Materials: Fatigue and Fracture (Third Volume)*, ASTM STP 1110, T. K. O'Brien, Ed., American Society for Testing and Materials, Philadelphia, 1991, pp. 340-358.
5. Armanios, E.A., Sriram, P., and Badir, A.M., "Fracture Analysis of Transverse Crack-Tip and Free Edge Delamination in Laminated Composites," *Composite Materials: Fatigue and Fracture (Third Volume)*, ASTM STP 1110, T. K. O'Brien, Ed., American Society for Testing and Materials, Philadelphia, 1991, pp. 269-286.
6. Berdichevsky, V., Armanios, E. A. and Badir, A., "Theory of Anisotropic Thin-walled Closed-cross-section Beams," *Composites Engineering*, Vol. 2, Nos. 5-7, pp. 411-432, 1992.

Conference Proceedings:

1. Armanios, E.A. and Rehfield, L.W., "Interlaminar Analysis of Laminated Composites Using a Sublaminar Approach," *Proceedings of the AIAA/ASME/ASCE/AHS 27th Structures, Structural Dynamics, and Materials (SDM) Conference*, San Antonio, Texas, 19-21 May, 1986. AIAA Paper No. 86-0969CP, Part 1, pp. 442-452.
2. Armanios, E.A. and Mahler, M.A., "Residual Thermal and Moisture Influences on the Free-Edge Delamination of Laminated Composites," *Proceedings of the AIAA/ASME/ASCE/AHS 19th Structures, Structural Dynamics and Materials (SDM) Conference*, Part 1, pp. 371-381, 1988.
3. Armanios, E.A. and Rehfield, L.W., "A Simplified Approach to Strain Energy Release Computations for Interlaminar Fracture of Composites," *Proceedings of the Fourth Japan-U.S. Conference on Composite Materials*, June 27-29, 1988, Washington, D.C., Technomic Publishing Co., pp. 285-296.
4. Armanios, E.A., Badir, A. and Sriram, P., "Sublaminar Analysis of Mode I Edge Delamination in Laminated Composites," *Proceedings of the AIAA/ASME/AHS/ASC 30th Structures, Structural Dynamics and Materials (SDM) Conference*, Mobile, Alabama, April 3-5, 1989, pp. 2109-2116.
5. Sriram, P., and Armanios, E.A., "Fracture Analysis of Local Delaminations in Laminated Composites," *Proceedings of the AIAA/ASME/ASCE/AHS/ASC 30th (SDM) Conference*, Mobile, Alabama, April 3-5, 1989, pp. 2109-2116.

6. Armanios, E.A. and Badir, A.M., "Hygrothermal Influence on the Edge Delamination in Composites," *Proceedings of the American Society for Composites Fourth Technical Conference*, V.P.I. Blacksburg, VA, October 3-5, 1989, pp. 944-950.

7. Armanios, E.A., Badir, A. and Berdichevsky, V., "Effect of Damage on Elastically Tailored Composite Laminates", *Proceedings of the AHS International Technical Specialists' Meeting on Rotorcraft Basic Research*, Atlanta, Georgia, March 25-27, 1991, pp. (48-1)-(48-11).

8. Badir, A. M., "Theory of Anisotropic Thin-Walled Closed- Section Beams with Hygrothermal Effects," *Proceedings of the 33rd AIAA/ASME/ASCE/AHS Structures, Structural Dynamics, and Materials (SDM) Conference*, San Antonio, Texas, 19-21 May, 1986. AIAA Paper No. 86-0969CP, Part 1, pp. 442-452.

Presentations:

1. Rehfield, L.W. and Armanios, E.A., "Sublaminar Analysis of Interlaminar Fracture in Composites," 1985 Grant and Contract Review Vol. II, NASA Langley Research Center, Materials Division, Fatigue and Fracture Branch, February 13-14, 1985.

2. Armanios, E.A., "Analytical Modeling of Interlaminar Fracture Behavior in the Edge Delamination Specimen (Extension)," NASA/AVSCOM/Bell Helicopter Meeting, Georgia Institute of Technology, Atlanta, GA, July 15-16, 1985.

3. Armanios, E.A., "Analytical Modeling of Interlaminar Fracture Behavior in the Edge Delamination Specimen (Bending and Combined Bending and Extension)," NASA/AVSCOM/Bell Helicopter Meeting, Georgia Institute of Technology, Atlanta, GA, July 15-16, 1985.

4. Armanios, E.A. and Rehfield, L.W., "Interlaminar Analysis of Laminated Composites using a Sublaminar Approach," *AIAA/ASME/ASCE/AHS 27th Structures, Structural Dynamics, and Materials (SDM) Conference*, San Antonio, Texas, May 19-21, 1986.

5. Armanios, E.A. and Mahler, M.A., "Residual Thermal and Moisture Influences on the Free-Edge Delamination of Laminated Composites," *Proceeding of the AIAA/ASME/AHS/ASC 29th Structures, Structural Dynamics and Materials (SDM) Conference*, Williamsburg, VA, April 18-20, 1988.

6. Armanios, E.A. and Rehfield, L.W., "A Simplified Approach to Strain Energy Release Computations for Interlaminar Fracture of Composites," *Fourth Japan-U.S. Conference on Composite Materials*, June 27-29, 1988, Washington , D.C.

7. Armanios, E.A., Badir, A., and Sriram, P., "Sublaminar Analysis of Mode I Edge Delamination in Laminated Composites," *AIAA/ASME/ASCE/AHS/ASC 30th Structures, Structural Dynamics and Materials (SDM) Conference*, Mobile, Alabama, April 3-5, 1989.

8. Sriram, P. and Armanios, E.A., "Fracture Analysis of Local Delamination in Laminated Composites," *AIAA/ASME/ASCE/AHS/ASC 30th Structures, Structural Dynamics and Materials (SDM) Conference*, Mobile, Alabama, April 3-5, 1989.

9. Armanios, E.A. and Badir, A.M., "Hygrothermal Influence on the Edge Delamination in Composites," *the American Society for Composites, Fourth Technical Conference*, V.P.I., Blacksburg, VA, October 3-5, 1989.

10. Armanios, E.A., "Analysis of Delamination Related Fracture Processes in Composites," *Review of NASA Langley Composites Grants*, NASA Langley Research Center, Materials Division, May 16-17, 1989.
11. Armanios, E.A., Sriram, P. and Badir, A., "Fracture Analysis of Matrix Crack-Tip and Free Edge Delamination in Laminated Composites," *Third Symposium on Composite Materials: Fatigue and Fracture*, Lake Buena Vista, Florida, November 6-7, 1989.
12. Armanios, E.A. and Parnas, L., "Delamination Analysis of Tapered Laminated Composites under Tensile Loading," *Third Symposium on Composite Materials: Fatigue and Fracture*, Lake Buena Vista, Florida, November 6-7, 1989.
13. Armanios, E.A. and Sriram, P., "Modeling of Transverse Cracks in Laminated Composites," *Fifteenth Southeastern Conference on Theoretical and Applied Mechanics (SECTAM)*, Atlanta, Georgia, March 22-23, 1990.
14. Armanios, E.A., Badir, A. and Berdichevsky, V., "Effect of Damage on Elastically Tailored Composite Laminates", *AHS International Technical Specialists' Meeting on Rotorcraft Basic Research*, Atlanta, Georgia, March 25-27, 1991.
15. Armanios, E.A., Badir, A. and Berdichevsky, V., "An Assessment of Thin-Walled Closed Sections Composite Beam Theories", *AIAA Aerospace Symposium*, Atlanta, Georgia, February 28-29, 1992.
16. Badir, A. M., "Analysis of Composite Rotor Blades," AIAA Southeastern Regional Student Conference, Orlando, Florida, April 11-13, 1991.
17. Badir, A. M. and Armanios, E. A. "Theory of Anisotropic Thin-Walled Opened-Cross-Section Beams with Hygrothermal Effects," To be presented *34th AIAA/ASME/ASCE/AHS Structures, Structural Dynamics, and Materials (SDM) Conference*, Lajolla, California, April 19-21, 1993

M.Sc. Special Problems:

1. Mahler, M., "A Study on the Thermal and Moisture Influences on the Free-edge Delamination of Laminated Composites," Special Problem Report Submitted in partial fulfillment of the requirements for the M.Sc. degree, School of Aerospace Engineering, Georgia Institute of Technology, September, 1987.
2. Badir, A. M., "Hygrothermal Influence on Mode I Edge Delamination in Composites," Special Problem Report Submitted in partial fulfillment of the requirements for the M.Sc. degree, School of Aerospace Engineering, Georgia Institute of Technology, June, 1989.

Ph. D. Theses:

1. Parnas, L., "Failure Mechanisms and Prediction in Advanced Composite Materials," Ph.D Thesis, School of Aerospace Engineering, Georgia Institute of Technology, March 1991.
2. Badir, A. M., "Analysis of Advanced Thin-Walled Composite Structures". Ph.D. Thesis, Georgia Institute of Technology, February 1992.

